BESTE SEYLA GÖÇKÜN

M.S. Thesis

JULY,2022

ON SOME OF THE FACTORS INFLUENCING THE ENGINEERING PROPERTIES OF IMPROVED CLAYEY SOILS

BESTE SEYLA GÖÇKÜN

IŞIK UNIVERSITY
JULY,2022

ON SOME OF THE FACTORS INFLUENCING THE ENGINEERING PROPERTIES OF IMPROVED CLAYEY SOILS

BESTE SEYLA GÖÇKÜN
B.S., Civil Engineering, Işık University, 2020
M.S., Civil Engineering, Işık University, 2022

Submitted to the Graduate School of Science and Engineering in partial fulfillment
of the requirements for the degree of Master of Science
in
Civil Engineering.

IŞIK UNIVERSITY
JULY, 2022

IŞIK UNIVERSITY
GRADUATE SCHOOL OF SCIENCE AND ENGINEERING

ON SOME OF THE FACTORS INFLUENCING THE ENGINEERING PROPERTIES OF IMPROVED CLAYEY SOILS

BESTE SEYLA GÖÇKÜN

APPROVED BY:

Assist. Prof. Ehsan ETMİNAN (Thesis Advisor)	Işık University
Prof. Aykut ŞENOL	Istanbul Technical University
Assist. Prof. Önder UMUT	Işık University

APPROVAL DATE: 04/07/2022

ON SOME OF THE FACTORS INFLUENCING THE ENGINEERING PROPERTIES OF IMPROVED CLAYEY SOILS

ABSTRACT

Alternative materials and techniques are constantly being investigated within the scope of innovative solutions for the construction of earth structures. Improvement of soft soils for the structures, such as subgrades of highway embankments and shallow foundation soils, can be critical for implementing sustainable and economic applications, especially in the cases where alternative materials are used in soft soils. During this thesis, the high plasticity clay was mixed with class C fly ash which is a recycled material, and two different synthetic fibers in order to stabilize clayey soil. Furthermore, fly ash combined with each copolymer and polypropylene fiber was added to the high plasticity clay to observe more effective improvement. In this thesis, findings from both laboratory and numerical analysis executed with particular emphasis on the use of mentioned alternative materials were represented. First, the compaction and unconfined compression tests were performed on all mixtures. On the other hand, the influence of adding alternative materials to high plasticity clayey soil was studied from analytical aspects by modifying and suggesting new versions of the Duncan-Chang hyperbolic model for the unconfined compression test results. After gathering the unconfined compression test results of mentioned mixtures, the initial tangent modulus (E_i) and the tangent modulus at half of the maximum stress (E_{t50}) were found using the modified Duncan-Chang model. Then, the secant modulus at failure point (E_{sf}) and the secant modulus at half of the maximum stress (E_{s50}) were determined by suggested new equations in terms of the initial tangent modulus and the tangent modulus at half of the maximum stress. The relationship between each soil moduli and the unconfined compression strength of all tested samples were also presented. Finally, obtained soil moduli values of high plasticity clay mixtures improved that mentioned alternative materials and increased the strength and load-deformation properties of high plasticity clayey soil with different percentages.

Keywords: Clayey Soil Stabilization, Fly Ash, Fiber Reinforcement, Modified Duncan-Chang Model, Deformation Modulus

İYİLEŞTİRİLMİŞ KİLLİ ZEMİNLERİN MÜHENDİSLİK ÖZELLİKLERİ ÜZERİNDE ETKİLİ OLAN BAZI FAKTÖRLER

ÖZET

Toprak yapıların inşası için yenilikçi çözümler geliştirme kapsamında sürekli alternatif malzeme ve teknikler araştırılmaktadır. Başta dayanımları olmak üzere elverişsiz mühendislik özelliklerine sahip olan yumuşak zeminlerin tekrar tasarlanarak geliştirilmesi zemin iyileştirme olarak tanımlanmaktadır. Zemin boşluklarının çeşitli bileşimdeki karışımlarla doldurularak zemin boşluk oranının azaltılması zemin iyileştirme yöntemlerinin temel amaçlarındandır. Otoyol dolgularının zeminleri ve yüzeysel temellerin zeminleri gibi yapılar için, özellikle alternatif malzemelerin kullanıldığı durumlarda yumuşak zeminlerin iyileştirilmesi sürdürülebilir ve ekonomik uygulamaların sağlanması için kritik olabilmektedir. Sonuç olarak, alternatif malzemelerle zayıf mühendislik özelliklerine sahip mevcut zeminin belirli oranlarda karıştırılması, sıkça kullanılan, maliyet ve zaman açısından büyük tasarruflara sebep olan bir yöntem olarak kullanılmaktadır.

Bu çalışma boyunca, yüksek plastisiteli kil, geri dönüştürülmüş bir malzeme olan C tipi uçucu kül ve iki farklı sentetik fiber ile killi zemini stabilize etmek için karıştırılmıştır. Ayrıca, hem kopolmer hem de polipropilen ile ayrı ayrı birleştirilmiş uçucu kül, daha verimli bir zemin iyileştirmesi gözlemlemek için yüksek plastisiteli kile karıştırılmıştır. Bu çalışmada, hem ekonomik hem de çevresel etkiler açısından azalmaya sebep olan bahsedilen alternatif malzemelerin kullanımına özel vurgu yapılarak uygulanan laboratuvar ve sayısal analizlerden elde edilen bulgular gösterilmiştir. Öncelikle, kompaksiyon ve serbest basınç deneyleri tüm karışımlar üzerinde uygulanmıştır. Bir diğer yandan, Duncan-Chang hiperbolik modeli serbest basınç deney sonuçları için modifiye edilerek ve yeni formüller önerilerek, yüksek plastisiteli killi zeminlere alternatif malzemeler eklenmesinin etkisi analitik yönlerden incelenmiştir. Bahsedilen karışımların serbest basınç deney sonuçları toplandıktan sonra, başlangıç tanjant modülü (E_i) ve maksimum aksiyel gerilmenin yarısındaki tanjant modülü (E_{t50}) modifiye edilmiş Duncan-Chang modeli kullanılarak bulunmuştur. Sonrasında, göçme noktasındaki sekant modülü (E_{sf}) ve maksimum

aksiyel gerilmenin yarısındaki sekant modülü (E_{s50}), başlangıç tanjant ve maksimum aksiyel gerilmenin yarısındaki tanjant modülleri cinsinden önerilen yeni formüller ile saptanmıştır. Deneye tabii tutulmuş tüm numuneler için, her bir zemin modülü ile serbest basınç dayanımı arasındaki ilişki ayrıca sunulmuştur. Son olarak, yüksek plastisiteli kil karışımlarının elde edilmiş zemin modül değerleri doğrultusunda, bahsedilen alternatif malzemelerin yüksek plastisiteli killi zeminin mukavemetini ve yük-deformasyon özelliklerini farklı yüzdelerde arttırdığı tespit edilmiştir.

Anahtar Kelimeler: Killi Zemin Stabilizasyonu, Uçucu Kül, Fiber Güçlendirme, Modifiye edilmiş Duncan-Chang Modeli, Deformasyon Modülü

ACKNOWLEDGEMENTS

First and foremost, I thank the respectful members of the Civil Engineering Department of Işık University for giving me the opportunity to study for my M.Sc. thesis. I would especially like to thank and tell my regards to my thesis advisor, Assist. Prof. Ehsan ETMİNAN, who contributed much to the development of this research, starting from the early stages of my dissertation work. I also would like to state that having the opportunity to work with him over the years was intellectually rewarding and fulfilling.

The last words of thanks go to my family. I thank my parents and my sister for their patience and encouragement. Any accomplishments of mine are due to their support.

Beste Seyla GÖÇKÜN

To my family…

TABLE OF CONTENTS

LIST OF TABLES

LIST OF FIGURES

LIST OF SYMBOLS

A	:	Area of the soil plane
A_o	:	Bottom or top surface area of the soil sample
b	:	Reciprocal of asymptotic value of stress difference
C_i	:	Initial moduli
CSL	:	Critical state line
c	:	Cohesion of soil
c’	:	Effective cohesion
c_{cm}	:	Cementation strength of soil
c_u	:	Undrained shear strength
c_{app}	:	Apparent cohesion
D	:	Diameter of the soil particles
D	:	Deviatoric tensor
d	:	Diameter of the sample
$d\gamma$	:	Incremental shear strain
$d\varepsilon_z$	:	Incremental vertical strain
E	:	Modulus of elasticity or Young’s modulus
E_i	:	Initial tangent modulus
E_s	:	Secant modulus
E_{s50}	:	Secant modulus at one-half the maximum stress
E_{sf}	:	Secant modulus at the maximum stress or failure
E_t	:	Tangent modulus
E_{t50}	:	Tangent modulus at the half of the maximum stress
E_u	:	Unloading modulus
E_r	:	Reloading modulus
E_c	:	Cyclic modulus
e_{cs}	:	Critical void ratio

e	:	Void ratio
e_o	:	Initial void ratio
e_{co}	:	Initial void ratio corresponding to critical state
e^e	:	Elastic component of the strain
e_y	:	Void ratio corresponding to yield stress
e_{so}	:	Initial void ratio corresponding to the initial net normal stress
e^e	:	Void ratio elastic rebound swelling on Barcelona Basic model
F	:	Resultant force
F	:	Finer percent
f	:	Plastic potential or the yield function
G	:	Shear modulus
H_o	:	Initial height of the soil sample
K	:	Modulus number
K	:	Bulk modulus
k	:	Constant of proportion
L	:	Length of the soil specimen
LL	:	Liquid limit
M	:	Constrained modulus
M	:	Critical state parameter on Modified Cam Clay model
M_i	:	Soil mass in *i*th sieve on sieve analysis
N	:	Normal force
NCL	:	Normal compression line
n	:	Exponent of variation rate
OCR	:	Over consolidation ratio
PI	:	Plasticity index
PL	:	Plastic limit
p_a	:	Atmospheric pressure
p’	:	Mean normal stress
p'_o	:	Initial effective stress
p'_y	:	Effective yield stress
p*	:	Net normal stress on Barcelona Basic model
p^*_o	:	Initial net normal stress
p	:	Total principal stress
q_u	:	Unconfined compression strength

q	:	Deviatoric stress
q	:	Deviator stress
$q_{u(undisturbed)}$	:	Unconfined compression strength in undisturbed state
$q_{u(remolded)}$	:	Unconfined compression strength in remolded state
R_f	:	Failure ratio
r_o	:	Initial radius of cylindrical soil sample
S	:	Spherical tensor
S	:	Fraction of strength on Duncan-Chang model
s	:	Net suction or water tension
T	:	Force tangent to the surface
TSP	:	Total stress path
t	:	Stress vector
u_a	:	Pore air pressure
u_w	:	Pore water pressure
v	:	Velocity of soil particles in hydrometer test
α	:	Fraction of the total area
α	:	Dilation angle
β	:	Fraction of the plane covered by air
γ_{ij}	:	Shear strains
γ_{max}	:	Maximum shear strain
γ_{dmax}	:	Maximum dry unit weight
ΔP	:	Normal force
Δx	:	Horizontal displacement
Δz	:	Length change of the soil sample in height
Δr	:	Length change of the soil sample in Radius
Δe	:	Change in void ratio from e_o
Δu	:	Change in porewater pressure
$\Delta\sigma_1$	:	Axial pressure increment
$\Delta\sigma_3$	:	Lateral pressure increment
$\Delta\varepsilon_1$	:	Axial strain increment
ε_p or ε_v	:	Volumetric strain
ε_r	:	Radial strain
ε_z	:	Vertical strain
ε_1	:	Major principal strain

ε_3 : Minor principal strain

ε_{50} : Axial strain at half of the maximum stress

ε_f : Axial strain at the maximum stress

ξ_o : Apparent friction angle

η : Viscosity of water

θ : Inclination angle of failure plane

κ : Swelling index

κ_s : Compression index

λ : Lame's constant

λ : Isotropic logarithmic compression index

λ_o : Compression index for zero suction

λ_s : Slope of NCL

μ_f : Static friction coefficient of sliding

ν : Poisson's ratio

ρ_s : Density of soil

ρ_w : Density of water

σ : Normal stress

σ' : Effective stress

σ_M : Mean normal stress

σ_1 : Major principal stress

σ_2 : Intermediate principal stress

σ_3 : Minor principal stresses

σ'_o : Effective overburden pressure

σ'_p : Preconsolidation pressure

σ'_v : Vertical effective stress

$(\sigma'_n)_f$: Normal effective stress on slip

$(\sigma'_1)_f$: Major principal effective stress

$(\sigma'_3)_f$: Minor principal effective stress

σ_m : Mean principal stress

$(\sigma_1 - \sigma_3)_f$: Stress difference at failure

$(\sigma_1 - \sigma_3)_{ult}$: Asymptotic value of stress difference

$(\sigma_1)_f$: Maximum stress in the stress-strain curve

τ : Shear stress

τ_{max} : Maximum shear stress

τ_f	:	Shear strength of soil
τ_{cs}	:	Critical state shear stress
τ_p	:	Peak shear stress
φ	:	Friction angle
φ'	:	Effective friction angle
φ^b	:	Angle in rate of shear strength increase with the matric suction
χ	:	Fraction of a unit cross sectional area in soil occupied by water
ω	:	Water content
ω_{opt}	:	Optimum water content
$\sum$	:	Strain tensor

CHAPTER 1

1. INTRODUCTION

Geotechnical engineering studies deal with soils under various types of loadings, such as earthquake and static loadings. If a certain amount of loading is applied to soil, it causes deformations in the applied loading direction. The type and amount of this deformation can be related to soil's different engineering properties and behaviors. For instance, clayey soils have more complex water and clay particle interactions than gravels, sands, and silty soils. Hence, it is obvious that the engineering properties of clayey soils should be studied. It should be noted that the inadequacy strength of the clayey soils can be led to catastrophic disasters such as the settlement of foundations and slope stability failure of highway road embankments. In general, laboratory tests are used to determine different engineering behavior of cohesive soils, and there are several methods for assessing the deformation characteristics of the soils. One of the methods is through the analysis of the deformation modulus, which provides useful information about the deformation features of the soils.

Another challenge in geotechnical engineering is that selecting appropriate materials is a primary problem in cost and engineering behavior aspects for subgrade and embankment constructions. Also, cohesive soils can result in excessive settlement on the foundation of structures. Therefore, investigating the engineering properties of the clayey soils under different loads plays an important role in the stability of earth structures. The total compressibility limits of cohesive soils may be limited or maintained by using alternative materials. Furthermore, the cohesive soils can be improved by stabilization techniques that enhance the engineering properties by adding soil-stabilized engineering materials into available materials. In addition, cementitious stabilization and soil reinforcement using synthetic fibers may be effective options to improve the strength features of cohesive soils (Etminan, 2012).

Stabilizing the soils with fly ash can be a good option for geotechnical engineers. It can be a solution to the exiguity of conventional construction materials and environmental and ecological issues. The usage of fly ash provides cost efficiency in a construction project in a significant way. Fly ash can be categorized based on the chemical composition of the type of coal burned, and it is generally used for cementitious stabilization in clayey soils. Also, the enhancement of strength and decreasing the amount of deformations can be provided by adding fly ash to available materials. It is suitable for many civil engineering applications because of its self-hardening characteristics.

As a second option for stabilizing clayey soils, fibers such as polypropylene and copolymer are used to improve the mechanical behavior in soil composition. Since the shear stresses in the fiber-reinforced soil are transported by tensile resistance in the fibers, it represents relatively high tensile strength compared with plain soils. Therefore, soil reinforcement seems to play an important role in improving the engineering properties, such as shear strength, compressibility, hydraulic conductivity, and density. For instance, reinforcing soil with polypropylene fiber increases strength, and using the copolymer as a reinforcement in the soil leads to an increase in durability. The main purposes of reinforcing soil are improving stability, increasing bearing capacity, reducing lateral deformations, and decreasing settlements.

Soil nature exhibits a nonlinear behavior, and also, the soil's stiffness and strength properties relate to its strain and stress levels. However, the stress and strain relationship is not simply due to the nonlinear behavior of soil. It should be noted that the deformation modulus is an essential parameter for the soft soils subjected to the stabilization techniques such as mixing the soil with fly ash or synthetic fibers. Nevertheless, relatively little is known about how and to what extent the deformation moduli are influenced when clayey soils are reinforced with synthetic fibers and stabilized with fly ash. Thus, it is obvious that setting up a numerical process of engineering properties in the soil is called the constitutive model. The illustration of stress-strain curves using mathematical functions and fitting methods, the nonlinear elasticity, and plasticity theories are methods used to propose the constitutive models. On the other hand, creating or modifying a constitutive model may lead to investigating the engineering properties of tested soils, and it can provide the proper and trustable results.

As a used constitutive model in this thesis, the Duncan-Chang model is the most common and widely used model for determining the nonlinear characteristics of various types of soils. In other words, the Duncan-Chang hyperbolic model is more suitable for most soil types by modifying under complicated stress states. It should be noted that the required parameters to apply the Duncan-Chang model can be obtained from the triaxial tests. In addition, it can be understood that the tangent modulus proposed by Duncan and Chang (1970) and the unconfined compression test coincide with the observation of the main feature of stress and strain relationships.

As a result, the material's excavation, loading, and transportation costs are the most important factors for the total cost during the construction process. The soft clayey soil is removed and replaced by gravel or crushed rock fill layer to reach higher bearing capacity values in the conventional approach. Recently, it has been found that using existing soft soil is the most economical way. Hence, it seems inevitable to stabilize and improve the engineering properties of the existing soft soil to satisfy the necessary criteria for engineering constructions. One of the main targets of this thesis is to find the best additive for clayey soils by performing laboratory experiments and analyzing their outcomes. It should be noted that fly ash, which is recycled material and different synthetic fibers that were used as additives during the experimental program from different soil moduli aspects, are selected in a way that provides economic benefits and reduces environmental impacts. As a next step, modifying the mentioned model to analyze the results of unconfined compression tests in more accessible and trustable ways. Initial tangent modulus (E_i), tangent modulus at half of the maximum stress (E_{t50}), secant modulus at half of the maximum stress (E_{s50}), and secant modulus at failure (E_{sf}) were determined by using the modified constitutive model. In the last part of the study, all soil moduli data of clayey soil mixtures were compared to investigate soft soil stabilization by using mentioned alternative materials to achieve a better amount of stabilization.

CHAPTER 2

2. STRESS AND STRAIN BEHAVIOUR OF CLAYEY SOILS

One of the essential factors in the behavior of clayey soils is understanding fundamental principles of mechanics in determining stress and strain conditions. Practically, constructions and geotechnical structures cause a change in stress and strain. Therefore, stress and strain behavior have to be understood by a geotechnical engineer. Furthermore, it is essential to calculate the ground settlement and estimate slope stability analysis of retaining structures.

Determination of stress and strain conditions in clayey soils may be difficult. In most cases, the nature of the soil is not homogeneous, elastic, and rigid. In general, we assume that the soil is an elastic material. This situation has advantages for the practical work and geotechnical tests. In this part of the thesis, the elastic behavior of the soil is explained. In the third part of the thesis, nonlinear and inelastic soil behavior are discussed in detail by constitutive models of soils.

2.1 Stress-Strain Response of Materials to Normal and Shear Forces

The stress and strain concepts are necessary to state the soil properties, such as the modulus of elasticity or Poisson's ratio. In general, the theories of stress and strain in soil refer to the theory of elasticity. The stress determined as force divided by area at a certain point is the intensity of loading. The strain defined as the change ratio of the original dimension is the intensity of deformation in the soil medium. Applied force on the soil medium may not be tangent or perpendicular to the area. Therefore, the stress vector on the given point in a soil medium is determined as:

$$\vec{t} = \lim_{A \to 0} \frac{\vec{F}}{A} \tag{2.1}$$

where F is the resultant force at a certain point, and A is the area of the plane where the resultant force is applied, t is the stress vector. If the soil mass is assumed that a cube and the applied forces are tangent or perpendicular to the area, the general formulation of the shear and normal stresses can be written as:

$$\sigma = \frac{N}{A} \tag{2.2}$$

$$\tau = \frac{T}{A} \tag{2.3}$$

where σ is the normal stress, N is subjected to the force that is normal to the surface of the soil area A, τ is the shear stress, and T is subjected to the force tangent to the soil area A. Figure 2.1 illustrates normal and shear stresses in the coordinate system.

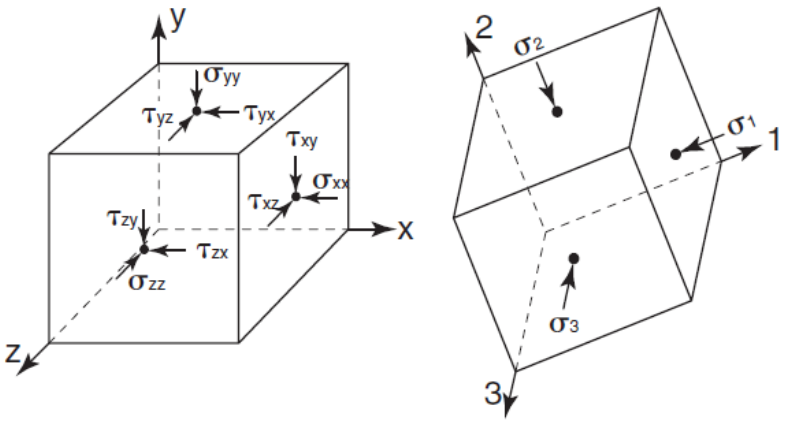

Figure 2.1 Normal and shear stresses on the cube (Briaud, 2013)

σ_x, σ_y, and σ_z are normal stresses acting on the planes normal to the x, y, z axes. τ_{ij} is the notation for shear stress that i denotes the stress acting on the normal plane and j denotes the parallel direction axis. τ_{xy}, τ_{yx}, τ_{yz}, τ_{zy}, τ_{xz} and τ_{zx} are shear stresses. For a moment of equilibrium:

$$\tau_{xy} = \tau_{yx} \tag{2.4}$$

$$\tau_{yz} = \tau_{zy} \tag{2.5}$$

$$\tau_{xz} = \tau_{zx} \tag{2.6}$$

Symmetry and equilibrium cause equal and opposite stresses on opposite faces. Typically, there are 18 stresses (6x3 stresses). However, the number of stresses is decreased by 6 independent stresses, which are 3 normal stresses and 3 shear stresses.

These stresses can be illustrated on a 3x3 symmetric matrix because the shear stresses on the perpendicular planes are equal to each other. Therefore, the stress tensor $\sum$ is written as:

$$\sum = \begin{bmatrix} \sigma_x & \tau_{xy} & \tau_{xz} \\ \tau_{yx} & \sigma_y & \tau_{yz} \\ \tau_{zx} & \tau_{zy} & \sigma_z \end{bmatrix} \tag{2.7}$$

The stress tensor $\sum$ can be assembled by deviatoric tensor D and spherical tensor S:

$$\sum = \begin{bmatrix} \sigma_x & \tau_{xy} & \tau_{xz} \\ \tau_{yx} & \sigma_y & \tau_{yz} \\ \tau_{zx} & \tau_{zy} & \sigma_z \end{bmatrix} = S + D = \begin{bmatrix} \sigma_M & 0 & 0 \\ 0 & \sigma_M & 0 \\ 0 & 0 & \sigma_M \end{bmatrix} + \begin{bmatrix} \sigma_x - \sigma_M & \tau_{xy} & \tau_{xz} \\ \tau_{yx} & \sigma_y - \sigma_M & \tau_{yz} \\ \tau_{zx} & \tau_{zy} & \sigma_z - \sigma_M \end{bmatrix} \tag{2.8}$$

where

$$\sigma_M = \frac{1}{3}(\sigma_x + \sigma_y + \sigma_z) \tag{2.9}$$

where σ_M is the mean normal stress. The spherical tensor denotes a confinement effect at the point in the soil medium. The deviatoric tensor denotes the effect of various shear stress, which disrupts with no mean normal stress (Briaud, 2013).

In Figure 2.1, there are three planes where the shear stresses are equal to zero, which are perpendicular to each other. They are called principal planes. The normal stresses on the principal planes are named principal stresses. The principal stresses are denoted by σ_1, σ_2, and σ_3. The largest stress in the principal stresses is named major principal stress, σ_1, and the smallest is named minor principal stress, σ_3. Also, the σ_2 is called intermediate principal stress (Briaud, 2013). Figure 2.2 shows a soil element subjected to shear and normal stresses.

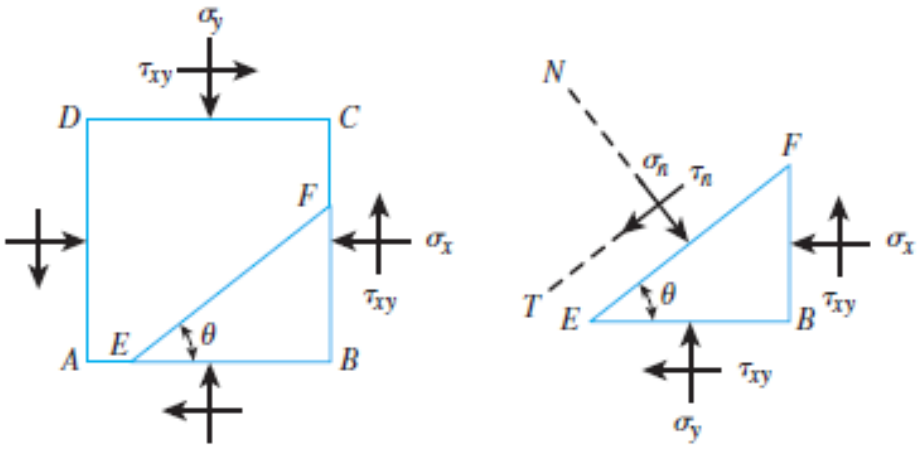

Figure 2.2 Normal and shear stresses acting on soil (Das, 2010)

It is seen that shear stress on the EF plane makes an angle θ with the AB plane. σ_n and τ_n are normal and shear stress (Das, 2010). σ_n and τ_n are considered by geometry, and the obtained formulation of these can be written as:

$$\sigma_n = \sigma_x \sin^2\theta + \sigma_y \cos^2\theta + 2\tau_{xy} \sin\theta \cos\theta \quad (2.10)$$

$$\sigma_n = \frac{\sigma y+\sigma x}{2} + \frac{\sigma y-\sigma x}{2} \cos 2\theta + \tau_{xy} \sin 2\theta \quad (2.11)$$

$$\tau_n = \frac{\sigma_y-\sigma_x}{2} \sin 2\theta - \tau_{xy} \cos 2\theta \quad (2.12)$$

Angle θ can be chosen as a value that makes the τ_n equal to zero. Substituting $\tau_n = 0$ into Eq.(2.12):

$$\tan 2\theta = \frac{2\tau_{xy}}{\sigma_y-\sigma_x} \quad (2.13)$$

In Eq. (2.13), chosen values of θ can make the two planes whose shear stresses are zero, respectively θ. That planes are called principal planes, and the normal stress acting on the principal planes is called principal stresses. The principal stresses can be written by substituting the Eq.(2.13) into Eq. (2.11):

$$\sigma_n=\sigma_1 = \frac{\sigma y+\sigma x}{2} + \sqrt{\left[\frac{(\sigma y-\sigma x)}{2}\right]^2 + {\tau_{xy}}^2} \quad (2.14)$$

$$\sigma_n= \sigma_3 = \frac{\sigma y+\sigma x}{2} - \sqrt{\left[\frac{(\sigma y-\sigma x)}{2}\right]^2 + {\tau_{xy}}^2} \quad (2.15)$$

where σ_1 is named as major principal stress written in Eq. (2.14) and σ_3 is named as minor principal stress written in Eq. (2.15), as mentioned.

The concept of strain should be understood clearly in geotechnical engineering studies. Again, if a volume of soil is considered due to given stress conditions in Figure 2.3, the displacements of the x, y, and z directions can be denoted by u, v, and w, respectively.

Then the equations of strains which in isotropic and elastic soil material can be written as:

$$\varepsilon_x = \frac{\partial u}{\partial x} \quad (2.16)$$

$$\varepsilon_y = \frac{\partial v}{\partial y} \quad (2.17)$$

$$\varepsilon_z = \frac{\partial w}{\partial z} \tag{2.18}$$

$$\gamma_{xy} = \frac{\partial v}{\partial x} + \frac{\partial u}{\partial y} \tag{2.19}$$

$$\gamma_{yz} = \frac{\partial w}{\partial y} + \frac{\partial v}{\partial z} \tag{2.20}$$

$$\gamma_{zx} = \frac{\partial u}{\partial z} + \frac{\partial w}{\partial x} \tag{2.21}$$

where ε_x, ε_y, and ε_z are normal strains in the x, y, and z directions. γ_{xy} is the shear strain between the xz and yz planes, γ_{yz} is the shear strain between the yx and zx planes, and γ_{zx} is the shear strain between the zy and xy planes.

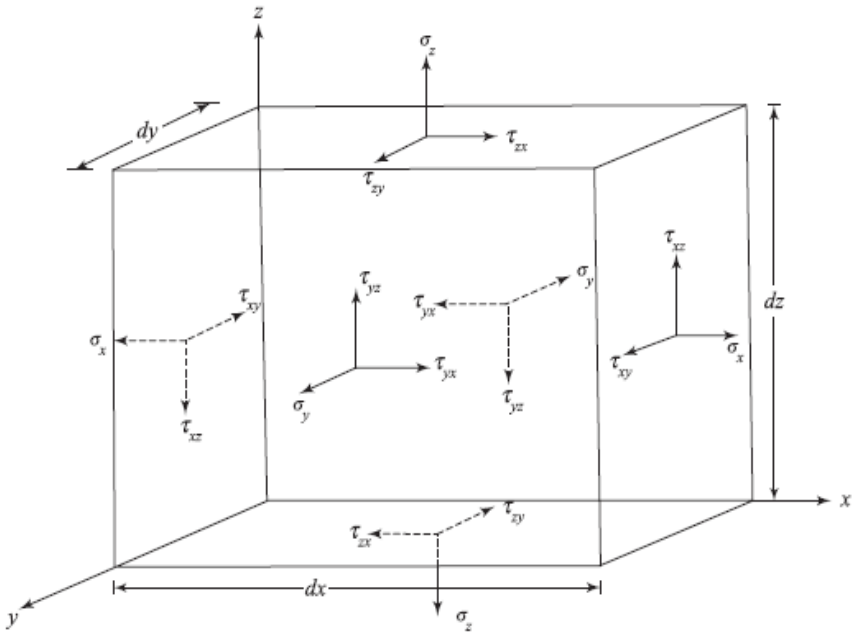

Figure 2.3 Concept of strain (Das and Ramana, 2011)

In addition to the concept of strain, the volumetric strain, which is denoted by ε_p can be written as:

$$\varepsilon_p = \varepsilon_x + \varepsilon_y + \varepsilon_z \tag{2.22}$$

On the other hand, Figure 2.4 shows displacements and forces on a cylindrical soil sample, as shown below.

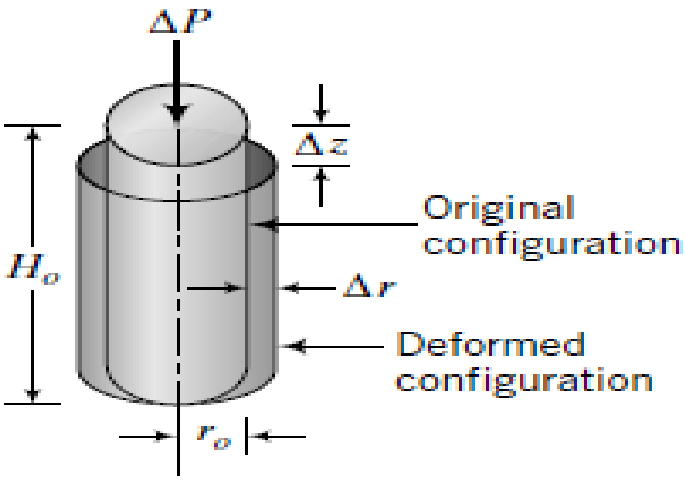

Figure 2.4 Displacements and forces on a cylindrical soil sample (Budhu, 2011)

Suppose the soil mass is assumed that a cylindrical sample and the applied force ΔP is normal to the soil sample area, and H_o is the original height of the soil sample. In that case, r_o is the original radius of the soil sample. Δz and Δr are the length change of the soil sample in height and radius, respectively. Then, the vertical strain, which is denoted by $\Delta\varepsilon_z$, in Eq.(2.23) and radial strain, which is denoted by $\Delta\varepsilon_r$, in Eq.(2.24), and the formulation of Poisson's ratio, which is marked by v, Eq.(2.25) can be written as:

$$\Delta\varepsilon_z = \frac{\Delta z}{H_o} \tag{2.23}$$

$$\Delta\varepsilon_r = \frac{\Delta r}{r_o} \tag{2.24}$$

$$v = \frac{-\Delta\varepsilon_r}{\Delta\varepsilon_z} \tag{2.25}$$

2.1.1 Mohr's Circle for Stress and Strain States

A single circle can be used to find stresses at a point on any soil plane. That technique was discovered by Otto Mohr. (Briaud, 2013). Shear stress and normal stress applied to any soil plane can be determined by Mohr's circle.

The shear stress on a soil plane is plotted on the vertical axis of the coordinates system, and the normal stress on the same soil plane is plotted on the horizontal axis.

All of the stress points obtained for all planes fall in an area bounded by three centered circles on a horizontal axis, as illustrated in Figure 2.5.

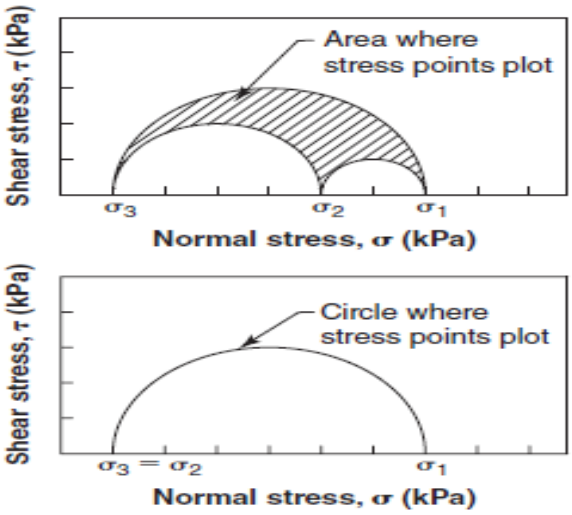

Figure 2.5 Shear stress, normal stress, and Mohr's circle (Briaud, 2013)

The shear stresses are equal on the perpendicular planes. Also, the circles' centers are placed on the horizontal axis. On the other hand, the intersecting points of the circle are on the normal stress axis, which is located on the x-axis. That points are named principal stress values, which are σ_1, σ_2, and σ_3. Moreover, the σ_2 that was called intermediate principal stress is equal to the major or minor principal stresses. Therefore, one circle has occurred in only two principal stresses. Indeed, that case can occur in some situations, such as the unconfined compression test studied in that thesis. In addition, the relationship between the stresses on Mohr's circle:

1. The stress points on the Mohr circle act on the soil plane
2. The stresses on the other plane
3. The direction of the other plane in two-dimensional space

where if 1 and 2 are known information on a situation, the stresses of another plane can be found (Briaud, 2013).

The sign convention of the Mohr circle can be explained as the compressive normal stresses being positive, and the shear stresses that act on the opposite face of soil element and counterclockwise rotation are considered positive. As a representation of Mohr's circle, M and R points, shown in Figure 2.6, represent the stresses on planes AB and AD, respectively, as shown in Figure 2.2.

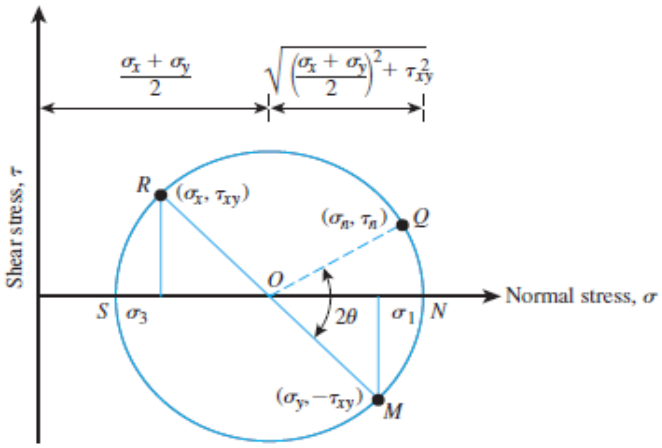

Figure 2.6 Representation of Mohr's circle (Das, 2010)

RM line intersects the normal stress axis, which is denoted by σ. The point of intersection is located on point O. It is the center of the Mohr circle, and the RM line can be called the diameter of the Mohr circle. The OR line can be called the radius of the Mohr circle, and stress conditions are considered to account for this. The radius of Mohr's circle is written as:

$$\sqrt{\left[\frac{(\sigma_y-\sigma_x)}{2}\right]^2 + \tau_{xy}{}^2} \tag{2.26}$$

The stress on the EF plane makes an angle θ with the AB plane in Figure 2.2, and that angle is determined in a counterclockwise direction from point M to point Q on Mohr's circle. The angle θ is twice that it represents in Mohr's circle, as 2θ. σ_n and τ_n are normal stress, and shear stress are given by the abscissa and ordinate of point Q in Figure 2.6 (Das, 2010).

In addition, soil planes as major and minor principal planes and representation of Mohr's circle are shown in Figure 2.7.

When AB and AD planes are major and minor principal planes, the shear and normal stresses can be found by substituting τ_{xy} as equal to zero. Then, σ_x and σ_y are become σ_1 and σ_3, respectively. Thus:

$$\sigma_n = \frac{\sigma_1+\sigma_3}{2} + \frac{\sigma_1-\sigma_3}{2}\cos 2\theta \tag{2.27}$$

$$\tau_n = \frac{\sigma_1-\sigma_3}{2}\sin 2\theta \tag{2.28}$$

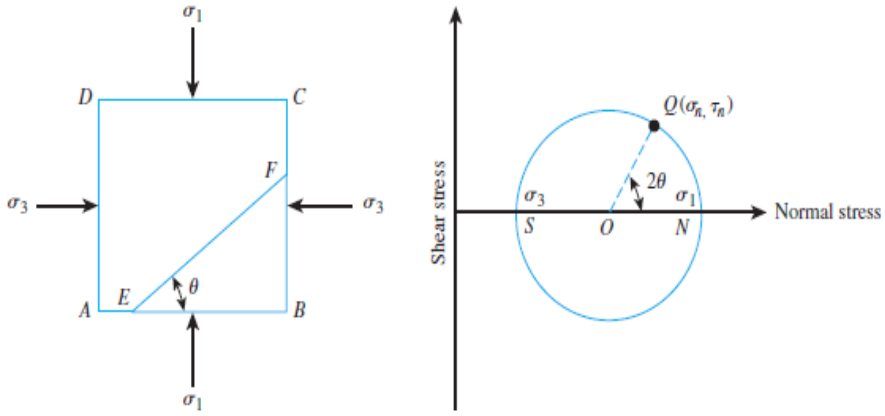

Figure 2.7 Soil planes as major and minor principal planes and representation of Mohr's circle (Das, 2010)

Another critical situation is the maximum (principal) shear stress which is a considerable case in the unconfined compression test. The maximum shear stress considered on top of the Mohr circle can be written as:

$$\tau_{max} = \frac{\sigma_1 - \sigma_3}{2} \tag{2.29}$$

If the strain state on Mohr's circle is examined, it is found that similar to the stress state. The strain states of Mohr's circle are shown in Figure 2.8.

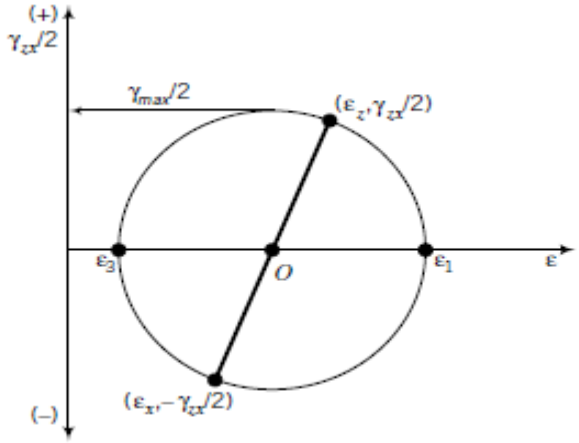

Figure 2.8 Strain states of Mohr's circle (Budhu, 2011)

Then the principal strains ε_1, named as the major principal strain, and ε_3 named as the minor principal strain, can be written as:

$$\varepsilon_1 = \frac{\varepsilon_z+\varepsilon_x}{2} + \sqrt{\left[\frac{(\varepsilon_z-\varepsilon_x)}{2}\right]^2 + \left[\frac{\gamma_{zx}}{2}\right]^2} \quad (2.30)$$

$$\varepsilon_3 = \frac{\varepsilon_z+\varepsilon_x}{2} - \sqrt{\left[\frac{(\varepsilon_z-\varepsilon_x)}{2}\right]^2 + \left[\frac{\gamma_{zx}}{2}\right]^2} \quad (2.31)$$

where γ_{zx} is commonly named the engineering shear strain or the simple shear strain (Budhu, 2011).

Another important situation is the maximum (simple) shear strain which is formulated as:

$$\gamma_{max} = \varepsilon_1 - \varepsilon_3 \quad (2.32)$$

The Pole method is an important and famous technique for solving soil stress problems in Mohr's circle along a plane. The pole in the Mohr circle is a point. A line on the circle passes through the point of stress and is parallel to the plane that acts on stress. Therefore, the method has three factors: the stress point on the circle, the pole on the circle, and the plane in which stresses act (Briaud, 2013). In Figure 2.9, the relationship between Mohr's circle and the physical space of soil in triaxial tests is illustrated.

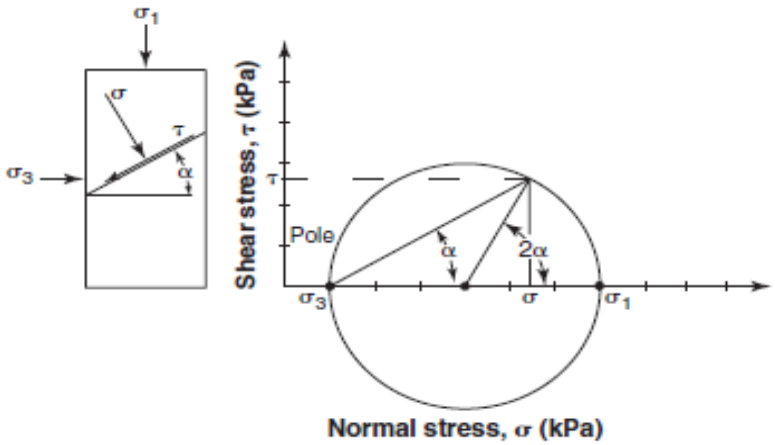

Figure 2.9 Relationship between Mohr's circle and physical space of soil in triaxial tests (Briaud, 2013)

It can be seen that an angle that moves to the two planes as α. Also, the unconfined compression test was investigated in this thesis, which is a type of triaxial test. Thus, the concept of Mohr's circle in Figure 2.9 is a significant case.

2.1.2 Yield Surface

Many loading conditions can act on the soil mediums. The yield surface can have different arrangements in geotechnical engineering studies because of the very different types of soils and very different types of loadings. The loading combinations or more complex situations have to be understood by geotechnical engineers. As mentioned in this thesis, the main data used to obtain engineering soil properties was given by the unconfined compression test. The more complex loading situations should be understood to be knowledgeable on the situation of uniaxial loading. If the more complex situation on a cylindrical sample is considered in Figure 2.10 below, the axial and radial stresses are applied, and these stresses become the principal stresses (Budhu, 2011).

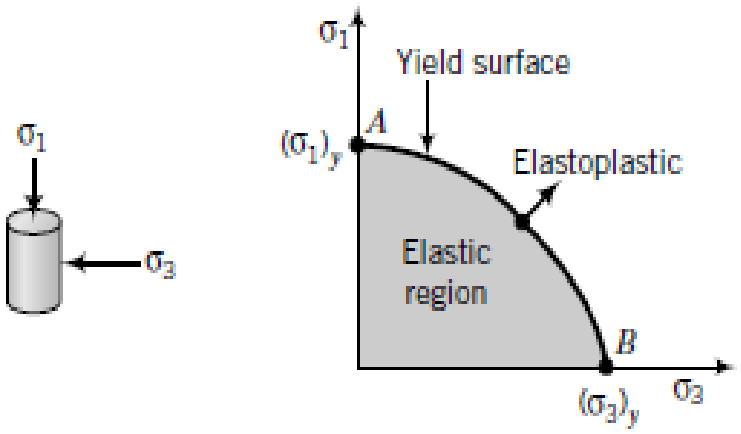

Figure 2.10 Illustration of yield surface in a soil sample (Budhu, 2011)

As the principal stresses, radial stress and axial stress can be presented with $\sigma_z = \sigma_1 = \sum\Delta\sigma_z$ and $\sigma_r = \sigma_3 = \sum\Delta\sigma_r$, respectively. For example, σ_1 is equal to zero, and σ_3 increases. In this situation, the soil material yields on the point of $(\sigma_3)_y$, which is represented by point B. On the other hand, σ_3 is equal to zero, and σ_1 increases. In this situation, the soil material yields on the point of $(\sigma_1)_y$, which is represented by point A (Budhu, 2011). The second condition that σ_3 is equal to zero and σ_1 increases is a significant case on the unconfined compression test.

2.1.3 Hooke's Law

If stresses and strains in soil are linear, isotropic, and elastic, it is directly related to formulations of Hooke's law. In this thesis, the unconfined compression test was

performed. According to confinement conditions of stress in the unconfined compression test, the initial tangent modulus can be determined by Hooke's law. Hence, Hooke's law is significant in the thesis, and the method of calculations was emphasized in the following chapters. For general states of stress in Hooke's law:

$$\begin{Bmatrix} \varepsilon_x \\ \varepsilon_y \\ \varepsilon_z \\ \gamma_{xy} \\ \gamma_{yz} \\ \gamma_{zx} \end{Bmatrix} = \frac{1}{E} \begin{bmatrix} 1 & -v & -v & 0 & 0 & 0 \\ -v & 1 & -v & 0 & 0 & 0 \\ -v & -v & 1 & 0 & 0 & 0 \\ 0 & 0 & 0 & 2(1+v) & 0 & 0 \\ 0 & 0 & 0 & 0 & 2(1+v) & 0 \\ 0 & 0 & 0 & 0 & 0 & 2(1+v) \end{bmatrix} \begin{Bmatrix} \sigma_x \\ \sigma_y \\ \sigma_z \\ \tau_{xy} \\ \tau_{yz} \\ \tau_{zx} \end{Bmatrix} \tag{2.33}$$

where E is called the elastic modulus or Young's modulus, and v is Poisson's ratio. Eq.(2.33) is named the elastic stress-strain constitutive equation. On the other hand, the tangent modulus or the secant modulus of nonlinearly elastic materials can be determined by Eq.(2.33). Equations of strains can be written as by Hooke's law:

$$\varepsilon_x = \frac{\partial u}{\partial x} = \frac{1}{E}[\sigma_x - v(\sigma_y + \sigma_z)] \tag{2.34}$$

$$\varepsilon_y = \frac{\partial v}{\partial y} = \frac{1}{E}[\sigma_y - v(\sigma_x + \sigma_z)] \tag{2.35}$$

$$\varepsilon_z = \frac{\partial w}{\partial z} = \frac{1}{E}[\sigma_z - v(\sigma_x + \sigma_y)] \tag{2.36}$$

$$\gamma_{xy} = \frac{\tau_{xy}}{G} \tag{2.37}$$

$$\gamma_{xz} = \frac{\tau_{xz}}{G} \tag{2.38}$$

$$\gamma_{yz} = \frac{\tau_{yz}}{G} \tag{2.39}$$

where E, v, and G are elastic parameters of soil, and G is the shear modulus of the material. Calculating Poisson's ratio of soils is not easy work, but if shear modulus can be obtained, the Poisson's ratio can be determined from shear modulus (Budhu, 2011). Equation of shear modulus, G, can be obtained from strains equations of Hooke's law:

$$G = \frac{E}{2(1+v)} \tag{2.40}$$

If the principal stresses on the soil are taken into account only, the number of Hooke's law equations reduce:

$$\begin{Bmatrix} \varepsilon_1 \\ \varepsilon_2 \\ \varepsilon_3 \end{Bmatrix} = \frac{1}{E} \begin{bmatrix} 1 & -v & -v \\ -v & 1 & -v \\ -v & -v & 1 \end{bmatrix} \begin{Bmatrix} \sigma_1 \\ \sigma_2 \\ \sigma_3 \end{Bmatrix} \tag{2.41}$$

The right-hand side matrix of Eq.(2.41) is named as compliance matrix, and the inverse of Eq.(2.41) is written as:

$$\begin{Bmatrix}\sigma_1\\ \sigma_2\\ \sigma_3\end{Bmatrix} = \frac{E}{(1+v)(1-2v)}\begin{bmatrix}1-v & v & v\\ v & 1-v & v\\ v & v & 1-v\end{bmatrix}\begin{Bmatrix}\varepsilon_1\\ \varepsilon_2\\ \varepsilon_3\end{Bmatrix} \tag{2.42}$$

The right-hand side matrix of Eq.(2.42) is named as stiffness matrix, and from the relations given by Eqs. (2.34), (2.35), and (2.36), the equations of stresses can be written as by Hooke's law (Das, 2008) :

$$\sigma_1 = \frac{vE}{(1+v)(1-2v)}(\varepsilon_1+\varepsilon_2+\varepsilon_3) + \frac{E}{1+v}\varepsilon_1 \tag{2.43}$$

$$\sigma_2 = \frac{vE}{(1+v)(1-2v)}(\varepsilon_1+\varepsilon_2+\varepsilon_3) + \frac{E}{1+v}\varepsilon_2 \tag{2.44}$$

$$\sigma_3 = \frac{vE}{(1+v)(1-2v)}(\varepsilon_1+\varepsilon_2+\varepsilon_3) + \frac{E}{1+v}\varepsilon_3 \tag{2.45}$$

In addition, if Lame's constant and Poisson's ratio equations are a requirement, Eqs. (2.34), (2.35), and (2.36) can be solved to switch normal stresses in terms of normal strains (Das and Ramana, 2011) :

$$\sigma_x = \lambda\bar{\varepsilon} + 2G\varepsilon_x \tag{2.46}$$

$$\sigma_y = \lambda\bar{\varepsilon} + 2G\varepsilon_y \tag{2.47}$$

$$\sigma_z = \lambda\bar{\varepsilon} + 2G\varepsilon_z \tag{2.48}$$

where

$$\bar{\varepsilon} = \varepsilon_x + \varepsilon_y + \varepsilon_z \tag{2.49}$$

where λ is known as the Lame's constant, and it is determined by the measurement of Poisson's ratio, v, and Young's modulus, E.

$$\lambda = \frac{vE}{(1+v)(1-2v)} \tag{2.50}$$

$$v = \frac{\lambda}{2(\lambda+G)} \tag{2.51}$$

2.1.4 Effective and Total Stress Mechanisms

The principle of effective stress was reconstituted by Terzaghi in the middle of the 1920s. Then, the principle of effective stress occurs only on normal stresses. In

other words, there is no effective stress in the shear stresses (Budhu, 2011). The principle of effective stress in the soil is illustrated in Figure 2.11.

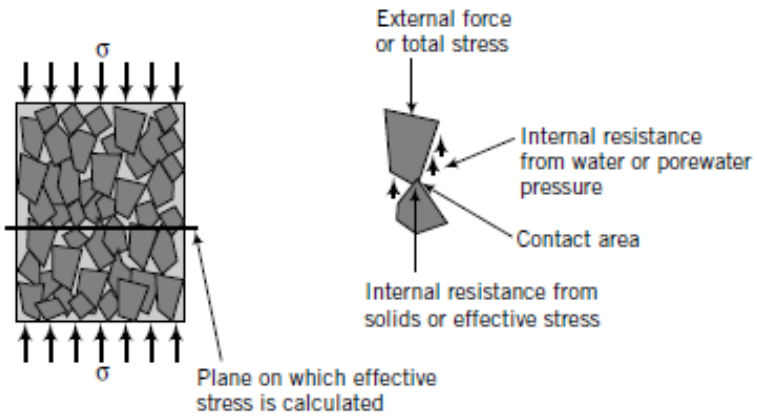

Figure 2.11 Principle of effective stress in soil (Budhu, 2011)

The void spaces are not continuous in partially saturated soil. At any point in a soil medium, the total stress is formed as intergranular, pore water pressure, and pore air pressure (Das, 2010). There is three phase system in a soil medium. These are specified as solid, pore water, and pore air, as shown in Figure 2.12.

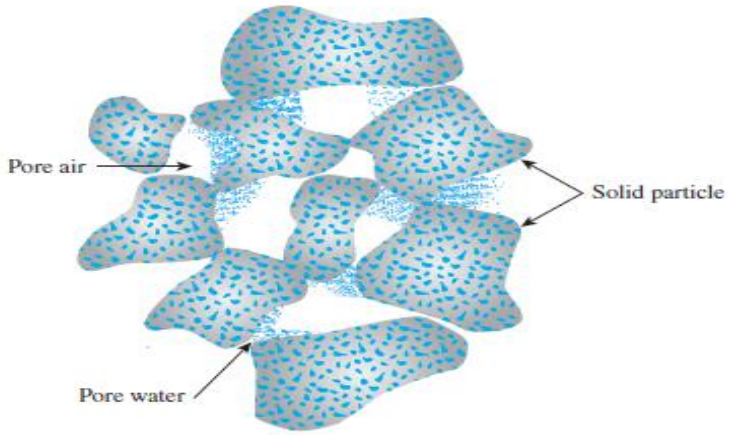

Figure 2.12 Representation of partially saturated soil (Das, 2010)

The stresses in the soil medium have to be equal and opposite because of Newton's third law. In partially saturated soil, the equation of effective stress from laboratory tests is determined as:

$$\sigma' = \sigma - u_a + \chi(u_a - u_w) \tag{2.52}$$

where σ' is effective stress, which leads to resistance and reactions by a combination of stresses from solid particles. σ is total stress, u_a is pore air pressure, u_w is the pore water pressure, and χ is the representation of the fraction of a unit cross-sectional area in soil occupied by water. χ is zero in dry soil, and χ is equal to 1 in saturated soil. In other words, intermediate values of χ are depended on the degree of saturation of soil denoted by S. However, χ is influenced by soil structures (Bishop et al., 1960).

In this form of Eq.(2.52), there are two independent states of stress to identify the effective stress, such as the normal total stress concerning air stress (σ-u_a) and the net water tension in excess over air stress (u_a-u_w). The stress tensor of a point in the soil is mentioned in Eq.(2.7), which does not contain information about air and water stress. As mentioned, shear stress can not affect water and air stress. The stress state should be identified again by the following two stress tensors, Σ_1 and Σ_2, in an unsaturated soil (Briaud, 2013):

$$\Sigma_1 = \begin{bmatrix} \sigma_x - u_a & \tau_{xy} & \tau_{xz} \\ \tau_{yx} & \sigma_y - u_a & \tau_{yz} \\ \tau_{zx} & \tau_{zy} & \sigma_z - u_a \end{bmatrix} \tag{2.53}$$

$$\Sigma_2 = \begin{bmatrix} u_a - u_w & 0 & 0 \\ 0 & u_a - u_w & 0 \\ 0 & 0 & u_a - u_w \end{bmatrix} \tag{2.54}$$

The stress state should be identified again by the following only one stress tensor, Σ_1, in saturated soil:

$$\Sigma_1 = \begin{bmatrix} \sigma_x - u_w & \tau_{xy} & \tau_{xz} \\ \tau_{yx} & \sigma_y - u_w & \tau_{yz} \\ \tau_{zx} & \tau_{zy} & \sigma_z - u_w \end{bmatrix} \tag{2.55}$$

The pore water pressure and the effective stress due to uniaxial loading were discussed in the next part of the thesis.

2.2 Shear Strength of Soils

In the past 80 years, excessive research has been done about the shear strength of soil, and these were beneficial research studies of soil strength. The main purpose is to provide knowledge about a framework or begin detailed studies of the shear strength of soil in sites (Duncan, Wright and Brandon, 2014). In geotechnical engineering studies, it may be an effective control mechanism to determine the ultimate loads. In other words, the safety conditions of almost all geotechnical

structures are related to soil strength. It provides to make an estimation of the bearing capacity of shallow foundations and piles, stress-strain characteristics of soil, stability of dams and embankments, and lateral earth pressure on retaining walls. When soil resists the shear forces, the shear strength is controlled in this situation. That soil behavior can be observed to be different in groups of soils, such as uncemented soils with weak interparticle bonds and cemented soils with strong interparticle bonds between the soil particles (Budhu, 2011). Therefore, the cemented soil particles have strong chemically bonded, such as a mixture of clay used for this thesis on an unconfined compression test.

The best way to determine the shear strength of soils is to apply laboratory tests performed on prepared soil specimens and in situ tests. When these tests are applied, the same stress conditions should be preserved within the field (Anochie-Boateng, 2007).

As mentioned, the shear strength and parameters of shear strength are determined by several laboratory test methods with soil specimens. These are briefly mentioned below;

- *Direct Shear Test (Shear Box):* Vertical and horizontal forces are applied, and when the horizontal force is applied to the specimen, the direct shear test is conducted by displacement control. In addition, the shear test can be conducted as stress-controlled and strain-controlled depending on the test equipment. Parameters of horizontal displacement, vertical displacement, vertical load, and horizontal loads are obtained and recorded. Also, the soil failure is determined if the soil specimen can not resist the horizontal forces. The shear box apparatus can not prevent drainage. However, if the specimen is fine-grained, unconfined compression strength can be obtained quickly (Budhu, 2011). An illustration of the direct shear test apparatus is given in Figure 2.13.

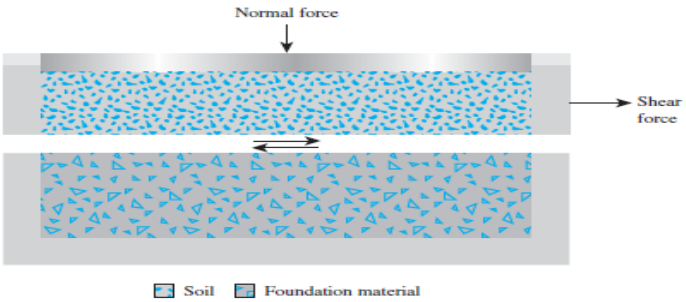

Figure 2.13 Illustration of the direct shear test apparatus (Das, 2010)

- *Triaxial Shear Tests:* The triaxial tests are the most reliable testing method for determining the shear strength, parameters of shear strength, and stress-strain behavior of soils. Generally, sand and clay type of soils are used in triaxial tests. There are three standard types of triaxial tests. One of them is the *consolidated-drained triaxial test* called the CD test. As a confining pressure σ_3 is applied all around the soil specimen, and if the drainage is prevented, the pore water pressure of the soil specimen increases. If the drainage of the apparatus is opened, pore water is dissipated, and consolidation has occurred. The consolidated-drained test is not used commonly. The *consolidated-undrained triaxial test* can be called the CU test as a confining pressure σ_3 is applied all around the soil specimen. The total stress and effective stress are not the same in the test because the pore water pressure is obtained at the failure of the soil. Another type of triaxial test is the unconsolidated-undrained triaxial test, which can be called the UU test. Due to the application of pressure σ_3 on soil specimens, the drainage is prevented. Also, the drainage is prevented at any stage of the unconsolidated-undrained test. The soil specimen is shearing to failure during to application of deviatoric stress. The UU test is always applied to the clayey types of soils (Das, 2010). An illustration of the triaxial test apparatus is given in Figure 2.14.

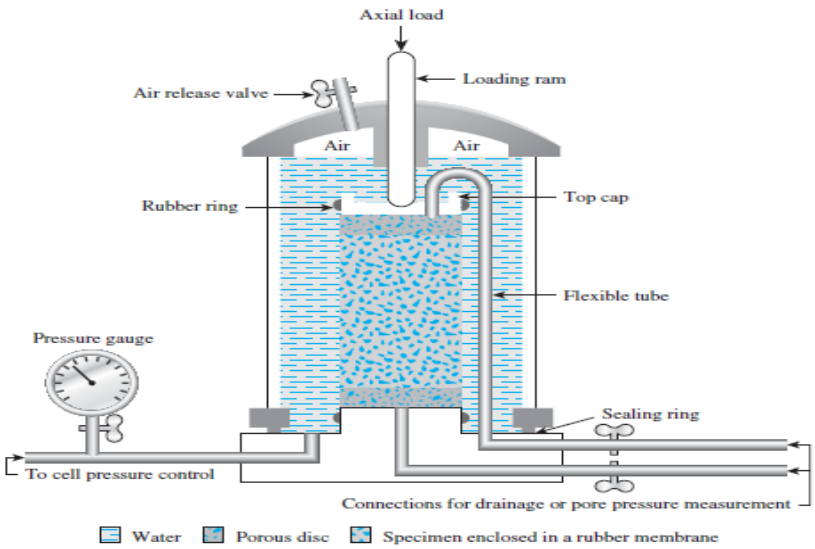

Figure 2.14 Illustration of the triaxial test apparatus (Das, 2010)

In addition, the unconfined compression test is a type of unconsolidated-undrained test which is commonly applied on clayey types of soils. The

confining pressure σ_3 is equal to zero. An axial load is applied to the specimen, and the failure of the specimen has occurred. The unconfined compression test was explained in detail in the next part of the thesis.

As mentioned, the shear strength and parameters of shear strength are determined by several field test methods. These are briefly mentioned below;

- *Vane Shear Test:* The vane shear test is a method of determining the undrained shear strength. This test is generally used in cohesive soils. Also, the vane shear test can be called the VST. The test method is determined as the vane is pushed into the soil site, and the torque is applied with the torque rod. The maximum torque causes the failure in the soil due to application, and the sum of the resisting moment by soil is named failure (Das, 2008).
- *Standard Penetration Test:* The standard penetration test can be called the SPT. This test should only be used to assess the relative shear strength on fine-grained soils (Budhu, 2011).
- *Cone Penetrometer Test:* The cone penetrometer test can be called the CPT. This test should be used only to provide the assessment of the undrained shear strength correlated with the cone resistance value. Also, the test results are correlated with peak friction angle (Robertson and Campanella, 1983).

The shear strength of soil can be described as internal resistance per unit area, which resists failure in the soil mass. The shear strength characteristics of soils and the factor of parameters are given as follows in the general case. Also, the details of the shear strength of soil were discussed in part of the failure criterion models in the thesis. The shear strength of soil can be composed due to friction and no water in the soil plane:

$$\tau_f = \sigma \tan \varphi \tag{2.56}$$

where τ_f is named the shear strength of soil, σ is the normal stress on the plane of failure, and φ is the friction angle that often varies between 0 and 1. If the cohesion exists in soil particles, the Eq.(2.56) becomes:

$$\tau_f = c + \sigma \tan \varphi \tag{2.57}$$

where c is the cohesion of soil. If the pore water that refers to voids between soil particles in 100% saturation is added, the normal stress is changed due to the water under a certain amount of water pressure. The normal stress transforms the effective

normal stress, σ', which is the difference between the total normal stress, σ, and the pore water pressure, u_w. Also, the cohesion transforms to the effective stress cohesion, c', and the friction angle transforms to the effective stress friction angle, φ'. Eq.(2.57) becomes (Briaud, 2013):

$$\tau_f = c' + (\sigma - u_w)\tan\varphi' = c' + \sigma'\tan\varphi' \tag{2.58}$$

If the pore water that refers to voids between soil particles can not reach full of saturation, a fraction of the total area, α, is added. Eq.(2.58) becomes:

$$\tau_f = c' + (\sigma - \alpha u_w)\tan\varphi' = c' + \sigma'\tan\varphi' \tag{2.59}$$

The shear strength envelope of soils is shown in Figure 2.15.

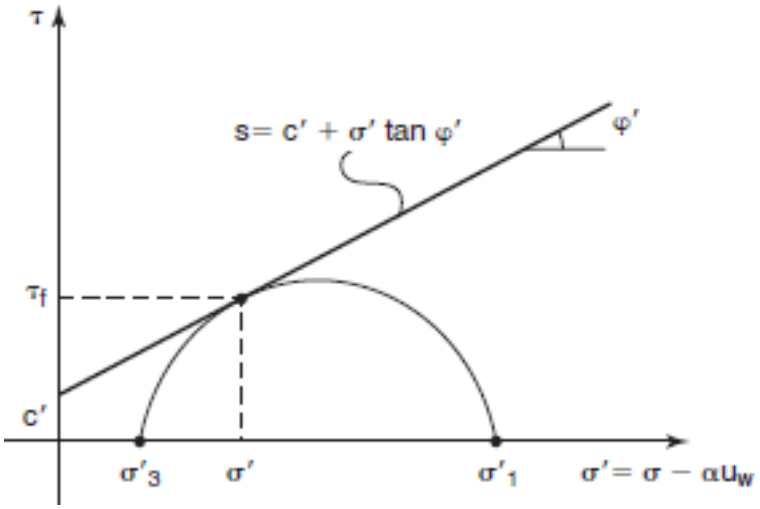

Figure 2.15 The shear strength envelope of soils (Briaud, 2013)

In addition, the general equation of shear strength in a soil that is saturated or unsaturated can be written as:

$$\tau_f = c' + (\sigma - \alpha u_w - \beta u_a)\tan\varphi' = c' + \sigma'\tan\varphi' \tag{2.60}$$

where u_a is called the air stress, and β is called a fraction of the plane covered by air. Also, the parameter of the water stress, u_w, can be taken as equal to the degree of saturation denoted by S. On the other hand, α and β parameters can be calculated as:

$$\alpha = \frac{\tan\varphi^b}{\tan\varphi'} \tag{2.61}$$

$$\beta = 1 - \frac{\tan\varphi^b}{\tan\varphi'} \tag{2.62}$$

where φ^b is an angle which is the rate of increase in shear strength respect to the matric suction (u_a-u_w).

As a result, the shear strength equation, τ_f, can be taken as Eq.(2.59) in all cases in saturated or unsaturated soils because of atmospheric air stress and zero gauge pressure (Briaud, 2013).

2.2.1 Factors Influencing on Shear Strength

The shear strength of the soil is a main significant parameter to geotechnical engineers. The safety of any geotechnical structures or infrastructures is related to the shear strength of the soils. If soil shear strength can not be analyzed beyond reproach, losing bearing capacity and failure situations on soil can occur. These cases lead to causing economic damage and danger to lives. Some of the factors influencing shear strength are discussed below:

- *Response of soils to shear forces:* For example, there are two types of soil samples. The first one, mostly loose sands or normally consolidated and lightly overconsolidated clays have an overconsolidation ratio that is less than 2 or equal to 2. That sample is called Type I in Figure 2.16. The other ones, mostly dense sands, and overconsolidated clays have an overconsolidation ratio greater than 2. That sample is called Type II in Figure 2.17. In Figure 2.16 and Figure 2.17, Δz is the vertical displacement, Δx is the horizontal displacement, H_o is the original height of the soil sample, and γ_{zx} is the shear strain.

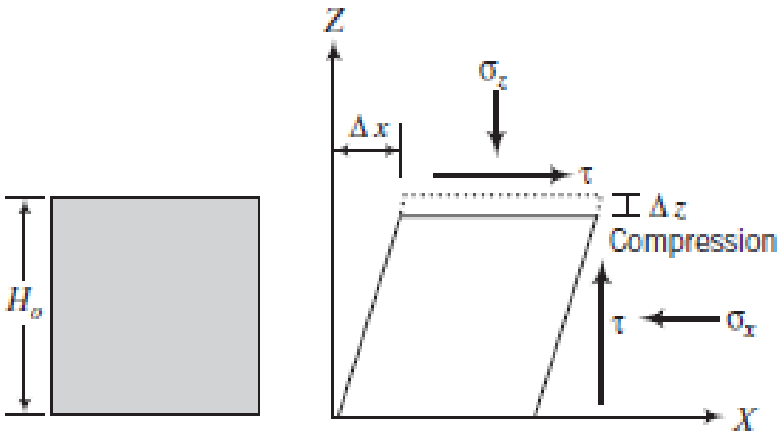

Figure 2.16 Original configuration of soil sample and shear deformation of Type I soils (Budhu, 2011)

Mostly loose sands or normally consolidated and lightly overconsolidated clays denoted by Type I soils respond to a gradual increase in shear stress like the shear strain increase due to reaching the approximately constant shear stress, called critical state shear stress τ_{cs}. That type of shear strain increases is called strain hardens. Also, Type I soils are responded to becoming denser due to reaching the approximately constant void ratio called the critical void ratio, e_{cs}.

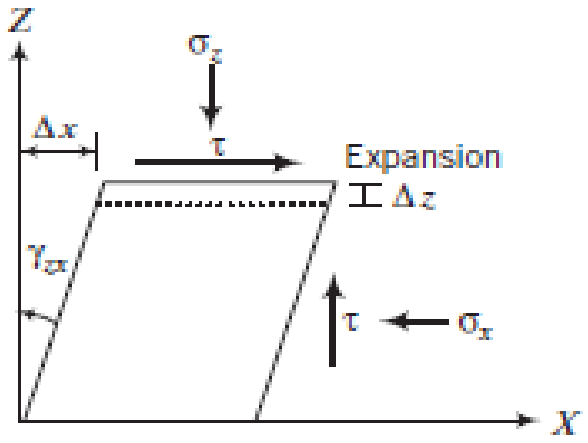

Figure 2.17 Shear deformation of Type II soils (Budhu, 2011)

Mostly dense sands and overconsolidated clays denoted by Type II soils are responded to an instantaneous increase in shear stress at a low increase of shear strain compared with the Type I soils. This increase is continued until reaching the peak value, τ_p. Beyond that point, Type II soils are responded to a decrease in shear stress at increasing shear strain. That type of shear strain increases is called strain softens. In general, the shear bands localized in the failure zone cause the strain softening response of the soils. When the shear bands are loosened, the shear stress can be reached the critical state. The creation of the shear bands can be related to homogeneity and grain size of soils, boundary conditions and initial density of soils, and uniformity of loads. Type II soils are responded to becoming looser due to reaching the approximately constant void ratio called the critical void ratio. All observations about the described soils above are illustrated in Figure 2.18.

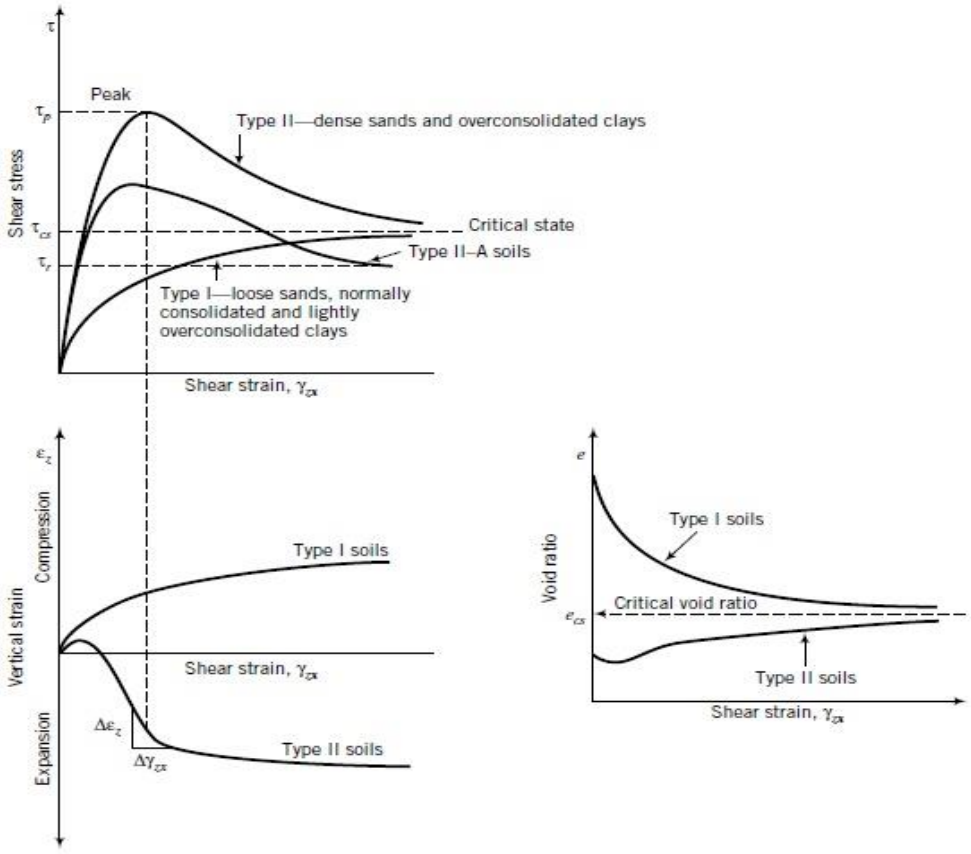

Figure 2.18 Response of Type I, Type II, and Type II-A soils (Budhu, 2011)

If a shear band occurs in some types of overconsolidated clays, it causes a decrease in the final shear stress below the critical state. These types of soils are illustrated in Figure 2.18 by Type II-A.

- *Effects of increase in normal effective stress:* The same types of soils have been valid as the section on the response of soils to shear forces. If the normal effective stress rises, the critical shear stress increases in mostly loose sands or normally consolidated and lightly overconsolidated clays. Again, if the normal effective stress rises, the peak shear stress tends to disappear, and the critical shear stress increases in mostly dense sands and overconsolidated clays. Also, if the normal effective stress versus shear stress graph is plotted, the critical state friction angle and the failure envelope can be obtained.
- *Effects of overconsolidation ratio:* Assume that two soil samples have the same type of soil and the same compositions. These two soil samples are overconsolidated soils, but they have different overconsolidation ratios. These

soil samples are illustrated in Figure 2.19. $(OCR)_1$ and $(OCR)_2$ represent the overconsolidation ratios where $(OCR)_2$ has a larger value than $(OCR)_1$.

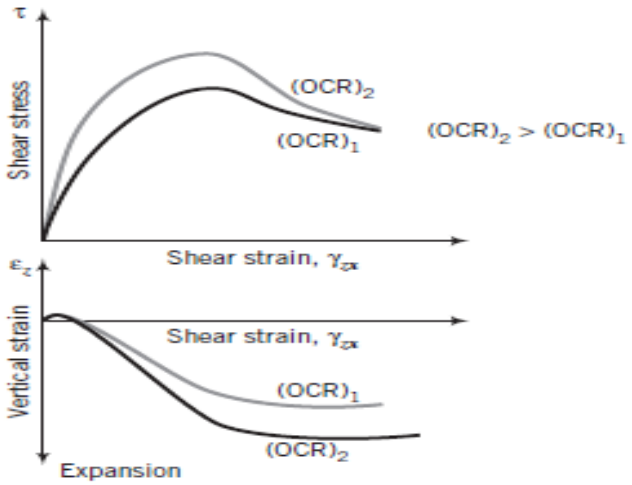

Figure 2.19 Effect of overconsolidation ratio (Budhu, 2011)

These two different overconsolidation ratios lead to a display of different volume expansions and different peak shear stresses. The greater volume expansion and the greater peak shear strength have occurred in higher overconsolidated soil.

- *Effects of drainage of porewater:* There are two different conditions for drainage on the soils. These are called drained and undrained conditions. If the porewater pressure is developed during the loadings of soil disseminates, that type of condition is called the drained condition. Therefore, Δu, called the porewater pressure, is equal to zero. The other one, if the pore water pressure can not be drained from the soil, it is named the undrained condition. The porewater pressure, Δu, is not equal to zero. The drained or undrained conditions of soils depend on the geological formations of soil types and types of loading. The dissemination rate of porewater pressure is frequently much faster than the loading rate under the undrained condition of soils. A soil that tends to compress has positive porewater pressure during the drained loading under undrained conditions. It causes to decrease in effective stress. On the other hand, soil that tends to expand has negative porewater pressure during the drained loading under drained conditions. It causes to increase in effective stress. In the undrained condition of soils, the volume and the void ratio are

constant. Therefore, the porewater pressure changes. In addition, there are two conditions on the geotechnical structures such as long-term conditions and short-term conditions. The dissemination of loading and drained conditions leads to developing the porewater pressure in long-term conditions. The dissemination of porewater pressure is fast in coarse-grained soils on static loading. However, fine-grained soils have low permeability, and the dissemination of porewater pressure takes more time, so the undrained condition of the soil is used.

- *Effects of cohesion on soils:* Cohesion is an essential term of geotechnical engineering. It is related to molecular forces in the soil. The cohesion is the explicit shear strength of the soil.
- *Effects of soil tension:* In unsaturated soils, the water surface tension in the soil can be identified by the soil tension. Negative porewater pressure from the capillary creates a pulling effect between soil particles. With this, the effective stress has to increase because of the negative porewater pressure, and it leads to creating resistance to shear. Therefore, it can be used as an advantage in geotechnical constructions. In saturated soils, the soil tension is equal to zero.
- *Effects of cementation on soils:* There are two groups of soil types of cementation. The uncemented soils have weak interparticle chemical bonds, and cemented soils have strong interparticle chemical bonds between the soil particles. The cementation can be classified by the degree of cementation in soils. Even if the normal effective stress equals zero, cemented soils have a shear strength. The shear strength of cementation can be effective at small strain levels, which is less than 0.001% (Budhu, 2011).

2.2.2 Failure Criterion Models

The shear resistance of soil is identified as the shear strength of soil at a certain shear stress value, as mentioned. Some of the factors affect the shear strength of the soils (Araz and Fitsum, 2011). According to the different assumptions, the failure criterion models were described to explain the response of the soils due to external impacts below.

2.2.2.1 Coulomb's Failure Criterion

Coulomb's failure criterion model is stringently based on failures of soil that take place in interfaces of two soil layers or interfaces of a geotechnical structure and a type of soil. In other words, Coulomb's frictional law is the fundamental case to apply that failure criterion for slipping between two bodies. According to Coulomb's frictional law, failure occurs due to the motion of the body relative to the other one. At this moment, Coulomb's failure criterion can be used in a critical state of soil behavior. In nature, the grains and structural organizations of soils are more complicated. However, Coulomb's failure criterion considered gathering dense and loose soils. The soil with loose assembly is leaned to act into the voids in the soil. The direction of motion of loose soils is downward, which is appraised as compression. The soil particles with dense assembly are leaned to push each other. The direction of motion of dense soils is upward, which is appraised as expansion. The shear strength of soil can be considered by the frictional law of Coulomb's, especially if the movement of shear is parallel to the movement of other soil body. The resulting formulations of Coulomb's failure criterion are presented as follows:

$$\tau_f = (\sigma'_n)_f \tan \varphi' \tag{2.63}$$

$$\tau_f = (\sigma'_n)_f \frac{\tan \varphi' + \tan \alpha}{1 - \tan \varphi' \tan \alpha} = (\sigma'_n)_f \tan(\varphi' + \alpha) \tag{2.64}$$

$$\tau_f = (\sigma'_n)_f \tan(\varphi' \mp \alpha) \tag{2.65}$$

$$\tau_f = c_{cm} + (\sigma'_n)_f \tan(\xi_o) \tag{2.66}$$

$$\alpha = \sin^{-1}\left(-\frac{\Delta\varepsilon_1 + \Delta\varepsilon_3}{\Delta\varepsilon_1 - \Delta\varepsilon_3}\right) = \sin^{-1}\left(-\frac{\Delta\varepsilon_1 + \Delta\varepsilon_3}{(\Delta\gamma_{zx})_{max}}\right) \tag{2.67}$$

where τ_f is the shear stress, $(\sigma'_n)_f$ is the normal effective stress on the slip denoted by failure, φ' is friction angle. Also, α is the dilation angle which is a change in volumetric strain with respect to the shear strain, and the positive value of the dilation angle is denoted by the expansion of soil. The negative value of the dilation angle is denoted by the contract of soil. The cementation strength of soil denotes c_{cm}, and ξ_o is the apparent friction angle. Eq.(2.63) is Coulomb's law in terms of stress. Eq.(2.65) is the general form of Eq.(2.64). If the dilation angle is equal to zero, the form of the equation is reduced to Eq.(2.63). However, if the dilation angle shows an increase, the shear strength enhances. If the normal effective stress increases, the value of the dilation

angle decreases. When the normal effective stress increases, the failure envelope of the soil tends to be curved, and the situations of dilation angle are shown in Figure 2.20 below. In Eq.(2.65), the positive sign denotes the upward direction of the motion of soil particles, and the negative sign denotes the downward direction of the motion of soil particles. Also, Coulomb's frictional law is applied to the cemented soils, and Eq.(2.66) is emphasized the cementation of soil (Budhu, 2011).

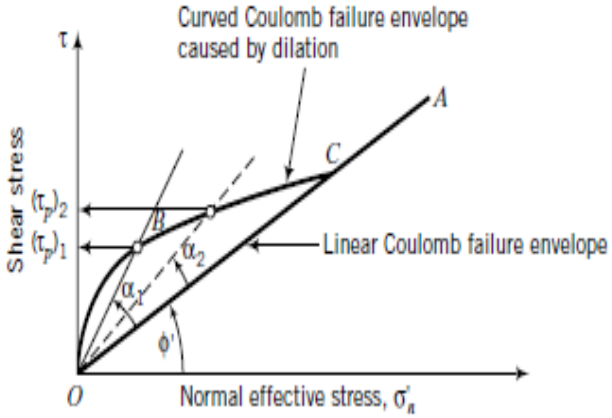

Figure 2.20 The dilation angle on Coulomb's failure envelope (Budhu, 2011)

2.2.2.2 Taylor's Failure Criterion

Taylor adopted the shear strength owing to the friction from the engagement of soil particles and shearing. Taylor's failure criterion model is used as an energy method to respond to the soil model. Taylor's failure criterion is not based on any assumption of soil failure. Therefore, it can be used in any case of loadings in homogeneous soil. The formulations of Taylor's failure criterion are presented as follows:

$$\tau d\gamma = \mu_f \sigma'_z d\gamma \mp \sigma'_z d\varepsilon_z \tag{2.68}$$

$$\frac{\tau}{\sigma'_z} = \mu f \mp \frac{d\varepsilon z}{d\gamma} \quad and \quad \alpha = \frac{d\varepsilon z}{d\gamma} \tag{2.69}$$

$$\left(\frac{\tau}{\sigma'_z}\right)_{cs} = \tan\varphi'_{cs} \quad and \quad \frac{d\varepsilon z}{d\gamma} = \tan\alpha_p \tag{2.70}$$

$$\left(\frac{\tau}{\sigma'_z}\right)_{p} = \tan\varphi'_{cs} + \tan\alpha_p \tag{2.71}$$

$$\tau_{cs} = (\sigma'_n)_f \tan\varphi'_{cs} \tag{2.72}$$

$$\tau_p = (\sigma'_n)_f (\tan\varphi'_{cs} + \tan\alpha_p) \tag{2.73}$$

where τ is the shear stress of soil, σ'_z is the vertical effective stress, dγ is the incremental shear strain, $d\varepsilon_z$ is incremental vertical strain, and μ_f is the static friction coefficient of sliding. The critical state is denoted by subscript of cs, and the peak is denoted by subscript of p. Tdγ represents the external energy, $\mu_f \sigma'_z d\gamma$ represents the internal energy that is work done by friction, and $\mp\sigma'_z d\varepsilon_z$ represents energy that is work done by engagement energy of soil against the vertical effective stress. The equilibrium equation of energy is given in Eq.(2.68). If Eq.(2.68) is organized, Eq.(2.69) is formed. In a critical state, there is no dilation. Eq.(2.70) represents the critical state and case of peak shear strength. The general forms of Taylor's failure criterion are represented in Eq.(2.72) and Eq.(2.73), the critical shear strength and the peak shear strength, respectively. The peak dilation angle of Taylor's failure criterion is greater than Coulomb's failure criterion (Budhu, 2011).

2.2.2.3 Mohr-Coulomb Failure Criterion

The Mohr-Coulomb failure criterion was formed to delineate the failure of isotropic soils with the principal stresses. The Mohr-Coulomb failure criterion was designed as the linear equations without including the intermediate principal stress denoted by σ_2. That failure criterion is viewed as a contribution from the stress state of Mohr's circle and the frictional law of Coulomb's. The shape of the failure envelope of soil and the case of the minor and major principal stresses are used in Mohr's condition, which can be linear or nonlinear. The linear failure envelope of soil at a critical state is used in Coulomb's condition (Labuz and Zang, 2012). The Mohr-Coulomb failure envelope in Figure 2.21 and the formulations of the Mohr-Coulomb failure criterion are presented as follows:

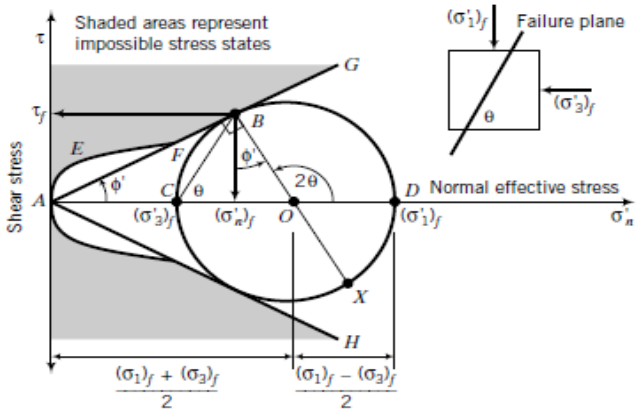

Figure 2.21 Illustration of the Mohr-Coulomb failure envelope (Budhu, 2011)

$$\sin\varphi' = \frac{OB}{OA} = \frac{\frac{(\varphi'_1)_f-(\varphi'_3)_f}{2}}{\frac{(\varphi'_1)_f+(\varphi'_3)_f}{2}} = \frac{(\varphi'_1)_f-(\varphi'_3)_f}{(\varphi'_1)_f+(\varphi'_3)_f} \quad (2.74)$$

$$\sin\varphi' = \frac{\frac{(\varphi'_1)_f}{(\varphi'_3)_f}-1}{\frac{(\varphi'_1)_f}{(\varphi'_3)_f}+1} \quad (2.75)$$

$$(\sigma'_n)_f = \frac{\sigma'_1+\sigma'_3}{2} - \frac{\sigma'_1-\sigma'_3}{2}\sin\varphi' \quad (2.76)$$

$$\tau_f = \frac{\sigma'_1-\sigma'_3}{2}\cos\varphi' \quad (2.77)$$

$$\tau_{max} = \left[\frac{\sigma'_1-\sigma'_3}{2}\right]_{max} \quad (2.78)$$

$$\theta = 45 + \frac{\varphi'}{2} = \frac{\pi}{4} + \frac{\varphi'}{2} \quad (2.79)$$

where $(\sigma'_1)_f$ and $(\sigma'_3)_f$ are the major and minor principal effective stresses, $(\sigma'_n)_f$ and τ_f are the failure stresses, τ_{max} is called as the maximum shear stress, and θ is the inclination of the failure plane. In Figure 2.21, the AB line is called the Coulomb frictional failure line, which intersects the principal effective stresses of Mohr's circle. The AG line represents the failure line of compression, and the AH line represents the failure line of extension. On the other hand, the failure envelope of dilating soils is represented by AEFB, and the failure envelope of nondilating soils is represented by the AFB line. If Eq.(2.74) is simplified, Eq.(2.75) is obtained for determining the maximum principal effective stress ratio of soil, $(\sigma'_1)_f / (\sigma'_3)_f$. The maximum shear stress is given in Eq.(2.78). The maximum shear stress is greater than the failure shear stress. The relationship between the inclination of the failure plane and the effective friction angle is given in Eq.(2.79) (Budhu, 2011). An illustration of the failure envelope and Mohr's circle is shown in Figure 2.22.

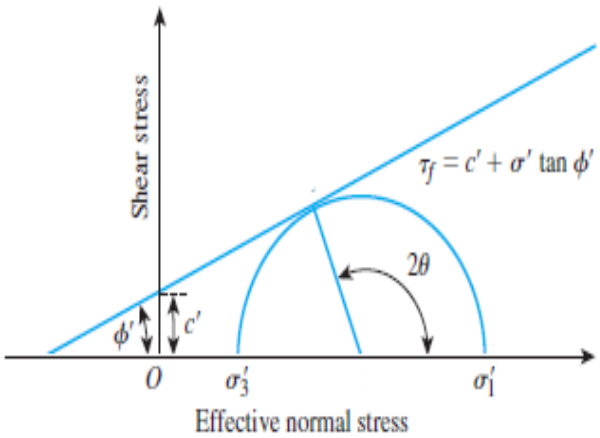

Figure 2.22 Illustration of failure envelope and Mohr's circle (Das, 2010)

Eq.(2.80) is determined as the Mohr-Coulomb failure criterion in terms of the total stress and the effective stress. Also, shear failure can occur if the shear stress applied on a plane in soil attains a value of given Eq.(2.80). When the inclination of the failure plane in terms of the friction angle is evaluated, the expressions in terms of total and effective stresses can be obtained as follows:

$$\tau_f = c + \sigma \tan\varphi \quad and \quad \tau_f = c' + \sigma' \tan\varphi' \tag{2.80}$$

$$\sigma_1 = \sigma_3 \tan^2\left(45 + \frac{\varphi}{2}\right) + 2c \tan\left(45 + \frac{\varphi}{2}\right) \tag{2.81}$$

$$\sigma'_1 = \sigma'_3 \tan^2\left(45 + \frac{\varphi'}{2}\right) + 2c \tan\left(45 + \frac{\varphi'}{2}\right) \tag{2.82}$$

where c is the cohesion parameter of soil (Das, 2010).

2.2.2.4 Tresca Failure Criterion

The Tresca Failure Criterion is formed to describe the failure load of fine-grained soils under undrained conditions. The Mohr-Coulomb failure and Tresca failure criteria are extensively used for linear and nonlinear analyses in geotechnical engineering studies. On the other hand, the Tresca failure criterion is a special case of the Mohr-Coulomb failure criterion. In addition, the Tresca failure criterion is used to define the shear strength, which is the undrained shear strength of soil (Taiebat and Carter, 2008).

The undrained shear strength is a representation of the radius of the Mohr's circle, and the magnitude of the undrained shear strength depends on the initial confining pressure and the initial void ratio of soils. The Mohr's circle of undrained condition in Figure 2.23 and the formulation of the Tresca failure criterion are presented as follows:

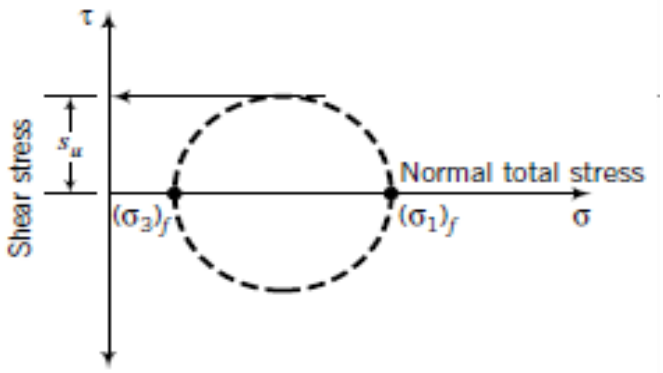

Figure 2.23 The illustration of Mohr's circle under undrained condition (Budhu, 2011)

$$s_u = \frac{(\sigma_1)_f - (\sigma_3)_f}{2} = \frac{(\sigma'_1)_f - (\sigma'_3)_f}{2} \quad (2.83)$$

where s_u is called the undrained shear strength of the soil. If the confining pressure called the initial normal effective stress increases, it reduces the initial void ratio. In that case, the change in porewater pressure occurs in the undrained condition of soils (Budhu, 2011).

2.2.3 Shear Strength of Unsaturated and Saturated Cohesive Soils

Generally, laboratory tests are used to determine the shear strength of cohesive soils, such as the direct shear test and triaxial tests. The triaxial tests are used in common. These tests were mentioned in previous sections. In addition, the equation of effective stress in partially saturated soils was given in Eq.(2.52), and the equation of shear strength in terms of the effective stress was given in Eq.(2.59). When the Eq.(2.52) is substituted into Eq.(2.59), this equation is obtained as follows:

$$\tau_f = c' + [\sigma - u_a + \chi(u_a - u_w)] \tan \varphi' \quad (2.84)$$

where the cohesion of cohesive soil is equal to zero if the soil is normally consolidated clay, but the cohesion parameter is greater than zero if the soil is overconsolidated clay. The representation of the fraction of a unit cross-sectional area in soil occupied by water, χ, depends on the degree of saturation. The determination of effective stress in unsaturated soil can not be possible by the mentioned laboratory tests. At this moment, the undrained triaxial test is used to measure the total stress in unsaturated soil. In that case, the failure envelope will be curved, but approximately, it can be shaped into a straight line. If the confining stress increases, it leads to compression on the voids of the soil specimens, and the degree of saturation increases. If the degree of saturation is reached a percentage of 100% by normal stress and shear stress, the failure envelope will be horizontal, which means that the friction angle of the soil is equal to zero (φ=0). The strength of unsaturated or partially saturated soils can not be used in the design of geotechnical studies (Das, 2010).

The clayey type of soil has complicated interactions between water and clay particles. Therefore, the strength attributes of clay should be analyzed cautiously by a geotechnical engineer. The deficiency strength of the clayey type of soil can be led to slope stability problems such as the stability of embankments. In particular, normally consolidated clays with low undrained strength and moderately overconsolidated clays

frequently induce stability problems. Therefore, evaluating the strength of clay soils is a requirement for the stability of clay. However, it is not easy because the many factors affect the laboratory and in situ tests of clays. These factors are considered as follows:

- *Disturbance:* The undisturbed clay samples incline to increase the pore water pressure and decrease the effective stress (Ladd and Lambe, 1963). Therefore, this situation can be induced to reduce the undrained shear strength of clay which is evaluated by the unconsolidated undrained triaxial test in the laboratory. The undrained shear strength of clay considered by the UU test can be lower than the undrained shear strength considered by the in situ tests.
- *Anisotropy:* It is related to the orientation of the failure plane of soil. There are two effects of anisotropy in clay: inherent anisotropy and stress system-induced anisotropy. The inherent anisotropy in entire clays tends to get perpendicular to the major principal strain direction during the consolidation. It is the result of stiffness and strength that is direction dependent. The stress system-induced anisotropy alters depending on the orientation of planes due to the applied magnitude of the stress on consolidation. The magnitude of the pore pressure in undrained loading conditions alters with the orientation of change in stress. These two results of anisotropy of clay vary with the principal stress orientation at failure and the failure plane. The laboratory tests to obtain the undrained strength of clay are performed on the undisturbed plane. These test results simulate the effects of stress orientations.
- *Strain rate:* The laboratory tests regard higher strain rates than most field conditions of soils. Loadings in the field condition comprise periods of weeks or months if it is compared with laboratory conditions. There is an inverse proportion in the failure times of the laboratory soil specimen and in situ soil deposit. The strain rate effects and the disturbance effects of the clay cancel each other on the unconsolidated undrained triaxial test.
- *Sensitivity and thixotropy:* The unconfined compression strength reduces when the tests are applied on a remolding clay sample without any moisture content change. This situation of clay is called sensitivity. The degree of sensitivity can be determined as:

$$S_t = \frac{q_{u(undisturbed)}}{q_{u(remolded)}} \tag{2.85}$$

where $q_{u(undisturbed)}$ represents the unconfined compression strength in an undisturbed state and $q_{u(remolded)}$ represents the unconfined compression strength in a remolded state. The differences in the unconfined strength of undisturbed and remolded states are shown in Figure 2.24.

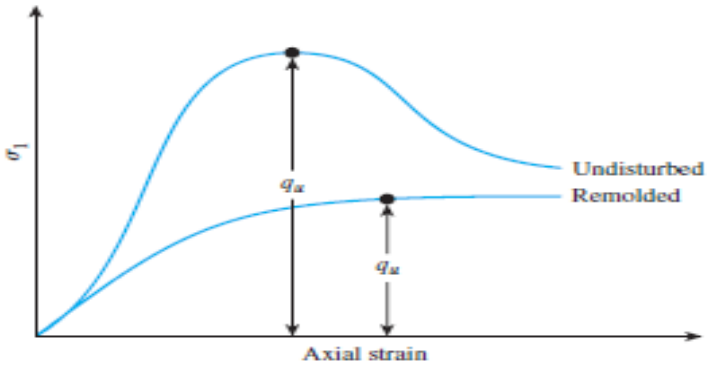

Figure 2.24 Unconfined compression strength of undisturbed and remolded clay (Das, 2010)

The degree of sensitivity on most clay samples ranges from about 1 to 8. The general classification is given in Figure 2.25.

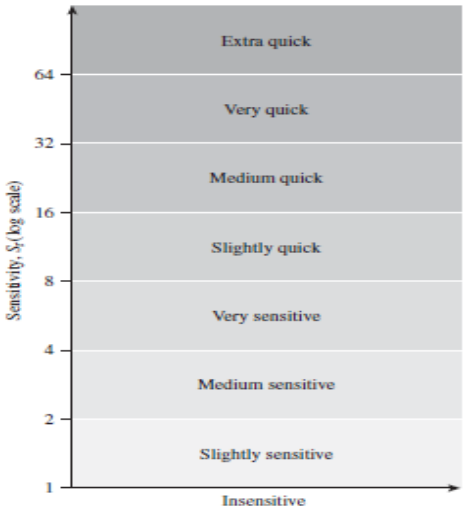

Figure 2.25 Sensitivity classification of clays (Das, 2010)

The devastation of the clay particle structure during sedimentation causes the loss of strength in clayey soils. If the soil specimen remains undisturbed after applied remolding, that soil specimen gains strength with time. This phenomenon is called thixotropy. It is a time-dependent and reversible process

in the soil. The loss of strength regains gradually if the soil specimen is allowed to rest, as shown in Figure 2.26 (a). However, if the soil specimen has partially thixotropic, the loss of strength caused by remolding can not be regained with time, as shown in Figure 2.26 (b) (Das, 2010)

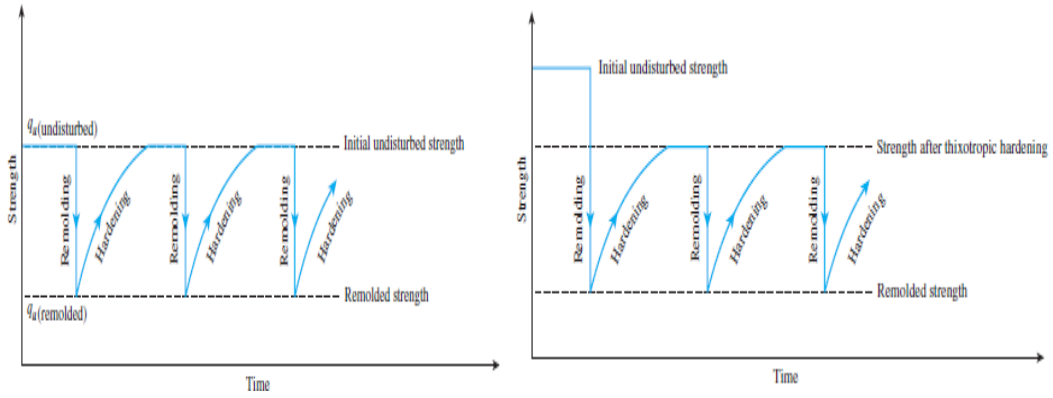

(a) (b)

Figure 2.26 Representation of (a) thixotropic and (b) partially thixotropic materials (Das, 2010)

- *Empirical relationship of undrained shear strength:* Many correlations are proposed to appraise clay's undrained shear strength. The earliest one was suggested by Skempton. It is related to the Plasticity Index, and it is for normally consolidated clay. The correlation was developed using the field vane shear and unconfined compression tests (Skempton, 1957). The relationship given by Skempton is written as:

$$\frac{s_u}{\sigma'_o} = 0.11 + 0.0037(PI) \quad (2.86)$$

where s_u is undrained shear strength, σ'_o is the effective overburden pressure, and PI represents the plasticity index (%). When the preconsolidation stress increases in clay, the undrained strength of saturated clays increases. The effect of preconsolidation pressure on the strength of clay was described (Mesri, 1989). This approximately linear relationship for clays is given as:

$$s_u = 0.22\sigma'_p \quad (2.87)$$

where σ'_p is the preconsolidation pressure or the maximum effective stress and the constant 0.22 is inferred undrained strength ratio in an overconsolidated condition. Another correlation is presented by Jamiliokowski. It is related to the overconsolidation ratio and the vertical effective stress. The undrained

strength ratio for the normally consolidated condition was 0.23 (Jamiliokowski et al., 1985). The equation is given as:

$$\frac{s_u}{\sigma'_v} = 0.23(OCR)^{0.8} \quad (2.88)$$

where σ'_v is the vertical effective stress of clay and OCR represents the overconsolidation ratio. This equation can be generalized as:

$$\frac{s_u}{\sigma'_v} = S(OCR)^m \quad (2.89)$$

where S is the undrained strength ratio of the normally consolidated condition, and m can be called an empirical exponent (Duncan et al., 2014).

When the loads applied to the soil are fast enough, the water has no time to drain from the soil. Also, if the drainage of the water is precluded in a laboratory test, the water can not drain from the soil. In that case, the shear strength of the soil is called the undrained shear strength, and it is denoted by s_u, as mentioned above. Some other factors are not emphasized in part of the shear strength of cohesive soils. The temperature and moisture content affect the undrained shear strength of clay. The temperature increase leads to decreased undrained shear strength with decreasing unconfined compression strength. The water content versus deviatoric stress at failure in log scale varies approximately linear on the normally consolidated clays. However, the variation is not linear on the overconsolidated clays (Das, 2008).

On the other hand, the variation of saturated and unsaturated cohesive soils can be expressed among four categories:

1. The soil is saturated when the water is in tension
2. The soil is saturated when the water is in compression
3. The degree of saturation, S, varies between 0.85 to 1 where the air is impeded, and the water is in tension
4. The degree of saturation, S, has a smaller value than 0.85 where the air has an uninterrupted path, and the water is in tension

On the other hand, categories 1, 2, and 3 are interpreted in the case of saturated cohesive soils. Category 4 is diagnosed in the case of unsaturated cohesive soils. In the case of saturated soil, the effective stress can not increase so, and the shear strength can not increase during the undrained loading on cohesive soils but the water stress increases. Therefore, the control instance of design for loadings is based on the undrained case called a short-term case. The water stress reduces due to the water drainage as time passes, and the shear strength of cohesive soil increases, respectively.

As mentioned above, the Eq.(2.60) becomes Eq.(2.90) in all cases, and the undrained case:

$$s_u = c' + \sigma' \tan \varphi' \tag{2.90}$$

The undrained shear strength of saturated soft or normally consolidated soils depends on the stress path, the stress history, and the stress level. However, the undrained shear strength is a constant. An illustration of undrained shear strength for soft and normally consolidated soils is shown in Figure 2.27.

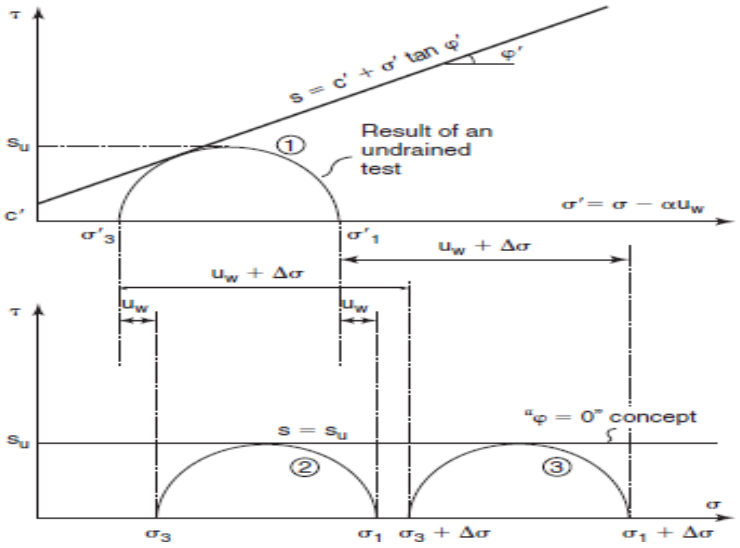

Figure 2.27 Illustration of undrained shear strength for soft and normally consolidated soils (Briaud, 2013)

If the undrained tests are applied on soft and normally consolidated soils, Mohr circle 1 is placed on the axes of the effective stress, and Mohr circle 2 is placed on the axes of the normal stress. The difference between these two stresses represents the water stress, u_w. If the undrained test is applied one more time on the same soil sample, the effective stress of the soil does not change, as shown in Mohr circle 3 in Figure 2.27. It explains why the undrained shear strength is constant and independent of the total stress. This case can be called as φ=0 concept. In the case of unsaturated cohesive soil, the total stress reassigns to the water with degrees of saturation of more or less about 0.85, and the effective stress can not increase. On the other hand, most of the total stress transfers to the soil in low degrees of saturation, and the shear strength increases with the total stress. In low degrees of saturation, if the confining pressure is high enough, the soil can conduct as saturated soil (Briaud, 2013).

2.3 Strain Levels and Characteristics

The structure deformations and ground movements are estimated by geotechnical engineers using analytical or empirical methods. Laboratory tests, in-situ tests, and analytical approaches are applied to determine the geotechnical parameters of soils. Many estimating methods of soil parameters assume that the soil behaves like linear elastic materials that conform to the energy conversation. In more complex soil models, it is assumed that the soil behaves like linear elastic up to the point of maximum shearing resistance. Beyond this point, the behavior of soil becomes perfectly plastic. However, in the nature of soils, primarily nonlinear and inelastic behaviors are valid. That complex behavior of soil is qualified by high constant stiffness at very small strains and decreasing stiffness with increasing strain. The nonlinearity and inelastic behavior of soils, and exhibition of modulus degradation with increasing strain may lead to errors in deformation predictions, especially in the normally and lightly overconsolidated clays. The strain range is an essential factor in the soil moduli predicted by laboratory tests. That soil moduli can be greater than the predicted moduli (Holman T.P., 2005).

The stiffness behavior of soils under the static loading analyzed by fields and laboratory works was classified according to strain levels. The strain levels are introduced into three categories which are very small strains (VSS), small strains (SS), and large strains (LS), as shown in Table 2.1 (Atkinson and Sallfors, 1991).

Table 2.1 Strain level categories and their limits (Atkinson and Sallfors, 1991)

Strain Category	Strain Limits (%)
Very Small Strain (VSS)	<0.001
Small Strain (SS)	0.1 to 0.001
Large Strain (LS)	>0.1

The characterization of the upper boundary in very small strains was obtained as 0.001%. If the strains are below this boundary, the assumption is based on induced by geophysical means. If the stress-strain properties are below this boundary, the assumption is generated by mechanical means. The stress-strain behavior of soil in the very small strain range exhibits linear elastic. When the strain level reaches the level

of threshold value near 0.001%, the stress-strain behavior of soil becomes nonlinear. The secant and tangent modulus of soil exposes a degradation in a hyperbolic fashion due to increasing strain. This region is characterized as a small strain in strains between 0.1% to 0.001%. The large strain behaviors of soils occur at about a strain of 0.1%. The tangent and secant modulus execute relatively small values, and the failure can occur in the large strain level of the soil. This characterization may not be applicable to all soil types (Cho, 2007; Holman T.P., 2005).

Another consideration about strain levels proposed by Ishihara (1996) that the soil deformation occurs as purely elastic and recoverable in the infinitesimal strains. The infinitesimal strains coincide with the strain limits of the very small strain levels that have the upper boundary of 0.001%. The second zone is intermediate strains where the soils behave like elasto-plastic and irrecoverable or permanent deformation. The dilation can occur in the intermediate strains. The intermediate strains coincide with the strain limits of the small strain levels that have the strains between 0.1% to 0.001%. The large strain is determined as the strains exceeding a few percent of the strain limits, and in that case, failure can take place in soils (Cho, 2007).

2.4 Deformation of Soft Soils

The geotechnical engineering studies can be related to the very different types of soils and very different types of loadings. If a certain amount of loading is applied to soil, it is led to deformation in the direction of applied loading. The value of deformation and the type of deformation can exhibit different behavior from one soil type to another. When an application of the same certain amount of loading is on soil, the soft soils deform in a different posture than the stiff soils. The structure and the bond between soil particles, water content, the origin of the soil, and so on significantly affect the deformation properties of any type of soil (Araz and Fitsum, 2011).

In fact, soft soils behave like nonlinear, plastic, and anisotropic deformation. However, in different geotechnical studies, the soft soil is assumed to have elastic, linear, and isotropic deformation. This assumption is valid for applying the theory of elasticity to understand the behavior of stress-strain relationships in soft soils. On the other hand, the elastic deformation is restricted to the pre-consolidation and yield stress for drained conditions and the shear strength for undrained conditions (Araz and Fitsum, 2011).

As an introduction to the soil moduli, the stress-strain graphs of elastic and elastoplastic materials are given below. Linear and nonlinear stress-strain graphs of elastic materials are illustrated in Figure 2.28.

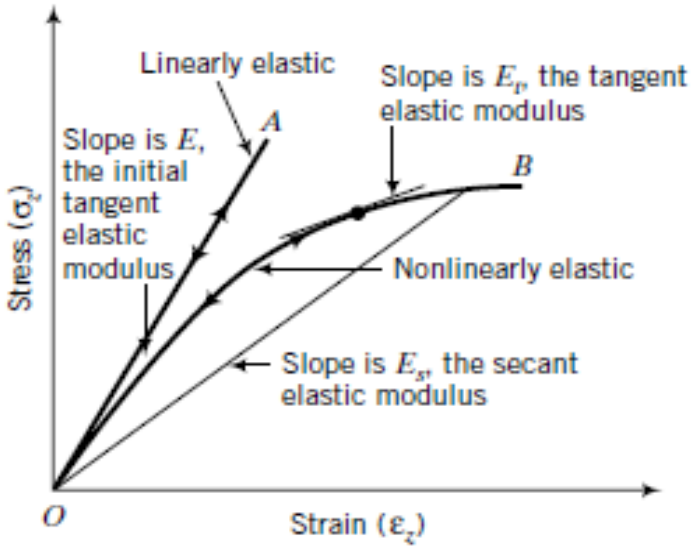

Figure 2.28 Linear and nonlinear stress-strain graphs of elastic materials (Budhu, 2011)

σ_z and ε_z are vertical stress and vertical strain, respectively. The same value of displacements in the vertical direction is obtained for equal increments of vertical loading difference. If the material is unloaded, it has become its original configuration. That relation is illustrated on the OA straight line called linear behavior of soil and the material called linearly elastic material in Figure 28. On the other hand, another case is for equal increments of vertical loading difference, but the different values of displacements in the vertical direction are obtained. Again, if the material is unloaded, it has become its original configuration. That relation is illustrated on the OB curve called nonlinear behavior of soil, and the material called nonlinearly elastic material in Figure 28. An elastic material always obeys the principle of superposition, such as two different loadings acting on elastic material, and there are two different displacements on material with the proportion of loading, respectively (Budhu, 2011).

Also, the initial tangent modulus, tangent modulus, and secant modulus are shown in Figure 28. More precision and true elastic moduli can be determined by small and incremental loadings. The soil moduli were discussed in detail by the following

explanation named as types of soil moduli. On the other hand, some materials, such as the soil, can not return to original configurations after the unloading situation, as illustrated in Figure 29.

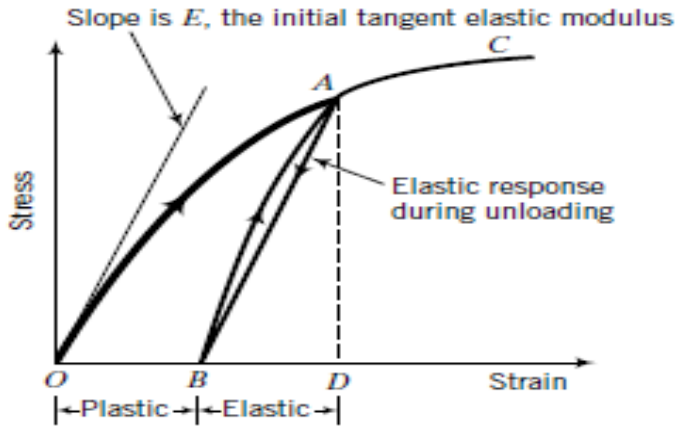

Figure 2.29 Stress-strain graphs of elastoplastic materials (Budhu, 2011)

OA curve is the response of loading. AB line is the response of unloading, and the BC curve is the response to reloading the material. The strains occur in two different parts that are elastic and plastic responses. Part of BD is denoted by elastic or recoverable portion, and part of OB is called plastic or unrecoverable part. These types of materials are named elastoplastic materials. Also, the elastic deformation case should be understood as a knowledgeable of plastic deformation case, which causes permanent deformation in the soil mediums (Budhu, 2011).

2.4.1 Types of Soil Moduli

When a certain amount of loading is applied to soil, the soil exhibits deformation in the direction of the load. The type of deformation can vary in the type of soil, the origin of the soil, and the bond between soil particles and water content. The laboratory tests can consider the deformation of soil with the soil samples or in-situ tests with direct measurements in the field (Araz and Fitsum, 2011).

The selection of appropriable laboratory or in-situ tests and the soil parameters to conceive a deformation problem in the field may not be an easy operation. One of the crucial processes in selecting the laboratory or in-situ test is detecting the deformation conditions of the soil at the element levels. There are several methods to

identify the deformation characteristics of the soil, and one of the methods is through the modulus of deformation (Briaud, 2013).

The deformation modulus is applicable in solving specific soil mechanics problems, such as the design of pavements, settlement of the foundation, and the stress distribution in a semi-infinite mass. There have been several investigators in the past, such as Janbu (1963), Duncan and Chang (1970), and O'Rourke and Crespo (1988). Moreover, the deformation modulus can be an essential parameter in the improved soils subjected to the stabilization techniques, for example, the soil mixtures stabilized by fly ash or synthetic fibers (Ghosh and Subbarao, 2012).

2.4.1.1 Soil Stiffness (Young's Modulus)

The soil stiffness is an essential parameter to figure out the behavioral analysis of substructures and the calculation of the elastic deformation due to the applied static loadings. In addition, it can be required to calculate soil settlement and distribution of stresses in the soil. The soil stiffness is defined as the modulus of elasticity or Young's modulus. Therefore, it can be obtained as the maximum elastic modulus in the slope of the tangent passing through the origin or the initial slope of the stress-strain curve of soil. Hence, it can be qualified as the initial tangent modulus of soil (Anochie-Boateng, 2007). The initial tangent modulus is illustrated in Figure 2.30.

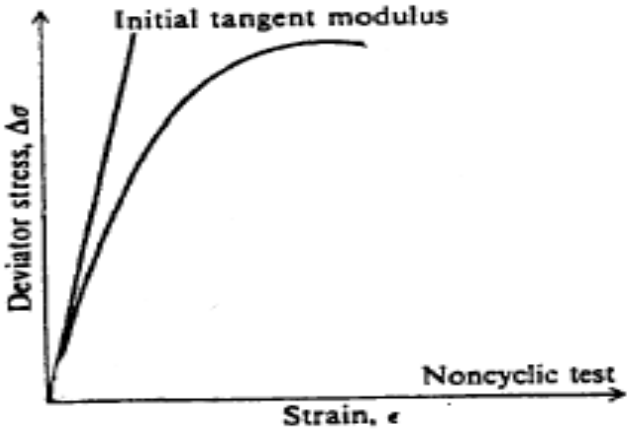

Figure 2.30 The initial tangent modulus in the stress-strain curve (Bejarano, 1999)

The tendency of the stress-strain curve for soil is generally nonlinear, depending on several factors. The beginning or early part of the curve may be approximately a

straight line. However, it does not exhibit nonlinear behavior at a very early stage in the stress-strain curve of the soil. Therefore, the using theory of elasticity becomes applicable to calculations. In that case, the Poisson's ratio that depends on chosen test conditions can be essential for Young's modulus. Note that the modulus may not be a slope of the line calculated as the increment of stress divided by strain increment. This case can be valid only if the loading is applied as unconfined such as in the unconfined compression tests. In the triaxial tests, Young's modulus or modulus of elasticity and the Poisson's ratio is given as:

$$E = \frac{\sigma_1 - 2v\sigma_3}{\varepsilon_1} \tag{2.91}$$

$$v = \frac{-\varepsilon_3\sigma_1 + \varepsilon_1\sigma_3}{\varepsilon_1\sigma_1 + \varepsilon_1\sigma_3 - 2\varepsilon_3\sigma_3} \tag{2.92}$$

where Young's modulus or the modulus of elasticity is denoted by E, σ_1 is the major principal stress, σ_3 is minor principal stress, Poisson's ratio is represented by v, ε_1 is the major principal strain. If the unconfined compression test is applied to the soil specimen, the slope and the Poisson's ratio are given as:

$$E = \frac{\sigma_1}{\varepsilon_1} \tag{2.93}$$

$$v = -\frac{\varepsilon_3}{\varepsilon_1} \tag{2.94}$$

Eq.(2.93) and Eq.(2.94) are available only if the minor principal stress, σ_3, is equal to zero (Briaud, 2013). As mentioned in Eq.(2.25), Poisson's ratio of soil is determined in Eq.(2.94)

The definition of the initial tangent modulus is defined by Janbu (1963), and it can be formulated as:

$$E_i = Kp_a\left(\frac{\sigma'_3}{p_a}\right)^n \tag{2.95}$$

where the initial tangent modulus of soil denotes E_i, σ'_3 is the minor effective principal stress, p_a is determined as atmospheric pressure, K is the modulus number, and n is the exponent determining the variation rate of the initial tangent modulus with the effective minor principal stress. The atmospheric pressure has the same pressure unit as the initial tangent modulus and the effective minor principal stress. The magnitude of K and n values can be considered from the results of the number of triaxial tests for a particular soil specimen. After that, the initial tangent modulus versus the effective

minor principle stress graph on a log-log scale is plotted. The magnitude of the modulus number, K, usually varies in the range of 300-2000 and n varies between 0.3 and 0.6 (Das, 2008).

In addition, in Eq.(2.95), the mean principal stress, which is denoted by σ_m ($\sigma_m=0.33(\sigma_1+ \sigma_2+ \sigma_3)$), can be written instead of the minor effective principal stress, σ'_3 (Briaud, 2013).

2.4.1.2 Secant Modulus

The nonlinearities of soil can be led to initial occlusion of soil pores and shearing close to the yield state of the soil. Hence, the irreversible changes are caused by the nonlinear stress-strain response of the soil. The secant modulus may be a way of analysis to involve the effects of irreversible changes in the internal structure of the tested soil sample. Therefore, the nonlinear nature of the deformation response can be interpreted by the secant modulus of soil. The slope of the straight line from the origin to a certain load level of the stress-strain response is the secant modulus of tested soil. In other words, the secant modulus is defined as the slope of a straight line drawn from the origin of the stress-strain curve to a specific stress level (Tutluoğlu, Öge and Karpuz, 2015).

The secant modulus of soil can predict the movement of a spread footing due to the first loading application. There are several determination ways of the secant modulus. Some geotechnical engineers prefer to consider the secant modulus by using the maximum stress point on the stress-strain curve or corresponding to a certain strain level, such as strain levels of 0.5% or 1%. Another approximation of the secant modulus commonly used is one-half the maximum stress corresponding to the stress-strain curve. It is denoted by E_{s50}. E_{sf} can represent the secant modulus considered by using the maximum stress point. The secant modulus is not a constant value that tends to decrease as the axial strain of soil increases (Budhu, 2011). The representation of the secant modulus on the stress-strain curve is shown in Figure 2.31.

The relation between deviatoric stress and strain in the secant modulus is shown above. Hence, it is clear that the secant modulus decreases with increasing strain. The general slope equation of the secant modulus in the soil can be written as:

$$E_s = \frac{\Delta\sigma}{\Delta\varepsilon} \tag{2.96}$$

where E_s is the secant modulus of soil at a certain stress level, $\Delta\sigma$ is denoted by a stress difference in the deviatoric stress, $\Delta\varepsilon$ is the strain difference from origin to a certain point on the stress-strain curve of soil. The type of stress can be altered according to applied in-situ or laboratory test conditions (Anochie-Boateng, 2007).

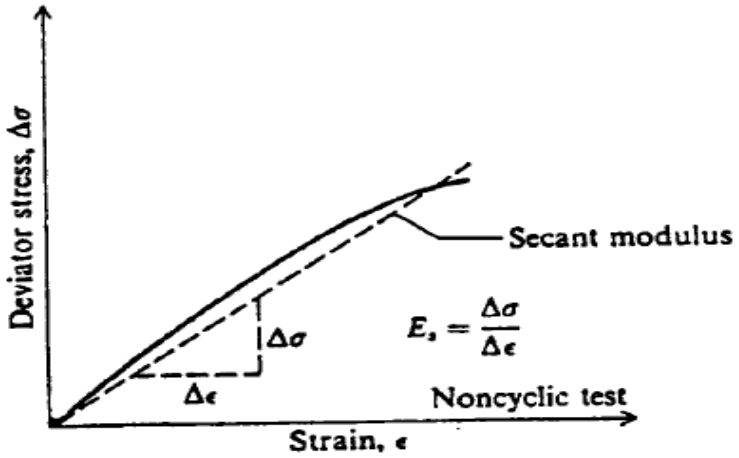

Figure 2.31 The secant modulus in the stress-strain curve (Bejarano, 1999)

Furthermore, the tested soil's initial tangent modulus and the secant modulus are shown in Figure 2.32 at the same stress-strain curve.

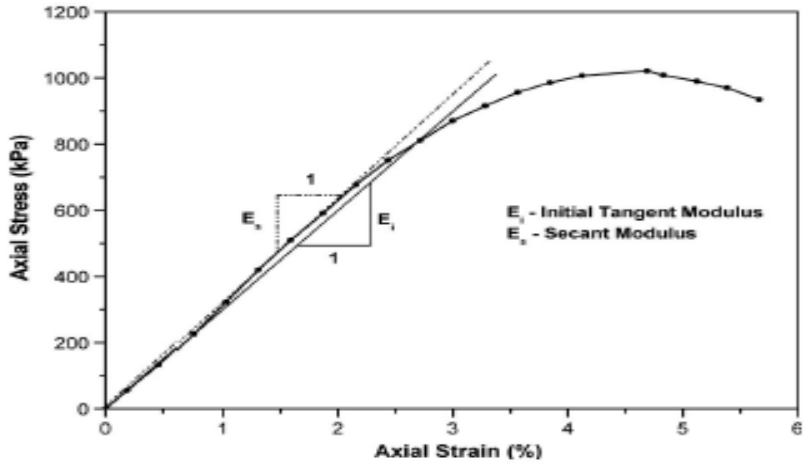

Figure 2.32 Determination of initial tangent modulus and secant modulus (Moghal, Obaid and Al-Refeai, 2014)

2.4.1.3 Tangent Modulus

The tangent modulus would analyze the incremental movement due to the incremental loading. When a tangent line is drawn on a point in the stress-strain curve

of soil, the tangent modulus can be obtained. It is denoted by E_t (Briaud, 2013). Also, if the tangent line is drawn in the half of maximum stress, the slope of the line can be called the tangent modulus of soil at the half of the maximum stress and can be denoted by E_{t50}. The representation of the tangent modulus on the stress-strain curve is shown in Figure 2.33.

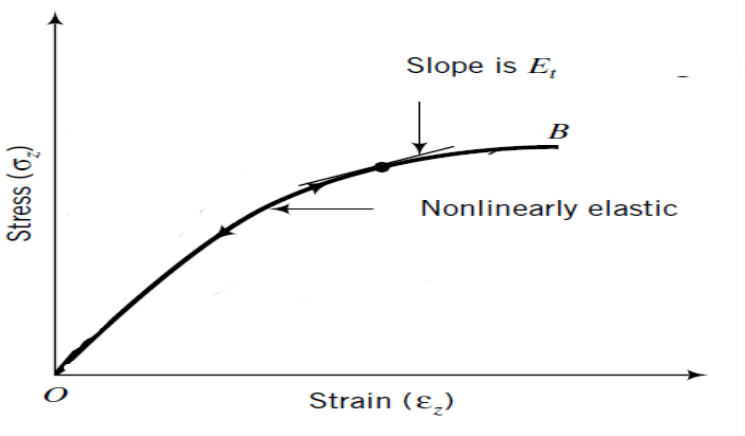

Figure 2.33 The tangent modulus in the stress-strain curve (Budhu, 2011)

The tangent modulus is used in the incremental stress analysis of a soil mass. The required soil parameters to calculate the tangent modulus can be determined from the laboratory test results. The type of stress can be altered according to applied laboratory or in-situ test conditions. The general equation of tangent modulus can be written as:

$$E_t = \frac{\partial(\sigma'_1 - \sigma'_3)}{\partial \varepsilon} \tag{2.97}$$

where E_t is the tangent modulus of soil, σ'_1 is the major effective principal stress, σ_3 is the minor effective principal stress, and ε is the strain rate of soil (Das, 2008).

Hence, it is clear that the tangent modulus is not a constant value that tends to decrease with the increasing strain. Kondner and Janbu's models were combined by Duncan and Chang (1970) to formulate a hyperbolic model (Anochie-Boateng, 2007). The hyperbolic model of Duncan and Chang was described in detail on the part of common constitutive models of soils.

2.4.1.4 Unloading Modulus, Reloading Modulus, Resilient Modulus, Cyclic Modulus

The nature of soil does not behave elastic, and the stress-strain curve can tend to be nonlinear. As mentioned, the slope of the stress-strain curve refers to the soil moduli. Many types of moduli can be determined from the triaxial tests. Different types of modulus can be defined depending on the conditions and properties of geotechnical studies. These types of modulus admit unloading modulus, reloading modulus, and cyclic modulus, as shown in Figure 2.34.

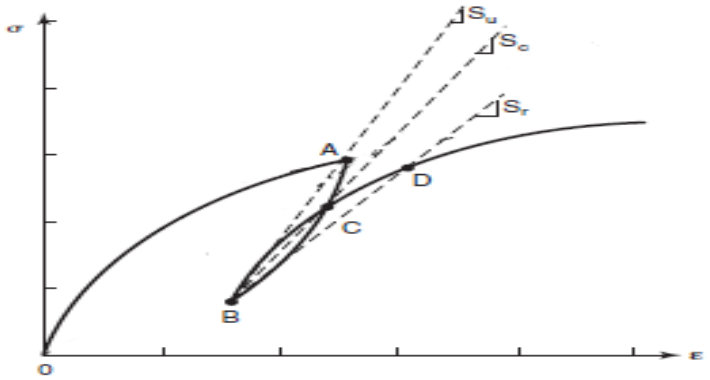

Figure 2.34 Definitions of unloading, reloading, resilient, and cyclic modulus (Briaud, 2013)

The unloading modulus is drawn in the line that passes through points A and B. S_u is denoted by the unloading slope, and the unloading modulus is calculated with the unloading slope. It is symbolized by E_u. The unloading modulus can be an essential parameter of excavation analysis if the deformation occurs at the bottom of the excavation. For example, the stress in the clay layer at the bottom of the excavation decreases when the unloading condition is valid. Therefore, the unloading modulus of soil tends to decline due to the decreasing stress. On the other hand, the initial value of the unloading modulus has larger due to the effect of creep. It decreases in the depth of excavation if it is normally or slightly consolidated clays (Araz and Fitsum, 2011).

The reloading modulus is drawn in the line that passes through points B and D. S_r is denoted by the slope of reloading, and the reloading modulus is calculated with this slope. It is symbolized by E_r. The reloading modulus can be an essential parameter to calculate the motion at the bottom of the excavation when the excavated soil is substituted in the excavation. Also, the reloading modulus can be used to calculate

movement in the pavement due to the reloading. Another type of modulus is the cyclic modulus. It is drawn in the line that passes through points B and C. S_c is denoted by the slope of the cyclic, and the cyclic modulus is calculated with this slope. It is symbolized by E_c. The cyclic modulus can be an essential parameter to calculate the function of the number of cycles and the movement of the pile foundations due to repeated loadings (Briaud, 2013).

The laboratory test determines the resilient modulus parameters and repeated load triaxial tests. Several repeated deviator stresses are applied to the cylindrical specimens due to the constant confining stress conditions. Therefore, the magnitude of stress level, number of applied loads, the moisture content of specimen, and the stress history affect the resilient modulus of soils. Also, liquid limit, plasticity index, water content, density, and specific gravity can be several factors related to the resilient modulus of soils (Bejarano and Thompson, 1999).

2.4.1.5 Shear Modulus, Bulk Modulus, Constrained Modulus

The soil moduli are required to analyze the mathematical representation of the soil behavior due to the applied loadings. It is related to the response of soil under applied stress. The theory of elasticity is associated with linear stresses and strains. Other types of soil moduli are shear, bulk, and constrained moduli. They are defined from the modulus of elasticity, E, and Poisson's ratio, v. The shear modulus is denoted by G. It can be found by the simple shear test, and the shear modulus can be determined as the ratio between the shear stress, τ, and the engineering shear strain, γ. The shear modulus relationships are given as follows:

$$\varepsilon_{xy} = \frac{1+v}{E}\tau_{xy} = \frac{\gamma_{xy}}{2} \tag{2.98}$$

$$G = \frac{\tau_{xy}}{\gamma_{xy}} = \frac{\tau_{xy}}{2\varepsilon_{xy}} = \frac{E}{2(1+v)} \tag{2.99}$$

where G is the shear modulus, E is the modulus of elasticity, and v is the Poisson's ratio (Briaud, 2013). The initial shear modulus, tangent shear modulus, and secant shear modulus are shown in Figure 2.35.

The constrained modulus is based on the vertical normal stress in a cylindrical sample, and it can preclude any lateral movements. The constrained modulus is the ratio between the applied normal stress and vertical strain caused by the stress, denoted by M (Briaud, 2013). The relationship of the constrained modulus can be given as:

$$M = \frac{\sigma_{xx}}{\varepsilon_{xx}} = \frac{E(1-v)}{(1+v)(1-2v)} \tag{2.100}$$

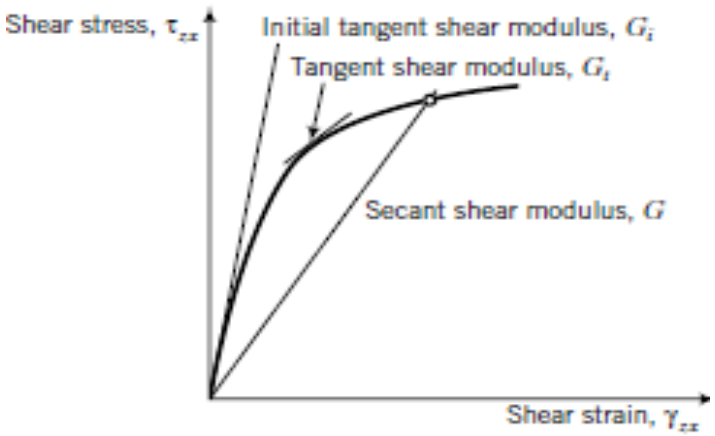

Figure 2.35 Representation of shear moduli (Budhu, 2011)

The bulk modulus occurs due to the hydrostatic pressure all around in a soil sample. It is denoted by K. The bulk modulus is described as the ratio between the pressure and the volumetric strain. The relationship of the bulk modulus can be given as:

$$K = \frac{\sigma}{\Delta V/V} = \frac{\frac{1}{3}(\sigma_{xx}+\sigma_{yy}+\sigma_{zz})}{(\varepsilon_{xx}+\varepsilon_{yy}+\varepsilon_{zz})} = \frac{E}{3(1-2v)} \tag{2.101}$$

where the volumetric strain is $\varepsilon_v=\Delta V/V$. Also, the nonlinear relationships of bulk modulus, the deviator stress, and the volumetric strain were determined by Duncan (1980). It was suggested by a conventional triaxial test with constant confining pressure. The relationship can be written as follows:

$$K = \left(\frac{\sigma_1+\sigma_3}{3\varepsilon_v}\right) \tag{2.102}$$

$$K = k_b P_a \left(\frac{\sigma_3}{P_a}\right)^m \tag{2.103}$$

where k_b is bulk modulus number, p_a is determined as atmospheric pressure, and m is bulk modulus exponent. m usually varies in the range of 0 and 1. Duncan (1980) proposed Eq(2.103) which is determined as a hyperbolic model for the variation of bulk modulus (Anochie-Boateng, 2007).

2.4.2 Influence of State Factors and Influence of Loading Factors

Several factors markedly act upon the moduli of soils. These factors may be separated into two categories related to the nature and history of soil and applied stress conditions. First, the nature and history of soil are related to the composition, soil grading, particle properties, soil density, and cementing of soil particles. Another one is related to drainage conditions, loading rates, and boundary conditions of loading (Atkinson and Sallfors, 1991; Tatsuoka et al., 1997).

The state factors of soil moduli are included the particle packing, organization of particles, the water content, the stress history, age and creep, and the cementation of soil. One of the factors is how the *particles* are closely *packed*. It is considered by measuring the dry density and porosity of the soil. Therefore, the soil moduli tend to increase when the particles are closely packed. The *particles organization* is mentioned in soil structures such as fine-grained or coarse-grained soils. For example, fine-grained soils have a nature of disseminated and flocculated structures. The *water content* significantly influences the soil moduli. The low water content in the soil causes water attachment in the soil particles. Therefore, the effective stress between the soil particles tends to increase due to the water tension, especially in fine-grained soils. It is related to why the clayey type of soil becomes very stiff and shrinks when it is in dry condition. In that case, the soil moduli tend to increase when the soil has low water content. Therefore, if the water lubrication rises due to the water content increasing, the soil moduli exhibit to increase due to the effect of compaction. In contrast, the soil moduli decrease due to increasing compressibility when the water content enhances beyond an optimum value. The *stress history* refers to what the soil has been applied to loading conditions in the past. If the soil has been applied the load in the past, this soil situation is called the overconsolidated. In that case, the soil moduli have a high value due to the reload part of the stress-strain curve. If the soil has a condition of equilibrium under stress, this soil situation can be called normally consolidated. In that case, the soil moduli have a lower value than the overconsolidated soil. Since the normally consolidated soil is on the first loading part of the stress-strain curve. The *cementation* factor of soil can be described as adhesiveness between the soil particles. As discussed earlier, the low water contents in the fine-grained soils caused the glue effect between particles due to the water tension of the soil. Another case of cementation is the chemical cementation in the soil adjunction. It leads to an

increase in the soil moduli (Briaud, 2013). The *age and creep* factor of soil significantly influences the soil moduli. The increase in undrained strength and the pre-consolidation pressure of soil induced by sustained aging and the increase in stiffness may not be described by decreasing the void ratio in the soil during the secondary compression. Understanding the microstructure and physical and chemical bonds is an essential factor due to the rearrangement of soil. The soil moduli tend to increase in a constant state of stress due to the small creep periods (Anderson and Stokoe, 1978).

The loading factors of soil moduli are included, such as the mean stress level, the stain level, the strain rate, the number of cycles in loading, and the drainage conditions. One of the factors is what the *mean stress level* is in the soil. The loading condition causes stress that can be shear or normal stresses and the combinations in the soil. The confinement effect can be defined as the mean of these three stresses. The soil modulus tends to be higher due to the confinement effect of soil. The *strain level* is caused by loading in the soil. The soil modulus has a dependence on the mean strain level due to the nonlinearity of the soil. Most of the soil modulus is leaned to a higher value where the strain level of soil increases. Also, the stress-strain curve obtained from the triaxial tests has a hyperbola up to the peak value of the curve. As mentioned before, this model is assigned by Duncan and Chang (1970). The *strain rate* refers to the strain per unit of time. The plotting of soil modulus versus strain rate on a log-log scale gives an approximately straight line. The values of this exponent alter from 0.02 in stiff clays and 0.1 in very soft clays. The nature of the soil is viscous, which leads to faster loaded and getting the stiffer situation. In that case, the soil modulus tends to have a higher value. The *number of cycles* by the soil has influenced the soil modulus. When the loading is applied a repeated number of times, this factor affects the soil. The *drainage condition* factor of soil can be categorized as drained and undrained loading. If drainage is not allowed during the laboratory test, the undrained condition takes place. The drainage depends on the soil type because of the time involved in completing the drainage. For example, when drainage is not allowed due to the loading of clay, the Poisson's ratio of soil is commonly assumed to equal 0.5 because of any volume change in the clay (Briaud, 2013).

2.4.3 Application Fields of Soil Modulus

The soil modulus is practicable to utilize in many geotechnical engineering studies. However, the soil modulus can have different properties from one field to another. For example, in the *shallow foundations*, the strain occurs first in the construction state, and then the loads are sustained by the foundation over many years. Therefore, the loading rate of the shallow foundation is slow. On the other hand, in the case of *deep foundation*, the friction on a pile sustains over a range of depths, and the main stresses level vary. Hence, the stain level of the pile has a generally smaller value than the shallow foundations. Furthermore, deep foundations are utilized in very different types of soils and loadings. Therefore, the soil moduli present a much more comprehensive range of values than the shallow foundations. The movements of *retaining structures and the slope stability* case are linked with the deformation of soil mass under the own weight of the structure. Therefore, the strains are generally minor, and the strain rates of the retaining structures and the slope is related due to the initial construction and long-term deformations. Therefore, the soil moduli tend to have a higher value than in structures of foundation engineering because of small strain levels. The strain levels are limited to long-term deformations in the *pavements*, and the mean stress levels are low in the subgrade (Briaud, 2013).

CHAPTER 3

3. COMMON CONSTITUTIVE MODELS OF SOILS

In reality, soil nature has a nonlinear behavior in which the stiffness and strength of soil depend on strain and stress levels. When dealing with the nonlinear behavior of soil, the stress and strain relationship is not simple. Setting up a numerical process of physical quantities in the soil is called the constitutive model. Evaluation and the application of nonlinear relations are essential in researching geotechnical problems. Nevertheless, some constitutive models have been produced that may receive many soil behavior characteristics. These provide a numerical approach to geotechnical engineering problems. The constitutive models are mainly applied to the reconstitution of soil and remolded materials. The constitutive models are facilitated by representing stress-strain curves using mathematical functions and fitting methods, nonlinear elasticity, and plasticity theories. Three common constitutive models that respond to relatively few soil parameters are presented in the following sections (Calvello, 2002; Desai and Christian, 1977).

The mechanical illustrations of an obtained stress-strain curve are bilinear and multilinear models in related nonlinearity. The initial moduli of soil are valid until the soil stress reaches the yield value and the incremental stress-strain relationship is applied up to the yield. That is related to the bilinear relation, which develops to alter Young's modulus from initial to yield value. The incremental stress-strain relationship in initial can be written as:

$$\{\Delta\sigma\} = [C_i]\{\Delta\varepsilon\} \tag{3.1}$$

where $[C_i]$ is the initial moduli. It refers to the initial value of Young's modulus denoted by E_i. The bilinear model of nonlinear materials is shown in Figure 3.1.

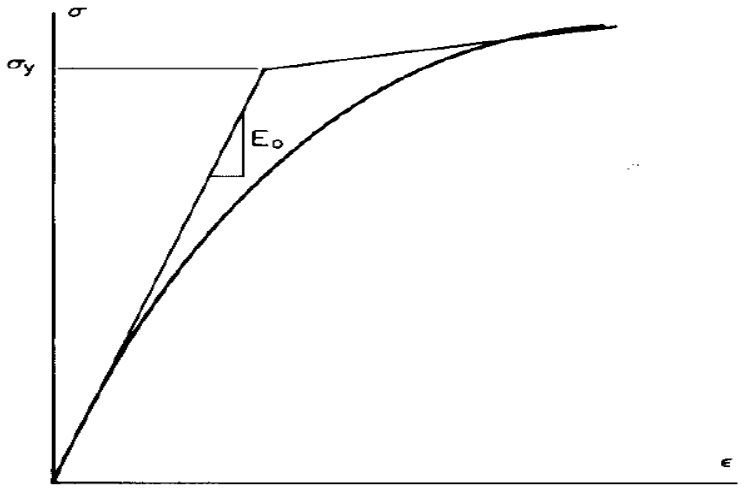

Figure 3.1 Illustration of bilinear model for nonlinear materials (Desai and Christian, 1977)

Another is the multilinear model, in which nonlinear curves are divided into several linear curves. It is a linear approach by the interpolation procedure that a set of points on a stress-strain curve can obtain the tangent moduli. For example, the multilinear model of nonlinear materials is shown in Figure 3.2, and the tangent modulus, that is the slope of two computed points, can be written as:

$$E_t = \frac{\sigma_i - \sigma_{i-1}}{\varepsilon_i - \varepsilon_{i-1}} \tag{3.2}$$

where E_i refers to the tangent modulus.

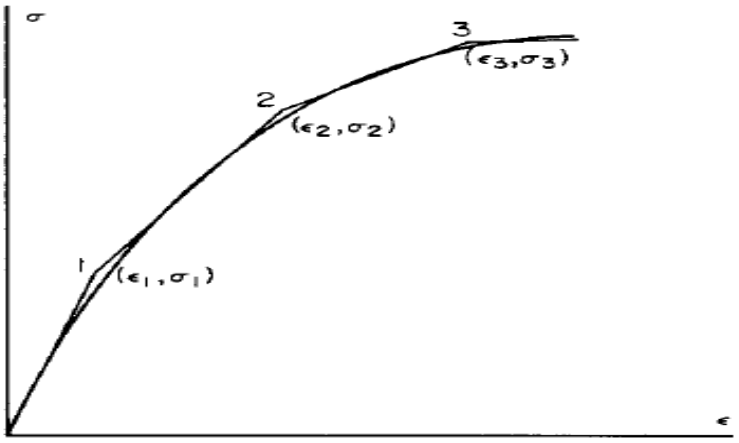

Figure 3.2 Illustration of multilinear model for nonlinear materials (Desai and Christian, 1977)

Using mathematical functions such as hyperbolas and polynomials provides accurate computations of the tangent modulus (Desai and Christian, 1977).

3.1 Duncan-Chang Hyperbolic Model

The Duncan-Chang model is the most common and widely used model used to determine nonlinear characteristics on various types of soils. It should be noted that Masin and Rott (2014) produced a hypo-plastic model for clays that regard the effect of stress paths. However, it does not apply to a wide range of soil types. On the contrary, the Duncan-Chang hyperbolic model was found to be more suitable for most soil types by revising under complicated stress states in order to obtain the stress-strain relationship between soil and the tangent modulus under the lateral unloading stress path (H.Huang, M.Huang and Ding, 2018).

In order to describe the nonlinear stress-strain analysis of the soil and originate the technique for this behavior of soil, the stress-strain relationship is taken into account the nonlinearity, the stress-dependency, and inelasticity of soil in the Duncan-Chang hyperbolic model. The soil parameters for the Duncan-Chang model have been easily received from the laboratory triaxial tests. The test conditions and the specimens are chosen to duplicate field conditions. Many factors of effect in the stress-strain relationship of soil can be described as over a wide range of stress in inelastic, nonlinearity, and the magnitude of confining pressures in the tests. The simplification of procedures and tests may be led to some loss of accuracy. Still, the obtained results by Duncan-Chang hyperbolic model are sufficiently accurate for many practical purposes (Duncan and Chang, 1970).

There are incremental procedures and iterative procedures to analyze the stress-strain relationship. The incremental procedure is investigated by changing loading with a series of increments. Approximately, the series of straight lines at the beginning of the new increment of loadings allows for analyzing the modulus values of stress and strain. The advantages of the incremental procedure are accounting for the initial stress easily, examining the influence of a given loading, and calculating the stresses and strains with smaller values. However, the defect of this procedure is unfeasible, simulating stress-strain relationships beyond the peak point of the graph. The incremental procedure examines the analysis of embankment and excavated slopes and

stresses in the simple shear specimens(Clough and Woodward, 1967; Dunlop and Duncan, 1970). The successive increments are shown in Figure 3.3.

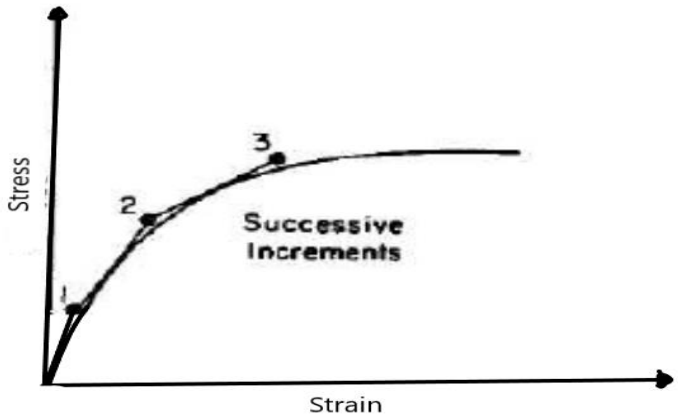

Figure 3.3 The successive increments (Duncan and Chang, 1970)

The iterative procedure is investigated to capture nonlinear relationships between stress and strain by stress and strain values. The new values of modulus are chosen for the subsequent analysis if these values do not represent. The advantage of the iterative procedure is representing the stress-strain relationships beyond the peak point of the graph. The shortcoming of this procedure is the difficulty of accounting for the non-zero initial stresses. The iterative procedure examines the analysis of footing settlements and the pavements (Duncan, Monismith and Wilson, 1968). The successive iterations are shown in Figure 3.4.

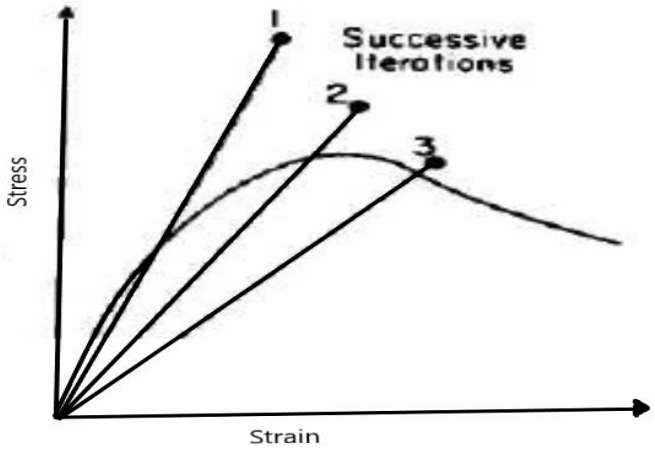

Figure 3.4 The successive iterations (Duncan and Chang, 1970)

The nonlinear stress and strain behavior of soil can be presented by hyperbolic stress-strain models widely used to model behavior in many soil types because of their adaptability, simplicity, and a high degree of accuracy. Kondner (1963) suggested the hyperbolic equation based on the quantity of triaxial tests. The hyperbolic equation is given as:

$$\sigma_1 - \sigma_3 = \frac{\varepsilon}{a+b\varepsilon} \tag{3.3}$$

where σ_1 is the major principal stress, σ_3 is the minor principal stress, ε is the axial strain, a and b are constants determined experimentally (Anochie-Boateng, 2007).

When the subscripts are removed from Eq.(3.3), σ and ε are vertical stress and vertical strain, respectively. Plotting the σ/ε versus ε controls whether the data fit a hyperbola from the triaxial test, as shown in Figure 3.6. In order to find the incremental stiffness of soil, the equation became at the very small strains:

$$\sigma = \frac{\varepsilon}{a} \tag{3.4}$$

where 1/a is denoted by the initial Young's modulus or initial tangent modulus. The equation became at the large strains:

$$\sigma = \frac{1}{b} \tag{3.5}$$

where 1/b is the compressive strength and the asymptote (Desai and Christian, 1977).

Duncan and Chang (1970) combined the models of Kondner (1963) and Janbu (1963) to formulate a hyperbolic model that expresses in terms of the tangent modulus. The proposed equation by Janbu is given in Eq. (2.95). The physical meanings of constants a and b are given that a is the reciprocal of the initial tangent modulus and b is the reciprocal of the asymptotic value of stress difference, as shown in Figure 3.5. The stress difference refers to the stress-strain curve approaches at the infinite strain written as $(\sigma_1 - \sigma_3)_{ult}$. The hyperbolic representations of the stress-strain curve are given in Figure 3.5 and Figure 3.6 as follows.

It is a usefully meaning of the nonlinear behavior of soil in the stress-stain curve. Then, if Eq.(3.3) is written in the following form:

$$\frac{\varepsilon}{\sigma_1-\sigma_3} = a + b\varepsilon \tag{3.6}$$

where the parameter a is the intercept and b is the slope of the resulting straight line, as shown in Figure 3.6.

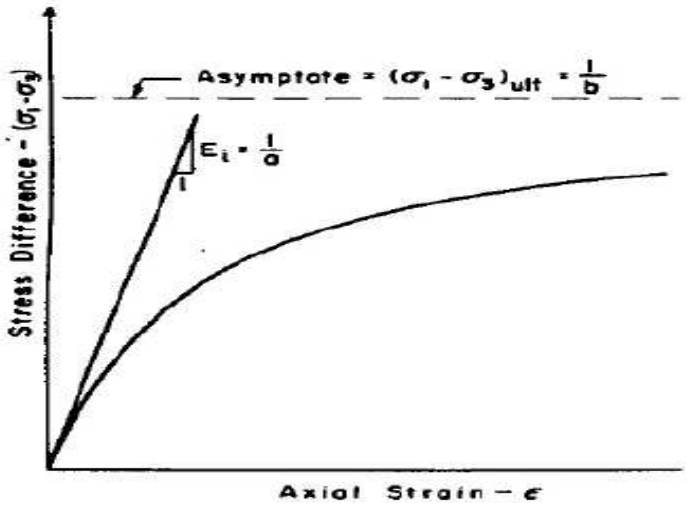

Figure 3.5 The representation of the hyperbolic stress-strain curve (Duncan and Chang, 1970)

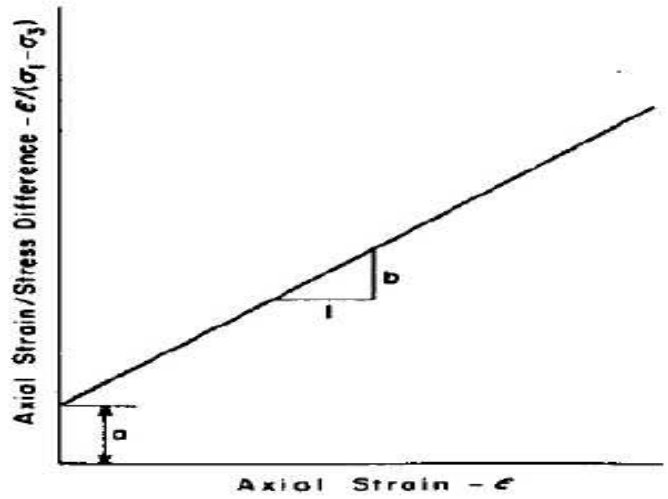

Figure 3.6 The representation of the transformed hyperbolic stress-strain curve (Duncan and Chang, 1970)

The asymptotic value of stress difference is larger than the compressive strength of the soil sample because the hyperbola stays below the asymptote. Therefore, the equation of this relationship in the asymptotic value and compressive strength of soil can be written as:

$$(\sigma_1 - \sigma_3)_f = R_f (\sigma_1 - \sigma_3)_{ult} \quad (3.7)$$

where $(\sigma_1 - \sigma_3)_f$ is the stress difference at failure or compressive strength, $(\sigma_1 - \sigma_3)_{ult}$ is the asymptotic value of stress difference. R_f is the failure ratio that always has a value less than unity, and it is independent of confining pressure proposed by Duncan and Chang (1970). Desai and Christian (1977) presented that the failure ratio can be found usually between 0.7 and 0.9. If parameters a and b are written in terms of initial tangent modulus and compressive strength, the Eq.(3.3) can be given as:

$$(\sigma 1 - \sigma 3) = \frac{\varepsilon}{\left[\frac{1}{Ei} + \frac{\varepsilon R_f}{(\sigma_1 - \sigma_3)_f}\right]} \tag{3.8}$$

where E_i is the initial tangent modulus of soil, as mentioned. If the performing the given differentiation in Eq.(2.97) with Eq.(3.8) and organized it, the expression can be written with the tangent modulus as follows:

$$E_t = \frac{\frac{1}{Ei}}{\left[\frac{1}{Ei} + \frac{\varepsilon R_f}{(\sigma_1 - \sigma_3)_f}\right]^2} \tag{3.9}$$

where E_t is the tangent modulus of soil, as mentioned before. The defect of this expression is that the tangent modulus refers to both stress difference and strain in the different reference states. While the reference state of stress difference may be specified precisely, such as $(\sigma_1 - \sigma_3)$ is equal to zero, the reference state of strain can be completely arbitrary such as ε is equal to zero. Therefore, the initial conditions should be selected as a reference state for strain, but it is not valid in the stress difference. Hence, the expression of tangent modulus is proper when it is established independent of stress or independent of strain. On the other hand, the stresses can be estimated more precisely than the strains in the geotechnical problems. Therefore, if the strain is eliminated and tangent modulus is written in terms of stress in Eq.(3.9) by rewriting Eq. (3.8), the expression became:

$$\varepsilon = \frac{\sigma_1 - \sigma_3}{E_i\left[1 - \frac{R_f(\sigma_1 - \sigma_3)}{(\sigma_1 - \sigma_3)_f}\right]} \tag{3.10}$$

and substituting Eq.(3.10) into Eq.(3.9) and simplifying the resulting equation, the tangent modulus may be expressed as:

$$E_t = (1 - R_f S)^2 E_i \tag{3.11}$$

where S is the stress level or fraction of the strength, and it can be written as:

$$S = \frac{(\sigma_1 - \sigma_3)}{(\sigma_1 - \sigma_3)_f} \quad (3.12)$$

where $(\sigma_1 - \sigma_3)$ is the stress difference at a certain point, and $(\sigma_1 - \sigma_3)_f$ is the stress difference at failure. The constant minor principal stress for total stress analyses is used to determine the parameters in the unconsolidated-undrained tests. The tangent modulus and the compressive strength of soil vary with the confining pressure except in the unconsolidated-undrained tests (Duncan and Chang, 1970).

The Duncan-Chang hyperbolic model uses the Mohr-Coulomb failure criterion that depends on the friction angle with confining stress and does not directly cover the dilatancy. The Mohr-Coulomb failure criterion at the failure can be written as follows:

$$(\sigma_1 - \sigma_3)_f = \frac{2c\cos\varphi + 2\sigma_3 \sin\varphi}{1 - \sin\varphi} \quad (3.13)$$

where c is the cohesion of soil and φ is the friction angle of soil specimen, as mentioned before (Desai and Christian, 1977).

When Eq.(3.12) and Eq.(3.13) are substituted into Eq.(3.11), the expression of tangent modulus for any stress conditions can be written as:

$$E_t = E_i \left[1 - \frac{Rf(1 - \sin\varphi)(\sigma_1 - \sigma_3)}{2c\cos\varphi + 2\sigma_3 \sin\varphi}\right]^2 \quad (3.14)$$

and the utility of Eq.(3.14) is based on two factors. First, the tangent modulus is defined in terms of only stress, so analyses of the geotechnical problem regard any initial stress conditions. Another one, the required parameters of the relationship are obtained easily by laboratory tests (Duncan and Chang, 1970).

3.2 Modified Cam Clay Model

Roscoe, Schofield and Wroth (1958) originated the Cam Clay model to evolve a complete stress-strain model using plasticity theory for normally consolidated and lightly overconsolidated saturated clays. The Cam Clay model was modified in 1965, and it is called as Modified Cam Clay (MCC) model. The Modified Cam Clay model is a non-linear, elastoplastic, isotropic, and strain hardening model (Roscoe and Burland, 1968).

The Modified Cam Clay model establishes the critical state theory that all stress paths finish at the failure. It regards a logarithmic relationship between the mean effective stress and the void ratio. The MCC model lets a linear stress-dependency of

stiffness in the normally consolidated clays. On the other hand, the hardening plasticity that the preconsolidation stress induces development in the plastic volumetric strain. The change in strength in soil with stress history and current effective stress can be connected by the Modified Cam Clay model (Atkinson, 1993; Brinkgreve, 2005).

No more variation in volume and stress on the critical state line exists on the graphs of e-Lnp' and the of q-p'. The deviator stress is denoted by q, p' is the mean normal stress, and e is the void ratio. The defined parameters of these two lines are shown in Figure 3.7. For the triaxial test, the deviatoric stress is defined as the differences between major principal stress and minor principal stress, respectively. On the same type of test, the mean normal stress equals $0.33(\sigma'_1+2\sigma'_3)$. Also, the shear modulus, G, is required. Besides, the initial state is defined by the initial void ratio of the soil, e_o, its initial overconsolidation ratio, OCR, and the initial effective stress, p'_o (Briaud, 2013).

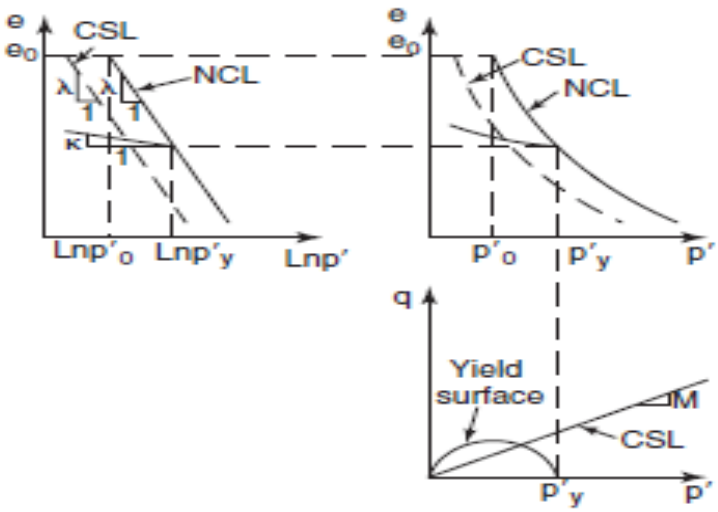

Figure 3.7 Representation graphs of Modified Cam Clay model (Briaud, 2013)

The equation of axial strain for the consolidation test can be given as:

$$\varepsilon = \frac{\Delta e}{1+e_o} \tag{3.15}$$

where Δe is the change in void ratio from e_o. The normal compression line that NCL denotes is identified as the stress-strain curve by a straight line on the e versus Lnp'. In that case, the mean effective stress, p' is equal to $0.33(\sigma'_1+\sigma'_2+\sigma'_3)$:

$$e = e_o - \lambda Ln\frac{p'}{p'_o} \tag{3.16}$$

where e is the void ratio with the current mean effective stress correspondingly, e_o is the initial void ratio with the initial mean effective stress, p'_o, correspondingly. The isotropic logarithmic compression index that identified the slope of the line is denoted by λ. The critical state line that CSL represents is determined the critical state by the same slope of the normal compression line on the e versus Lnp'. If the soil attains a condition that no more volume change and no more stress variation, the critical void ratio is determined at the end of the loading:

$$e_c = e_{co} - \lambda Ln \frac{p'}{p'_o} \tag{3.17}$$

where e_c is the critical void ratio, e_{co} is the initial void ratio corresponding to the critical state. In addition, the elastic component of the strain, e^e, is identified as part of the recovery strain due to unloading. The unload-reload line can be determined by a straight line on the e versus Lnp':

$$e^e = e_y - \kappa Ln \frac{p'}{p'_y} \tag{3.18}$$

where e_y is the void ratio with the yield stress, p'_y, correspondingly. The swelling index that identified the slope of the line is denoted by κ. As well as the critical state line on the deviator stress versus the mean confining stress plot can be written as:

$$q = Mp' \tag{3.19}$$

where M is the critical state parameter, and the mean confining stress equals $0.33(\sigma'_1+2\sigma'_3)$ for a triaxial test. Eventually, the yield function can be written in the following equation:

$$f = q^2 - M^2(p'(p'_y - p')) \tag{3.20}$$

where f is identified by the plastic potential or the yield function. When the yield function equals zero, the yield surface occurs. The yield surface is perpendicular to the direction of the plastic strain (Briaud, 2013).

3.3 Barcelona Basic Model

The Barcelona Basic model was proposed by Alonso, Gens and Josa (1990). It is related to the explanation of the behavior of the unsaturated soil. The Barcelona Basic Model (BBM) is based on the net normal stress denoted by p* equals σ-ua and

the net suction or water tension denoted by s equals u_w-u_a. Behavioral observations of the unsaturated soil are reversibleness of swelling, shrinking at low confining pressures, collapse mechanism at high pressures, and increase in yield stress that can be called preconsolidation pressure due to increasing net water tension. While the suction equals zero, the Barcelona Basic model has equality with the Modified Cam Clay model. As mentioned in the MCC model, a linear relationship in the void ratio, e, and the logarithm of net normal stress indicated by p* is identified by the normal compression loading curve in the BBM. In addition, representation graphs of the Barcelona Basic model are shown in Figure 3.8. There is another linear relationship between the natural logarithm of the suction and the void ratio denoted s or the net water tension, as shown in Figure 3.8 (b) (Briaud, 2013).

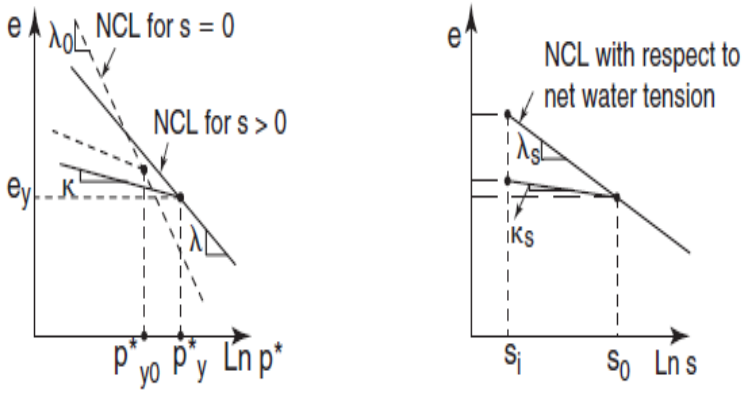

(a) (b)

Figure 3.8 Representation graphs of Barcelona Basic model (Briaud, 2013)

When the suction equals zero, shown in the NCL curve in the void ratio versus the natural logarithm of net normal stress plot in Figure 3.8 (a), the Barcelona Basic model can be represented by the same equation in the MCC model without the mean effective stress:

$$e = e_o - \lambda_o Ln \frac{p^*}{p^*_o} \tag{3.21}$$

where e is the void ratio with the net normal stress correspondingly, e_o is the initial void ratio with the initial net normal stress, p^*_o, correspondingly. The compression index for zero suction that identified the slope of the line is denoted by λ_o. If the suction does not equal zero, shown in the NCL curve, the equation becomes:

$$e = e_{so} - \lambda Ln \frac{p^*}{p^*_o} \quad (3.22)$$

where e_{so} is the initial void ratio corresponding to the initial net normal stress. A straight line can determine the unload-reload line:

$$e^e = e_y - \kappa Ln \frac{p^*}{p^*_y} \quad (3.23)$$

where e^e is the void ratio identified after elastic rebound swelling, and e_y is the void ratio with the yield stress, p^*_y, correspondingly. The swelling index that identified the slope of the line is denoted by κ. On the other hand, the void ratio versus the natural logarithm of the suction plot has the NCL curve. Hence, λ_s is the slope, κ_s is the compression index. λ_s and κ_s are determined concerning the water tension or suction, s, as shown in Figure 3.8b. The critical state line can be shown in the q-p' plot, as shown in Figure 3.9 (Briaud, 2013).

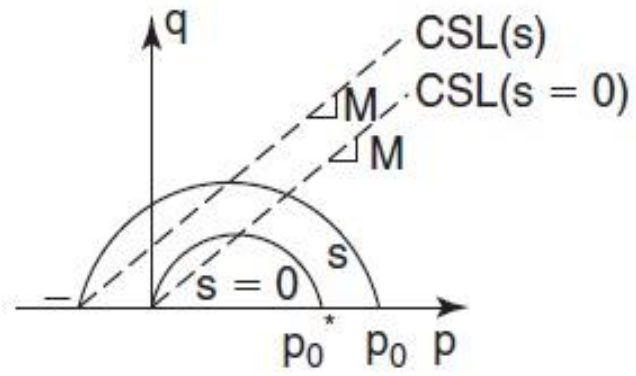

Figure 3.9 Representation of q-p' plot in Barcelona Basic model (Briaud, 2013)

The suction and the apparent cohesion have a linear relationship with each other:

$$c_{app} = ks \quad (3.24)$$

where c_{app} is the apparent cohesion and k is a constant of proportion. As well as the critical state line on the deviator stress versus the mean confining stress plot can be written as:

$$q = Mp^* + ks \quad (3.15)$$

where M is the critical state parameter, the CSL equation is modified by the contribution of suction with the apparent cohesion (Briaud, 2013).

CHAPTER 4

4. STABILIZATION TECHNIQUES OF CLAYEY SOILS

4.1 Cementitious Stabilization

Lime, portland cement, and fly ash can be used for cementitious stabilization and alterations of used materials in geotechnical constructions. On the other hand, portland cement and lime are manufacturable materials, and fly ash is a material that is the product of the burning of coal. Therefore, fly ash can be demonstrated by high variance when the other materials are compared. Processing of the stabilization techniques is required, such as site-specific, applicative standard test methods, analysis and design procedures, and originated acceptable results. These requirements with strict environmental constraints are critical conditions for project success. Retrenchment of the economy and resource sustainability of the cementitious material has visibly contributed to a construction project. Since it provides an extension of standard in situ soils (Ibanez, 2007).

The application of cementitious stabilizations is required for safety considerations. These applications can be led to float and impulsion of dust containing fly ash, lime, or cement over a short distance of the application area. In addition, heat or increasing temperature can occur during the chemical reaction between water, soil, and cementitious stabilization materials. Therefore, the following considerations should be taken into account due to the stabilization processes:

- A closed system that transports bulk products from pneumatic trailers to spreaders is used to prevent dust clouds. Also, the water trucks add the water to the mixer during the operate dust and improve the efficiency of the soil reaction. Therefore, these attempts can be led to the protection of undesirable drifts.

- When the soil stabilization materials begin to respond with water, the workers should protect their bodies from the unreacted materials.
- All workers need attention because of breathing the clouds of dust and touching distilled materials on the soil.
- Usage of the impervious coveralls can be necessary for the protection of liquids penetration.
- Using barrier creams and gloves can be necessary to protect arms, hands, and face (Transportation Research Board (TRB), 1987).

4.1.1 Soil Stabilization Using Lime

Workability and bearing characteristics of soil can be improved by using lime. Also, quicklime is generally used in dry wet soils to decrease time and provide a working surface. An example of used lime is modified and stabilized the soil beneath roads. Both quicklime and hydrated lime can be led to an increase in the impermeability, stability, and bearing capacity against the load on subgrades (Das, 2007).

Lime can be a brilliant option for the modification of soils. It can be used to modify nearly all fine-grained soils, but it has intense improvement in the high plasticity clay. Since calcium ions supplied by hydrated lime replaced the ions on the clay material. Using lime in clayey soils includes reducing plasticity, moisture, swell reduction in soil, stability improvement, and providing a workable area in the construction platform (Kumar, Walia and Bajaj, 2007).

If lime is contributed to the reactive soil to provide a long-term strength by pozzolanic reactions, in that case, the contributed lime is initiated the soil stabilization with the silicates and aluminates dissolved from the soil. This reaction case provides a mixed design protocol and confident construction practices (Little, 1995).

Lime is led to an increase in the soil resilient modulus. Also, when the lime is contributed to the soil, a considerable improvement in shear strength occurs. The advantages of using lime for stabilization can be described as; saving budget and time, reducing the environmental impact such as disturbance in construction areas, simple process, and less equipment necessity, and being a widely used technique (Qubain BS., 2000).

One of the advantages of lime stabilization is economic benefits, as mentioned. These benefits can be categorized into short-term and long-term. In the short term, the covering and existing subgrade soil with lime cause a reduction in cost rather than removing the subgrade material. Also, the lime-stabilized material provides an increase in strength. In the long term, the performance benefits of lime stabilization are gained to reduce maintenance costs (Ibanez, 2007).

In addition, the stabilization of lime has not a tricky process. First, the proper mix is designed thoroughly, and the tests are performed. Then, a reserved amount of lime is added to the soil and mixed to suited depth. The preliminary mixing can take over 24 to 28 hours of curing in the heavy clays. Also, the application of the correct compaction is essential. However, it is a requirement for providing maximum strength and durability of soil (Ibanez, 2007).

4.1.2 Soil Stabilization Using Portland Cement

Using cement in stabilization is an effective option on a wide range of soils, such as silts, clays, and granular materials. In addition, it can be a product of slag, fly ash, and waste materials such as powdered bituminous pavements and crushed concrete pieces. There is a classification in definitions and applications of cement-stabilized materials. These are soil-cement and cement-modified soil.

A mixture of powdered soil materials, aggregates, water, and a measured amount of portland cement is called soil-cement and compacted at a high density. Hardened material with an added amount of cement is essential to strength and durability on the primary structural base layer and flexible or rigid pavements (Bell, 2000).

Mix design can change depending on the aim. For example, when cement-stabilized materials are compared with each other, the soil-cement usually has more formidable necessities than the cement-modified soils. Hence, the durability and strength tests are typically used in the soil-cement bases. Freeze-thaw (ASTM D560) and the basis of maximum weight losses under wet-dry (ASTM D559) tests have been developed by the Portland Cement Association to originate necessities of AASHTO soils A-1 to A-7. It is led to find the durability of soil. In addition, many transportation departments demand minimum unconfined compressive strength testing (ASTM D1633). These strength tests have been applied more quickly and have fewer laboratory equipment requirements than durability tests (Kowalski and Starry, 2007).

The soil-cement materials are cement-treated aggregate base and recycled flexible pavements. A relatively small portion of portland cement has handled the aggregate materials. In contrast, more cement is required to develop hardened soil-cement. Cement-modified soils are generally used to evolve subgrade soils and treat local aggregates for using more costly transported aggregates (Bell, 2000).

Objectives and definitions that depend on cement requirements are selected by engineers for cement-modified soils. These are decreasing the plasticity index defined by Atterberg limits (ASTM D4318), increasing the shrinkage limit, decreasing the volume change of the soil, reducing the clay/silt-sized particles determined by hydrometer analysis, assembling strength values or indexes defined by California Bearing Ratio (ASTM D1883) or triaxial tests (ASTM D2850), and evolving the resilient modulus (Kowalski and Starry, 2007).

The composition of the calcium-silicates and calcium-aluminates is formed by the portland cement. When these are added to water, the hydrate form of calcium-silicate-hydrate, calcium-aluminate-hydrate, and calcium hydroxide, defined as lime, occurs. Portland cement can be a successful option for stabilizing both granular and fine-grained soils. Calcium hydroxide, soil alümina, and soil silica occur because of a pozzolanic reaction in the fine-grained clayey soils. The cement stabilized soils exhibits to decrease in permeability. These materials have become moisture-resistant materials that are more durable and resist over the long term by stabilization (Rawas and Goosen, 2006).

Application of soil-cement and cement-modified soil is a rapid process. There are several ways to contribute cement into the soil/aggregate. The most common way is disseminating dry cement into prepared soil/aggregate. Then, it is blended by a transverse single shaft mixer at an appropriate depth. Reducing the dusting and improvement of mixing with heavy clays are produced by cement slurries. It occurs with a combination of water and cement in a 50/50 blend (Halstead, 2011).

4.1.3 Soil Stabilization Using Fly Ash

Using coal fly ash in stabilization can be an effective option on the pavements. Stabilization of fly ash is preferred to qualify the engineering properties of available materials. Non-self-cementing and self-cementing coal ashes are utilized in the application of stabilization (Senol, Edil, Bin-Shafique, Acosta and Benson, 2006).

Fly ash is a residue that occurs with the burning of coal. It is generally produced from power plants. There are two types of ash: coal ash and bottom ash, which are removed from the undersurface of coal furnaces. According to the source and composition of burned coal, the constituent of fly ash can be varied substantially. Fly ash admits a considerable amount of silicon dioxide (SiO_2) and calcium oxide (CaO). Toxic institutes are arsenic, boron, beryllium, cadmium, thallium, chromium, cobalt, lead, mangasene, molybdenum, selenium, mercury, strontium, and vanadium with the dioxins chemical compounds. On the other hand, fly ash usage in concrete improves workability, decreases segregation, bleeding, permeability, increases sulfate resistance, and has significant ecological and economic benefits (Helmuth, 1987).

There are two majority classes of fly ash specified by ASTM C 618. These are indicated as: Class F developed from burning anthracite or bituminous coal, and Class C obtained from burning subbituminous coal and lignite. It is based on the chemical composition of the type of coal burned. Class C fly ash includes cementitious properties as well as pozzolanic properties due to free lime. Class F fly ash rarely contains cementitious properties if it is mixed alone with water (Adams, 1988). Class C fly ash and class F fly ash are shown in Figure 4.1 and Figure 4.2, respectively.

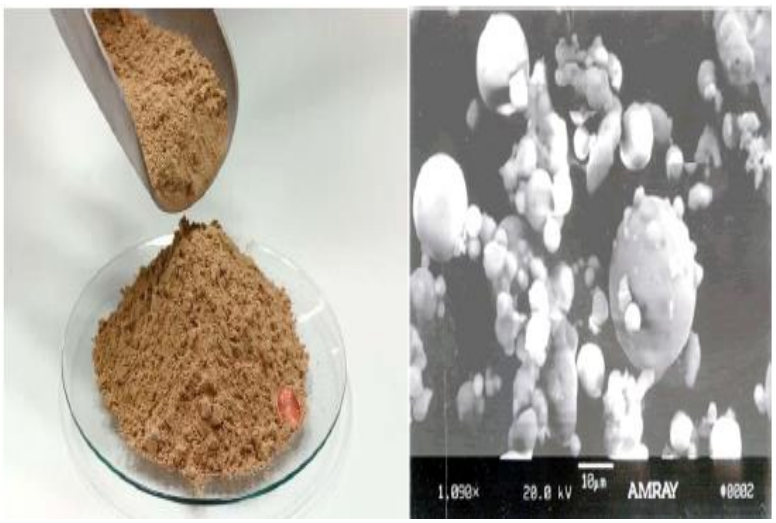

Figure 4.1 Class C fly ash (Etminan, 2012)

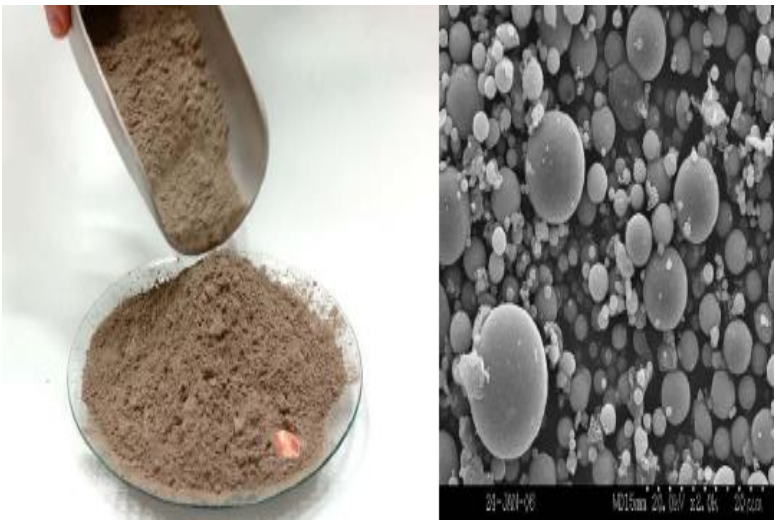

Figure 4.2 Class F fly ash (Etminan, 2012)

Using the other fuels in the plant can lead to contamination, and when the plant achieves an entirely efficient operation, it is caused to the inconsistency of carbon content. Therefore, the fly ash productions of start-up and shut-down have to be distinguished. In addition, there are differences in commonly used specifications such as ASTM C 618 and AASHTO M 295. The most crucial difference is some state transportation agencies. Otherwise, these specifications are fundamentally equivalenced. Although the specification in ASTM C 618 includes the classes of coal such as Class F fly ash and Class C fly ash. Identification of the specific type of coal is not specified for given fly ash classes (Halstead, 2011).

The world faces significant problems such as the exiguity of conventional construction materials, environmental issues, and ecological issues. However, the employment of fly ash in construction sites has reduced these problems and provided cost efficiency. For example, re-used fly ash in highway constructions can be provided significant cost savings (Ghosh and Dey, 2009).

Fly ash is suitable for many potential applications of geotechnical engineering because of having self-hardening characteristics. In addition, using fly ash in construction areas has been investigated by previous researchers because of its effects on strength and deformation. There are other fields of application to using fly ash, such as replacements of cement in concrete, land reclamation, injection grouting, and liner material (Ghosh and Subbarao, 2012).

4.2 Shredded Waste Tires Stabilization

Several industrial and public ventures have been established to have cognition and practices about using waste materials instead of raw materials in construction materials. On the other hand, methodologies to fitting the appraisal have been developed by scientific and standardization communities. However, the waste tire stockpiles can be led to health and environmental hazards due to rising air pollution. Although this approach exists, recent environmental legislating recommends that recycling and using of disposed of tires are increasing. Therefore, the resource by recycling waste tire stockpiles is the most suitable approach. These materials are generally very elastic and porous, have well vibration and damping attributes, and are easily compacted (Erol, 2008).

There are many advantages of shredded tires as lightweight filling material. Shredded tires exhibit non-biodegradable at below or above the water and low density, so this supplies a stable road base for a more extended time than the other lightweight filling materials. In addition, they have easy transportation and replacement on the construction site. Also, the shredded tires exhibit well porosity characteristics. Therefore, the proper drainage of the highway base is assisted by the shredded tires stabilization. Furthermore, it can be provided significant cost savings. Using shredded tires as a filling material instead of sand or gravel helps save costs. Finally, the shredded tires offer to complete work faster and inexpensively cost (Bosscher, Edil and Kuraoka, 1997).

Although shredded tires seem an effective option for the lightweight filling material, they have several disadvantages. First, using these materials for lightweight filling is recent concept, and there is no more information about their usage. Thus, there are limited design standards. Another is the preparation requirements before using the shredded tires to avoid soil and groundwater transmission. Finally, consideration of the general public is using the shredded tires, which is another way of burying them (Bosscher et al., 1997).

The shredded tire has several improvement effects as a lightweight filling. For example, the compacted shredded tire has more porous than washed gravel. Also, the usage of shredded tires provides drainage below the pavements, which leads to extending the life of a roadway. On the other hand, shredded tires are elastic material, allowing a better distribution of loads on the roadway. In contrast, the same features

can be led to higher deflections. Moreover, these are easily compacted and consolidated. Even though there is no design standard for shredded tires, the size of the tires is identified (Etminan, 2012).

4.3 Soil Reinforcement Using Fibers

In general, the types of soil have low shear and tensile strength, and the characteristics of soils are linked to environmental conditions. Also, these certain materials can be had lack reinforcements. Hence, soil reinforcement may be a requirement to advance the engineering properties such as shear strength, compressibility, hydraulic conductivity, and density. The fundamental aims of reinforced soil are improving stability, increasing bearing capacity, reducing lateral deformations, and decreasing settlements. The standard fiber-reinforced soil is identified as a mass of soil that comprises random distribution. Fibers are used to improve the mechanical behavior of soil composite, and fiber-reinforced soil exhibits relatively high tensile strength. On the other hand, the shear stresses of the soil are transported by tensile resistance in the fibers. Therefore, soil reinforcement using fibers leads to providing an artificial replication of vegetation effects. It was proved by laboratory and in-situ test results (Hejazi, Sheikhzadeh, Abtahi and Zadhoush, 2012).

Short fiber soil composite can be classified into two sides: the randomly implication of fibers into the soils and orienting fibrous materials such as geosynthetics. The soil reinforcements are classified into two categories by McGown (1978). These are ideally inextensible and ideally extensible inclusions. The category of ideally inextensible has high modulus metal strips, which strengthen the soil, whereas the ideally extensible inclusion has a relatively low modulus (Savastano, Warden and Coutts, 2000).

4.3.1 Natural Fibers

4.3.1.1 Coconut Fibers

The outer cover of an aged coconut is a fibrous material, and it is called coconut husk. These fibers have generally 50-350 mm long, and it is comprised of lignin, tannin, pectin, cellulose, and other water soluble contents. Hence, the coir degradation

occurs much more slowly than the other natural fibers due to the substance of lignin. Therefore, these fibers are more permanent, having a 4-10 years service life. In addition, if the coir is wet, it provides much more tensile strength. Although it has low viscidity, its elongation is much higher. The medium embedment and the climatic conditions can be let to the degradation of coirs. When it is replaced in the clay, the tensile strength of soil is retained percentage of 80% after 6 months. The reinforcement purposes of coir geotextiles are utilized economically. The coir fibers have a better resilient reaction against synthetic fibers because of the friction coefficient. For example, the coir fibers have a greater resilient modulus or strength in the soil than the synthetic fibers. The influence of random distribution in coir fibers is led to reducing the swelling tendency of soil. The coir-stabilized soils exhibit decreasing the maximum dry density due to the increasing amount of the coir and increasing the optimum moisture content value due to the expanding amount of the coir. In addition, the percentage of water absorption and tensile strength of coir-reinforced soil increases due to the increasing amount of the coir fibers (Babu et al., 2008).

4.3.1.2 Sisal Fibers

Sisal is identified as a lingo-cellulose fiber, and it is used to reinforcement for gypsum plaster sheets in building traditionally. The leaves of plants produce sisal fibers whose size varies between 6-10 cm in width and 50-250 cm in length. Generally, the leading producers of sisal fibers are Brazil, East African countries, and Indonesia. The containment of 4% sisal contributes to considerable ductility, and it is led to a slightly increased in the compressive strength reported by Ghavami et al. (1999). In addition, the sisal fibers decrease the dry density of the soil. On the other hand, increasing the fiber distance and increasing the amount of sisal fibers content cause the reduction of the soil's dry density. Furthermore, the shear stress increases due to the non-linear with an increase in the length of sisal fibers. Lastly, the inclusion of fiber content improves the shear strength (Etminan, 2012).

4.3.1.3 Palm Fibers

The production of palm fibers is based on filament textures. Its remarkable features have more economical, abundance in the region, durability, lightweight, tension capacity, and proportional strength against degradation. Decomposed palm

trees produce palm fibers that exhibit low tensile strength, brittle, low modulus of elasticity, and high water absorption. The palm fiber-reinforced soft soil significantly improves the failure deviator stress and the shear strength. Namely, the palm fibers cause to interlock between the soil particles, so the strength properties of soil are enhanced (Ahmad, Saman and Tahir, 2010).

4.3.1.4 Bamboo Fibers

Bamboo fibers are identified as cellulose fibers. It pullulates naturally without applying any pesticide. The scientists reported that bamboo has a unique anti-bacteria named Bamboo Kun. This bacteria is significant to root rhizomes that cause excellent ligature. As well as it prevents erosion in the soil mass. Although the bamboo fibers have strong tension, they have a low modulus of elasticity (Khedari, Watsanasathaporn and Hirunlabh, 2005).

4.3.1.5 Flax Fibers

Flax is known as the oldest textile fiber. Fibers of a blue flowered plant produce flax fibers. It seems as slender, and its seeds are in many places. The addition of flax fibers in the soil-cement composite is caused to improve the ductility. The fiber surface improves the interfacial bond strength between the soil. In addition, a flax machine is expended on altering the fast and mobile process of flax leaves (Segetin, Jayaraman and Xu, 2007).

4.3.2 Synthetic Fibers

4.3.2.1 Polyethylene Fibers

The feasibility of polyethylene-reinforced soil and PE strips has limited enlargement. It reported that the existence of a small fraction of polyethylene with high density causes fracture energy in the soil. It is generally mixed or blended into the type of sand or clay soil, and PP fibers are used as soil reinforcement. The tensile strength of soil increases due to the inclusion amount of PE fibers. In addition, the significant increase in toughness because of increasing strain capacity occurs due to the inclusion amount of PE fibers. The expected performance benefits of soil stress-strain behavior are due to the increasing toughness exhibited. Therefore, the polyethylene fibers

improve the tension. Inclusion in the amount of the PE fibers in local sand causes to increase in secant modulus (Khedari, Watsanasathaporn and Hirunlabh, 2005).

4.3.2.2 Nylon Fibers

The strength behavior of nylon fiber reinforced silty clay in different degrees of compaction is studied by Kumar and Tabor (2006). The study reported that the residual and peak strength of the soil for 90% compaction is more than the soil samples compacted at the higher densities. On the other hand, nylon fibers have a low cost because of carpet waste, so the usage of fiber-reinforced soil becomes much more expensive than nylon fiber (Segetin et al., 2007).

4.3.2.3 Steel Fibers

Steel fiber reinforcements are generally used in concrete and soil-cement composites. The steel fibers can be led to an improvement in the soil strength. However, it can not compare with using other types of fibers. Polyethylene fibers are preferable instead of steel fibers in cold climates due to the effects of freeze-thaw cycles. Because polyethylene fibers have a smaller unit weight than the steel fibers (Segetin et al., 2007).

4.3.2.4 Polyvinyl Alcohol Fibers

Polyvinyl alcohol fibers are identified as synthetic fibers used in fiber-reinforced concrete. It causes improved tensile strength, weather resistance, and chemical resistance, especially alkaline resistance. Polyvinyl alcohol fibers (PVA) have considerably lower shrinkage and high alkali characteristics. Therefore, using the PVA fibers as a soil reinforcement material is a suitable option. It can be an effective reinforcement to improve strength and ductility (Segetin et al., 2007).

CHAPTER 5

5. LABORATORY TESTS, MATERIALS, AND MODELING PROCEDURE ENGINEERING PROPERTIES OF MATERIALS

During this chapter, the used laboratory tests that specify the engineering properties of used engineering materials were described in detail. In addition, this chapter also discusses the engineering properties of studied clays and the physical and chemical properties of used alternative materials are discussed thoroughly in this chapter. Moreover, a suggested modified numerical model to obtain soil moduli is explained.

5.1 Laboratory Tests

Laboratory tests and in situ tests are crucial options to obtain the engineering properties of materials. The soil properties are a requirement for geotechnical engineering projects. In addition, these tests can contribute to the theoretical analysis. Some advantages of tests include that the boundary of drainage and loading conditions may be operated (Briaud, 2013). In other words, the experimental techniques provide to qualify the mechanical behavior of engineering materials. Furthermore, the testing procedures and devices, size and preparation process in the soil can be conformed to the project conditions (Hicher and Shao, 2008).

The geotechnical test results are used to determine the soil moduli by the proposed modified model. It should be noted that the experimental results used during this study were obtained with official permission. The tests were performed by Etminan (2012) in Istanbul Technical University's Prof. Dr. Hamdi Peynircioğlu laboratory of geotechnical engineering. The amount of improvement in the stabilized

clay by stabilizing engineering materials is evaluated by the results of the unconfined compression test. Also, a comparison of improvement in mentioned clay is related to the saturation of the soil samples. The optimum water contents of samples are obtained by the Harvard miniature compaction test. After seven days of curing, the unconfined test was conducted on at least five samples with different amount of water contents. The unconfined compression strength of other material and fly ash increases due to the increasing curing time resulting in cementitious stabilization. On the other hand, all the fibers used in clayey soil during the test contribute to the high tensile strength. Therefore, the length of the fibers directly affects the unconfined compression test results (Etminan, 2012).

5.1.1 Sieve and Hydrometer Analysis of Plain Soils

The sieve and hydrometer analysis provide to determine the size range of soil particles. In general, there are two methods to identify the particle-size distribution of soil, such as the sieve analysis and hydrometer analysis. The basic concept of the sieve and hydrometer analysis is discovered shortly in the followings.

The agitating the soil sample through several sets of sieves can describe the principles of *sieve analysis*. The sieves typically consist of 203 mm (8 in.) in diameter. Firstly, the soil becomes dry form from an oven. Next, the small lumps in the soil are broken. The set of sieves that are staked with decreasing openings size from top to bottom shakes. The smallest-sized sieve typically used for the U.S. No. 200 sieve. The soil mass held on each sieve of the set is specified after the soil is shaken. The set of sieves in a shaker in the laboratory is shown in Figure 5.1.

Figure 5.1 A set of sieves in the laboratory (Das, 2010)

If the analysis of cohesive soils is conducted, the process of breaking lumps in soil particles can not be easy. Therefore, these types of soils should be mixed with the water, and cohesive soil slurry is washed through the set of sieves. In order to determine the percentage of finer in soil, the followings should be applied:

1. Obtain the soil mass held on each sieve, for example, M_1, M_2,… M_n
2. Find the total mass of the soil:

$$M_1 + M_2 + \cdots + M_i + \cdots + M_n + M_p = \Sigma M \quad (5.1)$$

3. Obtain the cumulative soil mass held above each sieve. For example, M_1+M_2+… +M_i is for the *i*th sieve
4. The soil mass passed the *i*th sieve is:

$$\Sigma M - (M_1 + M_2 + \cdots + Mi) \quad (5.2)$$

5. The percentage of soil or percent finer passed the *i*th sieve is

$$F = \frac{\Sigma M - (M_1+M_2+\cdots+M_i)}{\Sigma M} \times 100 \quad (5.3)$$

where F is called percent finer.

The calculations of percent finer are platted on the semilogarithmic paper. Then, the percent finer is located on the ordinate, and the sieve opening size is situated on the abscissa, as shown in Figure 5.2. This plot refers to the particle-size distribution of the soil (Das, 2010).

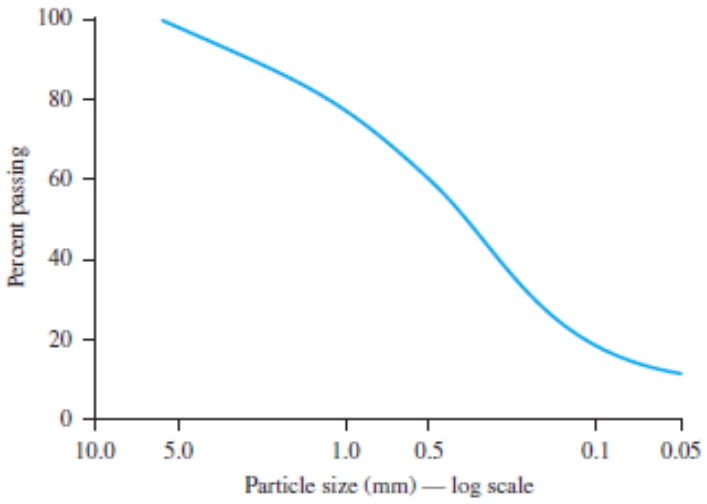

Figure 5.2 An example of the particle-size distribution curve (Das, 2010)

In principle, the sedimentation of soil grains with water can identify the *hydrometer analysis*. The soil specimen disseminates in water. The shape, size, viscosity of water, and weight affect the settlement of the soil particles with different

velocities. A sedimentation cylinder with 50 g or 100 g oven-dried samples is used in the hydrometer test. The sedimentation cylinder has 63.5 mm in diameter and 457 mm high. The volume of the disseminated soil is increased to 1000 ml due to adding distilled water. The time of soil suspension is measured from the beginning of sedimentation. The specific gravity of soil at a depth is measured by a hydrometer located on the soil suspension. Also, the specific gravity of soil can be determined as a function of the amount of soil particles per unit volume. The used hydrometers obtain the amount of soil in grams. In addition, it is assumed that all soil particles are given as spheres. Stoke's law refers to obtaining the velocity of soil particles, as written in Eq. (5.4):

$$v = \frac{\rho_s - \rho_w}{18\eta} D^2 \tag{5.4}$$

where v is the velocity of soil particles, ρ_s is the density of soil, ρ_w is the density of water, η is the viscosity of water, and D is the diameter of the soil particles. Also, in many cases, sieve and hydrometer analysis results are given in one graph for finer soil fractions, as shown in Figure 5.3.

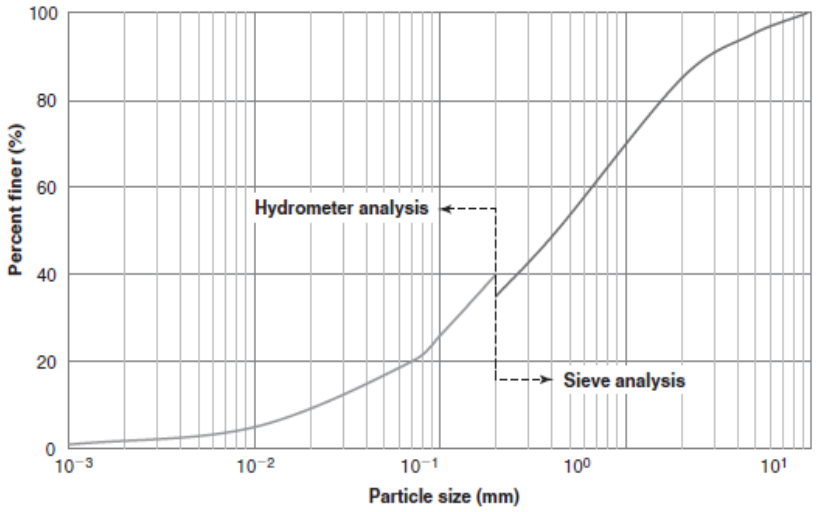

Figure 5.3 Particle-size distribution curve of sieve and hydrometer analysis on one graph (Briaud, 2013)

The hydrometer analysis provides the diameter of the equivalent sphere, and the sieve analysis provides the intermediate dimensions of the particle (Das, 2010).

5.1.2 Casagrande Test of Plain Soils

A method that discovers the limited consistency of fine-grained soils is based on moisture content. This method was developed by Atterberg. Hence, these limits include the liquid limit, the plastic limit, and the shrinkage limit. The liquid limit refers to the moisture content in percent due to the expressing the soil from a liquid state through a plastic state, as shown in Figure 5.4.

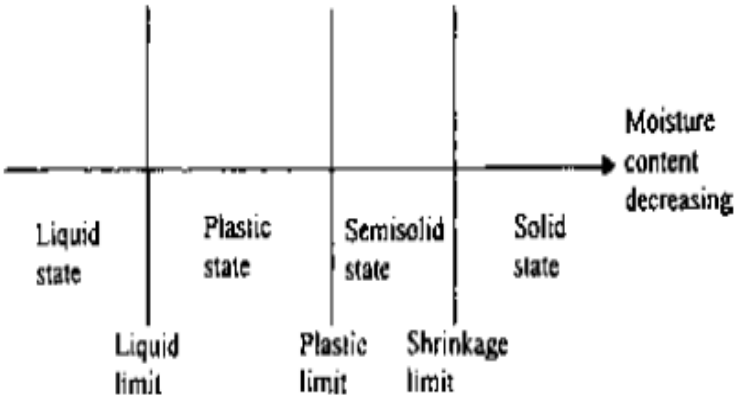

Figure 5.4 Consistency limits of cohesive soils (Das, 2008)

The Standard Casagrande device is generally used to define the liquid limit of soil. This device has a hard rubber base and a brass cup. The soil paste is located in the brass cup, and this cup is dropped into the base. Next, the center of soil is cut by a Groove with the standard grooving tool. The brass cup is lifted and dropped from a height of 10 mm during 25 blows. Then, to obtain the moisture content of the soil in percent, it is expected to close a distance of 12.7 mm along the bottom of the groove. The Standard Casagrande device is shown in Figure 5.5.

Figure 5.5 Liquid limit device (Briaud, 2013)

In addition, at least three times in the same soil paste is carried out at altering moisture contents with a varying number of blows between 10 and 35. The moisture content of the soil and the number of blows is plotted on a semilogarithmic graph (Das, 2008).

The plastic limit refers to the moisture content of the soil in percent due to rolling into threads of 3.2 mm in diameter. Therefore, the plastic limit is a lower limit in the plastic stage of the soil. The plastic limit test of soil is given in ASTM Test Designation D-4318, and it is performed by Rolling an ellipsoidal size soil mass. The test is repeated three to four times, and the altering moisture content is obtained. When the cone penetration equals 20 mm, it is the plastic limit of soil. On the other hand, the plasticity index of the soil is found by the differences between the liquid and the plastic limits, as written in Eq. (5.5):

$$PI = LL - PL \tag{5.5}$$

where PI is called the plasticity index, LL is the liquid limit, and Pl is the plastic limit of soil (Das, 2008).

5.1.3 Unconfined Compression Test

The unconfined compression test is a particular type of the unconsolidated undrained triaxial test, and the unconfined compression test is carried out to determine the undrained shear strength of the clay due to the unconfined condition. In other words, the unconfined compression strength, q_u, is identified by using the unconfined compression test. The unconfined compressive strength is determined as the compressive stress at failed unconfined cylindrical soil specimen in a compression test by ASTM standard. The unconfined compression strength includes the maximum load reached per unit area or the load per unit area under 15% axial strain. On the other hand, the undrained shear strength, s_u, is required to identify the bearing capacity of dams, foundations, etc. (ASTM D2166). In addition, there are application standards for the unconfined compression test. The measurements of diameter and length of soil specimen are done at three locations 120 degrees apart. The average of measured dimensions is recorded on the datasheet. The aspect ratio (L/d) of soil specimen should vary approximately between 2 and 2.5. L is the length of the soil specimen, and d is called the diameter of the sample. The soil specimen is located on the compression device, and the upper plate should contact the soil sample by setting zero loads and

deformation dial. When the load is applied to the specimen, an axial strain is produced at a rate of 0.5% to 2.0% per minute. Then, the load and deformation are read and recorded on datasheet at every 20 to 50 divisions of the deformation dial (Das, 1997). The unconfined compression test was used for the soil removed from the Harvard miniature compaction test. The unconfined compression test device is shown in Figure 5.6.

Figure 5.6 Unconfined compression test device (Etminan, 2012)

As mentioned, there is no confinement on the soil specimen, so the minor principal stress equals zero. In addition, a vertical load is conducted to the soil sample by pushing up the bottom platen at a constant displacement rate where the top platen is fixed. Therefore, this test can be determined as strain-controlled. Also, dividing the vertical load by the cross-sectional area of the sample determines the vertical total stress. Since the assumption described, there is no shear stress between the top and bottom of platen, and soil specimen. Therefore, this stress is named the major principal stress in the unconfined compression test (Briaud, 2013).

The unconfined compression test results are used to appraise the short-term bearing capacity in fine-grained soils for foundations, the short-term slope stability, and the stress-strain characteristics under undrained loading conditions. The advantages of this test are an estimation of soil strength quickly and cheaper performance that provides cost-effective application (Budhu, 2011).

One of the unconfined compression test results is a stress-strain curve that generally behaves nonlinearly. Therefore, some of the soil moduli can be determined due to the chosen certain stress levels by the stress-strain curve. Another advantage of the unconfined compression test is determining the undrained shear strength and

modulus of deformation on one test in fine-grained soils. The deformation modulus can be written in terms of unconfined compression strength. Drapper and Smith (1998) studied this equation form by using the study of scatter plots (Ghosh and Dey, 2009).

Generally, there are two types of failure in a soil sample carried out an unconfined compression test. The failure by shear and bulging can be obtained at the end of the unconfined compression test. The soil affected in failure by shear has lower plastic behavior than affected in the failure by bulging (Das, 2010). The failure by shear and bulging are shown in Figure 5.7.

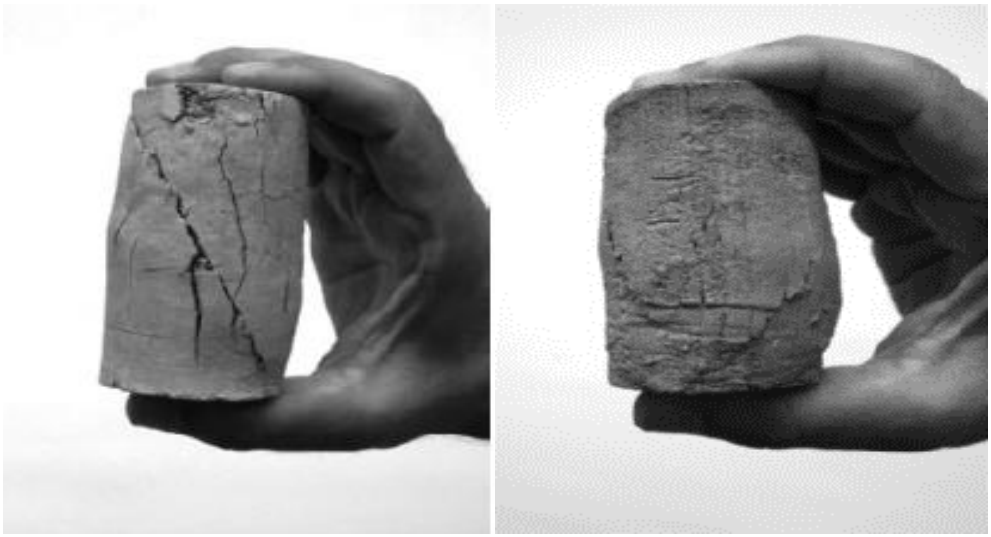

a) b)

Figure 5.7 a)Failure by shear and b)failure by bulging of unconfined compression test specimens (Das, 2010)

5.1.3.1 Saturated Soils

The intention of an unconfined compression test is to obtain the shear strength of saturated clays. The load is applied to the soil specimen rapidly. Therefore, there is no time to porewater drain from the soil, and there is no volume change in the soil. The total stress path can be considered as shown in Figure 5.8. In contrast, the effective stress path can not be determined from the unconfined compression test because the change of porewater pressure can not be evaluated.

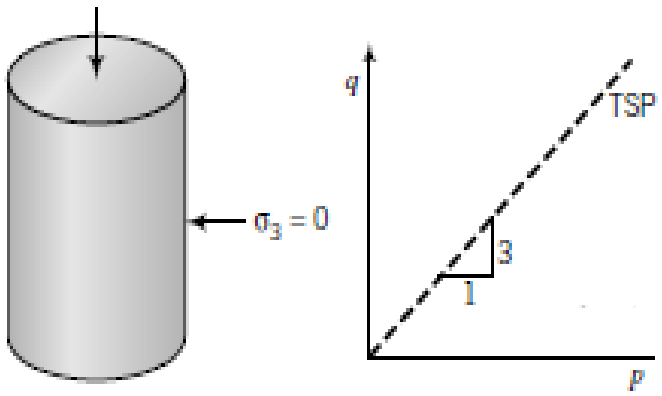

Figure 5.8 Total stress path in an unconfined compression test (Budhu, 2011)

The ratio of change in deviatoric stress and mean principal total stress for the unconfined compression test can be written as:

$$\Delta p = \frac{\Delta\sigma_1}{3} \; and \; \frac{\Delta q}{\Delta p} = 3 \tag{5.6}$$

where p is the total principal stress, and q is the deviatoric stress. TSP means the total stress path in Figure 5.8. Theoretically, the principle of effective stress can be written as:

$$\sigma'_3 = \sigma_3 - \Delta u = 0 - \Delta u = -\Delta u \tag{5.7}$$

where Δu is the change in porewater pressure. Therefore, the porewater pressure should be a negative value at the beginning of the test for saturated clays because of the capillary pressure. Mohr's circle of effective stress should be right side compared with the total stress. Also, area due to constant volume of soil can be written as:

$$A = \frac{A_o(1-\varepsilon_p)}{1-\varepsilon_1} \; and \; A = \frac{A_o}{1-\varepsilon_1} \tag{5.8}$$

where A_o is the bottom or top surface area of the soil sample. There is no volumetric strain due to the constant volume change (Budhu, 2011).

Since the minor principal stress equals to zero, the undrained shear strength in the saturated soil that is independent with the confining pressure:

$$\tau_f = \frac{\sigma_1}{2} = \frac{q_u}{2} = c_u \tag{5.9}$$

where c_u or s_u is the undrained shear strength of the soil. Also, Mohr's circle of the total stress in the unconfined compression test is shown in Figure 5.9.

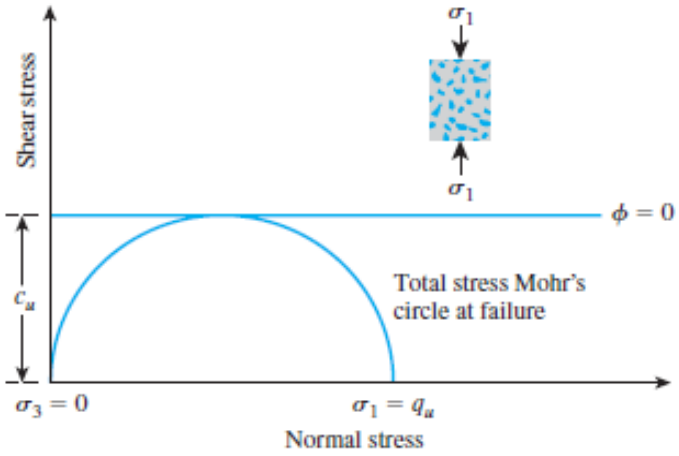

Figure 5.9 Mohr's circle in the unconfined compression test (Das, 2010)

The saturated clay sample should theoretically yield the same undrained shear strength value in the unconfined compression test and the unconsolidated-undrained triaxial test. However, the saturated clay practically yields a bit lower value in the unconfined compression test. However, the unconfined compression test results are accurate (Das, 2010).

5.1.3.2 Unsaturated Soils

The porewater pressure can not be measured in the unconfined compression test. Therefore, there is no change in the test procedure of unsaturated soils for the unconfined compression test. Also, the measurements and data reduction of this test do not need to change. However, the observational affair is an estimation of water tension by using the unconfined compression strength, q_u. The relationship between water tension and unconfined compression strength is shown in Figure 5.10.

The expressions of this relation are given in the followings. If the air stress is accepted to zero, the shear strength of unsaturated soils is written in Eq. (5.9). The horizontal total stress that is zero and vertical total stress at failure are given in Eqs. (5.10) and (5.11), respectively:

$$s = c' + (\sigma - \alpha u_w) \tan \varphi' \tag{5.9}$$

$$\sigma_h = 0 = \sigma'_h + \alpha u_w \ \ and \ \ \sigma'_h = -\alpha u_w \tag{5.10}$$

$$\sigma_v = q_u = \sigma'_v + \alpha u_w \;\; and \;\; \sigma'_v = q_u - \alpha u_w \tag{5.11}$$

where s is the shear strength of soil.

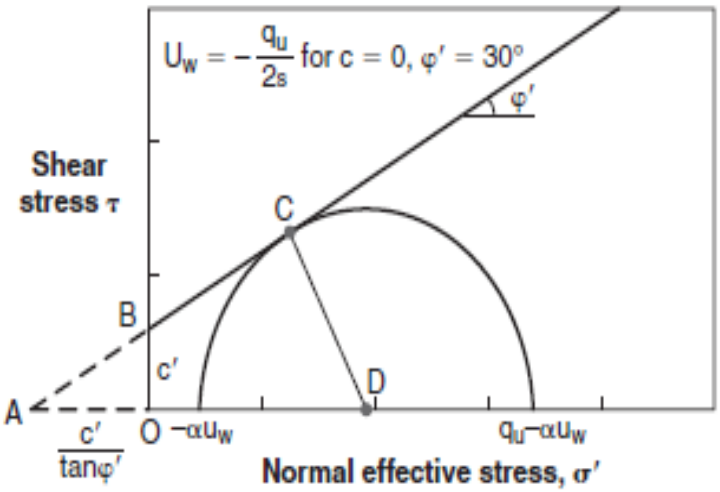

Figure 5.10 Relationship of water tension and unconfined compression strength in the unconfined compression test (Briaud, 2013)

The shear stress is identified as a point of tendency in Figure 5.10. Also, according to the ACD triangle:

$$\frac{CD}{AD} = \sin\varphi' = \frac{0.5((q_u - \alpha u_w) - (-\alpha u_w))}{0.5((q_u - \alpha u_w) + (-\alpha u_w)) + \frac{c'}{\tan\varphi'}} \tag{5.12}$$

where Eq. (5.12) is simplified and reorganized:

$$u_w = \frac{0.5 q_u (\sin\varphi' - 1) + c' \cos\varphi'}{\alpha \sin\varphi'} \tag{5.13}$$

where u_w the water tension at failure (Briaud, 2013).

5.2 Materials Used in Laboratory Tests

Cohesive soils may be led to excessive settlement on the foundation of structures. It is a crucial problem in the stability of structure and shear strength of the soil. Although the soil can resist the shear failure, the settlements can exceed the allowable limits. Therefore, total compressibility values of the cohesive soils should be maintained low to provide safety of structures. In addition, sample disturbance,

water content, dry density, strain rate, stress path, and amount and type of clayey soils are essential factors to affect the compressibility of clayey soils (Moghal et al., 2014).

Materials used in laboratory tests can be emphasized as fly ash, polypropylene, and copolymer. These materials are used with clayey soil to stabilize it. Therefore, several combinations of clayey soil with fly ash, polypropylene, and copolymer mixtures were prepared to apply mentioned the laboratory tests. In addition, the engineering properties of these mixtures were obtained. Then, evaluation of soil moduli was expressed by using test results, after obtained test results, and engineering properties of soils.

5.2.1 High Plasticity Clay Soil

A clayey soil was received from the Akpınar district of Istanbul, Turkey. The grain size distribution must be known to classify the received soil. The sieve analysis provides the determination of gradation in generally coarse-grained soils. It was applied to obtain conformity with verification specifications of the soil. In addition, to using the sieve analysis, the plain soil becomes oven-dry by $110 \pm 5^{\circ}$ for 24 hours. The contents of each sieve set were separated and weighed, as mentioned in part of the sieve analysis and hydrometer analysis of plain soils. The classification of the clayey soil is illustrated in Table 5.1.

Table 5.1 Classification of high plasticity clay soil (Etminan, 2012)

	Gravel	Sand	Silt	Clay
%	0	3	27	70

The hydrometer analysis provides the determination of grain size distribution smaller than the #200 sieve in fine-grained soils. This test includes the Stokes equation related to the velocity of a free-falling sphere in suspension, as mentioned in part of the sieve analysis and hydrometer analysis of plain soils. In the hydrometer test, 50 g of plain soil with added dispersion agent 100-150 ml passed through the #200 sieve. Also, sodium-hexametaphosphate $(NaPO_3)_6$ provided deflocculates to the plain soil. As a result, the grain-size distribution curve of plain soil was obtained by using both

sieve and hydrometer analysis, as shown in Figure 5.11. According to the grain-size distribution graph, the plain soil comprises 3% sand, 27% silt, and 70% clay.

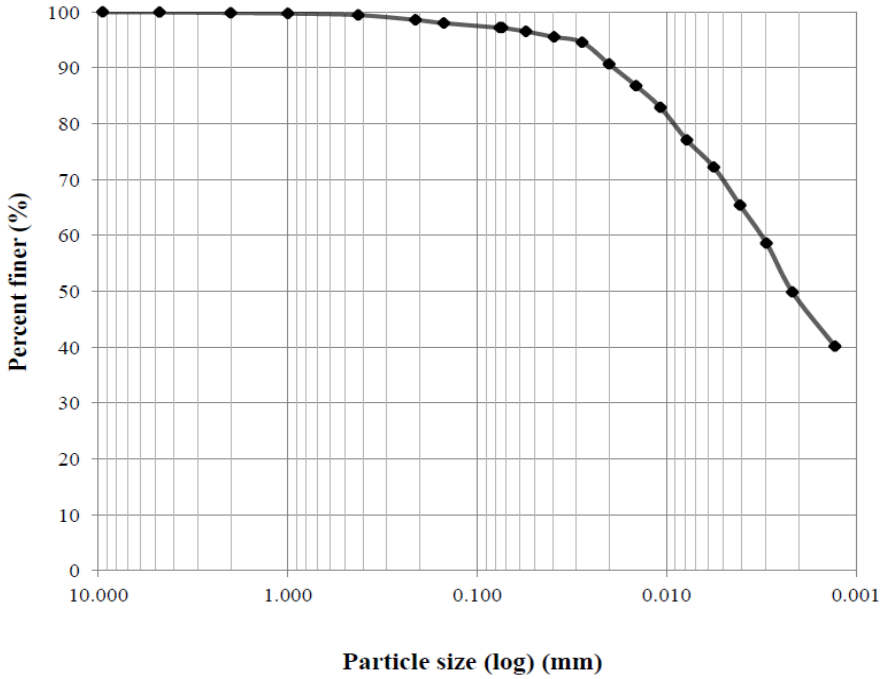

Figure 5.11 Grain-size distribution curve of high plasticity clay (Etminan, 2012)

The Atterberg limits must be defined for the plain soil of fine-grained. The Casagrande test determines the liquid limit of soil, and the procedures are discussed in the part of the Casagrande test of plain soils. Also, the determination of the plastic limit and the plasticity index is mentioned in the part of Casagrande test of plain soils. The Atterberg limits of plain soil are shown in Table 5.2.

Table 5.2 Atterberg limits of high plasticity clay soil (Etminan, 2012)

Liquid Limit	Plastic Limit	Plasticity Index
LL(%)	PL(%)	PI(%)
78	28	50

The liquid limit amount for plain soil is 78%. The plastic limit of plain soil is obtained 28%. Therefore, the plasticity index is %50. According to all obtained data from these experiments, the plain soil can be classified as CH (high plasticity clay) with respect to the Unified Soil Classification System (USCS).

5.2.2 Fly Ash

Fly ash is used for cementitious stabilization and alterations of clayey soils in geotechnical constructions. There are several advantages to the strength and deformation of clayey soil. The class C fly ash was used to apply the laboratory tests. As mentioned in section 4.1.3, Class C is obtained from burning subbituminous coal and lignite. Class C fly ash includes cementitious and pozzolanic properties due to free lime. The fly ash is the first alternative material for clayey soils, and it was obtained from the Çayırhan power station in Ankara, Turkey. The chemical and physical properties of class C fly ash are shown in Table 5.3 and Table 5.4.

Table 5.3 Chemical properties of class C fly ash (Etminan, 2012)

Parameter	Value(%)
$CaCO_3$+$MgCO_3$	1.25
H_2O	0.20
SiO_2	45.00
Al_2O_3	13.90
Fe_2O_3	8.26
CaO	15.11
MgO	6.68
SO_3	4.26
Na_2O	2.13
K_2O	2.78
Cl	0.006
Loss on ignition	0.22
S.CaO	0.15
TOTAL	100%

Table 5.4 Physical properties of class C fly ash (Etminan, 2012)

Specific Surface (cm/g)	Specific Gravity (g/cm^3)	Activity Index (%)
2100	2.34	83

In addition, sieve analysis and hydrometer analysis were applied to the fly ash. As a result, the grain-size distribution curve of fly ash was obtained by using both tests, as shown in Figure 5.12.

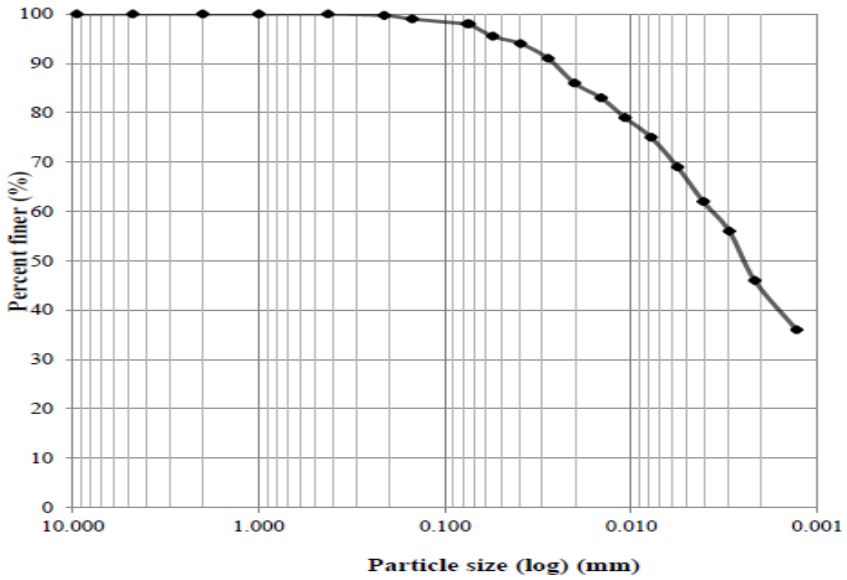

Figure 5.12 Grain-size distribution curve of fly ash (Etminan, 2012)

5.2.3 Polypropylene Fiber

Polypropylene fiber can be had a twisted fibrillating network form. It is made of 100% virgin materials. This fiber can be used to provide high-performance reinforcement in the concrete. In addition, polypropylene fiber improves shrinkage and impact strength, increases fatigue resistance, and increases the toughness of concrete. Polypropylene fiber is the second alternative material for clayey soils. Therefore, it was used to apply the laboratory tests with mixed clayey soils. The physical properties of polypropylene fiber are given in Table 5.5.

Table 5.5 Physical properties of polypropylene fiber (Etminan, 2012)

Properties of Polypropylene	Value
Color	White
Form	Fibrillated Fiber
Acid/Alkali Resistance	Excellent
Specific Gravity	0.91
Absorption	Nil
Tensile Strength	758
Length	54 mm
Compliance	ASTM C-1116

As mentioned, the polypropylene fiber can be consisting forms of deformed and twisted fibrillating networks. Both forms of polypropylene fibers are shown in Figure 5.13.

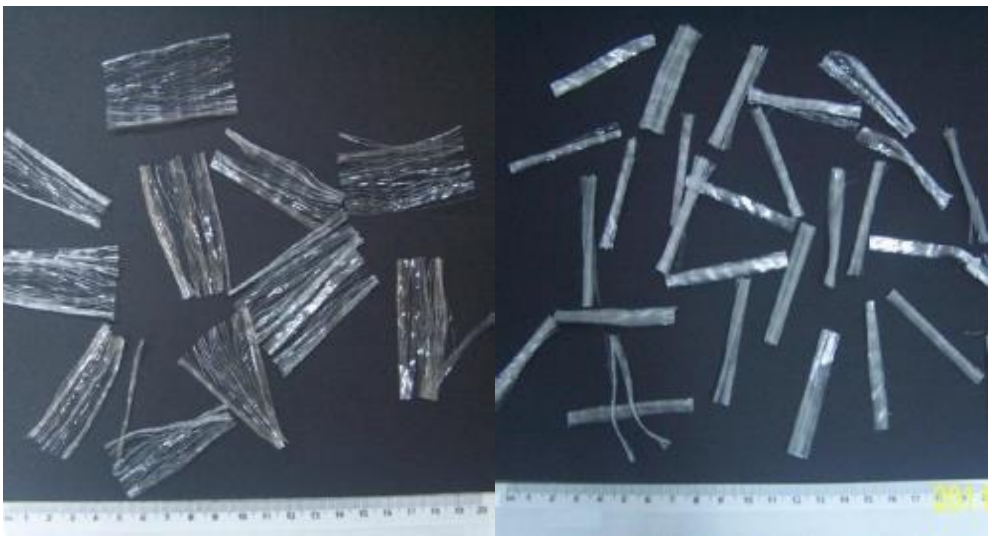

(a) Deformed form (b) Fibrillated form

Figure 5.13 (a) Deformed form and (b) fibrillated form of polypropylene fibers (Etminan, 2012)

5.2.4 Copolymer Fiber

Copolymer fiber can be had a fibrillating network form. It is made of 100% virgin materials. This fiber can be used to provide high-performance reinforcement in the concrete. In addition, copolymer fiber improves settlement shrinkage and impact

strength, increases durability, and increases the toughness of concrete. Also, it is used to extend the maximum long-term durability, and effective secondary temperature cracks control. Copolymer fiber is another alternative material for clayey soils. Therefore, it was used to apply the laboratory tests with mixed clayey soils. The physical properties of copolymer fiber are given in Table 5.6.

Table 5.6 Physical properties of copolymer fiber (Etminan, 2012)

Properties of Copolymer	Value
Color	Gray
Form	Monofilament Fiber
Acid/Alkali Resistance	Excellent
Specific Gravity	0.91
Absorption	Nil
Tensile Strength	758
Length	54 mm
Compliance	ASTM C-1116

As mentioned, the copolymer fiber can be consisting forms of deformed and monofilament fiber networks. Both forms of copolymer fibers are shown in Figure 5.14.

(a) Deformed form (b) Fibrillated form

Figure 5.14 (a) Deformed form and (b) fibrillated form of copolymer fibers (Etminan, 2012)

5.3 Modeling of Experiment Results and Numerical Model

The soil specimen can behave with very different characteristics concerning the type of performed test. Therefore, the experimental results are received by the different testing procedures and techniques. However, the same constitutive model describes the interaction between deformability and strength with different aspects. In order to observe the main feature of tested soil behavior, the creation or modification of a constitutive model can be considered (Hicher and Shao, 2008).

The hyperbolic function that expresses the stress-strain relationship of the soil was suggested and proved. The Duncan-Chang model is commonly used in the constitutive models related to the stress-strain relationship of soil. Because it is indicated the nonlinear behavior of soil. Also, it is applicable to a wide range of soil types. It provides to expand the usage of the Duncan-Chang model. Also, it leads to the improving application of engineering practices (Huang et al., 2018). A hyperbola can fit the stress-strain curves due to the different stress paths. Huang et al. (2018) modified the tangent modulus formula based on the Duncan-Chang model. The modifications were applied under lateral and axial unloading stress paths.

As mentioned in section 3.1, the tangent modulus can be expressed independent of stress or independent of strain. However, the stresses can be evaluated more accurately than the strains in many geotechnical problems. Therefore, the calculation of tangent modulus in the Duncan-Chang model was established by eliminating the strains and expressing in terms of stress only (Duncan and Chang, 1970). Also, the unconfined compression test can be determined as strain-controlled. Hence, the tangent modulus proposed by the Duncan-Chang model, and the unconfined compression test coincide with the observation of the main feature in stress and strain relationships.

The tangent modulus formula was demonstrated by using derivation in the Duncan-Chang model. In order to derive the evaluation of tangent modulus formulas, the unconfined compression test was performed on improved clayey soils, as mentioned in section 5.2. The modification of the Duncan-Chang model on the basis of the unconfined compression test conditions is given as follows.

As mentioned in section 3.1, Kondner (1963) proposed the hyperbolic equation based on the triaxial tests. The hyperbolic equation was given in Eq. (3.3). However, there is no confinement on the soil specimen when the unconfined compression test

conditions are regarded. Therefore, the minor principal stress equals zero ($\Delta\sigma_3$=0), and a vertical load is applied to the soil sample. Hence, Eq. (3.3) should be reorganized:

$$\sigma 1 = \frac{\varepsilon_1}{a+b\varepsilon_1} \tag{5.14}$$

In Eq. (5.14) is rearranged:

$$a + b\varepsilon_1 = \frac{\varepsilon_1}{\sigma_1} \tag{5.15}$$

when ε_1 and $\varepsilon_1/\ \sigma_1$ are taken as abscissa and coordinate in Figure 3.6 corresponding to a straight line, parameter a is called the linear intercept, and b denotes the slope of the line.

On the other hand, the slope of the stress-strain curves is denoted by E_0. Therefore, E_0 can be evaluated as:

$$E_0 = \frac{\Delta(\sigma_1-\sigma_3)}{\Delta\varepsilon_1} = \frac{(\Delta\sigma_1-\Delta\sigma_3)}{\Delta\varepsilon_1} \tag{5.16}$$

where $\Delta\sigma_1$ is the axial pressure increment, $\Delta\sigma_3$ is the lateral pressure increment, and $\Delta\varepsilon_1$ is the axial strain increment (Huang et al., 2018). Thus, during the axial loading condition, the parameter E_0 can be written as:

$$E_0 = \frac{\Delta\sigma_1}{\Delta\varepsilon_1} \tag{5.17}$$

where the lateral pressure increment is eliminated from Eq. (5.17).

Hooke's law was mentioned in section 2.1.3. Also, the intermediate principal stress can be assumed to be equal to the minor principal stress in the triaxial tests (Duncan and Chang, 1970). Loading conditions of the unconfined compression test include zero confining or minor principal stress. Therefore, if Eqs. (2.34) and (2.36) are generalized as:

$$\Delta\varepsilon 1 = \frac{1}{E_t}[\Delta\sigma 1 - v(\Delta\sigma 3 + \Delta\sigma 3)] \tag{5.18}$$

$$\Delta\varepsilon 3 = \frac{1}{E_t}[\Delta\sigma 3 - v(\Delta\sigma 1 + \Delta\sigma 1)] \tag{5.19}$$

where E_t is the tangent modulus of the soil, and v is the Poisson's ratio. If Eqs. (5.18) and (5.19) are reorganized to determine the tangent modulus of the soil, Eq. (5.20) can be obtained:

$$E_t = \frac{(\Delta\sigma_1-\Delta\sigma_3)(\Delta\sigma_1+2\Delta\sigma_3)}{\Delta\varepsilon_1\Delta\sigma_1+\Delta\sigma_3(\Delta\varepsilon_1-2\Delta\varepsilon_3)} \tag{5.20}$$

where $\Delta\sigma_1$ is the axial pressure increment, $\Delta\sigma_3$ is the lateral pressure increment, $\Delta\varepsilon_1$ is the axial strain increment, and $\Delta\varepsilon_3$ is the lateral strain increment. When the lateral pressure increment, $\Delta\sigma_3$, is eliminated from Eqs. (5.20), (5.18), and (5.19), respectively:

$$E_t = \frac{\Delta\sigma_1{}^2}{\Delta\varepsilon_1 \Delta\sigma_1} = \frac{\Delta\sigma_1}{\Delta\varepsilon_1} \tag{5.21}$$

$$\Delta\varepsilon 1 = \frac{1}{E_t}\Delta\sigma 1 \tag{5.22}$$

$$\Delta\varepsilon 3 = -\frac{1}{E_t}\nu\Delta\sigma 1 \tag{5.23}$$

where E_t, $\Delta\varepsilon_1$, and $\Delta\varepsilon_2$ were written only in terms of $\Delta\sigma_1$ which is called as the axial pressure increment. In Eq. (5.23) is written in terms of the axial strain increment by using Eq. (5.22), the expression became:

$$\Delta\varepsilon 3 = -\nu\Delta\varepsilon 1 \tag{5.24}$$

where the lateral strain increment is reorganized in terms of the axial strain increment. Eq. (5.24) is not a requirement in the unconfinement condition. In other words, when the lateral pressure increment is not equal to zero, Eq. (5.24) is used to express in terms of the axial strain increment in Eq. (5.21). However, when the soil sample is influenced due to only the axial loading, Eq. (5.21) does not need to be written about the lateral strain increment.

On the other hand, the slope of the stress-strain curves (E_0) and the tangent modulus (E_t) have the same expressions as shown in Eqs. (5.17) and (5.21). Therefore, it can be mentioned as:

$$E_t = E_0 \tag{5.25}$$

The slope of the stress-strain curve (E_0) can be found by taking the derivative with respect to the stress-strain curve, and expressions are given as follows:

$$E_0 = \frac{d(\sigma_1 - \sigma_3)}{d\varepsilon_1} \tag{5.26}$$

where $(\sigma_1 - \sigma_3)$ is the stress difference. Then, the hyperbolic equation of Kondner (1963) that is mentioned in Eq. (5.14) can be substituted into Eq. (5.26):

$$E_0 = \frac{d\left(\frac{\varepsilon_1}{a+b\varepsilon_1}\right)}{d\varepsilon_1} \tag{5.27}$$

When the evaluation of derivative in the slope of the stress-strain curve is applied, the expression becomes as:

$$E_0 = \frac{1}{a+b\varepsilon_1} - \frac{b\varepsilon_1}{(a+b\varepsilon_1)^2} = \frac{a}{(a+b\varepsilon_1)^2} \tag{5.28}$$

In addition, when Eq. (5.14) is simplified, the following expressions are obtained:

$$\varepsilon_1 = a\sigma_1 + b\sigma_1\varepsilon_1 \tag{5.29}$$

$$\frac{a\sigma_1}{\varepsilon_1} = 1 - b\sigma_1 \tag{5.30}$$

$$\varepsilon_1 = \frac{a\sigma_1}{1-b\sigma_1} = \frac{a}{\frac{1}{\sigma_1}-b} \tag{5.31}$$

When Eq. (5.31) is inserted into Eq. (5.28), the following expressions and simplification steps are obtained:

$$E_0 = \frac{a}{\left(a+\frac{ab}{\frac{1}{\sigma_1}-b}\right)^2} = \frac{a}{a^2\left(1+\frac{b\sigma_1}{1-b\sigma_1}\right)^2} \tag{5.32}$$

$$E_0 = \frac{1}{a\left(\frac{1}{1-b\sigma_1}\right)^2} \tag{5.33}$$

$$E_0 = \frac{1}{a}(1 - b\sigma_1)^2 \tag{5.34}$$

On the other hand, the initial tangent modulus is proposed by Janbu (1963), and it was given in Eq. (2.95) in section 2.4.1.1. Also, this equation can be modified concerning the basis of the unconfined compression test condition. The expressions can be given as follows:

$$\frac{E_i}{p_a} = K\left(\frac{\sigma_m}{p_a}\right)^n \tag{5.35}$$

$$\log\left(\frac{E_i}{p_a}\right) = \log K + n\log\left(\frac{\sigma_1}{p_a}\right) \tag{5.36}$$

$$n = \frac{\Delta\log\left(\frac{E_i}{p_a}\right)}{\Delta\log\left(\frac{\sigma_1}{p_a}\right)} \tag{5.37}$$

where the initial tangent modulus of soil denotes E_i, σ_m is the mean principal stress, p_a is determined as atmospheric pressure, K is the modulus number, and n is the exponent determining the variation rate.

In addition, the failure ratio (R_f) was given in Eq. (3.7), and the stress level (S) was mentioned in Eq. (3.12). On the other hand, a and b were discussed in section 3.1. They can be written as:

$$E_i = \frac{1}{a} \tag{5.38}$$

$$(\sigma_1 - \sigma_3)_{ult} = \frac{1}{b} \tag{5.39}$$

where a and b are written with respect to the representation of the hyperbolic stress-strain curve, as mentioned in Figure 3.5 and Figure 3.6.

When parameters a and b are modified due to only the axial loading and submitted into Eq. (5.34), the following equation can be obtained:

$$E_0 = E_i \left(1 - \frac{\sigma_1}{(\sigma_1)_{ult}}\right)^2 \tag{5.40}$$

Then, if Eq. (3.7) and Eq. (3.12) that defined as equations of the failure ratio and the stress level inserted into Eq. (5.40), the following equation can be found as:

$$E_0 = E_i[1 - R_f S]^2 \tag{5.41}$$

Due to regarding the unconfined compression test conditions, Eq. (5.25) shows that Eq. (5.41) can be identified as the tangent modulus of the soil, and the expression is written as:

$$E_t = E_i[1 - R_f S]^2 \tag{5.42}$$

The Duncan-Chang hyperbolic model is proposed by including the Mohr-Coulomb failure criterion that depends on the friction angle, and it was written in Eq. (3.13). When it is generalized and organized, the Mohr-Coulomb failure criterion can be mentioned as:

$$\frac{(\sigma_1 - \sigma_3)_f}{2} = c \cos\varphi + \frac{(\sigma_1 - \sigma_3)_f}{2} \sin\varphi \tag{5.43}$$

where φ is the soil's friction angle. The friction angle equals zero if the unconfined compression test is applied to the saturated soil sample. Also, the minor principal stress is zero because of the unconfinement. Therefore, the Mohr-Coulomb failure criterion became:

$$\frac{(\sigma_1)_f}{2} = c_u = \frac{q_u}{2} \quad or \quad (\sigma_1)_f = 2c_u = q_u \tag{5.44}$$

where q_u is the unconfined compression strength, and c_u is the undrained shear strength. On the other hand, if the stress level Eq. (3.12) is submitted by Eq. (5.44), the stress level is found that:

$$S = \frac{(\sigma_1)}{q_u} \tag{5.45}$$

where (σ_1) is a certain level of axial stress of the soil specimen, and it can vary about the stress-strain curve of the soil in the unconfined compression test results. For instance, when the tangent modulus at half of the maximum stress is calculated, the stress level equals 0.5. According to loading conditions of the unconfined compression test, the tangent modulus of soil can be written by using Eq. (5.42):

$$E_t = E_i \left[1 - R_f \frac{(\sigma_1)}{q_u}\right]^2 \tag{5.46}$$

where E_t is the modified tangent modulus of tested soil specimens concerning the loading conditions of the unconfined compression test.

As a result, modifying a constitutive model may be regarded to detect the main feature of tested soil behavior, as shown above. Furthermore, it shows that the improvement of the used constitutive model can provide the proper observation to indicate the engineering properties of received soils.

Moreover, the relationship between the secant modulus at maximum stress, the tangent and secant modulus at half of the maximum stress, and the initial tangent modulus can be considered by the secant and tangent modulus expressions due to the unconfined compression test conditions. Therefore, the creation of the relationships between soil moduli on the basis of the unconfined compression test conditions and the modified Duncan-Chang model can be given as follows.

As mentioned in section 2.4.1.2, the secant modulus is based on the deviatoric stress and soil strain. Therefore, if the secant modulus at one-half of the maximum stress is modified according to the stress-strain curve of the unconfined compression test results, the expression can be written as:

$$E_{s50} = \frac{(\sigma_1)_f/_2}{\varepsilon_{50}} \quad or \quad (\sigma_1)_f = 2E_{s50}\,\varepsilon_{50} \tag{5.47}$$

where E_{s50} is the secant modulus at half of the maximum stress, $(\sigma_1)_f$ is the maximum stress in the stress-strain curve of soil, and ε_{50} is the axial strain at half of the maximum stress. Moreover, if the secant modulus at the maximum stress or failure is altered

concerning the stress-strain curve of the unconfined compression test results, the formulation can be written as:

$$E_{sf} = \frac{(\sigma_1)_f}{\varepsilon_f} \quad or \quad (\sigma_1)_f = E_{sf}\,\varepsilon_f \tag{5.48}$$

where E_{sf} is the secant modulus at the maximum stress, and ε_f is the axial strain at the maximum stress. When Eq. (5.48) is inserted in Eq. (5.47), the expression becomes:

$$E_{s50} = \frac{E_{sf}}{2}\frac{\varepsilon_f}{\varepsilon_{50}} \tag{5.49}$$

where the secant modulus at half of the maximum stress was identified in terms of the secant modulus at the failure. The crucial case is the determination of the axial strain at half of the maximum stress after defining the secant modulus at the maximum stress.The axial strain at half of the maximum stress was determined in this study by interpolation between pre-point and post-point of the half of the maximum stress point.

On the other hand, the tangent modulus formulation in Eq. (5.41) should be composed of an open form to modify it. In other words, if the tangent modulus is written without denoted failure ratio (R_f) and stress level (S), the expression can be emphasized as:

$$E_t = E_i\left[1 - \frac{(\sigma_1)_f}{(\sigma_1)_{ult}}\frac{(\sigma_1)}{(\sigma_1)_f}\right]^2 \tag{5.50}$$

where (σ_1) is a certain level of axial stress. Also, when the tangent modulus at half of the maximum stress is settled in Eq. (5.50), the following expressions and simplification steps are obtained:

$$E_{t50} = E_i\left[1 - \frac{(\sigma_1)_f}{(\sigma_1)_{ult}}\frac{(\sigma_1)_f/_2}{(\sigma_1)_f}\right]^2 \tag{5.51}$$

$$E_{t50} = E_i\left[1 - 0.5\,\frac{(\sigma_1)_f}{(\sigma_1)_{ult}}\right]^2 \tag{5.52}$$

$$E_{t50} = 0.25E_i\left[2 - \frac{(\sigma_1)_f}{(\sigma_1)_{ult}}\right]^2 \tag{5.53}$$

where $(\sigma_1)_f$ /2 is half of maximum stress, and E_{t50} is the tangent modulus at half of the maximum stress. Eq. (5.53) can describe the relationships between the tangent modulus at half of the maximum stress and the initial tangent modulus. However, the failure ratio should be controlled whether it has less or more than unity.

Furthermore, the secant modulus at the failure can be written in terms of the tangent modulus at half of the maximum stress and the initial tangent modulus. In other words, the relationships between the secant modulus at the failure, the tangent modulus at half of the maximum stress, and the initial tangent modulus are described by using Eq. (5.53). When Eq. (5.48) is inserted into Eq. (5.53), the following expressions and simplification steps are obtained:

$$E_{t50} = 0.25E_i\left[2 - \frac{E_{sf}\,\varepsilon_f}{(\sigma_1)_{ult}}\right]^2 \tag{5.54}$$

$$\sqrt{E_{t50}} = \sqrt{0.25}\sqrt{E_i}\left[2 - \frac{E_{sf}\,\varepsilon_f}{(\sigma_1)_{ult}}\right] \tag{5.55}$$

$$\frac{E_{sf}\,\varepsilon_f}{(\sigma_1)_{ult}} = 2 - 2\sqrt{E_{t50}/E_i} \tag{5.56}$$

where $1/(\sigma_1)_{ult}$ is determined by parameter b, as mentioned in Eq. (5.39). Therefore, the resulting expression can be written as:

$$E_{sf} = \frac{2\left[1-\sqrt{E_{t50}/E_i}\right]}{b\,\varepsilon_f} \tag{5.57}$$

where E_{sf} is the secant modulus at the maximum stress. However, the failure ratio (R_f) should be controlled whether it has less or more than unity.

In addition, the secant modulus at half of the maximum stress can be written in terms of the tangent modulus at half of the maximum stress and the initial tangent modulus. In other words, the relationships between the secant and tangent modulus at half of the maximum stress and the initial tangent modulus are described by using Eq. (5.53). When Eq. (5.47) is inserted into Eq. (5.53), the following expressions and simplification steps are obtained:

$$E_{t50} = 0.25E_i\left[2 - \frac{2E_{s50}\,\varepsilon_{50}}{(\sigma_1)_{ult}}\right]^2 \tag{5.58}$$

$$E_{t50} = E_i\left[1 - \frac{E_{s50}\,\varepsilon_{50}}{(\sigma_1)_{ult}}\right]^2 \tag{5.59}$$

where $1/(\sigma_1)_{ult}$ is determined by parameter b, as mentioned in Eq. (5.39). Therefore, Eq. (5.59) can be written and simplified as:

$$E_{t50} = E_i[1 - bE_{s50}\,\varepsilon_{50}]^2 \tag{5.60}$$

$$\sqrt{E_{t50}} = \sqrt{E_i}[1 - bE_{s50}\,\varepsilon_{50}] \tag{5.61}$$

Then, the resulting equation about the secant modulus at half of the maximum stress can be written as:

$$E_{s50} = \frac{1-\sqrt{E_{t50}/E_i}}{b\varepsilon_{50}} \tag{5.62}$$

where E_{s50} is the secant modulus at half of the maximum stress. However, the failure ratio (R_f) should be controlled whether it has less or more than unity.

As a control mechanism of the relationship between the secant modulus at maximum stress, the tangent and secant modulus at half of the maximum stress, and the initial tangent modulus can be obtained by equalizing Eqs. (5.54) and (5.59). Then, the following expressions and simplification steps are received:

$$E_{t50} = 0.25E_i\left[2-\frac{E_{sf}\,\varepsilon_f}{(\sigma_1)_{ult}}\right]^2 = E_i\left[1-\frac{E_{s50}\,\varepsilon_{50}}{(\sigma_1)_{ult}}\right]^2 \tag{5.63}$$

$$\sqrt{0.25\left[2-\frac{E_{sf}\,\varepsilon_f}{(\sigma_1)_{ult}}\right]^2} = \sqrt{\left[1-\frac{E_{s50}\,\varepsilon_{50}}{(\sigma_1)_{ult}}\right]^2} \tag{5.64}$$

$$0.5\,\frac{E_{sf}\,\varepsilon_f}{(\sigma_1)_{ult}} = \frac{E_{s50}\,\varepsilon_{50}}{(\sigma_1)_{ult}} \tag{5.65}$$

$$E_{sf}\,\varepsilon_f = 2E_{s50}\,\varepsilon_{50} \tag{5.66}$$

Eq. (5.66) shows that the modified expressions of soil moduli are consistent. Therefore, Eqs. (5.51), (5.57), and (5.62) are reasonable to calculate the soil moduli by using the unconfined compression test results in which the stress-strain curve of the stabilized clayey soil. Therefore, Eq. (5.51) was used for obtaining the tangent modulus at half of the maximum stress, Eq. (5.57) was used to determine the secant modulus at maximum stress, and Eq. (5.62) was employed to settle the secant modulus at half of the maximum stress.

Consequently, the enhancement of clayey soil stabilized by the alternative materials' initial tangent, secant, and tangent moduli will be obtained using the mentioned expressions from the constitutive model. Then, the discovered results from remarked terms will be used to compare and understand the improvement of stabilized clayey soils with different types and amounts of alternative materials.

CHAPTER 6

6. EVALUATION OF RESULTS AND DISCUSSION

The laboratory tests mentioned in section 5 were performed by Etminan (2012) in Istanbul Technical University's Prof. Dr. Hamdi Peynircioğlu laboratory of geotechnical engineering. The results of unconfined compression and the compaction test were used during this study to determine the deformation modulus of high plasticity clay and its mixtures blended with three different alternative materials. In addition, the soil moduli were calculated using the modified Duncan-Chang model, which is mentioned in section 5.3. The comparison of the amount of improvement in high plasticity clay when mixed with three different alternative materials is discussed in this section. Table 6.1 exhibit the different mixtures of high plasticity clay and the amount of alternative materials used during tests.

Table 6.1 Type of alternative materials and amount of them

No.	Materials	1	2	3	4	5
1	Fly Ash	5%	10%	15%	-	-
2	Polypropylene	0.25%	0.5%	0.75%	1%	-
3	Copolymer	0.5%	0.75%	1%	1.25%	1.5%
4	Fly Ash+	10%	10%	10%	-	-
	Polypropylene	0.25%	0.5%	0.75%	-	-
5	Fly Ash+	10%	10%	10%	-	-
	Copolymer	0.75%	1%	1.25%	-	-

6.1 High Plasticity Clay Soil

During the experimental program of this study, the high plasticity clay soil was used. The high plasticity clay (CH) was obtained from the Akpınar district of Istanbul, Turkey. The compaction and the unconfined compression tests were performed on the high plasticity clay soil, and the outcomes of these experiments are illustrated in Table 6.2. With respect to data obtained from mentioned tests, it can be seen that the value of ω_{opt} and γ_{dmax} obtained at 27% and 15.0 kN/m^3, respectively.

Table 6.2 Results of experiments executed with high plasticity clay soil

Sample No.	ω (%)	γ_d (kN/m^3)	q_u (kN/m^2)
1	20	13.30	96.5
2	23	14.40	156.0
3	27	15.00	174.7
4	30	14.50	113.3
5	39	13.30	28.8

The axial stress-axial strain curves of five different high plasticity clay samples are shown in Figure 6.1. Besides, Figure 6.2 exhibits the tested high plasticity clay soil sample, which has the highest value of the maximum unconfined compression strength. According to data obtained from the unconfined compression test of plain CH soil samples, it can be inferred that the maximum unconfined compression strength was obtained in the third sample of high plasticity clay, and it was obtained as 174.7 kN/m^2.

It should be noted that the reciprocal of the initial tangent modulus (a), reciprocal of the asymptotic value of stress difference (b), asymptotic value of stress difference $(\sigma_1)_{ult}$, compressive strength $(\sigma_1)_f$, failure ratio (R_f), axial strain value at failure (ε_f) and axial strain value at 50% of maximum stress (ε_{50}) are required parameters to obtain soil moduli. These parameters were derived from unconfined compression test results and transformed hyperbolic stress-strain curves of high plasticity clay samples. Mentioned engineering parameters are given in Table 6.3.

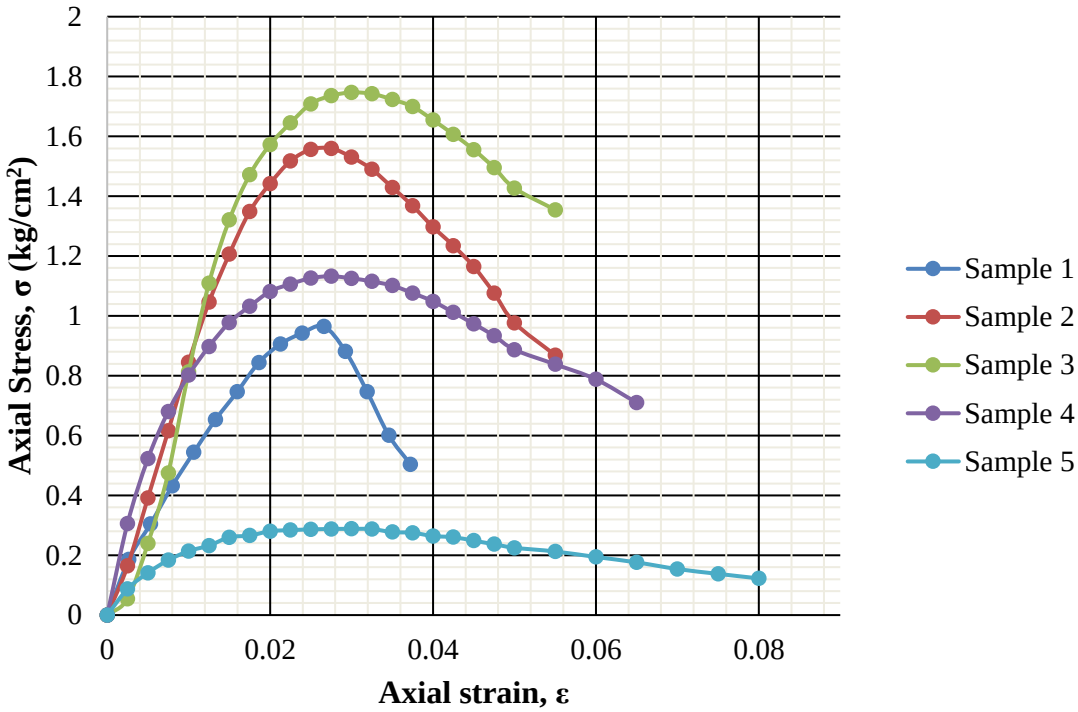

Figure 6.1 Results of unconfined compression tests of high plasticity clay soil

Table 6.3 Calculated engineering parameters of high plasticity clay soil

Sample No.	a (cm^2/kg)	b (cm^2/kg)	$(\sigma_1)_{ult}$ (kg/cm^2)	$(\sigma_1)_f$ (kg/cm^2)	R_f -	ε_f -	ε_{50} -
1	0.0141	0.4749	2.1057	0.965	0.46	0.0266	0.0092
2	0.0089	0.2779	3.5984	1.560	0.43	0.0275	0.0093
3	0.0079	0.2768	3.6127	1.747	0.48	0.0300	0.0105
4	0.0062	0.6331	1.5795	1.133	0.72	0.0275	0.0057
5	0.0210	2.6153	0.3824	0.288	0.75	0.0275	0.0052

It is obvious that, when the values of strains are between 0.1% to 0.001%, this region is categorized as a small strain. Furthermore, it should be noted that the strain level of high plasticity clay is classified as small strain (SS) because the maximum axial strain was determined in the fifth sample of high plasticity clay, and it was obtained as 0.08%. Thus, it can be concluded that nonlinear behaviour was observed for the tested high plasticity clay soil samples.

Initial tangent modulus, tangent modulus at 50% of maximum stress, secant modulus at failure, secant modulus at 50% of maximum stress, and unconfined

compression strength of five different high plasticity clay samples are given in Table 6.4.

Table 6.4 Soil moduli and unconfined compression strength of high plasticity clay soil

Sample No.	E_i (kN/m^2)	E_{t50} (kN/m^2)	E_{sf} (kN/m^2)	E_{s50} (kN/m^2)	q_u (kN/m^2)
1	7092.2	4214.4	3627.8	5260.4	96.5
2	11236.0	6892.8	5672.7	8395.8	156.0
3	12658.2	7277.1	5823.3	8310.4	174.7
4	16129.0	6634.3	4120.0	9939.1	113.3
5	4761.9	1850.6	1047.3	2782.9	28.8

It should be noted that the initial tangent modulus can be used to analyze stress distribution in soil samples. According to the data obtained, the maximum modulus values are observed in the initial tangent modulus compared with other soil moduli in all five high plasticity clay samples due to the initial slope of the stress-strain curves. In other words, the axial stress increases up to a certain point very sharply. Then, this sharp increasing trend suddenly starts to slow down, and during this slowing trend, the axial strain increases rapidly.

Figure 6.2 Peak point of high plasticity clay soil (ω =27%, q_u=174.7 kN/m^2) (Etminan, 2012)

Transformed hyperbolic stress-strain curves for five different high plasticity clay samples are illustrated in Figures 6.3, 6.4, 6.5, 6.6, and 6.7.

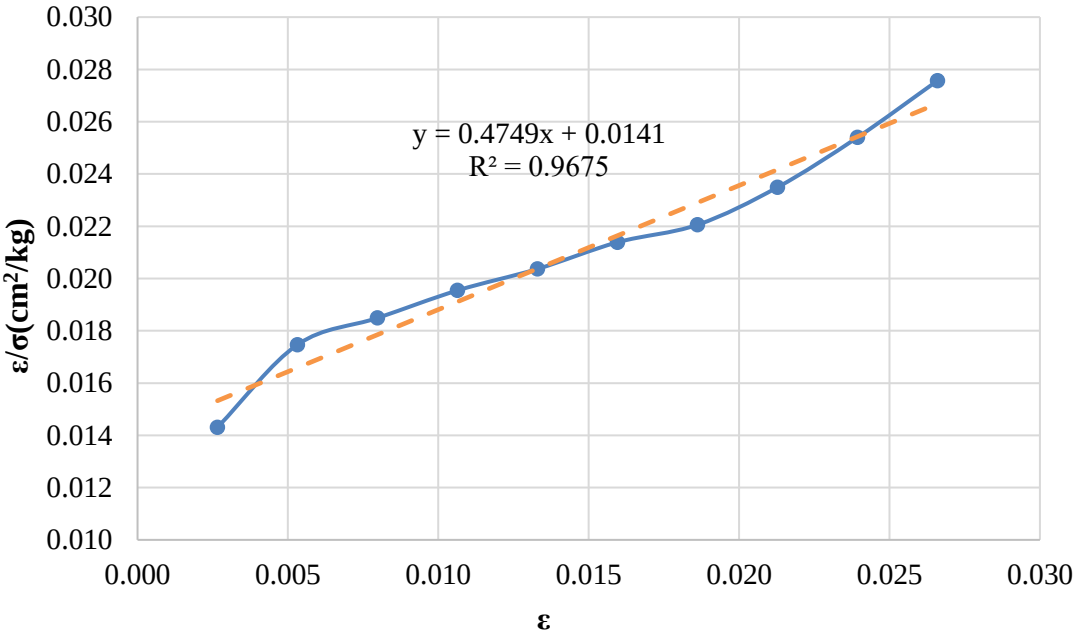

Figure 6.3 Transformed hyperbolic stress-strain curve for sample 1 (CH)

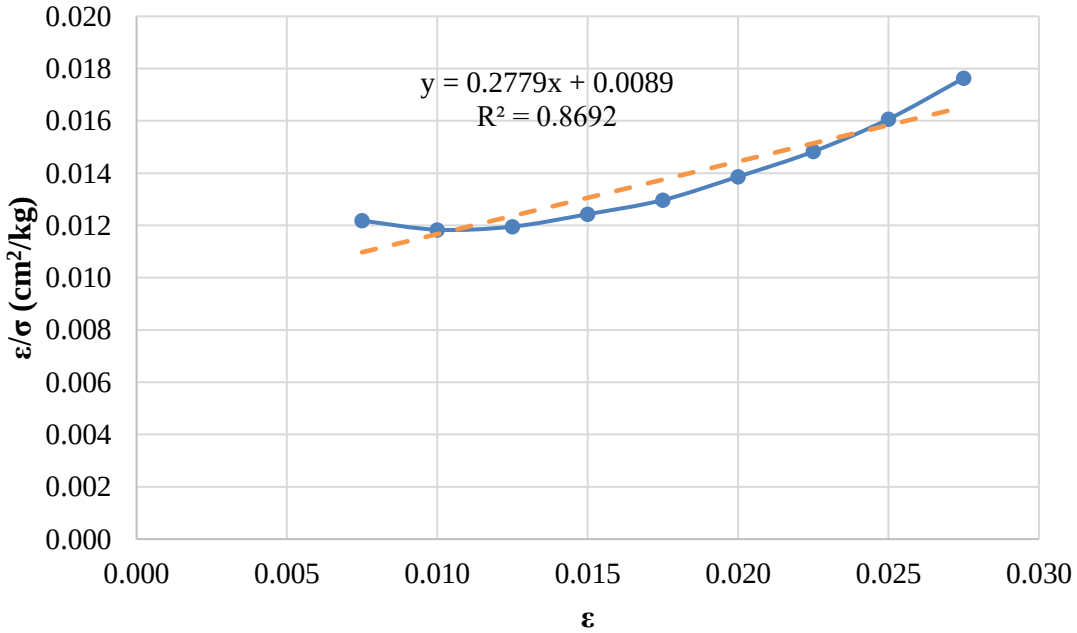

Figure 6.4 Transformed hyperbolic stress-strain curve for sample 2 (CH)

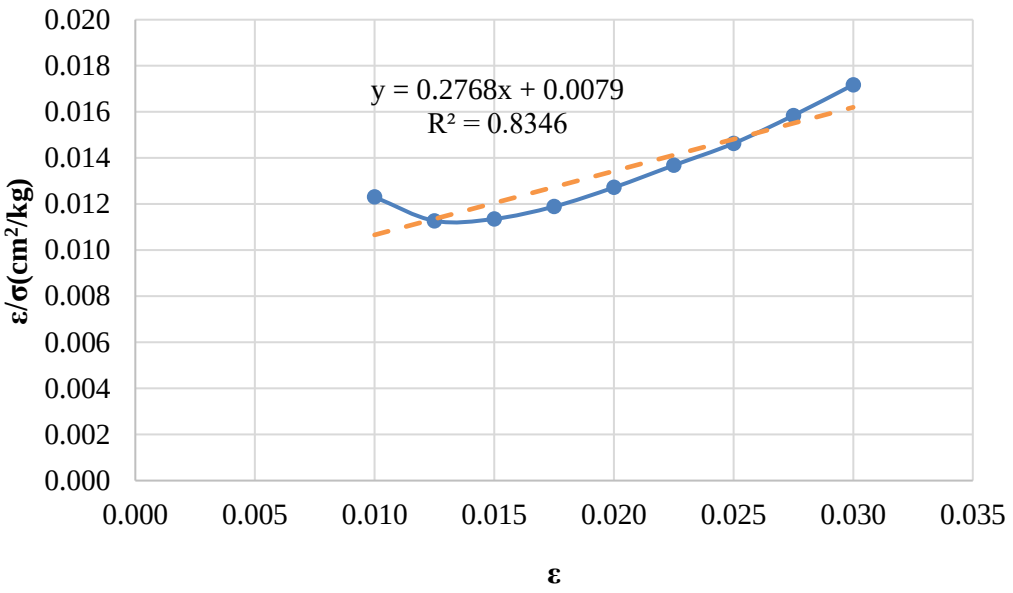

Figure 6.5 Transformed hyperbolic stress-strain curve for sample 3 (CH)

According to data obtained from Figures 6.3, 6.4, and 6.5, it can be concluded that the low and high values of axial strains in samples 1, 2, and 3 are not precisely hyperbolic. In other words, these points can not be fitted in a straight line. On the other hand, it was possible to estimate the actual stress-strain curves by a hyperbola. Therefore, it is found to have a reasonable degree of accuracy.

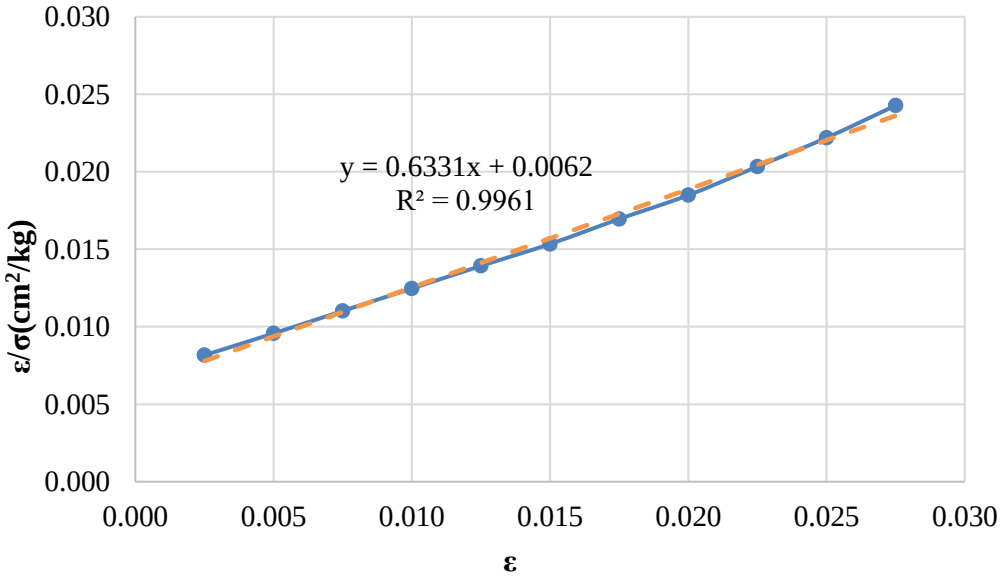

Figure 6.6 Transformed hyperbolic stress-strain curve for sample 4 (CH)

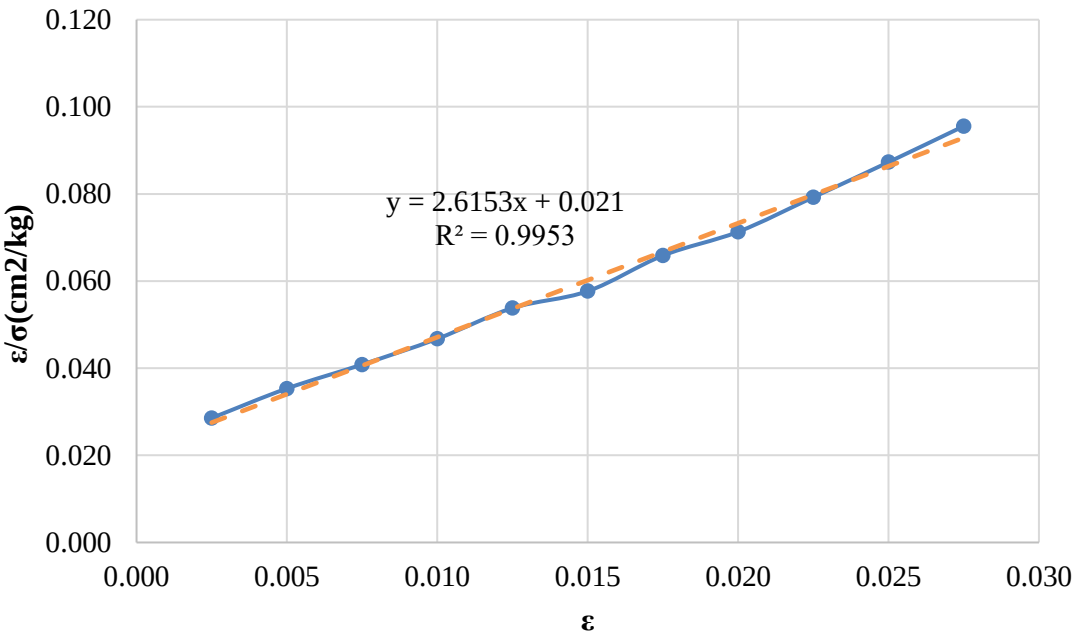

Figure 6.7 Transformed hyperbolic stress-strain curve for sample 5 (CH)

Transformed hyperbolic stress-strain curves in samples 4 and 5 showed hyperbolic behavior, as shown in Figures 6.6 and 6.7. In other words, these points can be best-fitted in a straight line.

On the other hand, the relationship between the secant modulus at 50% of maximum stress and the initial tangent modulus of high plasticity clay samples is shown in Figure 6.8. According to the data, it can be inferred that the initial tangent modulus increases with the secant modulus at 50% of maximum stress. Therefore, it was best suited for estimating these soil moduli by a power model. Furthermore, the initial tangent modulus (E_i) is related to the beginning of high plasticity clay samples' stress-strain curve, and the secant modulus at 50% of maximum stress (E_{s50}) is linked to the axial strain value at 50% maximum stress. Thus, these soil moduli refer to the hardening of high plasticity clay samples.

Furthermore, the relationship between the secant modulus at failure (E_{sf}) and the tangent modulus at 50% of maximum stress (E_{t50}) of high plasticity clay samples is shown in Figure 6.9.

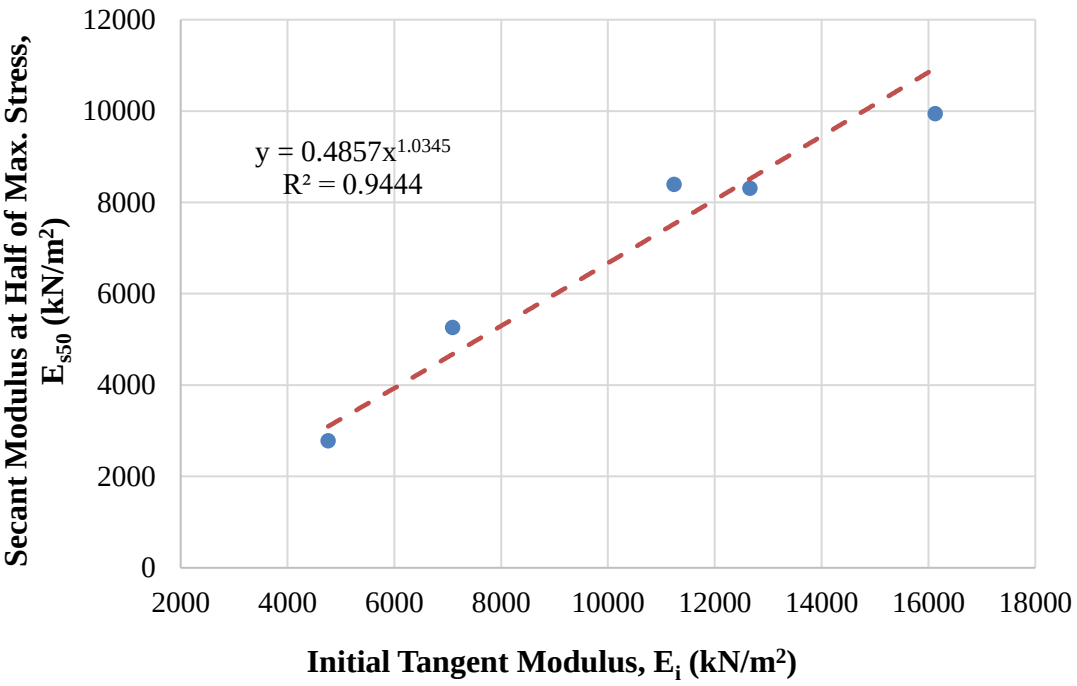

Figure 6.8 Relationship between secant modulus at 50% of maximum stress and initial tangent modulus (CH)

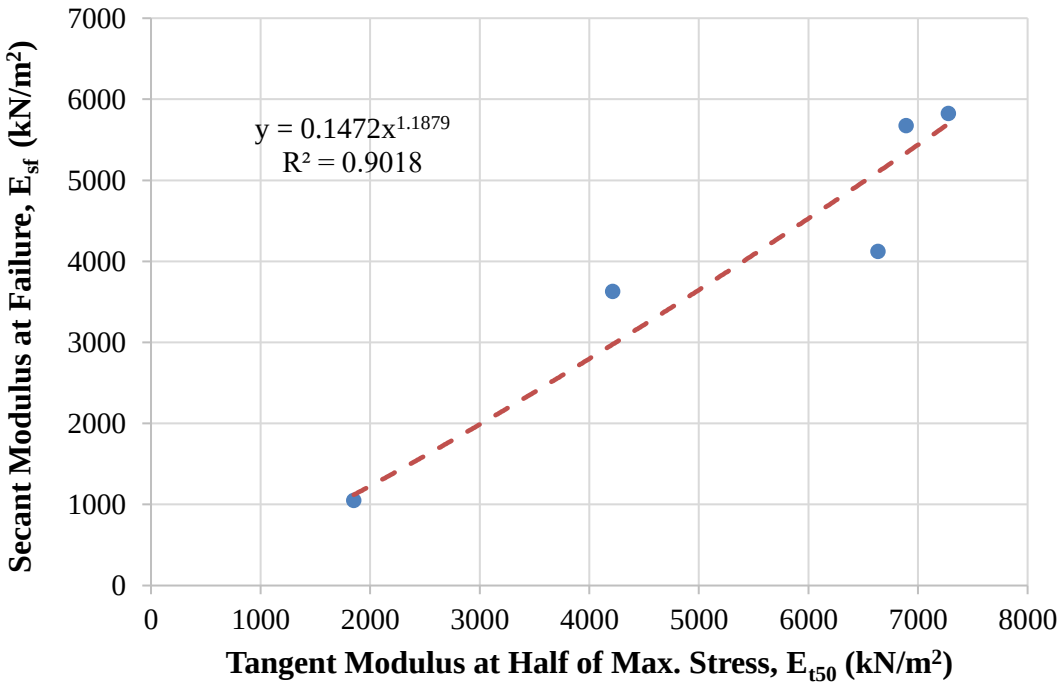

Figure 6.9 Relationship between secant modulus at failure point and tangent modulus at 50% of maximum stress (CH)

The tangent modulus at 50% of maximum stress increases with the secant modulus at failure. Therefore, it was best suited for estimating these soil moduli by a power model.

In addition, the relationship between initial tangent modulus (E_i) and unconfined compression strength of high plasticity clay samples is shown in Figure 6.10.

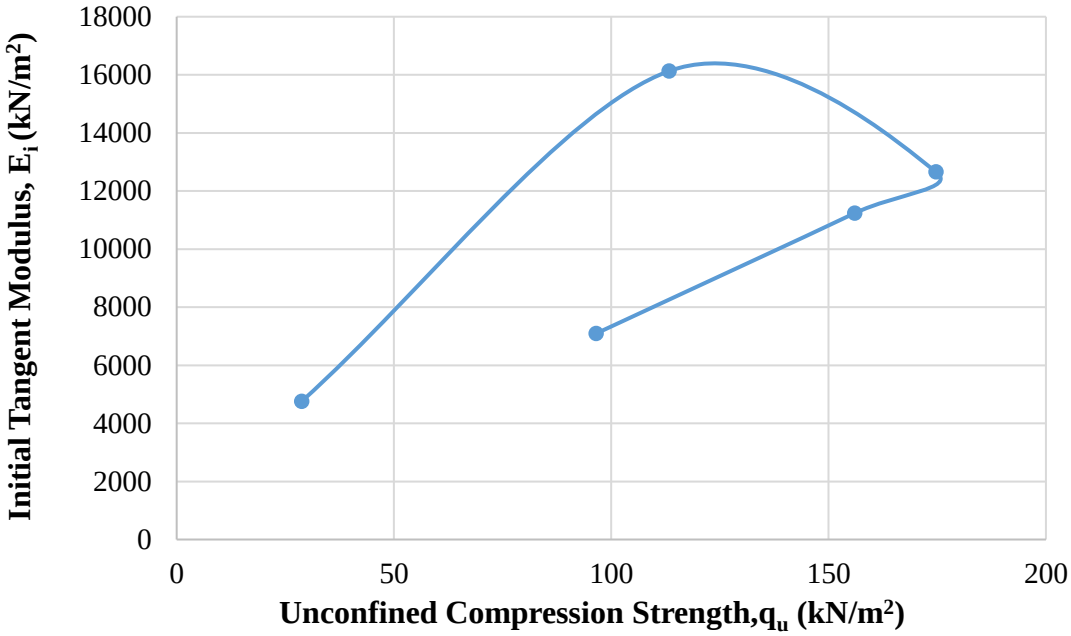

Figure 6.10 Relationship between initial tangent modulus and unconfined compression strength (CH)

According to data, the maximum initial tangent modulus is obtained in sample 4 as 16129 kN/m^2 for high plasticity clay. It should be noted that the water content is 30%, the dry unit weight is 14.5 kN/m^3, and the unconfined compression strength is 113.3 kN/m^2 when the initial tangent modulus is the maximum value for high plasticity clay.

In addition, the relationship between secant modulus at 50% of maximum stress (E_{s50}) and unconfined compression strength of high plasticity clay samples is shown in Figure 6.11.

The maximum secant modulus at 50% of maximum stress is obtained in sample 4 as 9939.1 kN/m^2 for high plasticity clay. It should be noted that the water content is 30%, the dry unit weight is 14.5 kN/m^3, and the unconfined compression strength is

113.3 kN/m^2 when the secant modulus at 50% of maximum stress is the maximum value for high plasticity clay.

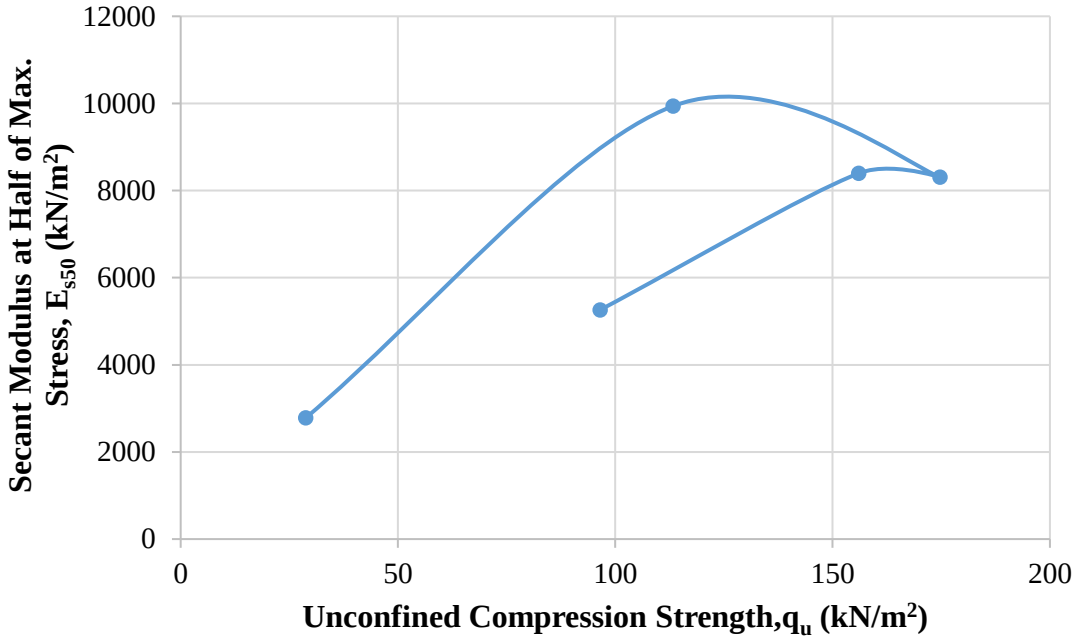

Figure 6.11 Relationship between secant modulus at 50% of maximum stress and unconfined compression strength (CH)

With respect to the results of the initial tangent modulus and secant modulus at 50% of maximum stress, it seems that the maximum values of these moduli are not obtained at maximum unconfined compression strength (sample 3 for high plasticity clay) since the beginning of the stress-strain curve of sample 4 has rapidly increased in axial stress. That increase can be related to the compaction in sample 4 for high plasticity clay.

On the other hand, the relationship between tangent modulus at 50% of maximum stress (E_{t50}) and secant modulus at failure point (E_{sf}) with the unconfined compression strength of high plasticity clay samples is shown in Figures 6.12, and 6.13.

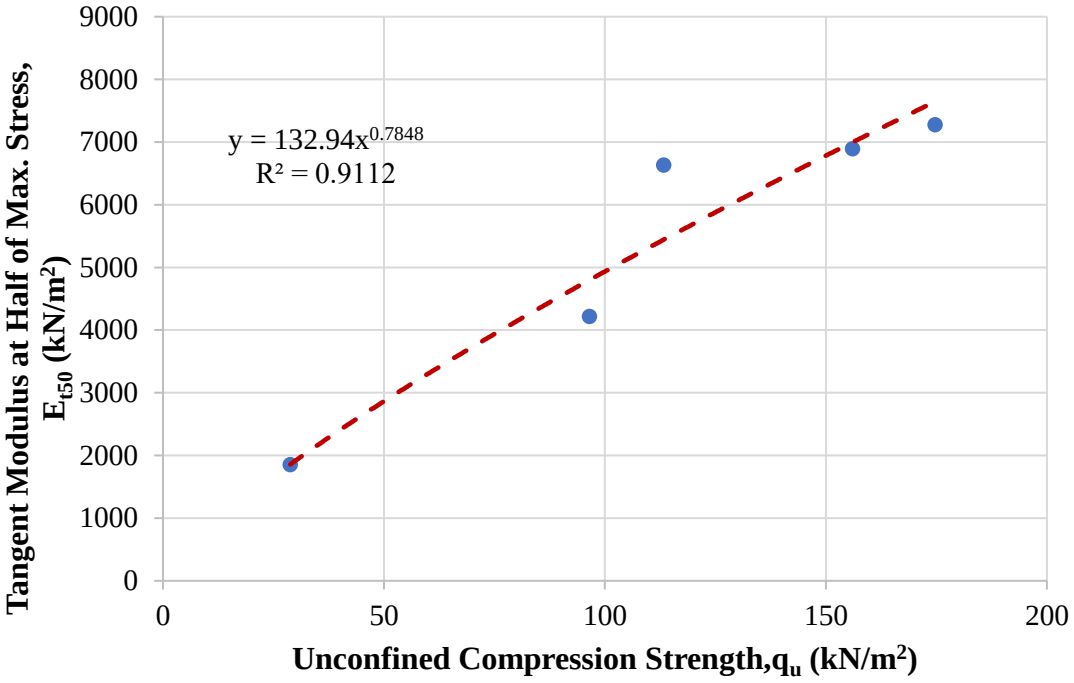

Figure 6.12 Relationship between tangent modulus at 50% of maximum stress and unconfined compression strength (CH)

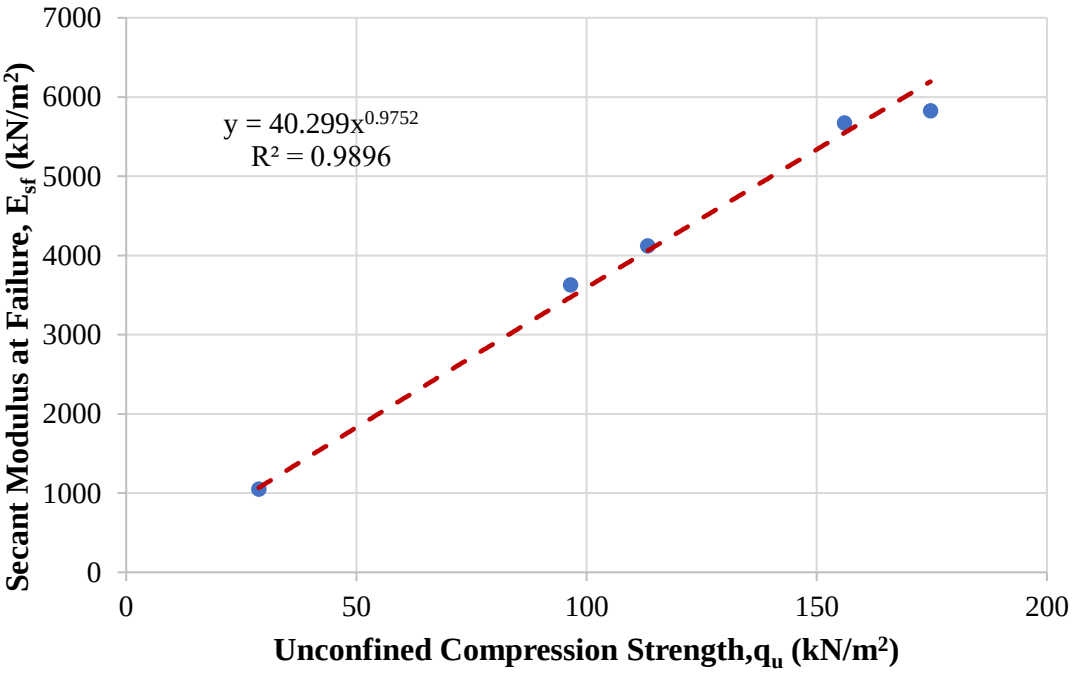

Figure 6.13 Relationship between secant modulus at failure point and unconfined compression strength (CH)

Maximum tangent modulus at 50% of maximum stress, and the maximum secant modulus at failure are found in sample 3 for high plasticity clay as 7277.1 kN/m^2 and 5823.3 kN/m^2, respectively. When the tangent modulus at 50% of maximum stress (E_{t50}) and secant modulus at failure point (E_{sf}) have the maximum value for high plasticity clay, the water content is equal to the optimum water content (w_{opt}=27%), the dry unit weight is equal to the maximum dry unit weight (γ_{dmax}=15 kN/m^3), and the unconfined compression strength is equal to the maximum unconfined compression strength (174.7 kN/m^2).

6.2 Fly Ash Mixtures with High Plasticity Clay Soil

Class C fly ash used in tests was obtained from the Çayırhan power station in Ankara, Turkey. Three different amounts of fly ash (5%, 10%, and 15%) were added to the high plasticity clay to study the effects of mixing fly ash with designated soil. In addition, the amounts of fly ash compared to whole mixtures in terms of soil moduli, the unconfined compression strength, and relationships in these engineering parameters. In other words, the amount of soil improvement of high plasticity clay was examined with added fly ash.

6.2.1 High Plasticity Clay Soil Mixture with 5% of Fly Ash

During the experimental program of this study, the amount of 5% fly ash mixed with high plasticity clay soil was used. The compaction and the unconfined compression tests were performed on the 5% fly ash mixed with high plasticity clay soil, and the outcomes of these experiments are illustrated in Table 6.5. With respect to data obtained from mentioned tests, it can be seen that the value of ω_{opt} and γ_{dmax} obtained as 24.3% and 15.60 kN/m^3, respectively.

The axial stress-axial strain curves of six different 5% fly ash-added high plasticity clay samples are shown in Figure 6.14. According to data obtained from the unconfined compression test of 5% fly ash-added high plasticity clay samples, it can be inferred that the maximum unconfined compression strength was obtained in the second sample of high plasticity clay, and it was obtained as 313.9 kN/m^2.

Table 6.5 Results of experiments executed with CH+5% fly ash

Sample No.	ω (%)	γ_d (kN/m^3)	q_u (kN/m^2)
1	18	14.30	164.5
2	22	15.16	313.9
3	25	15.55	292.3
4	27	15.30	229.2
5	30	14.76	138.6
6	33	13.67	74.9

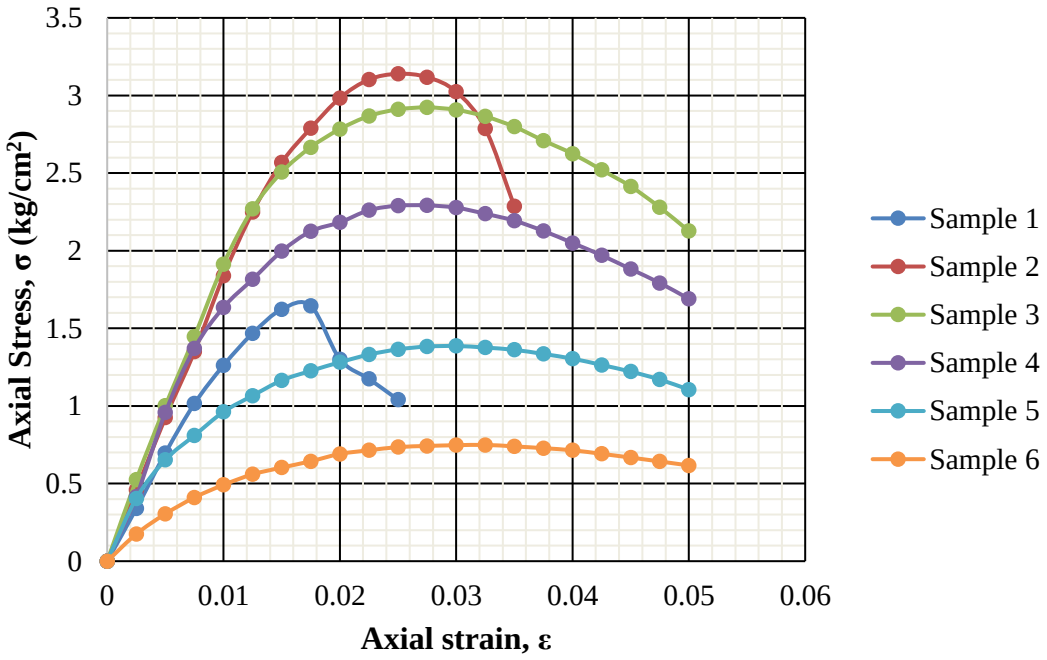

Figure 6.14 Results of unconfined compression tests of CH+5% fly ash

It should be noted that the reciprocal of the initial tangent modulus (a) and reciprocal of the asymptotic value of stress difference (b) were received from transformed hyperbolic stress-strain curves of 5% fly ash-added high plasticity clay samples. In addition, the asymptotic value of stress difference $(\sigma_1)_{ult}$, compressive strength $(\sigma_1)_f$, axial strain value at failure (ε_f), and axial strain value at 50% of maximum stress (ε_{50}) were obtained from unconfined compression test results. Lastly, the failure ratio (R_f) was calculated from unconfined compression test results. Mentioned engineering parameters to get soil moduli are given in Table 6.6.

Table 6.6 Calculated engineering parameters of CH+5% fly ash

Sample No.	a (cm^2/kg)	b (cm^2/kg)	$(\sigma_1)_{ult}$ (kg/cm^2)	$(\sigma_1)_f$ (kg/cm^2)	R_f -	ε_f -	ε_{50} -
1	0.0062	0.2151	4.649	1.645	0.35	0.0175	0.0060
2	0.0047	0.107	9.346	3.139	0.34	0.0250	0.0086
3	0.0037	0.1839	5.438	2.923	0.54	0.0275	0.0076
4	0.0039	0.2676	3.737	2.292	0.61	0.0275	0.0061
5	0.0049	0.5443	1.837	1.386	0.75	0.0300	0.0056
6	0.0110	0.9491	1.054	0.749	0.71	0.0325	0.0067

It should be noted that the strain level of 5% fly ash-added high plasticity clay is classified as small strain (SS) because the maximum axial strain was determined in samples 3, 4, 5, and 6 of 5% fly ash-added high plasticity clay. The maximum axial strain was received as 0.05%. Thus, it can be concluded that nonlinear behaviour was observed for the tested 5% fly ash-added high plasticity clay soil samples.

Initial tangent modulus (E_i), tangent modulus at 50% of maximum stress (E_{t50}), secant modulus at failure (E_{sf}), secant modulus at 50% of maximum stress (E_{s50}), and unconfined compression strength (q_u) of six different 5% fly ash-added high plasticity clay samples are given in Table 6.7.

Table 6.7 Soil moduli and unconfined compression strength of CH+5% fly ash

Sample No.	E_i (kN/m^2)	E_{t50} (kN/m^2)	E_{sf} (kN/m^2)	E_{s50} (kN/m^2)	q_u (kN/m^2)
1	16129.0	10926.8	9400.0	13728.1	164.5
2	21276.6	14730.4	12556.0	18203.0	313.9
3	27027.0	14451.3	10629.1	19287.1	292.3
4	25641.0	12325.8	8334.5	18660.5	229.2
5	20408.2	7915.9	4620.0	12293.9	138.6
6	9090.9	3776.9	2304.6	5627.5	74.9

According to the data obtained, it can be concluded that the maximum modulus values are observed in the initial tangent modulus compared with other soil moduli in all six 5% fly ash-added high plasticity clay samples due to the initial slope of the stress-strain curve. In other words, the axial stress begins rapidly increase up to a certain point.

On the other hand, transformed hyperbolic stress-strain curves for six different 5% fly ash-added high plasticity clay samples are illustrated in Figures 6.15, 6.16, 6.17, 6.18, 6.19, and 6.20.

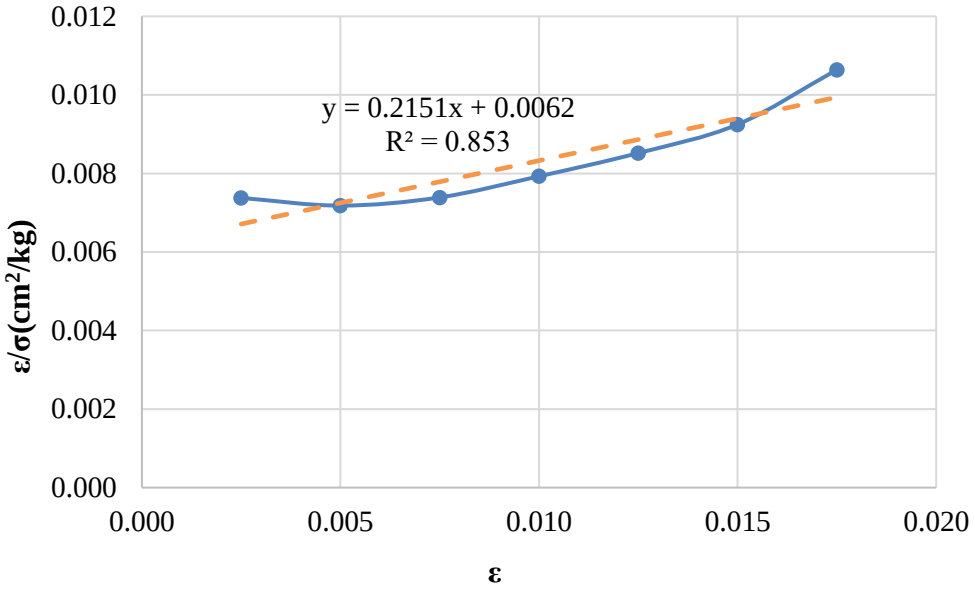

Figure 6.15 Transformed hyperbolic stress-strain curve for sample 1 (CH+5% Fly Ash)

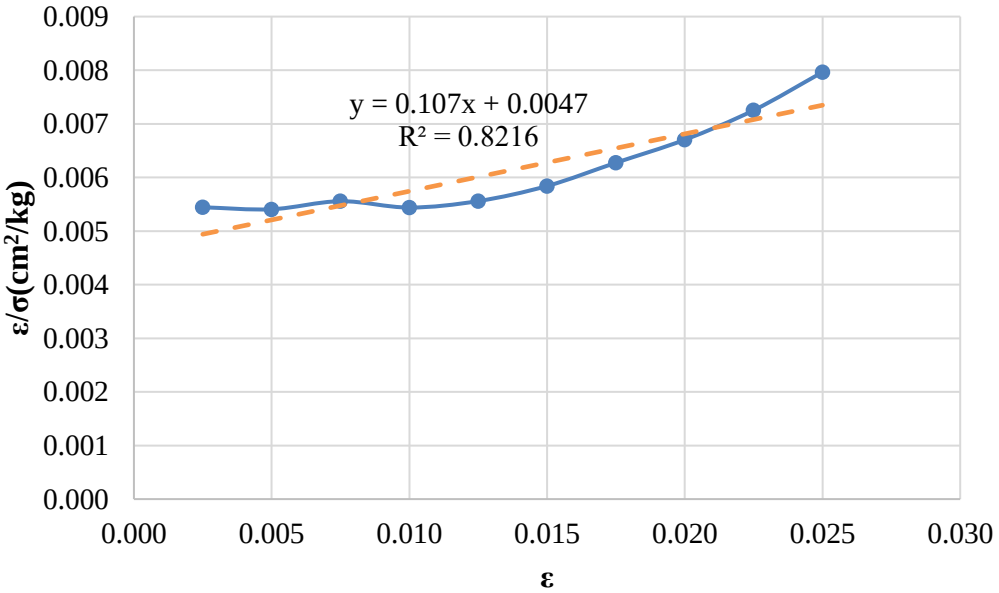

Figure 6.16 Transformed hyperbolic stress-strain curve for sample 2 (CH+5% Fly Ash)

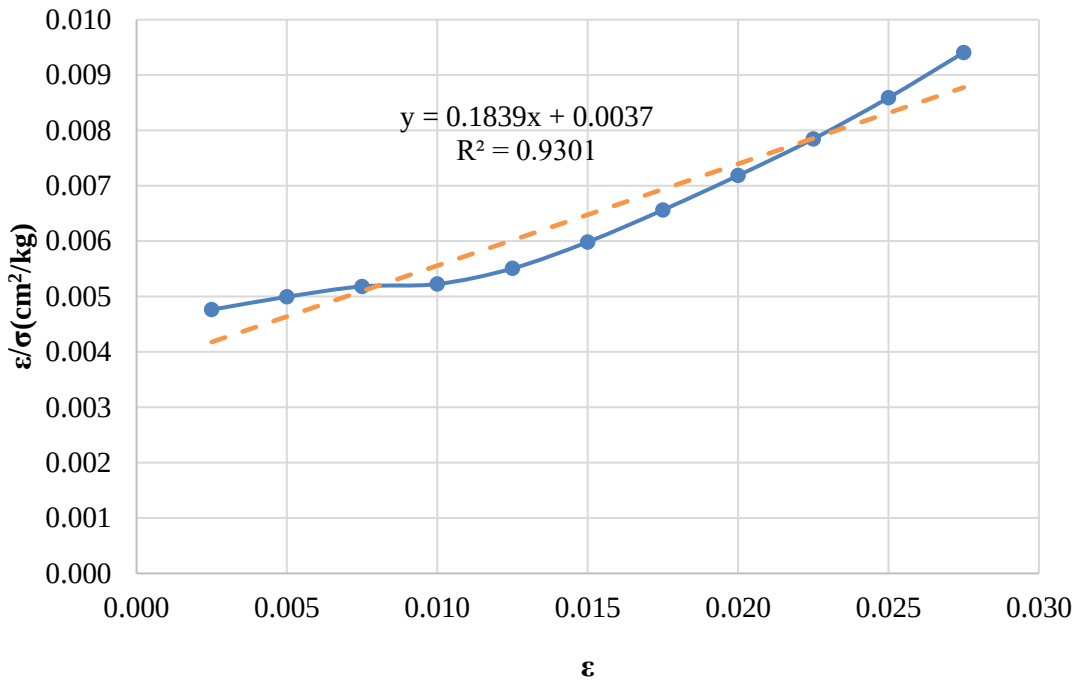

Figure 6.17 Transformed hyperbolic stress-strain curve for sample 3 (CH+5% Fly Ash)

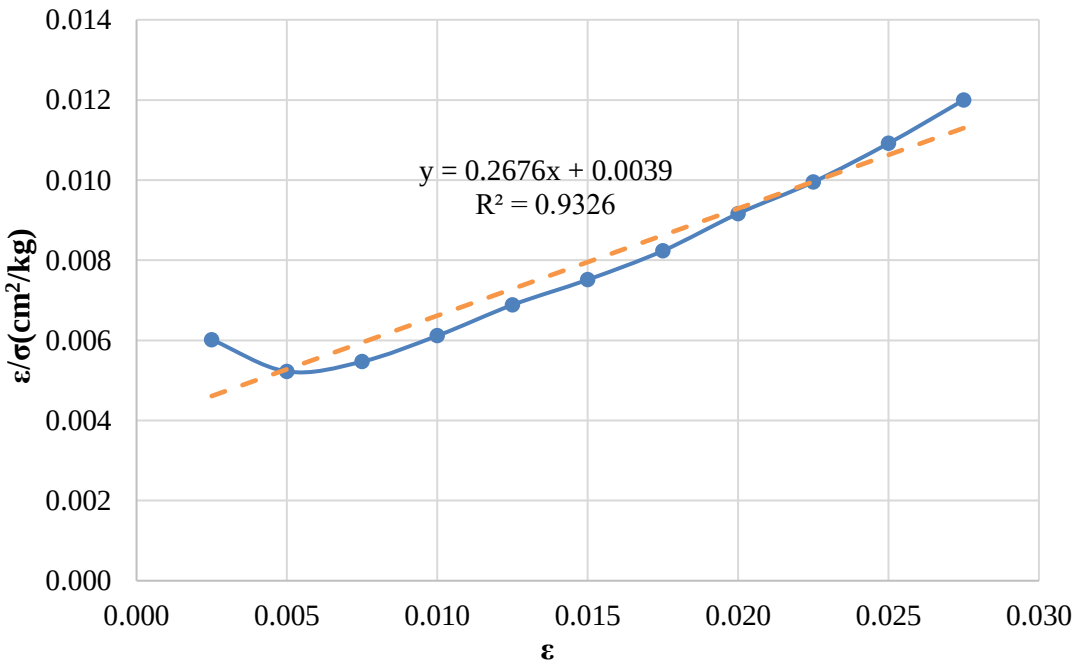

Figure 6.18 Transformed hyperbolic stress-strain curve for sample 4 (CH+5% Fly Ash)

According to data obtained from Figures 6.15, 6.16, 6.17, and 6.18, it was found that low and high values of axial strains in samples 1, 2, 3, and 4 are not precisely hyperbolic. In other words, these points can not be fitted in a straight line. However, it was possible to estimate the actual stress-strain curves by a hyperbola. Thus, it is found to have a reasonable degree of accuracy.

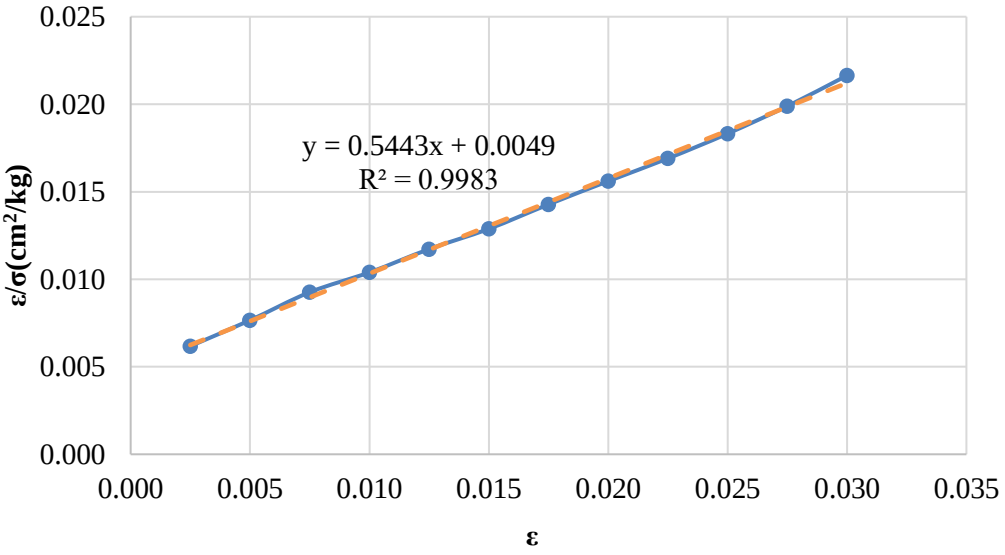

Figure 6.19 Transformed hyperbolic stress-strain curve for sample 5 (CH+5% Fly Ash)

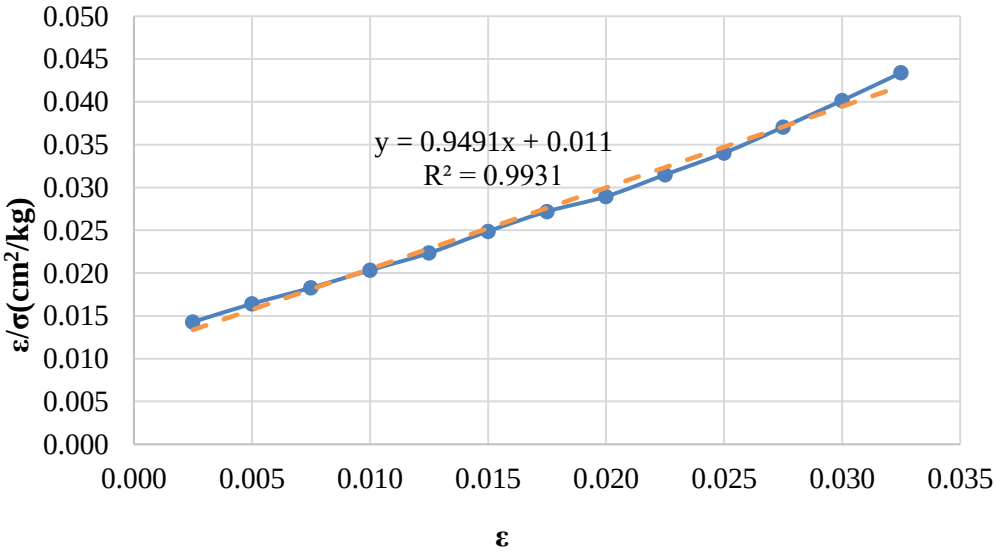

Figure 6.20 Transformed hyperbolic stress-strain curve for sample 6 (CH+5% Fly Ash)

On the other hand, transformed hyperbolic stress-strain curves in samples 5 and 6 showed hyperbolic behavior, as shown in Figures 6.19 and 6.20. In other words, these points can be best-fitted in a straight line.

On the other hand, the relationship between the secant modulus at 50% of maximum stress (E_{s50}) and the initial tangent modulus (E_i) of 5% fly ash-added high plasticity clay samples is shown in Figure 6.21.

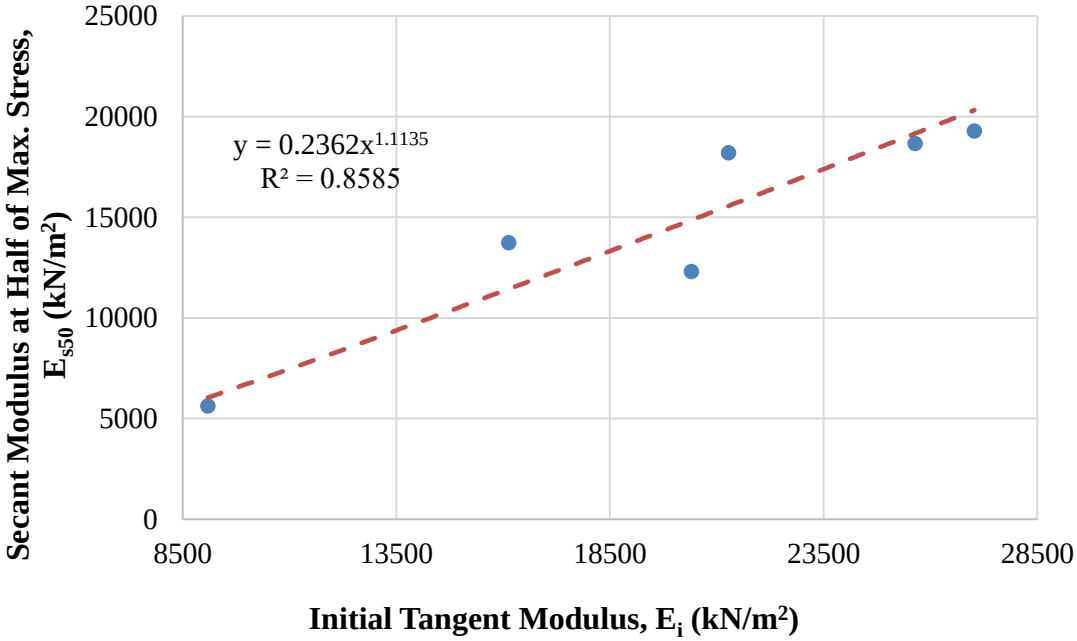

Figure 6.21 Relationship between secant modulus at 50% of maximum stress and initial tangent modulus (CH+5% Fly Ash)

According to the data, it can be inferred that the initial tangent modulus increases with the secant modulus at 50% of maximum stress. Thus, it was best suited for estimating these soil moduli by a power model. Furthermore, these soil moduli refer to the hardening of 5% fly ash-added high plasticity clay samples.

In addition, the relationship between the secant modulus at failure (E_{sf}) and the tangent modulus at 50% of maximum stress (E_{t50}) of 5% fly ash-added high plasticity clay samples are shown in Figure 6.22.

The tangent modulus at 50% of maximum stress increases with the secant modulus at failure. Thus, it was best suited for estimating these soil moduli by a power model.

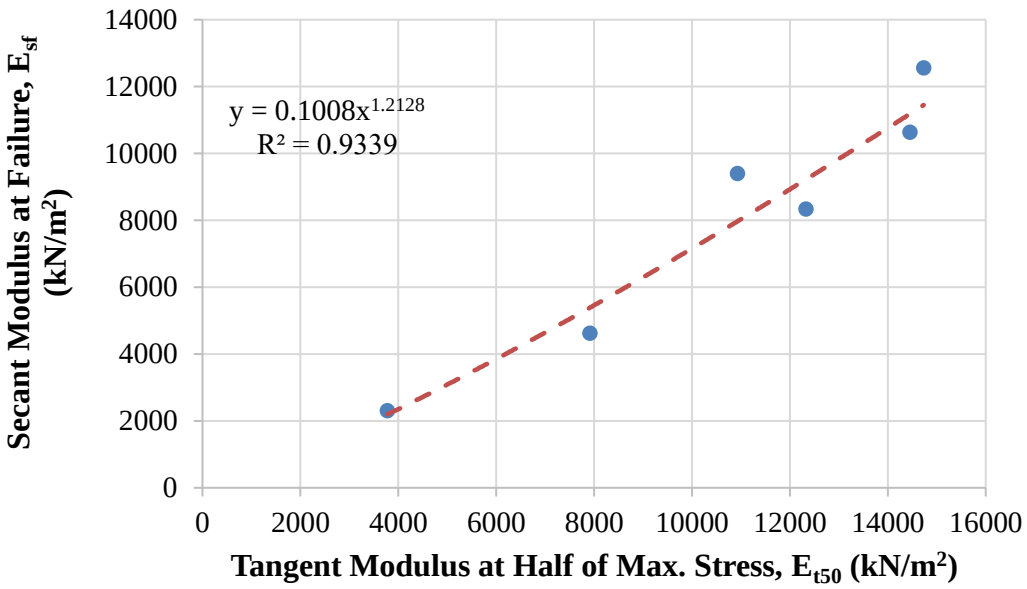

Figure 6.22 Relationship between secant modulus at failure point and tangent modulus at 50% of maximum stress (CH+5% Fly Ash)

Furthermore, the relationship between initial tangent modulus (E_i) and unconfined compression strength of 5% fly ash-added high plasticity clay samples is shown in Figure 6.23.

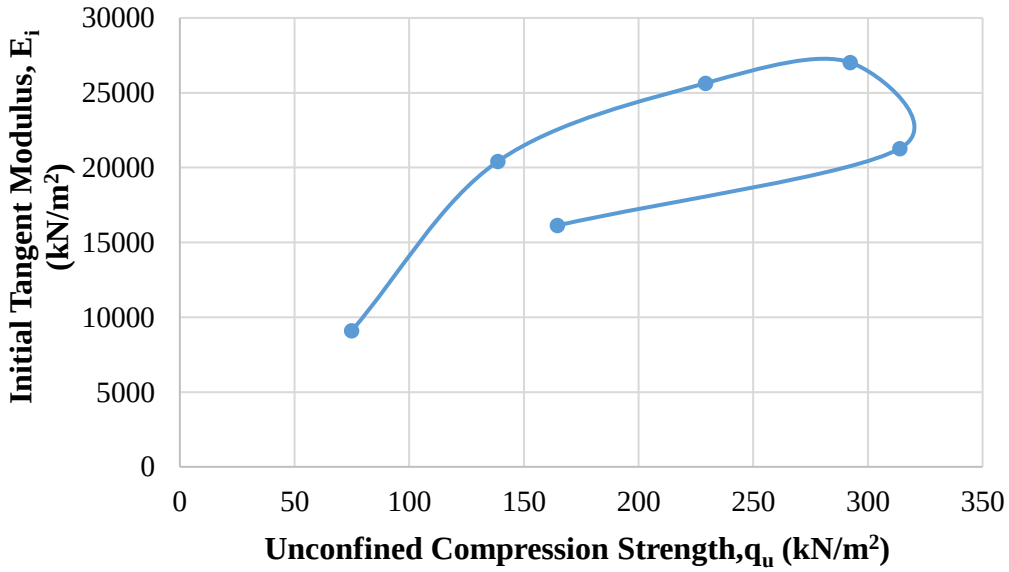

Figure 6.23 Relationship between initial tangent modulus and unconfined compression strength (CH+5% Fly Ash)

According to data, the maximum initial tangent modulus is obtained in sample 3 as 27027 kN/m^2 for 5% fly ash-added high plasticity clay. It should be noted that the water content is 25%, the dry unit weight is 15.55 kN/m^3, and the unconfined compression strength is 292.3 kN/m^2 when the initial tangent modulus is the maximum value for 5% fly ash-added high plasticity clay. When the initial tangent modulus has the maximum value for 5% fly ash-added high plasticity clay, the water content is close to the optimum water content (w_{opt}=24.3%), and the dry unit weight is relative to the maximum dry unit weight (γ_{dmax}=15.60 kN/m^3).

In addition, the relationship between secant modulus at 50% of maximum stress (E_{s50}) and unconfined compression strength of 5% fly ash-added high plasticity clay samples is shown in Figure 6.24.

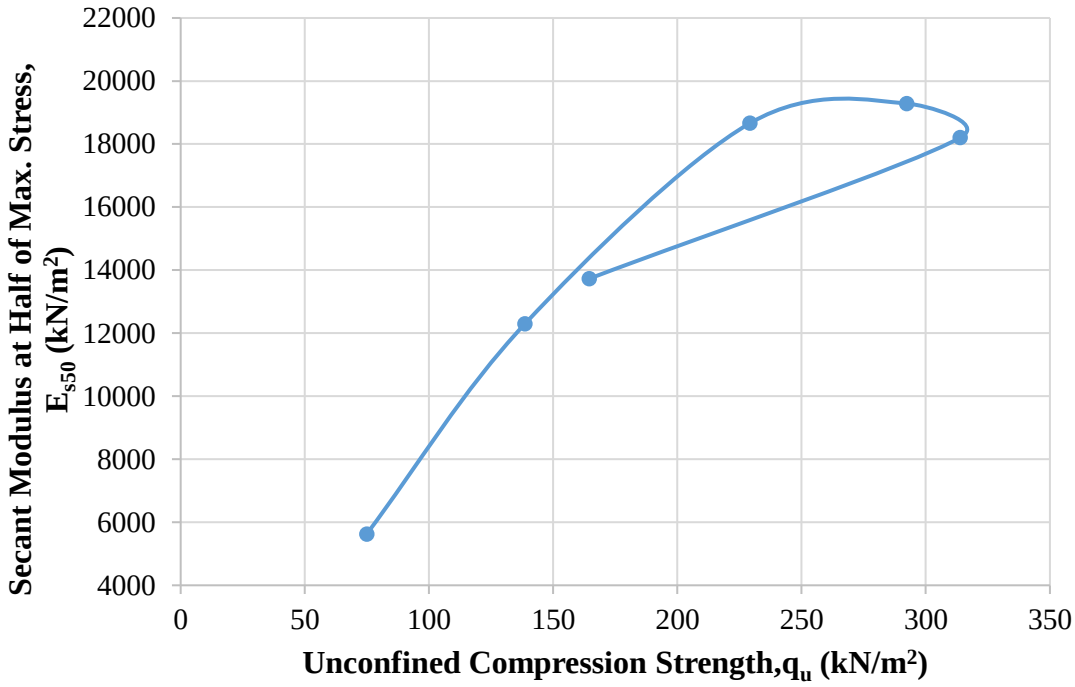

Figure 6.24 Relationship between secant modulus at 50% of maximum stress and unconfined compression strength (CH+5% Fly Ash)

The maximum secant modulus at 50% of maximum stress is obtained in sample 3 as 19287.1 kN/m^2 for 5% fly ash-added high plasticity clay. It should be noted that the water content is 25%, the dry unit weight is 15.55 kN/m^3, and the unconfined compression strength is 292.3 kN/m^2. Therefore, when the secant modulus at 50% of maximum stress has the maximum value for 5% fly ash-added high plasticity clay, the

water content is close to the optimum water content (w_{opt}=24.3%), and the dry unit weight is relative to the maximum dry unit weight (γ_{dmax}=15.60 kN/m^3).

In addition, concerning the results of the initial tangent modulus and secant modulus at 50% of maximum stress, it seems that the maximum values of these moduli are not obtained at maximum unconfined compression strength (sample 2 for 5% fly ash-added high plasticity clay) since the beginning of the stress-strain curve of sample 3 has rapidly increased in axial stress.

On the other hand, the relationship between tangent modulus at 50% of maximum stress (E_{t50}) and secant modulus at failure point (E_{sf}) with the unconfined compression strength of 5% fly ash-added high plasticity clay samples is shown in Figures 6.25, and 6.26.

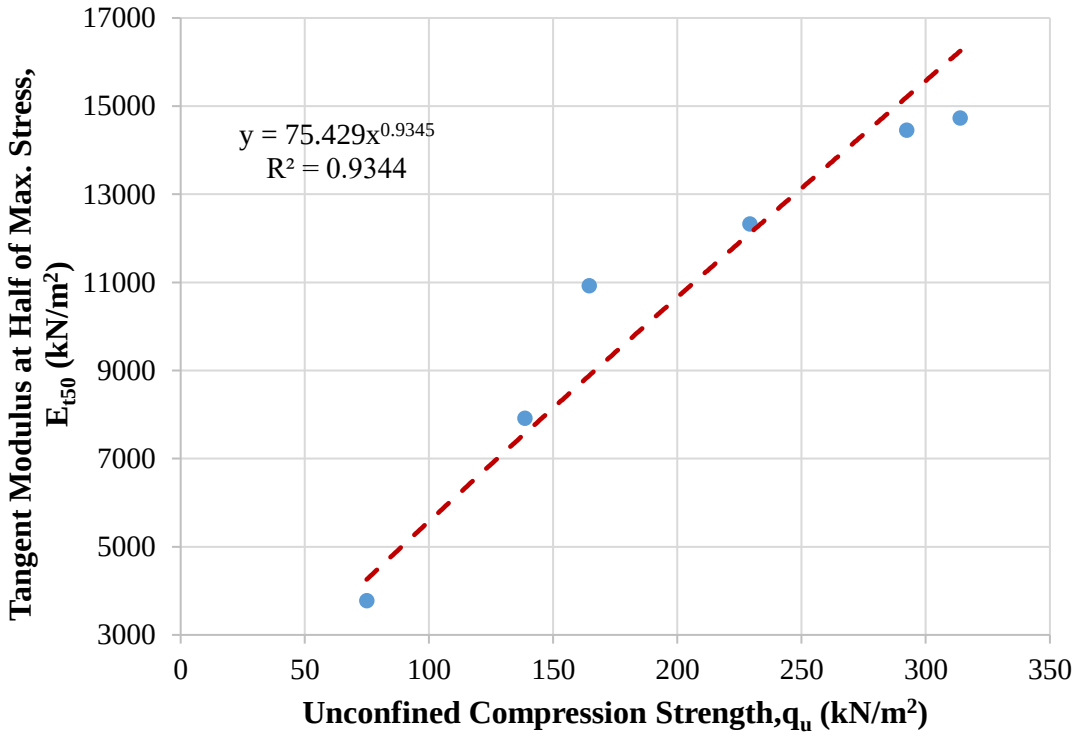

Figure 6.25 Relationship between tangent modulus at 50% of maximum stress and unconfined compression strength (CH+5% Fly Ash)

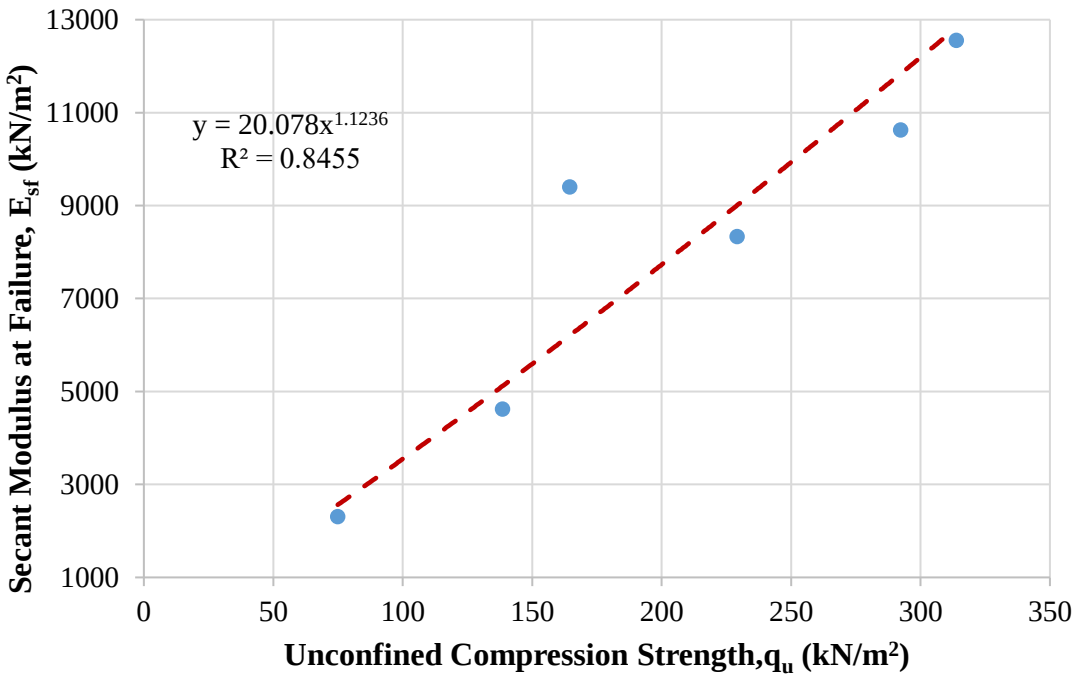

Figure 6.26 Relationship between secant modulus at failure point and unconfined compression strength (CH+5% Fly Ash)

Maximum tangent modulus at 50% of maximum stress, and the maximum secant modulus at failure are found in sample 2 for 5% fly ash-added high plasticity clay as 14730.4 kN/m^2 and 12556 kN/m^2, respectively. When the tangent modulus at 50% of maximum stress (E_{t50}) and secant modulus at failure point (E_{sf}) have the maximum values for 5% fly ash-added high plasticity clay, the water content is 22%, the dry unit weight is 15.16 kN/m^3, and the unconfined compression strength is equal to the maximum unconfined compression strength (313.9 kN/m^2). Values of water content and the dry unit weight are less than the optimum water content and the maximum dry unit weight because low water content can lead to glue effect and chemical cementation in fly ash mixed clayey soils.

6.2.2 High Plasticity Clay Soil Mixture with 10% of Fly Ash

During the experimental program of this study, the amount of 10% fly ash mixed with high plasticity clay soil was used. The compaction and the unconfined compression tests were performed on the 10% fly ash mixed with high plasticity clay soil, and the outcomes of these experiments are illustrated in Table 6.8. With respect

to data obtained from mentioned tests, it can be seen that the value of ω_{opt} and γ_{dmax} obtained at 23.7% and 15.60 kN/m^3, respectively.

Table 6.8 Results of experiments executed with CH+10% fly ash

Sample No.	ω (%)	γ_d (kN/m^3)	q_u (kN/m^2)
1	15	14.89	99.2
2	17	14.51	234.0
3	20	15.06	475.2
4	22	15.50	389.8
5	24	15.60	324.8
6	33	14.06	68.4
7	37	13.01	44.5

The axial stress-axial strain curves of seven different 10% fly ash-added high plasticity clay samples are shown as a graph in Figure 6.27. According to data obtained from the unconfined compression test of 10% fly ash mixed with high plasticity clay soil samples, it can be inferred that the maximum unconfined compression strength was obtained in the third sample, and it was obtained as 475.2 kN/m^2.

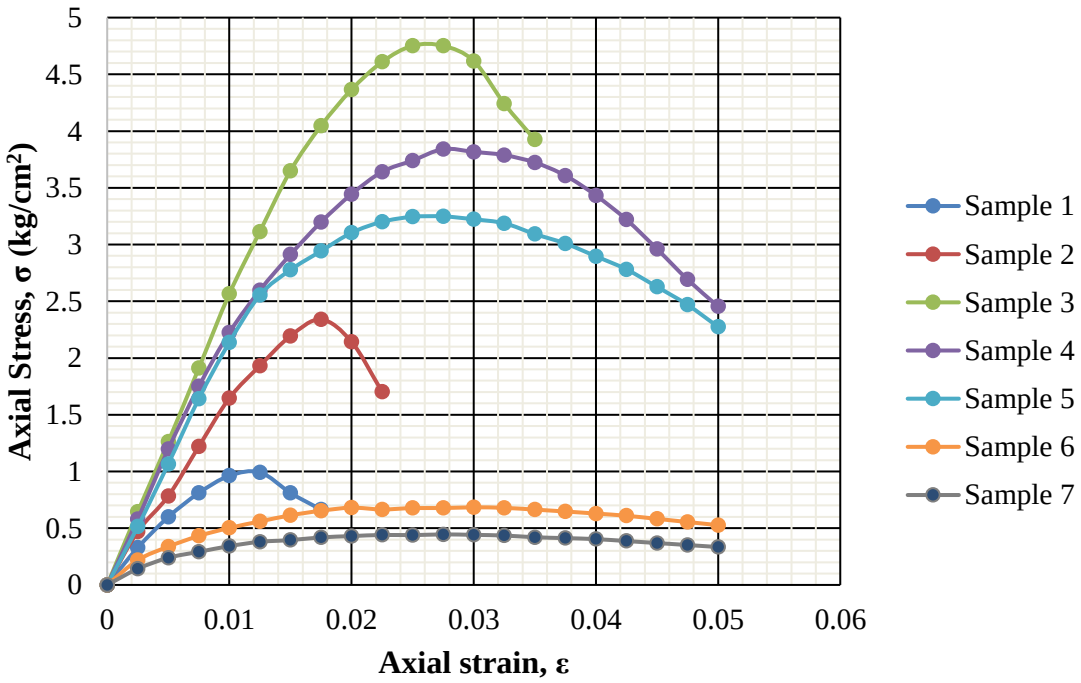

Figure 6.27 Results of unconfined compression tests of CH+10% fly ash

It should be noted that the reciprocal of the initial tangent modulus (a) and reciprocal of the asymptotic value of stress difference (b) were received from transformed hyperbolic stress-strain curves of 10% fly ash-added high plasticity clay samples. In addition, the asymptotic value of stress difference $(\sigma_1)_{ult}$, compressive strength $(\sigma_1)_f$, axial strain value at failure (ε_f), and axial strain value at 50% of maximum stress (ε_{50}) were obtained from unconfined compression test results. Lastly, the failure ratio (R_f) was calculated from unconfined compression test results. Mentioned engineering parameters are given in Table 6.9.

Table 6.9 Calculated engineering parameters of CH+10% fly ash

Sample No.	a (cm^2/kg)	b (cm^2/kg)	$(\sigma_1)_{ult}$ (kg/cm^2)	$(\sigma_1)_f$ (kg/cm^2)	R_f -	ε_f -	ε_{50} -
1	0.0060	0.4796	2.085	0.992	0.48	0.0125	0.0041
2	0.0053	0.1103	9.066	2.340	0.26	0.0175	0.0072
3	0.0034	0.0597	16.750	4.752	0.28	0.0250	0.0093
4	0.0035	0.1189	8.410	3.898	0.46	0.0275	0.0086
5	0.0036	0.1529	6.540	3.248	0.50	0.0275	0.0074
6	0.0082	1.1444	0.874	0.684	0.78	0.0300	0.0051
7	0.0120	1.7616	0.568	0.445	0.78	0.0275	0.0046

It should be noted that the strain level of 10% fly ash-added high plasticity clay is classified as small strain (SS) because the maximum axial strain was determined in samples 4, 5, 6, and 7 of 10% fly ash-added high plasticity clay. The maximum axial strain was obtained as 0.05%. Thus, it can be concluded that nonlinear behaviour was observed for the tested 10% fly ash-added high plasticity clay soil samples.

Initial tangent modulus (E_i), tangent modulus at 50% of maximum stress (E_{t50}), secant modulus at failure (E_{sf}), secant modulus at 50% of maximum stress (E_{s50}), and unconfined compression strength (q_u) of seven different 10% fly ash-added high plasticity clay samples are given in Table 6.10.

In addition, it can be concluded that the maximum modulus values are observed in the initial tangent modulus compared with other soil moduli in all seven 10% fly ash-added high plasticity clay samples since the initial slope of the stress-strain curve. In other words, the axial stress increases up to a certain point very sharply. Then, this

sharp increasing trend suddenly starts to slow down, and during this slowing trend, the axial strain increases rapidly.

Table 6.10 Soil moduli and unconfined compression strength of CH+10% fly ash

Sample No.	E_i (kN/m^2)	E_{t50} (kN/m^2)	E_{sf} (kN/m^2)	E_{s50} (kN/m^2)	q_u (kN/m^2)
1	16666.7	9680.4	7936.0	12230.1	99.2
2	18867.9	14312.3	13371.4	16218.6	234.0
3	29411.8	21659.6	19008.0	25617.8	475.2
4	28571.4	16863.7	14174.5	22788.3	389.8
5	27777.8	15695.5	11810.9	21868.9	324.8
6	12195.1	4517.2	2280.0	6664.6	68.4
7	8333.3	3081.0	1618.2	4863.7	44.5

On the other hand, transformed hyperbolic stress-strain curves for seven different 10% fly ash-added high plasticity clay samples are illustrated in Figures 6.28, 6.29, 6.30, 6.31, 6.32, 6.33, and 6.34.

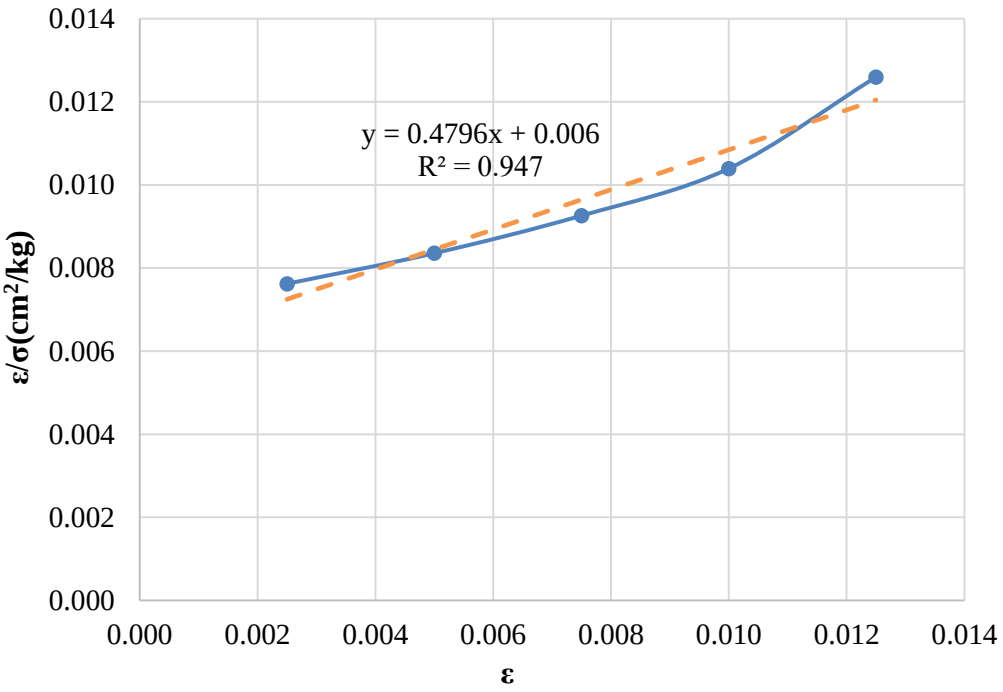

Figure 6.28 Transformed hyperbolic stress-strain curve for sample 1 (CH+10% Fly Ash)

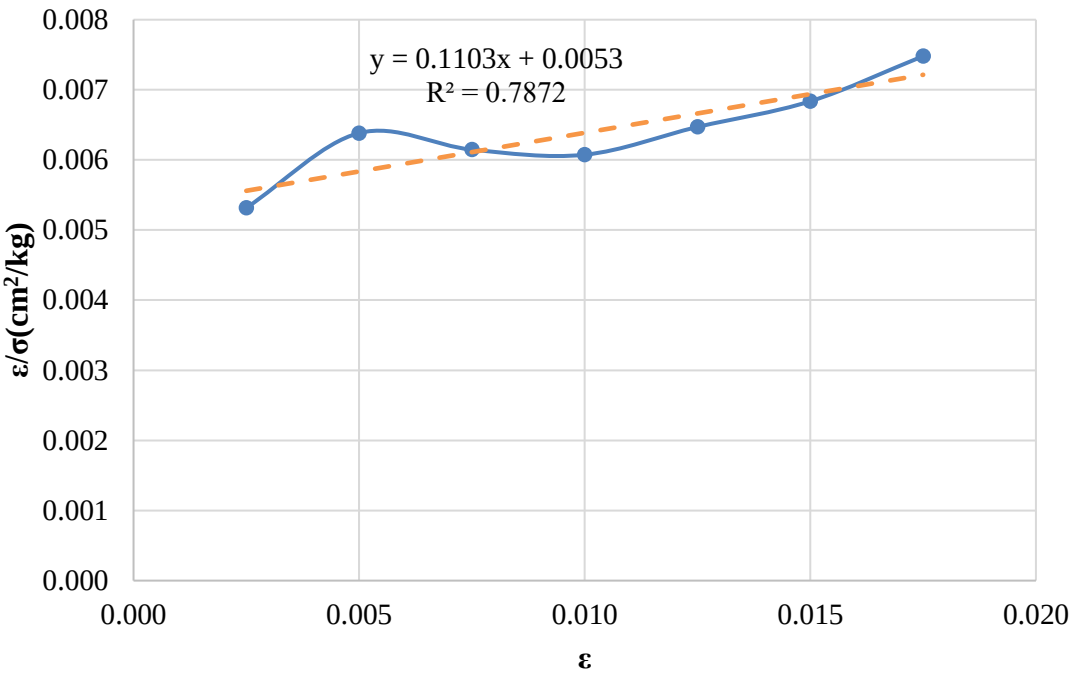

Figure 6.29 Transformed hyperbolic stress-strain curve for sample 2 (CH+10% Fly Ash)

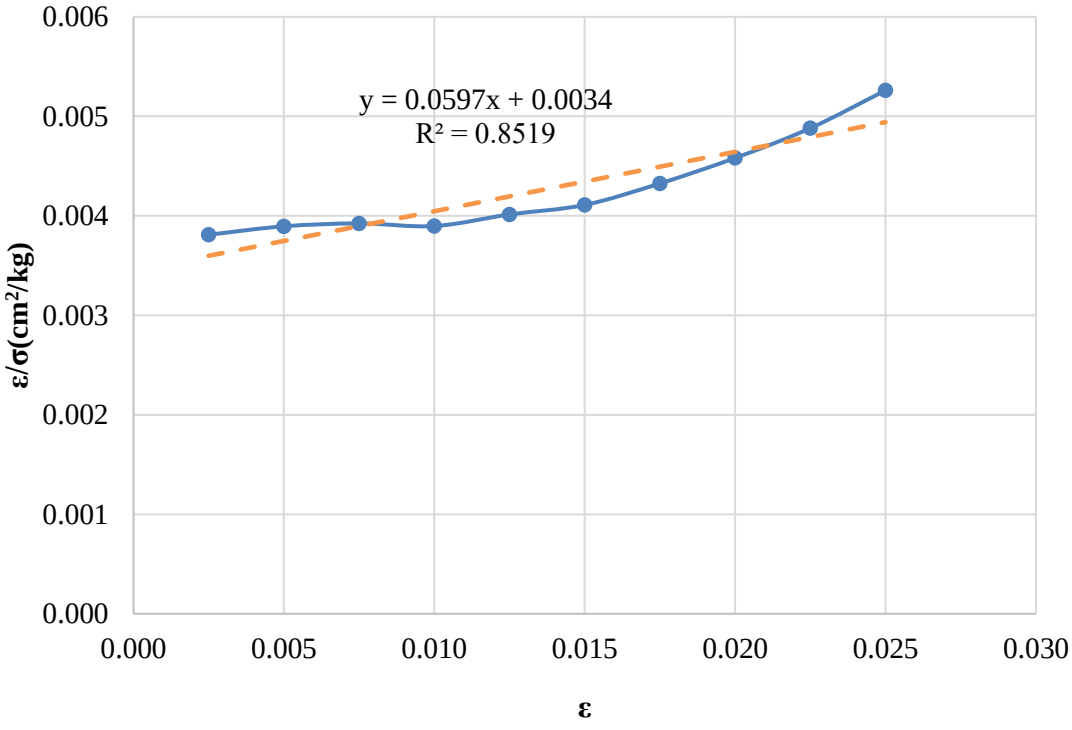

Figure 6.30 Transformed hyperbolic stress-strain curve for sample 3 (CH+10% Fly Ash)

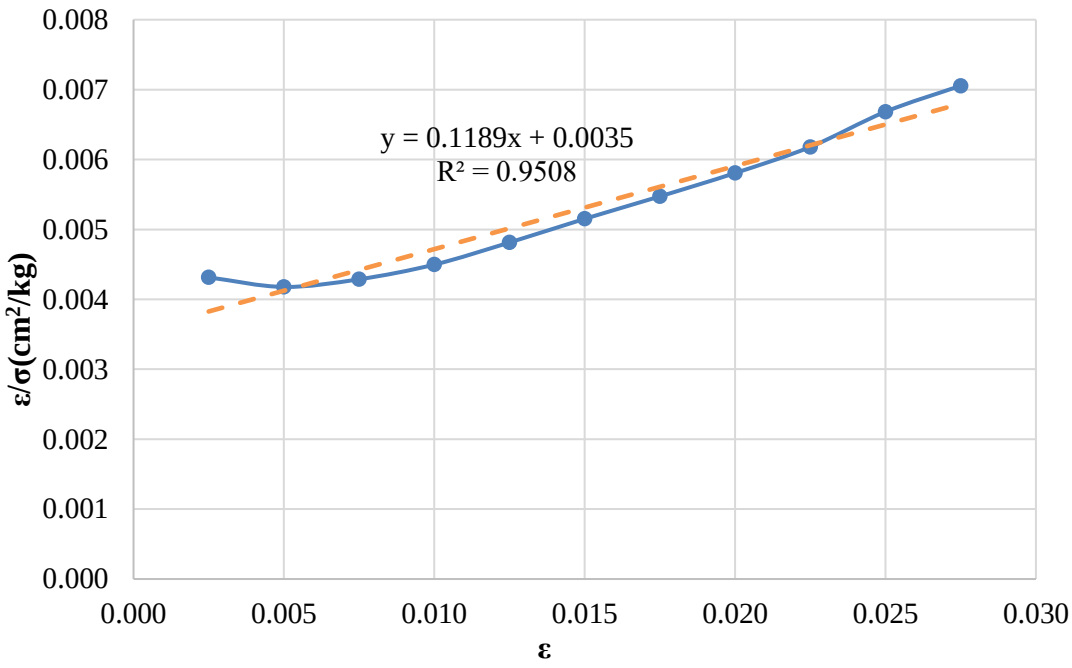

Figure 6.31 Transformed hyperbolic stress-strain curve for sample 4 (CH+10% Fly Ash)

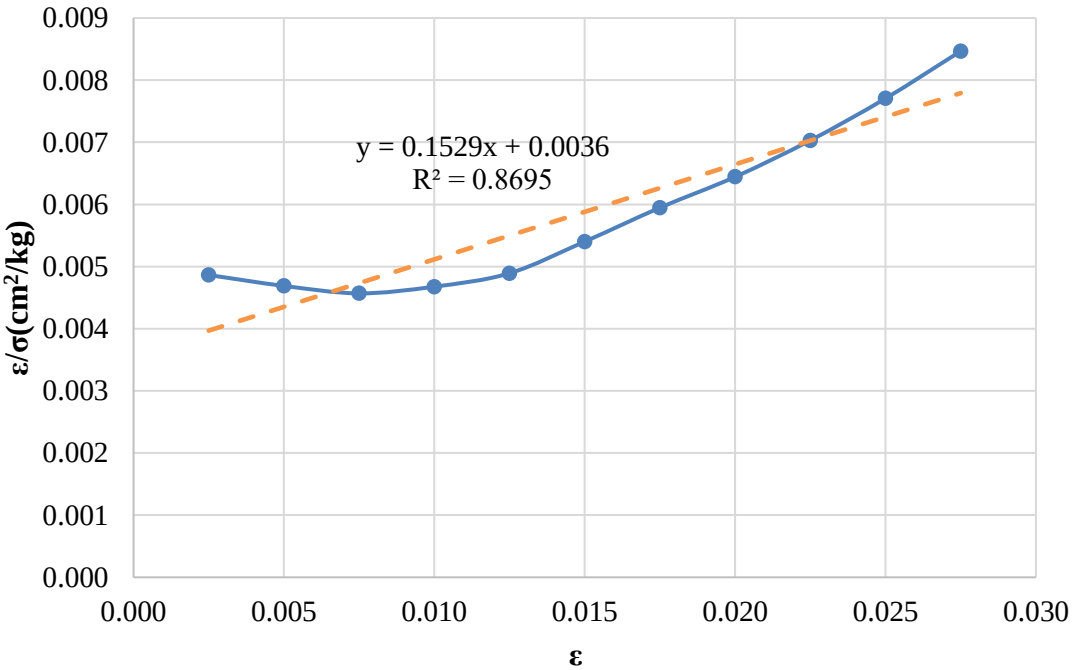

Figure 6.32 Transformed hyperbolic stress-strain curve for sample 5 (CH+10% Fly Ash)

It was found that low and high values of axial strains in samples 1, 2, 3, 4, and 5 are not precisely hyperbolic, as shown in Figures 6.28, 6.29, 6.30, 6.31, and 6.32. In other words, these points can not be fitted in a straight line. On the other hand, it was possible to estimate the actual stress-strain curves by a hyperbola. Therefore, it is found to have a reasonable degree of accuracy.

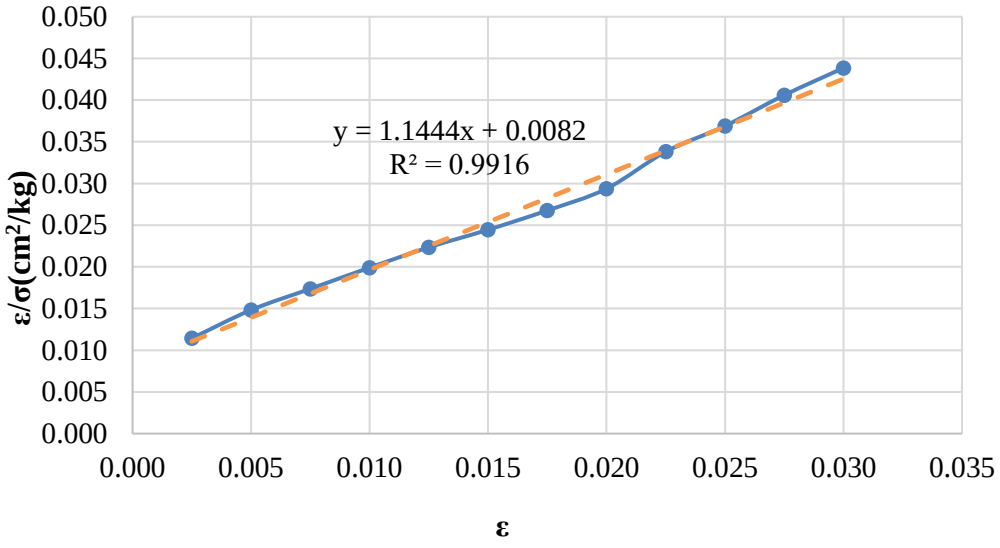

Figure 6.33 Transformed hyperbolic stress-strain curve for sample 6 (CH+10% Fly Ash)

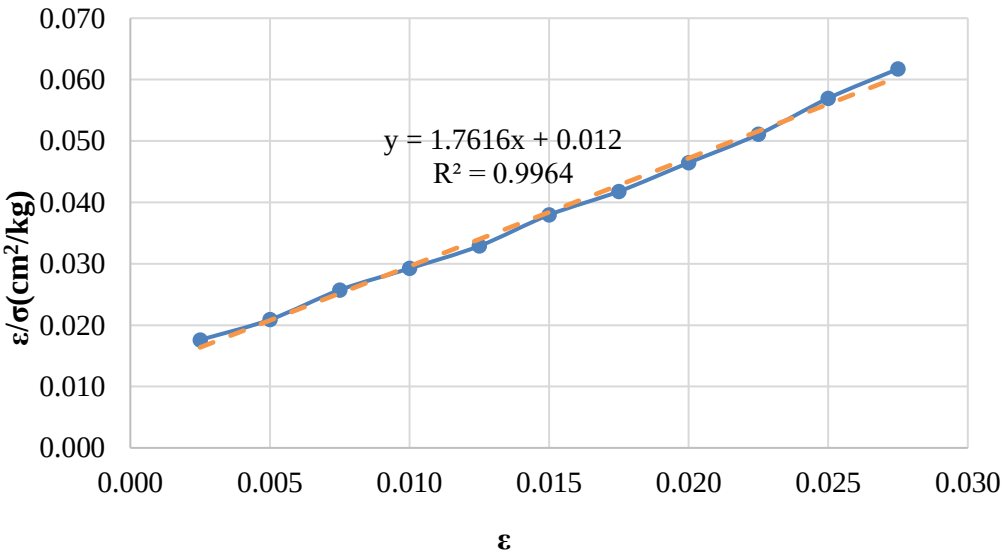

Figure 6.34 Transformed hyperbolic stress-strain curve for sample 7 (CH+10% Fly Ash)

Transformed hyperbolic stress-strain curves in samples 6 and 7 showed hyperbolic behavior, as shown in Figures 6.33 and 6.34. In other words, these points can be best-fitted in a straight line.

On the other hand, the relationship between the secant modulus at 50% of maximum stress (E_{s50}) and the initial tangent modulus (E_i) of 10% fly ash-added high plasticity clay samples is shown in Figure 6.35.

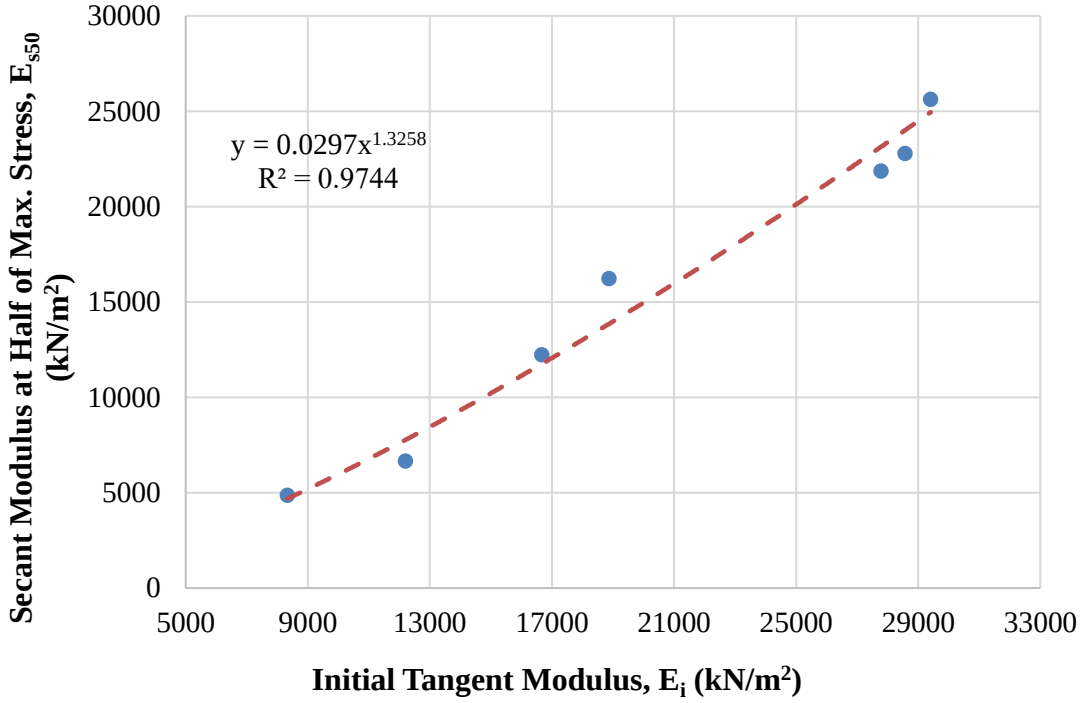

Figure 6.35 Relationship between secant modulus at 50% of maximum stress and initial tangent modulus (CH+10% Fly Ash)

It can be inferred that these soil moduli can be related to the hardening of 10% fly ash-added high plasticity clay samples. Thus, the initial tangent modulus increases with increasing the secant modulus at 50% of maximum stress. Furthermore, it was best suited for estimating these soil moduli by a power model.

Furthermore, the relationship between the secant modulus at failure (E_{sf}) and the tangent modulus at 50% of maximum stress (E_{t50}) of 10% fly ash-added high plasticity clay samples are shown in Figure 6.36.

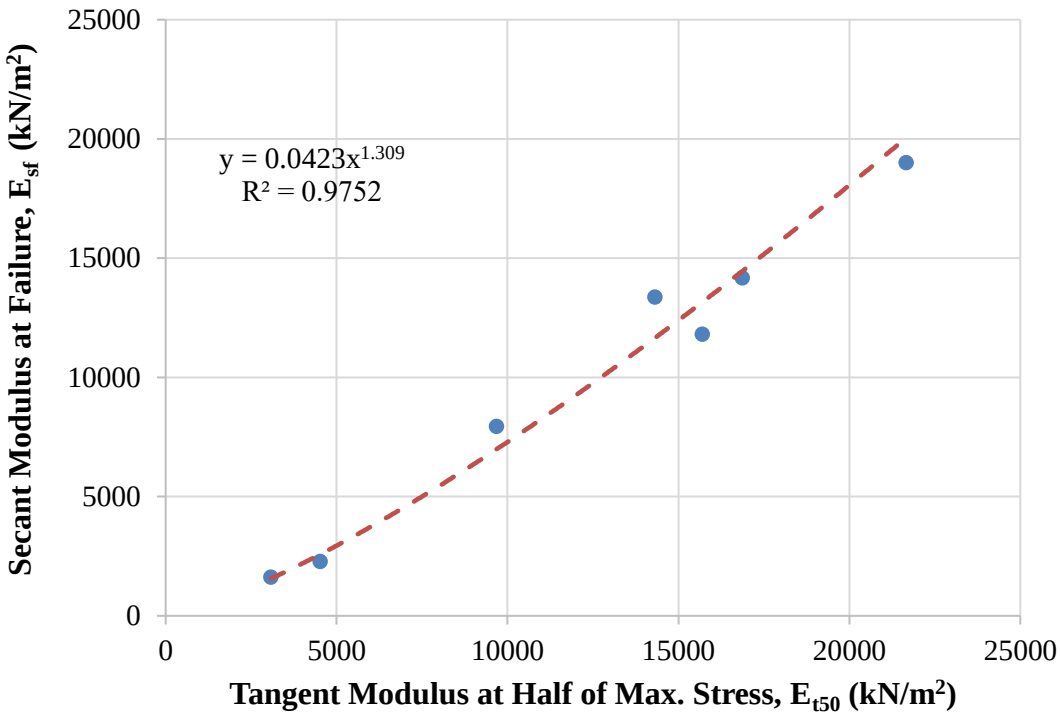

Figure 6.36 Relationship between secant modulus at failure point and tangent modulus at 50% of maximum stress (CH+10% Fly Ash)

The tangent modulus at 50% of maximum stress increases with increasing secant modulus at failure. Thus, it was best suited for estimating these soil moduli by a power model.

In addition, the relationship between initial tangent modulus (E_i) and unconfined compression strength of 10% fly ash-added high plasticity clay samples is shown in Figure 6.37.

According to data, the maximum initial tangent modulus is obtained in sample 3 as 29411.8 kN/m^2 for 10% fly ash-added high plasticity clay. It should be noted that the water content is 20%, the dry unit weight is 15.06 kN/m^3, and the unconfined compression strength is 475.2 kN/m^2 when the initial tangent modulus is the maximum value for 10% fly ash-added high plasticity clay.

In addition, the relationship between secant modulus at 50% of maximum stress (E_{s50}) and unconfined compression strength of 10% fly ash-added high plasticity clay samples is shown in Figure 6.38.

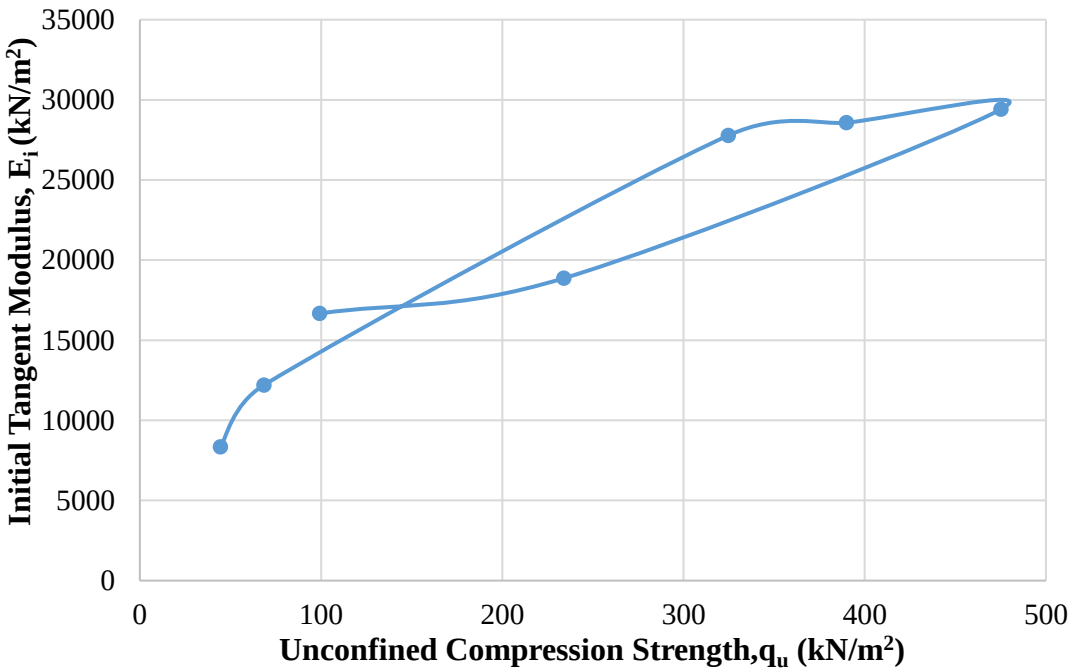

Figure 6.37 Relationship between initial tangent modulus and unconfined compression strength (CH+10% Fly Ash)

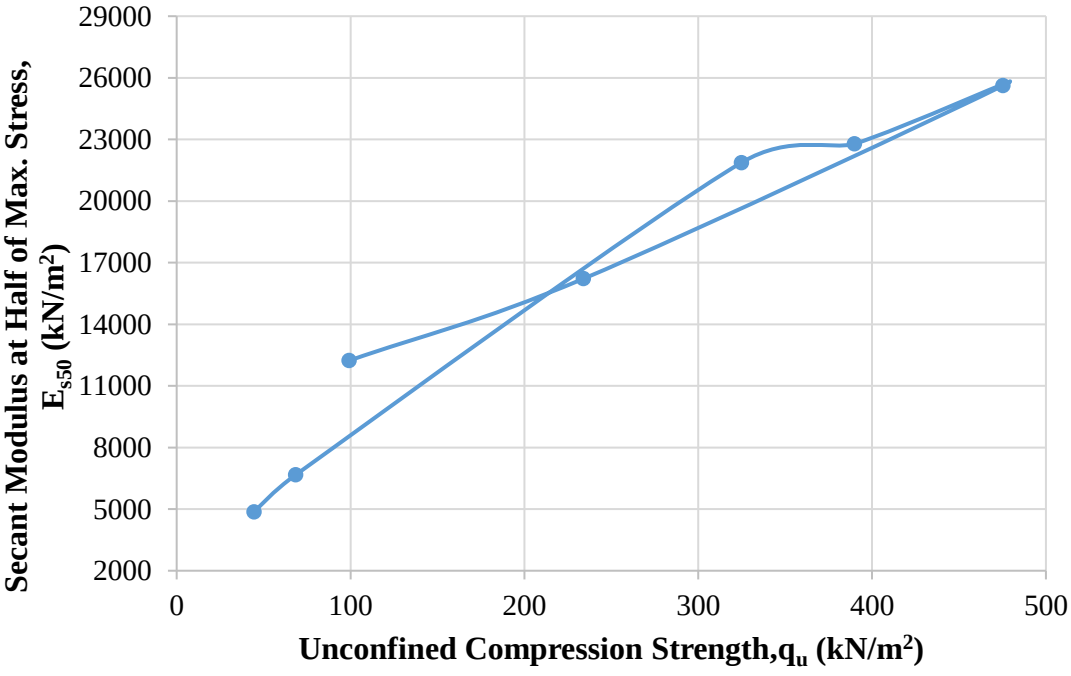

Figure 6.38 Relationship between secant modulus at 50% of maximum stress and unconfined compression strength (CH+10% Fly Ash)

The maximum secant modulus at 50% of maximum stress is obtained in sample 3 as 25617.8 kN/m^2 for 10% fly ash-added high plasticity clay. It should be noted that the water content is 20%, the dry unit weight is 15.06 kN/m^3, and the unconfined compression strength is 475.2 kN/m^2 when the secant modulus at 50% of maximum stress is the maximum value for 10% fly ash-added high plasticity clay.

On the other hand, the relationship between tangent modulus at 50% of maximum stress (E_{t50}) and unconfined compression strength of 10% fly ash-added high plasticity clay samples is shown in Figure 6.39.

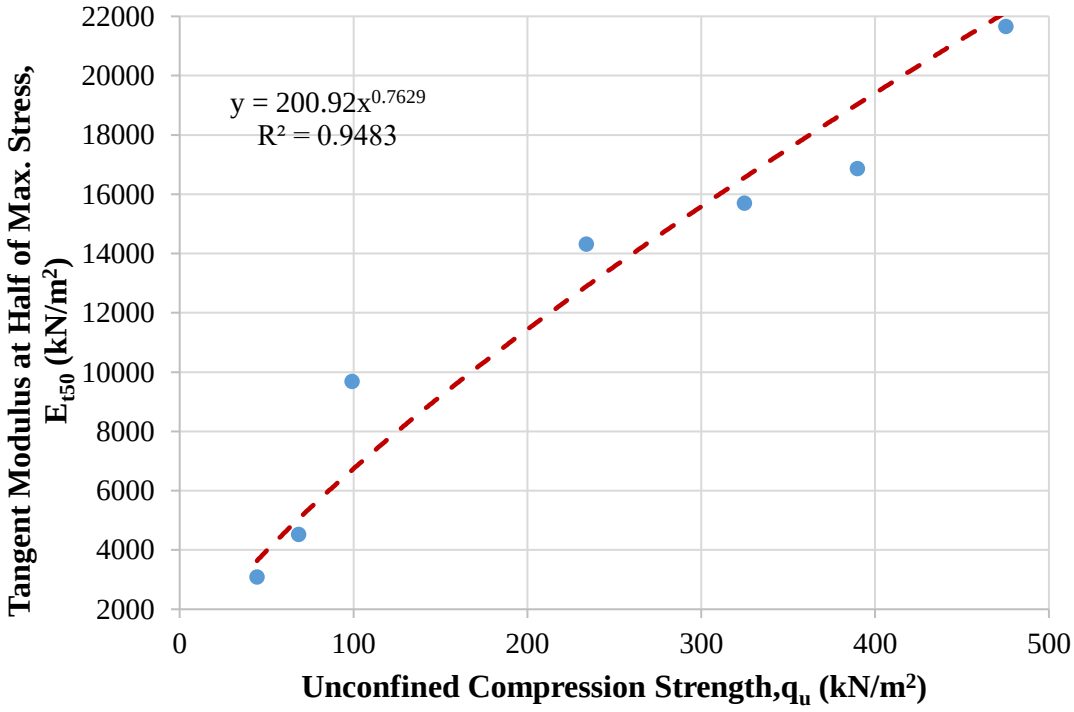

Figure 6.39 Relationship between tangent modulus at 50% of maximum stress and unconfined compression strength (CH+10% Fly Ash)

The maximum tangent modulus at 50% of maximum stress is obtained in sample 3 as 21659.6 kN/m^2 for 10% fly ash-added high plasticity clay. It should be noted that the water content is 20%, the dry unit weight is 15.06 kN/m^3, and the unconfined compression strength is 475.2 kN/m^2 when the tangent modulus at 50% of maximum stress is the maximum value for 10% fly ash-added high plasticity clay.

Furthermore, the relationship between secant modulus at failure point (E_{sf}) and unconfined compression strength of 10% fly ash-added high plasticity clay samples is shown in Figure 6.40.

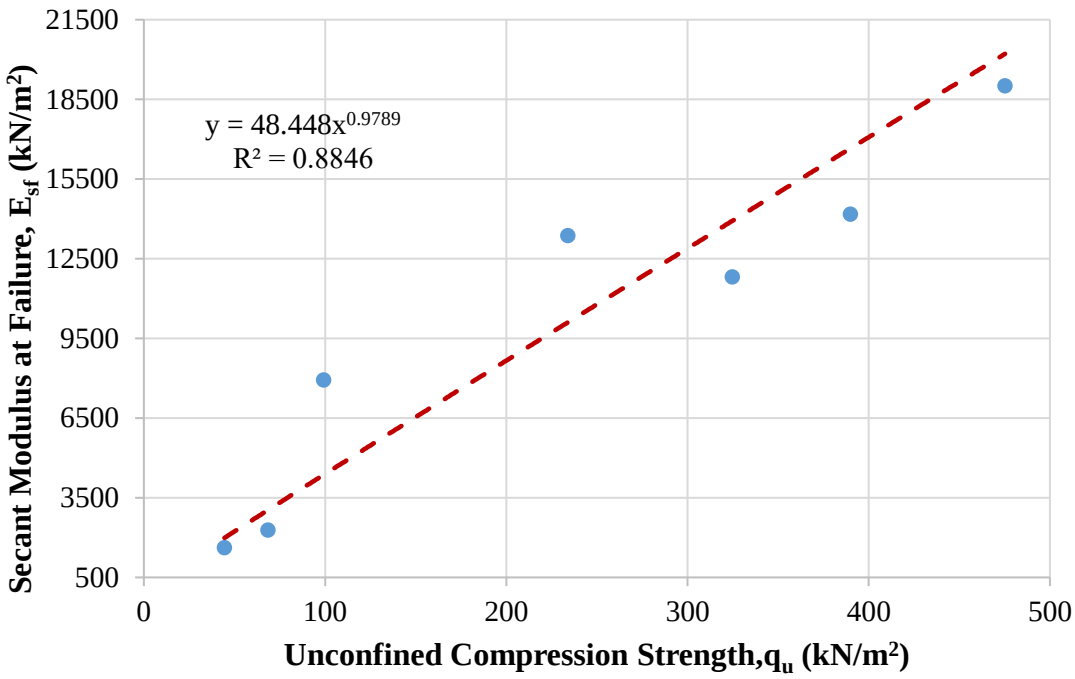

Figure 6.40 Relationship between secant modulus at failure point and unconfined compression strength (CH+10% Fly Ash)

The maximum secant modulus at failure point is obtained in sample 3 as 19008 kN/m^2 for 10% fly ash-added high plasticity clay. It should be noted that the water content is 20%, the dry unit weight is 15.06 kN/m^3, and the unconfined compression strength is 475.2 kN/m^2 when the secant modulus at failure point is the maximum value for 10% fly ash-added high plasticity clay.

With respect to the results of all soil moduli, it seems that the maximum values are obtained at maximum unconfined compression strength (sample 3 for 10% fly ash-added high plasticity clay). However, values of water content and the dry unit weight are less than the optimum water content (w_{opt}=23.7%) and the maximum dry unit weight (γ_{dmax}=15.60 kN/m^3) because low water content can lead to glue effect and chemical cementation in fly ash mixed clayey soils.

6.2.3 High Plasticity Clay Soil Mixture with 15% of Fly Ash

During the experimental program of this study, the amount of 15% fly ash mixed with high plasticity clay soil was used. The compaction and the unconfined compression tests were performed on the 15% fly ash mixed with high plasticity clay

soil, and the outcomes of these experiments are illustrated in Table 6.11. With respect to data obtained from mentioned tests, it can be seen that the value of ω_{opt} and γ_{dmax} obtained as 25.1% and 15.52 kN/m^3, respectively.

Table 6.11 Results of experiments executed with CH+15% fly ash

Sample No.	ω (%)	γ_d (kN/m^3)	q_u (kN/m^2)
1	16	13.50	184.1
2	21	14.65	316.4
3	23	15.40	326.3
4	25	15.52	235.8
5	28	14.46	153.6
6	32	13.70	79.2

The axial stress-axial strain curves of six different 15% fly ash-added high plasticity clay samples are shown in Figure 6.41. According to data obtained from the unconfined compression test of 15% fly ash-added high plasticity clay samples, it can be inferred that the maximum unconfined compression strength was obtained in the third sample, and it was obtained as 326.3 kN/m^2.

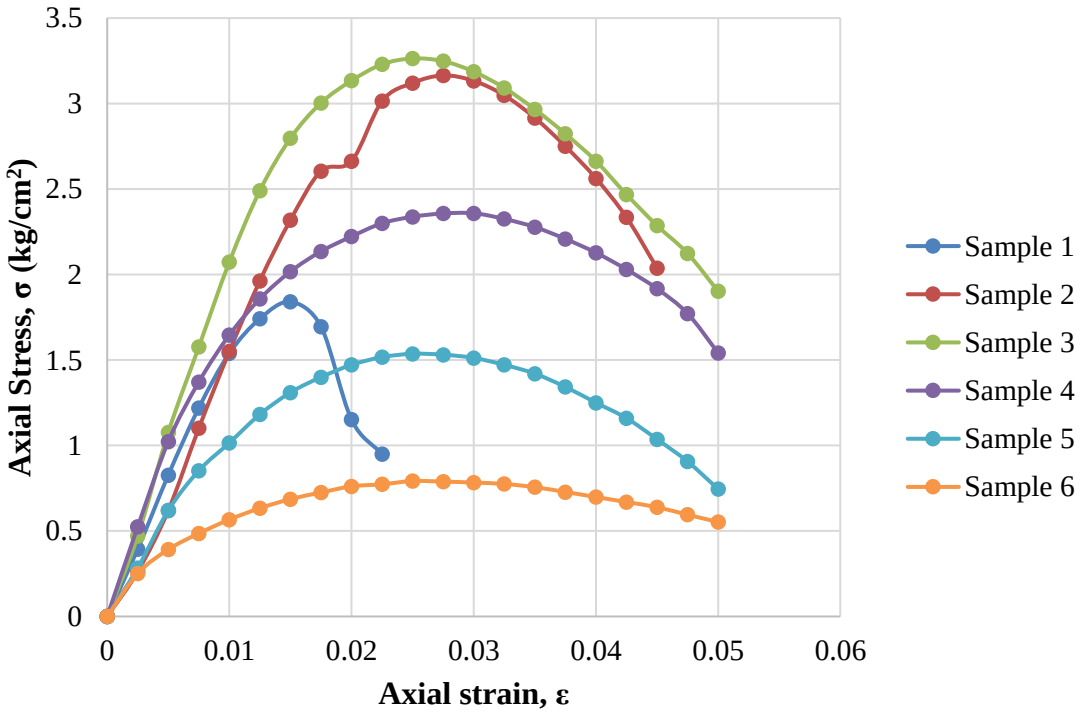

Figure 6.41 Results of unconfined compression tests of CH+15% fly ash

It should be noted that the reciprocal of the initial tangent modulus (a), reciprocal of the asymptotic value of stress difference (b), asymptotic value of stress difference $(\sigma_1)_{ult}$, compressive strength $(\sigma_1)_f$, failure ratio (R_f), axial strain value at failure (ε_f) and axial strain value at 50% of maximum stress (ε_{50}) are required parameters to obtain soil moduli. These parameters were derived from unconfined compression test results and transformed hyperbolic stress-strain curves of 15% fly ash-added high plasticity clay samples. Mentioned engineering parameters are given in Table 6.12.

Table 6.12 Calculated engineering parameters of CH+15% fly ash

Sample No.	a	b	$(\sigma_1)_{ult}$	$(\sigma_1)_f$	R_f	ε_f	ε_{50}
	(cm^2/kg)	(cm^2/kg)	(kg/cm^2)	(kg/cm^2)	-	-	-
1	0.0055	0.1455	6.873	1.841	0.27	0.0150	0.0056
2	0.0047	0.1318	7.587	3.164	0.42	0.0275	0.0102
3	0.0035	0.1509	6.627	3.263	0.49	0.0250	0.0078
4	0.0033	0.2954	3.385	2.358	0.70	0.0300	0.0061
5	0.0066	0.3577	2.796	1.536	0.55	0.0250	0.0066
6	0.0080	0.9328	1.072	0.792	0.74	0.0250	0.0051

It should be noted that the strain level of 15% fly ash-added high plasticity clay is classified as small strain (SS) because the maximum axial strain was determined in samples 3, 4, 5, and 6 of 15% fly ash-added high plasticity clay. The maximum axial strain was obtained as 0.05%. Thus, it can be concluded that nonlinear behaviour was observed for the tested 15% fly ash-added high plasticity clay soil samples.

Initial tangent modulus (E_i), tangent modulus at 50% of maximum stress (E_{t50}), secant modulus at failure (E_{sf}), secant modulus at 50% of maximum stress (E_{s50}), and unconfined compression strength (q_u) of six different 15% fly ash-added high plasticity clay samples are given in Table 6.13.

According to the data obtained, it can be concluded that the maximum modulus values are observed in the initial tangent modulus compared with other soil moduli in all six 15% fly ash-added high plasticity clay samples due to the initial slope of the stress-strain curve. In other words, the axial stress increases up to a certain point very sharply. Then, this sharp increasing trend suddenly starts to slow down, and during this slowing trend, the axial strain increases rapidly.

Table 6.13 Soil moduli and unconfined compression strength of CH+15% fly ash

Sample No.	E_i (kN/m^2)	E_{t50} (kN/m^2)	E_{sf} (kN/m^2)	E_{s50} (kN/m^2)	q_u (kN/m^2)
1	18181.8	13637.7	12273.3	16452.8	184.1
2	21276.6	13328.9	11505.5	15520.1	316.4
3	28571.4	16235.0	13052.0	20986.2	326.3
4	30303.0	12871.0	7860.0	19262.5	235.8
5	15151.5	7970.3	6144.0	11657.6	153.6
6	12500.0	4970.9	3168.0	7755.0	79.2

In addition, transformed hyperbolic stress-strain curves for six different 15% fly ash-added high plasticity clay samples are illustrated in Figures 6.42, 6.43, 6.44, 6.45, 6.46, and 6.47.

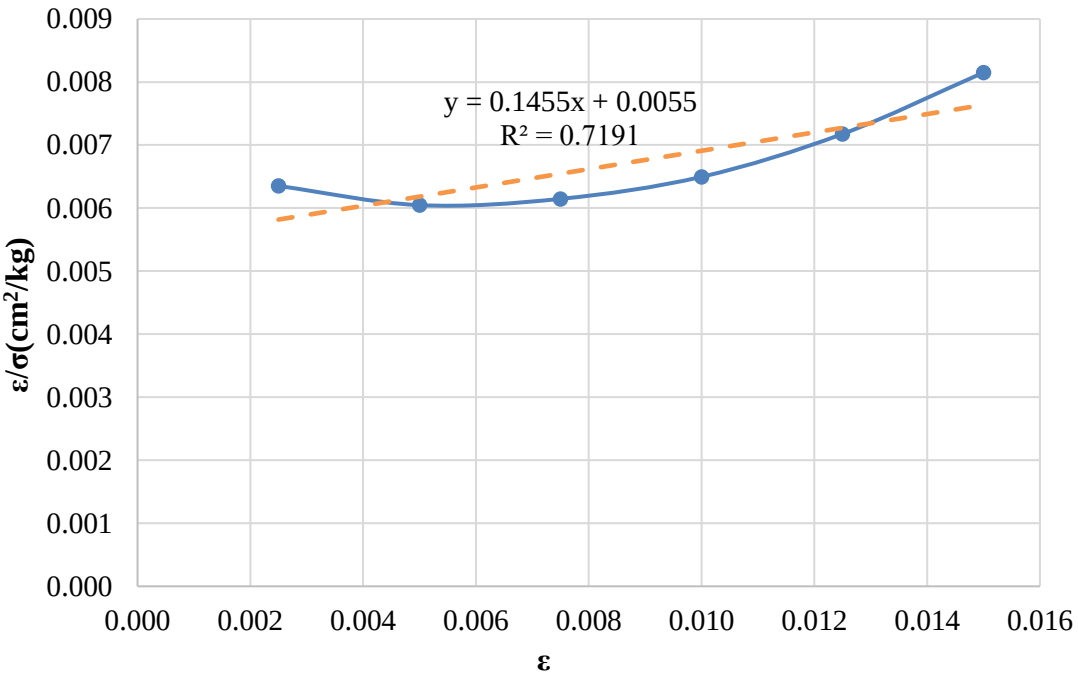

Figure 6.42 Transformed hyperbolic stress-strain curve for sample 1 (CH+15% Fly Ash)

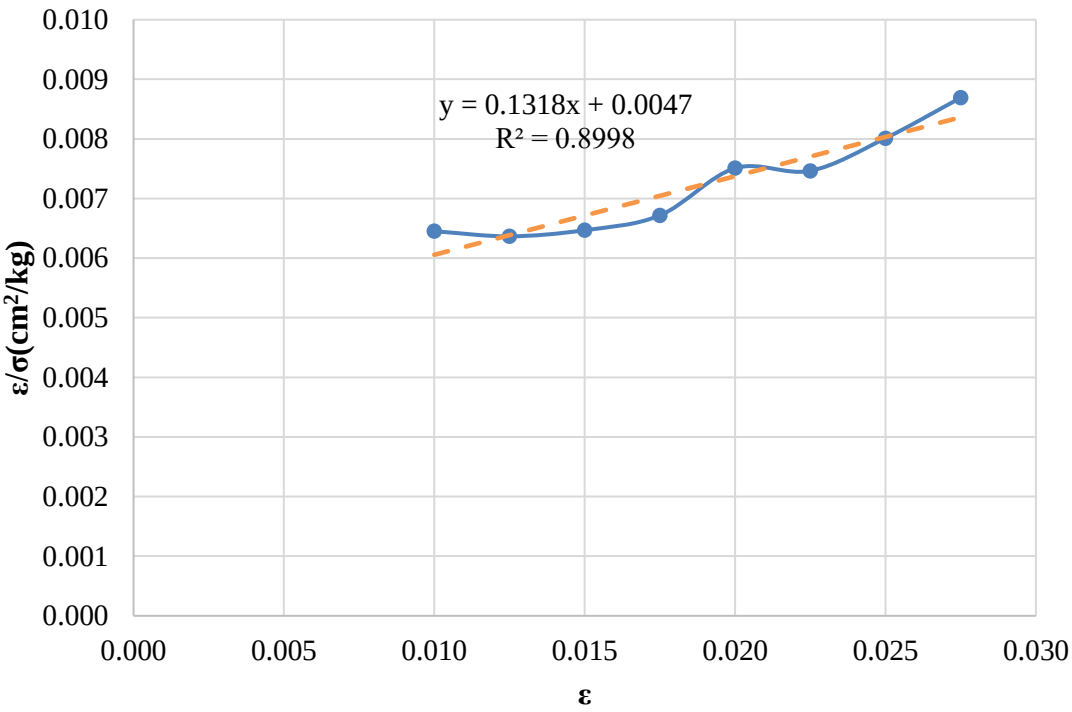

Figure 6.43 Transformed hyperbolic stress-strain curve for sample 2 (CH+15% Fly Ash)

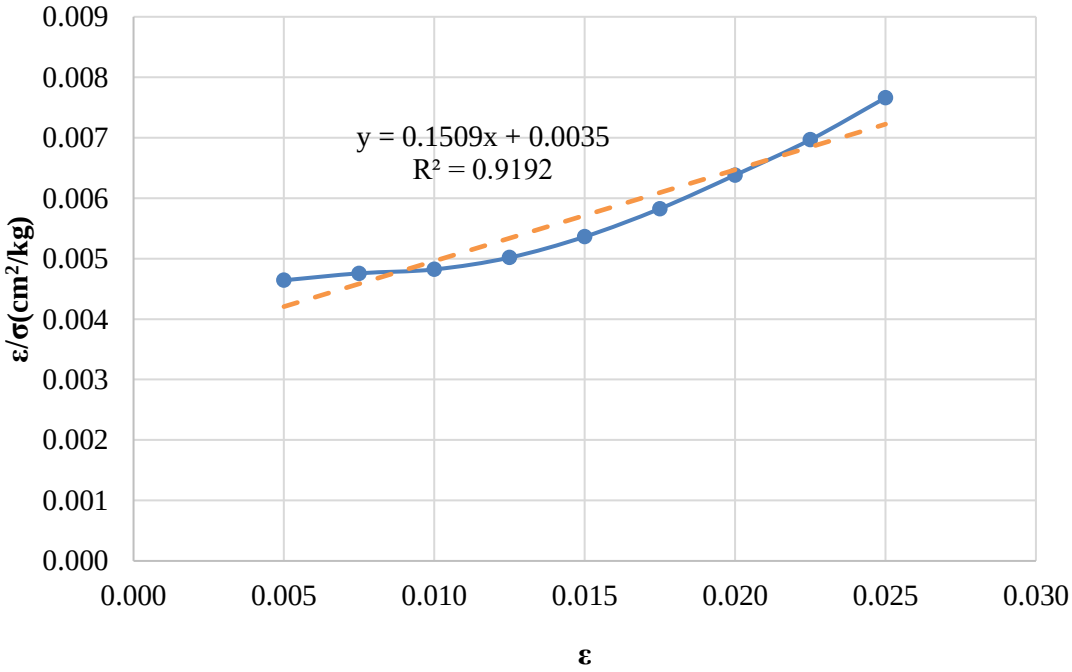

Figure 6.44 Transformed hyperbolic stress-strain curve for sample 3 (CH+15% Fly Ash)

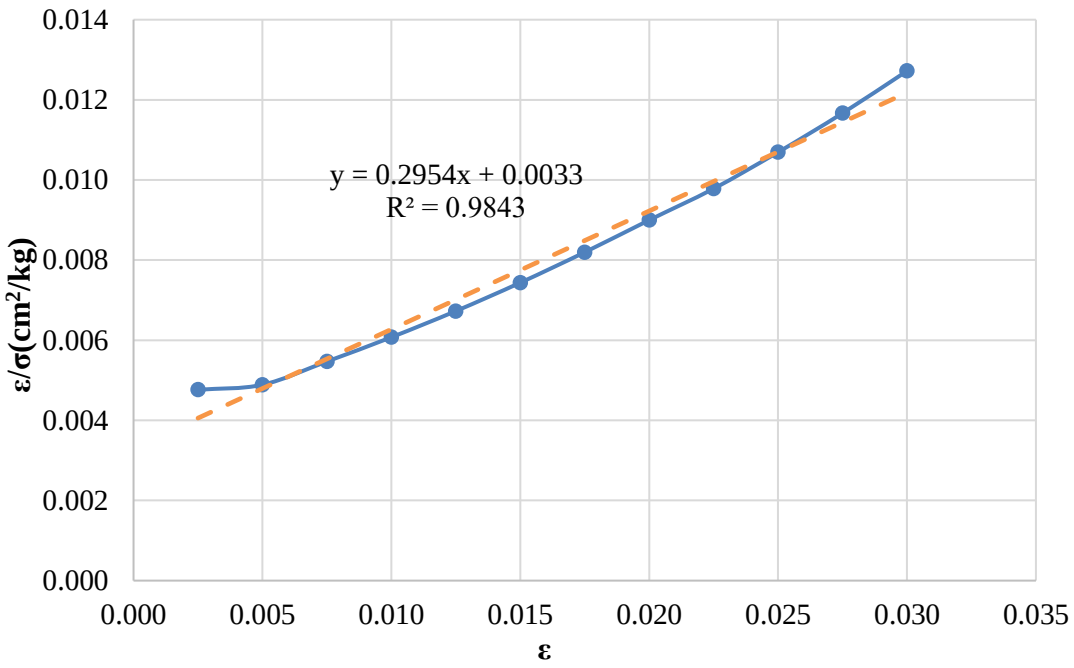

Figure 6.45 Transformed hyperbolic stress-strain curve for sample 4 (CH+15% Fly Ash)

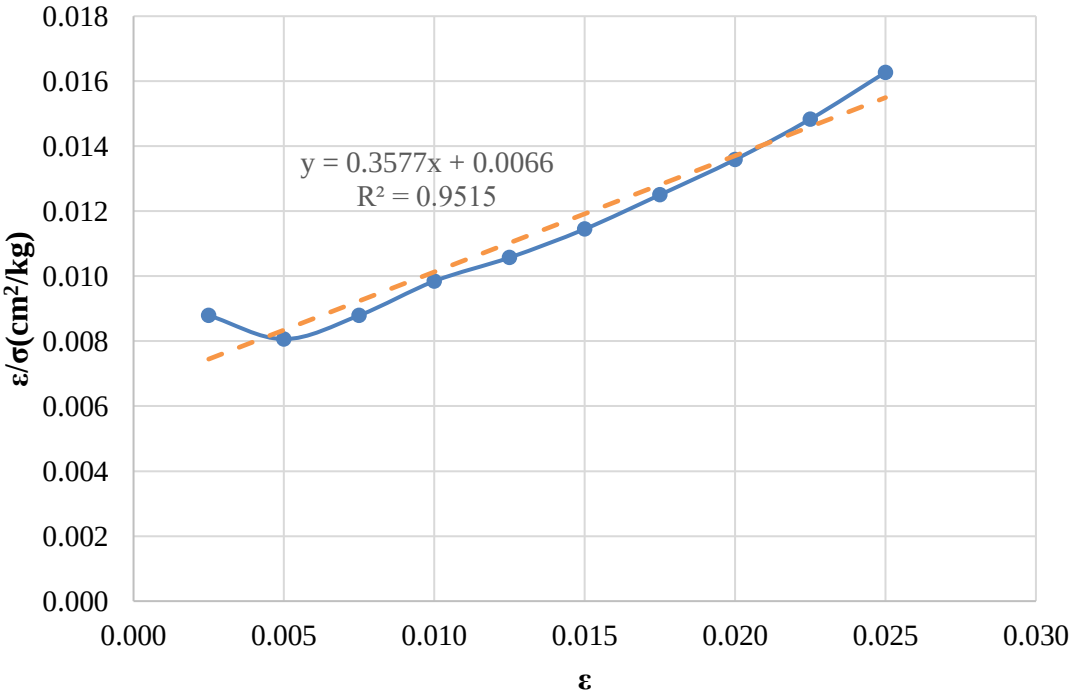

Figure 6.46 Transformed hyperbolic stress-strain curve for sample 5 (CH+15% Fly Ash)

It was found that low and high values of axial strains in samples 1, 2, 3, 4, and 5 are not precisely hyperbolic, as shown in Figures 6.42, 6.43, 6.44, 6.45, and 6.46. In other words, these points can not be fitted in a straight line. On the other hand, it was possible to estimate the actual stress-strain curves by a hyperbola. Therefore, it is found to have a reasonable degree of accuracy.

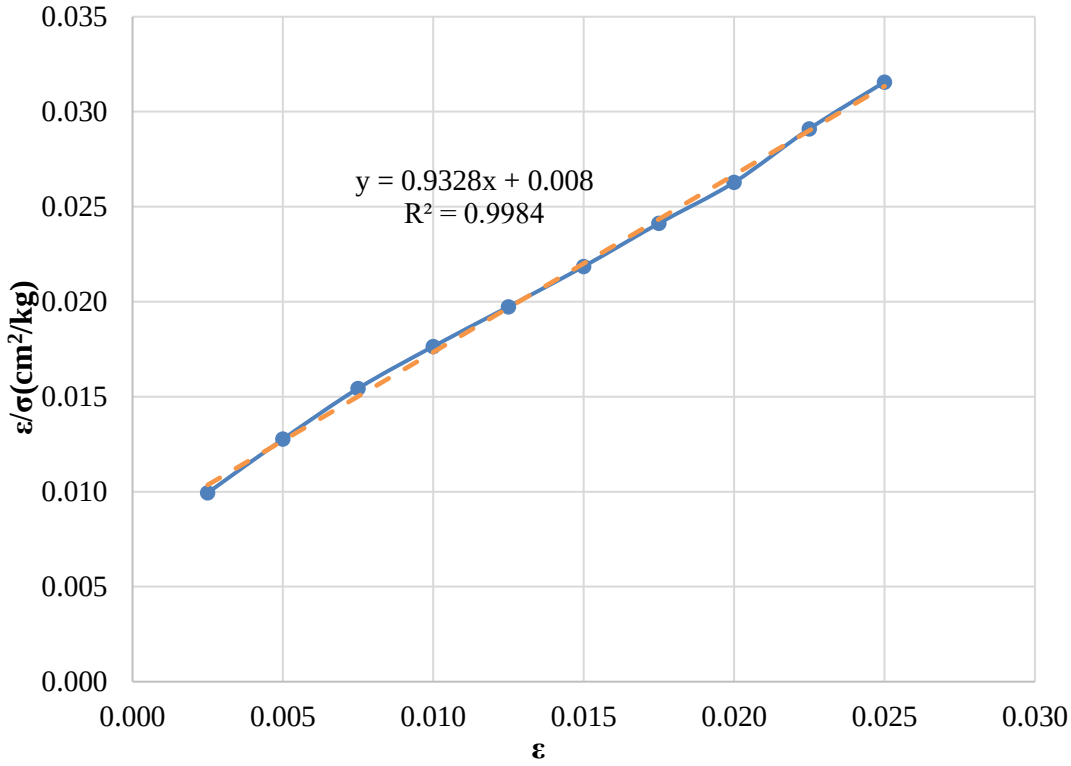

Figure 6.47 Transformed hyperbolic stress-strain curve for sample 6 (CH+15% Fly Ash)

On the other hand, the transformed hyperbolic stress-strain curve in sample 6 showed hyperbolic behavior, as shown in Figure 6.48. In other words, these points can be best-fitted in a straight line.

The relationship between the secant modulus at 50% of maximum stress (E_{s50}) and the initial tangent modulus (E_i) of 15% fly ash-added high plasticity clay samples is shown in Figure 6.48.

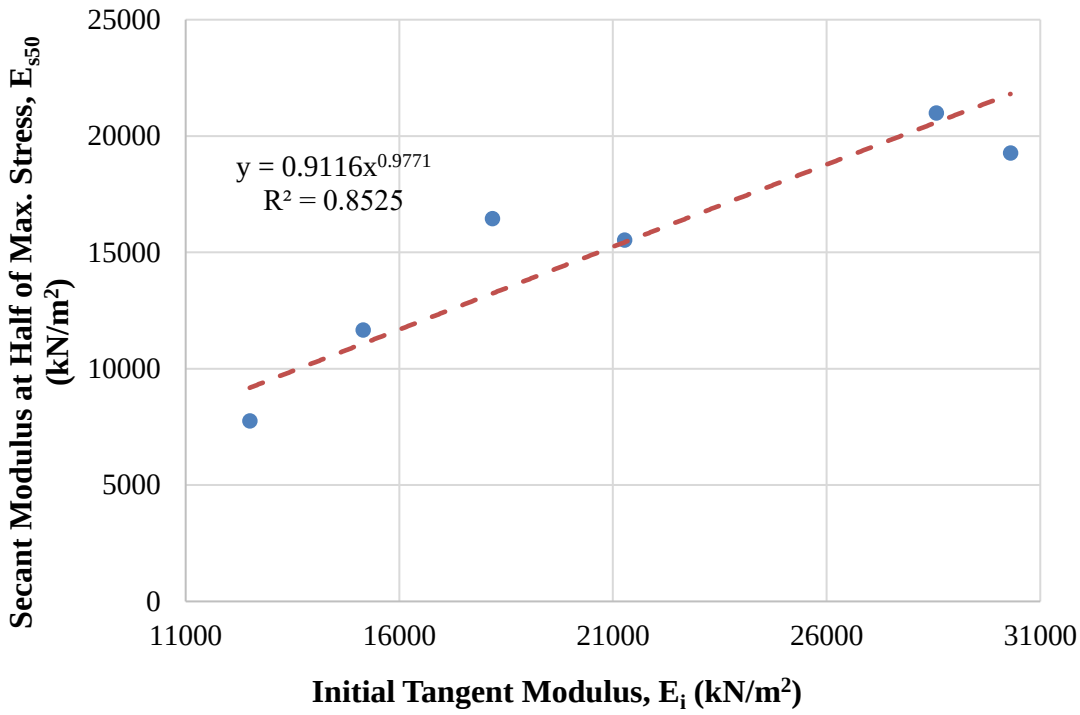

Figure 6.48 Relationship between secant modulus at 50% of maximum stress and initial tangent modulus (CH+15% Fly Ash)

According to the data, it can be inferred that these soil moduli can be related to the hardening of 15% fly ash-added high plasticity clay samples. Thus, the initial tangent modulus increases with the increasing secant modulus at 50% of maximum stress. Furthermore, it was best suited for estimating these soil moduli by a power model.

Furthermore, the relationship between the secant modulus at failure (E_{sf}) and the tangent modulus at 50% of maximum stress (E_{t50}) of 15% fly ash-added high plasticity clay samples are shown in Figure 6.49.

The tangent modulus at 50% of maximum stress increases with the increasing secant modulus at failure. Thus, it was best suited for estimating these soil moduli by a power model.

In addition, the relationship between initial tangent modulus (E_i) and unconfined compression strength of 15% fly ash-added high plasticity clay samples is shown in Figure 6.50.

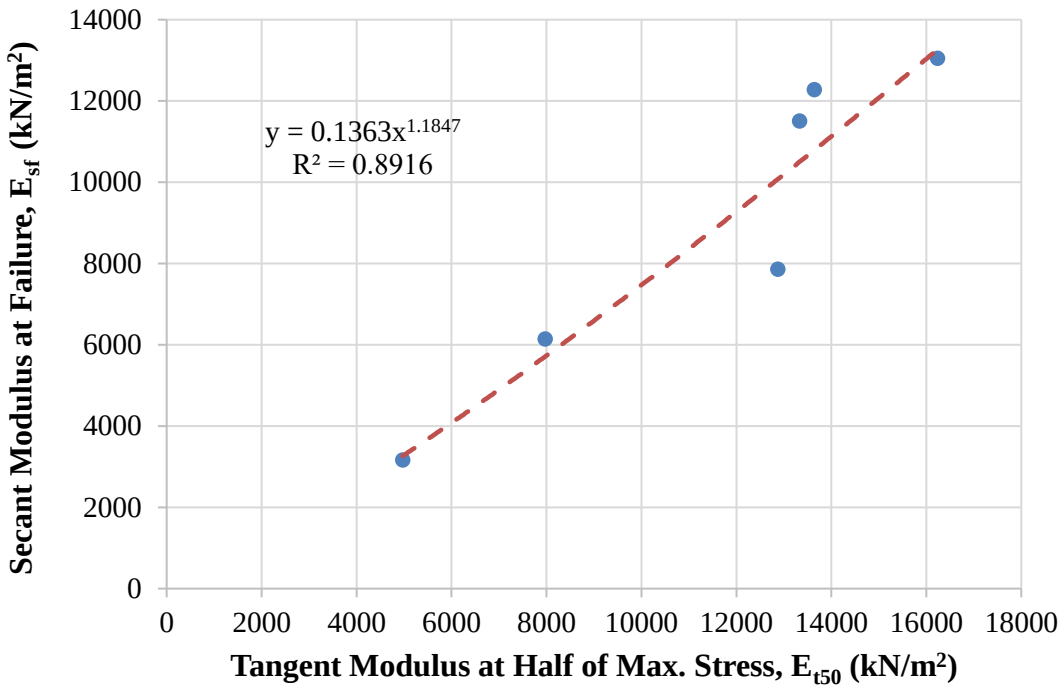

Figure 6.49 Relationship between secant modulus at failure point and tangent modulus at 50% of maximum stress (CH+15% Fly Ash)

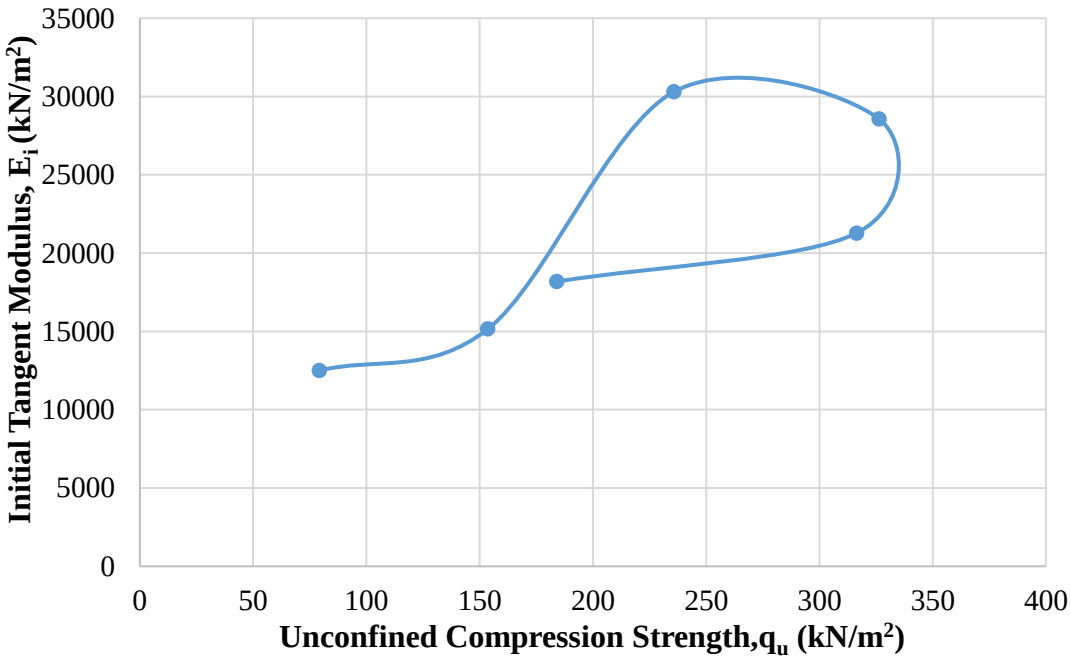

Figure 6.50 Relationship between initial tangent modulus and unconfined compression strength (CH+15% Fly Ash)

According to data, the maximum initial tangent modulus is obtained in sample 4 as 30303 kN/m^2 for 15% fly ash-added high plasticity clay. It should be noted that the water content is 25%, the dry unit weight is 15.52 kN/m^3, and the unconfined compression strength is 235.8 kN/m^2 when the initial tangent modulus is the maximum value for 15% fly ash-added high plasticity clay. On the other hand, when the initial tangent modulus has the maximum value for 15% fly ash-added high plasticity clay, the water content is close to the optimum water content (w_{opt}=25.1%), and the dry unit weight is equal to the maximum dry unit weight (γ_{dmax}=15.52 kN/m^3).

In addition, with respect to the results of the initial tangent modulus, it seems that the maximum value is not obtained at maximum unconfined compression strength (sample 3 for 15% fly ash-added high plasticity clay) since the beginning of sample 4's stress-strain curve has been rapidly increased in axial stress. That increase can be related to the compaction in sample 4 for 15% fly ash-added high plasticity clay.

The relationship between secant modulus at 50% of maximum stress (E_{s50}) and unconfined compression strength of 15% fly ash-added high plasticity clay samples is shown in Figure 6.51.

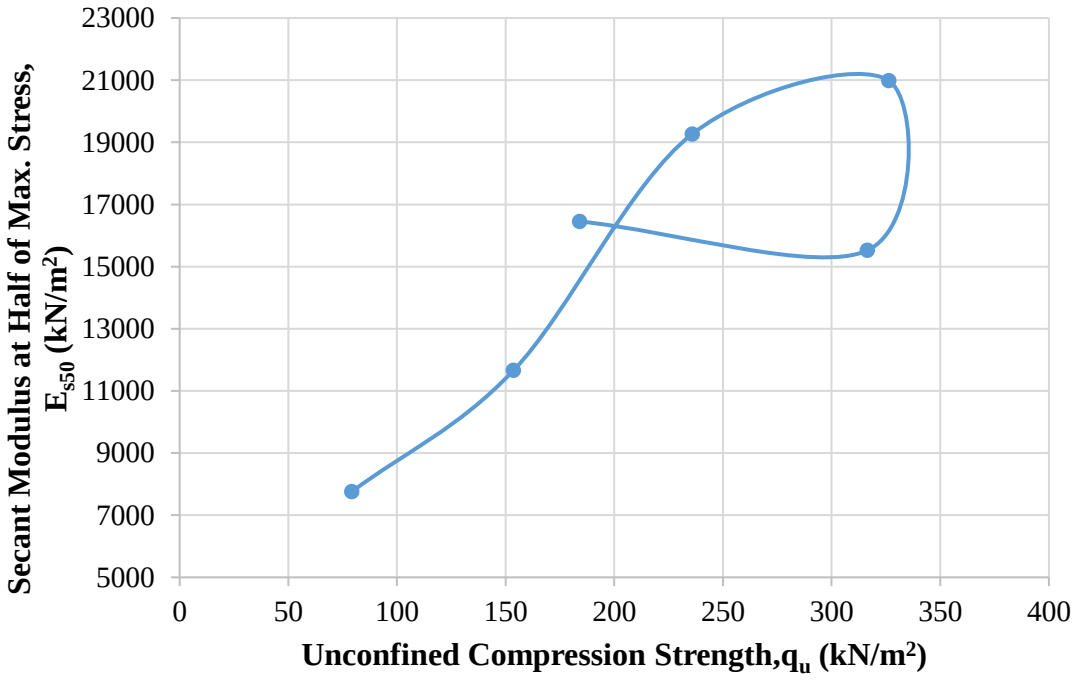

Figure 6.51 Relationship between secant modulus at 50% of maximum stress and unconfined compression strength (CH+15% Fly Ash)

The maximum secant modulus at 50% of maximum stress is obtained in sample 3 as 20986.2 kN/m^2 for 15% fly ash-added high plasticity clay. It should be noted that the water content is 23%, the dry unit weight is 15.40 kN/m^3, and the unconfined compression strength is 326.3 kN/m^2 when the secant modulus at 50% of maximum stress has the maximum value of 15% fly ash-added high plasticity clay.

On the other hand, the relationship between tangent modulus at 50% of maximum stress (E_{t50}) and unconfined compression strength of 15% fly ash-added high plasticity clay samples is shown in Figure 6.52.

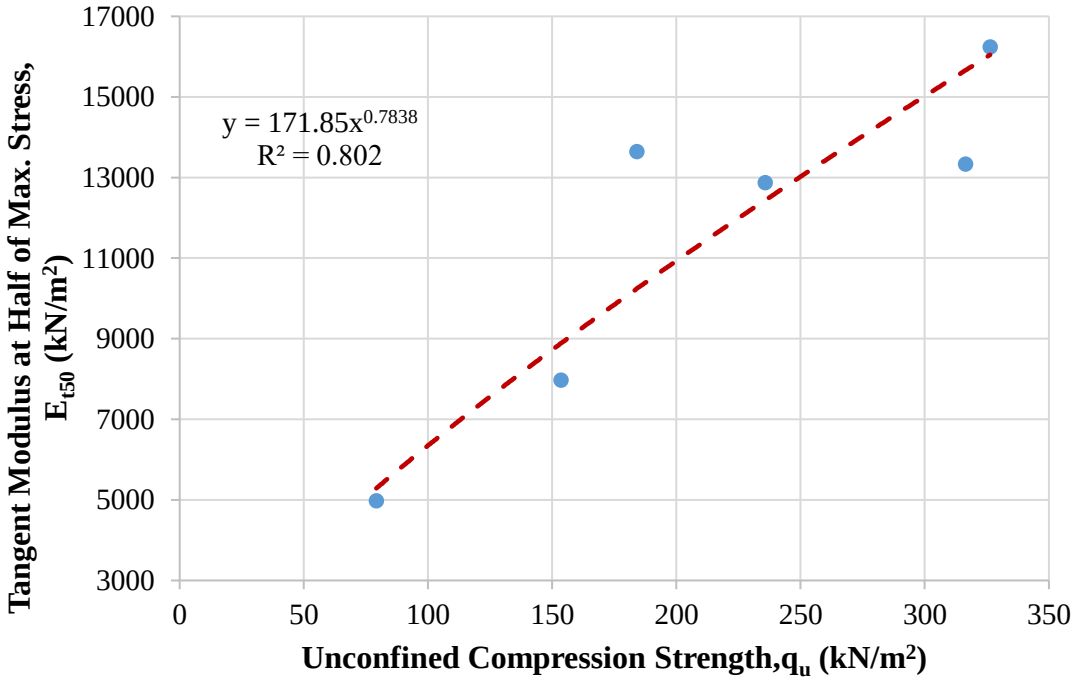

Figure 6.52 Relationship between tangent modulus at 50% of maximum stress and unconfined compression strength (CH+15% Fly Ash)

It is obvious that the maximum tangent modulus at 50% of maximum stress is obtained in sample 3 as 16235 kN/m^2 for 15% fly ash-added high plasticity clay. It should be noted that the water content is 23%, the dry unit weight is 15.40 kN/m^3, and the unconfined compression strength is 326.6 kN/m^2 when the tangent modulus at 50% of maximum stress is the maximum value for 15% fly ash-added high plasticity clay. In addition, the relationship between secant modulus at failure point (E_{sf}) and unconfined compression strength of 15% fly ash-added high plasticity clay samples is shown in Figure 6.53.

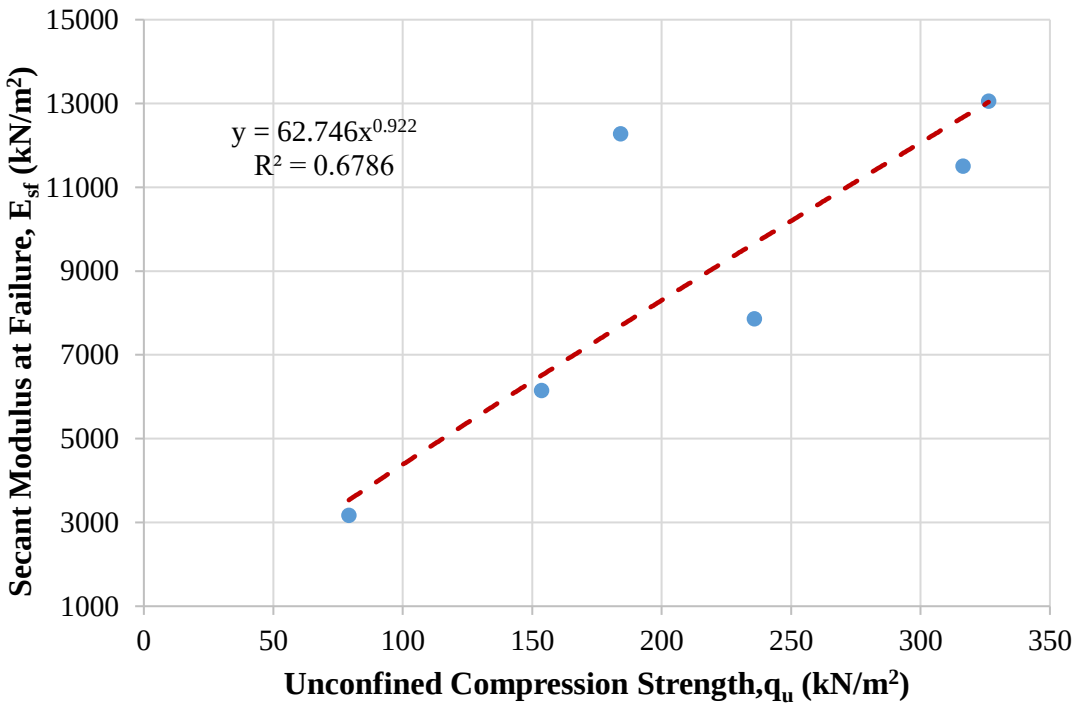

Figure 6.53 Relationship between secant modulus at failure point and unconfined compression strength (CH+15% Fly Ash)

The maximum secant modulus at failure point is obtained in sample 3 as 13052 kN/m^2 for 15% fly ash-added high plasticity clay. It should be noted that the water content is 23%, the dry unit weight is 15.40 kN/m^3, and the unconfined compression strength is 326.3 kN/m^2 when the secant modulus at failure point is the maximum value for 15% fly ash-added high plasticity clay.

With respect to the results of the tangent modulus at 50% of maximum stress, secant modulus at 50% of maximum stress, and secant modulus at failure, it seems that the maximum values of these moduli are obtained at maximum unconfined compression strength (sample 3 for 15% fly ash-added high plasticity clay). However, values of water content and the dry unit weight are less than the optimum water content (w_{opt}=25.1%) and the maximum dry unit weight (γ_{dmax}=15.52 kN/m^3) because low water content can lead to glue effect and chemical cementation in fly ash mixed clayey soils.

6.2.4 Comparison of Three Different Fly Ash Mixtures with High Plasticity Clay Soil

Three different amounts of fly ash (5%, 10%, and 15%) mixed with high plasticity clay soil were prepared to analyze deformation moduli. The soil moduli of the mentioned high plasticity clay-fly ash mixtures are compared with the plain high plasticity clay. Figure 6.54 exhibits the relationship between the maximum initial tangent modulus and different fly ash content of CH.

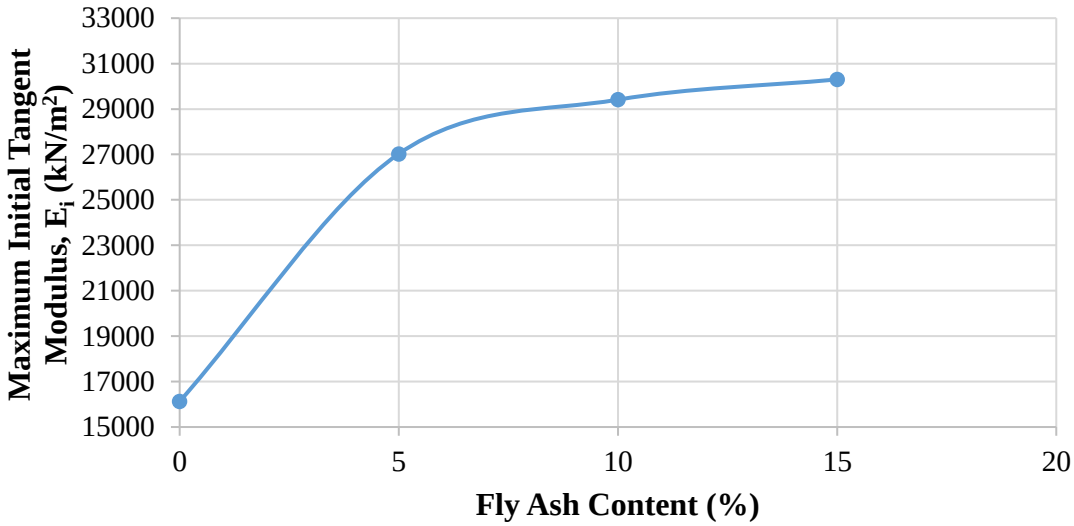

Figure 6.54 Relationship between maximum initial tangent modulus and different fly ash contents of CH

After analyzing all initial tangent modulus of high plasticity clay-fly ash mixtures and comparing them in a graph, it can be seen that the maximum initial tangent modulus was obtained in the mixture with 15% of fly ash. In addition, the initial tangent modulus increases up to 88% in the mixture with 15% of fly ash. In other words, the initial tangent modulus increases with the increasing fly ash content in the high plasticity clay-fly ash mixture.

As the next step, all secant modulus at 50% of maximum stress of high plasticity clay-fly ash mixtures were gathered and compared in Figure 6.55.

It can be seen that the maximum secant modulus at 50% of maximum stress was obtained in the mixture with 10% of fly ash. In addition, the secant modulus at 50% of maximum stress increases up to 158% for the mixture with 10% of fly ash. In other

words, the optimum value of secant modulus at 50% of maximum stress was determined in the 10% fly ash content of the high plasticity clay-fly ash mixture.

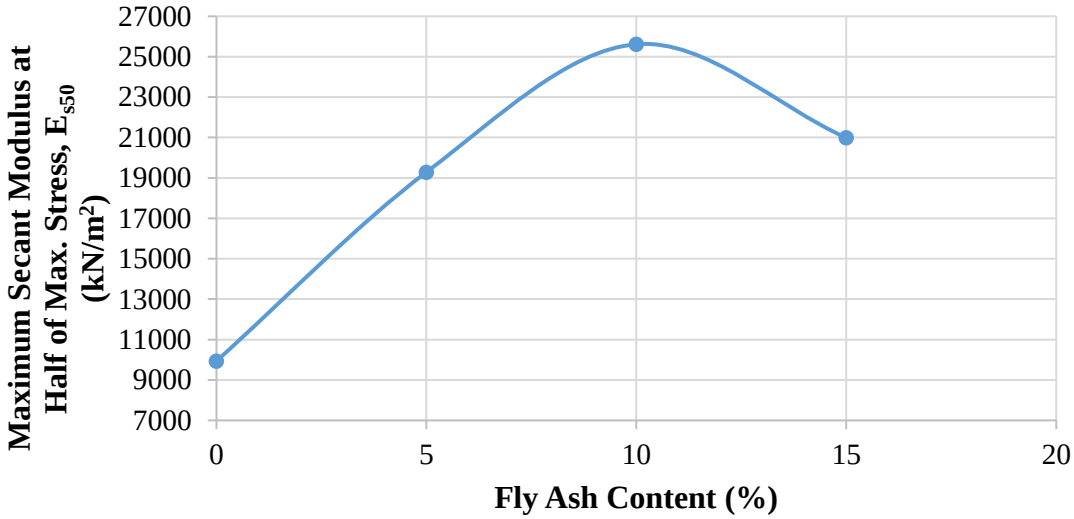

Figure 6.55 Relationship between maximum secant modulus at 50% of maximum stress and different fly ash contents of CH

Furthermore, after gathering all tangent modulus at 50% of maximum stress of high plasticity clay-fly ash mixtures were shown and compared them in Figure 6.56.

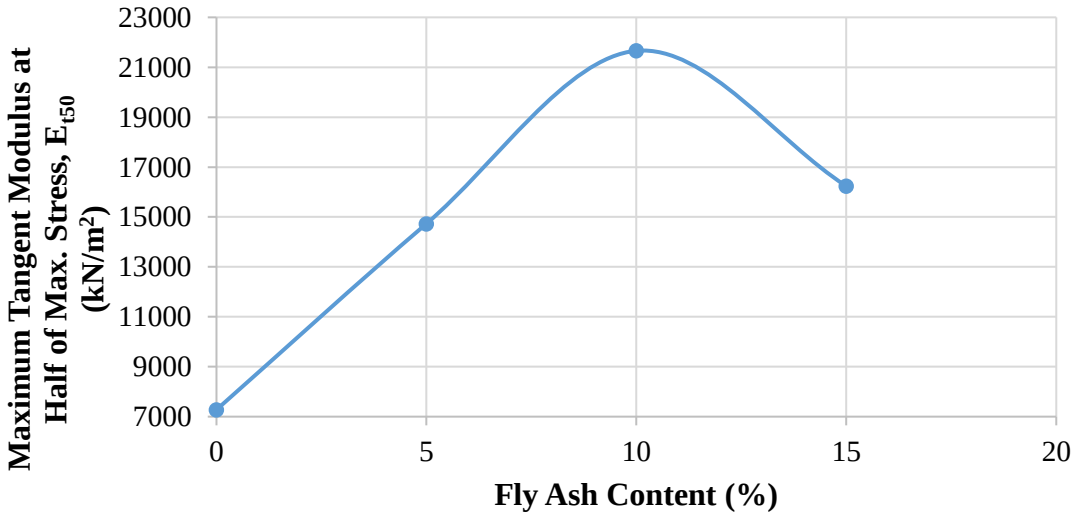

Figure 6.56 Relationship between maximum tangent modulus at 50% of maximum stress and different fly ash contents of CH

It can be seen that the maximum tangent modulus at 50% of maximum stress was obtained in the mixture with 10% of fly ash. In addition, the tangent modulus at 50% of maximum stress increases up to 198% in the mixture with 10% of fly ash. In other words, the optimum value of tangent modulus at 50% of maximum stress was determined in the 10% fly ash content of the high plasticity clay-fly ash mixture.

Moreover, Figure 6.57 exhibits the relationship between the maximum secant modulus at failure point and different fly ash contents of CH.

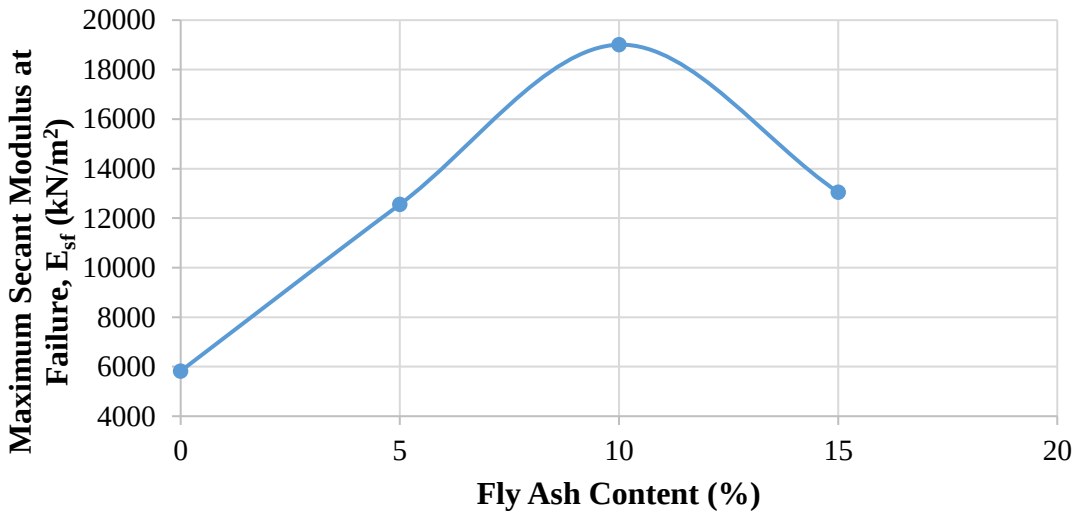

Figure 6.57 Relationship between maximum secant modulus at failure point and different fly ash contents of CH

After gathering all secant modulus at failure point of high plasticity clay-fly ash mixtures and comparing them in a graph, it can be seen that the maximum secant modulus at failure point was obtained in the mixture with 10% of fly ash (sample 3, 19008 kN/m^2). In addition, the secant modulus at failure point increases up to 124% in the mixture with 10% of fly ash. In other words, the optimum value of secant modulus at failure point was determined in the 10% fly ash content of the high plasticity clay-fly ash mixture.

6.3 Polypropylene Mixtures with High Plasticity Clay Soil

Polypropylene fiber can be had a twisted fibrillating network form, which is made of 100% virgin materials. Four different amounts of polypropylene (0.25%, 0.5%, 0.75%, and 1%) were added to the high plasticity clay to study the effects of

mixing polypropylene with designated soil. In addition, the amounts of polypropylene compared to whole mixtures in terms of soil moduli, the unconfined compression strength, and relationships in these engineering parameters. In other words, the amount of soil improvement of high plasticity clay was examined with added polypropylene.

6.3.1 High Plasticity Clay Soil Mixture with 0.25% of Polypropylene

During the experimental program of this study, the amount of 0.25% polypropylene mixed with high plasticity clay soil was used. The compaction and the unconfined compression tests were performed on the 0.25% polypropylene mixed with high plasticity clay, and the outcomes of these experiments are illustrated in Table 6.14. With respect to data obtained from mentioned tests, it can be seen that the value of ω_{opt} and γ_{dmax} obtained at 26% and 14.60 kN/m^3, respectively.

Table 6.14 Results of experiments executed with CH+0.25% polypropylene

Sample No.	ω (%)	γ_d (kN/m^3)	q_u (kN/m^2)
1	20	13.50	212.4
2	24	14.20	254.9
3	26	14.50	224.2
4	28	14.60	178.2
5	31	14.00	122.5
6	33	13.40	74.9

The axial stress-axial strain curves of six different 0.25% polypropylene-added high plasticity clay samples are shown in Figure 6.58. Besides, Figure 6.59 exhibits the tested 0.25% polypropylene-added high plasticity clay sample, which has the highest value of the maximum unconfined compression strength. Therefore, according to data obtained from the unconfined compression test of the 0.25% polypropylene-added high plasticity clay sample, it can be inferred that the maximum unconfined compression strength was obtained in the second sample, and it was obtained as 254.9 kN/m^2.

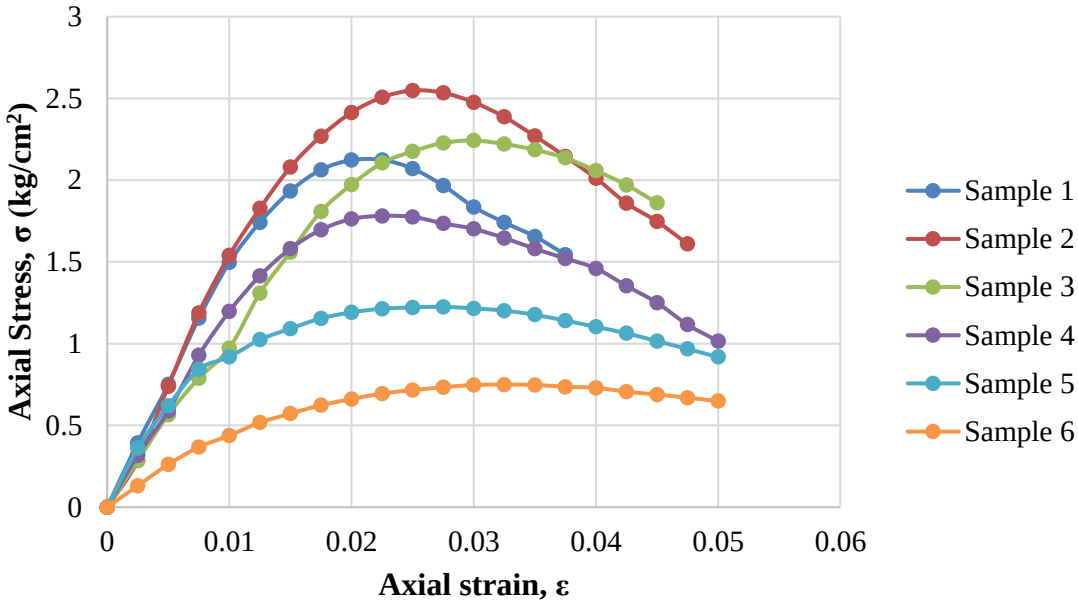

Figure 6.58 Results of unconfined compression tests of CH+0.25% polypropylene

Reciprocal of the initial tangent modulus (a) and reciprocal of the asymptotic value of stress difference (b) were derived from transformed hyperbolic stress-strain curves of 0.25% polypropylene-added high plasticity clay samples. In addition, the asymptotic value of stress difference $(\sigma_1)_{ult}$, compressive strength $(\sigma_1)_f$, axial strain value at failure (ε_f), and axial strain value at 50% of maximum stress (ε_{50}) were obtained from unconfined compression test results. Lastly, the failure ratio (R_f) was calculated from unconfined compression test results. Mentioned engineering parameters are given in Table 6.15.

Table 6.15 Calculated engineering parameters of CH+0.25% polypropylene

Sample No.	a (cm^2/kg)	b (cm^2/kg)	$(\sigma_1)_{ult}$ (kg/cm^2)	$(\sigma_1)_f$ (kg/cm^2)	R_f -	ε_f -	ε_{50} -
1	0.0052	0.2021	4.948	2.124	0.43	0.0225	0.0069
2	0.0051	0.1644	6.083	2.549	0.42	0.0250	0.0081
3	0.0081	0.1396	7.163	2.242	0.31	0.0300	0.0111
4	0.0067	0.2208	4.529	1.782	0.39	0.0225	0.0072
5	0.0047	0.6213	1.610	1.225	0.76	0.0275	0.0049
6	0.0146	0.8266	1.210	0.749	0.62	0.0325	0.0078

It should be noted that the strain level of 0.25% polypropylene-added high plasticity clay is categorized as small strain (SS) because the maximum axial strain was determined in samples 4, 5, and 6 of 0.25% polypropylene-added high plasticity clay. The maximum axial strain was obtained as 0.05%. Thus, it can be concluded that nonlinear behaviour was observed for the tested 0.25% polypropylene-added high plasticity clay soil samples.

Initial tangent modulus (E_i), tangent modulus at 50% of maximum stress (E_{t50}), secant modulus at failure (E_{sf}), secant modulus at 50% of maximum stress (E_{s50}), and unconfined compression strength (q_u) of six different 0.25% polypropylene-added high plasticity clay samples are given in Table 6.16.

Table 6.16 Soil moduli and unconfined compression strength of CH+0.25% polypropylene

Sample No.	E_i (kN/m^2)	E_{t50} (kN/m^2)	E_{sf} (kN/m^2)	E_{s50} (kN/m^2)	q_u (kN/m^2)
1	19230.8	11861.6	9440.0	15336.8	212.4
2	19607.8	12251.9	10196.0	15706.7	254.9
3	12345.7	8784.0	7473.3	10101.0	224.2
4	14925.4	9630.4	7920.0	12338.3	178.2
5	21276.6	8164.3	4454.5	12430.0	122.5
6	6849.3	3265.1	2304.6	4823.5	74.9

According to the data obtained, it can be concluded that the maximum modulus values are observed in the initial tangent modulus compared with other soil moduli in all six 0.25% polypropylene-added high plasticity clay samples due to the initial slope of the stress-strain curves. In other words, the axial stress increases up to a certain point very sharply. Then, this sharp increasing trend suddenly starts to slow down, and during this slowing trend, the axial strain increases rapidly.

Figure 6.59 Peak point of CH+0.25% polypropylene (ω =24%, q_u=254.9 kN/m^2) (Etminan, 2012)

In addition, transformed hyperbolic stress-strain curves for six different 0.25% polypropylene-added high plasticity clay samples are illustrated in Figure 6.60.

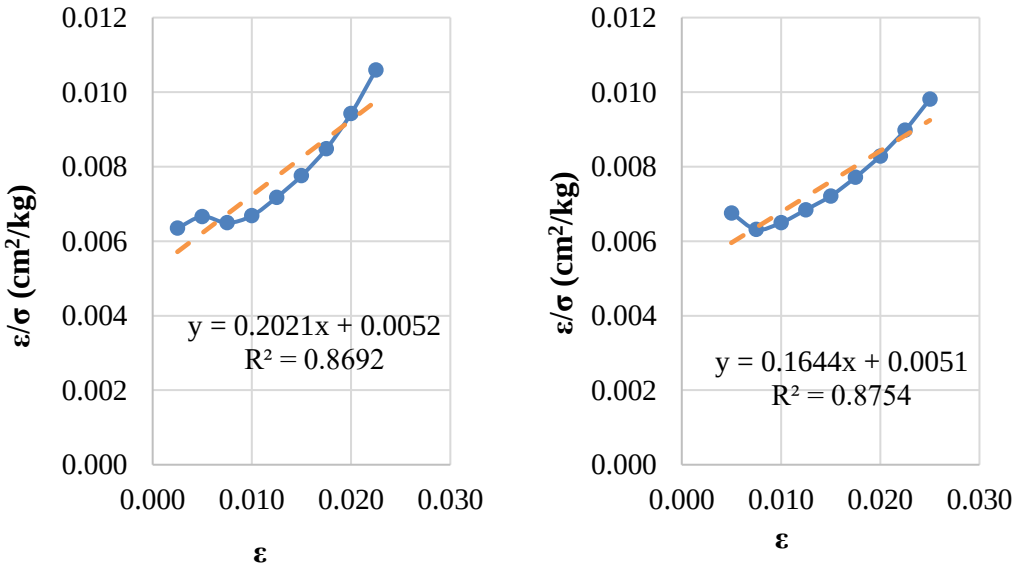

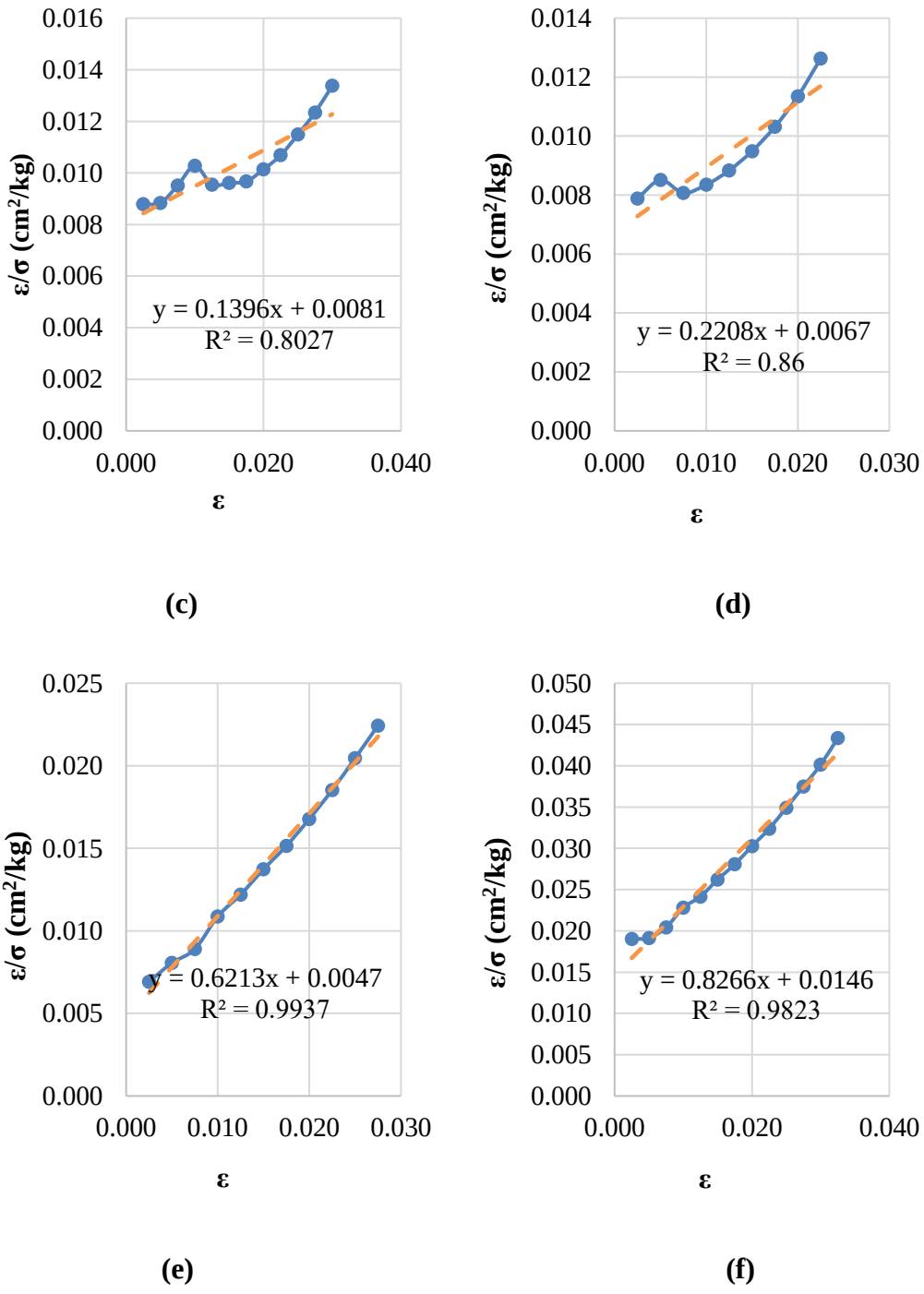

Figure 6.60 Transformed hyperbolic stress-strain curves for (a) sample 1, (b) sample 2, (c) sample 3, (d) sample 4, (e) sample 5, and (f) sample 6 (CH+0.25% Polypropylene)

It was found that low and high values of axial strains in samples 1, 2, 3, and 4 are not precisely hyperbolic, as shown in Figures 6.60 (a, b, c, and d). In other words, these points can not be fitted in a straight line. However, it was possible to estimate

the actual stress-strain curves by a hyperbola. Thus, it is found to have a reasonable degree of accuracy. On the other hand, the transformed hyperbolic stress-strain curve in samples 5 and 6 showed hyperbolic behavior, as shown in Figures 6.60 (e and f). In other words, these points can be best-fitted in a straight line.

The relationship between the secant modulus at 50% of maximum stress (E_{s50}) and the initial tangent modulus (E_i) of 0.25% polypropylene-added high plasticity clay samples is shown in Figure 6.61.

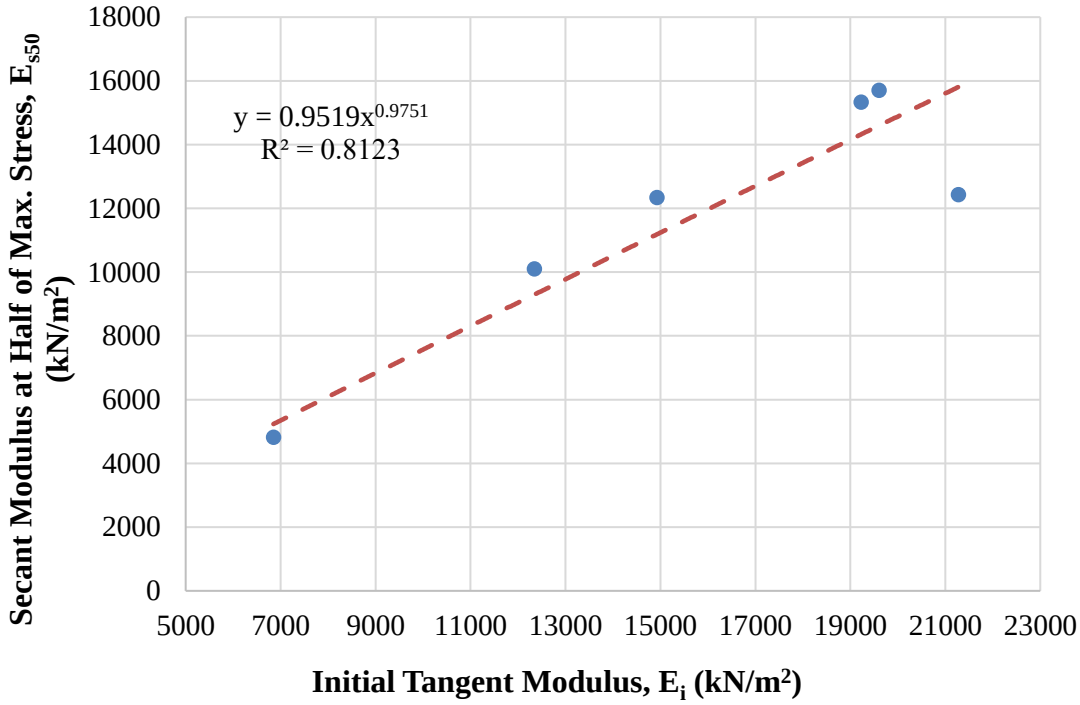

Figure 6.61 Relationship between secant modulus at 50% of maximum stress and initial tangent modulus (CH+0.25% Polypropylene)

According to the data, it can be inferred that these soil moduli refer to the hardening of 0.25% polypropylene-added high plasticity clay samples. Thus, the initial tangent modulus increases with the increasing secant modulus at 50% of maximum stress. Furthermore, it was best suited for estimating these soil moduli by a power model.

The relationship between the secant modulus at failure (E_{sf}) and the tangent modulus at 50% of maximum stress (E_{t50}) of 0.25% polypropylene-added high plasticity clay samples are shown in Figure 6.62.

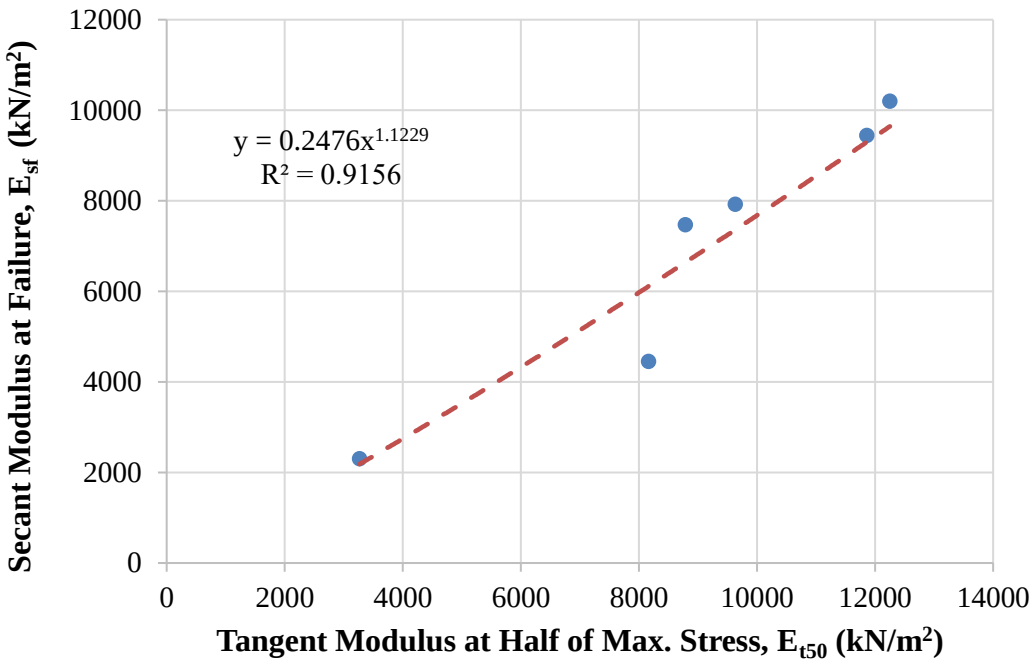

Figure 6.62 Relationship between secant modulus at failure point and tangent modulus at 50% of maximum stress (CH+0.25% Polypropylene)

Furthermore, the relationship between initial tangent modulus (E_i) and unconfined compression strength of 0.25% polypropylene-added high plasticity clay samples is shown in Figure 6.63.

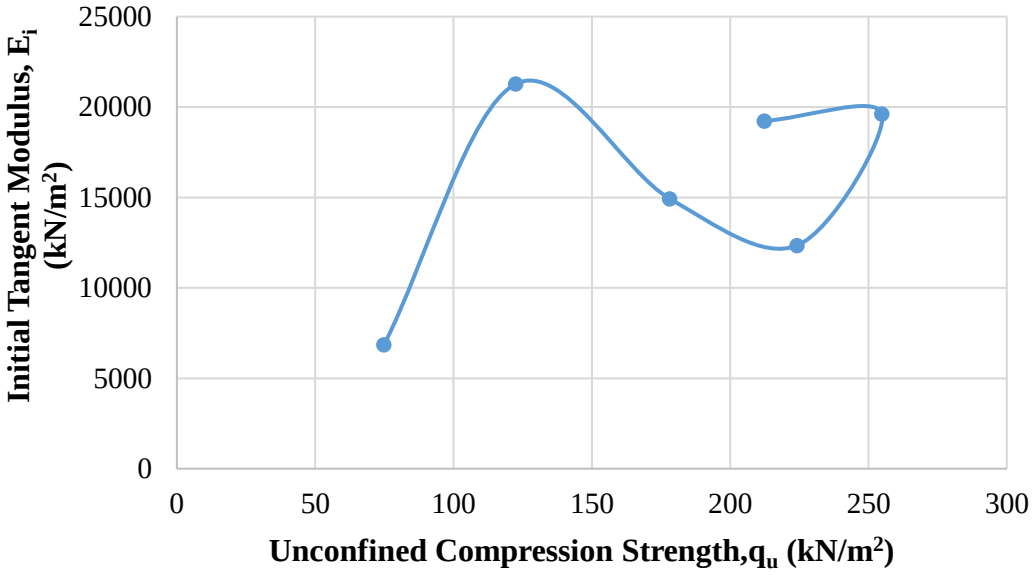

Figure 6.63 Relationship between initial tangent modulus and unconfined compression strength (CH+0.25% Polypropylene)

The maximum initial tangent modulus is obtained in sample 5 as 21276.6 kN/m^2 for 0.25% polypropylene-added high plasticity clay. It should be noted that the water content is 31%, the dry unit weight is 14.00 kN/m^3, and the unconfined compression strength is 122.5 kN/m^2 when the initial tangent modulus is the maximum value for 0.25% polypropylene-added high plasticity clay.

In addition, with respect to the results of the initial tangent modulus, it seems that the maximum value is not obtained at maximum unconfined compression strength (sample 2 for 0.25% polypropylene-added high plasticity clay) since the beginning of sample 5's stress-strain curve has been rapidly increased in axial stress.

The relationship between secant modulus at 50% of maximum stress (E_{s50}) and unconfined compression strength of 0.25% polypropylene-added high plasticity clay samples is shown in Figure 6.64.

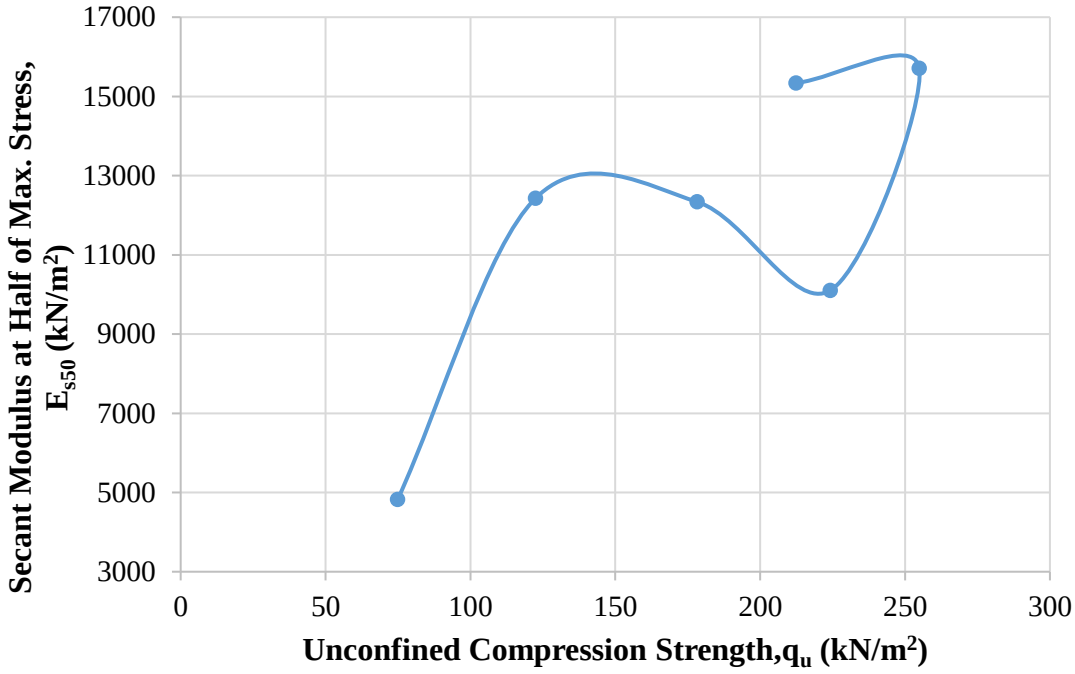

Figure 6.64 Relationship between secant modulus at 50% of maximum stress and unconfined compression strength (CH+0.25% Polypropylene)

The maximum secant modulus at 50% of maximum stress is obtained in sample 2 as 15706.7 kN/m^2 for 0.25% polypropylene-added high plasticity clay. It should be noted that the water content is 24%, the dry unit weight is 14.20 kN/m^3, and the unconfined compression strength is 254.9 kN/m^2 when the secant modulus at 50% of

maximum stress has the maximum value of 0.25% polypropylene-added high plasticity clay.

On the other hand, the relationship between tangent modulus at 50% of maximum stress (E_{t50}) and unconfined compression strength of 0.25% polypropylene-added high plasticity clay samples is shown in Figure 6.65.

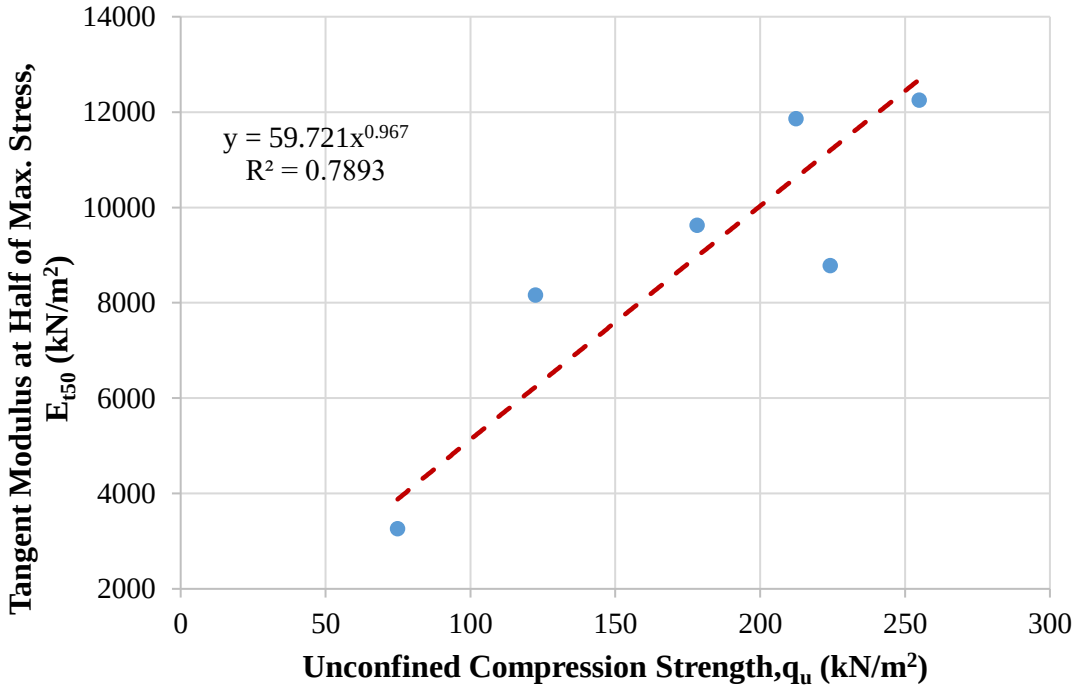

Figure 6.65 Relationship between tangent modulus at 50% of maximum stress and unconfined compression strength (CH+0.25% Polypropylene)

The maximum tangent modulus at 50% of maximum stress is obtained in sample 2 as 12251.9 kN/m^2 for 0.25% polypropylene-added high plasticity clay. It should be noted that the water content is 24%, the dry unit weight is 14.20 kN/m^3, and the unconfined compression strength is 254.9 kN/m^2 when the tangent modulus at 50% of maximum stress is the maximum value for 0.25% polypropylene-added high plasticity clay.

In addition, the relationship between secant modulus at failure point (E_{sf}) and unconfined compression strength of 0.25% polypropylene-added high plasticity clay samples is shown in Figure 6.66.

The maximum secant modulus at failure point is obtained in sample 2 as 10196 kN/m^2 for 0.25% polypropylene-added high plasticity clay. It should be noted that the water content is 24%, the dry unit weight is 14.20 kN/m^3, and the unconfined

compression strength is 254.9 kN/m^2 when the secant modulus at failure point is the maximum value for 0.25% polypropylene-added high plasticity clay.

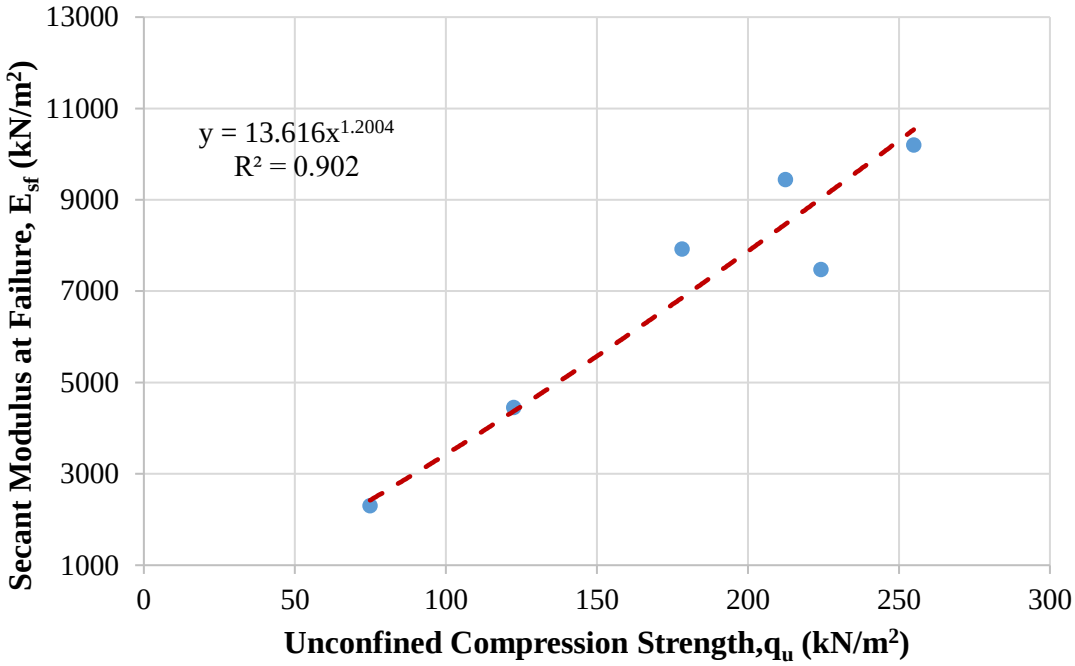

Figure 6.66 Relationship between secant modulus at failure point and unconfined compression strength (CH+0.25% Polypropylene)

With respect to the results of the tangent modulus at 50% of maximum stress, the secant modulus at 50% of maximum stress, and the secant modulus at failure, it seems that the maximum values of these moduli are obtained at maximum unconfined compression strength (sample 2 for 0.25% polypropylene-added high plasticity clay). However, values of water content and the dry unit weight are less than the optimum water content (w_{opt}=26%) and the maximum dry unit weight (γ_{dmax}=14.60 kN/m^3). Its reasons can be explained as the glue effect in polypropylene mixed clayey soils because of low water content. When polypropylene mixed with clayey soil is in dry condition, the soil can become stiffer. Also, high plasticity clayey soil's strength and load-deformation properties are improved by reinforcing with polypropylene fiber.

6.3.2 High Plasticity Clay Soil Mixture with 0.5% of Polypropylene

During the experimental program of this study, the amount of 0.5% polypropylene mixed with high plasticity clay soil was used. The compaction and the unconfined compression tests were performed on the 0.5% polypropylene mixed with

high plasticity clay, and the outcomes of these experiments are illustrated in Table 6.17. With respect to data obtained from mentioned tests, it can be seen that the value of ω_{opt} and γ_{dmax} obtained at 25.4% and 14.50 kN/m^3, respectively.

Table 6.17 Results of experiments executed with CH+0.5% polypropylene

Sample No.	ω (%)	γ_d (kN/m^3)	q_u (kN/m^2)
1	22	13.80	243.0
2	25	14.40	274.4
3	29	14.50	162.1
4	32	13.90	99.3
5	34	13.30	63.9

The axial stress-axial strain curves of five different 0.5% polypropylene-added high plasticity clay samples are shown in Figure 6.67. According to data obtained from the unconfined compression test of 0.5% polypropylene-added high plasticity clay soil samples, it can be inferred that the maximum unconfined compression strength was obtained in the second sample, and it was obtained as 274.4 kN/m^2.

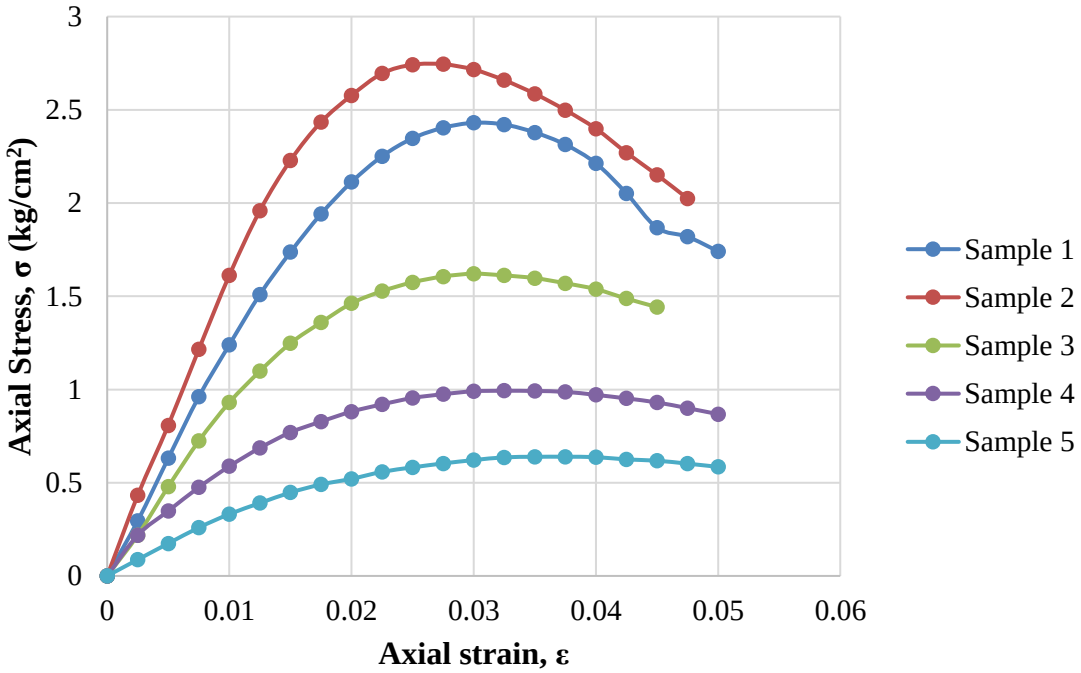

Figure 6.67 Results of unconfined compression tests of CH+0.5% polypropylene

It should be noted that the reciprocal of the initial tangent modulus (a) and the reciprocal of the asymptotic value of stress difference (b) were derived from transformed hyperbolic stress-strain curves of 0.5% polypropylene-added high plasticity clay samples. In addition, the asymptotic value of stress difference $(\sigma_1)_{ult}$, compressive strength $(\sigma_1)_f$, axial strain value at failure (ε_f), and axial strain value at 50% of maximum stress (ε_{50}) were obtained from unconfined compression test results. Lastly, the failure ratio (R_f) was calculated from unconfined compression test results. Mentioned engineering parameters are given in Table 6.18.

Table 6.18 Calculated engineering parameters of CH+0.5% polypropylene

Sample No.	a (cm^2/kg)	b (cm^2/kg)	$(\sigma_1)_{ult}$ (kg/cm^2)	$(\sigma_1)_f$ (kg/cm^2)	R_f -	ε_f -	ε_{50} -
1	0.0069	0.1508	6.631	2.430	0.37	0.0300	0.0098
2	0.0049	0.1576	6.345	2.744	0.43	0.0275	0.0085
3	0.0086	0.2857	3.500	1.621	0.46	0.0300	0.0085
4	0.0101	0.6603	1.514	0.993	0.66	0.0325	0.0080
5	0.0229	0.8324	1.201	0.639	0.53	0.0350	0.0096

It should be noted that the strain level of 0.5% polypropylene-added high plasticity clay is classified as small strain (SS) because the maximum axial strain was determined in samples 1, 4, and 5 of 0.5% polypropylene-added high plasticity clay. The maximum axial strain was obtained as 0.05%. Thus, it can be concluded that nonlinear behaviour was observed for the tested 0.5% polypropylene-added high plasticity clay soil samples.

Initial tangent modulus (E_i), tangent modulus at 50% of maximum stress (E_{t50}), secant modulus at failure (E_{sf}), secant modulus at 50% of maximum stress (E_{s50}), and unconfined compression strength (q_u) of five different 0.5% polypropylene-added high plasticity clay samples are given in Table 6.19.

According to the data obtained, it can be concluded that the maximum modulus values are observed in the initial tangent modulus compared with other soil moduli in all five 0.5% polypropylene-added high plasticity clay samples due to the initial slope of the stress-strain curve. In other words, the axial stress increases up to a certain point

very sharply. Then, this sharp increasing trend suddenly starts to slow down, and during this slowing trend, the axial strain increases rapidly.

Table 6.19 Soil moduli and unconfined compression strength of CH+0.5% polypropylene

Sample No.	E_i (kN/m^2)	E_{t50} (kN/m^2)	E_{sf} (kN/m^2)	E_{s50} (kN/m^2)	q_u (kN/m^2)
1	14492.8	9668.5	8100.0	12428.4	243.0
2	20408.2	12536.7	9978.2	16167.5	274.4
3	11627.9	6866.3	5403.3	9479.8	162.1
4	9901.0	4473.3	3055.4	6225.2	99.3
5	4366.8	2353.0	1825.7	3337.9	63.9

In addition, transformed hyperbolic stress-strain curves for five different 0.5% polypropylene-added high plasticity clay samples are illustrated in Figure 6.68.

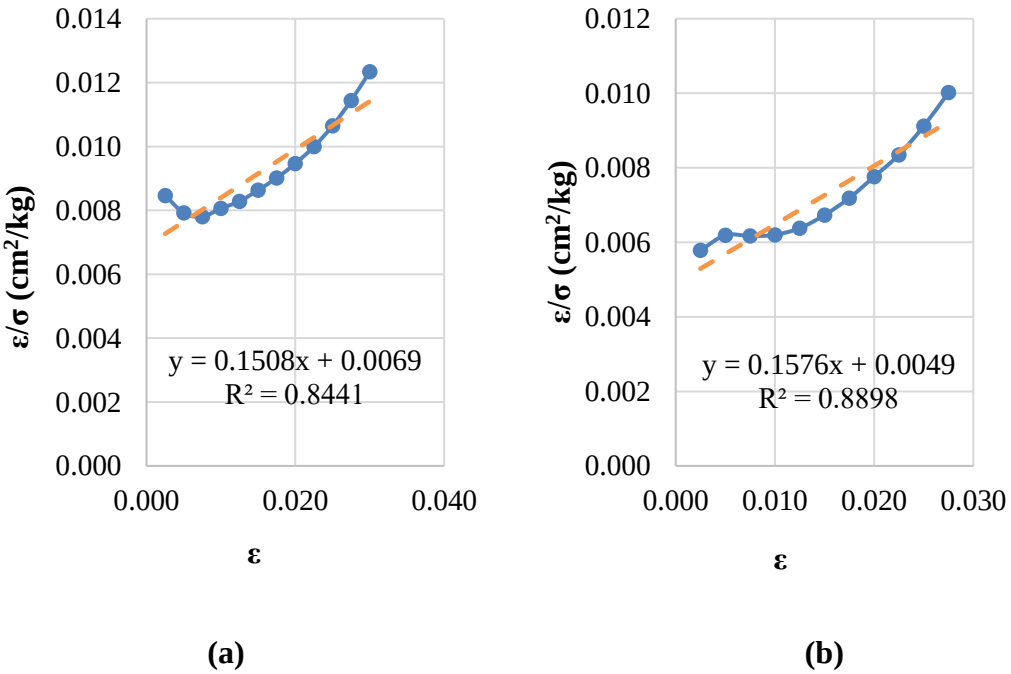

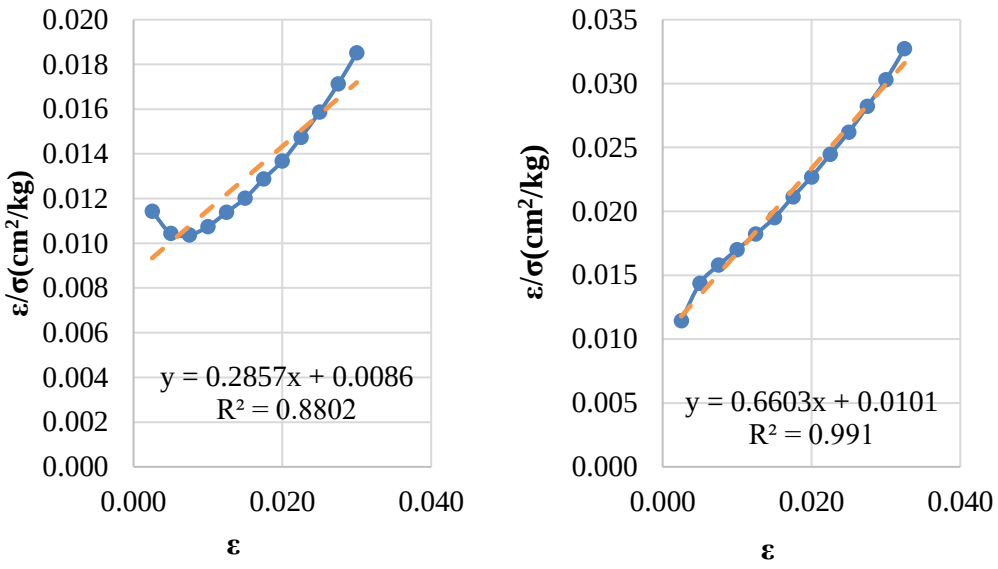

(c) **(d)**

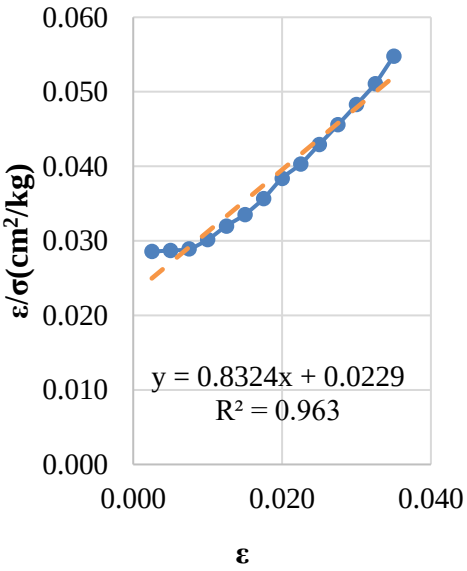

(e)

Figure 6.68 Transformed hyperbolic stress-strain curves for (a) sample 1, (b) sample 2, (c) sample 3, (d) sample 4, and (e) sample 5 (CH+0.5% Polypropylene)

It was found that low and high values of axial strains in samples 1, 2, and 3 are not precisely hyperbolic, as shown in Figures 6.68 (a, b, and c). In other words, these points can not be fitted in a straight line. However, it was possible to estimate the actual stress-strain curves by a hyperbola. Thus, it is found to have a reasonable degree of

accuracy. On the other hand, the transformed hyperbolic stress-strain curve in samples 4 and 5 is hyperbolic, as shown in Figures 6.68 (d and e). In other words, these points can be best-fitted in a straight line.

The relationship between the secant modulus at 50% of maximum stress (E_{s50}) and the initial tangent modulus (E_i) of 0.5% polypropylene-added high plasticity clay samples is shown in Figure 6.69.

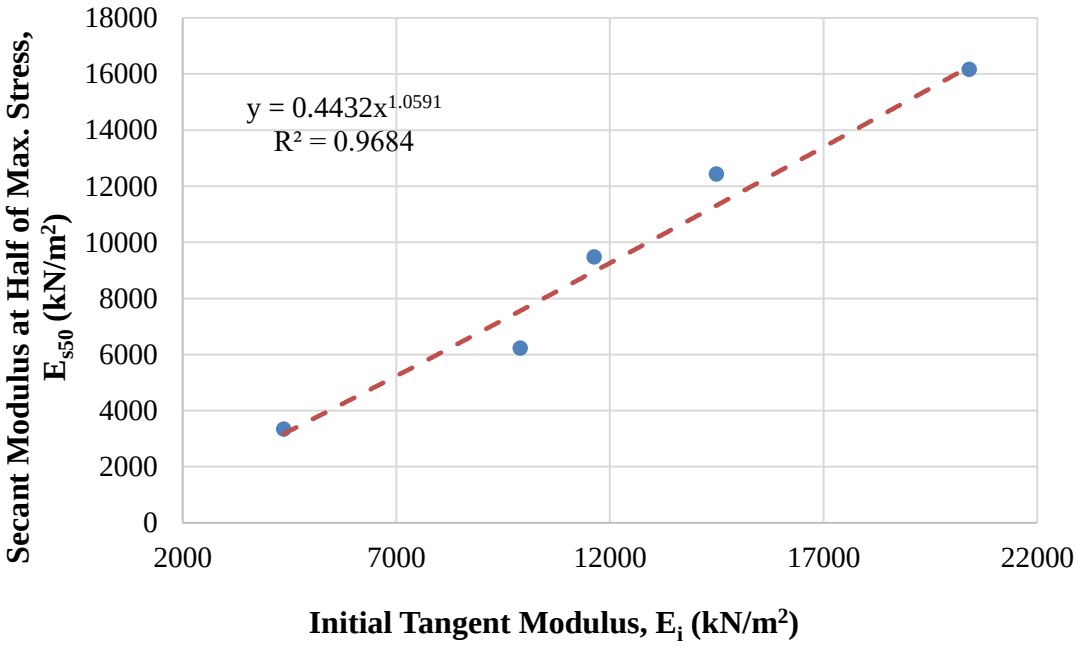

Figure 6.69 Relationship between secant modulus at 50% of maximum stress and initial tangent modulus (CH+0.5% Polypropylene)

According to the data, it can be inferred that these soil moduli refer to the hardening of 0.5% polypropylene-added high plasticity clay samples. Thus, the initial tangent modulus increases with the increasing secant modulus at 50% of maximum stress. Furthermore, it was best suited for estimating these soil moduli by a power model.

The relationship between the secant modulus at failure (E_{sf}) and the tangent modulus at 50% of maximum stress (E_{t50}) of 0.5% polypropylene-added high plasticity clay samples are shown in Figure 6.70.

The tangent modulus at 50% of maximum stress increases with the increasing secant modulus at failure. Thus, it was best suited for estimating these soil moduli by a power model.

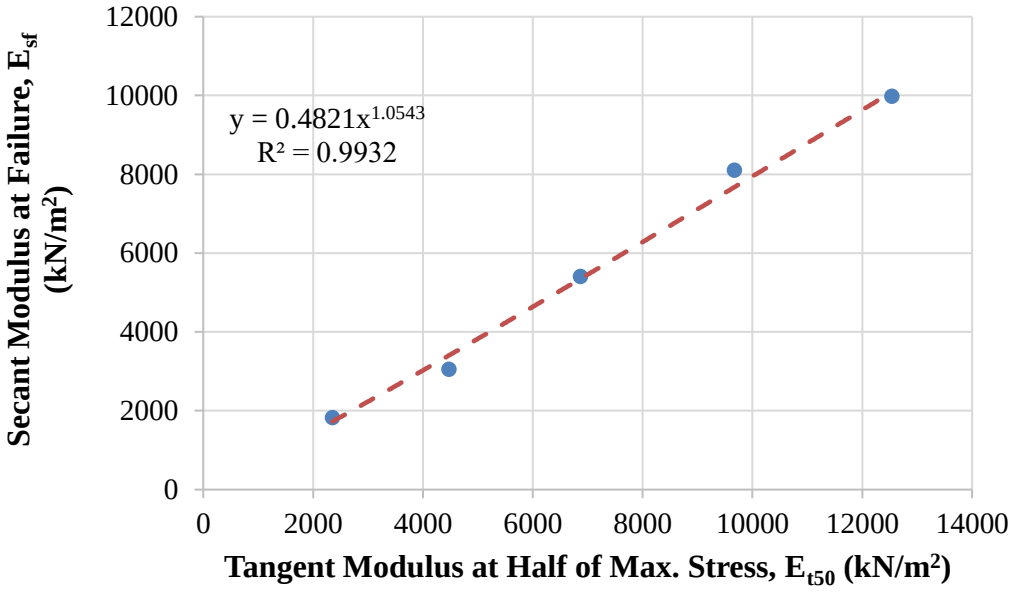

Figure 6.70 Relationship between secant modulus at failure point and tangent modulus at 50% of maximum stress (CH+0.5% Polypropylene)

Furthermore, the relationship between initial tangent modulus (E_i) and unconfined compression strength of 0.5% polypropylene-added high plasticity clay samples is shown in Figure 6.71.

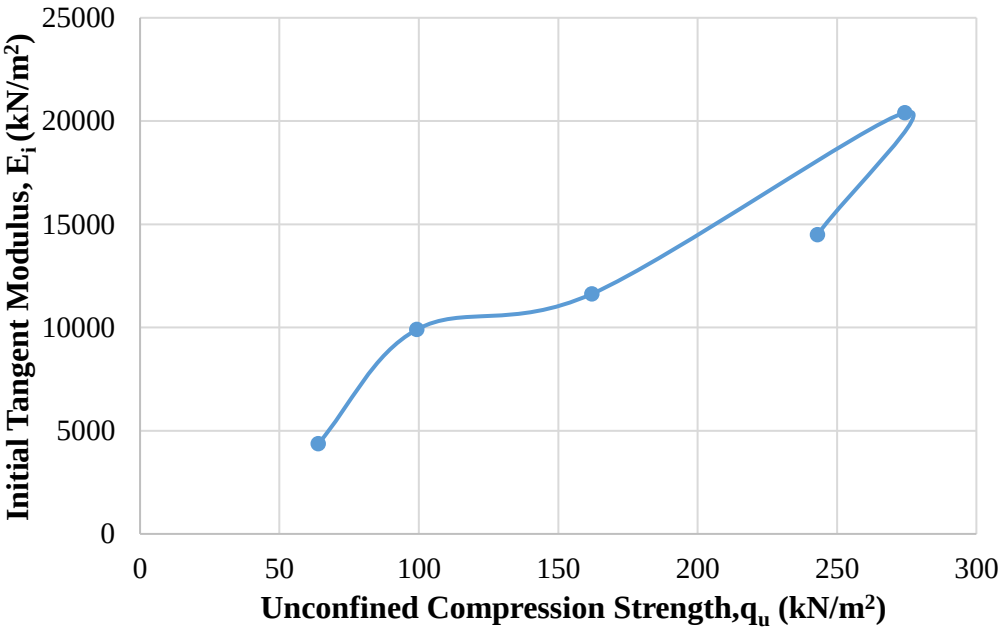

Figure 6.71 Relationship between initial tangent modulus and unconfined compression strength (CH+0.5% Polypropylene)

According to data, the maximum initial tangent modulus is obtained in sample 2 as 20408.2 kN/m^2 for 0.5% polypropylene-added high plasticity clay. It should be noted that the water content is 25%, the dry unit weight is 14.40 kN/m^3, and the unconfined compression strength is 274.4 kN/m^2 when the initial tangent modulus is the maximum value for 0.5% polypropylene-added high plasticity clay.

The relationship between secant modulus at 50% of maximum stress (E_{s50}) and unconfined compression strength of 0.5% polypropylene-added high plasticity clay samples is shown in Figure 6.72.

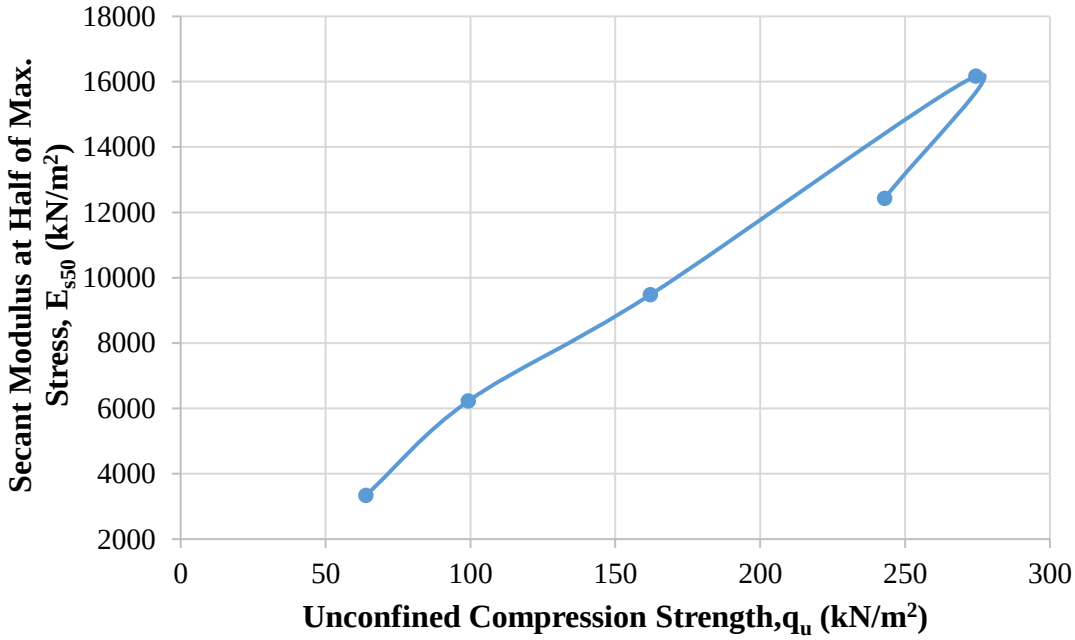

Figure 6.72 Relationship between secant modulus at 50% of maximum stress and unconfined compression strength (CH+0.5% Polypropylene)

The maximum secant modulus at 50% of maximum stress is obtained in sample 2 as 16167.5 kN/m^2 for 0.5% polypropylene-added high plasticity clay. It should be noted that the water content is 25%, the dry unit weight is 14.40 kN/m^3, and the unconfined compression strength is 274.4 kN/m^2 when the secant modulus at 50% of maximum stress has the maximum value of 0.5% polypropylene-added high plasticity clay.

On the other hand, the relationship between tangent modulus at 50% of maximum stress (E_{t50}) and unconfined compression strength of 0.5% polypropylene-added high plasticity clay samples is shown in Figure 6.73.

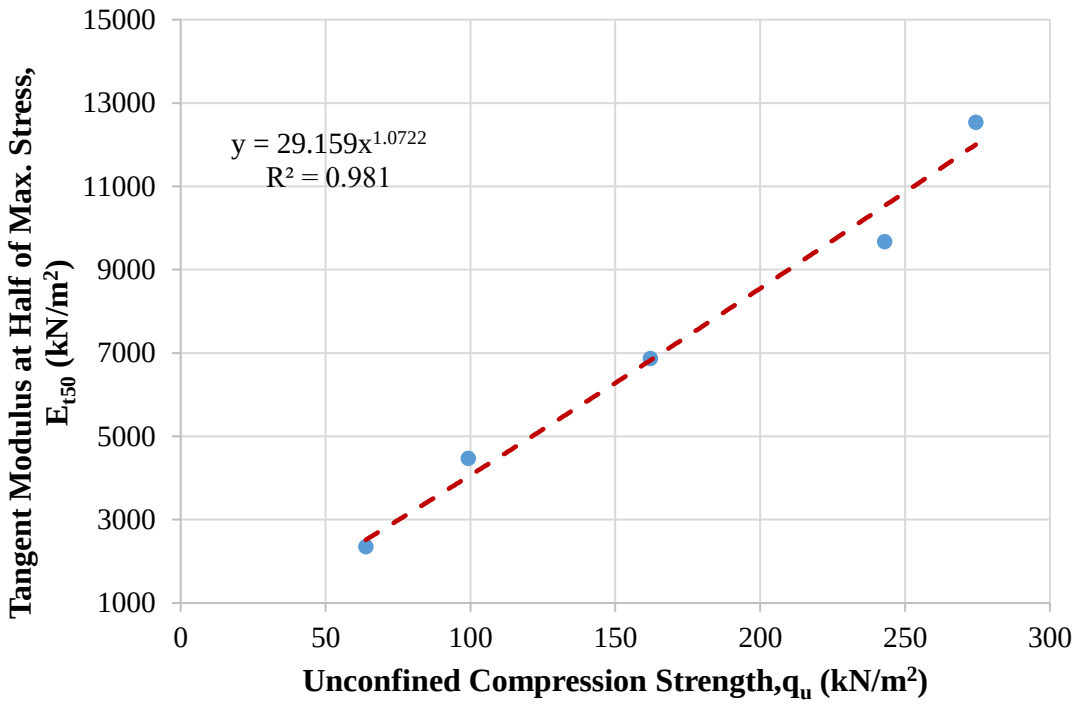

Figure 6.73 Relationship between tangent modulus at 50% of maximum stress and unconfined compression strength (CH+0.5% Polypropylene)

The maximum tangent modulus at 50% of maximum stress is obtained in sample 2 as 12536.7 kN/m^2 for 0.5% polypropylene-added high plasticity clay. It should be noted that the water content is 25%, the dry unit weight is 14.40 kN/m^3, and the unconfined compression strength is 274.4 kN/m^2 when the tangent modulus at 50% of maximum stress is the maximum value for the 0.5% polypropylene-added high plasticity clay.

In addition, the relationship between secant modulus at failure point (E_{sf}) and unconfined compression strength of 0.5% polypropylene-added high plasticity clay samples is shown in Figure 6.74.

It is obvious that the maximum secant modulus at failure point is obtained in sample 2 as 9978.2 kN/m^2 for 0.5% polypropylene-added high plasticity clay. It should be noted that the water content is 25%, the dry unit weight is 14.40 kN/m^3, and the unconfined compression strength is 274.4 kN/m^2 when the secant modulus at failure point is the maximum value for 0.5% polypropylene-added high plasticity clay.

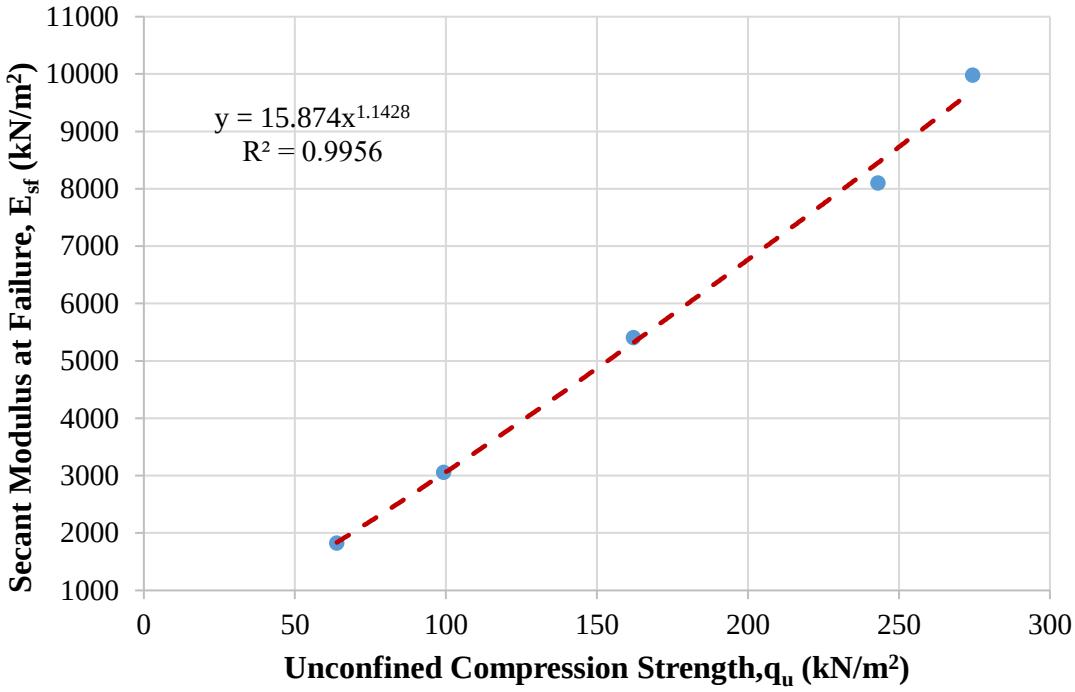

Figure 6.74 Relationship between secant modulus at failure point and unconfined compression strength (CH+0.5% Polypropylene)

With respect to the results of all calculated soil moduli, it seems that the maximum values of these moduli are obtained at maximum unconfined compression strength (sample 2 for 0.5% polypropylene-added high plasticity clay). On the other hand, when all calculated soil moduli have the maximum value for 0.5% polypropylene-added high plasticity clay, the water content is close to the optimum water content (w_{opt}=25.4%), and the dry unit weight is near to the maximum dry unit weight (γ_{dmax}=14.50 kN/m^3). Also, high plasticity clayey soil's strength and load-deformation properties are improved by reinforcing with polypropylene fiber.

6.3.3 High Plasticity Clay Soil Mixture with 0.75% of Polypropylene

During the experimental program of this study, the amount of 0.75% polypropylene mixed with high plasticity clay soil was used. The compaction and the unconfined compression tests were performed on the 0.75% polypropylene mixed with high plasticity clay, and the outcomes of these experiments are illustrated in Table 6.20. With respect to data obtained from mentioned tests, it can be seen that the value of ω_{opt} and γ_{dmax} obtained at 25% and 14.50 kN/m^3, respectively.

Table 6.20 Results of experiments executed with CH+0.75% polypropylene

Sample No.	ω (%)	γ_d (kN/m^3)	q_u (kN/m^2)
1	18	13.79	298.7
2	24	14.40	317.0
3	29	14.50	155.1
4	34	13.63	71.4
5	40	12.23	28.8

The axial stress-axial strain curves of five different 0.75% polypropylene-added high plasticity clay samples are shown in Figure 6.75. Besides, Figure 6.76 exhibits the tested 0.75% polypropylene-added high plasticity clay sample, which has the highest value of the maximum unconfined compression strength. Therefore, according to data obtained from the unconfined compression test of the 0.75% polypropylene-added high plasticity clay sample, it can be inferred that the maximum unconfined compression strength was obtained in the second sample, and it was obtained as 317 kN/m^2.

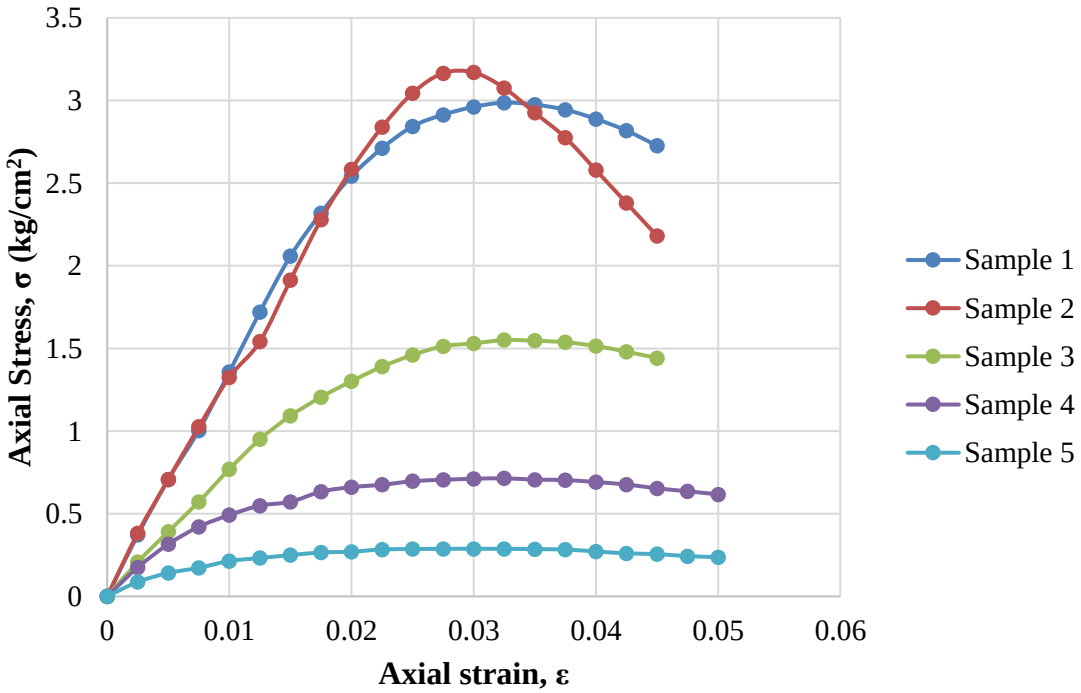

Figure 6.75 Results of unconfined compression tests of CH+0.75% polypropylene

It should be noted that the reciprocal of the initial tangent modulus (a) and the reciprocal of the asymptotic value of stress difference (b) were derived from transformed hyperbolic stress-strain curves of 0.75% polypropylene-added high plasticity clay samples. In addition, the asymptotic value of stress difference $(\sigma_1)_{ult}$, compressive strength $(\sigma_1)_f$, axial strain value at failure (ε_f), and axial strain value at 50% of maximum stress (ε_{50}) were obtained from unconfined compression test results. Lastly, the failure ratio (R_f) was calculated from unconfined compression test results. Mentioned engineering parameters are given in Table 6.21.

Table 6.21 Calculated engineering parameters of CH+0.75% polypropylene

Sample No.	a	b	$(\sigma_1)_{ult}$	$(\sigma_1)_f$	R_f	ε_f	ε_{50}
	(cm^2/kg)	(cm^2/kg)	(kg/cm^2)	(kg/cm^2)	-	-	-
1	0.0060	0.1210	8.264	2.987	0.36	0.0325	0.0109
2	0.0066	0.0753	13.280	3.170	0.24	0.0300	0.0128
3	0.0104	0.2816	3.551	1.551	0.44	0.0325	0.0101
4	0.0102	1.0448	0.957	0.714	0.75	0.0325	0.0060
5	0.0218	2.6067	0.384	0.288	0.75	0.0275	0.0052

It is obvious that, when the values of strains are between 0.1% to 0.001%, this region is categorized as a small strain. Furthermore, it should be noted that the strain level of 0.75% polypropylene-added high plasticity clay is classified as small strain (SS) because the maximum axial strain was determined in samples 4 and 5 of 0.75% polypropylene-added high plasticity clay, and it was obtained as 0.05%. Thus, it can be concluded that nonlinear behaviour was observed for the tested 0.75% polypropylene-added high plasticity clay.

Initial tangent modulus (E_i), tangent modulus at 50% of maximum stress (E_{t50}), secant modulus at failure (E_{sf}), secant modulus at 50% of maximum stress (E_{s50}), and unconfined compression strength (q_u) of five different 0.75% polypropylene-added high plasticity clay samples are given in Table 6.22.

According to the data obtained, it can be concluded that the maximum modulus values are observed in the initial tangent modulus compared with other soil moduli in all five 0.75% polypropylene-added high plasticity clay samples due to the initial slope of the stress-strain curve. In other words, the axial stress increases up to a certain point

very sharply. Then, this sharp increasing trend suddenly starts to slow down, and during this slowing trend, the axial strain increases rapidly.

Table 6.22 Soil moduli and unconfined compression strength of CH+0.75% polypropylene

Sample No.	E_i (kN/m^2)	E_{t50} (kN/m^2)	E_{sf} (kN/m^2)	E_{s50} (kN/m^2)	q_u (kN/m^2)
1	16666.7	11187.2	9190.8	13660.2	298.7
2	15151.5	11750.7	10566.7	12393.5	317.0
3	9615.4	5874.3	4772.3	7696.2	155.1
4	9803.9	3854.3	2196.9	5973.7	71.4
5	4587.2	1789.8	1047.3	2751.0	28.8

Figure 6.76 Peak point of CH+0.75% polypropylene (ω =25%, q_u=317 kN/m^2) (Etminan, 2012)

In addition, transformed hyperbolic stress-strain curves for five different 0.75% polypropylene-added high plasticity clay samples are illustrated in Figure 6.77.

It was found that low and high values of axial strains in samples 1, 2, and 3 are not precisely hyperbolic, as shown in Figures 6.77 (a, b, and c). In other words, these points can not be fitted in a straight line. However, it was possible to estimate the actual stress-strain curves by a hyperbola. Thus, it is found to have a reasonable degree of accuracy. On the other hand, the transformed hyperbolic stress-strain curve in samples

4 and 5 is hyperbolic, as shown in Figures 6.77 (d and e). In other words, these points can be best-fitted in a straight line.

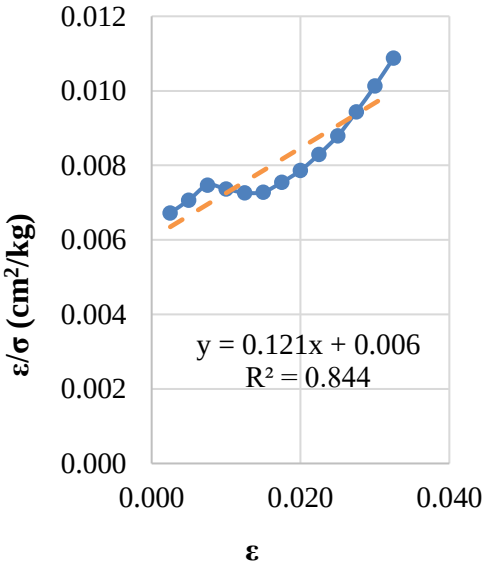

(a)

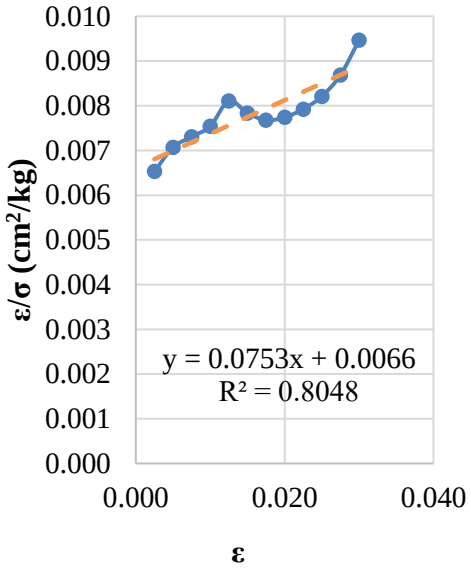

(b)

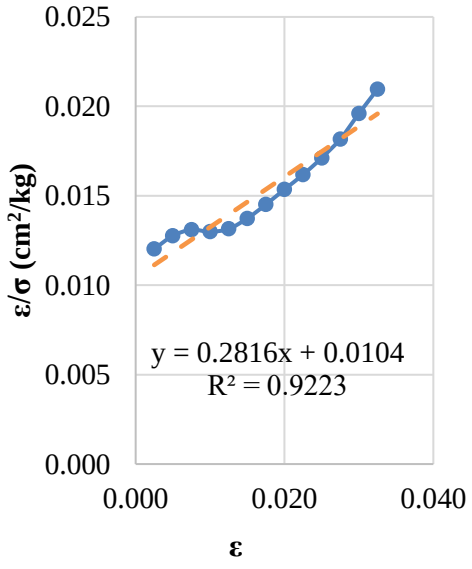

(c)

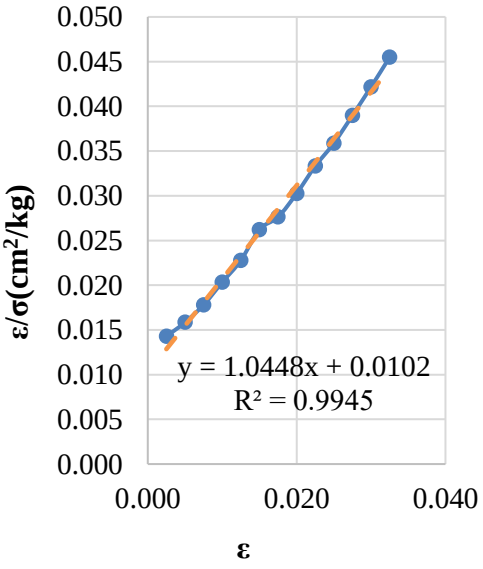

(d)

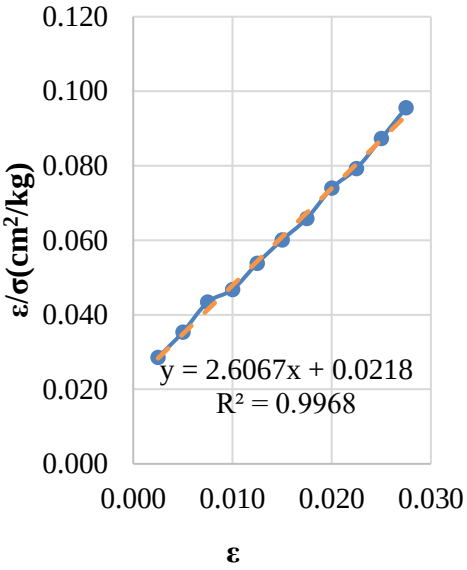

(e)

Figure 6.77**:** Transformed hyperbolic stress-strain curves for (a) sample 1, (b) sample 2, (c) sample 3, (d) sample 4, and (e) sample 5 (CH+0.75% Polypropylene)

The relationship between the secant modulus at 50% of maximum stress (E_{s50}) and the initial tangent modulus (E_i) of 0.75% polypropylene-added high plasticity clay samples is shown in Figure 6.78.

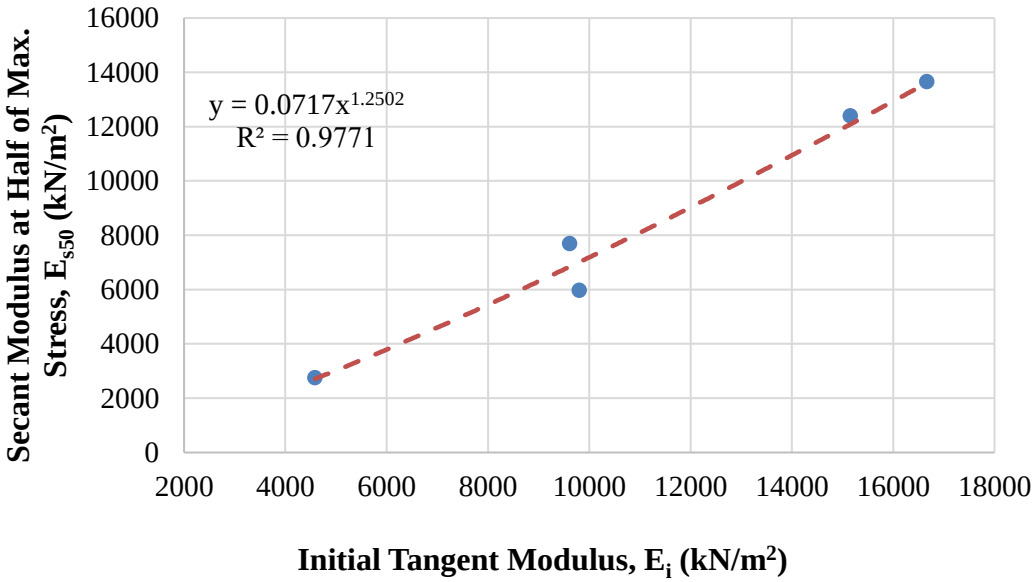

Figure 6.78 Relationship between secant modulus at 50% of maximum stress and initial tangent modulus (CH+0.75% Polypropylene)

According to the data, it can be inferred that these soil moduli refer to the hardening of 0.75% polypropylene-added high plasticity clay samples. Thus, the initial tangent modulus increases with the increasing secant modulus at 50% of maximum stress. Furthermore, it was best suited for estimating these soil moduli by a power model.

The relationship between the secant modulus at failure (E_{sf}) and the tangent modulus at 50% of maximum stress (E_{t50}) of 0.75% polypropylene-added high plasticity clay samples are shown in Figure 6.79.

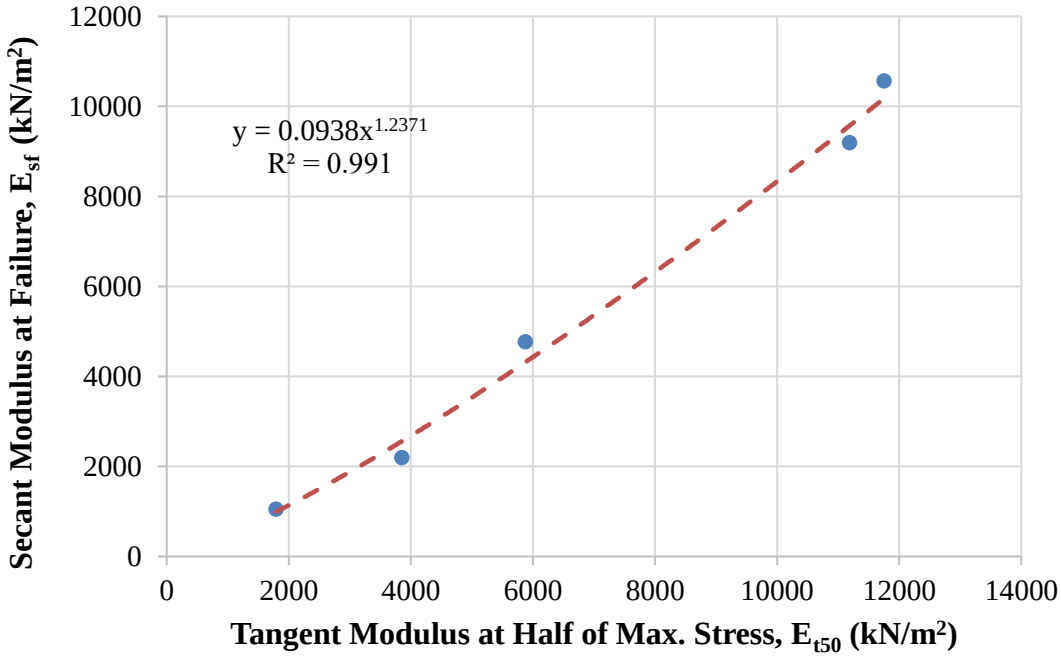

Figure 6.79 Relationship between secant modulus at failure point and tangent modulus at 50% of maximum stress (CH+0.75% Polypropylene)

The tangent modulus at 50% of maximum stress increases with the increasing secant modulus at failure. Thus, it was best suited for estimating these soil moduli by a power model.

Furthermore, the relationship between initial tangent modulus (E_i) and unconfined compression strength of 0.75% polypropylene-added high plasticity clay samples is shown in Figure 6.80.

According to data, the maximum initial tangent modulus is obtained in sample 1 as 16666.7 kN/m^2 for 0.75% polypropylene-added high plasticity clay. It should be noted that the water content is 18%, the dry unit weight is 13.79 kN/m^3, and the

unconfined compression strength is 298.7 kN/m^2 when the initial tangent modulus is the maximum value for 0.75% polypropylene-added high plasticity clay.

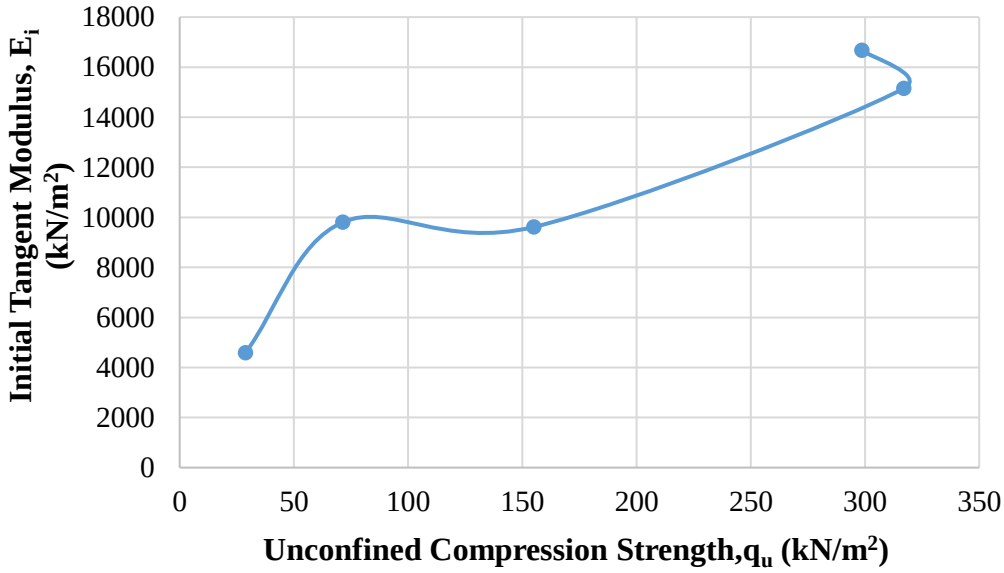

Figure 6.80 Relationship between initial tangent modulus and unconfined compression strength (CH+0.75% Polypropylene)

The relationship between secant modulus at 50% of maximum stress (E_{s50}) and unconfined compression strength of 0.75% polypropylene-added high plasticity clay samples is shown in Figure 6.81.

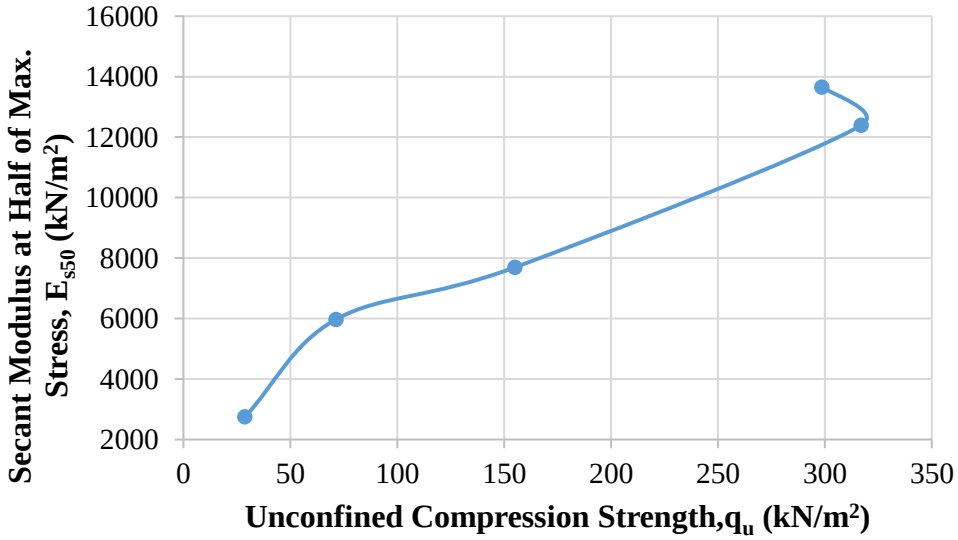

Figure 6.81 Relationship between secant modulus at 50% of maximum stress and unconfined compression strength (CH+0.75% Polypropylene)

The maximum secant modulus at 50% of maximum stress is obtained in sample 1 as 13660.2 kN/m^2 for 0.75% polypropylene-added high plasticity clay. It should be noted that the water content is 18%, the dry unit weight is 13.79 kN/m^3, and the unconfined compression strength is 298.7 kN/m^2 when the secant modulus at 50% of maximum stress has the maximum value of 0.75% polypropylene-added high plasticity clay.

With respect to the results of the initial tangent modulus and secant modulus at 50% of maximum stress, it seems that the maximum values of these moduli are not obtained at maximum unconfined compression strength (sample 2 for 0.75% polypropylene-added high plasticity clay) since the beginning of the stress-strain curve of sample 1 has rapidly increased in axial stress. On the other hand, when calculated initial tangent modulus and secant modulus at 50% of maximum stress have the maximum value for 0.75% polypropylene-added high plasticity clay, the water content is not equal to the optimum water content (w_{opt}=25%), and the dry unit weight is not equal to the maximum dry unit weight (γ_{dmax}=14.50 kN/m^3). High plasticity clay soil reinforced with polypropylene became stiffer when it was drier. Therefore, high plasticity clayey soil's strength and load-deformation properties are improved by reinforcing with polypropylene fiber.

On the other hand, the relationship between tangent modulus at 50% of maximum stress (E_{t50}) and unconfined compression strength of 0.75% polypropylene-added high plasticity clay samples is shown in Figure 6.82.

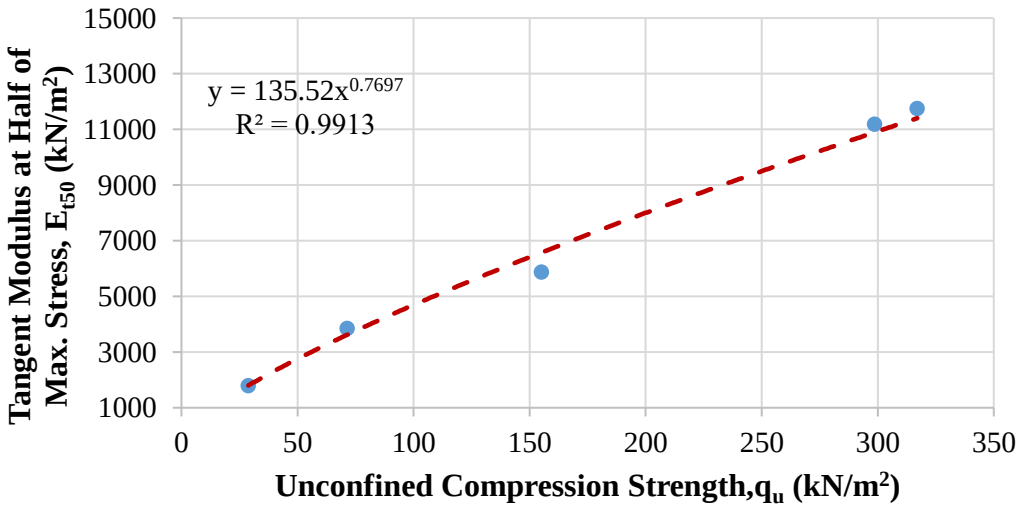

Figure 6.82 Relationship between tangent modulus at 50% of maximum stress and unconfined compression strength (CH+0.75% Polypropylene)

The maximum tangent modulus at 50% of maximum stress is obtained in sample 2 as 11750.7 kN/m^2 for 0.75% polypropylene-added high plasticity clay. It should be noted that the water content is 24%, the dry unit weight is 14.40 kN/m^3, and the unconfined compression strength is 317 kN/m^2 when the tangent modulus at 50% of maximum stress is the maximum value for the 0.75% polypropylene-added high plasticity clay.

In addition, the relationship between secant modulus at failure point (E_{sf}) and unconfined compression strength of 0.75% polypropylene-added high plasticity clay samples is shown in Figure 6.83.

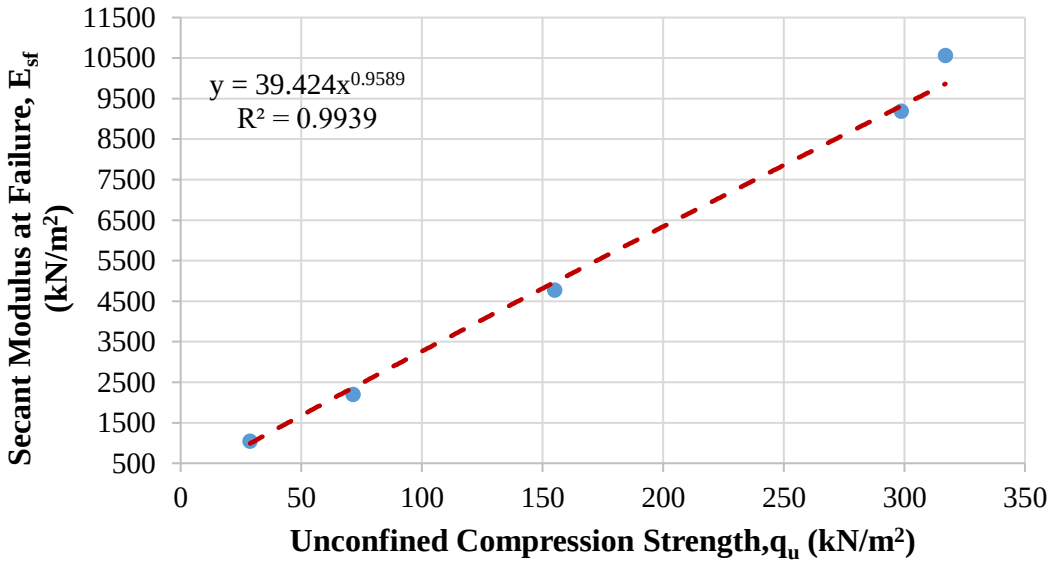

Figure 6.83 Relationship between secant modulus at failure point and unconfined compression strength (CH+0.75% Polypropylene)

It is obvious that the maximum secant modulus at failure point is obtained in sample 2 as 10566.7 kN/m^2 for 0.75% polypropylene-added high plasticity clay. It should be noted that the water content is 24%, the dry unit weight is 14.40 kN/m^3, and the unconfined compression strength is 317 kN/m^2 when the secant modulus at failure point is the maximum value for 0.75% polypropylene-added high plasticity clay.

With respect to the results of the calculated tangent modulus at 50% of maximum stress and secant modulus at failure point, it seems that the maximum values of these moduli are obtained at maximum unconfined compression strength (sample 2 for 0.75% polypropylene-added high plasticity clay). On the other hand, when all calculated soil moduli have the maximum value for 0.75% polypropylene-added high

plasticity clay, the water content is close to the optimum water content (w_{opt}=25%), and the dry unit weight is near to the maximum dry unit weight (γ_{dmax}=14.50 kN/m^3). Also, high plasticity clayey soil's strength and load-deformation properties are improved by reinforcing with polypropylene fiber.

6.3.4 High Plasticity Clay Soil Mixture with 1% of Polypropylene

During the experimental program of this study, the amount of 1% polypropylene mixed with high plasticity clay soil was used. The compaction and the unconfined compression tests were performed on the 1% polypropylene mixed with high plasticity clay, and the outcomes of these experiments are illustrated in Table 6.23. With respect to data obtained from mentioned tests, it can be seen that the value of ω_{opt} and γ_{dmax} obtained at 25.7% and 14.60 kN/m^3, respectively.

Table 6.23 Results of experiments executed with CH+1% polypropylene

Sample No.	ω (%)	γ_d (kN/m^3)	q_u (kN/m^2)
1	17	13.20	196.6
2	21	14.25	315.4
3	25	14.58	234.4
4	29	14.20	116.0
5	32	13.55	77.5

The axial stress-axial strain curves of five different 1% polypropylene-added high plasticity clay samples are shown in Figure 6.84. Besides, Figure 6.85 exhibits the tested 1% polypropylene-added high plasticity clay sample, which has the highest value of the maximum unconfined compression strength. Therefore, according to data obtained from the unconfined compression test of the 1% polypropylene-added high plasticity clay sample, it can be inferred that the maximum unconfined compression strength was obtained in the second sample, and it was obtained as 315.4 kN/m^2.

It should be noted that the reciprocal of the initial tangent modulus (a), reciprocal of the asymptotic value of stress difference (b), asymptotic value of stress difference $(\sigma_1)_{ult}$, compressive strength $(\sigma_1)_f$, failure ratio (R_f), axial strain value at failure (ε_f) and axial strain value at 50% of maximum stress (ε_{50}) are required parameters to obtain soil moduli. These parameters were derived from unconfined compression test results

and transformed hyperbolic stress-strain curves of 1% polypropylene-added high plasticity clay samples. Mentioned engineering parameters are given in Table 6.24.

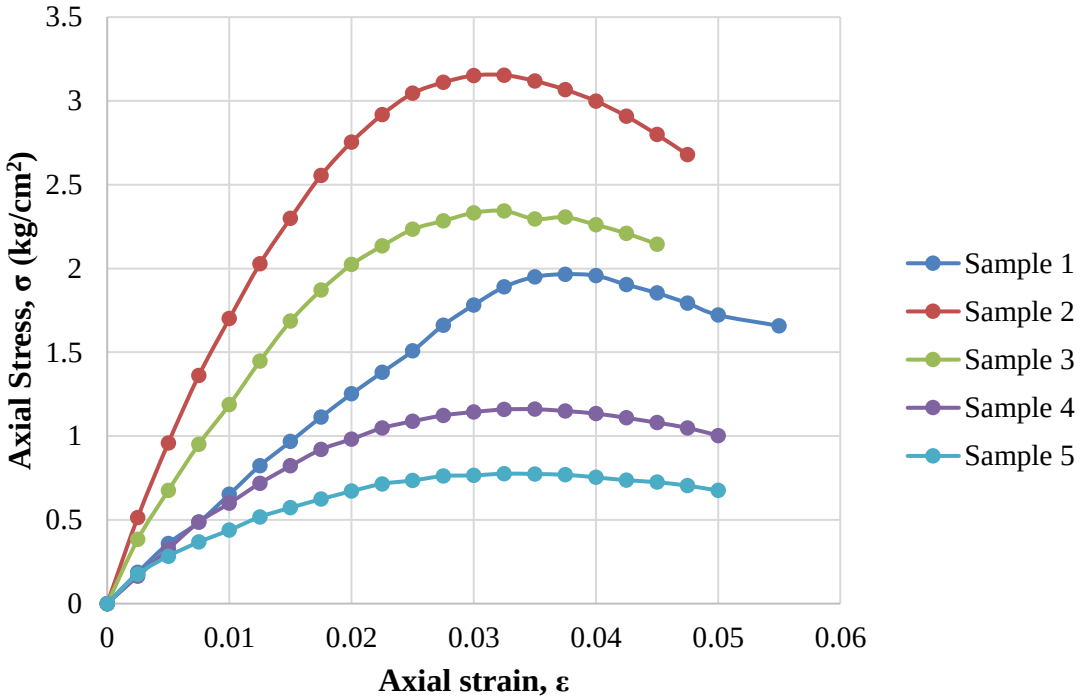

Figure 6.84 Results of unconfined compression tests of CH+1% polypropylene

Table 6.24 Calculated engineering parameters of CH+1% polypropylene

Sample No.	a (cm^2/kg)	b (cm^2/kg)	$(\sigma_1)_{ult}$ (kg/cm^2)	$(\sigma_1)_f$ (kg/cm^2)	R_f -	ε_f -	ε_{50} -
1	0.0136	0.1217	8.217	1.966	0.24	0.0375	0.0153
2	0.0041	0.1721	5.811	3.154	0.54	0.0325	0.0091
3	0.0059	0.2220	4.505	2.344	0.52	0.0325	0.0098
4	0.0121	0.4614	2.167	1.160	0.54	0.0350	0.0096
5	0.0132	0.8530	1.172	0.775	0.66	0.0325	0.0082

It is obvious that, when the values of strains are between 0.1% to 0.001%, this region is categorized as a small strain. Furthermore, it should be noted that the strain level of 1% polypropylene-added high plasticity clay is classified as small strain (SS) because the maximum axial strain was determined in the first sample of 1% polypropylene-added high plasticity clay, and it was obtained as 0.055%. Thus, it can

be concluded that nonlinear behaviour was observed for the tested 1% polypropylene-added high plasticity clay.

Initial tangent modulus, tangent modulus at 50% of maximum stress, secant modulus at failure, secant modulus at 50% of maximum stress, and unconfined compression strength of five different 1% polypropylene-added high plasticity clay samples are given in Table 6.25.

Table 6.25 Soil moduli and unconfined compression strength of CH+1% polypropylene

Sample No.	E_i (kN/m^2)	E_{t50} (kN/m^2)	E_{sf} (kN/m^2)	E_{s50} (kN/m^2)	q_u (kN/m^2)
1	7352.9	5698.9	5242.7	6436.6	196.6
2	24390.2	12947.7	9704.6	17343.2	315.4
3	16949.2	9276.7	7212.3	11909.2	234.4
4	8264.5	4433.0	3314.3	6054.5	116.0
5	7575.8	3395.3	2384.6	4713.1	77.5

According to the data obtained, it can be concluded that the maximum modulus values are observed in the initial tangent modulus compared with other soil moduli in all five 1% polypropylene-added high plasticity clay samples due to the initial slope of the stress-strain curve. In other words, the axial stress increases up to a certain point very sharply. Then, this sharp increasing trend suddenly starts to slow down, and during this slowing trend, the axial strain increases rapidly.

Figure 6.85 Peak point of CH+1% polypropylene (ω =25.7%, q_u=315.4 kN/m^2) (Etminan, 2012)

In addition, transformed hyperbolic stress-strain curves for five different 1% polypropylene-added high plasticity clay samples are illustrated in Figure 6.86.

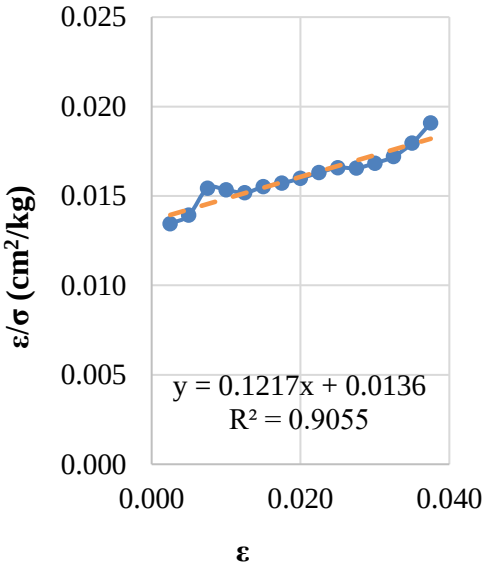

(a)

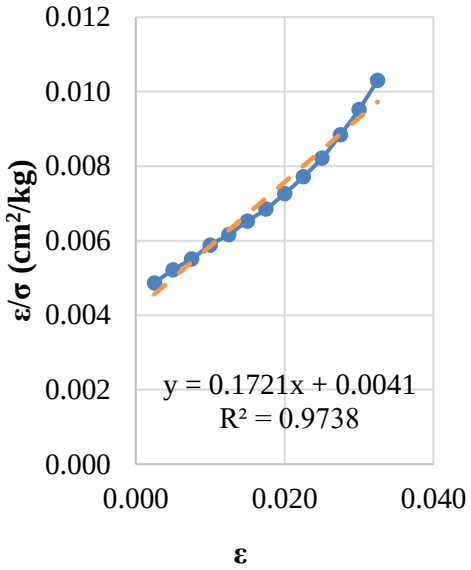

(b)

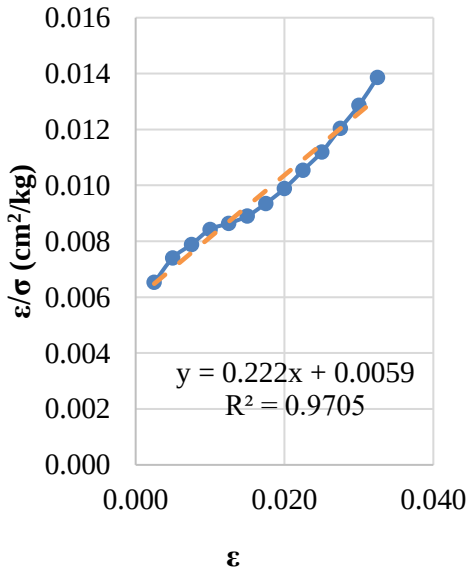

(c)

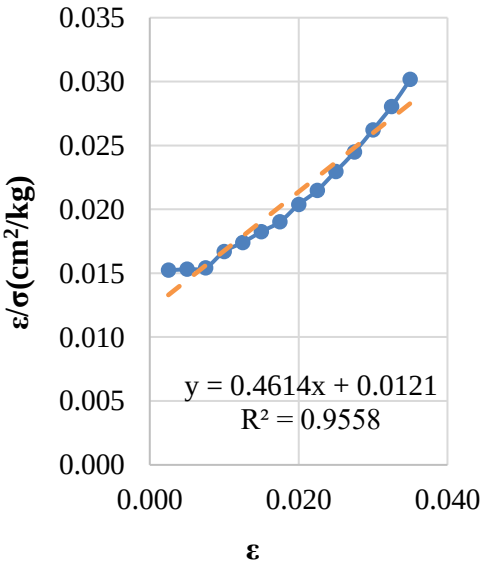

(d)

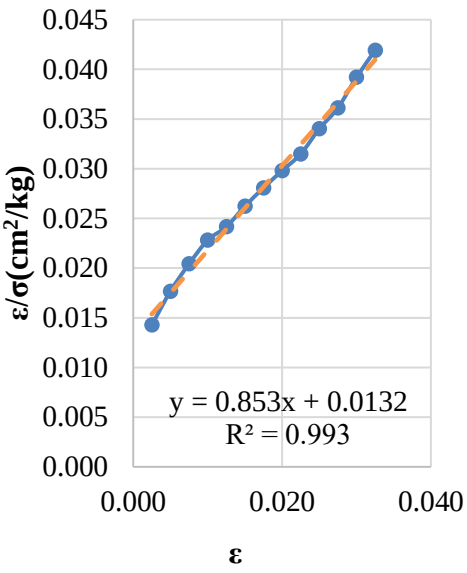

(e)

Figure 6.86 Transformed hyperbolic stress-strain curves for (a) sample 1, (b) sample 2, (c) sample 3, (d) sample 4, and (e) sample 5 (CH+1% Polypropylene)

It was found that low and high values of axial strains in samples 1 and 4 are not precisely hyperbolic, as shown in Figures 6.86 (a and d). In other words, these points can not be fitted in a straight line. However, it was possible to estimate the actual stress-strain curves by a hyperbola. Thus, it is found to have a reasonable degree of accuracy. On the other hand, the transformed hyperbolic stress-strain curve in samples 2, 3, and 5 is hyperbolic, as shown in Figures 6.86 (b, c, and e). In other words, these points can be best-fitted in a straight line.

The relationship between the secant modulus at 50% of maximum stress (E_{s50}) and the initial tangent modulus (E_i) of 1% polypropylene-added high plasticity clay samples is shown in Figure 6.87.

According to the data, it can be inferred that these soil moduli refer to the hardening of 1% polypropylene-added high plasticity clay samples. Thus, the initial tangent modulus increases with the increasing secant modulus at 50% of maximum stress. Furthermore, it was best suited for estimating these soil moduli by a power model.

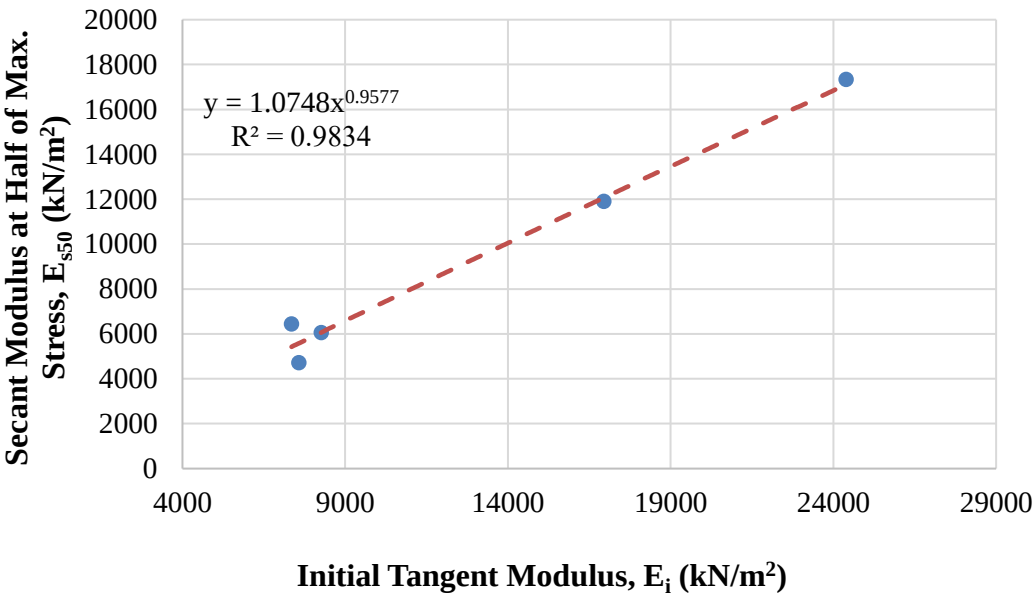

Figure 6.87 Relationship between secant modulus at 50% of maximum stress and initial tangent modulus (CH+1% Polypropylene)

The relationship between the secant modulus at failure (E_{sf}) and the tangent modulus at 50% of maximum stress (E_{t50}) of 1% polypropylene-added high plasticity clay samples is shown in Figure 6.88.

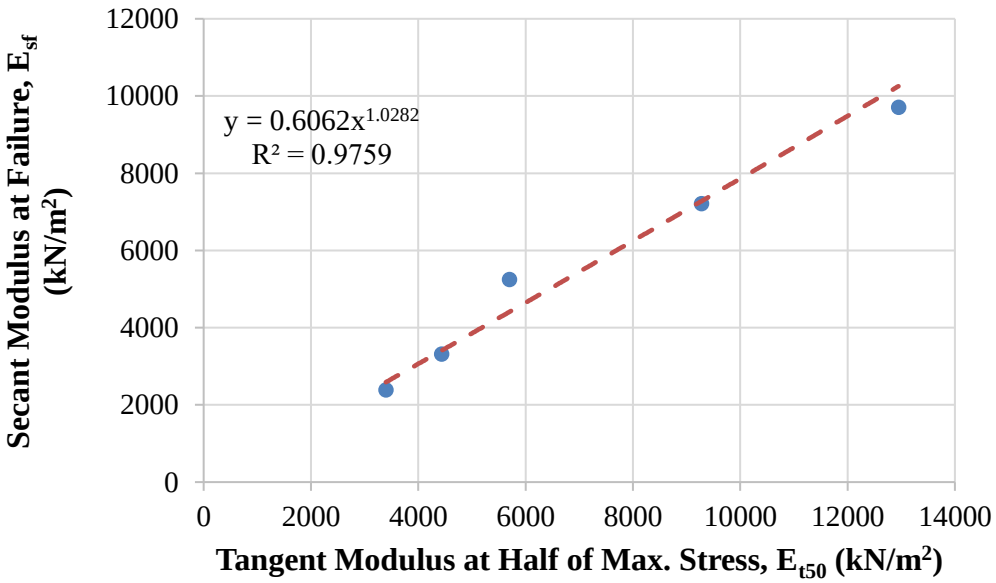

Figure 6.88 Relationship between secant modulus at failure point and tangent modulus at 50% of maximum stress (CH+1% Polypropylene)

The tangent modulus at 50% of maximum stress increases with the increasing secant modulus at failure. Thus, it was best suited for estimating these soil moduli by a power model.

Furthermore, the relationship between initial tangent modulus (E_i) and unconfined compression strength of 1% polypropylene-added high plasticity clay samples is shown in Figure 6.89.

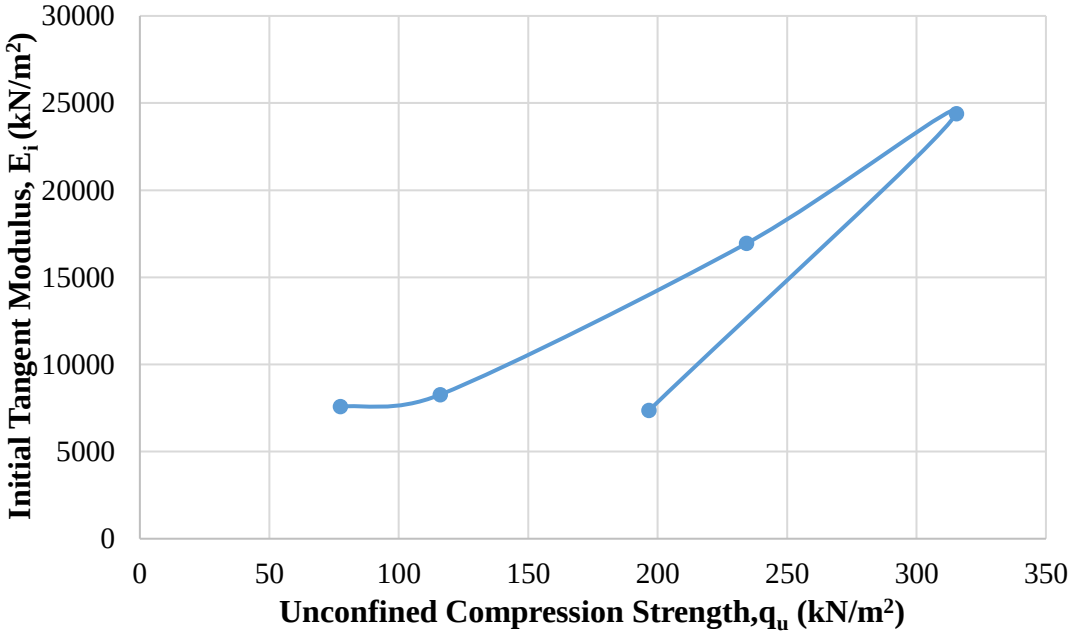

Figure 6.89 Relationship between initial tangent modulus and unconfined compression strength (CH+1% Polypropylene)

According to data, the maximum initial tangent modulus is obtained in sample 2 as 24390.2 kN/m^2 for 1% polypropylene-added high plasticity clay. It should be noted that the water content is 21%, the dry unit weight is 14.25 kN/m^3, and the unconfined compression strength is 315.4 kN/m^2 when the initial tangent modulus is the maximum value for 1% polypropylene-added high plasticity clay.

The relationship between secant modulus at 50% of maximum stress (E_{s50}) and unconfined compression strength of 1% polypropylene-added high plasticity clay samples is shown in Figure 6.90.

The maximum secant modulus at 50% of maximum stress is obtained in sample 2 as 17343.2 kN/m^2 for 1% polypropylene-added high plasticity clay. It should be noted that the water content is 21%, the dry unit weight is 14.25 kN/m^3, and the

unconfined compression strength is 315.4 kN/m^2 when the secant modulus at 50% of maximum stress has the maximum value of 1% polypropylene-added high plasticity clay.

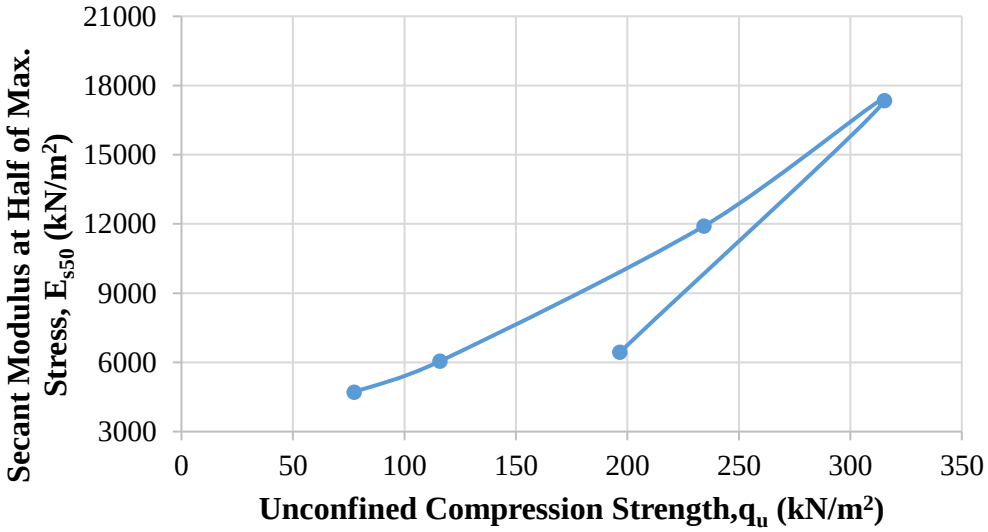

Figure 6.90 Relationship between secant modulus at 50% of maximum stress and unconfined compression strength (CH+1% Polypropylene)

On the other hand, the relationship between tangent modulus at 50% of maximum stress (E_{t50}) and unconfined compression strength of 1% polypropylene-added high plasticity clay samples is shown in Figure 6.91.

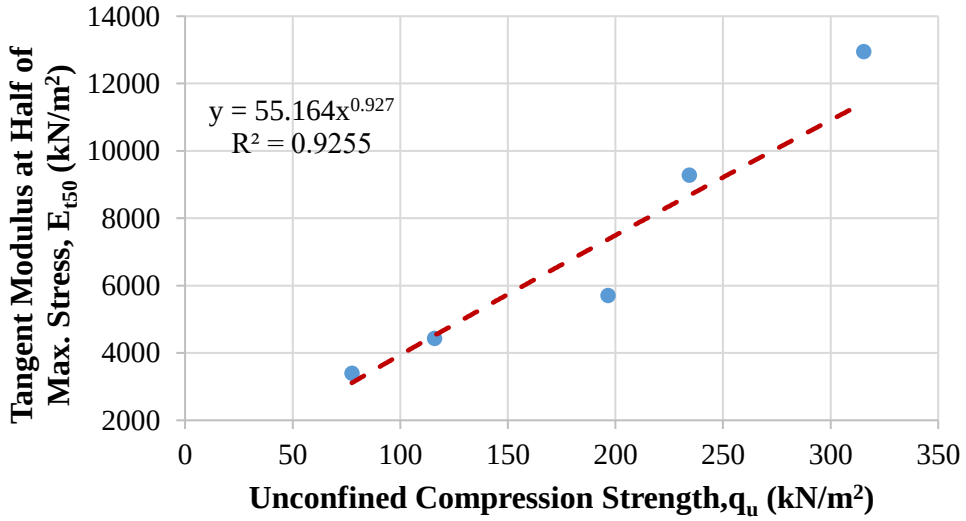

Figure 6.91 Relationship between tangent modulus at 50% of maximum stress and unconfined compression strength (CH+1% Polypropylene)

According to data, the maximum tangent modulus at 50% of maximum stress is obtained in sample 2 as 12947.2 kN/m^2 for 1% polypropylene-added high plasticity clay. It should be noted that the water content is 21%, the dry unit weight is 14.25 kN/m^3, and the unconfined compression strength is 315.4 kN/m^2 when the tangent modulus at 50% of maximum stress is the maximum value for the 1% polypropylene-added high plasticity clay.

In addition, the relationship between secant modulus at failure point (E_{sf}) and unconfined compression strength of 1% polypropylene-added high plasticity clay samples is shown in Figure 6.92.

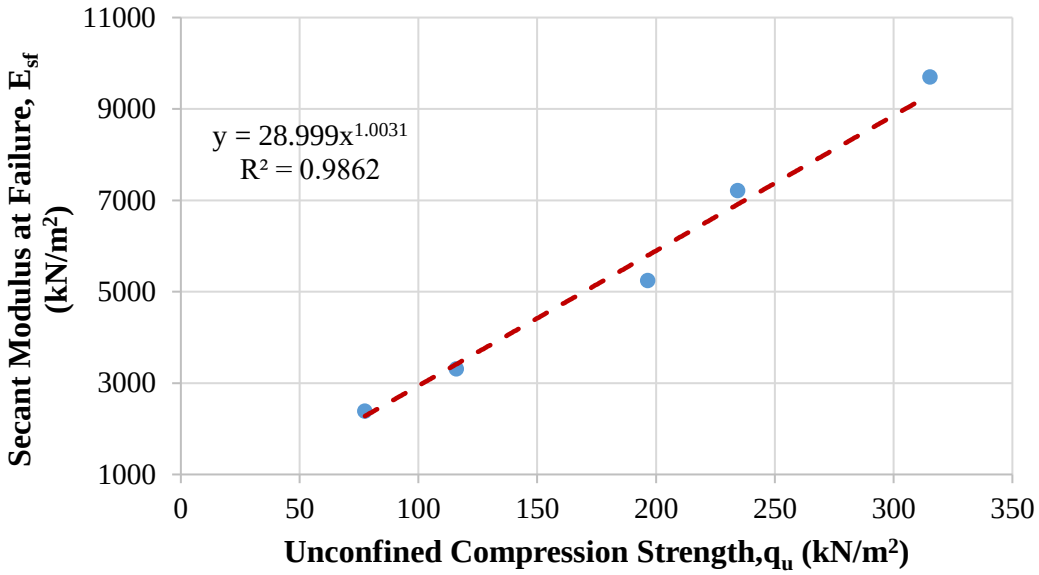

Figure 6.92 Relationship between secant modulus at failure point and unconfined compression strength (CH+1% Polypropylene)

It is obvious that the maximum secant modulus at failure point is obtained in sample 2 as 9704.6 kN/m^2 for 1% polypropylene-added high plasticity clay. It should be noted that the water content is 21%, the dry unit weight is 14.25 kN/m^3, and the unconfined compression strength is 315.4 kN/m^2 when the secant modulus at failure point is the maximum value for 1% polypropylene-added high plasticity clay.

With respect to the results of all calculated soil moduli, it seems that the maximum values of these moduli are obtained at maximum unconfined compression strength (sample 2 for 1% polypropylene-added high plasticity clay). On the other hand, when all calculated soil moduli have the maximum value for 1% polypropylene-

added high plasticity clay, the water content is not equal to the optimum water content (w_{opt}=25.7%), and the dry unit weight is close to the maximum dry unit weight (γ_{dmax}=14.60 kN/m^3). High plasticity clay soil reinforced with polypropylene became stiffer when it was drier. Also, high plasticity clayey soil's strength and load-deformation properties are improved by reinforcing with polypropylene fiber.

6.3.5 Comparison of Four Different Polypropylene Mixtures with High Plasticity Clay Soil

Four different amounts of polypropylene (0.25%, 0.5%, 0.75%, and 1%) mixed with high plasticity clay soil were prepared to analyze deformation moduli. The soil moduli of the mentioned high plasticity clay-polypropylene mixtures are compared with the plain high plasticity clay. Figure 6.93 exhibits the relationship between the maximum initial tangent modulus and different polypropylene content of CH.

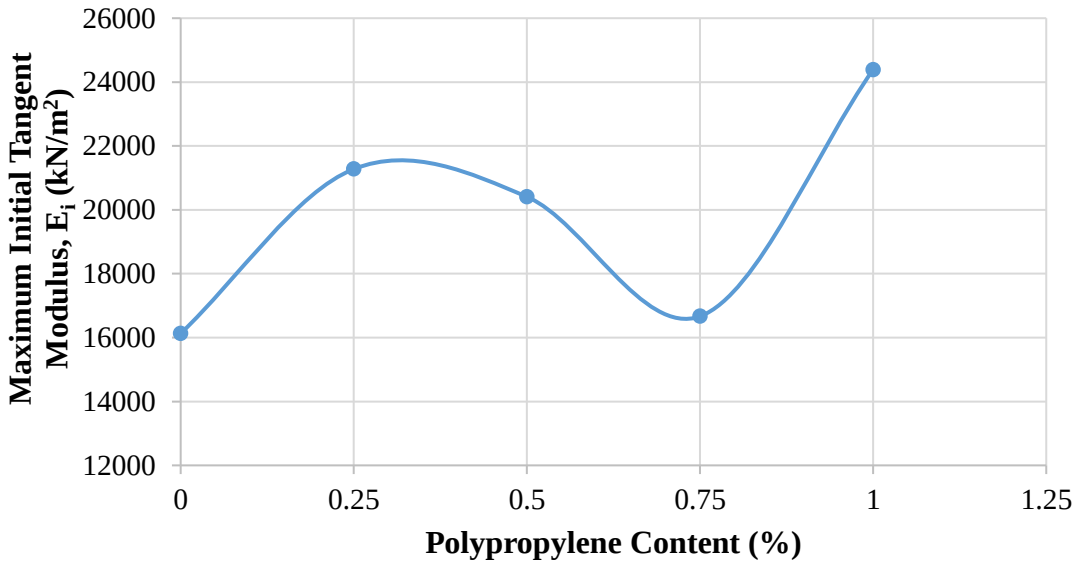

Figure 6.93 Relationship between maximum initial tangent modulus and different polypropylene contents of CH

After analyzing all initial tangent modulus of high plasticity clay-polypropylene mixtures and comparing them in a graph, it can be seen that the maximum initial tangent modulus was obtained in the mixture with 1% of polypropylene. In addition, the initial tangent modulus increases up to 51% in the mixture with 1% of polypropylene. In other words, the initial tangent modulus increases up to the mixture

with 0.25% of polypropylene. Then, it started to decrease with the increasing polypropylene content up to the mixture with 0.75% of polypropylene.

As the next step, all secant modulus at 50% of maximum stress of high plasticity clay- polypropylene mixtures were gathered and compared in Figure 6.94.

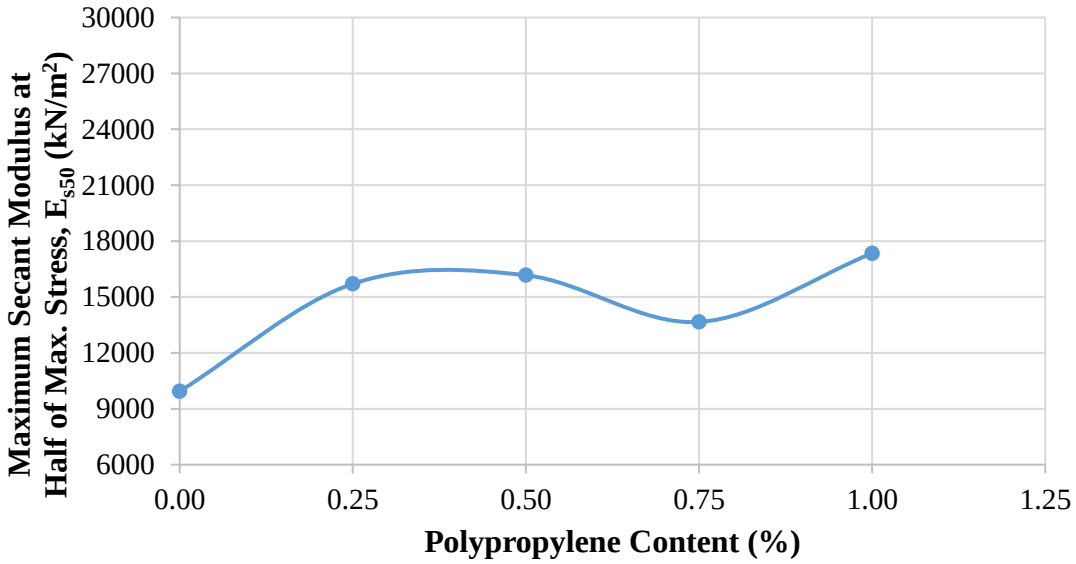

Figure 6.94 Relationship between maximum secant modulus at 50% of maximum stress and different polypropylene contents of CH

It can be seen that the maximum secant modulus at 50% of maximum stress was obtained in the mixture with 1% of polypropylene. In addition, the secant modulus at 50% of maximum stress increases up to 74% for the mixture with 1% of polypropylene. In other words, the initial tangent modulus increases up to the mixture with 0.25% of polypropylene. Then, it started to decrease with the increasing polypropylene content up to the mixture with 0.75% of polypropylene.

Furthermore, after gathering all tangent modulus at 50% of maximum stress of high plasticity clay- polypropylene mixtures were shown and compared them in Figure 6.95.

It can be seen that the maximum tangent modulus at 50% of maximum stress was obtained in the mixture with 1% of polypropylene. In addition, the tangent modulus at 50% of maximum stress increases up to 78% in the mixture with 1% of polypropylene. In other words, the initial tangent modulus increases up to the mixture with 0.25% of polypropylene. Then, it started to decrease with the increasing polypropylene content up to the mixture with 0.75% of polypropylene.

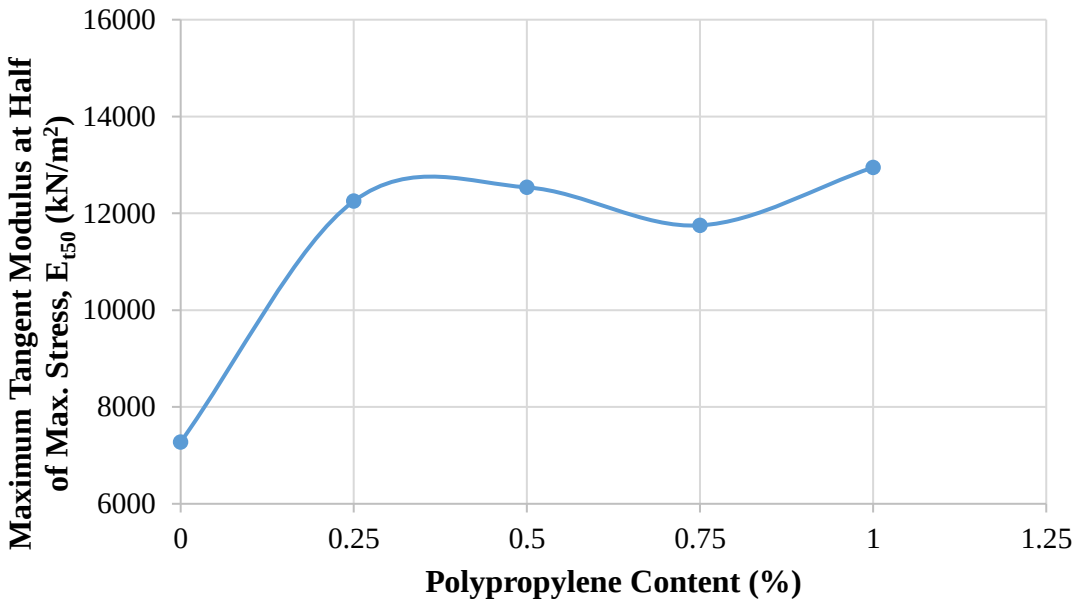

Figure 6.95 Relationship between maximum tangent modulus at 50% of maximum stress and different polypropylene contents of CH

Moreover, Figure 6.96 exhibits the relationship between the maximum secant modulus at failure point and different polypropylene contents of CH.

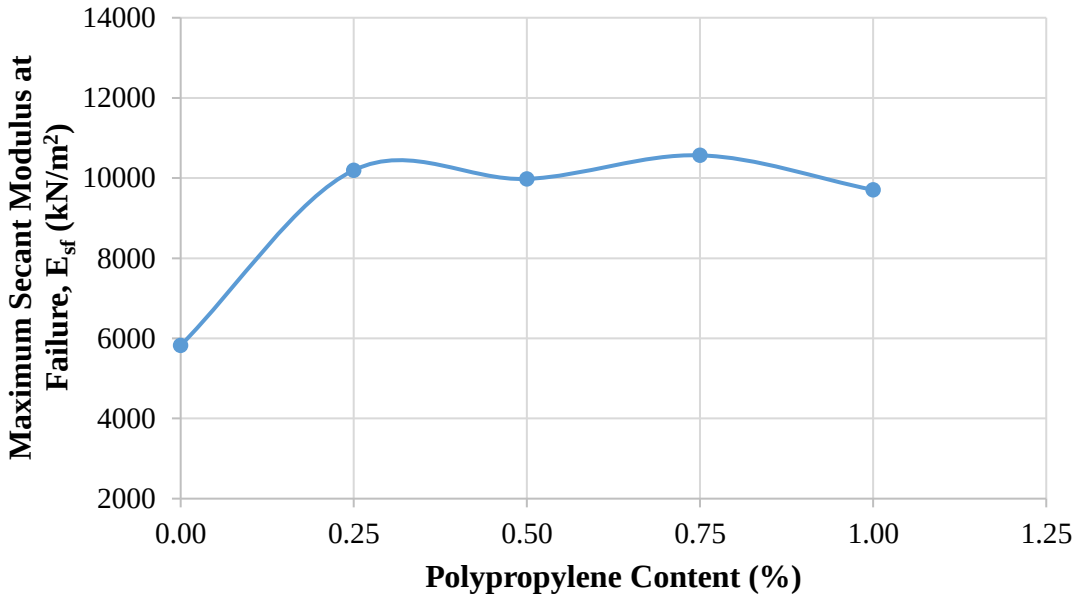

Figure 6.96 Relationship between maximum secant modulus at failure point and different polypropylene contents of CH

After gathering all secant modulus at failure point of high plasticity clay-polypropylene mixtures and comparing them in a graph, it can be seen that the maximum secant modulus at failure point was obtained in the mixture with 0.75% of polypropylene. In addition, the secant modulus at failure point increases up to 81% in the mixture with 0.75% of polypropylene. In other words, the initial tangent modulus increases up to the mixture with 0.25% of polypropylene. Then, it fluctuated with the increasing polypropylene content up to the mixture with 1% of polypropylene.

6.4 Copolymer Mixtures with High Plasticity Clay Soil

Copolymer fiber can be had a fibrillating network form, which is made of 100% virgin materials. Five different amounts of copolymer (0.5%, 0.75%, 1%, 1.25%, and 1.5%) were added to the high plasticity clay to study the effects of mixing copolymer with designated soil. In addition, the amounts of copolymer compared to whole mixtures in terms of soil moduli, the unconfined compression strength, and relationships in these engineering parameters. In other words, the amount of soil improvement of high plasticity clay was examined with the added copolymer.

6.4.1 High Plasticity Clay Soil Mixture with 0.5% of Copolymer

During the experimental program of this study, the amount of 0.5% copolymer mixed with high plasticity clay soil was used. The compaction and the unconfined compression tests were performed on the 0.5% copolymer mixed with high plasticity clay, and the outcomes of these experiments are illustrated in Table 6.26. With respect to data obtained from mentioned tests, it can be seen that the value of ω_{opt} and γ_{dmax} obtained at 26% and 15.23 kN/m^3, respectively.

Table 6.26 Results of experiments executed with CH+0.5% copolymer

Sample No.	ω (%)	γ_d (kN/m^3)	q_u (kN/m^2)
1	16	14.24	165.2
2	24	14.96	236.1
3	28	15.23	136.0
4	33	13.59	68.8
5	37	13.02	36.0

The axial stress-axial strain curves of five different 0.5% copolymer-added high plasticity clay samples are shown in Figure 6.97. According to data obtained from the unconfined compression test of 0.5% copolymer-added high plasticity clay soil samples, it can be inferred that the maximum unconfined compression strength was obtained in the second sample, and it was obtained as 236.1 kN/m^2.

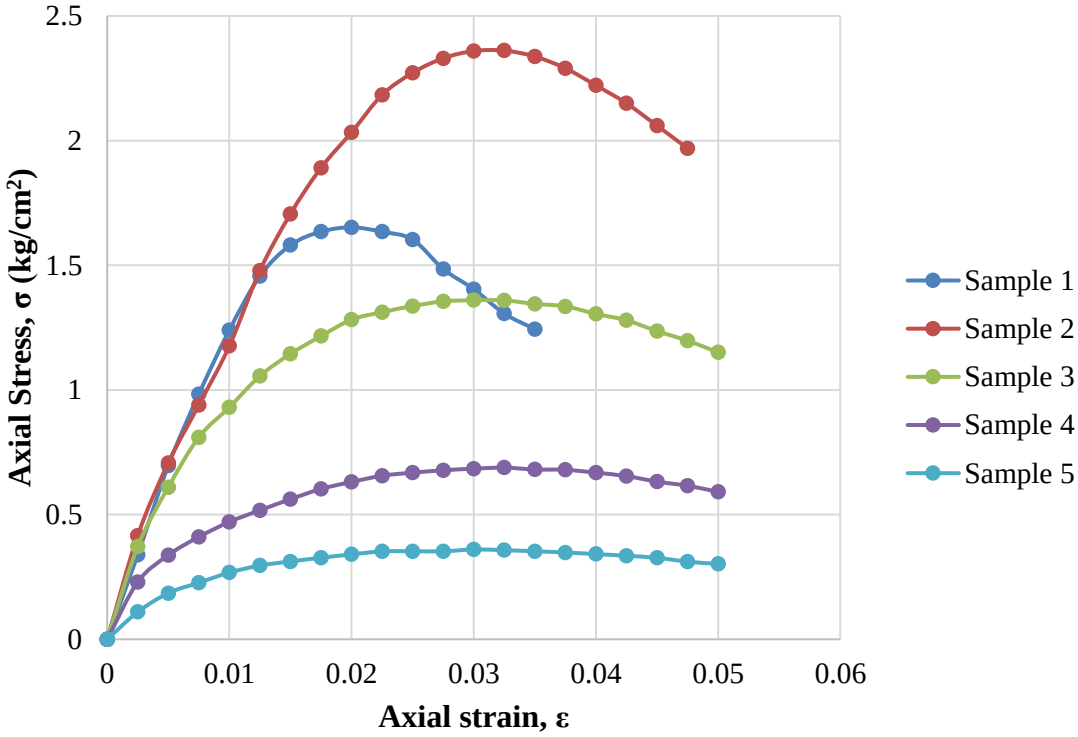

Figure 6.97 Results of unconfined compression tests of CH+0.5% copolymer

It should be noted that the reciprocal of the initial tangent modulus (a) and the reciprocal of the asymptotic value of stress difference (b) were derived from transformed hyperbolic stress-strain curves of 0.5% copolymer-added high plasticity clay samples. In addition, the asymptotic value of stress difference $(\sigma_1)_{ult}$, compressive strength $(\sigma_1)_f$, axial strain value at failure (ε_f), and axial strain value at 50% of maximum stress (ε_{50}) were obtained from unconfined compression test results. Lastly, the failure ratio (R_f) was calculated from unconfined compression test results. Mentioned engineering parameters are given in Table 6.27.

Table 6.27 Calculated engineering parameters of CH+0.5% copolymer

Sample No.	a (cm^2/kg)	b (cm^2/kg)	$(\sigma_1)_{ult}$ (kg/cm^2)	$(\sigma_1)_f$ (kg/cm^2)	R_f -	ε_f -	ε_{50} -
1	0.0058	0.2706	3.695	1.652	0.45	0.0200	0.0061
2	0.0057	0.2248	4.448	2.361	0.53	0.0325	0.0100
3	0.0052	0.5430	1.842	1.360	0.74	0.0300	0.0059
4	0.0090	1.1563	0.865	0.688	0.80	0.0325	0.0052
5	0.0158	2.2017	0.454	0.360	0.79	0.0300	0.0048

It is obvious that, when the values of strains are between 0.1% to 0.001%, this region is categorized as a small strain. Furthermore, it should be noted that the strain level of 0.5% copolymer-added high plasticity clay is classified as small strain (SS) because the maximum axial strain was determined in samples 3, 4, and 5 of 0.5% copolymer-added high plasticity clay, and it was obtained as 0.05%. Thus, it can be concluded that nonlinear behaviour was observed for the tested 0.5% copolymer-added high plasticity clay soil samples.

Initial tangent modulus (E_i), tangent modulus at 50% of maximum stress (E_{t50}), secant modulus at failure (E_{sf}), secant modulus at 50% of maximum stress (E_{s50}), and unconfined compression strength (q_u) of five different 0.5% copolymer-added high plasticity clay soil samples are given in Table 6.28.

Table 6.28 Soil moduli and unconfined compression strength of CH+0.5% copolymer

Sample No.	E_i (kN/m^2)	E_{t50} (kN/m^2)	E_{sf} (kN/m^2)	E_{s50} (kN/m^2)	q_u (kN/m^2)
1	17241.4	10395.3	8260.0	13469.4	165.2
2	17543.9	9467.9	7264.6	11761.2	236.1
3	19230.8	7651.1	4533.3	11574.5	136.0
4	11111.1	4029.8	2116.9	6565.2	68.8
5	6329.1	2306.6	1200.0	3722.4	36.0

According to the data obtained, it can be concluded that the maximum modulus values are observed in the initial tangent modulus compared with other soil moduli in

all five 0.5% copolymer-added high plasticity clay samples due to the initial slope of the stress-strain curve. In other words, the axial stress increases up to a certain point very sharply. Then, this sharp increasing trend suddenly starts to slow down, and during this slowing trend, the axial strain increases rapidly.

In addition, transformed hyperbolic stress-strain curves for five different 0.5% copolymer-added high plasticity clay samples are illustrated in Figure 6.98.

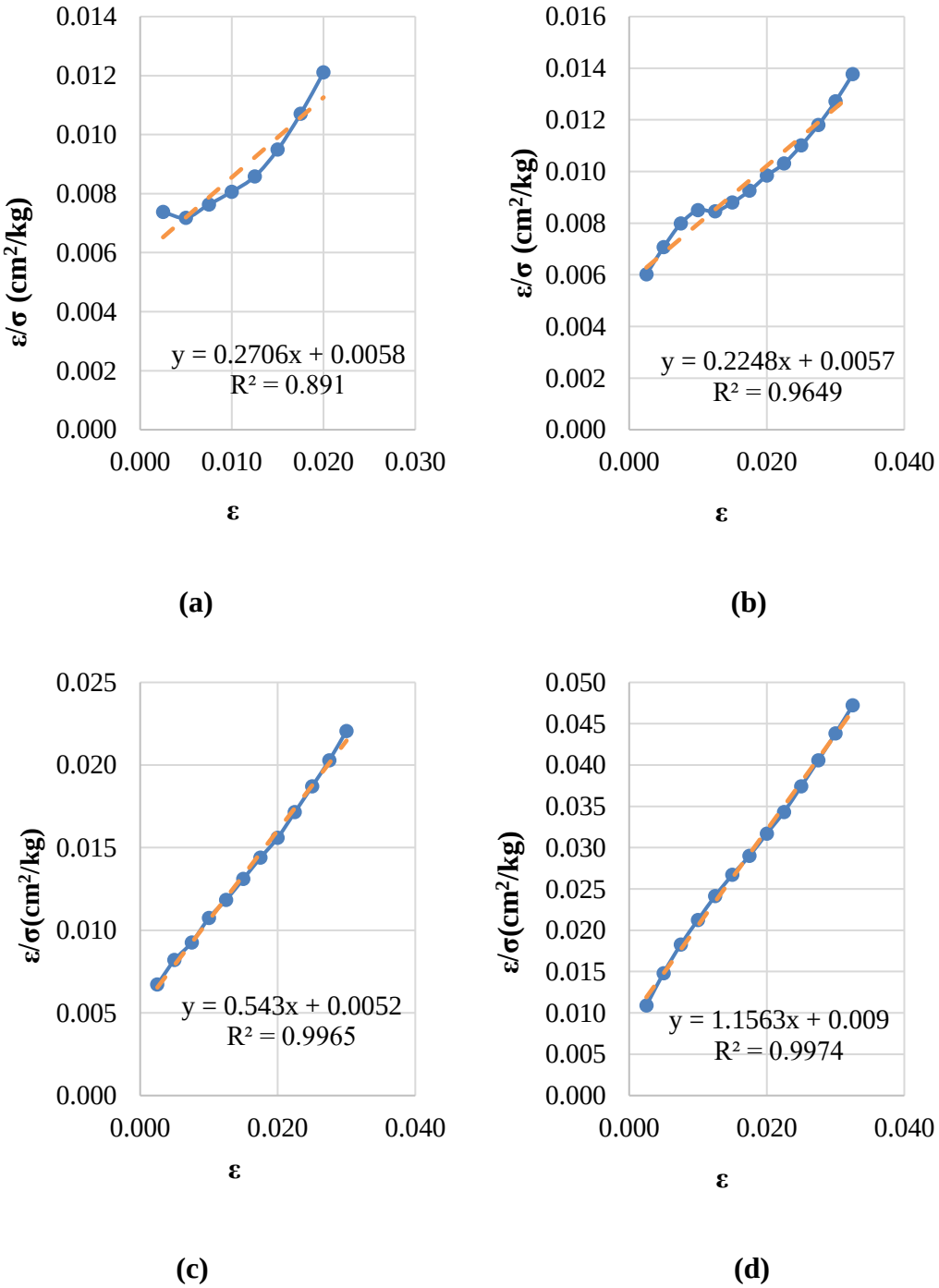

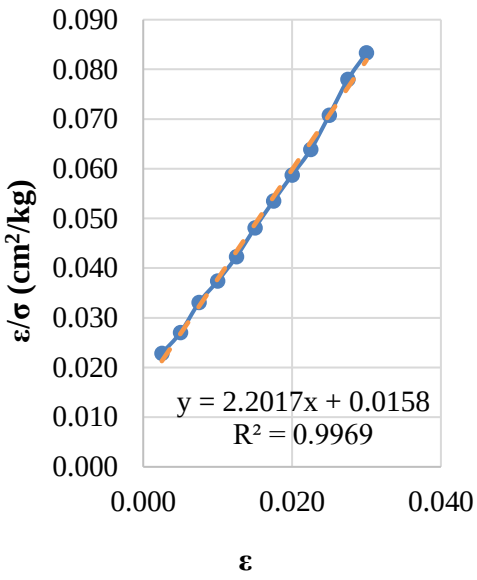

(e)

Figure 6.98 Transformed hyperbolic stress-strain curves for (a) sample 1, (b) sample 2, (c) sample 3, (d) sample 4, and (e) sample 5 (CH+0.5% Copolymer)

It was found that low and high values of axial strains in samples 1 and 2 are not precisely hyperbolic, as shown in Figures 6.98 (a and b). In other words, these points can not be fitted in a straight line. However, it was possible to estimate the actual stress-strain curves by a hyperbola. Thus, it is found to have a reasonable degree of accuracy. On the other hand, the transformed hyperbolic stress-strain curve in samples 3, 4, and 5 is hyperbolic, as shown in Figures 6.98 (c, d, and e). In other words, these points can be best-fitted in a straight line.

The relationship between the secant modulus at 50% of maximum stress (E_{s50}) and the initial tangent modulus (E_i) of 0.5% copolymer-added high plasticity clay samples is shown in Figure 6.99.

According to the data, it can be inferred that these soil moduli refer to the hardening of 0.5% copolymer-added high plasticity clay samples. Thus, the initial tangent modulus increases with the increasing secant modulus at 50% of maximum stress. Furthermore, it was best suited for estimating these soil moduli by a power model.

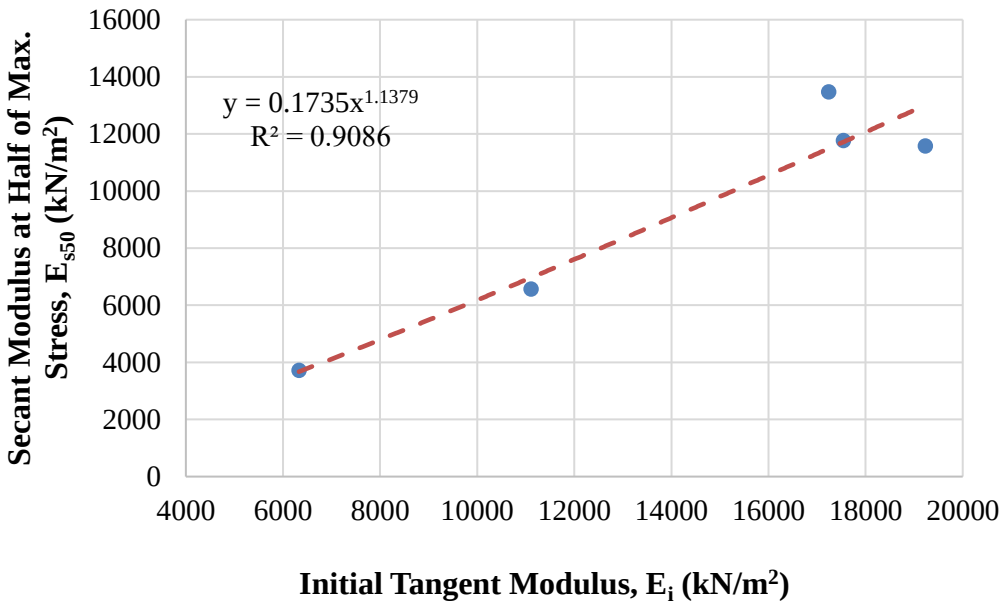

Figure 6.99 Relationship between secant modulus at 50% of maximum stress and initial tangent modulus (CH+0.5% Copolymer)

The relationship between the secant modulus at failure (E_{sf}) and the tangent modulus at 50% of maximum stress (E_{t50}) of 0.5% copolymer-added high plasticity clay samples is shown in Figure 6.100.

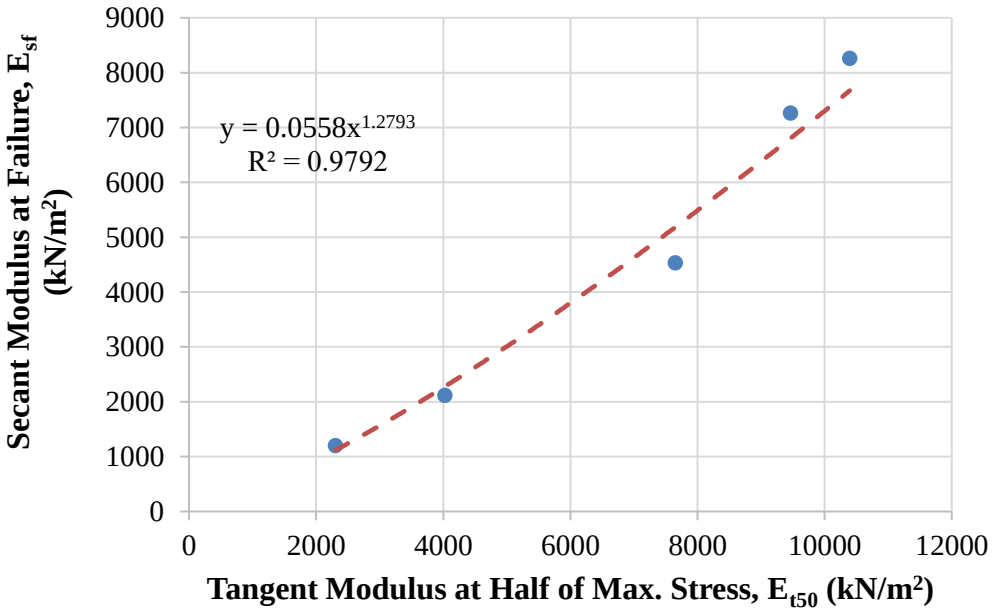

Figure 6.100 Relationship between secant modulus at failure point and tangent modulus at 50% of maximum stress (CH+0.5% Copolymer)

The tangent modulus at 50% of maximum stress increases with the increasing secant modulus at failure. Thus, it was best suited for estimating these soil moduli by a power model.

Furthermore, the relationship between initial tangent modulus (E_i) and unconfined compression strength of 0.5% copolymer-added high plasticity clay samples is shown in Figure 6.101.

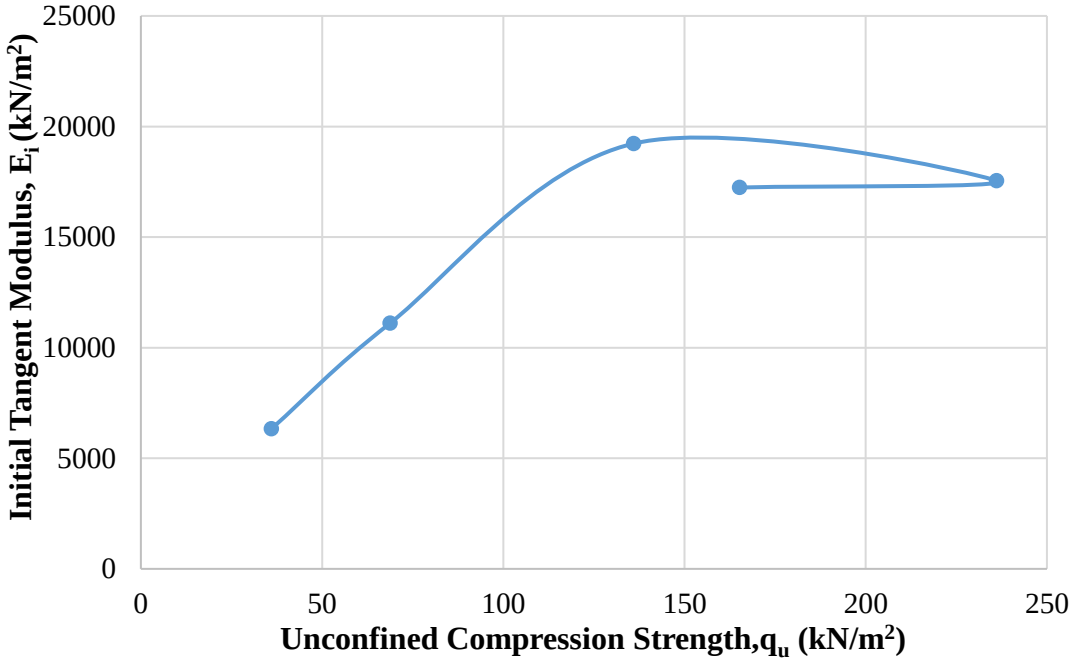

Figure 6.101 Relationship between initial tangent modulus and unconfined compression strength (CH+0.5% Copolymer)

According to data, the maximum initial tangent modulus is obtained in sample 3 as 19230.8 kN/m^2 for 0.5% copolymer-added high plasticity clay. It should be noted that the water content is 28%, the dry unit weight is 15.23 kN/m^3, and the unconfined compression strength is 136 kN/m^2 when the initial tangent modulus is the maximum value for 0.5% copolymer-added high plasticity clay.

With respect to the results of the initial tangent modulus, it seems that the maximum values of these moduli are not obtained at maximum unconfined compression strength (sample 2 for 0.5% copolymer-added high plasticity clay) since the beginning of the stress-strain curve of the sample 3 has rapidly increased in axial stress.

The relationship between secant modulus at 50% of maximum stress (E_{s50}) and unconfined compression strength of 0.5% copolymer-added high plasticity clay samples is shown in Figure 6.102.

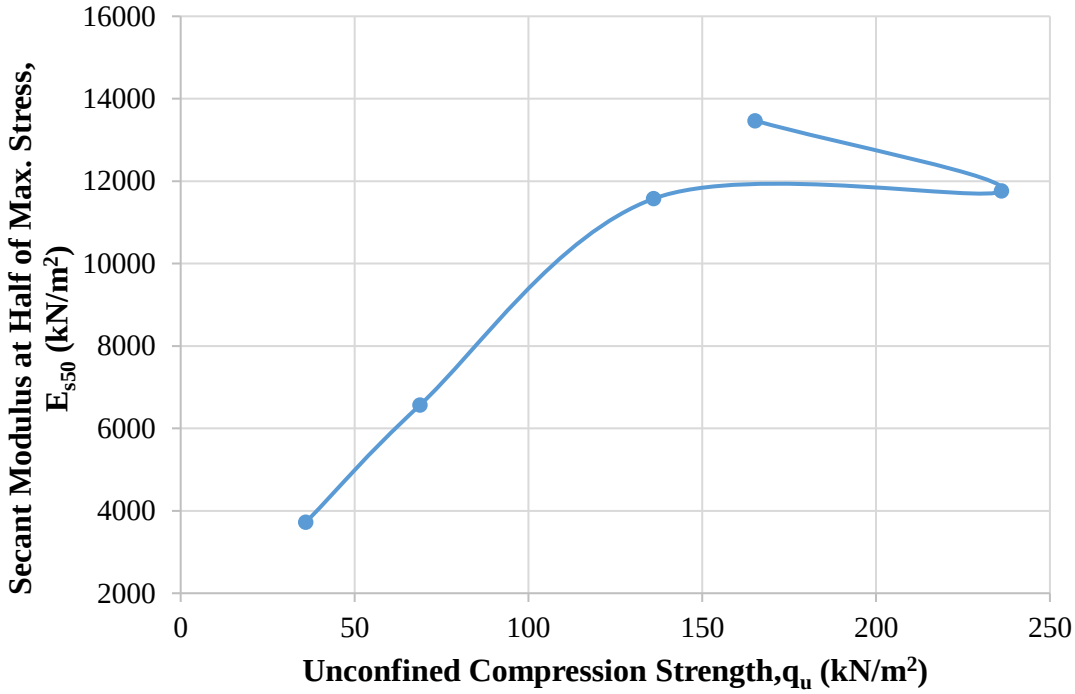

Figure 6.102 Relationship between secant modulus at 50% of maximum stress and unconfined compression strength (CH+0.5% Copolymer)

The maximum secant modulus at 50% of maximum stress is obtained in sample 1 as 13469.4 kN/m^2 for 0.5% copolymer-added high plasticity clay. It should be noted that the water content is 16%, the dry unit weight is 14.24 kN/m^3, and the unconfined compression strength is 165.2 kN/m^2 when the secant modulus at 50% of maximum stress has the maximum value of 0.5% copolymer-added high plasticity clay.

On the other hand, the relationship between tangent modulus at 50% of maximum stress (E_{t50}) and unconfined compression strength of 0.5% copolymer-added high plasticity clay samples is shown in Figure 6.103.

The maximum tangent modulus at 50% of maximum stress is obtained in sample 1 as 10395.3 kN/m^2 for 0.5% copolymer-added high plasticity clay. It should be noted that the water content is 16%, the dry unit weight is 14.24 kN/m^3, and the unconfined compression strength is 165.2 kN/m^2 when the tangent modulus at 50% of maximum stress is the maximum value for the 0.5% copolymer-added high plasticity clay.

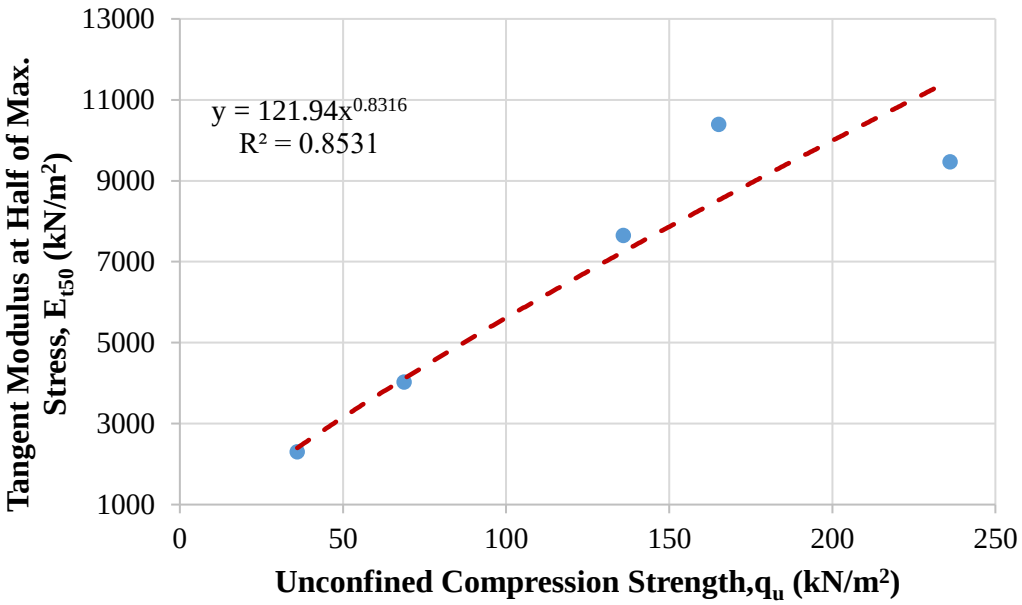

Figure 6.103 Relationship between tangent modulus at 50% of maximum stress and unconfined compression strength (CH+0.5% Copolymer)

In addition, the relationship between secant modulus at failure point (E_{sf}) and unconfined compression strength of 0.5% copolymer-added high plasticity clay samples is shown in Figure 6.104.

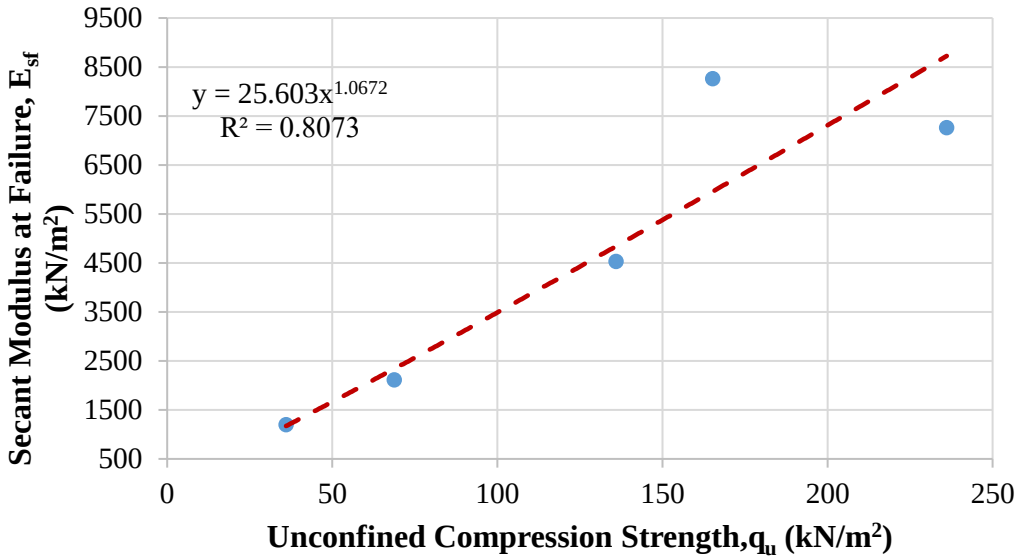

Figure 6.104 Relationship between secant modulus at failure point and unconfined compression strength (CH+0.5% Copolymer)

It is obvious that the maximum secant modulus at failure point is obtained in sample 1 as 8260 kN/m^2 for 0.5% copolymer-added high plasticity clay. It should be noted that the water content is 16%, the dry unit weight is 14.24 kN/m^3, and the unconfined compression strength is 165.2 kN/m^2 when the secant modulus at failure point is the maximum value for 0.5% copolymer-added high plasticity clay.

With respect to the results of the initial tangent modulus, secant modulus at 50% of maximum stress, and secant modulus at failure point, it seems that the maximum values of these moduli are not obtained at maximum unconfined compression strength (sample 2 for 0.5% copolymer-added high plasticity clay) since the beginning of the stress-strain curve of sample 1 has rapidly increased in axial stress. On the other hand, when calculated initial tangent modulus, secant modulus at 50% of maximum stress, and secant modulus at failure point have the maximum value for 0.5% copolymer-added high plasticity clay, the water content is not equal to the optimum water content (w_{opt}=26%), and the dry unit weight is not equal to the maximum dry unit weight (γ_{dmax}=15.23 kN/m^3). High plasticity clay soil reinforced with copolymer became stiffer when it was drier. Therefore, high plasticity clayey soil's strength and load-deformation properties are improved by reinforcing with copolymer fiber.

6.4.2 High Plasticity Clay Soil Mixture with 0.75% of Copolymer

During the experimental program of this study, the amount of 0.75% copolymer mixed with high plasticity clay soil was used. The compaction and the unconfined compression tests were performed on the 0.75% copolymer mixed with high plasticity clay, and the outcomes of these experiments are illustrated in Table 6.29. With respect to data obtained from mentioned tests, it can be seen that the value of ω_{opt} and γ_{dmax} obtained at 25.2% and 15.10 kN/m^3, respectively.

Table 6.29 Results of experiments executed with CH+0.75% copolymer

Sample No.	ω (%)	γ_d (kN/m^3)	q_u (kN/m^2)
1	18	13.90	147.0
2	21	14.75	249.6
3	24	15.10	228.6
4	33	14.80	54.8
5	35	13.80	36.3

The axial stress-axial strain curves of five different 0.75% copolymer-added high plasticity clay samples are shown in Figure 6.105. According to data obtained from the unconfined compression test of 0.75% copolymer-added high plasticity clay soil samples, it can be inferred that the maximum unconfined compression strength was obtained in the second sample, and it was obtained as 249.6 kN/m^2.

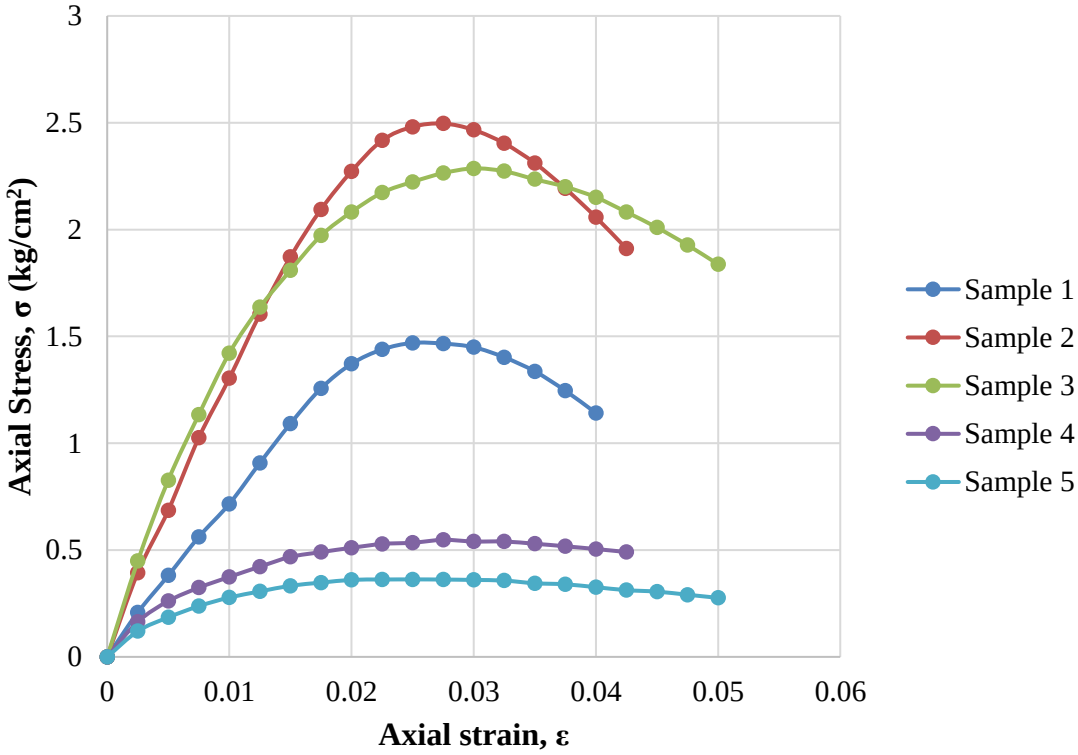

Figure 6.105 Results of unconfined compression tests of CH+0.75% copolymer

It should be noted that the reciprocal of the initial tangent modulus (a) and the reciprocal of the asymptotic value of stress difference (b) were derived from transformed hyperbolic stress-strain curves of 0.75% copolymer-added high plasticity clay samples. In addition, the asymptotic value of stress difference $(\sigma_1)_{ult}$, compressive strength $(\sigma_1)_f$, axial strain value at failure (ε_f), and axial strain value at 50% of maximum stress (ε_{50}) were obtained from unconfined compression test results. Lastly, the failure ratio (R_f) was calculated from unconfined compression test results. Mentioned engineering parameters are given in Table 6.30.

Table 6.30 Calculated engineering parameters of CH+0.75% copolymer

Sample No.	a	b	$(\sigma_1)_{ult}$	$(\sigma_1)_f$	R_f	ε_f	ε_{50}
	(cm^2/kg)	(cm^2/kg)	(kg/cm^2)	(kg/cm^2)	-	-	-
1	0.0118	0.1657	6.035	1.470	0.24	0.0250	0.0102
2	0.0060	0.1574	6.353	2.496	0.39	0.0275	0.0095
3	0.0045	0.2705	3.697	2.286	0.62	0.0300	0.0076
4	0.0123	1.3626	0.734	0.548	0.75	0.0275	0.0055
5	0.0156	2.0514	0.487	0.363	0.74	0.0250	0.0049

It is obvious that, when the values of strains are between 0.1% to 0.001%, this region is categorized as a small strain. Furthermore, it should be noted that the strain level of 0.75% copolymer-added high plasticity clay is classified as small strain (SS) because the maximum axial strain was determined in samples 3 and 5 of 0.75% copolymer-added high plasticity clay, and it was obtained as 0.05%. Thus, it can be concluded that nonlinear behaviour was observed for the tested 0.75% copolymer-added high plasticity clay soil samples.

Initial tangent modulus (E_i), tangent modulus at 50% of maximum stress (E_{t50}), secant modulus at failure (E_{sf}), secant modulus at 50% of maximum stress (E_{s50}), and unconfined compression strength (q_u) of five different 0.75% copolymer-added high plasticity clay soil samples are given in Table 6.31.

Table 6.31 Soil moduli and unconfined compression strength of CH+0.75% copolymer

Sample No.	E_i	E_{t50}	E_{sf}	E_{s50}	q_u
	(kN/m^2)	(kN/m^2)	(kN/m^2)	(kN/m^2)	(kN/m^2)
1	8474.6	6536.0	5880.0	7172.6	147.0
2	16666.7	10761.9	9076.4	13141.8	249.6
3	22222.2	10605.1	7620.0	15082.9	228.6
4	8130.1	3192.6	1992.7	4967.5	54.8
5	6410.3	2525.5	1452.0	3730.4	36.3

According to the data obtained, it can be concluded that the maximum modulus values are observed in the initial tangent modulus compared with other soil moduli in

all five 0.75% copolymer-added high plasticity clay samples due to the initial slope of the stress-strain curve. In other words, the axial stress increases up to a certain point very sharply. Then, this sharp increasing trend suddenly starts to slow down, and during this slowing trend, the axial strain increases rapidly.

In addition, transformed hyperbolic stress-strain curves for five different 0.75% copolymer-added high plasticity clay samples are illustrated in Figure 6.106.

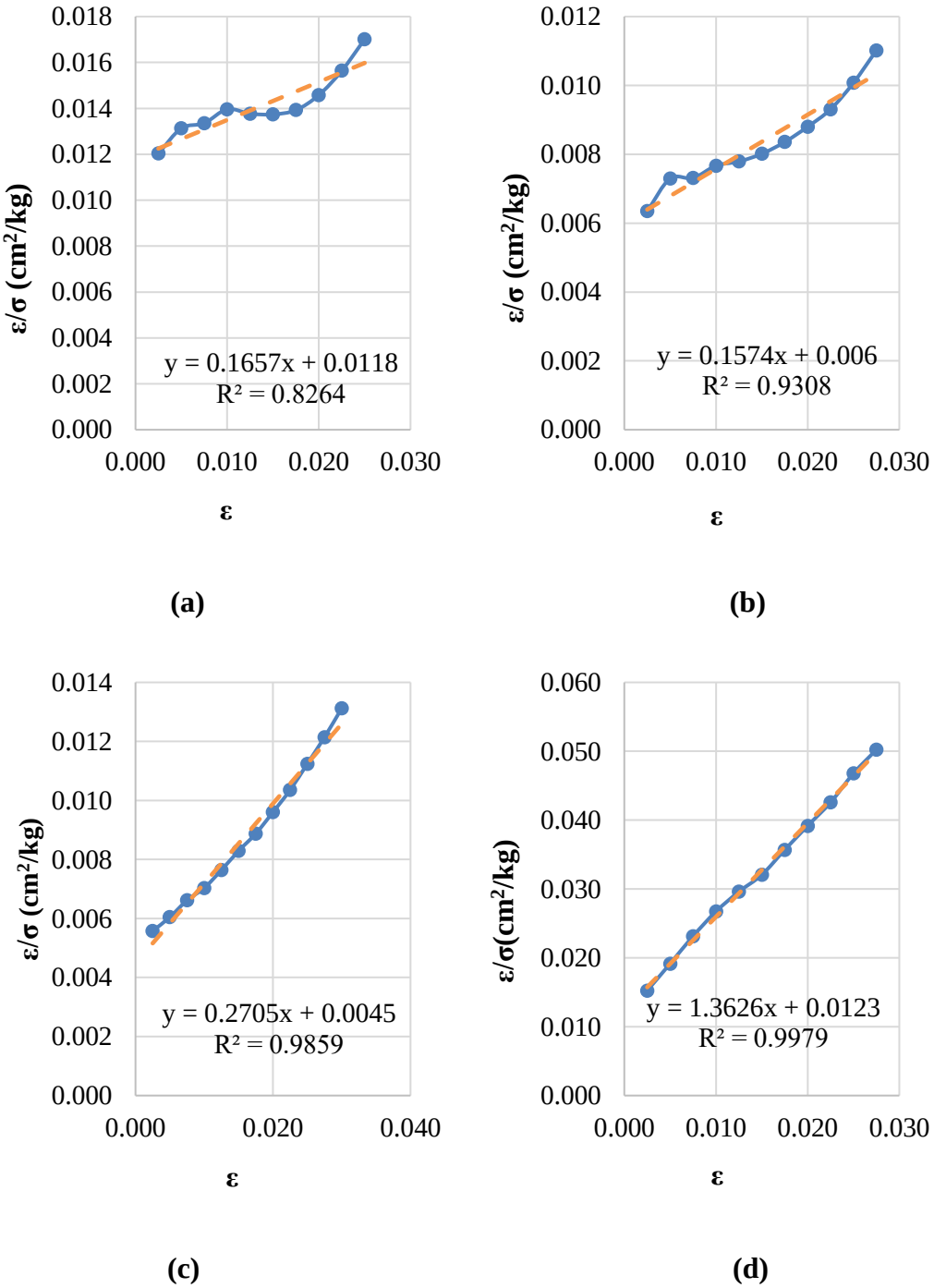

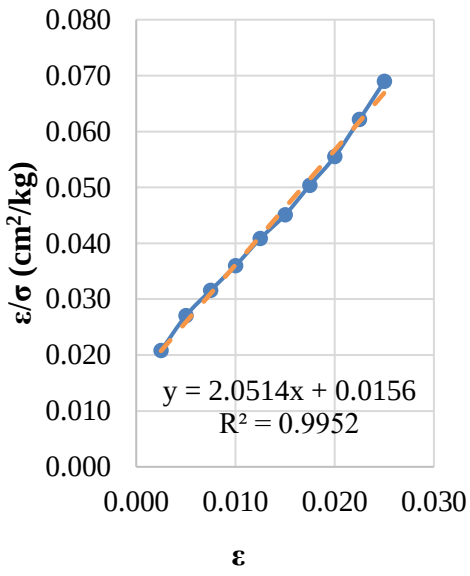

(e)

Figure 6.106 Transformed hyperbolic stress-strain curves for (a) sample 1, (b) sample 2, (c) sample 3, (d) sample 4, and (e) sample 5 (CH+0.75% Copolymer)

It was found that low and high values of axial strains in samples 1 and 2 are not precisely hyperbolic, as shown in Figures 6.107 (a and b). In other words, these points can not be fitted in a straight line. However, it was possible to estimate the actual stress-strain curves by a hyperbola. Thus, it is found to have a reasonable degree of accuracy. On the other hand, the transformed hyperbolic stress-strain curve in samples 3, 4, and 5 is hyperbolic, as shown in Figures 6.107 (c, d, and e). In other words, these points can be best-fitted in a straight line.

The relationship between the secant modulus at 50% of maximum stress (E_{s50}) and the initial tangent modulus (E_i) of 0.75% copolymer-added high plasticity clay samples is shown in Figure 6.107.

According to the data, it can be inferred that these soil moduli refer to the hardening of 0.75% copolymer-added high plasticity clay samples. Thus, the initial tangent modulus increases with the increasing secant modulus at 50% of maximum stress. Furthermore, it was best suited for estimating these soil moduli by a power model.

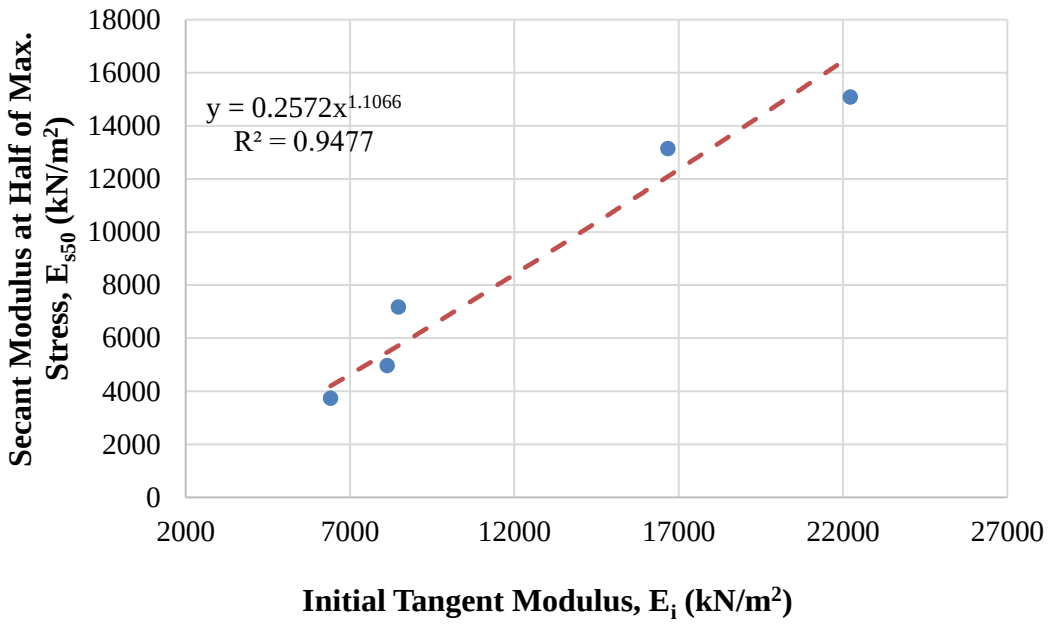

Figure 6.107 Relationship between secant modulus at 50% of maximum stress and initial tangent modulus (CH+0.75% Copolymer)

The relationship between the secant modulus at failure (E_{sf}) and the tangent modulus at 50% of maximum stress (E_{t50}) of 0.75% copolymer-added high plasticity clay samples is shown in Figure 6.108.

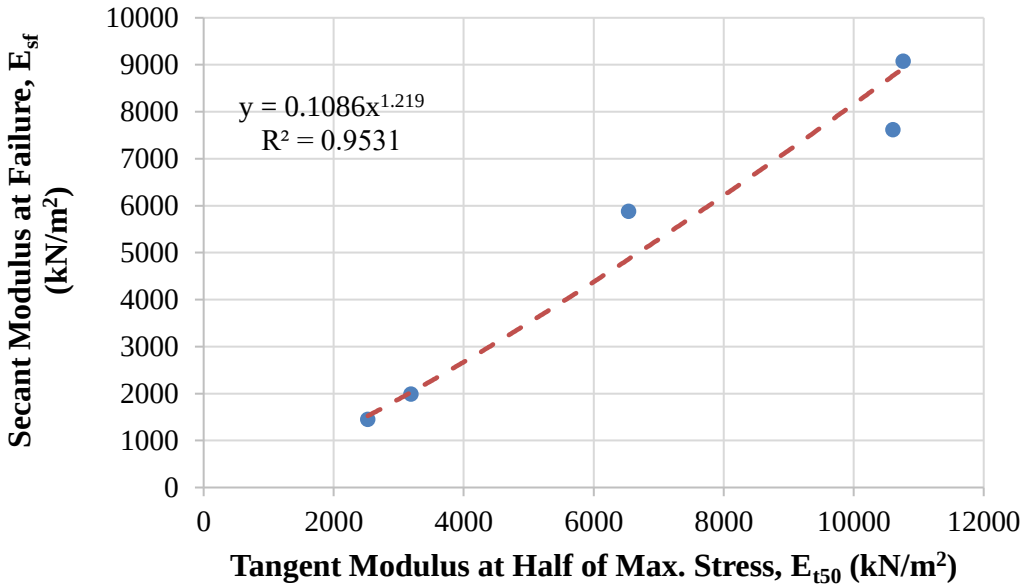

Figure 6.108 Relationship between secant modulus at failure point and tangent modulus at 50% of maximum stress (CH+0.75% Copolymer)

The tangent modulus at 50% of maximum stress increases with the increasing secant modulus at failure. Thus, it was best suited for estimating these soil moduli by a power model.

Furthermore, the relationship between initial tangent modulus (E_i) and unconfined compression strength of 0.75% copolymer-added high plasticity clay samples is shown in Figure 6.109.

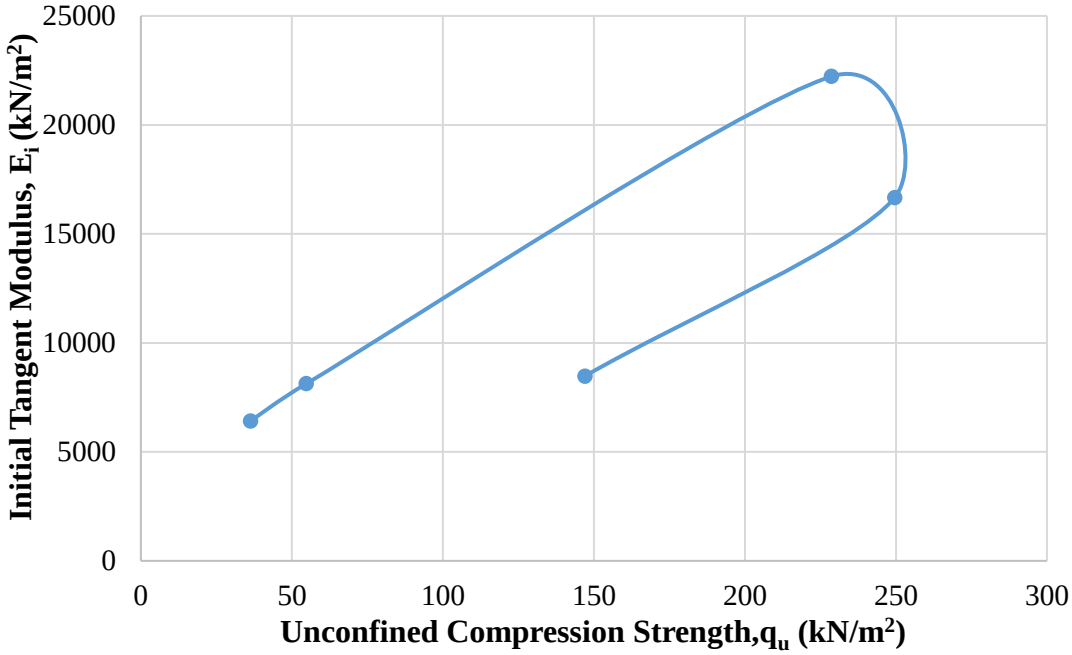

Figure 6.109 Relationship between initial tangent modulus and unconfined compression strength (CH+0.75% Copolymer)

According to data, the maximum initial tangent modulus is obtained in sample 3 as 22222.2 kN/m^2 for 0.75% copolymer-added high plasticity clay. It should be noted that the water content is 24%, the dry unit weight is 15.10 kN/m^3, and the unconfined compression strength is 228.6 kN/m^2 when the initial tangent modulus is the maximum value for 0.75% copolymer-added high plasticity clay.

With respect to the results, it seems that the maximum values of the initial tangent modulus are not obtained at maximum unconfined compression strength (sample 2 for 0.75% copolymer-added high plasticity clay) since the beginning of the stress-strain curve of sample 3 has rapidly increased in axial stress. On the other hand, when the calculated initial tangent modulus has the maximum value for 0.75% copolymer-added high plasticity clay, the water content is close to the optimum water

content (w_{opt}=25.2%), and the dry unit weight is equal to the maximum dry unit weight (γ_{dmax}=15.10 kN/m^3).

The relationship between secant modulus at 50% of maximum stress (E_{s50}) and unconfined compression strength of 0.75% copolymer-added high plasticity clay samples is shown in Figure 6.110.

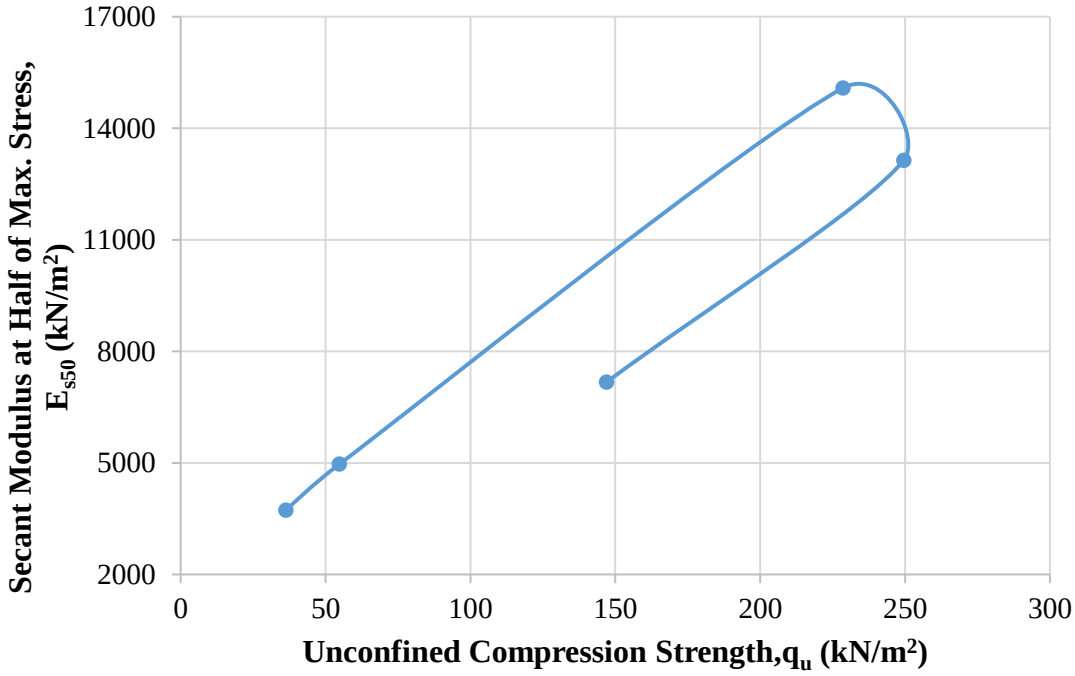

Figure 6.110 Relationship between secant modulus at 50% of maximum stress and unconfined compression strength (CH+0.75% Copolymer)

The maximum secant modulus at 50% of maximum stress is obtained in sample 2 as 13141.8 kN/m^2 for 0.75% copolymer-added high plasticity clay. It should be noted that the water content is 21%, the dry unit weight is 14.75 kN/m^3, and the unconfined compression strength is 249.6 kN/m^2 when the secant modulus at 50% of maximum stress has the maximum value of 0.75% copolymer-added high plasticity clay.

On the other hand, the relationship between tangent modulus at 50% of maximum stress (E_{t50}) and unconfined compression strength of 0.75% copolymer-added high plasticity clay samples is shown in Figure 6.111.

The maximum tangent modulus at 50% of maximum stress is obtained in sample 2 as 10761.9 kN/m^2 for 0.75% copolymer-added high plasticity clay. It should be noted that the water content is 21%, the dry unit weight is 14.75 kN/m^3, and the unconfined

compression strength is 249.6 kN/m^2 when the tangent modulus at 50% of maximum stress is the maximum value for the 0.75% copolymer-added high plasticity clay.

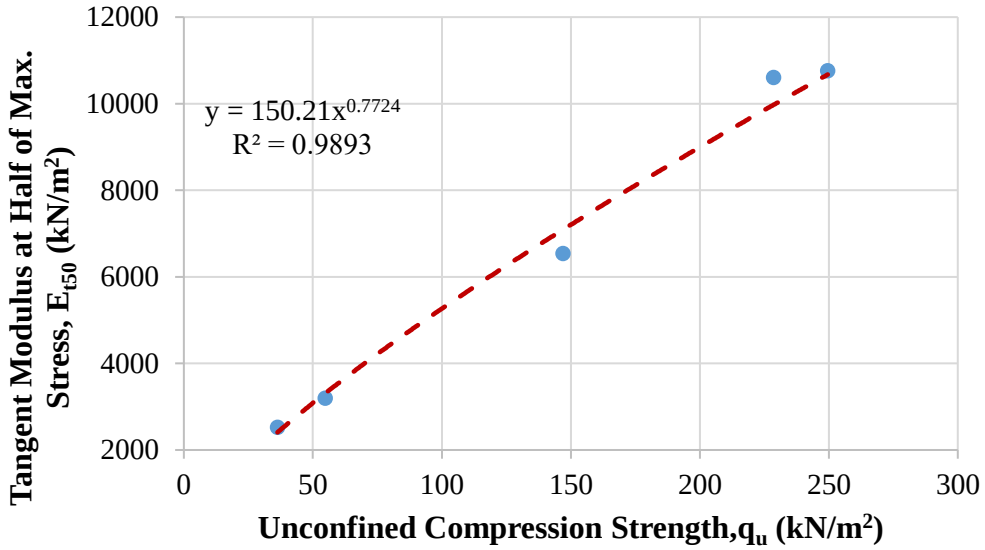

Figure 6.111 Relationship between tangent modulus at 50% of maximum stress and unconfined compression strength (CH+0.75% Copolymer)

In addition, the relationship between secant modulus at failure point (E_{sf}) and unconfined compression strength of 0.75% copolymer-added high plasticity clay samples is shown in Figure 6.112.

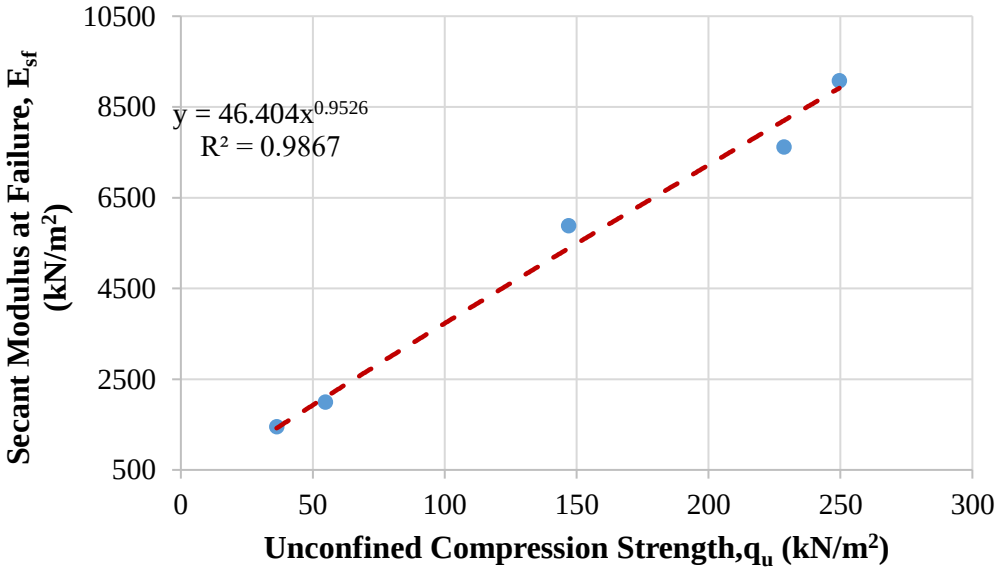

Figure 6.112 Relationship between secant modulus at failure point and unconfined compression strength (CH+0.75% Copolymer)

It is obvious that the maximum secant modulus at failure point is obtained in sample 2 as 9076.4 kN/m^2 for 0.75% copolymer-added high plasticity clay. It should be noted that the water content is 21%, the dry unit weight is 14.75 kN/m^3, and the unconfined compression strength is 249.6 kN/m^2 when the secant modulus at failure point is the maximum value for 0.75% copolymer-added high plasticity clay.

With respect to the results of the secant modulus at 50% of maximum stress, tangent modulus at 50% of maximum stress, and secant modulus at failure point, it seems that the maximum values are obtained at maximum unconfined compression strength (sample 2 for the 0.75% copolymer-added high plasticity clay). However, the value of water content is less than the optimum water content (w_{opt}=25.2%), and the dry unit weight is close to the maximum dry unit weight (γ_{dmax}=15.10 kN/m^3). High plasticity clay soil reinforced with copolymer became stiffer when it was drier. Therefore, high plasticity clayey soil's strength and load-deformation properties are improved by reinforcing with copolymer fiber.

6.4.3 High Plasticity Clay Soil Mixture with 1% of Copolymer

During the experimental program of this study, the amount of 1% copolymer mixed with high plasticity clay soil was used. The compaction and the unconfined compression tests were performed on the 1% copolymer mixed with high plasticity clay, and the outcomes of these experiments are illustrated in Table 6.32. With respect to data obtained from mentioned tests, it can be seen that the value of ω_{opt} and γ_{dmax} obtained at 26% and 15.00 kN/m^3, respectively.

Table 6.32 Results of experiments executed with CH+1% copolymer

Sample No.	ω (%)	γ_d (kN/m^3)	q_u (kN/m^2)
1	15	13.74	112.5
2	24	15.00	244.6
3	31	14.00	71.4
4	35	13.39	40.8
5	39	12.35	23.5

The axial stress-axial strain curves of five different 1% copolymer-added high plasticity clay samples are shown in Figure 6.113. According to data obtained from the unconfined compression test of 1% copolymer-added high plasticity clay soil

samples, it can be inferred that the maximum unconfined compression strength was obtained in the second sample, and it was obtained as 244.6 kN/m^2.

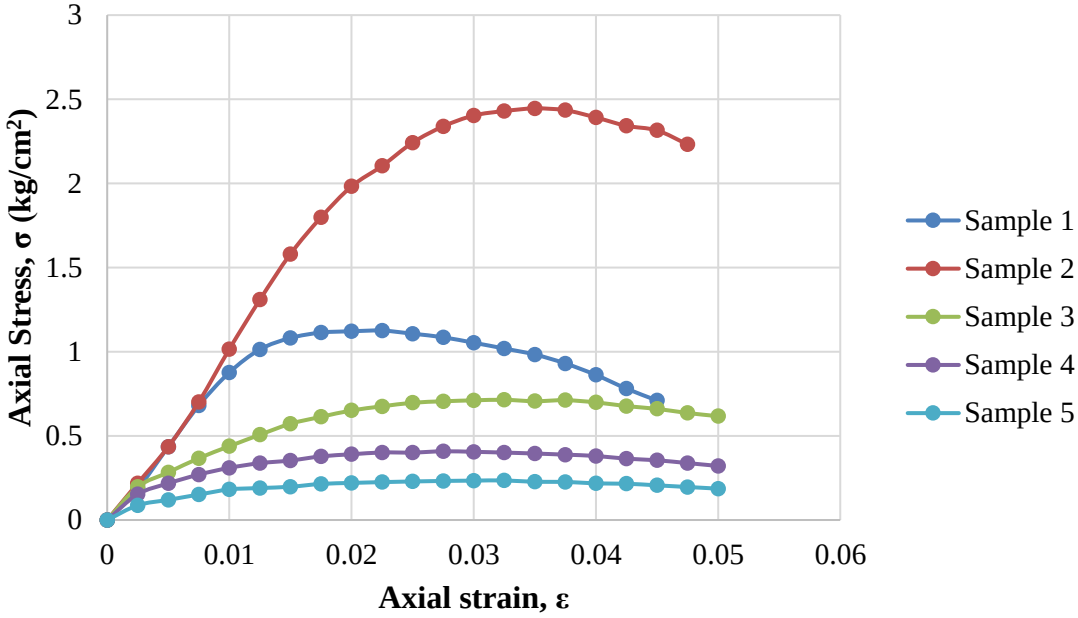

Figure 6.113 Results of unconfined compression tests of CH+1% copolymer

It should be noted that the reciprocal of the initial tangent modulus (a) and the reciprocal of the asymptotic value of stress difference (b) were derived from transformed hyperbolic stress-strain curves of 1% copolymer-added high plasticity clay samples. In addition, the asymptotic value of stress difference $(\sigma_1)_{ult}$, compressive strength $(\sigma_1)_f$, axial strain value at failure (ε_f), and axial strain value at 50% of maximum stress (ε_{50}) were obtained from unconfined compression test results. Lastly, the failure ratio (R_f) was calculated from unconfined compression test results. Mentioned engineering parameters are given in Table 6.33.

Table 6.33 Calculated engineering parameters of CH+1% copolymer

Sample No.	a (cm^2/kg)	b (cm^2/kg)	$(\sigma_1)_{ult}$ (kg/cm^2)	$(\sigma_1)_f$ (kg/cm^2)	R_f -	ε_f -	ε_{50} -
1	0.0071	0.5144	1.944	1.125	0.58	0.0225	0.0063
2	0.0069	0.1881	5.316	2.446	0.46	0.0350	0.0118
3	0.0117	0.9993	1.001	0.714	0.71	0.0325	0.0072
4	0.0123	1.9811	0.505	0.408	0.81	0.0275	0.0045
5	0.0213	3.5411	0.282	0.235	0.83	0.0325	0.0048

It is obvious that, when the values of strains are between 0.1% to 0.001%, this region is categorized as a small strain. Furthermore, it should be noted that the strain level of 1% copolymer-added high plasticity clay is classified as small strain (SS) because the maximum axial strain was determined in samples 3, 4, and 5 of 1% copolymer-added high plasticity clay, and it was obtained as 0.05%. Thus, it can be concluded that nonlinear behaviour was observed for the tested 1% copolymer-added high plasticity clay soil samples.

Initial tangent modulus (E_i), tangent modulus at 50% of maximum stress (E_{t50}), secant modulus at failure (E_{sf}), secant modulus at 50% of maximum stress (E_{s50}), and unconfined compression strength (q_u) of five different 1% copolymer-added high plasticity clay soil samples are given in Table 6.34.

Table 6.34 Soil moduli and unconfined compression strength of CH+1% copolymer

Sample No.	E_i (kN/m^2)	E_{t50} (kN/m^2)	E_{sf} (kN/m^2)	E_{s50} (kN/m^2)	q_u (kN/m^2)
1	14084.5	7113.0	5000.0	8927.1	112.5
2	14492.8	8591.7	6988.6	10394.2	244.6
3	8547.0	3536.5	2196.9	4956.7	71.4
4	8130.1	2886.5	1483.6	4572.4	40.8
5	4694.8	1600.8	723.1	2442.5	23.5

According to the data obtained, it can be concluded that the maximum modulus values are observed in the initial tangent modulus compared with other soil moduli in all five 1% copolymer-added high plasticity clay samples due to the initial slope of the stress-strain curve. In other words, the axial stress increases up to a certain point very sharply. Then, this sharp increasing trend suddenly starts to slow down, and during this slowing trend, the axial strain increases rapidly.

In addition, transformed hyperbolic stress-strain curves for five different 1% copolymer-added high plasticity clay samples are illustrated in Figure 6.114.

It was found that low and high values of axial strains in samples 1 and 2 are not precisely hyperbolic, as shown in Figures 6.114 (a and b). In other words, these points can not be fitted in a straight line. However, it was possible to estimate the actual stress-strain curves by a hyperbola. Thus, it is found to have a reasonable degree of

accuracy. On the other hand, the transformed hyperbolic stress-strain curve in samples 3, 4, and 5 is hyperbolic, as shown in Figures 6.114 (c, d, and e). In other words, these points can be best-fitted in a straight line.

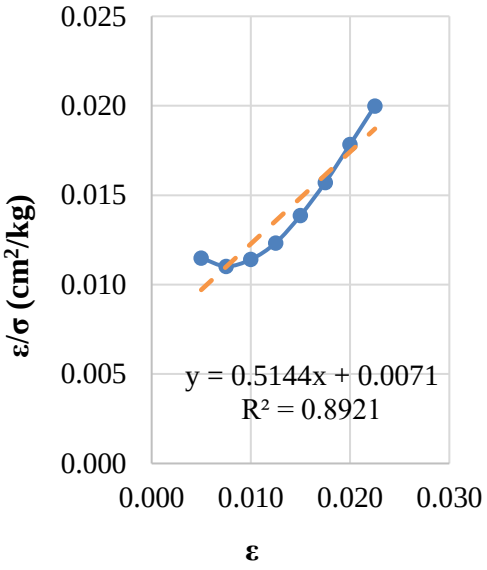

(a)

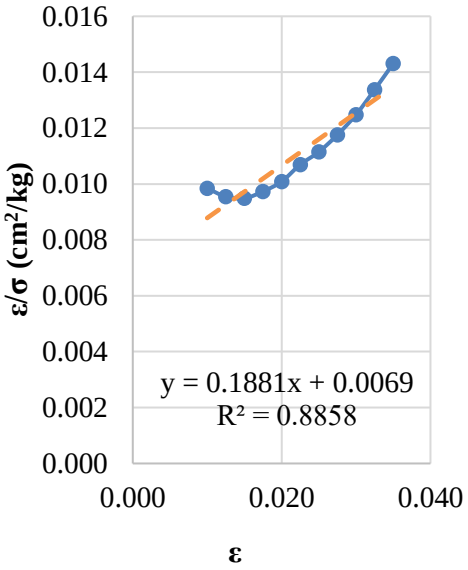

(b)

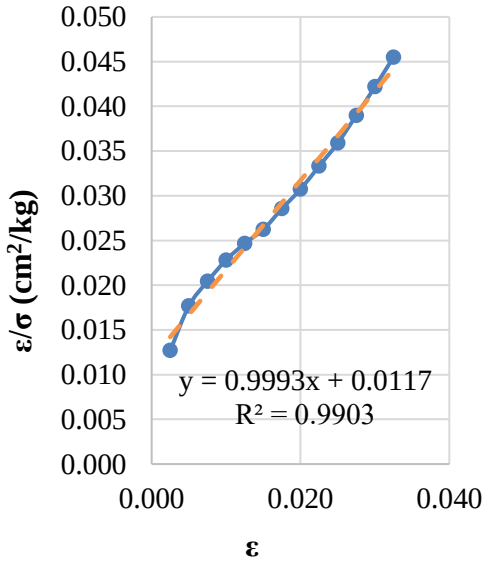

(c)

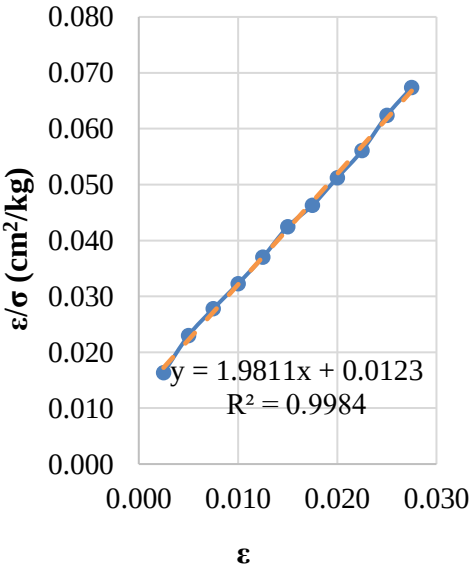

(d)

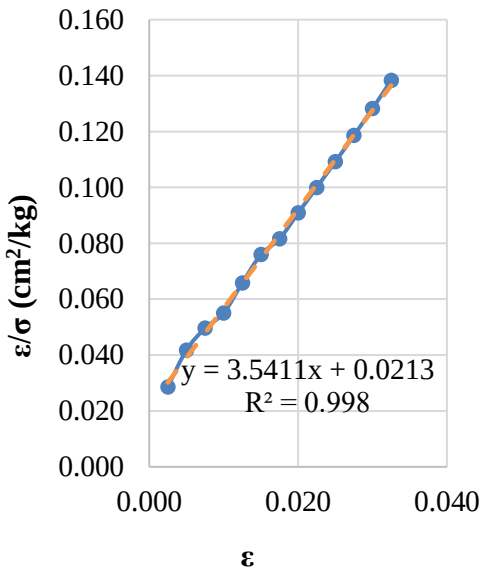

(e)

Figure 6.114 Transformed hyperbolic stress-strain curves for (a) sample 1, (b) sample 2, (c) sample 3, (d) sample 4, and (e) sample 5 (CH+1% Copolymer)

The relationship between the secant modulus at 50% of maximum stress (E_{s50}) and the initial tangent modulus (E_i) of 1% copolymer-added high plasticity clay samples is shown in Figure 6.115.

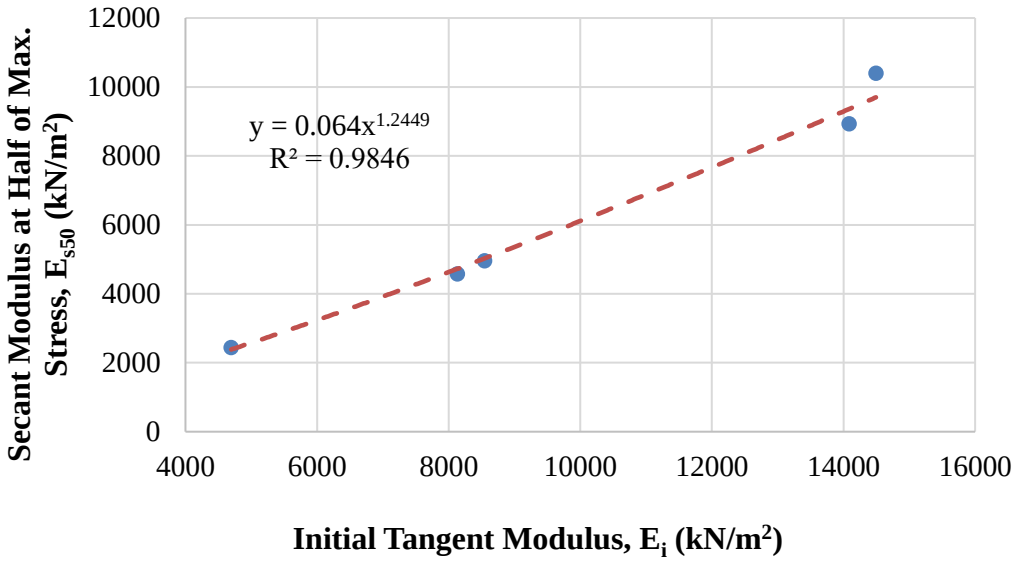

Figure 6.115 Relationship between secant modulus at 50% of maximum stress and initial tangent modulus (CH+1% Copolymer)

According to the data, it can be inferred that these soil moduli refer to the hardening of 1% copolymer-added high plasticity clay samples. Thus, the initial tangent modulus increases with the increasing secant modulus at 50% of maximum stress. Furthermore, it was best suited for estimating these soil moduli by a power model.

The relationship between the secant modulus at failure (E_{sf}) and the tangent modulus at 50% of maximum stress (E_{t50}) of 1% copolymer-added high plasticity clay samples is shown in Figure 6.116.

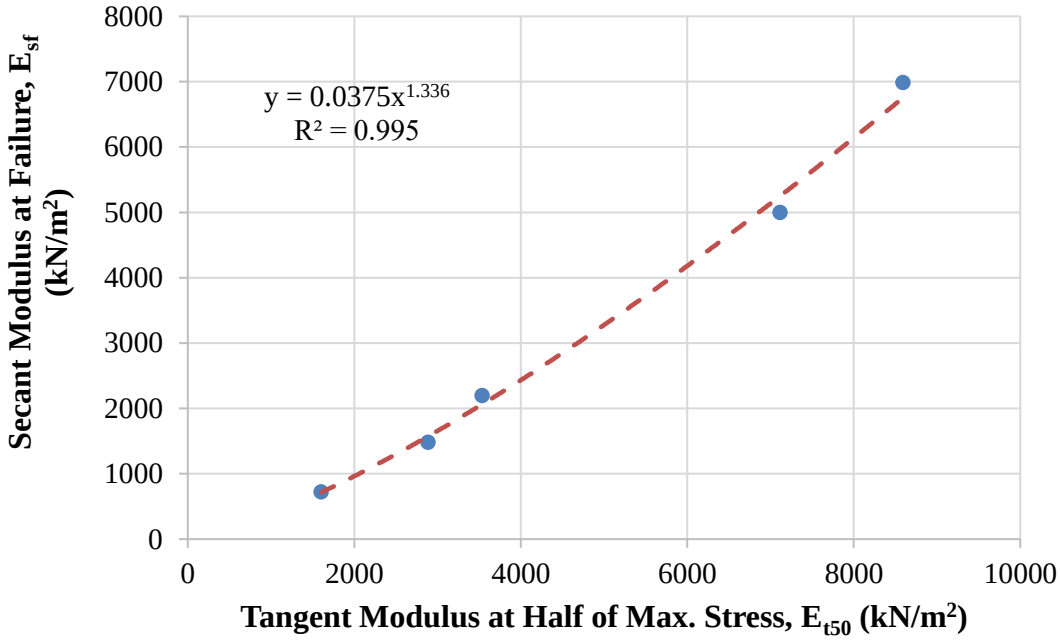

Figure 6.116 Relationship between secant modulus at failure point and tangent modulus at 50% of maximum stress (CH+1% Copolymer)

The tangent modulus at 50% of maximum stress increases with the increasing secant modulus at failure. Thus, it was best suited for estimating these soil moduli by a power model.

Furthermore, the relationship between initial tangent modulus (E_i) and unconfined compression strength of 1% copolymer-added high plasticity clay samples is shown in Figure 6.117.

According to data, the maximum initial tangent modulus is obtained in sample 2 as 14492.8 kN/m^2 for 1% copolymer-added high plasticity clay. It should be noted that the water content is 24%, the dry unit weight is 15.00 kN/m^3, and the unconfined

compression strength is 244.6 kN/m^2 when the initial tangent modulus is the maximum value for 1% copolymer-added high plasticity clay.

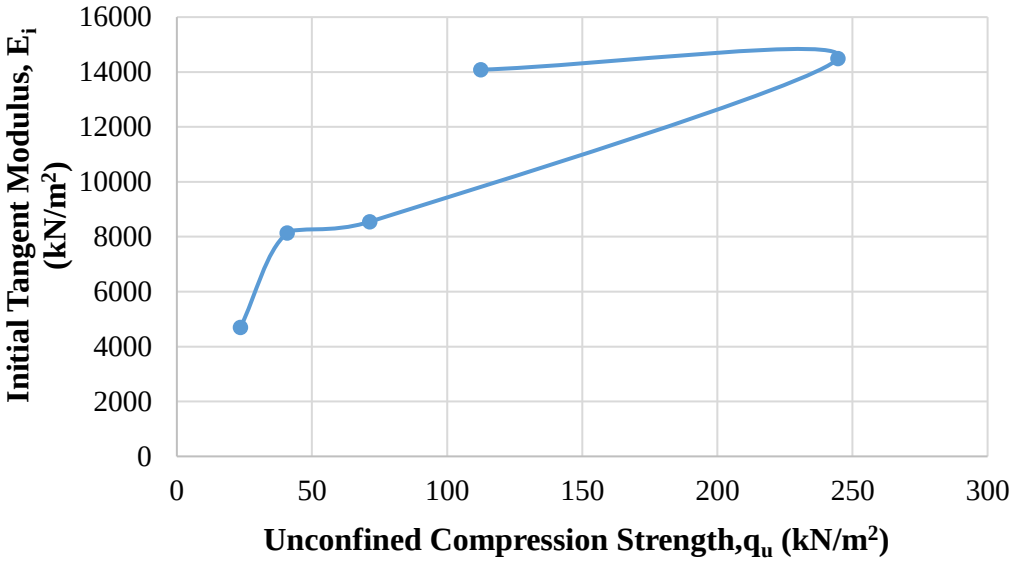

Figure 6.117 Relationship between initial tangent modulus and unconfined compression strength (CH+1% Copolymer)

The relationship between secant modulus at 50% of maximum stress (E_{s50}) and unconfined compression strength of 1% copolymer-added high plasticity clay samples is shown in Figure 6.118.

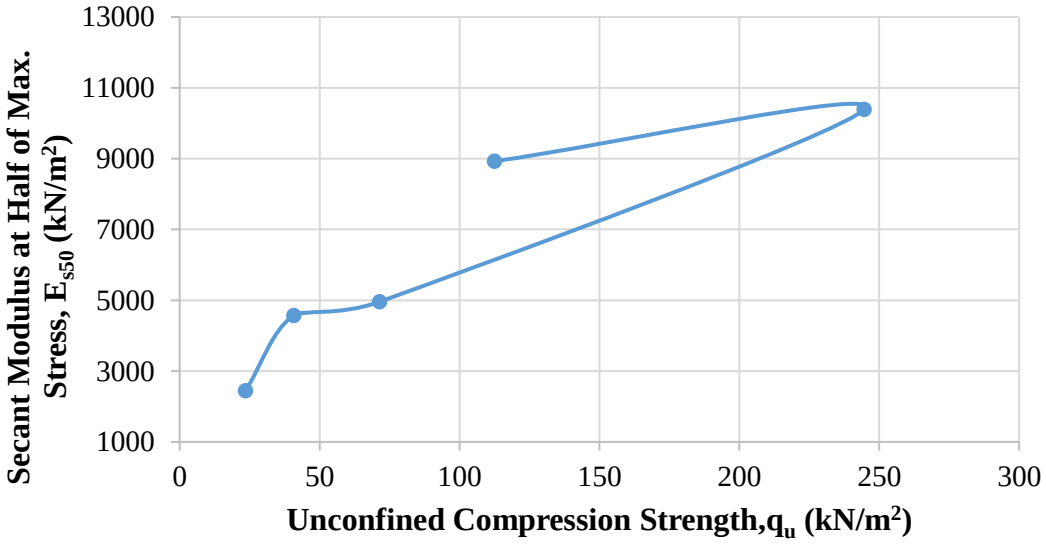

Figure 6.118 Relationship between secant modulus at 50% of maximum stress and unconfined compression strength (CH+1% Copolymer)

The maximum secant modulus at 50% of maximum stress is obtained in sample 2 as 10394.2 kN/m^2 for 1% copolymer-added high plasticity clay. It should be noted that the water content is 24%, the dry unit weight is 15.00 kN/m^3, and the unconfined compression strength is 244.6 kN/m^2 when the secant modulus at 50% of maximum stress has the maximum value of 1% copolymer-added high plasticity clay.

On the other hand, the relationship between tangent modulus at 50% of maximum stress (E_{t50}) and unconfined compression strength of 1% copolymer-added high plasticity clay samples is shown in Figure 6.119.

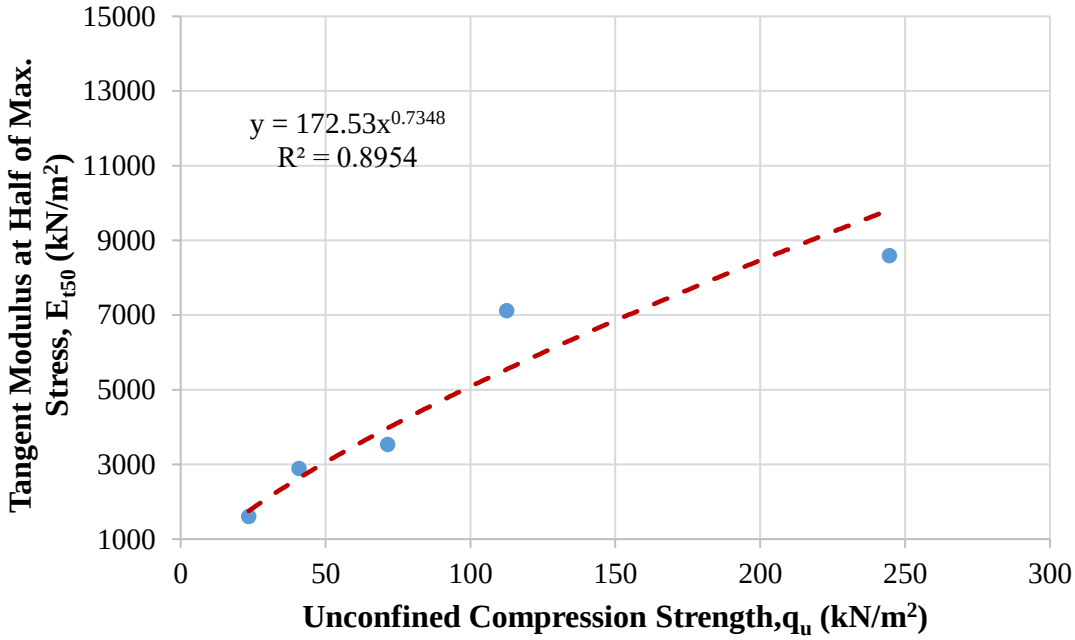

Figure 6.119 Relationship between tangent modulus at 50% of maximum stress and unconfined compression strength (CH+1% Copolymer)

According to data, the maximum tangent modulus at 50% of maximum stress is obtained in sample 2 as 8591.7 kN/m^2 for 1% copolymer-added high plasticity clay. It should be noted that the water content is 24%, the dry unit weight is 15.00 kN/m^3, and the unconfined compression strength is 244.6 kN/m^2 when the tangent modulus at 50% of maximum stress is the maximum value for the 1% copolymer-added high plasticity clay.

In addition, the relationship between secant modulus at failure point (E_{sf}) and unconfined compression strength of 1% copolymer-added high plasticity clay samples is shown in Figure 6.120.

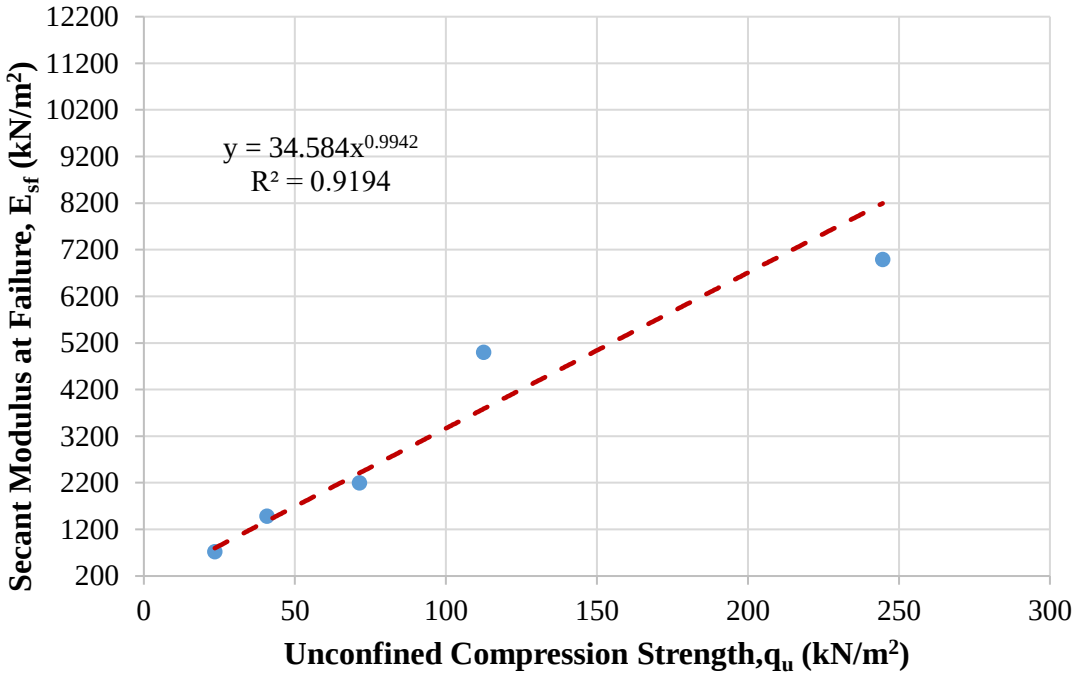

Figure 6.120 Relationship between secant modulus at failure point and unconfined compression strength (CH+1% Copolymer)

It is obvious that the maximum secant modulus at failure point is obtained in sample 2 as 6988.6 kN/m^2 for 1% copolymer-added high plasticity clay. It should be noted that the water content is 24%, the dry unit weight is 15.00 kN/m^3, and the unconfined compression strength is 244.6 kN/m^2 when the secant modulus at failure point is the maximum value for 1% copolymer-added high plasticity clay.

With respect to the results of all calculated soil moduli, it seems that the maximum values of these moduli are obtained at maximum unconfined compression strength (sample 2 for 1% copolymer-added high plasticity clay). On the other hand, when all calculated soil moduli have the maximum value for 1% copolymer-added high plasticity clay, the water content is not equal to the optimum water content (w_{opt}=26%), but the dry unit weight is equal to the maximum dry unit weight (γ_{dmax}=15.00 kN/m^3). Therefore, high plasticity clay soil reinforced with copolymer became stiffer when it was drier. Also, high plasticity clayey soil's strength and load-deformation properties are improved by reinforcing with copolymer fiber.

6.4.4 High Plasticity Clay Soil Mixture with 1.25% of Copolymer

During the experimental program of this study, the amount of 1.25% copolymer mixed with high plasticity clay soil was used. The compaction and the unconfined compression tests were performed on the 1.25% copolymer mixed with high plasticity clay, and the outcomes of these experiments are illustrated in Table 6.35. With respect to data obtained from mentioned tests, it can be seen that the value of ω_{opt} and γ_{dmax} obtained at 26% and 15.00 kN/m^3, respectively.

Table 6.35 Results of experiments executed with CH+1.25% copolymer

Sample No.	ω (%)	γ_d (kN/m^3)	q_u (kN/m^2)
1	17	13.56	120.6
2	20	14.30	234.0
3	24	15.00	237.0
4	29	14.60	132.4
5	31	14.10	85.8
6	34	13.50	59.2

The axial stress-axial strain curves of six different 1.25% copolymer-added high plasticity clay samples are shown in Figure 6.121. According to data obtained from the unconfined compression test of 1.25% copolymer-added high plasticity clay soil samples, it can be inferred that the maximum unconfined compression strength was obtained in the third sample, and it was obtained as 237 kN/m^2.

It should be noted that the reciprocal of the initial tangent modulus (a) and the reciprocal of the asymptotic value of stress difference (b) were derived from transformed hyperbolic stress-strain curves of 1.25% copolymer-added high plasticity clay samples. In addition, the asymptotic value of stress difference $(\sigma_1)_{ult}$, compressive strength $(\sigma_1)_f$, axial strain value at failure (ε_f), and axial strain value at 50% of maximum stress (ε_{50}) were obtained from unconfined compression test results. Lastly, the failure ratio (R_f) was calculated from unconfined compression test results. Mentioned engineering parameters are given in Table 6.36.

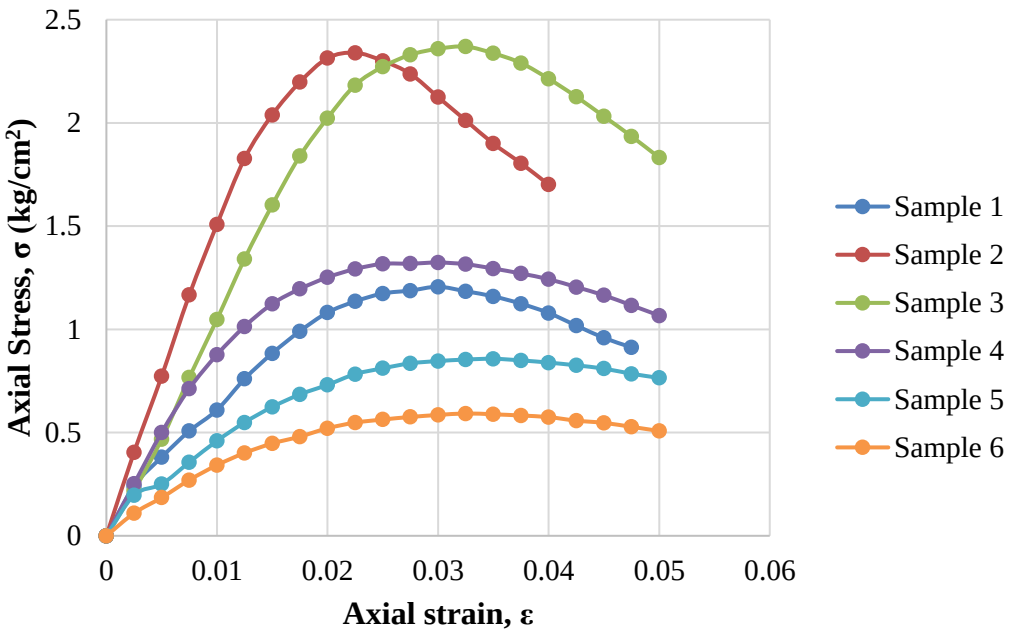

Figure 6.121 Results of unconfined compression tests of CH+1.25% copolymer

Table 6.36 Calculated engineering parameters of CH+1.25% copolymer

Sample No.	a	b	$(\sigma_1)_{ult}$	$(\sigma_1)_f$	R_f	ε_f	ε_{50}
	(cm^2/kg)	(cm^2/kg)	(kg/cm^2)	(kg/cm^2)	-	-	-
1	0.0105	0.4462	2.241	1.206	0.54	0.0300	0.0099
2	0.0053	0.1605	6.231	2.340	0.38	0.0225	0.0075
3	0.0067	0.1901	5.260	2.370	0.45	0.0325	0.0112
4	0.0071	0.4746	2.107	1.324	0.63	0.0300	0.0069
5	0.0136	0.7283	1.373	0.858	0.62	0.0350	0.0093
6	0.0195	1.0184	0.982	0.592	0.60	0.0325	0.0084

It is obvious that, when the values of strains are between 0.1% to 0.001%, this region is categorized as a small strain. Furthermore, it should be noted that the strain level of 1.25% copolymer-added high plasticity clay is classified as small strain (SS) because the maximum axial strain was determined in samples 3, 4, 5, and 6 of 1.25% copolymer-added high plasticity clay, and it was obtained as 0.05%. Thus, it can be concluded that nonlinear behaviour was observed for the tested 1.25% copolymer-added high plasticity clay soil samples.

Initial tangent modulus (E_i), tangent modulus at 50% of maximum stress (E_{t50}), secant modulus at failure (E_{sf}), secant modulus at 50% of maximum stress (E_{s50}), and unconfined compression strength (q_u) of six different 1.25% copolymer-added high plasticity clay soil samples are given in Table 6.37.

Table 6.37 Soil moduli and unconfined compression strength of CH+1.25% copolymer

Sample No.	E_i (kN/m^2)	E_{t50} (kN/m^2)	E_{sf} (kN/m^2)	E_{s50} (kN/m^2)	q_u (kN/m^2)
1	9523.8	5088.3	4020.0	6120.9	120.6
2	18867.9	12447.0	10400.0	15554.4	234.0
3	14925.4	8958.3	7292.3	10609.8	237.0
4	14084.5	6624.5	4413.3	9596.2	132.4
5	7352.9	3476.0	2451.4	4635.4	85.8
6	5128.2	2502.4	1821.5	3522.6	59.2

According to the data obtained, it can be concluded that the maximum modulus values are observed in the initial tangent modulus compared with other soil moduli in all six 1.25% copolymer-added high plasticity clay samples due to the initial slope of the stress-strain curve. In other words, the axial stress increases up to a certain point very sharply. Then, this sharp increasing trend suddenly starts to slow down, and during this slowing trend, the axial strain increases rapidly.

In addition, transformed hyperbolic stress-strain curves for six different 1.25% copolymer-added high plasticity clay samples are illustrated in Figure 6.122.

It was found that low and high values of axial strains in samples 1, 2, 3, 4, and 5 are not precisely hyperbolic, as shown in Figures 6.122 (a, b, c, d, and e). In other words, these points can not be fitted in a straight line. However, it was possible to estimate the actual stress-strain curves by a hyperbola. Thus, it is found to have a reasonable degree of accuracy. On the other hand, the transformed hyperbolic stress-strain curve in sample 6 is hyperbolic, as shown in Figures 6.122 (e). In other words, these points can be best-fitted in a straight line.

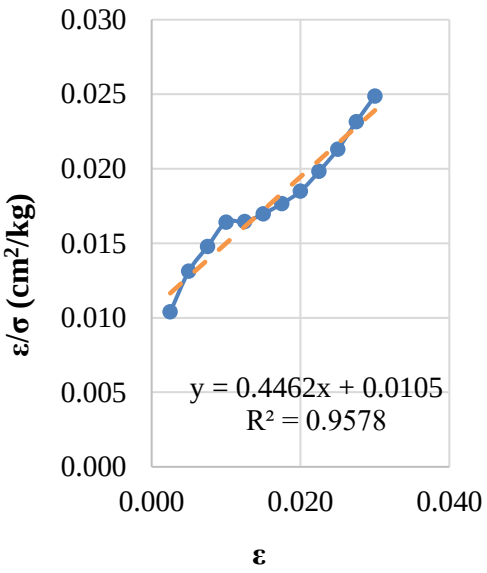
0.030
0.025
0.020
0.015
0.010
0.005
0.000
ε/σ (cm²/kg)
y = 0.4462x + 0.0105
R² = 0.9578
0.000
0.020
0.040
ε

(a)

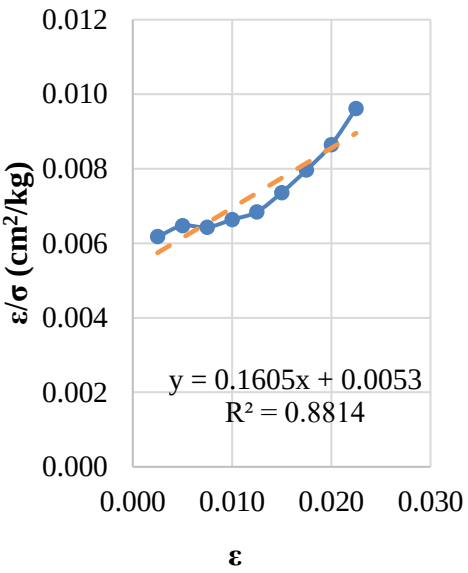
0.012
0.010
0.008
0.006
0.004
0.002
0.000
ε/σ (cm²/kg)
y = 0.1605x + 0.0053
R² = 0.8814
0.000
0.010
0.020
0.030
ε

(b)

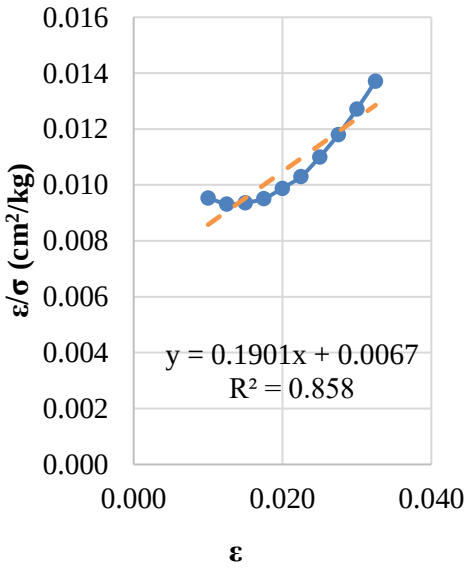
0.016
0.014
0.012
0.010
0.008
0.006
0.004
0.002
0.000
ε/σ (cm²/kg)
y = 0.1901x + 0.0067
R² = 0.858
0.000
0.020
0.040
ε

(c)

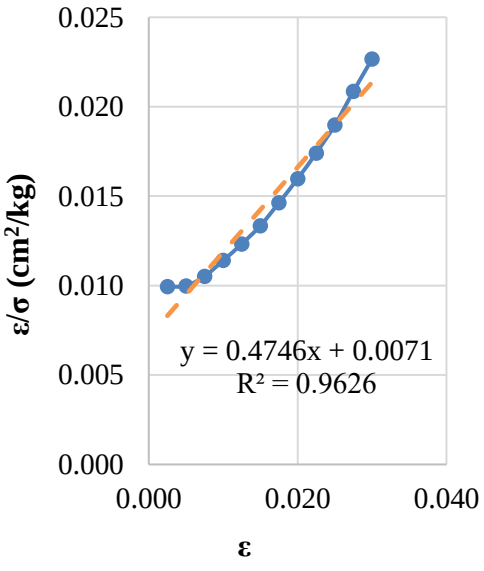
0.025
0.020
0.015
0.010
0.005
0.000
ε/σ (cm²/kg)
y = 0.4746x + 0.0071
R² = 0.9626
0.000
0.020
0.040
ε

(d)

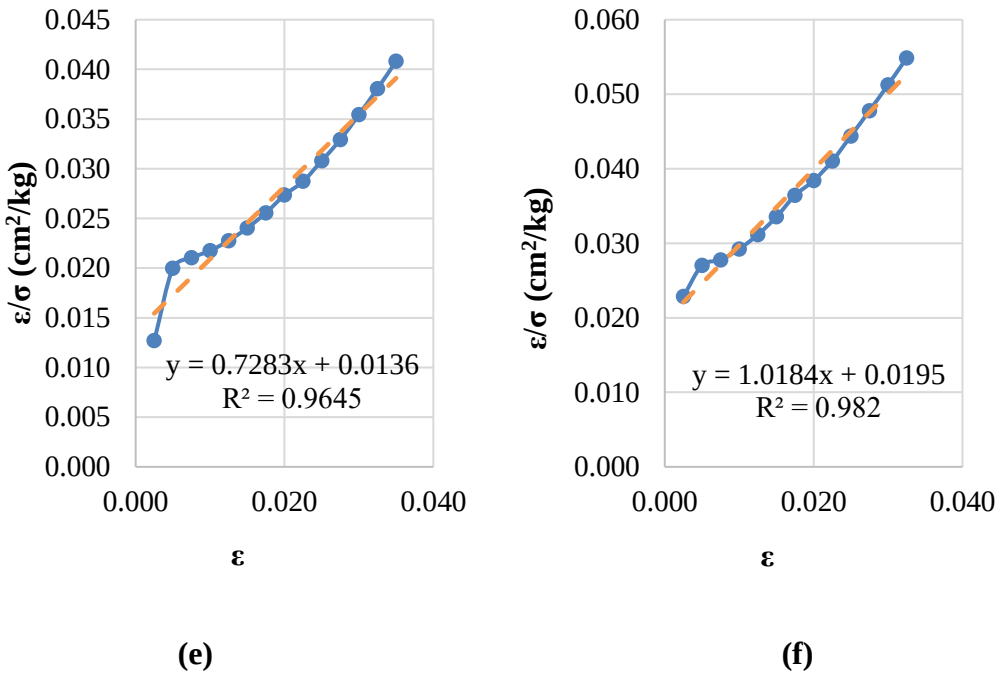

Figure 6.122 Transformed hyperbolic stress-strain curves for (a) sample 1, (b) sample 2, (c) sample 3, (d) sample 4, (e) sample 5, and (f) sample 6 (CH+1.25% Copolymer)

The relationship between the secant modulus at 50% of maximum stress (E_{s50}) and the initial tangent modulus (E_i) of 1.25% copolymer-added high plasticity clay samples is shown in Figure 6.123.

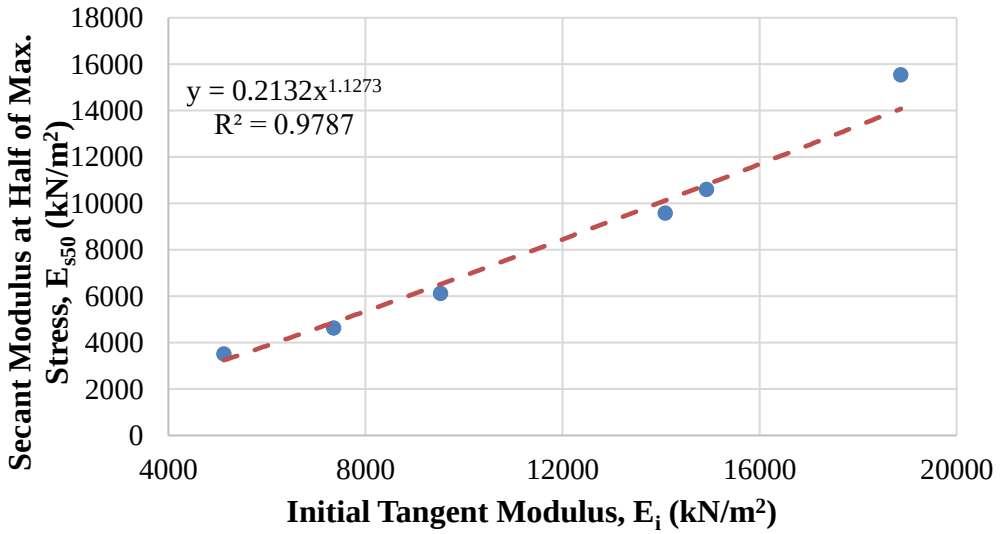

Figure 6.123 Relationship between secant modulus at 50% of maximum stress and initial tangent modulus (CH+1.25% Copolymer)

According to the data, it can be inferred that these soil moduli refer to the hardening of 1.25% copolymer-added high plasticity clay samples. Thus, the initial tangent modulus increases with the increasing secant modulus at 50% of maximum stress. Furthermore, it was best suited for estimating these soil moduli by a power model.

The relationship between the secant modulus at failure (E_{sf}) and the tangent modulus at 50% of maximum stress (E_{t50}) of 1.25% copolymer-added high plasticity clay samples is shown in Figure 6.124.

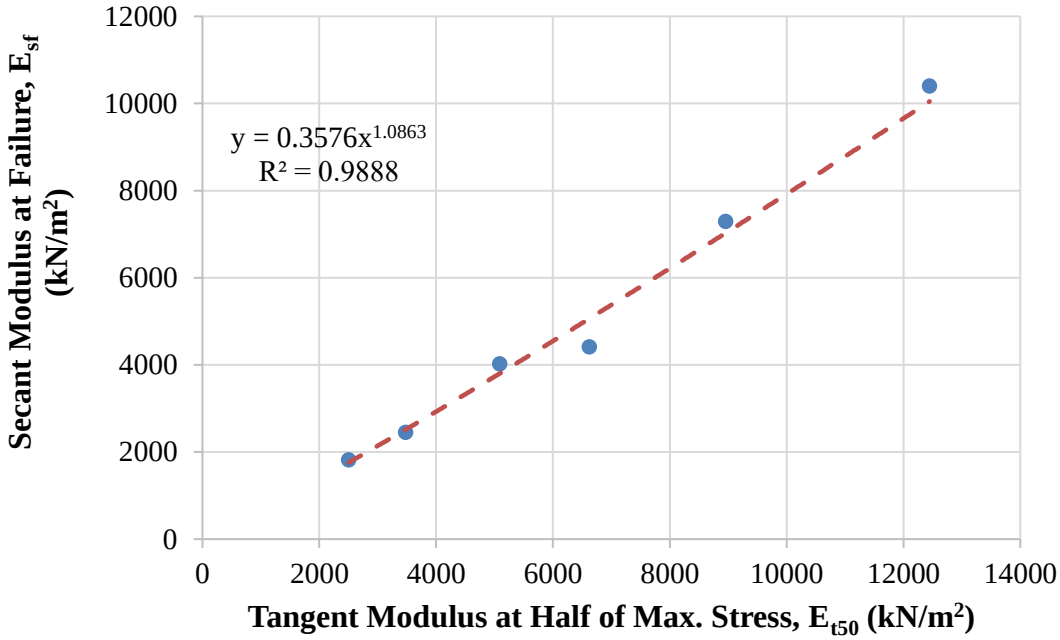

Figure 6.124 Relationship between secant modulus at failure point and tangent modulus at 50% of maximum stress (CH+1.25% Copolymer)

The tangent modulus at 50% of maximum stress increases with the increasing secant modulus at failure. Thus, it was best suited for estimating these soil moduli by a power model.

Furthermore, the relationship between initial tangent modulus (E_i) and unconfined compression strength of 1.25% copolymer-added high plasticity clay samples is shown in Figure 6.125.

According to data, the maximum initial tangent modulus is obtained in sample 2 as 18867.9 kN/m^2 for 1.25% copolymer-added high plasticity clay. It should be noted that the water content is 20%, the dry unit weight is 14.30 kN/m^3, and the unconfined

compression strength is 234 kN/m^2 when the initial tangent modulus is the maximum value for 1.25% copolymer-added high plasticity clay.

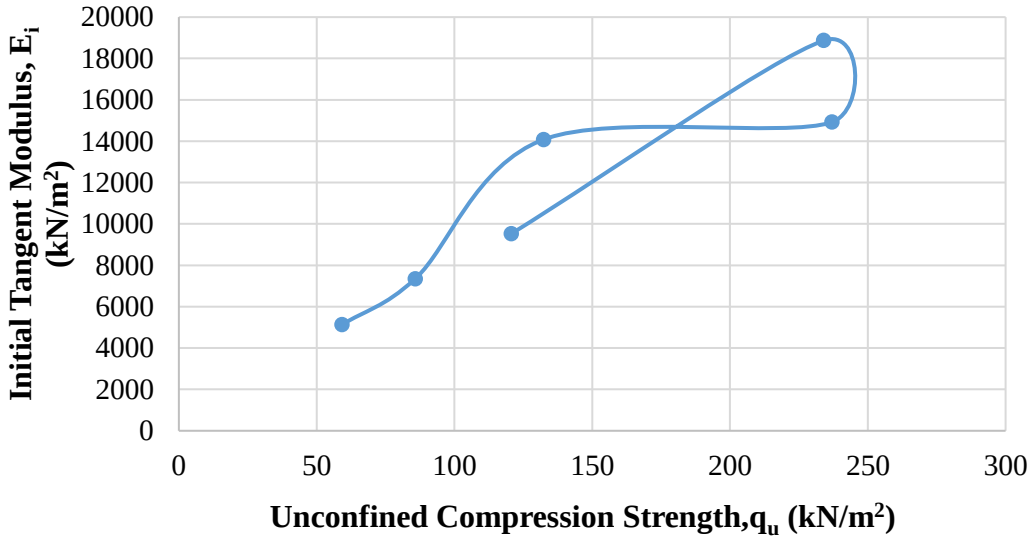

Figure 6.125 Relationship between initial tangent modulus and unconfined compression strength (CH+1.25% Copolymer)

The relationship between secant modulus at 50% of maximum stress (E_{s50}) and unconfined compression strength of 1.25% copolymer-added high plasticity clay samples is shown in Figure 6.126.

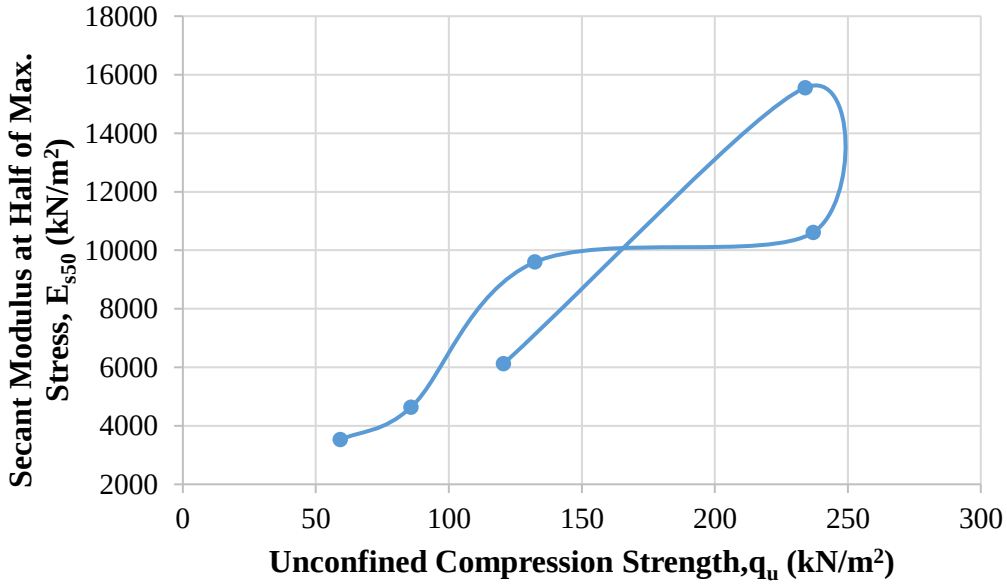

Figure 6.126 Relationship between secant modulus at 50% of maximum stress and unconfined compression strength (CH+1.25% Copolymer)

The maximum secant modulus at 50% of maximum stress is obtained in sample 2 as 15554.4 kN/m^2 for 1.25% copolymer-added high plasticity clay. It should be noted that the water content is 20%, the dry unit weight is 14.30 kN/m^3, and the unconfined compression strength is 234 kN/m^2 when the secant modulus at 50% of maximum stress has the maximum value of 1.25% copolymer-added high plasticity clay.

On the other hand, the relationship between tangent modulus at 50% of maximum stress (E_{t50}) and unconfined compression strength of 1.25% copolymer-added high plasticity clay samples is shown in Figure 6.127.

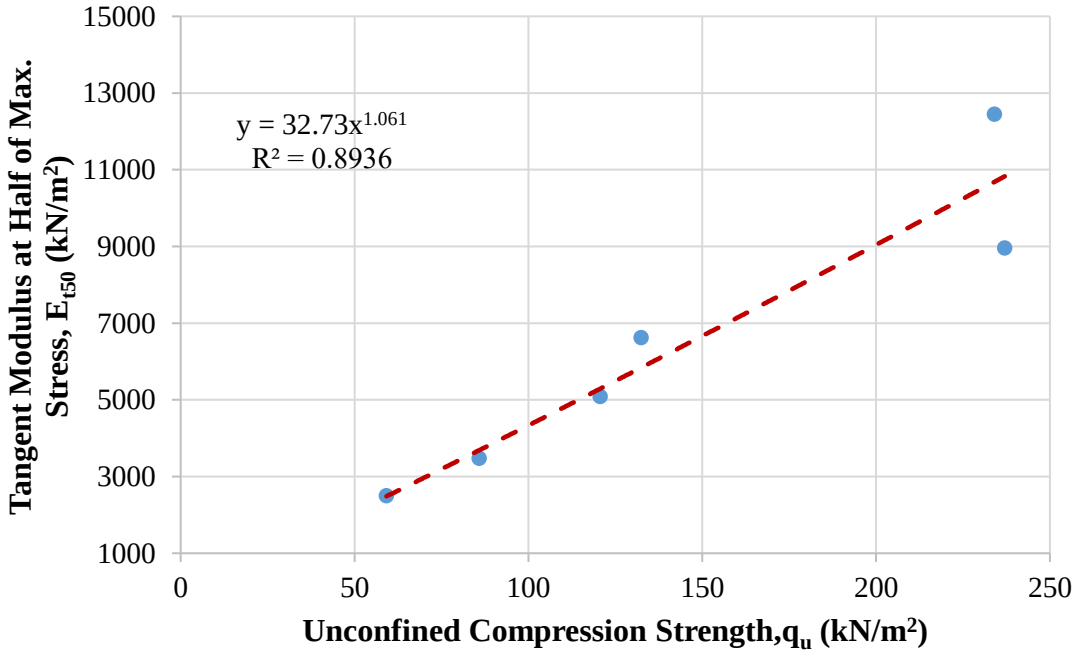

Figure 6.127 Relationship between tangent modulus at 50% of maximum stress and unconfined compression strength (CH+1.25% Copolymer)

According to data, the maximum tangent modulus at 50% of maximum stress is obtained in sample 2 as 12447 kN/m^2 for 1.25% copolymer-added high plasticity clay. It should be noted that the water content is 20%, the dry unit weight is 14.30 kN/m^3, and the unconfined compression strength is 234 kN/m^2 when the tangent modulus at 50% of maximum stress is the maximum value for the 1.25% copolymer-added high plasticity clay.

In addition, the relationship between secant modulus at failure point (E_{sf}) and unconfined compression strength of 1.25% copolymer-added high plasticity clay samples is shown in Figure 6.128.

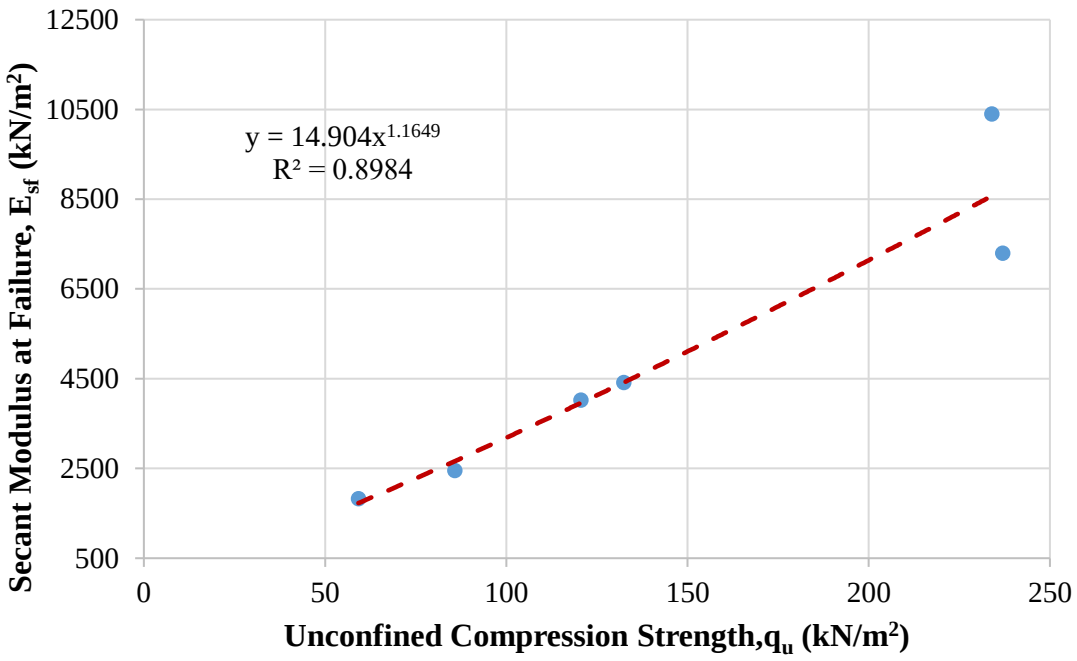

Figure 6.128 Relationship between secant modulus at failure point and unconfined compression strength (CH+1.25% Copolymer)

It is obvious that the maximum secant modulus at failure point is obtained in sample 2 as 104000 kN/m^2 for 1.25% copolymer-added high plasticity clay. It should be noted that the water content is 20%, the dry unit weight is 14.30 kN/m^3, and the unconfined compression strength is 234 kN/m^2 when the secant modulus at failure point is the maximum value for 1.25% copolymer-added high plasticity clay.

With respect to the results of all calculated soil moduli, it seems that the maximum values of these moduli are not obtained at the maximum unconfined compression strength (sample 3 for 1.25% copolymer-added high plasticity clay) since the beginning of the stress-strain curve of sample 2 has rapidly increased in axial stress. However, samples 2 and 3 slightly differ in the unconfined compression strength values. On the other hand, when all calculated soil moduli have the maximum value for 1.25% copolymer-added high plasticity clay, the water content is not equal to the optimum water content (w_{opt}=26%), and the dry unit weight is close to the maximum dry unit weight (γ_{dmax}=15.00 kN/m^3). Furthermore, high plasticity clay soil reinforced with copolymer became stiffer when it was drier. Therefore, high plasticity clayey soil's strength and load-deformation properties are improved by reinforcing with copolymer fiber.

6.4.5 High Plasticity Clay Soil Mixture with 1.5% of Copolymer

During the experimental program of this study, the amount of 1.5% copolymer mixed with high plasticity clay soil was used. The compaction and the unconfined compression tests were performed on the 1.5% copolymer mixed with high plasticity clay, and the outcomes of these experiments are illustrated in Table 6.38. With respect to data obtained from mentioned tests, it can be seen that the value of ω_{opt} and γ_{dmax} obtained at 26% and 14.80 kN/m^3, respectively.

Table 6.38 Results of experiments executed with CH+1.5% copolymer

Sample No.	w of q_u (%)	γ_d (kN/m^3)	q_u (kN/m^2)
1	16	13.26	85.0
2	20	14.10	171.9
3	22	14.80	169.3
4	29	14.34	103.9
5	33	13.40	45.0
6	35	12.85	39.6

The axial stress-axial strain curves of six different 1.5% copolymer-added high plasticity clay samples are shown in Figure 6.129. According to data obtained from the unconfined compression test of 1.5% copolymer-added high plasticity clay soil samples, it can be inferred that the maximum unconfined compression strength was obtained in the second sample, and it was obtained as 171.9 kN/m^2.

It should be noted that the reciprocal of the initial tangent modulus (a) and the reciprocal of the asymptotic value of stress difference (b) were derived from transformed hyperbolic stress-strain curves of 1.5% copolymer-added high plasticity clay samples. In addition, the asymptotic value of stress difference $(\sigma_1)_{ult}$, compressive strength $(\sigma_1)_f$, axial strain value at failure (ε_f), and axial strain value at 50% of maximum stress (ε_{50}) were obtained from unconfined compression test results. Lastly, the failure ratio (R_f) was calculated from unconfined compression test results. Mentioned engineering parameters are given in Table 6.39.

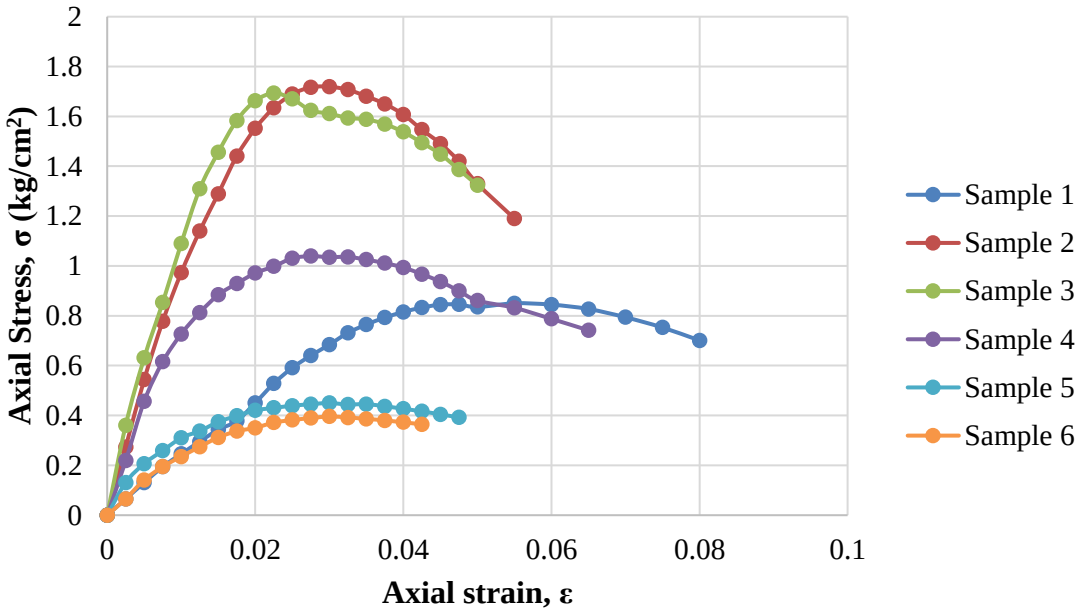

Figure 6.129 Results of unconfined compression tests of CH+1.5% copolymer

Table 6.39 Calculated engineering parameters of CH+1.5% copolymer

Sample No.	a (cm^2/kg)	b (cm^2/kg)	$(\sigma_1)_{ult}$ (kg/cm^2)	$(\sigma_1)_f$ (kg/cm^2)	R_f -	ε_f -	ε_{50} -
1	0.0353	0.4045	2.472	0.850	0.34	0.0550	0.0191
2	0.0075	0.2973	3.364	1.719	0.51	0.0300	0.0086
3	0.0063	0.2895	3.454	1.693	0.49	0.0225	0.0074
4	0.0079	0.6421	1.557	1.039	0.67	0.0275	0.0060
5	0.0154	1.6688	0.599	0.450	0.75	0.0300	0.0059
6	0.0286	1.4652	0.683	0.396	0.58	0.0300	0.0077

It is obvious that, when the values of strains are between 0.1% to 0.001%, this region is categorized as a small strain. Furthermore, it should be noted that the strain level of 1.5% copolymer-added high plasticity clay is classified as small strain (SS) because the maximum axial strain was determined in sample 1 of 1.5% copolymer-added high plasticity clay, and it was obtained as 0.08%. Thus, it can be concluded that nonlinear behaviour was observed for the tested 1.5% copolymer-added high plasticity clay soil samples.

Initial tangent modulus (E_i), tangent modulus at 50% of maximum stress (E_{t50}), secant modulus at failure (E_{sf}), secant modulus at 50% of maximum stress (E_{s50}), and

unconfined compression strength (q_u) of six different 1.5% copolymer-added high plasticity clay soil samples are given in Table 6.40.

Table 6.40 Soil moduli and unconfined compression strength of CH+1.5% copolymer

Sample No.	E_i (kN/m^2)	E_{t50} (kN/m^2)	E_{sf} (kN/m^2)	E_{s50} (kN/m^2)	q_u (kN/m^2)
1	2832.9	1942.6	1545.5	2224.0	85.0
2	13333.3	7389.8	5730.0	10049.9	171.9
3	15873.0	9046.5	7524.4	11397.9	169.3
4	12658.2	5621.9	3778.2	8683.4	103.9
5	6493.5	2532.6	1500.0	3836.1	45.0
6	3496.5	1762.0	1320.0	2556.9	39.6

According to the data obtained, it can be concluded that the maximum modulus values are observed in the initial tangent modulus compared with other soil moduli in all six 1.5% copolymer-added high plasticity clay samples due to the initial slope of the stress-strain curve. In other words, the axial stress increases up to a certain point very sharply. Then, this sharp increasing trend suddenly starts to slow down, and during this slowing trend, the axial strain increases rapidly.

In addition, transformed hyperbolic stress-strain curves for six different 1.5% copolymer-added high plasticity clay samples are illustrated in Figure 6.130.

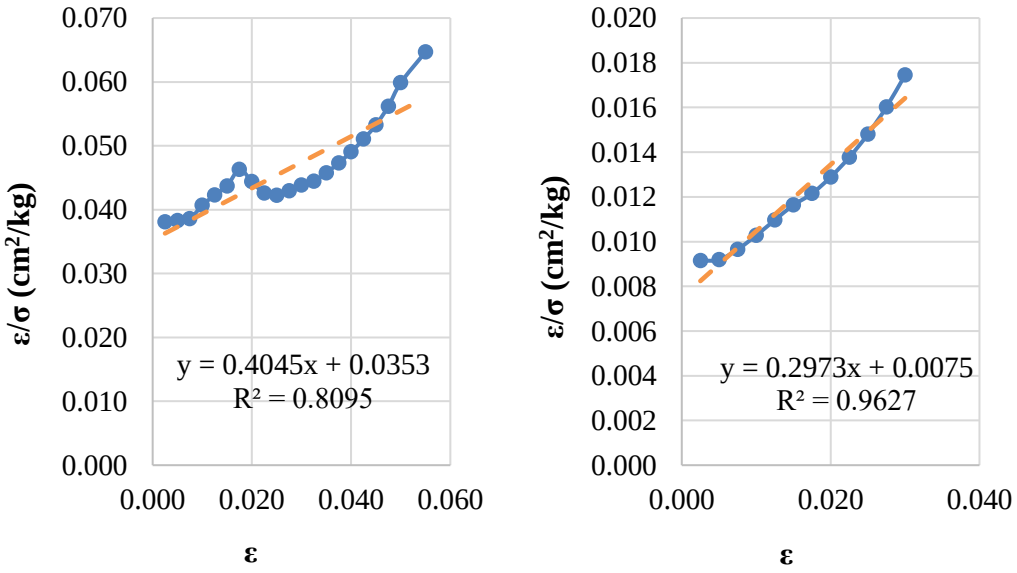

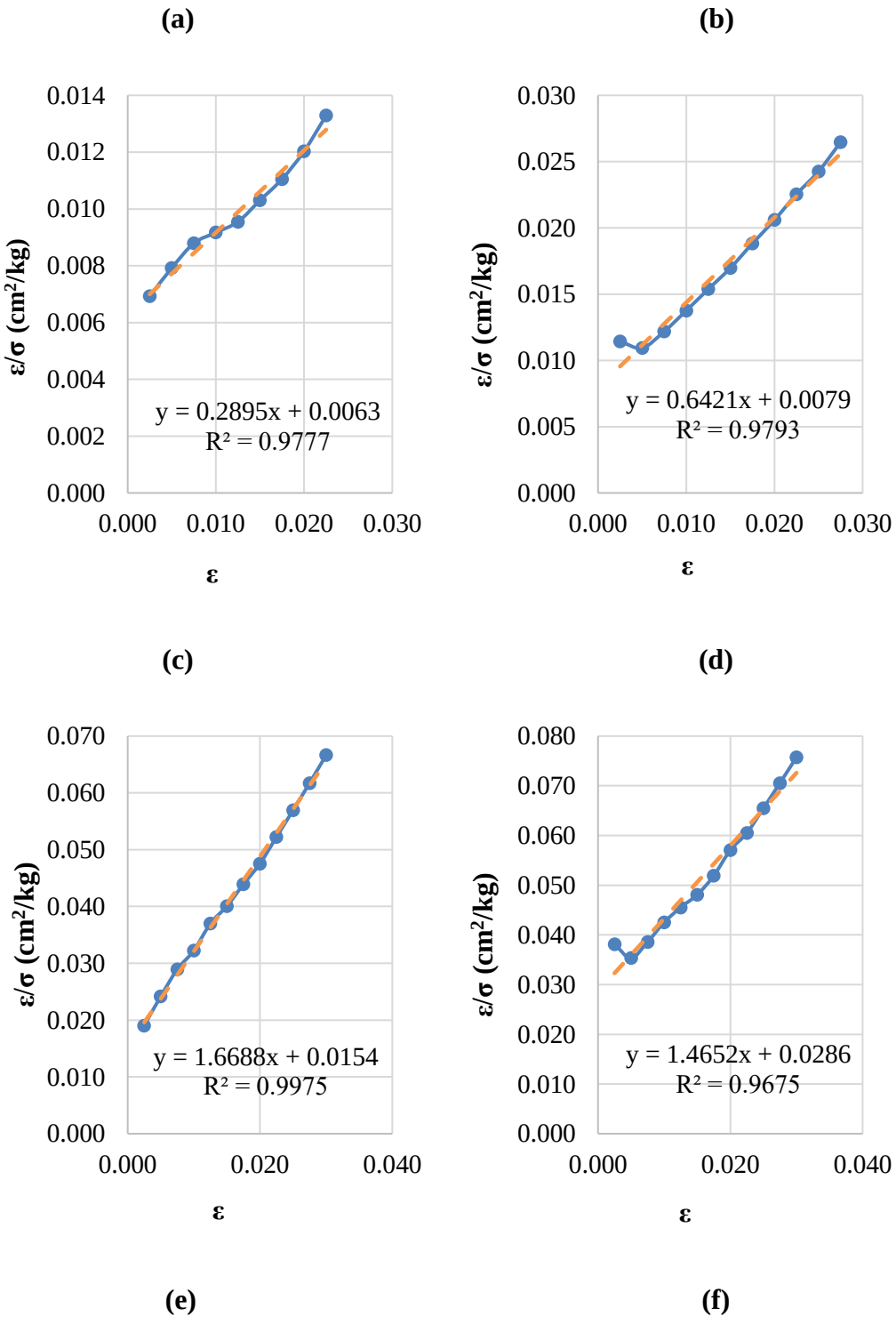

Figure 6.130 Transformed hyperbolic stress-strain curves for (a) sample 1, (b) sample 2, (c) sample 3, (d) sample 4, (e) sample 5, and (f) sample 6 (CH+1.5% Copolymer)

It was found that low and high values of axial strains in samples 1, 2, and 6 are not precisely hyperbolic, as shown in Figures 6.130 (a, b, and f). In other words, these

points can not be fitted in a straight line. However, it was possible to estimate the actual stress-strain curves by a hyperbola. Thus, it is found to have a reasonable degree of accuracy. On the other hand, the transformed hyperbolic stress-strain curve in samples 3, 4, and 5 is hyperbolic, as shown in Figures 6.130 (c, d, and e). In other words, these points can be best-fitted in a straight line.

The relationship between the secant modulus at 50% of maximum stress (E_{s50}) and the initial tangent modulus (E_i) of 1.5% copolymer-added high plasticity clay samples is shown in Figure 6.131.

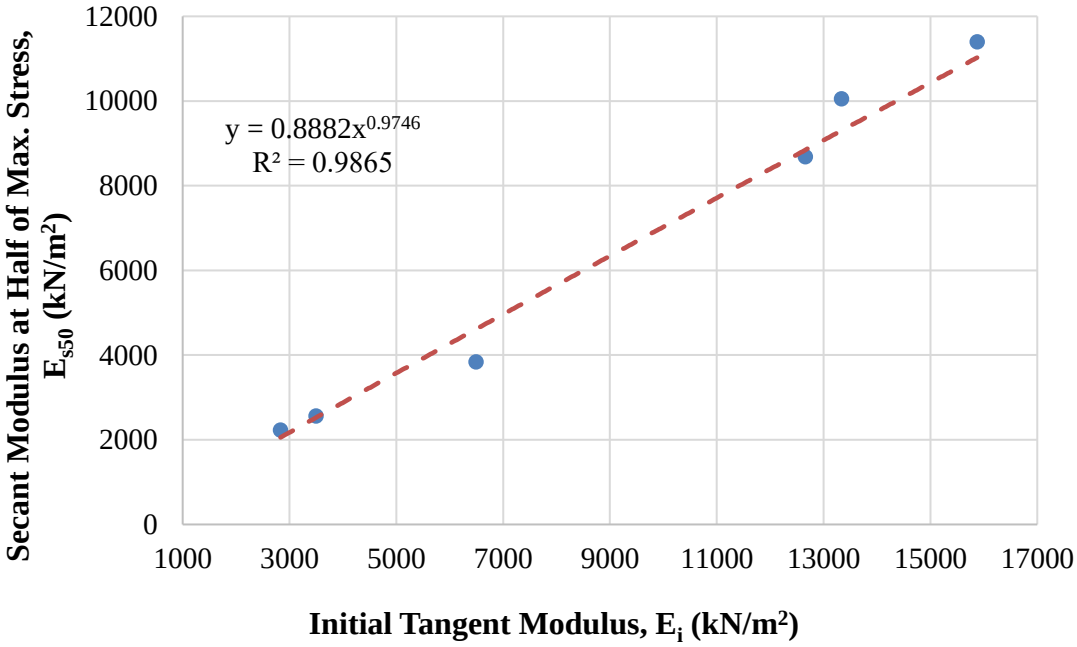

Figure 6.131 Relationship between secant modulus at 50% of maximum stress and initial tangent modulus (CH+1.5% Copolymer)

According to the data, it can be inferred that these soil moduli refer to the hardening of 1.5% copolymer-added high plasticity clay samples. Thus, the initial tangent modulus increases with the increasing secant modulus at 50% of maximum stress. Furthermore, it was best suited for estimating these soil moduli by a power model.

The relationship between the secant modulus at failure (E_{sf}) and the tangent modulus at 50% of maximum stress (E_{t50}) of 1.5% copolymer-added high plasticity clay samples is shown in Figure 6.132.

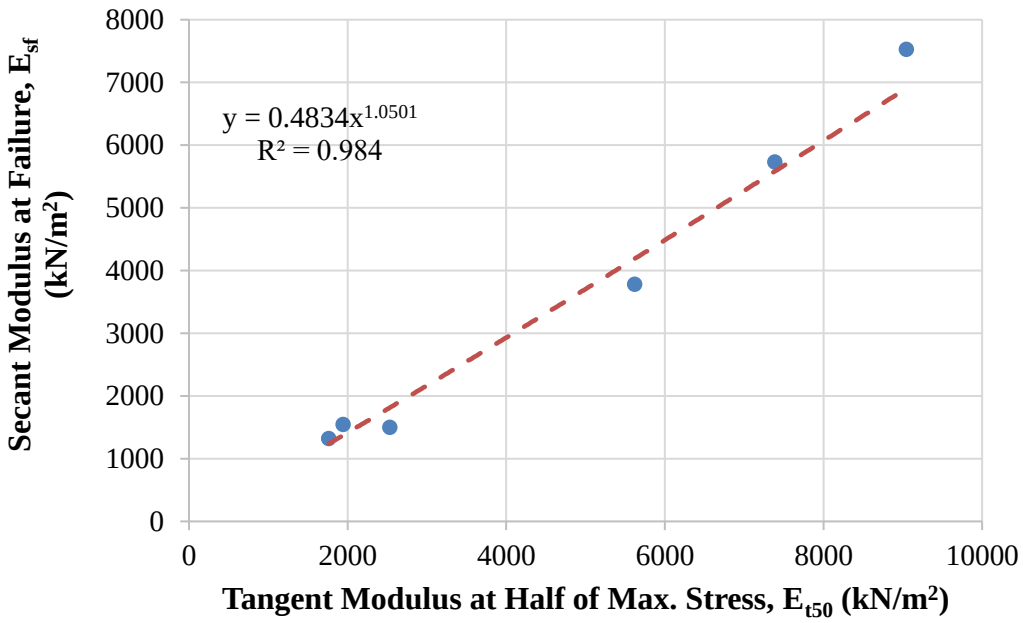

Figure 6.132 Relationship between secant modulus at failure point and tangent modulus at 50% of maximum stress (CH+1.5% Copolymer)

Furthermore, the relationship between initial tangent modulus (E_i) and unconfined compression strength of 1.5% copolymer-added high plasticity clay samples is shown in Figure 6.133.

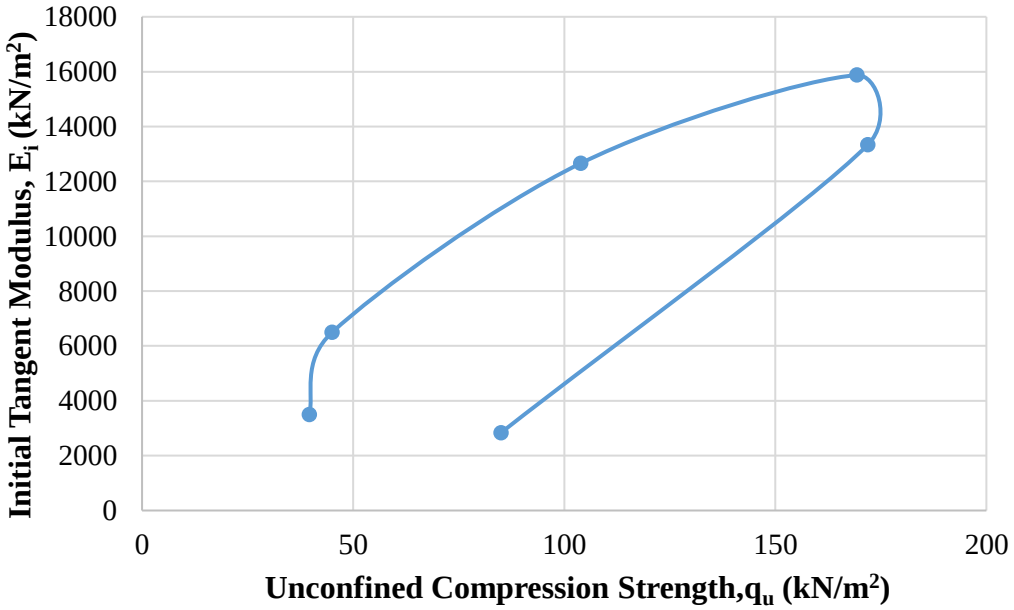

Figure 6.133 Relationship between initial tangent modulus and unconfined compression strength (CH+1.5% Copolymer)

According to data, the maximum initial tangent modulus is obtained in sample 3 as 15873 kN/m^2 for 1.5% copolymer-added high plasticity clay. It should be noted that the water content is 22%, the dry unit weight is 14.80 kN/m^3, and the unconfined compression strength is 169.3 kN/m^2 when the initial tangent modulus is the maximum value for 1.5% copolymer-added high plasticity clay.

The relationship between secant modulus at 50% of maximum stress (E_{s50}) and unconfined compression strength of 1.5% copolymer-added high plasticity clay samples is shown in Figure 6.134.

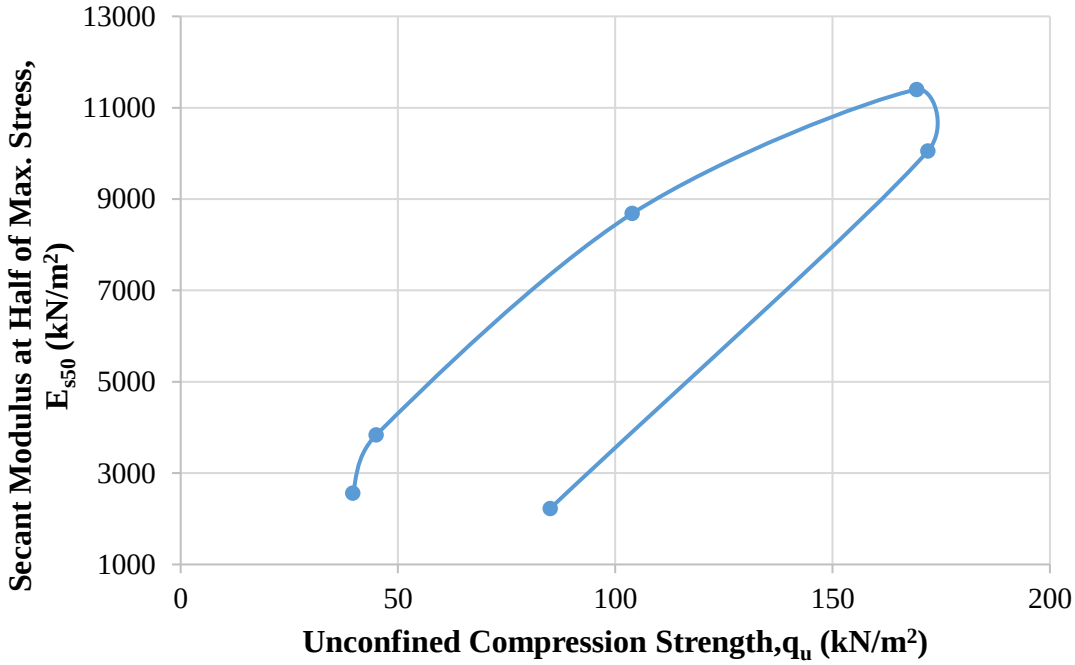

Figure 6.134 Relationship between secant modulus at 50% of maximum stress and unconfined compression strength (CH+1.5% Copolymer)

The maximum secant modulus at 50% of maximum stress is obtained in sample 3 as 11397.9 kN/m^2 for 1.5% copolymer-added high plasticity clay. It should be noted that the water content is 22%, the dry unit weight is 14.80 kN/m^3, and the unconfined compression strength is 169.3 kN/m^2 when the secant modulus at 50% of maximum stress has the maximum value of 1.5% copolymer-added high plasticity clay.

On the other hand, the relationship between tangent modulus at 50% of maximum stress (E_{t50}) and unconfined compression strength of 1.5% copolymer-added high plasticity clay samples is shown in Figure 6.135.

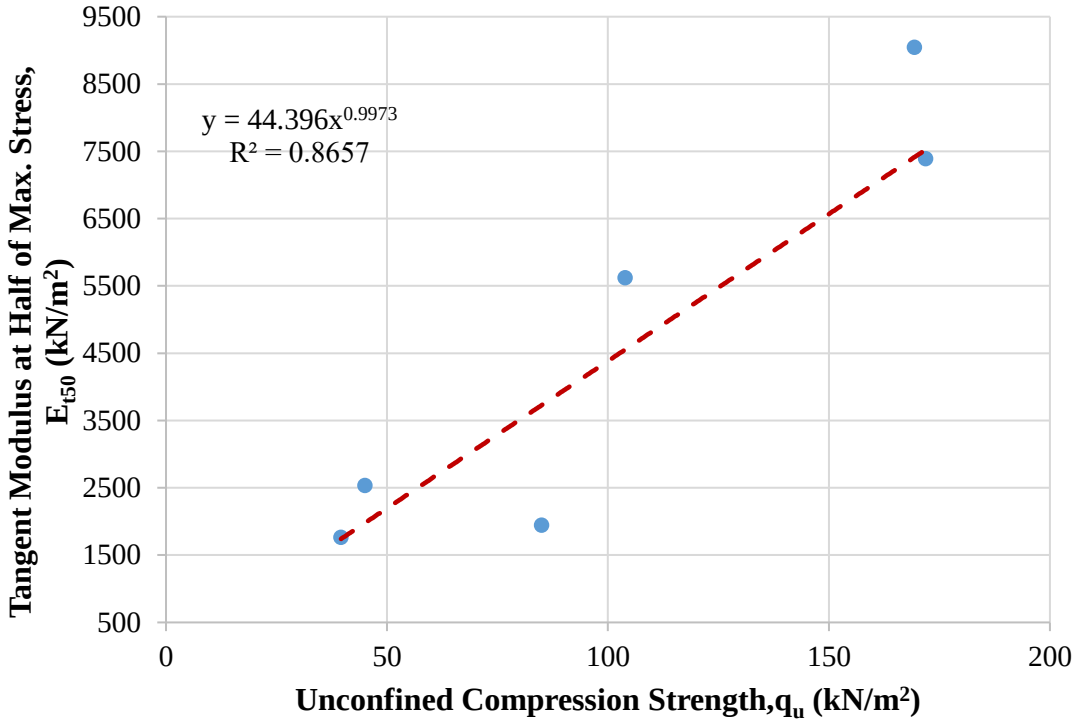

Figure 6.135 Relationship between tangent modulus at 50% of maximum stress and unconfined compression strength (CH+1.5% Copolymer)

The maximum tangent modulus at 50% of maximum stress is obtained in sample 3 as 9046.5 kN/m^2 for 1.5% copolymer-added high plasticity clay. It should be noted that the water content is 22%, the dry unit weight is 14.80 kN/m^3, and the unconfined compression strength is 169.3 kN/m^2 when the tangent modulus at 50% of maximum stress is the maximum value for the 1.5% copolymer-added high plasticity clay.

In addition, the relationship between secant modulus at failure point (E_{sf}) and unconfined compression strength of 1.5% copolymer-added high plasticity clay samples is shown in Figure 6.136.

It is obvious that the maximum secant modulus at failure point is obtained in sample 3 as 7524.4 kN/m^2 for 1.5% copolymer-added high plasticity clay. It should be noted that the water content is 22%, the dry unit weight is 14.80 kN/m^3, and the unconfined compression strength is 169.3 kN/m^2 when the secant modulus at failure point is the maximum value for 1.5% copolymer-added high plasticity clay.

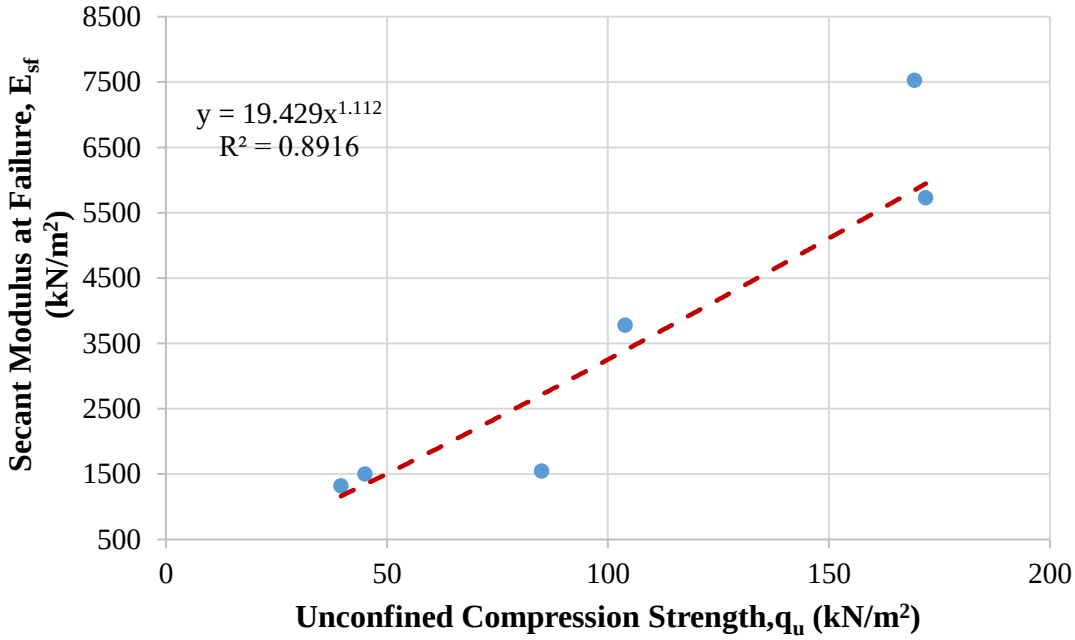

Figure 6.136 Relationship between secant modulus at failure point and unconfined compression strength (CH+1.5% Copolymer)

With respect to the results of all calculated soil moduli, it seems that the maximum values of these moduli are not obtained at the obtained maximum unconfined compression strength (sample 2 for 1.5% copolymer-added high plasticity clay) since the beginning of the stress-strain curve of sample 3 has rapidly increased in axial stress. However, samples 2 and 3 slightly differ in the unconfined compression strength values. On the other hand, when all calculated soil moduli have the maximum value for 1.5% copolymer-added high plasticity clay, the water content is not equal to the optimum water content (w_{opt}=26%), and the dry unit weight is equal to the maximum dry unit weight (γ_{dmax}=14.80 kN/m^3). Furthermore, high plasticity clay soil reinforced with copolymer became stiffer when it was drier. Therefore, high plasticity clayey soil's strength and load-deformation properties are improved by reinforcing with copolymer fiber.

6.4.6 Comparison of Five Different Copolymer Mixtures with High Plasticity Clay Soil

Five different amounts of copolymer (0.5%, 0.75%, 1%, 1.25%, and 1.5%) mixed with high plasticity clay soil were prepared to analyze deformation moduli. The soil moduli of the mentioned high plasticity clay-copolymer mixtures are compared

with the plain high plasticity clay. Figure 6.137 exhibits the relationship between the maximum initial tangent modulus and different copolymer content of CH.

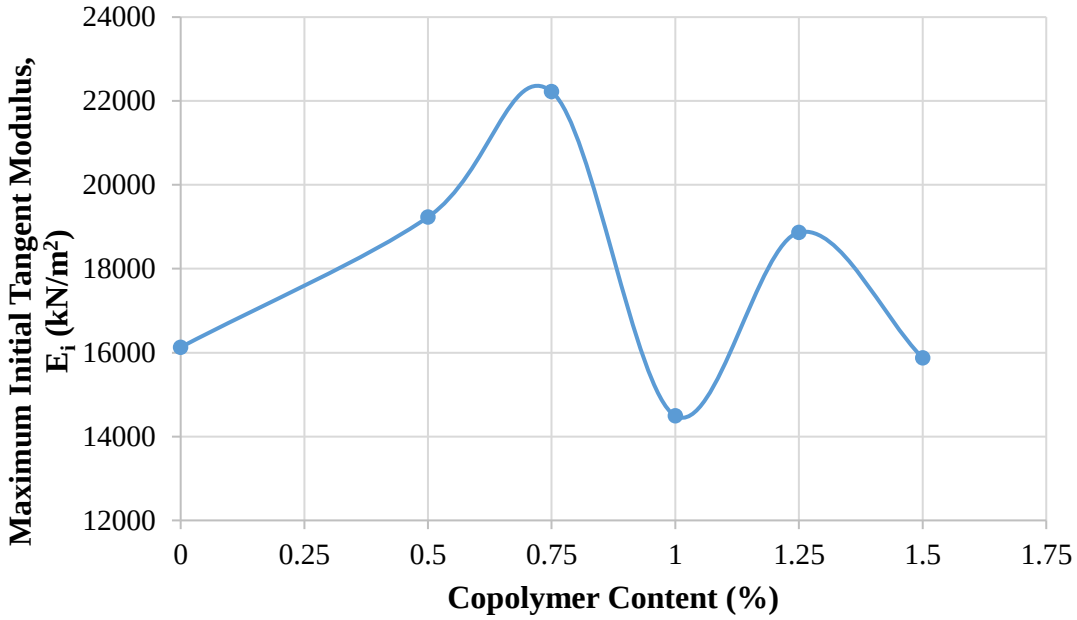

Figure 6.137 Relationship between maximum initial tangent modulus and different copolymer contents of CH

After analyzing all initial tangent modulus of high plasticity clay-copolymer mixtures and comparing them in a graph, it can be seen that the maximum initial tangent modulus was obtained in the mixture with 0.75% of copolymer. In addition, the initial tangent modulus increases up to 38% in the mixture with 0.75% of copolymer. In other words, it is found that the initial tangent modulus increases up to the mixture with 0.75% of copolymer. Then, it fluctuated with the increasing copolymer content up to the mixture with 1.5% of copolymer.

As the next step, all secant modulus at 50% of maximum stress of high plasticity clay-copolymer mixtures were gathered and compared in Figure 6.138.

It can be seen that the maximum secant modulus at 50% of maximum stress was obtained in the mixture with 1.25% of copolymer. In addition, the secant modulus at 50% of maximum stress increases up to 56% in the mixture with 1.25% of copolymer. In other words, it is found that the secant modulus at 50% of maximum stress increases up to the mixture with 0.75% of copolymer. Then, it fluctuated with the increasing copolymer content up to the mixture with 1.5% of copolymer.

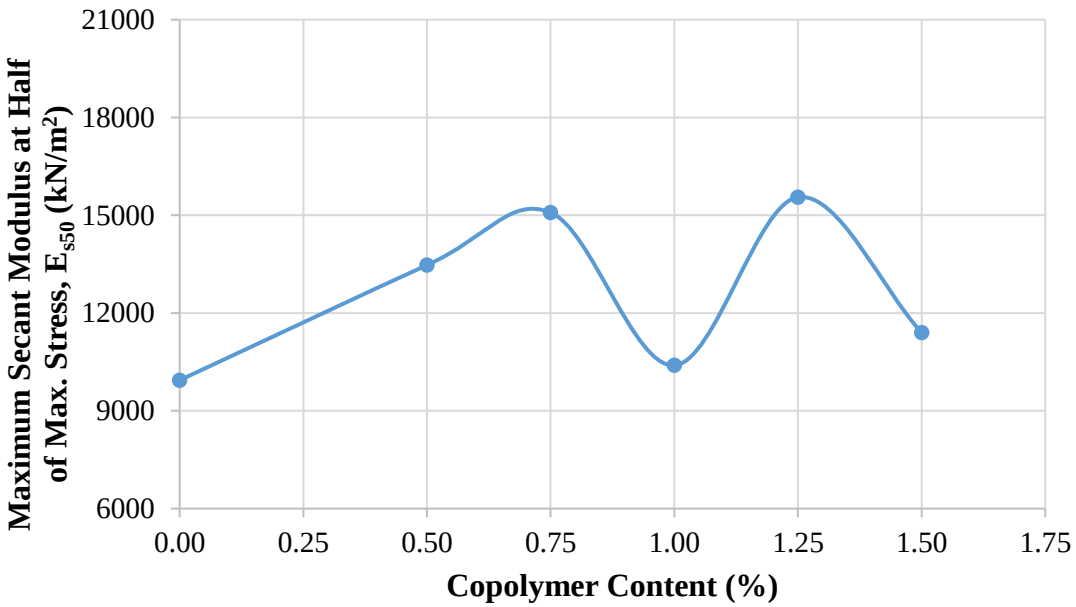

Figure 6.138 Relationship between maximum secant modulus at 50% of maximum stress and different copolymer contents of CH

Furthermore, after gathering all tangent modulus at 50% of maximum stress of high plasticity clay-copolymer mixtures were shown and compared them in Figure 6.139.

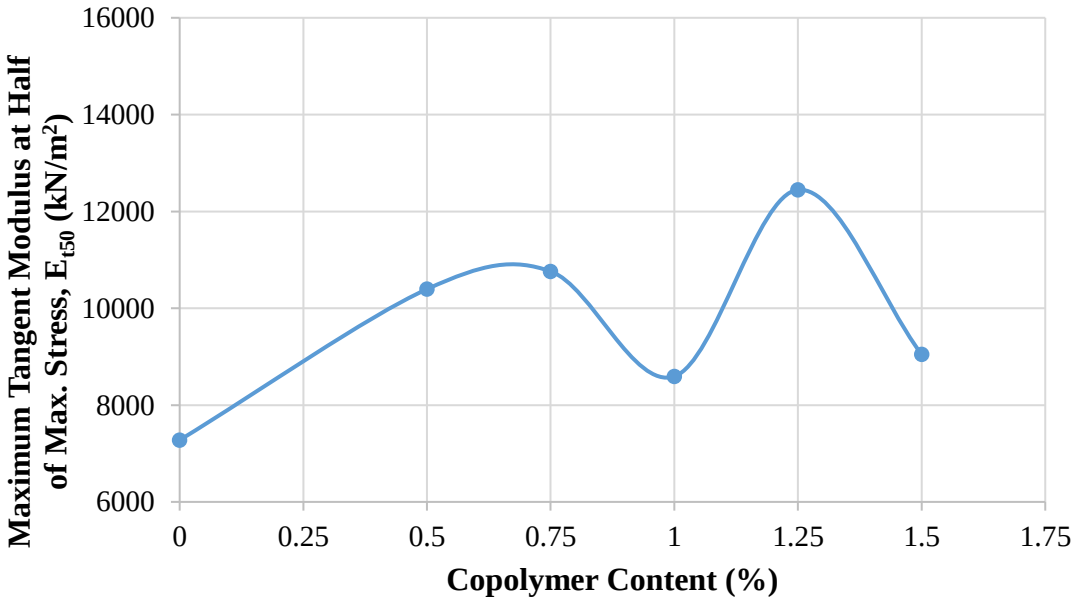

Figure 6.139 Relationship between maximum tangent modulus at 50% of maximum stress and different copolymer contents of CH

It can be seen that the maximum tangent modulus at 50% of maximum stress was obtained in the mixture with 1.25% of copolymer. In addition, the tangent modulus at 50% of maximum stress increases up to 71% in the mixture with 1.25% of copolymer. In other words, it is found that the tangent modulus at 50% of maximum stress increases up to the mixture with 0.75% of copolymer. Then, it fluctuated with the increasing copolymer content up to the mixture with 1.5% of copolymer.

Moreover, Figure 6.140 exhibits the relationship between the maximum secant modulus at failure point and different copolymer contents of CH.

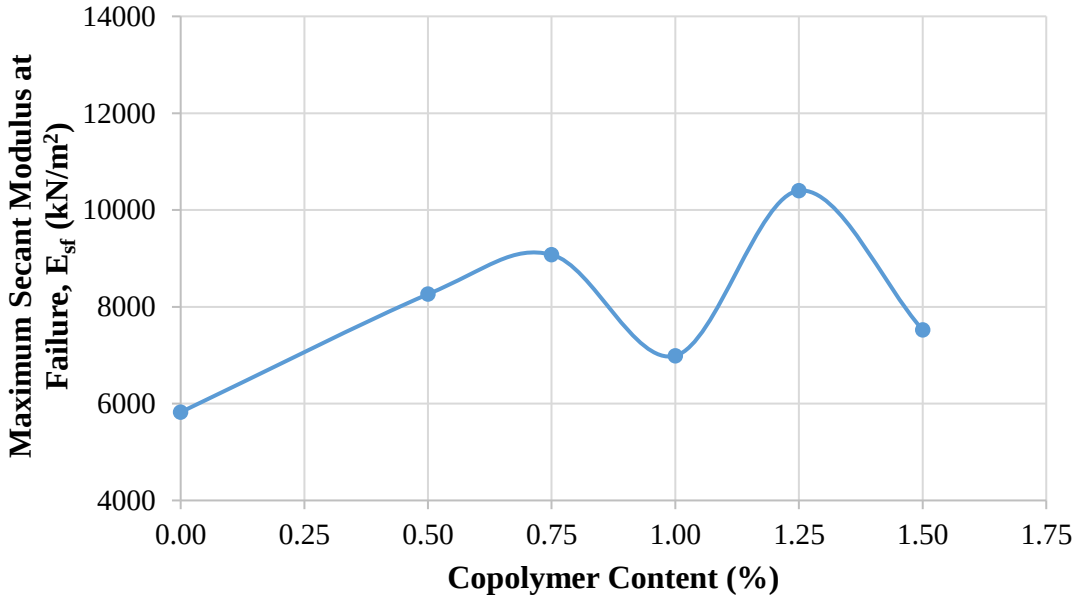

Figure 6.140 Relationship between maximum secant modulus at failure point and different copolymer contents of CH

After gathering all secant modulus at failure point of high plasticity clay-copolymer mixtures and comparing them in a graph, it can be seen that the maximum secant modulus at 50% of maximum stress was obtained in the mixture with 1.25% of copolymer. In addition, the secant modulus at 50% of maximum stress increases up to 79% in the mixture with 1.25% of copolymer. In other words, it is found that the secant modulus at 50% of maximum stress increases up to the mixture with 0.75% of copolymer. Then, it fluctuated with the increasing copolymer content up to the mixture with 1.5% of copolymer.

6.5 Fly Ash-Polypropylene Mixtures with High Plasticity Clay Soil

Three different amounts of polypropylene (0.25%, 0.5%, and 0.75%) and an amount of 10% fly ash were added to the high plasticity clay to study the effects of mixing polypropylene and fly ash with designated soil. In addition, the amounts of polypropylene with fly ash compared to whole mixtures in terms of soil moduli, the unconfined compression strength, and relationships in these engineering parameters. In other words, the amount of soil improvement of high plasticity clay was examined with added polypropylene and fly ash.

6.5.1 High Plasticity Clay Soil Mixture with 10% of Fly Ash and 0.25% of Polypropylene

During the experimental program of this study, the amount of 0.25% polypropylene and 10% fly ash mixed with high plasticity clay soil was used. The compaction and the unconfined compression tests were performed on the 0.25% polypropylene and 10% fly ash mixed with high plasticity clay, and the outcomes of these experiments are illustrated in Table 6.41. With respect to data obtained from mentioned tests, it can be seen that the value of ω_{opt} and γ_{dmax} obtained at 25% and 15.10 kN/m^3, respectively.

Table 6.41 Results of experiments executed with CH+10% fly ash+0.25% polypropylene

Sample No.	ω (%)	γ_d (kN/m^3)	q_u (kN/m^2)
1	16	13.77	198.7
2	21	15.10	342.4
3	25	14.90	235.0
4	28	14.37	148.5
5	30	13.95	90.9

The axial stress-axial strain curves of five different 0.25% polypropylene and 10% fly ash-added high plasticity clay samples are shown in Figure 6.141. Besides, Figure 6.142 exhibits the tested 0.25% polypropylene and 10% fly ash-added high plasticity clay sample, which has the highest value of the maximum unconfined

compression strength. Therefore, according to data obtained from the unconfined compression test of the 0.25% polypropylene and 10% fly ash-added high plasticity clay sample, it can be inferred that the maximum unconfined compression strength was obtained in the second sample, and it was obtained as 342.4 kN/m^2.

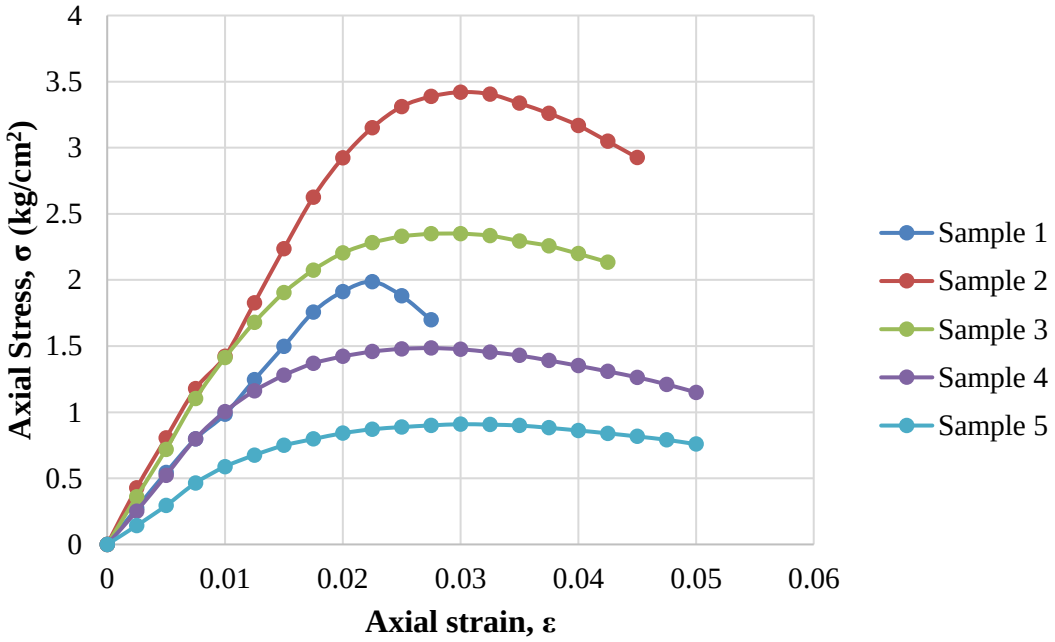

Figure 6.141 Results of unconfined compression tests of CH+10% fly ash+0.25% polypropylene

Some of the required parameters were calculated to apply the modified and mentioned numerical model. Calculated engineering parameters to obtain soil moduli are given in Table 6.42.

Table 6.42 Calculated engineering parameters of CH+10% fly ash+0.25% polypropylene

Sample No.	a (cm^2/kg)	b (cm^2/kg)	$(\sigma_1)_{ult}$ (kg/cm^2)	$(\sigma_1)_f$ (kg/cm^2)	R_f -	ε_f -	ε_{50} -
1	0.0088	0.0901	11.099	1.987	0.18	0.0225	0.0101
2	0.0057	0.0810	12.346	3.424	0.28	0.0300	0.0118
3	0.0053	0.2151	4.649	2.350	0.51	0.0300	0.0081
4	0.0072	0.3658	2.734	1.485	0.54	0.0275	0.0070
5	0.0125	0.6116	1.635	0.909	0.56	0.0300	0.0074

It is obvious that, when the values of strains are between 0.1% to 0.001%, this region is categorized as a small strain. Furthermore, it should be noted that the strain level of 0.25% polypropylene and 10% fly ash-added high plasticity clay is classified as small strain (SS) because the maximum axial strain was determined in samples 4 and 5 of 0.25% polypropylene and 10% fly ash-added high plasticity clay, and it was obtained as 0.05%. Thus, it can be concluded that nonlinear behaviour was observed for the tested 0.25% polypropylene and 10% fly ash-added high plasticity clay soil samples.

Initial tangent modulus (E_i), tangent modulus at 50% of maximum stress (E_{t50}), secant modulus at failure (E_{sf}), secant modulus at 50% of maximum stress (E_{s50}), and unconfined compression strength (q_u) of five different 0.25% polypropylene and 10% fly ash -added high plasticity clay soil samples are given in Table 6.43.

Table 6.43 Soil moduli and unconfined compression strength of CH+10% fly ash+0.25% polypropylene

Sample No.	E_i (kN/m^2)	E_{t50} (kN/m^2)	E_{sf} (kN/m^2)	E_{s50} (kN/m^2)	q_u (kN/m^2)
1	11363.6	9420.3	8831.1	9845.7	198.7
2	17543.9	13015.5	11413.3	14515.2	342.4
3	18867.9	10535.7	7833.3	14526.4	235.0
4	13888.9	7368.8	5400.0	10622.2	148.5
5	8000.0	4170.6	3030.0	6175.0	90.9

According to the data obtained, it can be concluded that the maximum modulus values are observed in the initial tangent modulus compared with other soil moduli in all five 0.25% polypropylene and 10% fly ash-added high plasticity clay samples due to the initial slope of the stress-strain curve. In other words, the axial stress increases up to a certain point very sharply. Then, this sharp increasing trend suddenly starts to slow down, and during this slowing trend, the axial strain increases rapidly.

Figure 6.142 Peak point of CH+10% fly ash+0.25% polypropylene

In addition, transformed hyperbolic stress-strain curves for five different 0.25% polypropylene and 10% fly ash-added high plasticity clay samples are illustrated in Figure 6.143.

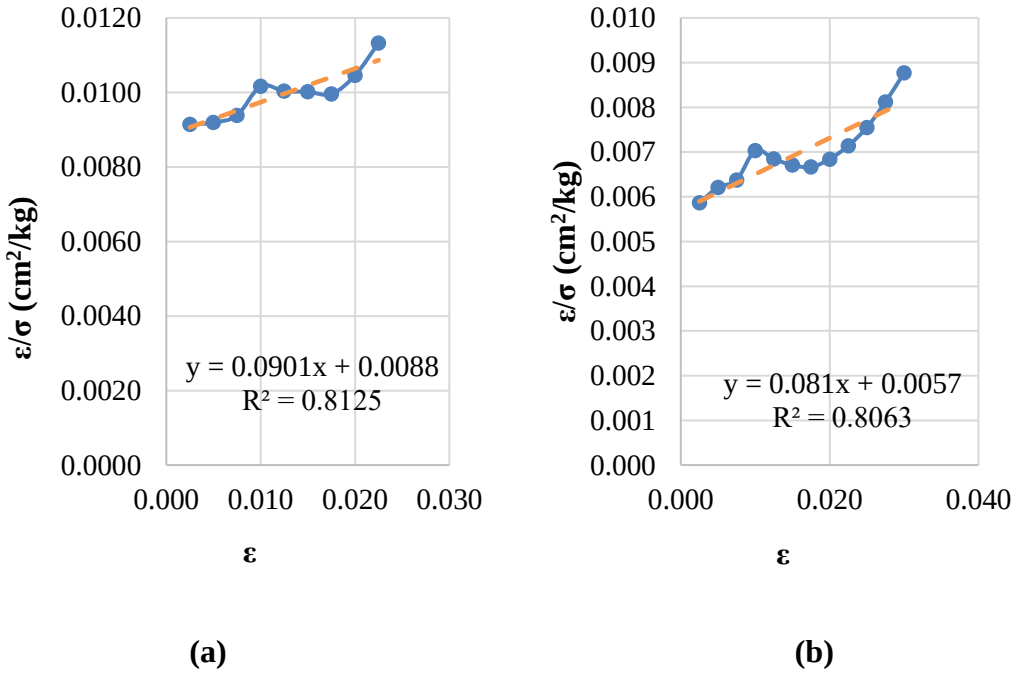

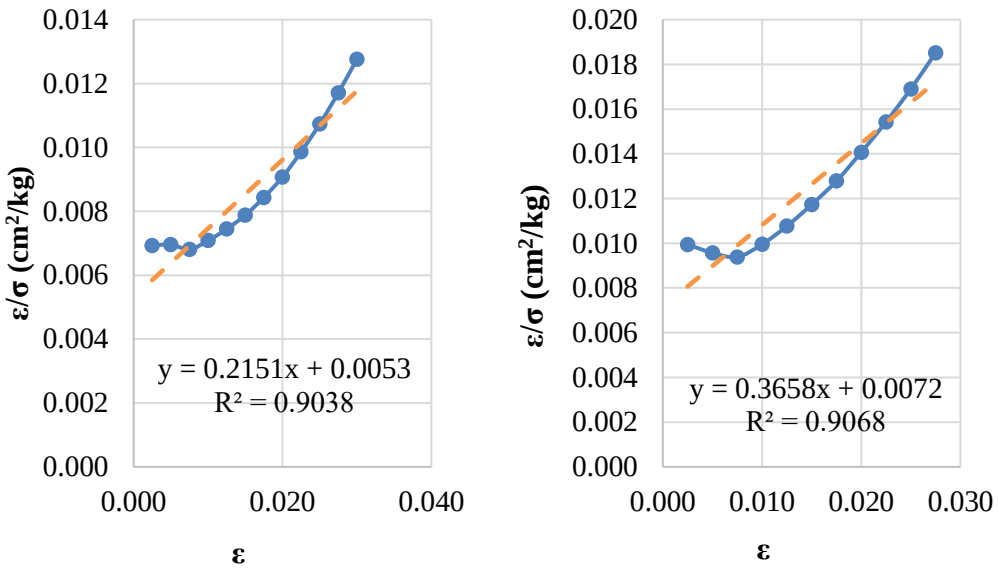

(c) **(d)**

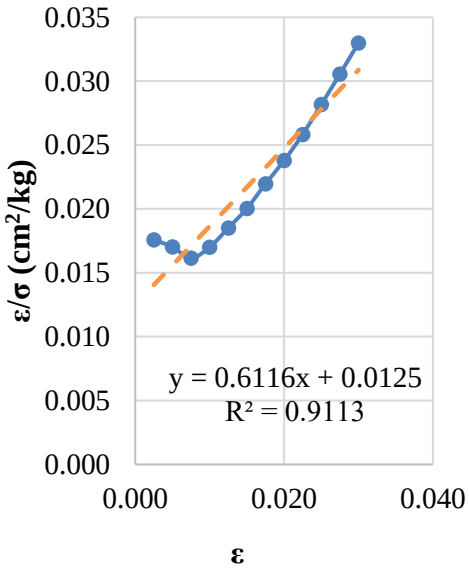

(e)

Figure 6.143 Transformed hyperbolic stress-strain curves for (a) sample 1, (b) sample 2, (c) sample 3, (d) sample 4, and (e) sample 5 (CH+10% Fly Ash+0.25% Polypropylene)

It was found that low and high values of axial strains in all samples are not precisely hyperbolic, as shown in Figures 6.143 (a, b, c, d, and e). In other words, these points can not be fitted in a straight line. However, it was possible to estimate the actual

stress-strain curves by a hyperbola. Thus, it is found to have a reasonable degree of accuracy.

The relationship between the secant modulus at 50% of maximum stress (E_{s50}) and the initial tangent modulus (E_i) of the designated mixture of high plasticity clay samples (0.25% polypropylene and 10% fly ash-added CH) is shown in Figure 6.144.

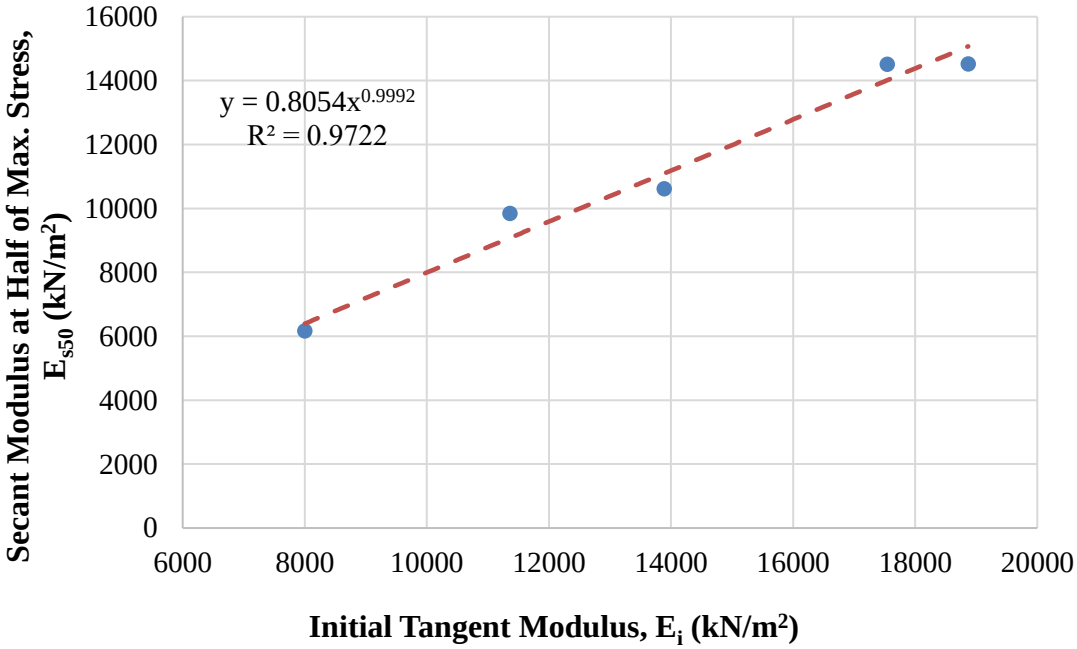

Figure 6.144 Relationship between secant modulus at 50% of maximum stress and initial tangent modulus (CH+10% Fly Ash+0.25% Polypropylene)

According to the data, it can be inferred that these soil moduli refer to the hardening of 0.25% polypropylene and 10% fly ash-added high plasticity clay samples. Thus, the initial tangent modulus increases with the increasing secant modulus at 50% of maximum stress. Furthermore, it was best suited for estimating these soil moduli by a power model.

The relationship between the secant modulus at failure (E_{sf}) and the tangent modulus at 50% of maximum stress (E_{t50}) of the designated mixture of high plasticity clay samples (0.25% polypropylene and 10% fly ash-added CH) is shown in Figure 6.145.

The tangent modulus at 50% of maximum stress increases with the increasing secant modulus at failure. Thus, it was best suited for estimating these soil moduli by a power model.

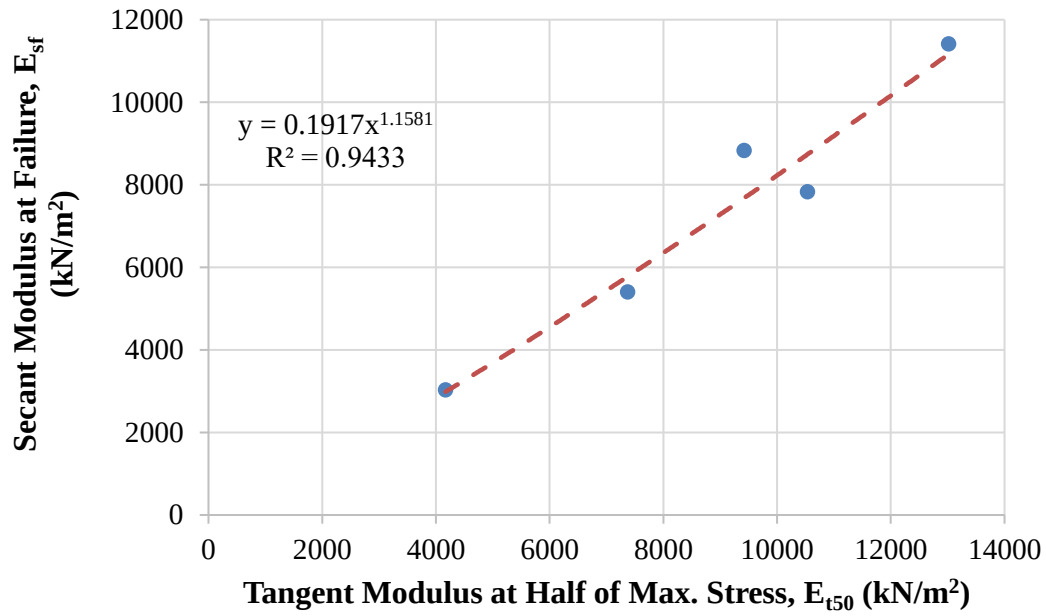

Figure 6.145 Relationship between secant modulus at failure point and tangent modulus at 50% of maximum stress (CH+10% Fly Ash +0.25% Polypropylene)

Furthermore, the relationship between the initial tangent modulus (E_i) and unconfined compression strength of the designated mixture of high plasticity clay samples (0.25% polypropylene and 10% fly ash-added CH) is shown in Figure 6.146.

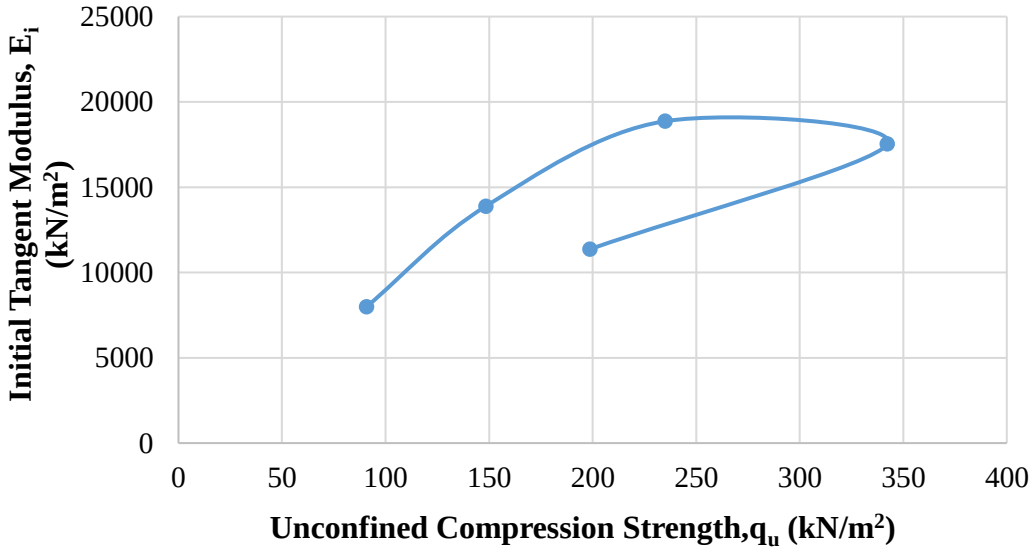

Figure 6.146 Relationship between initial tangent modulus and unconfined compression strength (CH+10% Fly Ash +0.25% Polypropylene)

According to data, the maximum initial tangent modulus is obtained in sample 3 as 18867.9 kN/m^2 for 0.25% polypropylene and 10% fly ash-added high plasticity clay. It should be noted that the water content is 25%, the dry unit weight is 14.90 kN/m^3, and the unconfined compression strength is 235 kN/m^2 when the initial tangent modulus is the maximum value for 0.25% polypropylene and 10% fly ash-added high plasticity clay.

The relationship between secant modulus at 50% of maximum stress (E_{s50}) and unconfined compression strength of the designated mixture of high plasticity clay samples (0.25% polypropylene and 10% fly ash-added CH) is shown in Figure 6.147.

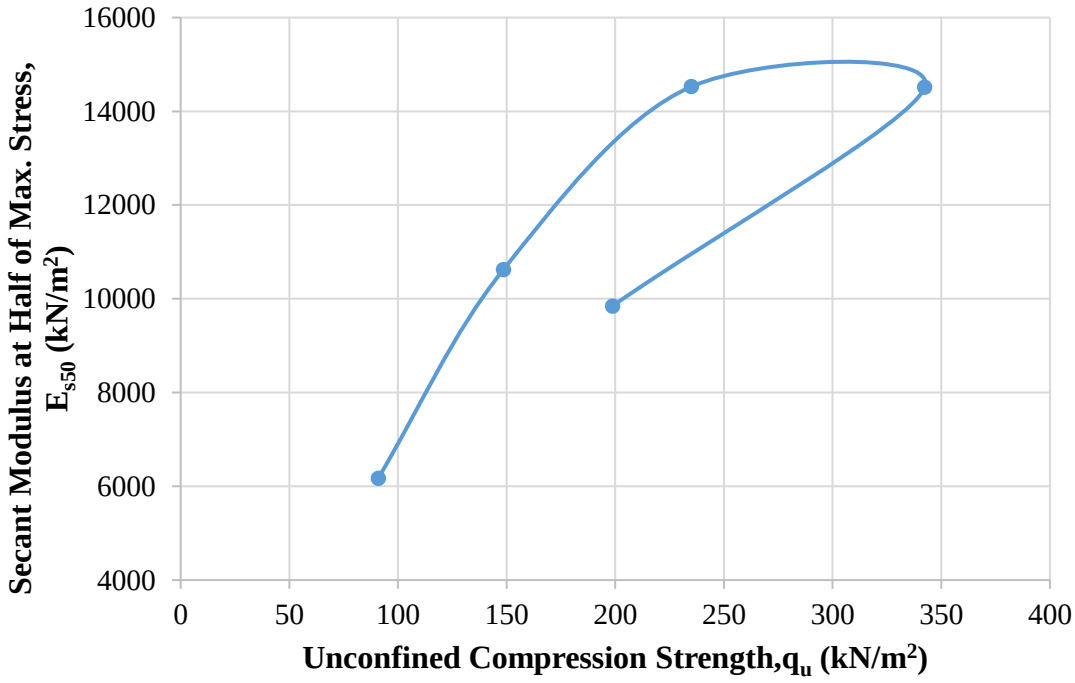

Figure 6.147 Relationship between secant modulus at 50% of maximum stress and unconfined compression strength (CH+10% Fly Ash +0.25% Polypropylene)

The maximum secant modulus at 50% of maximum stress is obtained in sample 3 as 14526.4 kN/m^2 for 0.25% polypropylene and 10% fly ash-added high plasticity clay. It should be noted that the water content is 25%, the dry unit weight is 14.90 kN/m^3, and the unconfined compression strength is 235 kN/m^2 when the secant modulus at 50% of maximum stress has the maximum value of 0.25% polypropylene and 10% fly ash-added high plasticity clay.

In addition, concerning the results of the initial tangent modulus and secant modulus at 50% of maximum stress, it seems that the maximum values of these moduli

are not obtained at maximum unconfined compression strength (sample 2 for 0.25% polypropylene and 10% fly ash-added high plasticity clay) since the beginning of the stress-strain curve of sample 3 has rapidly increased in axial stress. On the other hand, when calculated initial tangent modulus and secant modulus at 50% of maximum stress have the maximum values for 0.25% polypropylene and 10% fly ash-added high plasticity clay, the water content is equal to the optimum water content (w_{opt}=25%), and the dry unit weight is less than the maximum dry unit weight (γ_{dmax}=15.10 kN/m^3).

On the other hand, the relationship between tangent modulus at 50% of maximum stress (E_{t50}) and unconfined compression strength of the designated mixture of high plasticity clay samples (0.25% polypropylene and 10% fly ash-added CH) is shown in Figure 6.148.

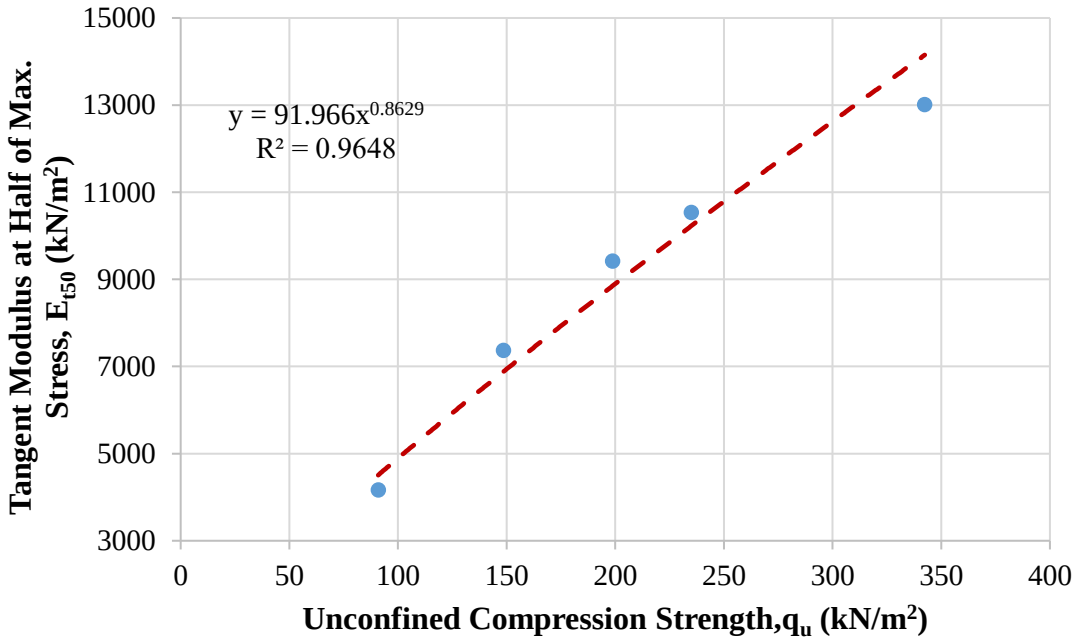

Figure 6.148 Relationship between tangent modulus at 50% of maximum stress and unconfined compression strength (CH+10% Fly Ash +0.25% Polypropylene)

The maximum tangent modulus at 50% of maximum stress is obtained in sample 2 as 13015.5 kN/m^2 for 0.25% polypropylene and 10% fly ash-added high plasticity clay. It should be noted that the water content is 21%, the dry unit weight is 15.10 kN/m^3, and the unconfined compression strength is 342.4 kN/m^2 when the tangent

modulus at 50% of maximum stress is the maximum value for the 0.25% polypropylene and 10% fly ash-added high plasticity clay.

In addition, the relationship between secant modulus at failure point (E_{sf}) and unconfined compression strength of the designated mixture of high plasticity clay samples (0.25% polypropylene and 10% fly ash-added CH) is shown in Figure 6.149.

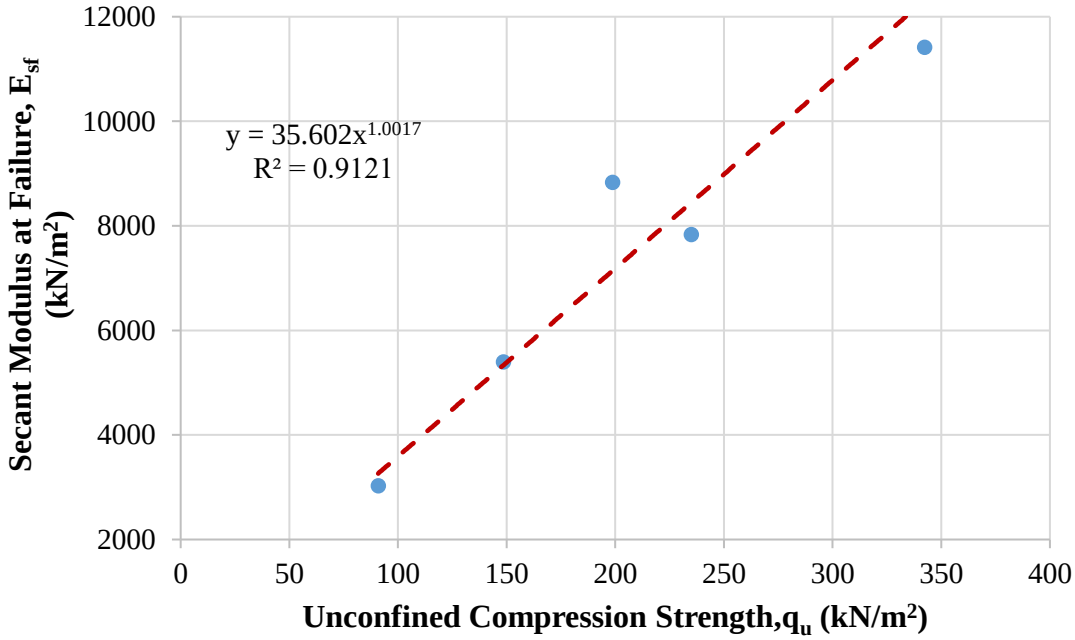

Figure 6.149 Relationship between secant modulus at failure point and unconfined compression strength (CH+10% Fly Ash +0.25% Polypropylene)

It is obvious that the maximum secant modulus at failure point is obtained in sample 2 as 11413.3 kN/m^2 for 0.25% polypropylene and 10% fly ash-added high plasticity clay. It should be noted that the water content is 21%, the dry unit weight is 15.10 kN/m^3, and the unconfined compression strength is 342.4 kN/m^2 when the secant modulus at failure point is the maximum value for 0.25% polypropylene and 10% fly ash-added high plasticity clay.

With respect to the results of the calculated tangent modulus at 50% of maximum stress and secant modulus at failure point, it seems that the maximum values of these moduli are obtained at maximum unconfined compression strength (sample 2 for 0.25% polypropylene and 10% fly ash-added high plasticity clay). On the other hand, when these moduli have the maximum value for 0.25% polypropylene and 10% fly ash-added high plasticity clay, the water content is less than the optimum water content (w_{opt}=25%), and the dry unit weight is equal to the maximum dry unit weight

(γ_{dmax}=15.10 kN/m^3). Also, high plasticity clayey soil's strength and load-deformation properties are improved by reinforcing with polypropylene fiber and stabilized with fly ash.

6.5.2 High Plasticity Clay Soil Mixture with 10% of Fly Ash and 0.5% of Polypropylene

During the experimental program of this study, the amount of 0.5% polypropylene and 10% fly ash mixed with high plasticity clay soil was used. The compaction and the unconfined compression tests were performed on the 0.5% polypropylene and 10% fly ash mixed with high plasticity clay, and the outcomes of these experiments are illustrated in Table 6.44. With respect to data obtained from mentioned tests, it can be seen that the value of ω_{opt} and γ_{dmax} obtained at 24% and 14.81 kN/m^3, respectively.

Table 6.44 Results of experiments executed with CH+10% fly ash+0.5% polypropylene

Sample No.	ω (%)	γ_d (kN/m^3)	q_u (kN/m^2)
1	ω	13.76	264.7
2	20	14.52	327.9
3	24	14.81	200.8
4	27	14.32	128.1

The axial stress-axial strain curves of four different 0.5% polypropylene and 10% fly ash-added high plasticity clay samples are shown in Figure 6.150. Besides, Figure 6.151 exhibits the tested 0.5% polypropylene and 10% fly ash-added high plasticity clay sample, which has the highest value of the maximum unconfined compression strength. Therefore, according to data obtained from the unconfined compression test of the 0.5% polypropylene and 10% fly ash-added high plasticity clay sample, it can be inferred that the maximum unconfined compression strength was obtained in the second sample, and it was obtained as 327.9 kN/m^2.

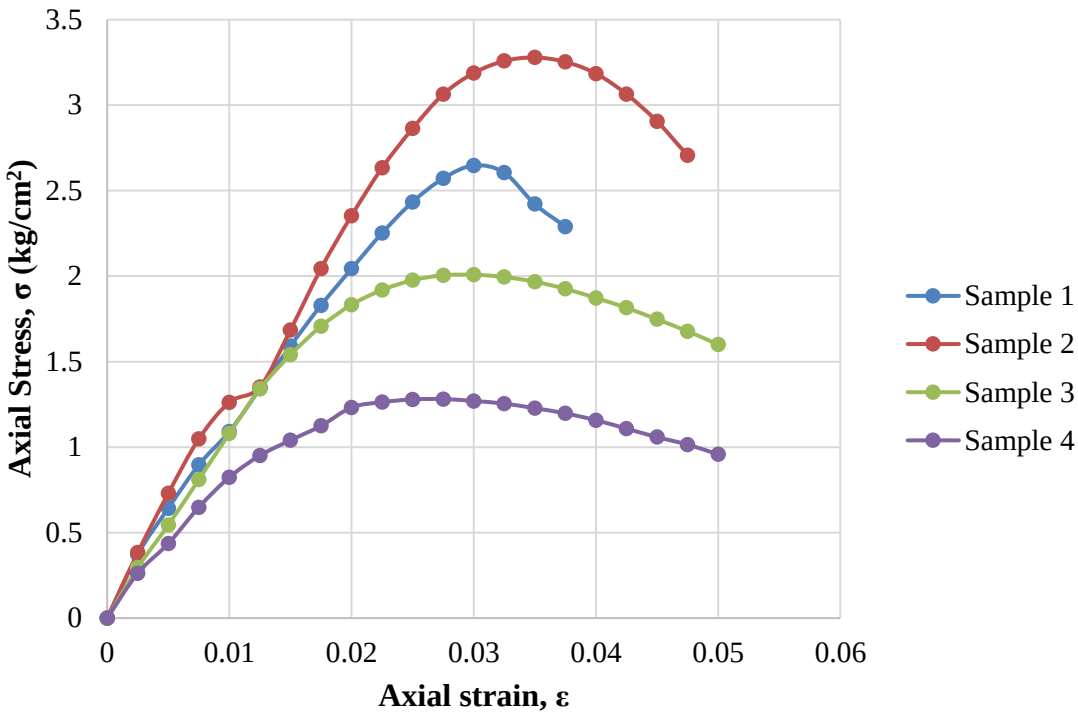

Figure 6.150 Results of unconfined compression tests of CH+10% fly ash+0.5% polypropylene

Some of the required parameters were calculated to apply the modified and mentioned numerical model. Calculated engineering parameters to obtain soil moduli are given in Table 6.45.

Table 6.45 Calculated engineering parameters of CH+10% fly ash+0.5% polypropylene

Sample No.	a (cm^2/kg)	b (cm^2/kg)	$(\sigma_1)_{ult}$ (kg/cm^2)	$(\sigma_1)_f$ (kg/cm^2)	R_f -	ε_f -	ε_{50} -
1	0.0072	0.1341	7.457	2.647	0.35	0.0300	0.0123
2	0.0067	0.0986	10.142	3.279	0.32	0.0350	0.0147
3	0.0073	0.2145	4.662	2.008	0.43	0.0300	0.0093
4	0.0082	0.4410	2.268	1.281	0.56	0.0275	0.0074

It should be noted that the strain level of 0.5% polypropylene and 10% fly ash-added high plasticity clay is classified as small strain (SS) because the maximum axial strain was determined in samples 3 and 4. The maximum axial strain was obtained as

0.05%. Thus, it can be concluded that nonlinear behaviour was observed for the tested 0.5% polypropylene and 10% fly ash-added high plasticity clay samples.

Initial tangent modulus (E_i), tangent modulus at 50% of maximum stress (E_{t50}), secant modulus at failure (E_{sf}), secant modulus at 50% of maximum stress (E_{s50}), and unconfined compression strength (q_u) of four different 0.5% polypropylene and 10% fly ash -added high plasticity clay soil samples are given in Table 6.46.

Table 6.46 Soil moduli and unconfined compression strength of CH+10% fly ash+0.5% polypropylene

Sample No.	E_i (kN/m^2)	E_{t50} (kN/m^2)	E_{sf} (kN/m^2)	E_{s50} (kN/m^2)	q_u (kN/m^2)
1	13888.9	9396.3	8823.3	10738.3	264.7
2	14925.4	10489.9	9368.6	11184.7	327.9
3	13698.6	8433.7	6693.3	10800.0	200.8
4	12195.1	6278.8	4658.2	8641.4	128.1

According to the data obtained, it can be concluded that the maximum modulus values are observed in the initial tangent modulus compared with other soil moduli in all four 0.5% polypropylene and 10% fly ash-added high plasticity clay samples due to the initial slope of the stress-strain curve. In other words, the axial stress increases up to a certain point very sharply. Then, this sharp increasing trend suddenly starts to slow down, and during this slowing trend, the axial strain increases rapidly.

Figure 6.151 Peak point of CH+10% fly ash+0.5% polypropylene

In addition, transformed hyperbolic stress-strain curves for four different 0.5% polypropylene and 10% fly ash-added high plasticity clay samples are illustrated in Figure 6.152.

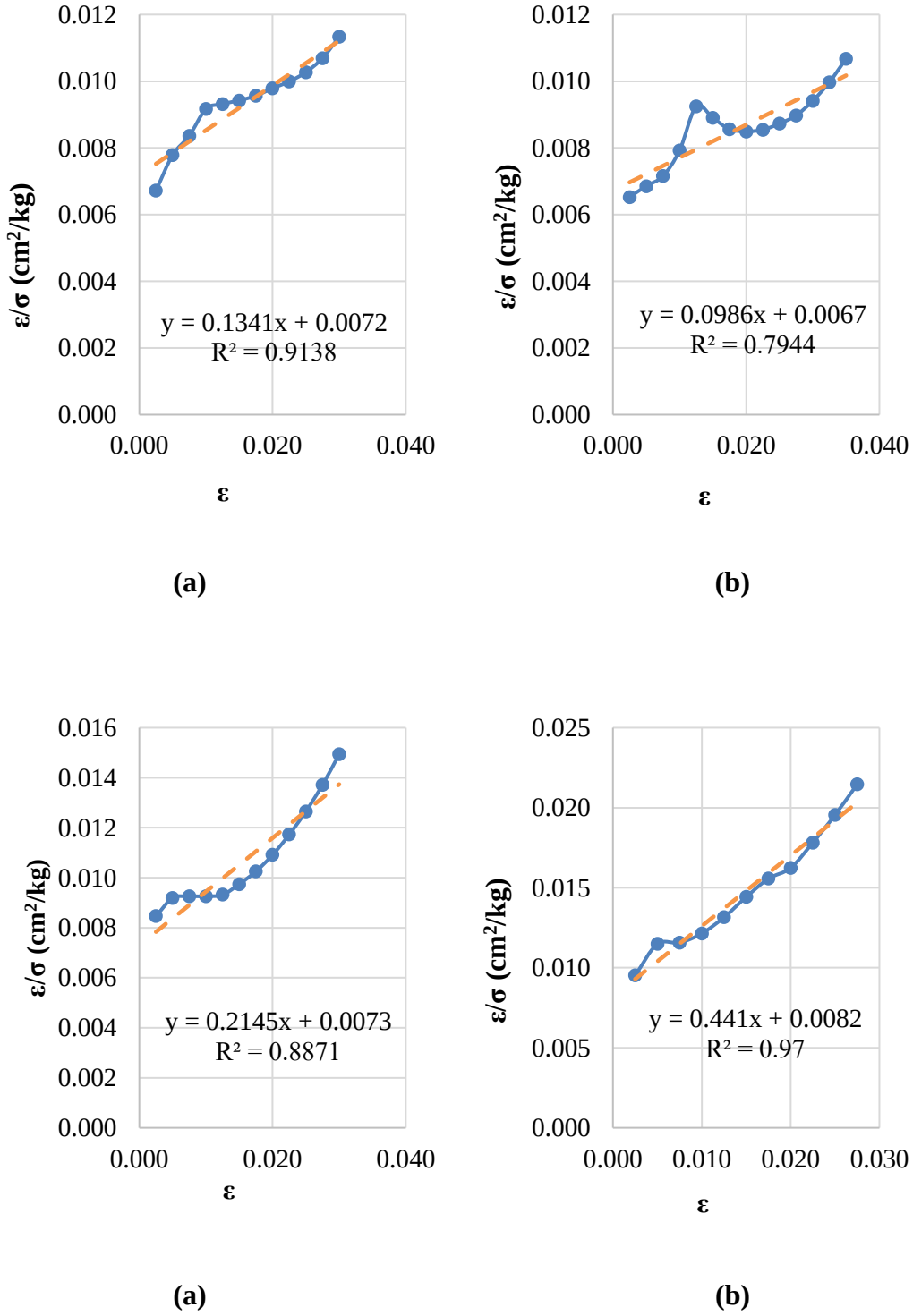

Figure 6.152 Transformed hyperbolic stress-strain curves for (a) sample 1, (b) sample 2, (c) sample 3, and (d) sample 4 (CH+10% Fly Ash+0.5% Polypropylene)

It was found that low and high values of axial strains in samples 1, 2, and 3 are not precisely hyperbolic, as shown in Figures 6.152 (a, b, and c). In other words, these points can not be fitted in a straight line. However, it was possible to estimate the actual stress-strain curves by a hyperbola. Thus, it is found to have a reasonable degree of accuracy. On the other hand, the transformed hyperbolic stress-strain curve in sample 4 is hyperbolic, as shown in Figure 6.152 (d). In other words, these points can be best-fitted in a straight line.

The relationship between the secant modulus at 50% of maximum stress (E_{s50}) and the initial tangent modulus (E_i) of the designated mixture of high plasticity clay samples (0.5% polypropylene and 10% fly ash-added CH) is shown in Figure 6.153.

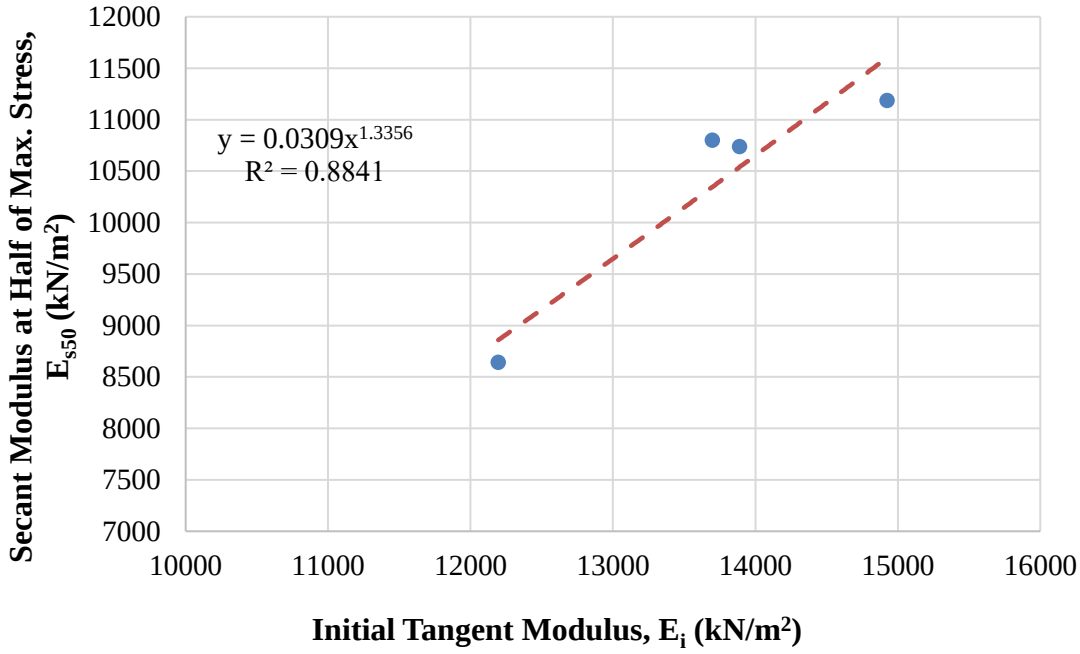

Figure 6.153 Relationship between secant modulus at 50% of maximum stress and initial tangent modulus (CH+10% Fly Ash+0.5% Polypropylene)

According to the data, it can be inferred that these soil moduli refer to the hardening of 0.5% polypropylene and 10% fly ash-added high plasticity clay samples. Thus, the initial tangent modulus increases with the increasing secant modulus at 50% of maximum stress. Furthermore, it was best suited for estimating these soil moduli by a power model.

The relationship between the secant modulus at failure (E_{sf}) and the tangent modulus at 50% of maximum stress (E_{t50}) of the designated mixture of high plasticity

clay samples (0.5% polypropylene and 10% fly ash-added CH) is shown in Figure 6.154.

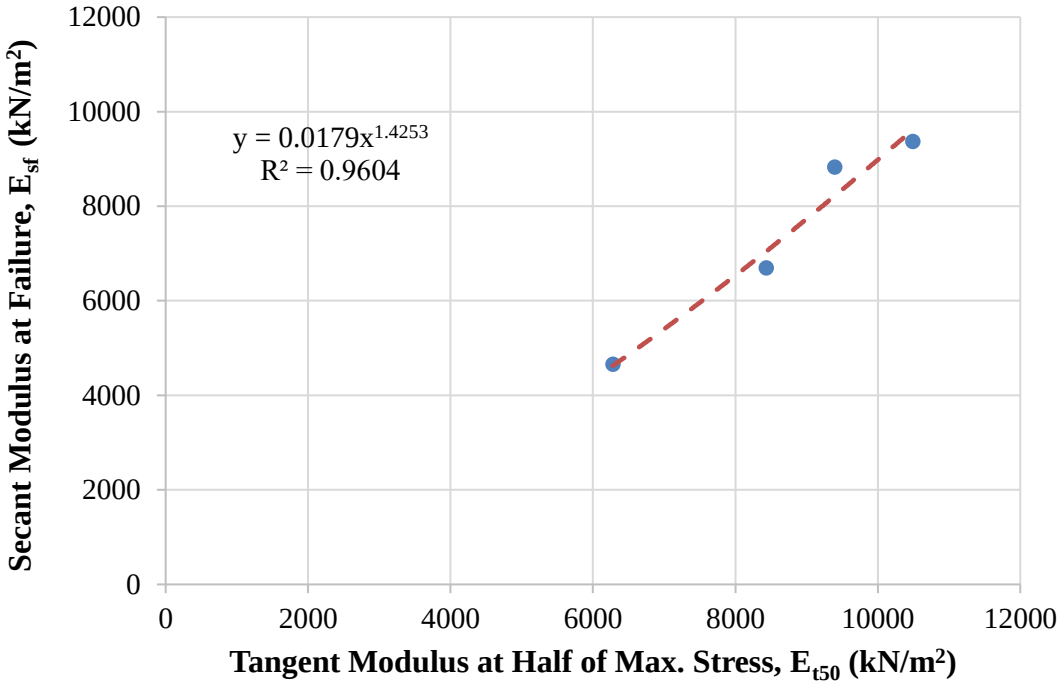

Figure 6.154 Relationship between secant modulus at failure point and tangent modulus at 50% of maximum stress (CH+10% Fly Ash +0.5% Polypropylene)

The tangent modulus at 50% of maximum stress increases with the increasing secant modulus at failure. Thus, it was best suited for estimating these soil moduli by a power model.

Furthermore, the relationship between the initial tangent modulus (E_i) and unconfined compression strength of the designated mixture of high plasticity clay samples (0.5% polypropylene and 10% fly ash-added CH) is shown in Figure 6.155.

According to data, the maximum initial tangent modulus is obtained in sample 2 as 14925.4 kN/m^2 for 0.5% polypropylene and 10% fly ash-added high plasticity clay. It should be noted that the water content is 20%, the dry unit weight is 14.52 kN/m^3, and the unconfined compression strength is 327.9 kN/m^2 when the initial tangent modulus is the maximum value for 0.5% polypropylene and 10% fly ash-added high plasticity clay.

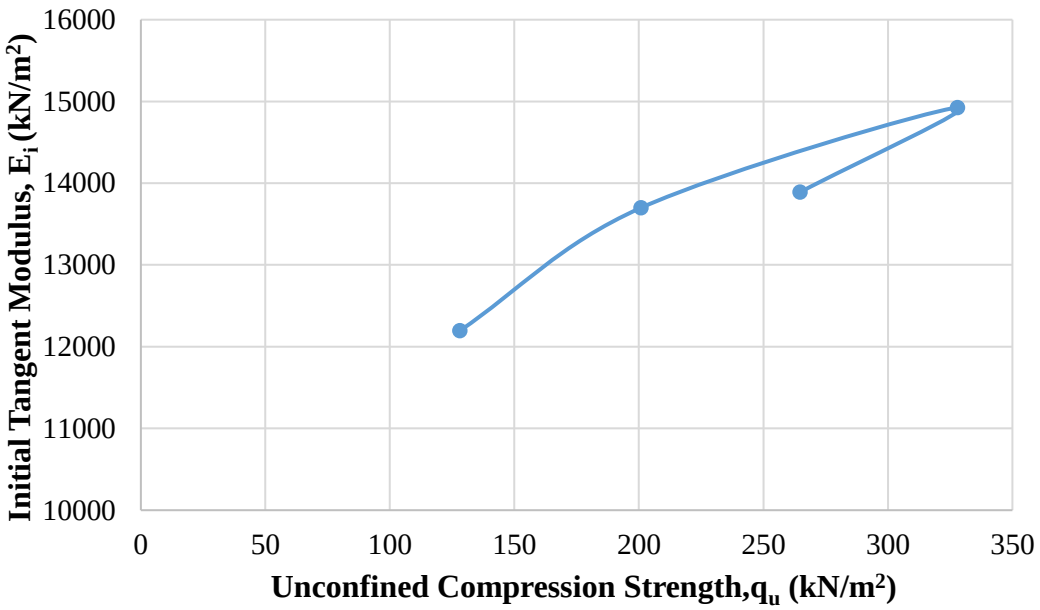

Figure 6.155 Relationship between initial tangent modulus and unconfined compression strength (CH+10% Fly Ash +0.5% Polypropylene)

The relationship between secant modulus at 50% of maximum stress (E_{s50}) and unconfined compression strength of the designated mixture of high plasticity clay samples (0.5% polypropylene and 10% fly ash-added CH) is shown in Figure 6.156.

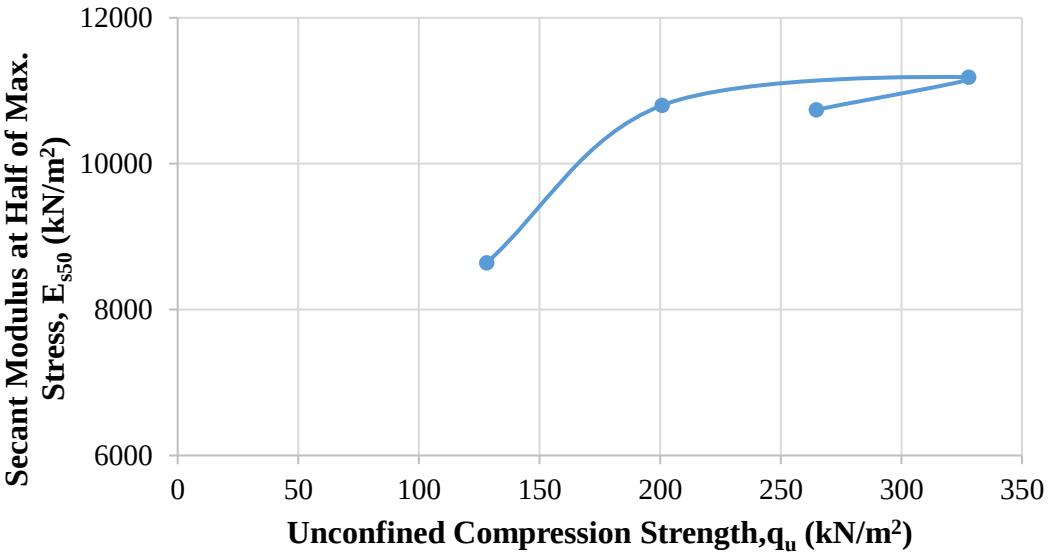

Figure 6.156 Relationship between secant modulus at 50% of maximum stress and unconfined compression strength (CH+10% Fly Ash +0.5% Polypropylene)

The maximum secant modulus at 50% of maximum stress is obtained in sample 2 as 11184.7 kN/m^2 for 0.5% polypropylene and 10% fly ash-added high plasticity clay. It should be noted that the water content is 20%, the dry unit weight is 14.52 kN/m^3, and the unconfined compression strength is 327.9 kN/m^2 when the secant modulus at 50% of maximum stress has the maximum value of 0.5% polypropylene and 10% fly ash-added high plasticity clay.

On the other hand, the relationship between tangent modulus at 50% of maximum stress (E_{t50}) and unconfined compression strength of the designated mixture of high plasticity clay samples (0.5% polypropylene and 10% fly ash-added CH) is shown in Figure 6.157.

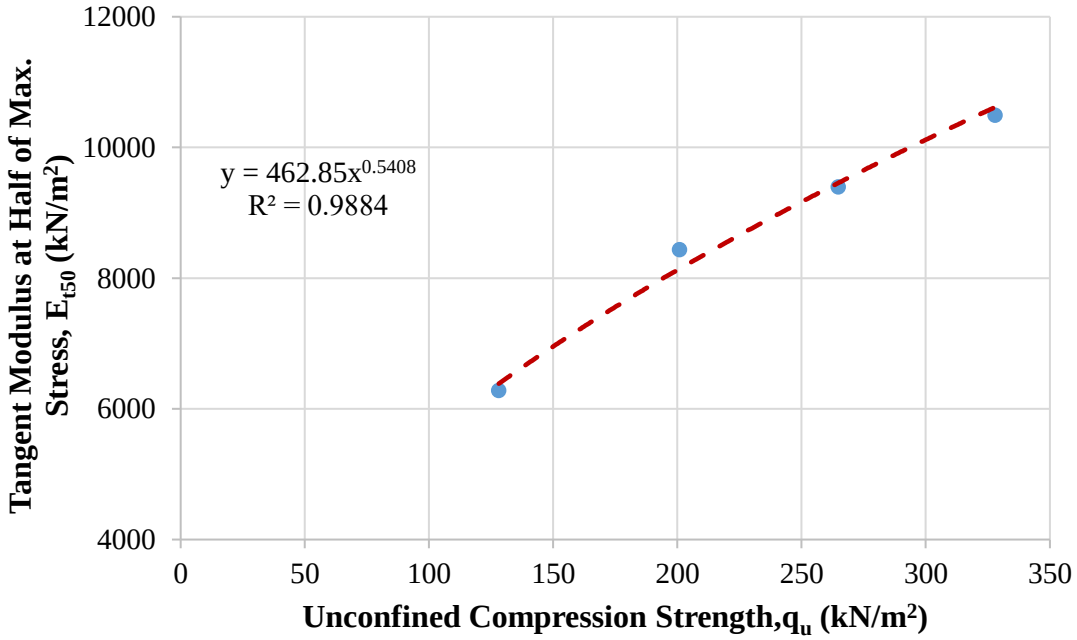

Figure 6.157 Relationship between tangent modulus at 50% of maximum stress and unconfined compression strength (CH+10% Fly Ash +0.5% Polypropylene)

The maximum tangent modulus at 50% of maximum stress is obtained in sample 2 as 10489.9 kN/m^2 for 0.5% polypropylene and 10% fly ash-added high plasticity clay. It should be noted that the water content is 20%, the dry unit weight is 14.52 kN/m^3, and the unconfined compression strength is 327.9 kN/m^2 when the tangent modulus at 50% of maximum stress is the maximum value for the 0.5% polypropylene and 10% fly ash-added high plasticity clay.

In addition, the relationship between secant modulus at failure point (E_{sf}) and unconfined compression strength of the designated mixture of high plasticity clay samples (0.5% polypropylene and 10% fly ash-added CH) is shown in Figure 6.158.

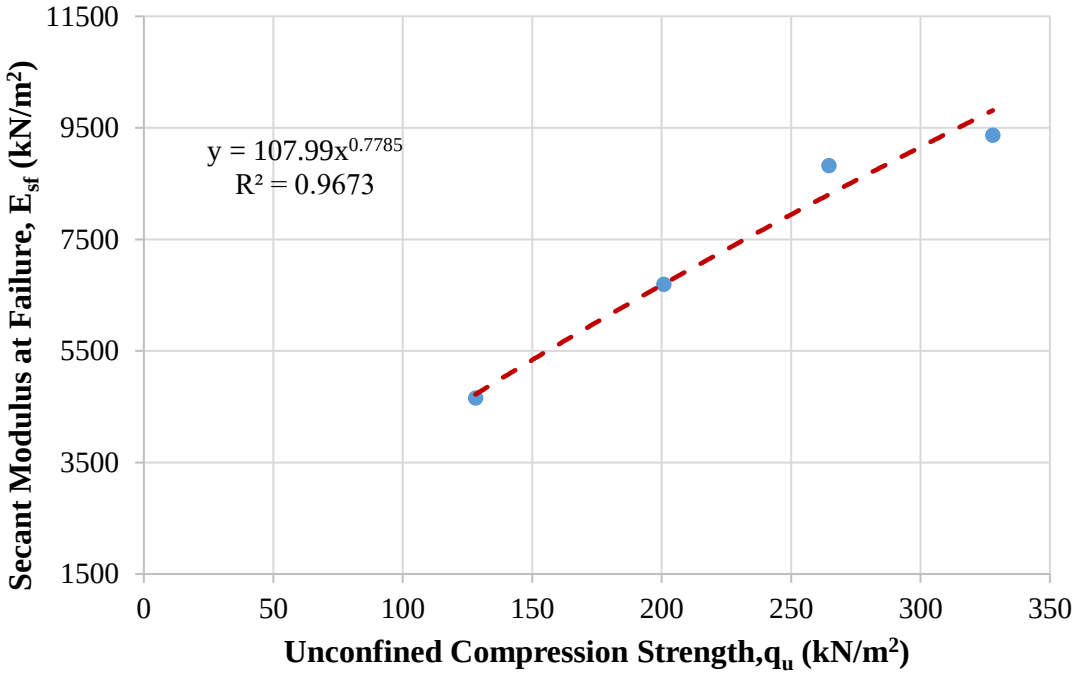

Figure 6.158 Relationship between secant modulus at failure point and unconfined compression strength (CH+10% Fly Ash +0.5% Polypropylene)

It is obvious that the maximum secant modulus at failure point is obtained in sample 2 as 9368.6 kN/m^2 for 0.5% polypropylene and 10% fly ash-added high plasticity clay. It should be noted that the water content is 20%, the dry unit weight is 14.52 kN/m^3, and the unconfined compression strength is 327.9 kN/m^2 when the secant modulus at failure point is the maximum value for 0.5% polypropylene and 10% fly ash-added high plasticity clay.

With respect to the results of the all calculated moduli, it seems that the maximum values of these moduli are obtained at maximum unconfined compression strength (sample 2 for 0.5% polypropylene and 10% fly ash-added high plasticity clay). On the other hand, when these moduli have the maximum value for 0.5% polypropylene and 10% fly ash-added high plasticity clay, the water content is less than the optimum water content (w_{opt}=24%), and the dry unit weight is close to the maximum dry unit weight (γ_{dmax}=14.81 kN/m^3). Also, high plasticity clayey soil's

strength and load-deformation properties are improved by reinforcing with polypropylene fiber and stabilized with fly ash.

6.5.3 High Plasticity Clay Soil Mixture with 10% of Fly Ash and 0.75% of Polypropylene

During the experimental program of this study, the amount of 0.75% polypropylene and 10% fly ash mixed with high plasticity clay soil was used. The compaction and the unconfined compression tests were performed on the 0.75% polypropylene and 10% fly ash mixed with high plasticity clay, and the outcomes of these experiments are illustrated in Table 6.47. With respect to data obtained from mentioned tests, it can be seen that the value of ω_{opt} and γ_{dmax} obtained at 25% and 15.10 kN/m^3, respectively.

Table 6.47 Results of experiments executed with CH+10% fly ash+0.75% polypropylene

Sample No.	ω (%)	γ_d (kN/m^3)	q_u (kN/m^2)
1	18	14.16	330.9
2	22	14.87	342.2
3	24	15.05	272.9
4	28	14.47	156.0
5	31	13.71	78.4

The axial stress-axial strain curves of five different 0.75% polypropylene and 10% fly ash-added high plasticity clay samples are shown in Figure 6.159. Besides, Figure 6.160 exhibits the tested 0.75% polypropylene and 10% fly ash-added high plasticity clay sample, which has the highest value of the maximum unconfined compression strength. Therefore, according to data obtained from the unconfined compression test of the 0.75% polypropylene and 10% fly ash-added high plasticity clay sample, it can be inferred that the maximum unconfined compression strength was obtained in the second sample, and it was obtained as 342.2 kN/m^2.

Some of the required parameters were calculated to apply the modified and mentioned numerical model. Calculated engineering parameters to obtain soil moduli are given in Table 6.48.

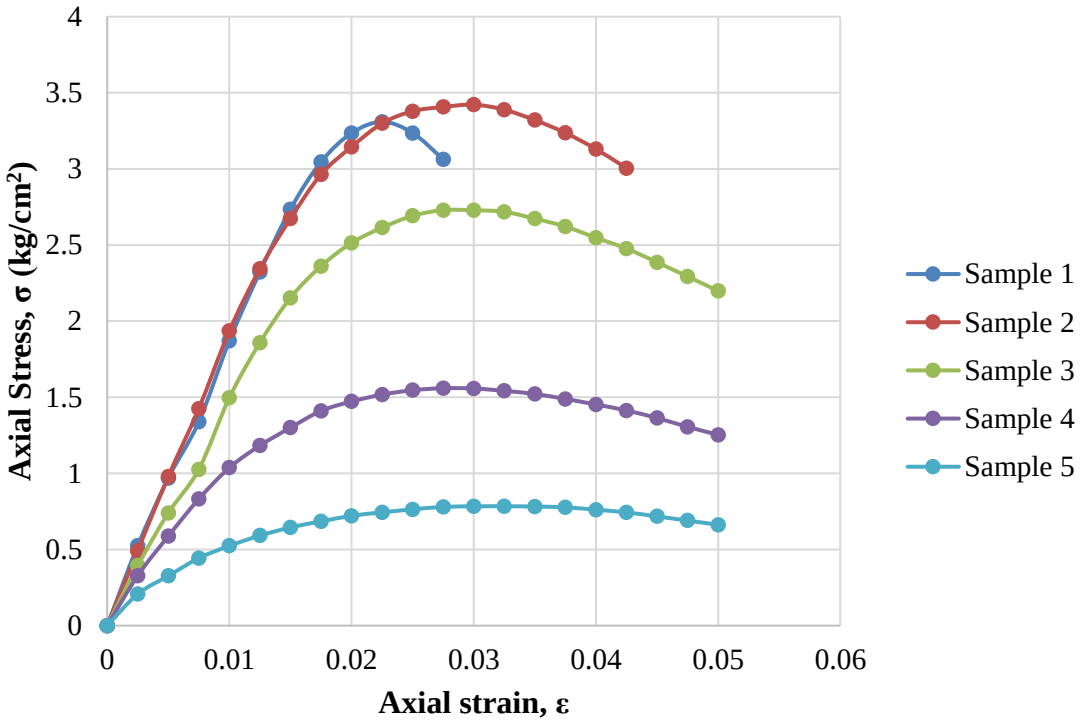

Figure 6.159 Results of unconfined compression tests of CH+10% fly ash+0.75% polypropylene

Table 6.48 Calculated engineering parameters of CH+10% fly ash+0.75% polypropylene

Sample No.	a (cm^2/kg)	b (cm^2/kg)	$(\sigma_1)_{ult}$ (kg/cm^2)	$(\sigma_1)_f$ (kg/cm^2)	R_f -	ε_f -	ε_{50} -
1	0.0046	0.0776	12.887	3.309	0.26	0.0225	0.0090
2	0.0041	0.1313	7.616	3.422	0.45	0.0300	0.0089
3	0.0057	0.1305	7.663	2.729	0.36	0.0275	0.0093
4	0.0061	0.3923	2.549	1.560	0.61	0.0275	0.0070
5	0.0096	0.9415	1.062	0.784	0.74	0.0325	0.0064

It should be noted that the strain level of 0.75% polypropylene and 10% fly ash-added high plasticity clay is classified as small strain (SS) because the maximum axial strain was determined in samples 3, 4, and 5. The maximum axial strain was obtained as 0.05%. Thus, it can be concluded that nonlinear behaviour was observed for the tested 0.75% polypropylene and 10% fly ash-added high plasticity clay samples.

Initial tangent modulus (E_i), tangent modulus at 50% of maximum stress (E_{t50}), secant modulus at failure (E_{sf}), secant modulus at 50% of maximum stress (E_{s50}), and unconfined compression strength (q_u) of five different 0.75% polypropylene and 10% fly ash -added high plasticity clay soil samples are given in Table 6.49.

Table 6.49 Soil moduli and unconfined compression strength of CH+10% fly ash+0.75% polypropylene

Sample No.	E_i (kN/m^2)	E_{t50} (kN/m^2)	E_{sf} (kN/m^2)	E_{s50} (kN/m^2)	q_u (kN/m^2)
1	21739.1	16515.3	14706.7	18424.6	330.9
2	24390.2	14662.5	11406.7	19231.1	342.2
3	17543.9	11852.2	9923.6	14677.2	272.9
4	16393.4	7895.8	5672.7	11195.3	156.0
5	10416.7	4146.6	2412.3	6124.2	78.4

According to the data obtained, it can be concluded that the maximum modulus values are observed in the initial tangent modulus compared with other soil moduli in all five 0.75% polypropylene and 10% fly ash-added high plasticity clay samples due to the initial slope of the stress-strain curve. In other words, the axial stress increases up to a certain point very sharply. Then, this sharp increasing trend suddenly starts to slow down, and during this slowing trend, the axial strain increases rapidly.

Figure 6.160 Peak point of CH+10% fly ash+0.75% polypropylene

In addition, transformed hyperbolic stress-strain curves for five different 0.75% polypropylene and 10% fly ash-added high plasticity clay samples are illustrated in Figure 6.161.

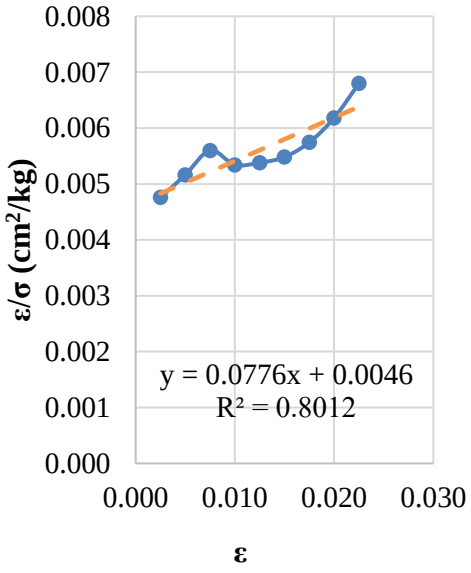

(a)

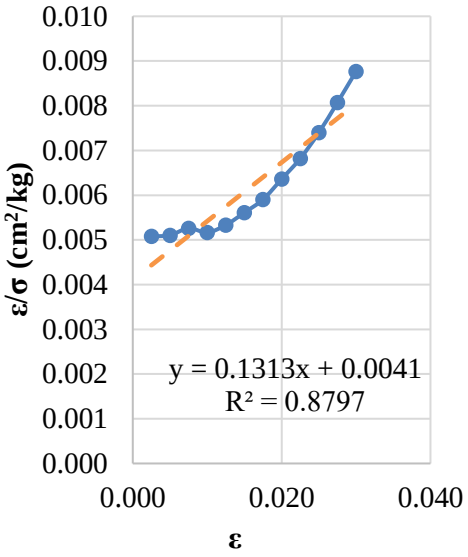

(b)

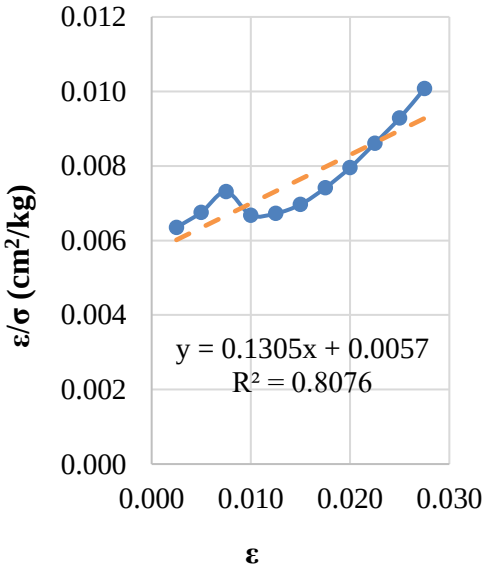

(c)

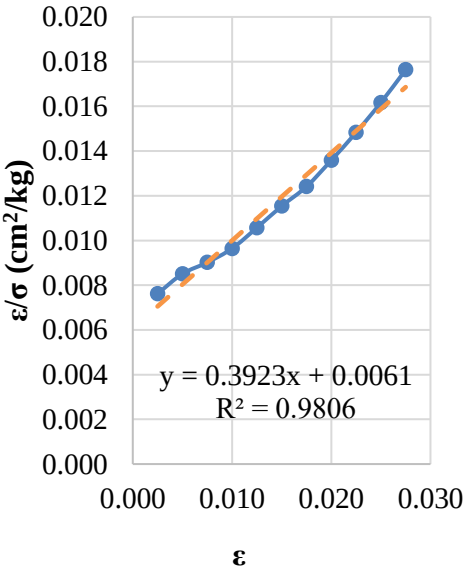

(d)

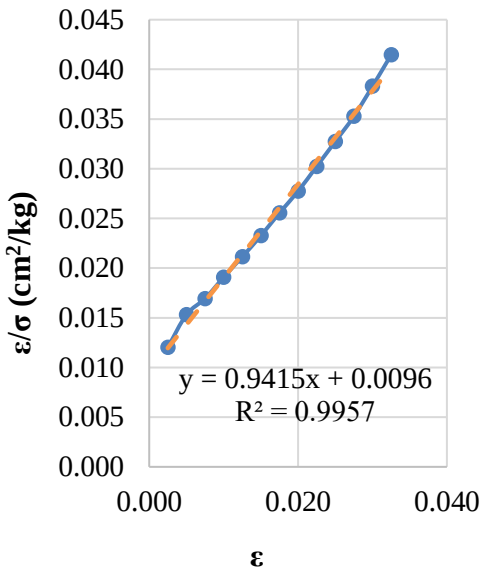

(e)

Figure 6.161 Transformed hyperbolic stress-strain curves for (a) sample 1, (b) sample 2, (c) sample 3, (d) sample 4, and (e) sample 5 (CH+10% Fly Ash+0.75% Polypropylene)

It was found that low and high values of axial strains in samples 1, 2, and 3 are not precisely hyperbolic, as shown in Figures 6.161 (a, b, and c). In other words, these points can not be fitted in a straight line. However, it was possible to estimate the actual stress-strain curves by a hyperbola. Thus, it is found to have a reasonable degree of accuracy. On the other hand, the transformed hyperbolic stress-strain curve in samples 4 and 5 is hyperbolic, as shown in Figures 6.161 (d and e). In other words, these points can be best-fitted in a straight line.

The relationship between the secant modulus at 50% of maximum stress (E_{s50}) and the initial tangent modulus (E_i) of the designated mixture of high plasticity clay samples (0.75% polypropylene and 10% fly ash-added CH) is shown in Figure 6.162.

According to the data, it can be inferred that these soil moduli refer to the hardening of 0.75% polypropylene and 10% fly ash-added high plasticity clay samples. Thus, the initial tangent modulus increases with the increasing secant modulus at 50% of maximum stress. Furthermore, it was best suited for estimating these soil moduli by a power model.

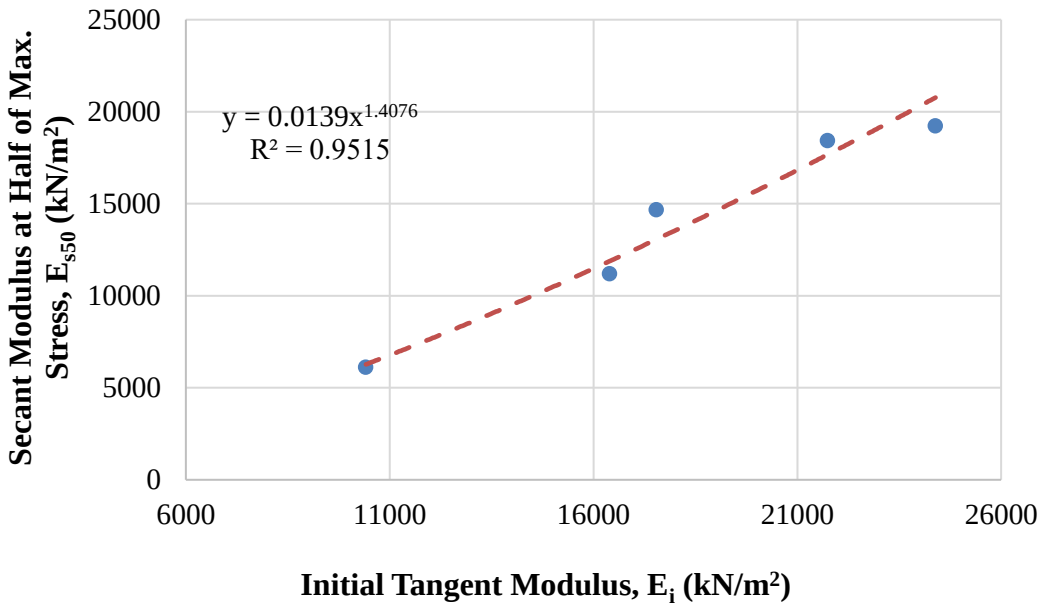

Figure 6.162 Relationship between secant modulus at 50% of maximum stress and initial tangent modulus (CH+10% Fly Ash+0.75% Polypropylene)

The relationship between the secant modulus at failure (E_{sf}) and the tangent modulus at 50% of maximum stress (E_{t50}) of the designated mixture of high plasticity clay samples (0.75% polypropylene and 10% fly ash-added CH) is shown in Figure 6.163.

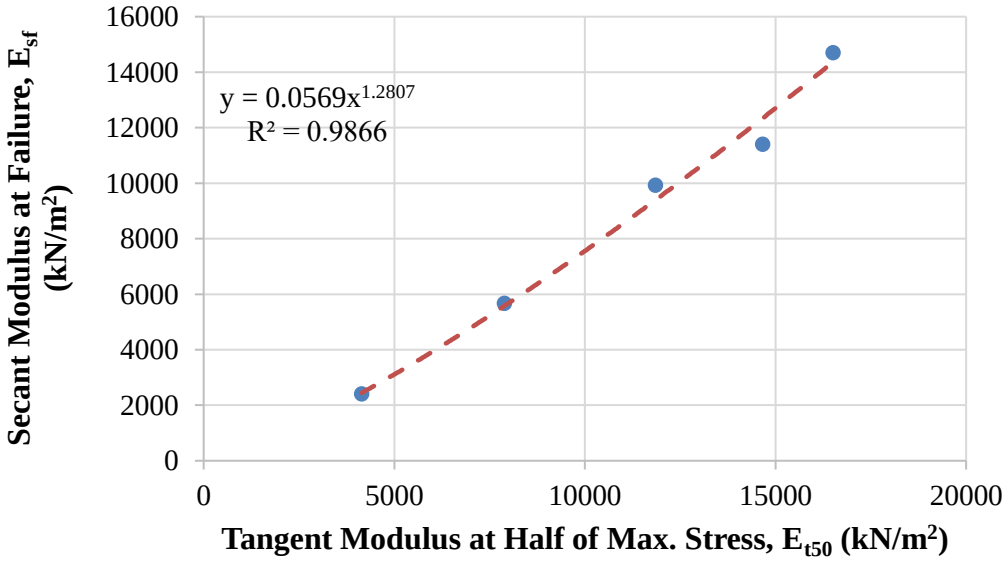

Figure 6.163 Relationship between secant modulus at failure point and tangent modulus at 50% of maximum stress (CH+10% Fly Ash +0.75% Polypropylene)

The tangent modulus at 50% of maximum stress increases with the increasing secant modulus at failure. Thus, it was best suited for estimating these soil moduli by a power model.

Furthermore, the relationship between the initial tangent modulus (E_i) and unconfined compression strength of the designated mixture of high plasticity clay samples (0.75% polypropylene and 10% fly ash-added CH) is shown in Figure 6.164.

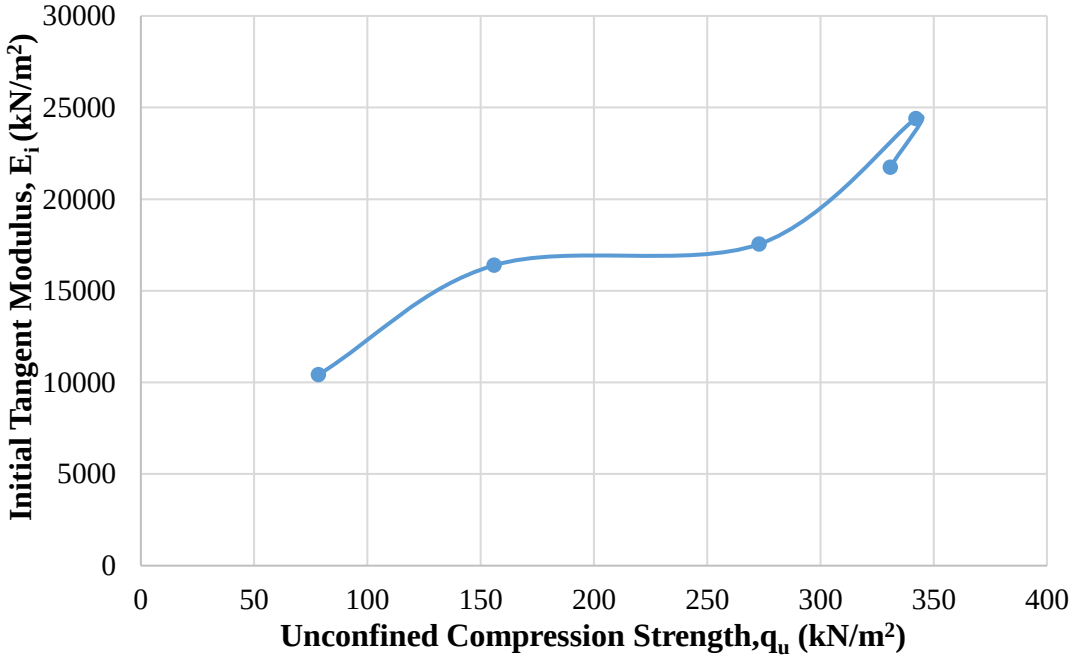

Figure 6.164 Relationship between initial tangent modulus and unconfined compression strength (CH+10% Fly Ash +0.75% Polypropylene)

According to data, the maximum initial tangent modulus is obtained in sample 2 as 24390.2 kN/m^2 for 0.75% polypropylene and 10% fly ash-added high plasticity clay. It should be noted that the water content is 22%, the dry unit weight is 14.87 kN/m^3, and the unconfined compression strength is 342.2 kN/m^2 when the initial tangent modulus is the maximum value for 0.75% polypropylene and 10% fly ash-added high plasticity clay.

The relationship between secant modulus at 50% of maximum stress (E_{s50}) and unconfined compression strength of the designated mixture of high plasticity clay samples (0.75% polypropylene and 10% fly ash-added CH) is shown in Figure 6.165.

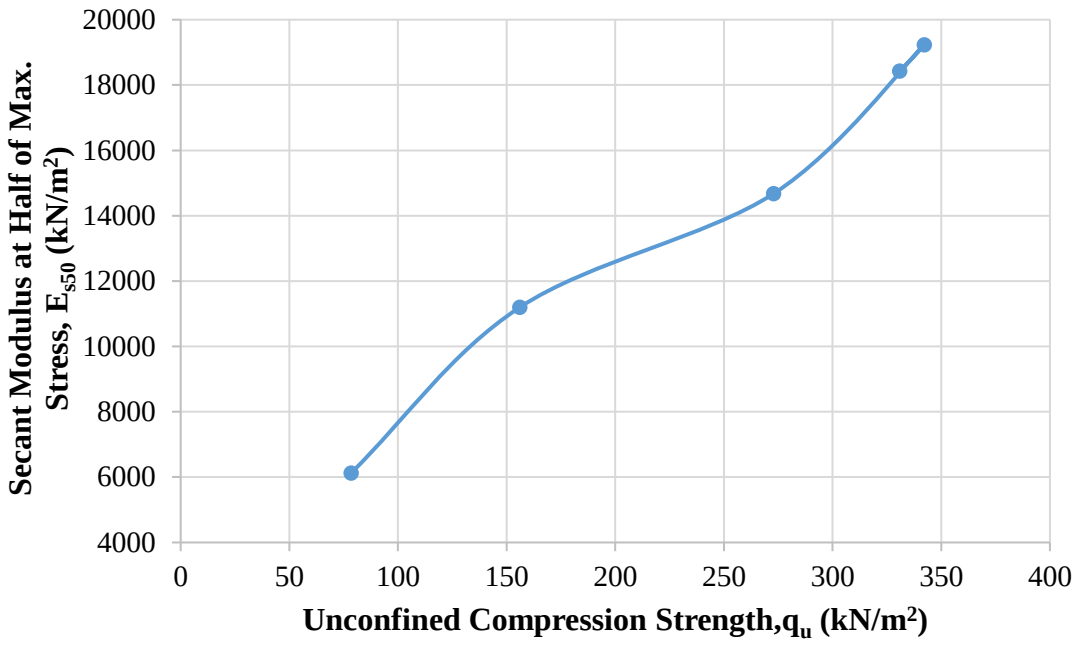

Figure 6.165 Relationship between secant modulus at 50% of maximum stress and unconfined compression strength (CH+10% Fly Ash +0.75% Polypropylene)

The maximum secant modulus at 50% of maximum stress is obtained in sample 2 as 19231.1 kN/m^2 for 0.75% polypropylene and 10% fly ash-added high plasticity clay. It should be noted that the water content is 22%, the dry unit weight is 14.87 kN/m^3, and the unconfined compression strength is 342.2 kN/m^2 when the secant modulus at 50% of maximum stress has the maximum value of 0.75% polypropylene and 10% fly ash-added high plasticity clay.

In addition, concerning the results of the initial tangent modulus and secant modulus at 50% of maximum stress, it seems that the maximum values of these moduli are obtained at maximum unconfined compression strength (sample 2 for 0.75% polypropylene and 10% fly ash-added high plasticity clay). On the other hand, when calculated initial tangent modulus and secant modulus at 50% of maximum stress have the maximum values for 0.75% polypropylene and 10% fly ash-added high plasticity clay, the water content is not equal to the optimum water content (w_{opt}=25%), and the dry unit weight is less than the maximum dry unit weight (γ_{dmax}=15.10 kN/m^3).

On the other hand, the relationship between tangent modulus at 50% of maximum stress (E_{t50}) and unconfined compression strength of the designated mixture

of high plasticity clay samples (0.75% polypropylene and 10% fly ash-added CH) is shown in Figure 6.166.

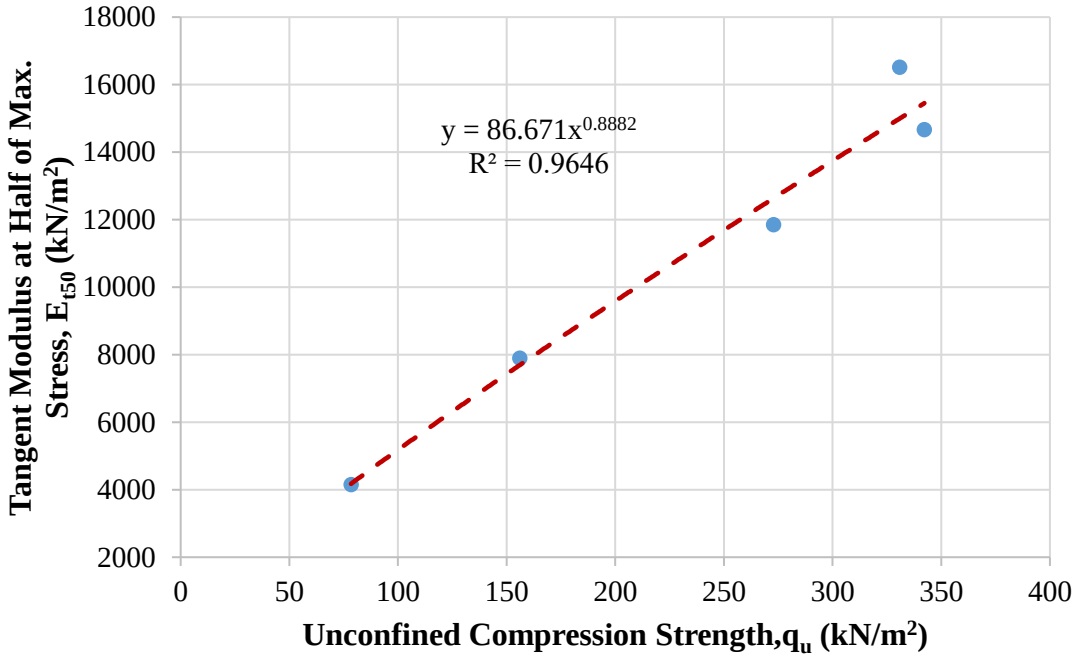

Figure 6.166 Relationship between tangent modulus at 50% of maximum stress and unconfined compression strength (CH+10% Fly Ash +0.75% Polypropylene)

The maximum tangent modulus at 50% of maximum stress is obtained in sample 1 as 16515.3 kN/m^2 for 0.75% polypropylene and 10% fly ash-added high plasticity clay. It should be noted that the water content is 18%, the dry unit weight is 14.16 kN/m^3, and the unconfined compression strength is 330.9 kN/m^2 when the tangent modulus at 50% of maximum stress is the maximum value for the 0.75% polypropylene and 10% fly ash-added high plasticity clay.

In addition, the relationship between secant modulus at failure point (E_{sf}) and unconfined compression strength of the designated mixture of high plasticity clay samples (0.75% polypropylene and 10% fly ash-added CH) is shown in Figure 6.167.

It is obvious that the maximum secant modulus at failure point is obtained in sample 1 as 14706.7 kN/m^2 for 0.75% polypropylene and 10% fly ash-added high plasticity clay. It should be noted that the water content is 18%, the dry unit weight is 14.16 kN/m^3, and the unconfined compression strength is 330.9 kN/m^2 when the secant modulus at failure point is the maximum value for 0.75% polypropylene and 10% fly ash-added high plasticity clay.

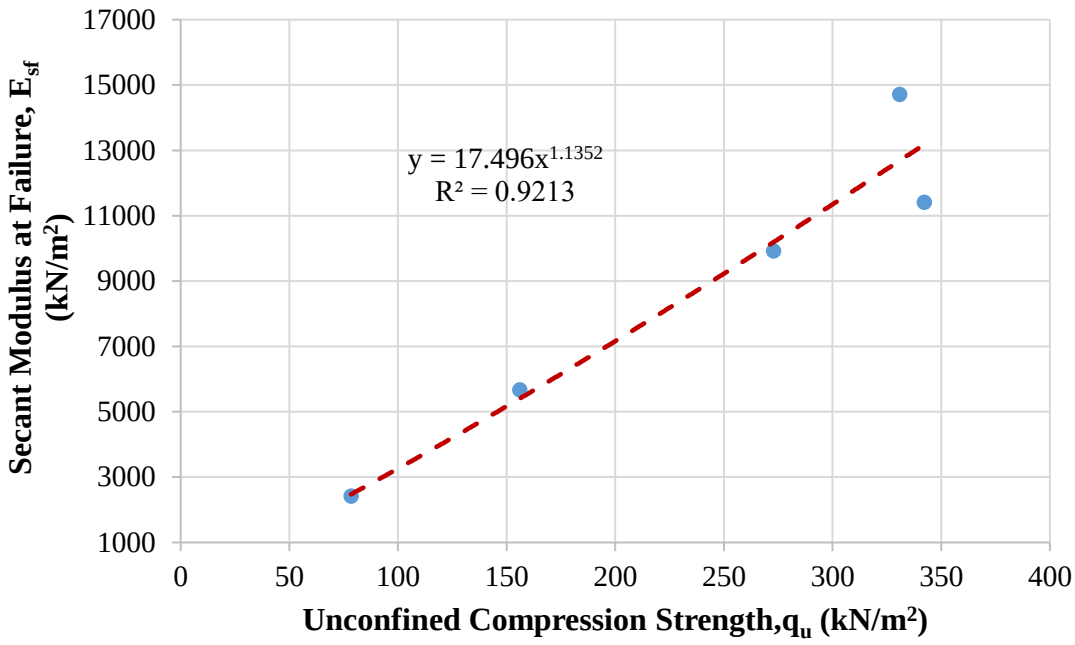

Figure 6.167 Relationship between secant modulus at failure point and unconfined compression strength (CH+10% Fly Ash +0.75% Polypropylene)

With respect to the results of the calculated tangent modulus at 50% of maximum stress and secant modulus at failure point, it seems that the maximum values of these moduli are not obtained at the maximum unconfined compression strength (sample 2 for 0.75% polypropylene and 10% fly ash-added high plasticity clay) since the beginning of the stress-strain curve of sample 1 has rapidly increased in axial stress. On the other hand, when these moduli have the maximum value for 0.75% polypropylene and 10% fly ash-added high plasticity clay, the water content is not equal to the optimum water content (w_{opt}=25%), and the dry unit weight is not equal to the maximum dry unit weight (γ_{dmax}=15.10 kN/m^3). Also, high plasticity clayey soil's strength and load-deformation properties are improved by reinforcing with polypropylene fiber and stabilized with fly ash.

6.5.4 Comparison of Three Different Fly Ash-Polypropylene Mixtures with High Plasticity Clay Soil

Three different amounts of polypropylene (0.25%, 0.5%, and 0.75%) mixed with 10% fly ash-added high plasticity clay soils were prepared to analyze deformation moduli. The soil moduli of the mentioned amounts of polypropylene and 10% fly ash-

added high plasticity clay mixtures are compared with the plain high plasticity clay. Figure 6.168 exhibits the relationship between the maximum initial tangent modulus and different polypropylene content of 10% fly ash-added CH mixtures.

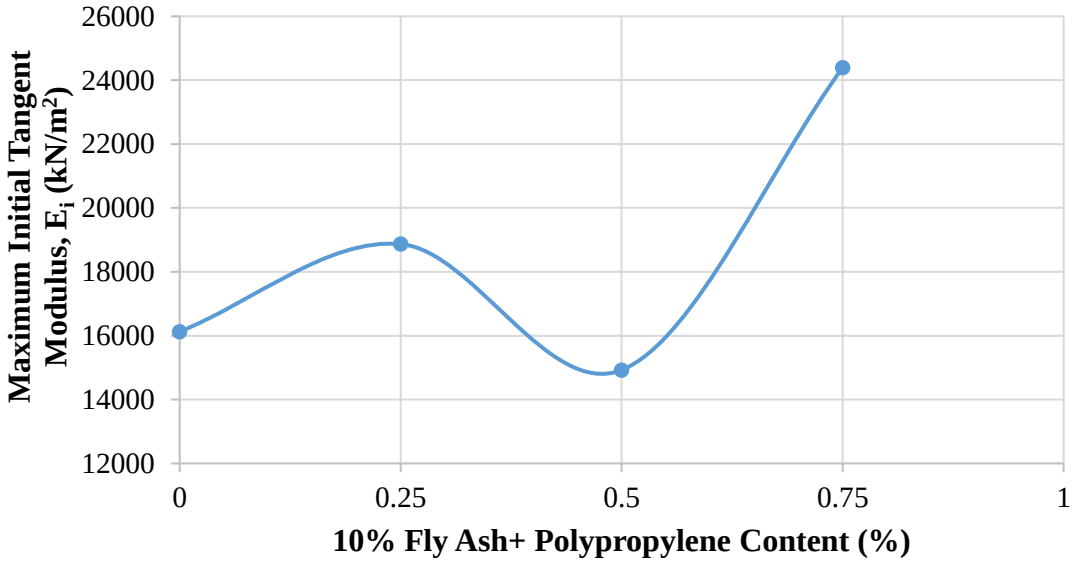

Figure 6.168 Relationship between maximum initial tangent modulus and different polypropylene contents of 10% fly ash-added CH mixture

After analyzing all initial tangent modulus of amounts of polypropylene and 10% fly ash-added high plasticity clay mixtures, and comparing them in a graph, it can be seen that the maximum initial tangent modulus was obtained in the mixture with 0.75% of polypropylene. In addition, the initial tangent modulus increases up to 51% in the mixture with 0.75% of polypropylene. In other words, the initial tangent modulus increases up to the mixture with 0.25% of polypropylene. Then, it started to decrease with the increasing polypropylene content up to the mixture with 0.5% of polypropylene.

As the next step, all secant modulus at 50% of maximum stress of polypropylene and 10% fly ash-added high plasticity clay mixtures were gathered and compared in Figure 6.169.

It can be seen that the maximum secant modulus at 50% of maximum stress was obtained in the mixture with 0.75% of polypropylene. In addition, the secant modulus at 50% of maximum stress increases up to 93% for the mixture with 0.75% of polypropylene. In other words, the initial tangent modulus increases up to the mixture

with 0.25% of polypropylene. Then, it started to decrease with the increasing polypropylene content up to the mixture with 0.5% of polypropylene.

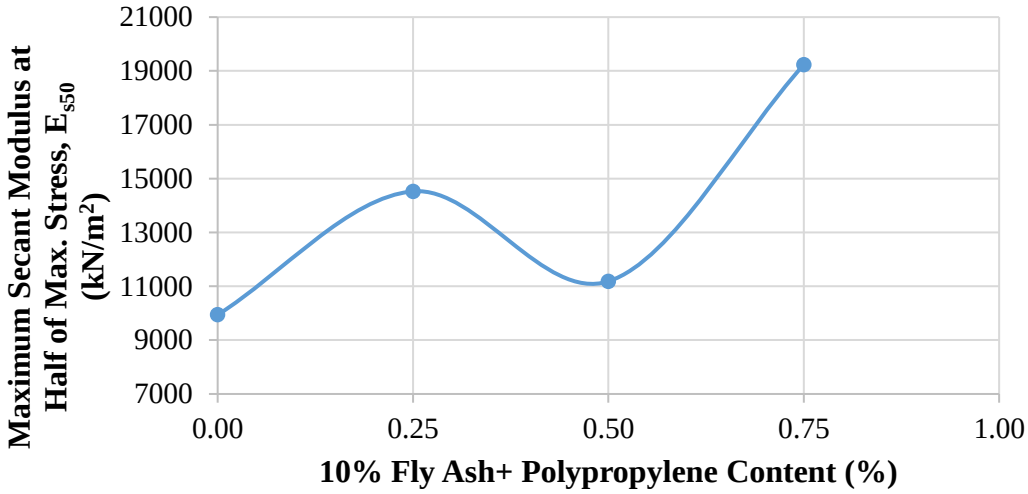

Figure 6.169 Relationship between maximum secant modulus at 50% of maximum stress and different polypropylene contents of 10% fly ash-added CH mixture

Furthermore, all tangent modulus at 50% of maximum stress of polypropylene and 10% fly ash-added high plasticity clay mixtures were gathered and compared in Figure 6.170.

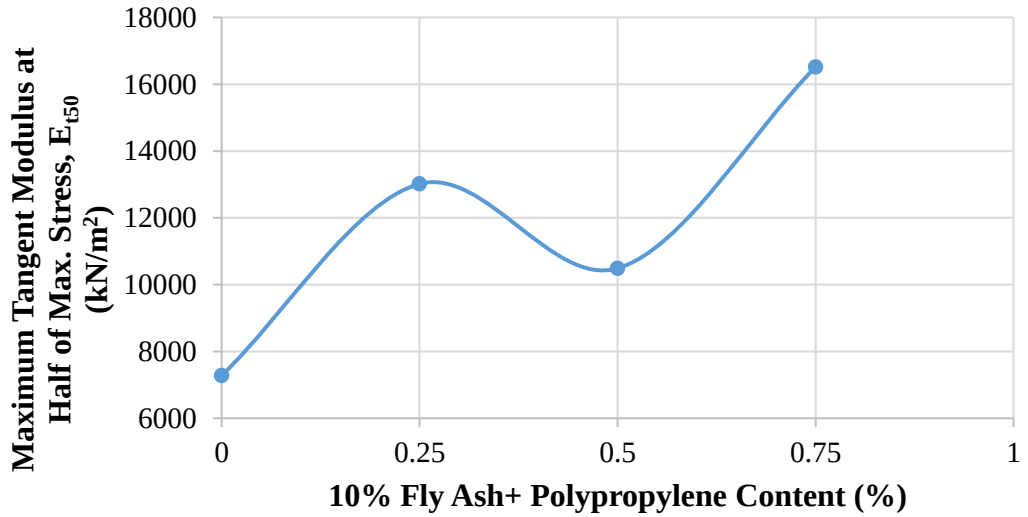

Figure 6.170 Relationship between maximum tangent modulus at 50% of maximum stress and different polypropylene contents of 10% fly ash-added CH mixture

It can be seen that the maximum tangent modulus at 50% of maximum stress was obtained in the mixture with 0.75% of polypropylene. In addition, the tangent modulus at 50% of maximum stress increases up to 127% in the mixture with 0.75% of polypropylene. In other words, the initial tangent modulus increases up to the mixture with 0.25% of polypropylene. Then, it started to decrease with the increasing polypropylene content up to the mixture with 0.5% of polypropylene.

Moreover, Figure 6.171 exhibits the relationship between the maximum secant modulus at failure point and different polypropylene content of 10% fly ash-added CH mixtures.

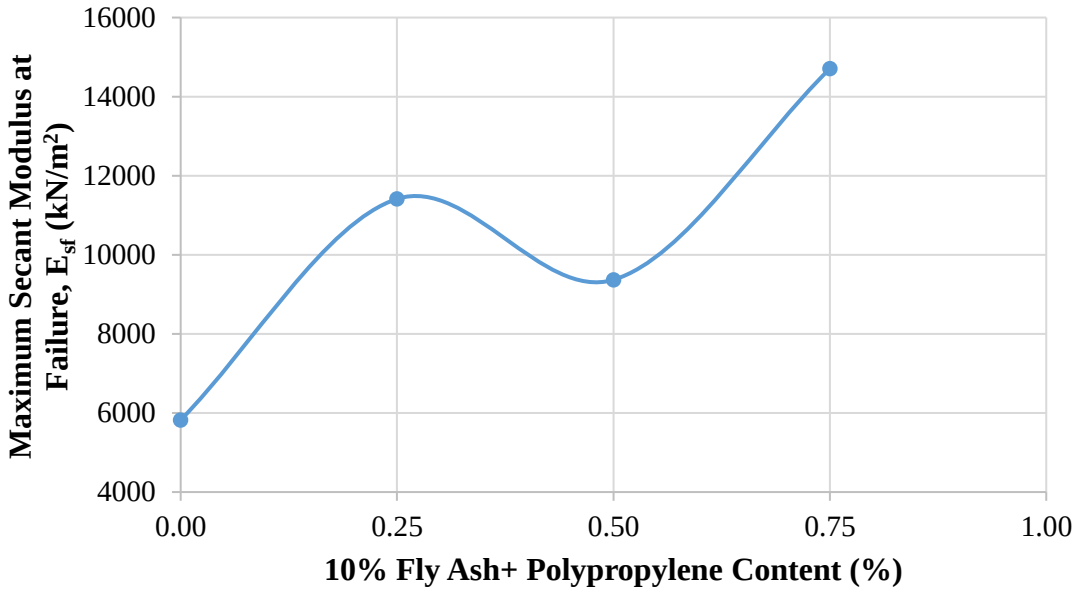

Figure 6.171 Relationship between maximum secant modulus at failure point and different polypropylene contents of 10% fly ash-added CH mixture

After gathering all secant modulus at failure point of amounts of polypropylene and 10% fly ash-added high plasticity clay mixtures, and comparing them in a graph, it can be seen that the maximum secant modulus at failure point was obtained in the mixture with 0.75% of polypropylene. In addition, the secant modulus at failure point increases up to 153% in the mixture with 0.75% of polypropylene. In other words, the initial tangent modulus increases up to the mixture with 0.25% of polypropylene. Then, it started to decrease with the increasing polypropylene content up to the mixture with 0.5% of polypropylene.

6.6 Fly Ash-Copolymer Mixtures with High Plasticity Clay Soil

Three different amounts of copolymer (0.75%, 1%, and 1.25%) and an amount of 10% fly ash were added to the high plasticity clay to study the effects of mixing copolymer and fly ash with designated soil. In addition, the amounts of copolymer with fly ash compared to whole mixtures in terms of soil moduli, the unconfined compression strength, and relationships in these engineering parameters. In other words, the amount of soil improvement of high plasticity clay was examined with added copolymer and fly ash.

6.6.1 High Plasticity Clay Soil Mixture with 10% of Fly Ash and 0.75% of Copolymer

During the experimental program of this study, the amount of 0.75% copolymer and 10% fly ash mixed with high plasticity clay soil was used. The compaction and the unconfined compression tests were performed on the 0.75% copolymer and 10% fly ash mixed with high plasticity clay, and the outcomes of these experiments are illustrated in Table 6.50. With respect to data obtained from mentioned tests, it can be seen that the value of ω_{opt} and γ_{dmax} obtained at 23.10% and 15.11 kN/m^3, respectively.

Table 6.50 Results of experiments executed with CH+10% fly ash+0.75% copolymer

Sample No.	ω (%)	γ_d (kN/m^3)	q_u (kN/m^2)
1	20	14.60	318.8
2	23	15.10	278.5
3	24	14.84	227.4
4	27	14.37	156.9

The axial stress-axial strain curves of four different 0.75% copolymer and 10% fly ash-added high plasticity clay samples are shown in Figure 6.172. Besides, Figure 6.173 exhibits the tested 0.75% copolymer and 10% fly ash-added high plasticity clay sample, which has the highest value of the maximum unconfined compression strength. Therefore, according to data obtained from the unconfined compression test of the 0.75% copolymer and 10% fly ash-added high plasticity clay sample, it can be

inferred that the maximum unconfined compression strength was obtained in the first sample, and it was obtained as 318.8 kN/m^2.

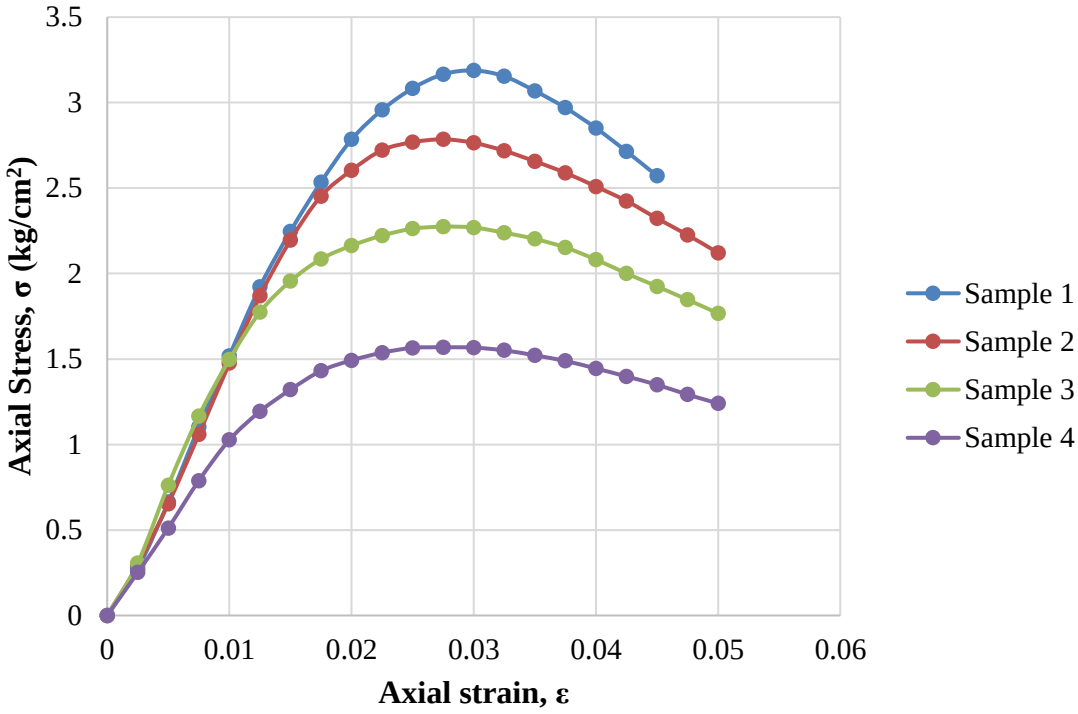

Figure 6.172 Results of unconfined compression tests of CH+10% fly ash+0.75% copolymer

Some of the required parameters were calculated to apply the modified and mentioned numerical model. Calculated engineering parameters to obtain soil moduli are given in Table 6.51.

Table 6.51 Calculated engineering parameters of CH+10% fly ash+0.75% copolymer

Sample No.	a	b	$(\sigma_1)_{ult}$	$(\sigma_1)_f$	R_f	ε_f	ε_{50}
	(cm^2/kg)	(cm^2/kg)	(kg/cm^2)	(kg/cm^2)	-	-	-
1	0.0047	0.1428	7.003	3.188	0.46	0.0300	0.0105
2	0.0051	0.1462	6.840	2.785	0.41	0.0275	0.0095
3	0.0043	0.2586	3.867	2.274	0.59	0.0275	0.0073
4	0.0075	0.3171	3.154	1.569	0.50	0.0275	0.0075

It should be noted that the strain level of 0.75% copolymer and 10% fly ash-added high plasticity clay is classified as small strain (SS) because the maximum axial strain was determined in samples 2, 3, and 4. The maximum axial strain was obtained as 0.05%. Thus, it can be concluded that nonlinear behaviour was observed for the tested 0.75% copolymer and 10% fly ash-added high plasticity clay samples.

Initial tangent modulus (E_i), tangent modulus at 50% of maximum stress (E_{t50}), secant modulus at failure (E_{sf}), secant modulus at 50% of maximum stress (E_{s50}), and unconfined compression strength (q_u) of four different 0.75% copolymer and 10% fly ash -added high plasticity clay soil samples are given in Table 6.52.

Table 6.52 Soil moduli and unconfined compression strength of CH+10% fly ash+0.75% copolymer

Sample No.	E_i (kN/m^2)	E_{t50} (kN/m^2)	E_{sf} (kN/m^2)	E_{s50} (kN/m^2)	q_u (kN/m^2)
1	21276.6	12692.9	10626.7	15231.3	318.8
2	19607.8	12436.8	10127.3	14658.8	278.5
3	23255.8	11590.6	8269.1	15543.8	227.4
4	13333.3	7524.7	5705.5	10517.0	156.9

According to the data obtained, it can be concluded that the maximum modulus values are observed in the initial tangent modulus compared with other soil moduli in all four 0.75% copolymer and 10% fly ash-added high plasticity clay samples due to the initial slope of the stress-strain curve. In other words, the axial stress increases up to a certain point very sharply. Then, this sharp increasing trend suddenly starts to slow down, and during this slowing trend, the axial strain increases rapidly.

In addition, transformed hyperbolic stress-strain curves for four different 0.75% copolymer and 10% fly ash-added high plasticity clay samples are illustrated in Figure 6.174.

Figure 6.173 Peak point of CH+10% fly ash+0.75% copolymer

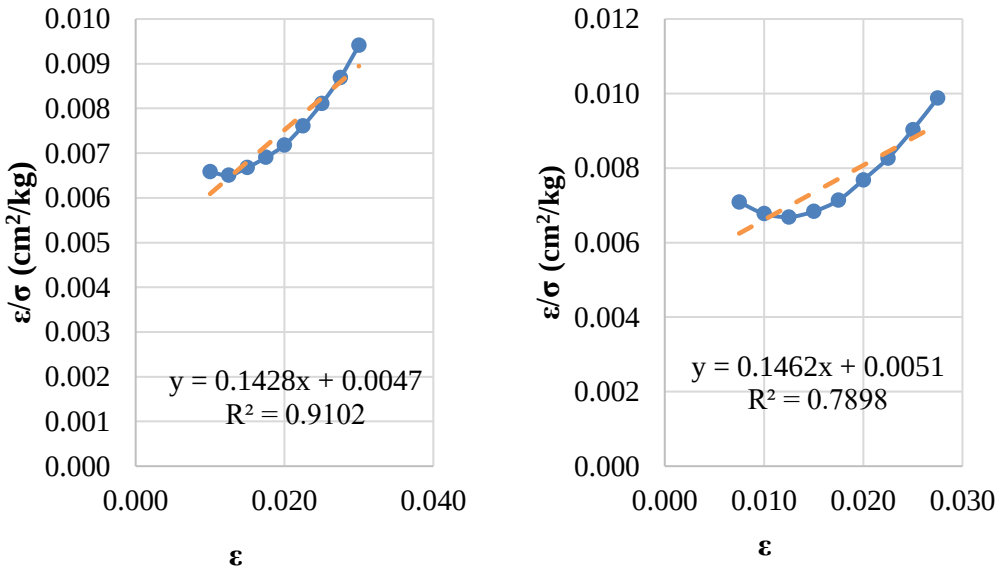

(a) **(b)**

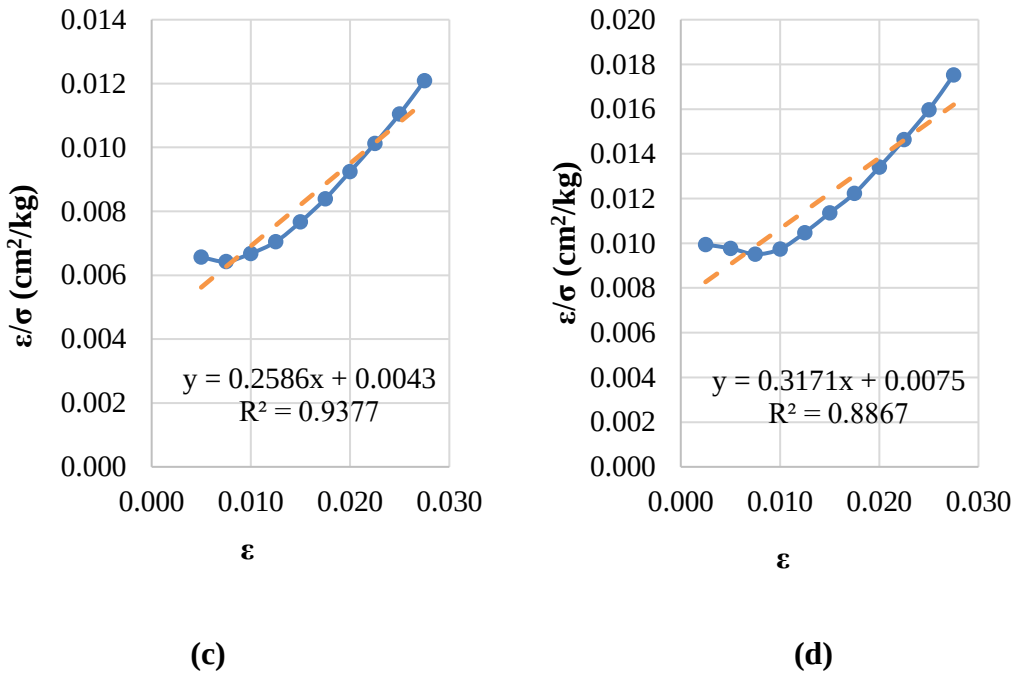

Figure 6.174 Transformed hyperbolic stress-strain curves for (a) sample 1, (b) sample 2, (c) sample 3, and (d) sample 4 (CH+10% Fly Ash+0.75% Copolymer)

It was found that low and high values of axial strains in all samples are not precisely hyperbolic, as shown in Figures 6.174 (a, b, c, and d). In other words, these points can not be fitted in a straight line. However, it was possible to estimate the actual stress-strain curves by a hyperbola. Thus, it is found to have a reasonable degree of accuracy.

The relationship between the secant modulus at 50% of maximum stress (E_{s50}) and the initial tangent modulus (E_i) of the designated mixture of high plasticity clay samples (0.75% copolymer and 10% fly ash-added CH) is shown in Figure 6.175.

According to the data, it can be inferred that these soil moduli refer to the hardening of 0.75% copolymer and 10% fly ash-added high plasticity clay samples. Thus, the initial tangent modulus increases with the increasing secant modulus at 50% of maximum stress. Furthermore, it was best suited for estimating these soil moduli by a power model.

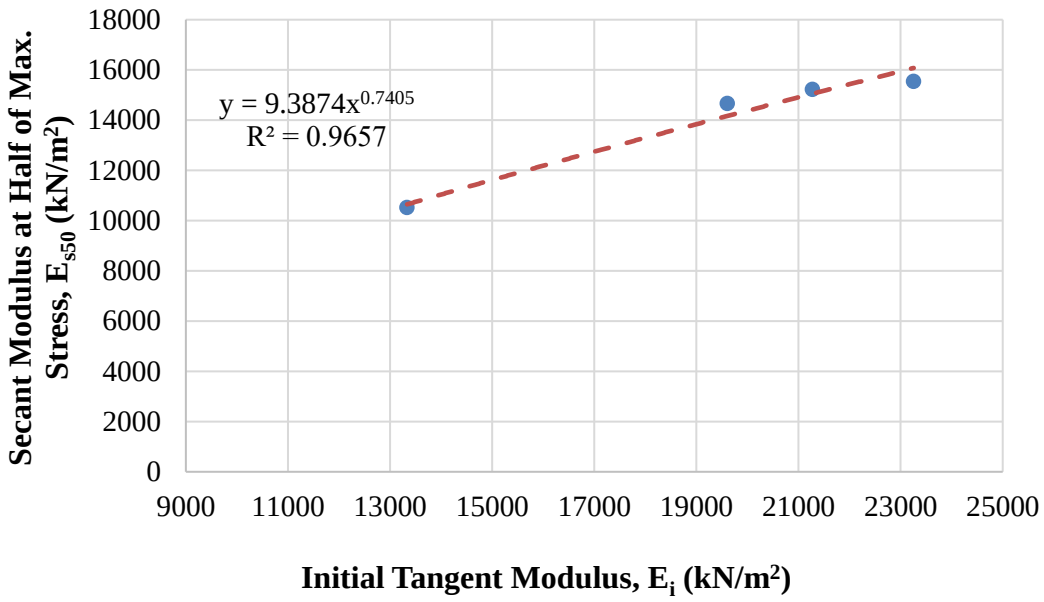

Figure 6.175 Relationship between secant modulus at 50% of maximum stress and initial tangent modulus (CH+10% Fly Ash+0.75% Copolymer)

The relationship between the secant modulus at failure (E_{sf}) and the tangent modulus at 50% of maximum stress (E_{t50}) of the designated mixture of high plasticity clay samples (0.75% copolymer and 10% fly ash-added CH) is shown in Figure 6.176.

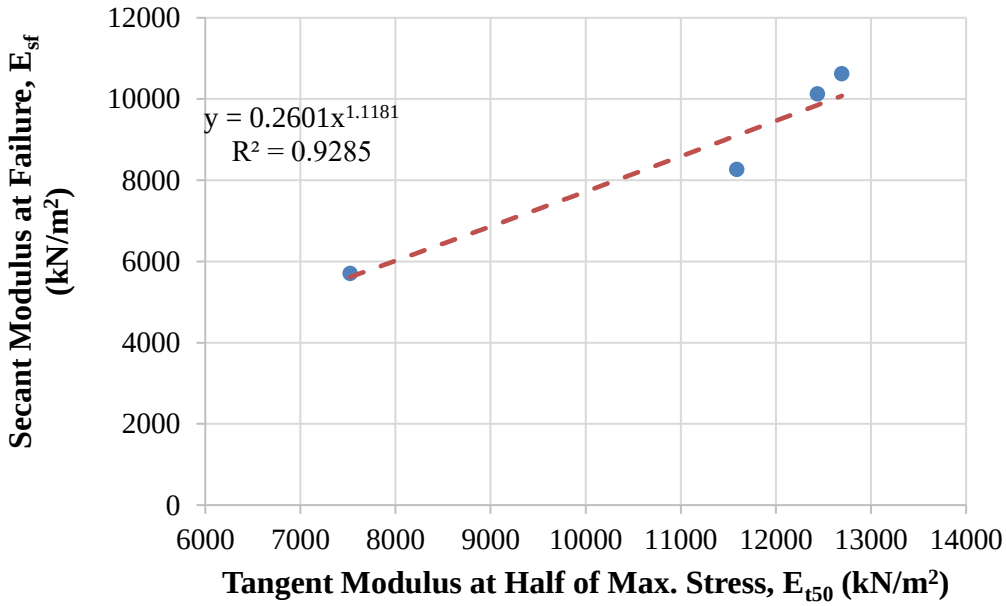

Figure 6.176 Relationship between secant modulus at failure point and tangent modulus at 50% of maximum stress (CH+10% Fly Ash +0.75% Copolymer)

The tangent modulus at 50% of maximum stress increases with the increasing secant modulus at failure. Thus, it was best suited for estimating these soil moduli by a power model.

Furthermore, the relationship between the initial tangent modulus (E_i) and unconfined compression strength of the designated mixture of high plasticity clay samples (0.75% copolymer and 10% fly ash-added CH) is shown in Figure 6.177.

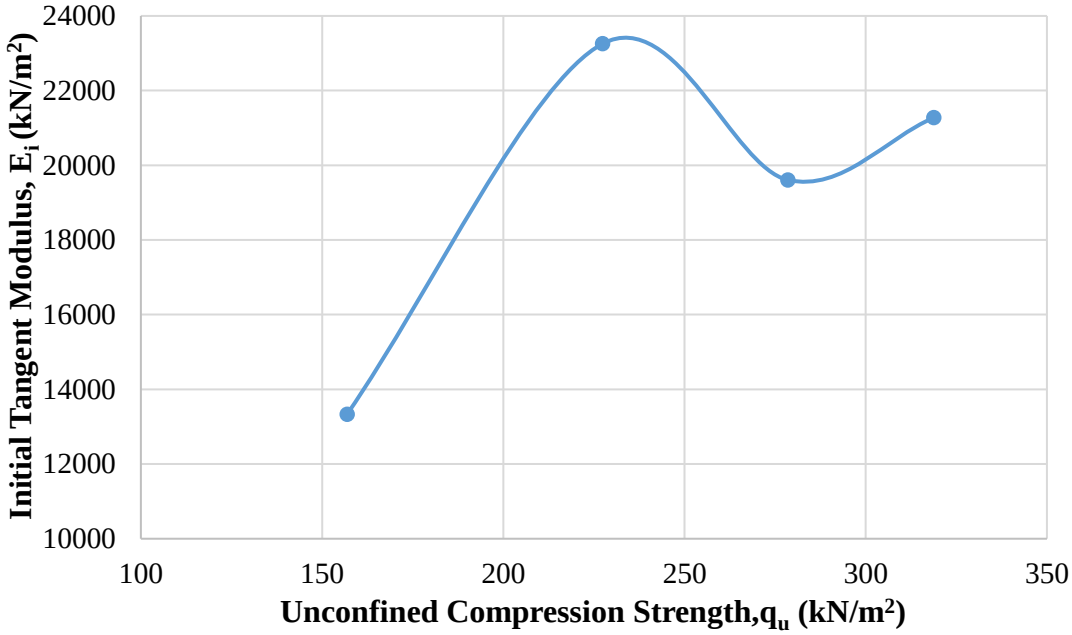

Figure 6.177 Relationship between initial tangent modulus and unconfined compression strength (CH+10% Fly Ash +0.75% Copolymer)

According to data, the maximum initial tangent modulus is obtained in sample 3 as 23255.8 kN/m^2 for 0.75% copolymer and 10% fly ash-added high plasticity clay. It should be noted that the water content is 24%, the dry unit weight is 14.84 kN/m^3, and the unconfined compression strength is 227.4 kN/m^2 when the initial tangent modulus is the maximum value for 0.75% copolymer and 10% fly ash-added high plasticity clay.

The relationship between secant modulus at 50% of maximum stress (E_{s50}) and unconfined compression strength of the designated mixture of high plasticity clay samples (0.75% copolymer and 10% fly ash-added CH) is shown in Figure 6.178.

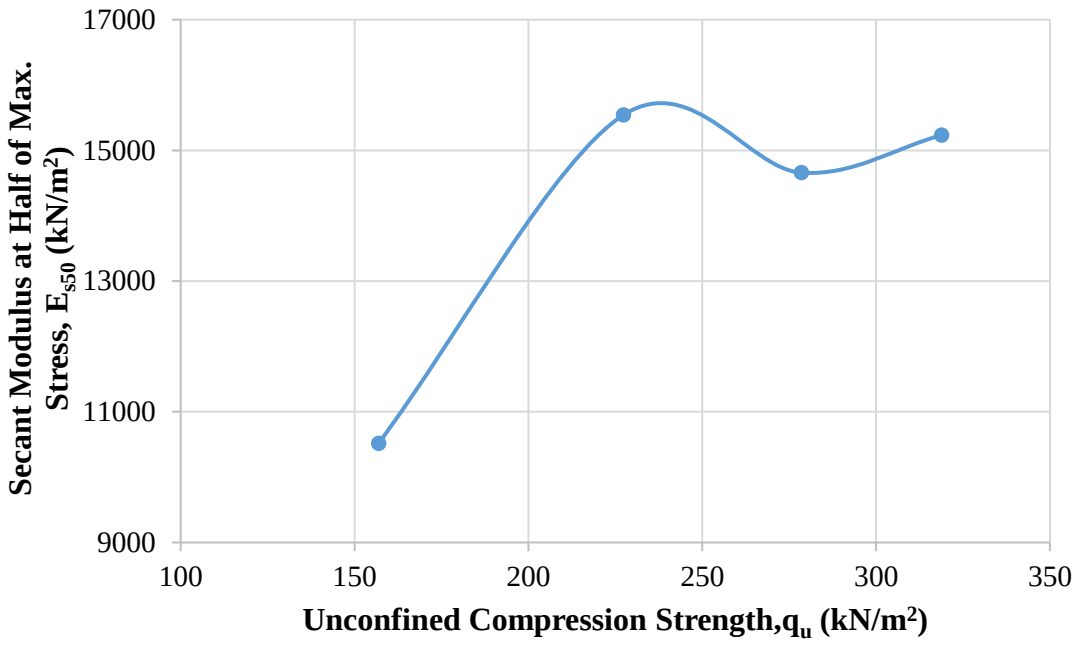

Figure 6.178 Relationship between secant modulus at 50% of maximum stress and unconfined compression strength (CH+10% Fly Ash +0.75% Copolymer)

The maximum secant modulus at 50% of maximum stress is obtained in sample 3 as 15543.8 kN/m^2 for 0.75% copolymer and 10% fly ash-added high plasticity clay. It should be noted that the water content is 24%, the dry unit weight is 14.84 kN/m^3, and the unconfined compression strength is 227.4 kN/m^2 when the secant modulus at 50% of maximum stress has the maximum value of 0.75% copolymer and 10% fly ash-added high plasticity clay.

In addition, concerning the results of the initial tangent modulus and secant modulus at 50% of maximum stress, it seems that the maximum values of these moduli are not obtained at maximum unconfined compression strength (sample 1 for 0.75% copolymer and 10% fly ash-added high plasticity clay) since the beginning of the stress-strain curve of sample 3 has rapidly increased in axial stress. On the other hand, when calculated initial tangent modulus and secant modulus at 50% of maximum stress have the maximum values for 0.75% copolymer and 10% fly ash-added high plasticity clay, the water content is close to the optimum water content (w_{opt}=23.1%), and the dry unit weight is less than the maximum dry unit weight (γ_{dmax}=15.11 kN/m^3).

On the other hand, the relationship between tangent modulus at 50% of maximum stress (E_{t50}) and unconfined compression strength of the designated mixture

of high plasticity clay samples (0.75% copolymer and 10% fly ash-added CH) is shown in Figure 6.179.

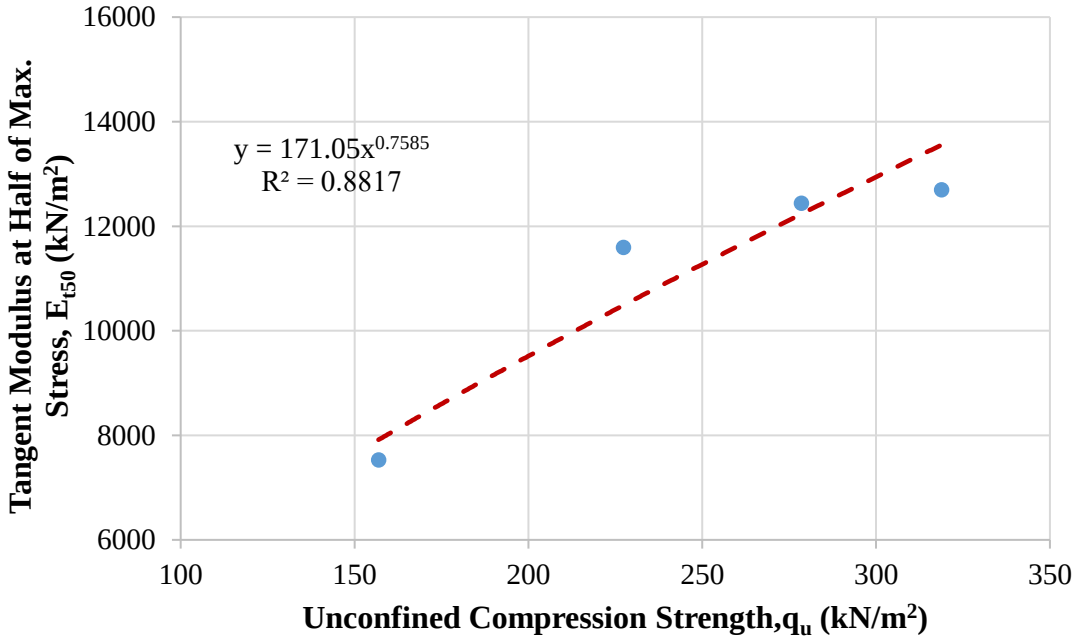

Figure 6.179 Relationship between tangent modulus at 50% of maximum stress and unconfined compression strength (CH+10% Fly Ash +0.75% Copolymer)

The maximum tangent modulus at 50% of maximum stress is obtained in sample 1 as 12692.9 kN/m^2 for 0.75% copolymer and 10% fly ash-added high plasticity clay. It should be noted that the water content is 20%, the dry unit weight is 14.60 kN/m^3, and the unconfined compression strength is 318.8 kN/m^2 when the tangent modulus at 50% of maximum stress is the maximum value for the 0.75% copolymer and 10% fly ash-added high plasticity clay.

In addition, the relationship between secant modulus at failure point (E_{sf}) and unconfined compression strength of the designated mixture of high plasticity clay samples (0.75% copolymer and 10% fly ash-added CH) is shown in Figure 6.180.

It is obvious that the maximum secant modulus at failure point is obtained in sample 1 as 10626.7 kN/m^2 for 0.75% copolymer and 10% fly ash-added high plasticity clay. It should be noted that the water content is 20%, the dry unit weight is 14.60 kN/m^3, and the unconfined compression strength is 318.8 kN/m^2 when the secant modulus at failure point is the maximum value for 0.75% copolymer and 10% fly ash-added high plasticity clay.

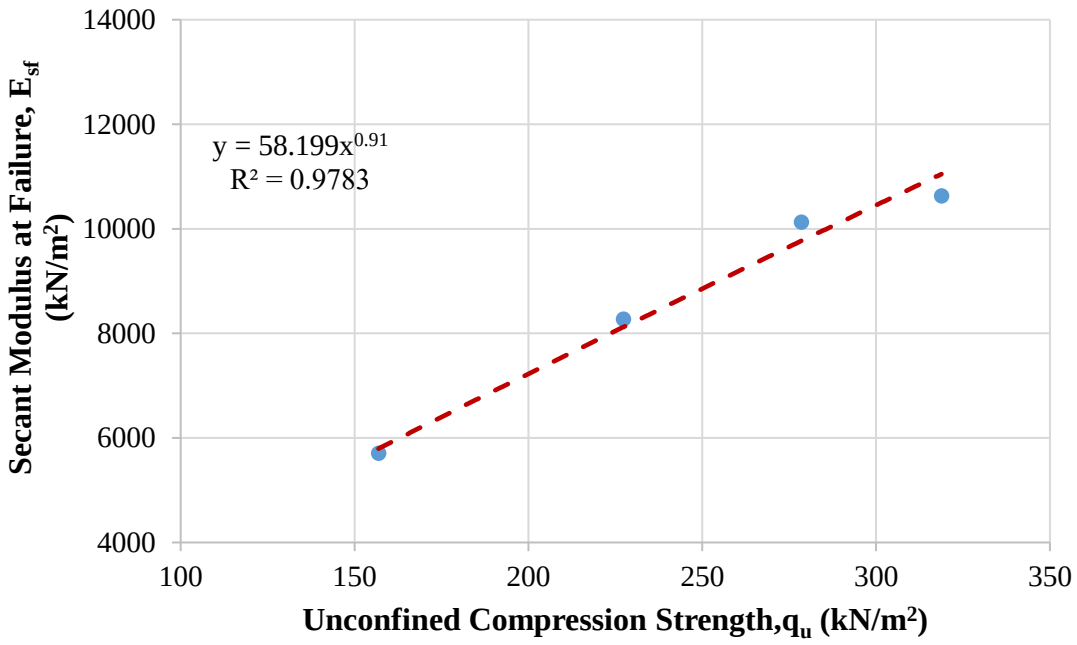

Figure 6.180 Relationship between secant modulus at failure point and unconfined compression strength (CH+10% Fly Ash +0.75% Copolymer)

With respect to the results of the calculated tangent modulus at 50% of maximum stress and secant modulus at failure point, it seems that the maximum values of these moduli are obtained at maximum unconfined compression strength (sample 1 for 0.75% copolymer and 10% fly ash-added high plasticity clay). On the other hand, when these moduli have the maximum value for 0.75% copolymer and 10% fly ash-added high plasticity clay, the water content is less than the optimum water content (w_{opt}=23.1%), and the dry unit weight is less than the maximum dry unit weight (γ_{dmax}=15.11 kN/m^3). Also, high plasticity clayey soil's strength and load-deformation properties are improved by reinforcing with copolymer fiber and stabilized with fly ash.

6.6.2 High Plasticity Clay Soil Mixture with 10% of Fly Ash and 1% of Copolymer

During the experimental program of this study, the amount of 1% copolymer and 10% fly ash mixed with high plasticity clay soil was used. The compaction and the unconfined compression tests were performed on the 1% copolymer and 10% fly ash mixed with high plasticity clay, and the outcomes of these experiments are illustrated

in Table 6.53. With respect to data obtained from mentioned tests, it can be seen that the value of ω_{opt} and γ_{dmax} obtained at 24.30% and 14.83 kN/m^3, respectively.

Table 6.53 Results of experiments executed with CH+10% fly ash+1% copolymer

Sample No.	ω (%)	γ_d (kN/m^3)	q_u (kN/m^2)
1	21	14.71	390.8
2	25	14.83	243.1
3	27	14.65	163.0
4	30	14.06	107.9
5	33	13.85	65.0

The axial stress-axial strain curves of five different 1% copolymer and 10% fly ash-added high plasticity clay samples are shown in Figure 6.181. Besides, Figure 6.182 exhibits the tested 1% copolymer and 10% fly ash-added high plasticity clay sample, which has the highest value of the maximum unconfined compression strength. Therefore, according to data obtained from the unconfined compression test of the 1% copolymer and 10% fly ash-added high plasticity clay sample, it can be inferred that the maximum unconfined compression strength was obtained in the first sample, and it was obtained as 390.8 kN/m^2.

Some of the required parameters were calculated to apply the modified and mentioned numerical model. Calculated engineering parameters to obtain soil moduli are given in Table 6.54.

It should be noted that the strain level of 1% copolymer and 10% fly ash-added high plasticity clay is classified as small strain (SS) because the maximum axial strain was determined in samples 3, 4, and 5. The maximum axial strain was obtained as 0.05%. Thus, it can be concluded that nonlinear behaviour was observed for the tested 1% copolymer and 10% fly ash-added high plasticity clay samples.

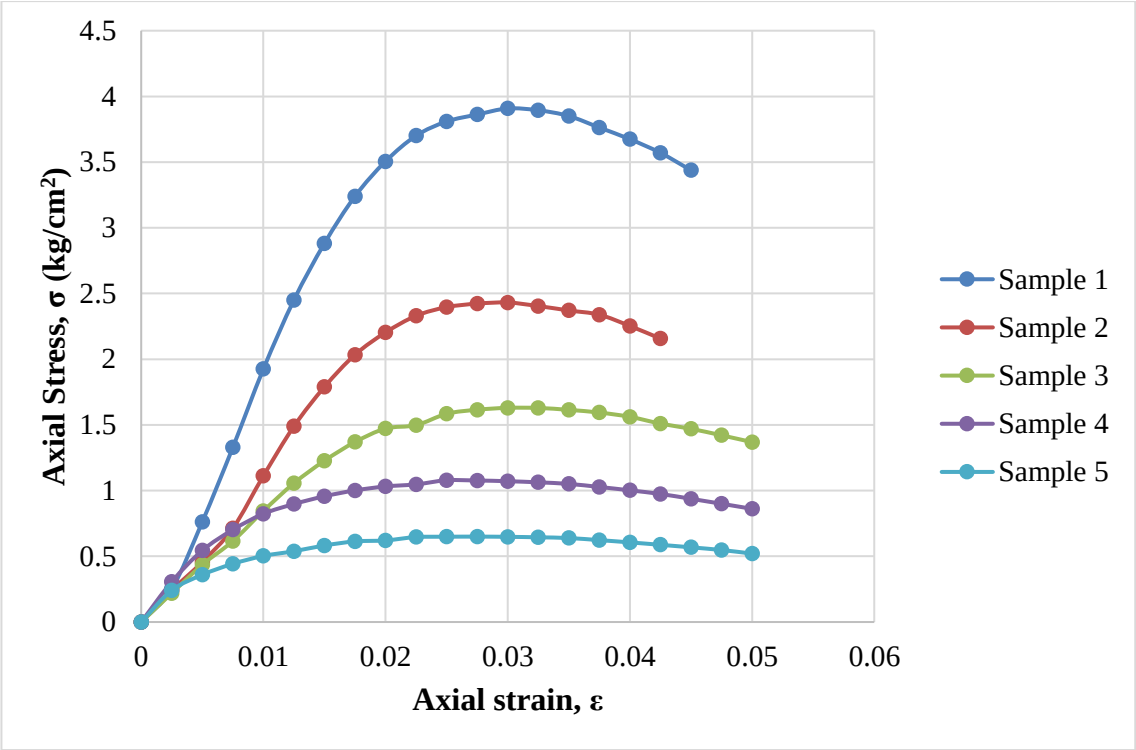

Figure 6.181 Results of unconfined compression tests of CH+10% fly ash+1% copolymer

Table 6.54 Calculated engineering parameters of CH+10% fly ash+1% copolymer

Sample No.	a (cm^2/kg)	b (cm^2/kg)	$(\sigma_1)_{ult}$ (kg/cm^2)	$(\sigma_1)_f$ (kg/cm^2)	R_f -	ε_f -	ε_{50} -
1	0.0034	0.1292	7.740	3.908	0.50	0.0300	0.0101
2	0.0060	0.1827	5.473	2.431	0.44	0.0300	0.0107
3	0.0097	0.2427	4.120	1.630	0.40	0.0300	0.0097
4	0.0057	0.6847	1.460	1.079	0.74	0.0250	0.0050
5	0.0074	1.2423	0.805	0.650	0.81	0.0275	0.0043

Initial tangent modulus (E_i), tangent modulus at 50% of maximum stress (E_{t50}), secant modulus at failure (E_{sf}), secant modulus at 50% of maximum stress (E_{s50}), and unconfined compression strength (q_u) of five different 1% copolymer and 10% fly ash -added high plasticity clay soil samples are given in Table 6.55.

Table 6.55 Soil moduli and unconfined compression strength of CH+10% fly ash+1% copolymer

Sample No.	E_i (kN/m^2)	E_{t50} (kN/m^2)	E_{sf} (kN/m^2)	E_{s50} (kN/m^2)	q_u (kN/m^2)
1	29411.8	16435.9	13026.7	19273.8	390.8
2	16666.7	10086.2	8103.3	11374.3	243.1
3	10309.3	6634.3	5433.3	8426.0	163.0
4	17543.9	6976.5	4316.0	10893.0	107.9
5	13513.5	4804.3	2363.6	7594.1	65.0

According to the data obtained, it can be concluded that the maximum modulus values are observed in the initial tangent modulus compared with other soil moduli in all five 1% copolymer and 10% fly ash-added high plasticity clay samples due to the initial slope of the stress-strain curve. In other words, the axial stress increases up to a certain point very sharply. Then, this sharp increasing trend suddenly starts to slow down, and during this slowing trend, the axial strain increases rapidly.

Figure 6.182 Peak point of CH+10% fly ash+1% copolymer

In addition, transformed hyperbolic stress-strain curves for five different 1% copolymer and 10% fly ash-added high plasticity clay samples are illustrated in Figure 6.183.

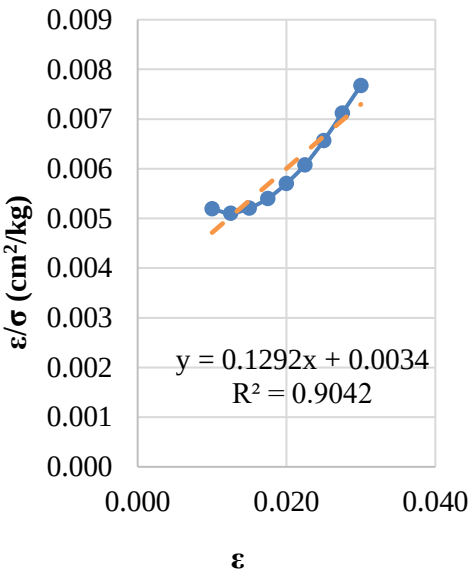
0.009
0.008
0.007
0.006
0.005
0.004
0.003
0.002
0.001
0.000
ε/σ (cm²/kg)
y = 0.1292x + 0.0034
R² = 0.9042
0.000
0.020
0.040
ε

(c)

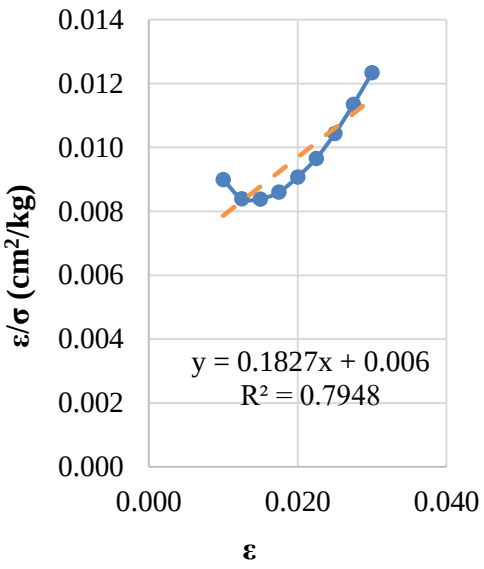
0.014
0.012
0.010
0.008
0.006
0.004
0.002
0.000
ε/σ (cm²/kg)
y = 0.1827x + 0.006
R² = 0.7948
0.000
0.020
0.040
ε

(d)

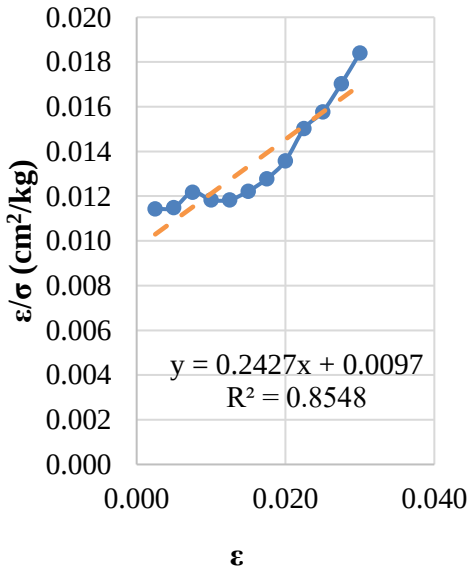
0.020
0.018
0.016
0.014
0.012
0.010
0.008
0.006
0.004
0.002
0.000
ε/σ (cm²/kg)
y = 0.2427x + 0.0097
R² = 0.8548
0.000
0.020
0.040
ε

(c)

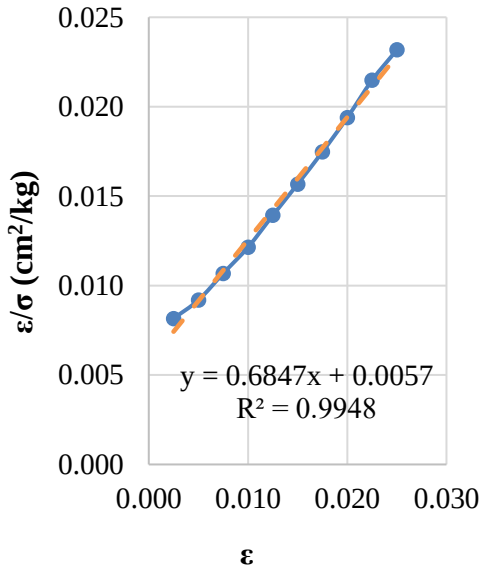
0.025
0.020
0.015
0.010
0.005
0.000
ε/σ (cm²/kg)
y = 0.6847x + 0.0057
R² = 0.9948
0.000
0.010
0.020
0.030
ε

(d)

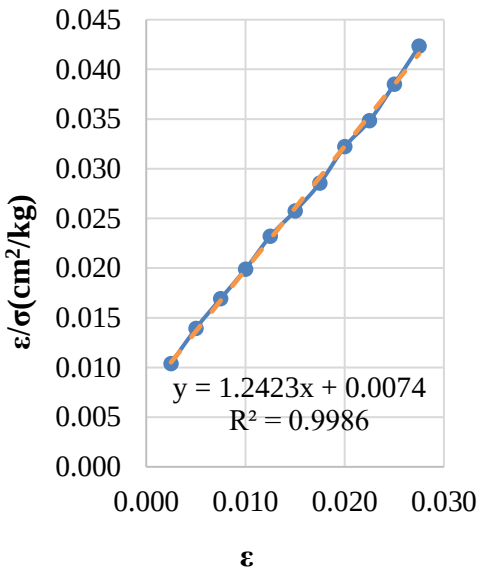

(e)

Figure 6.183 Transformed hyperbolic stress-strain curves for (a) sample 1, (b) sample 2, (c) sample 3, (d) sample 4, and (e) sample 5 (CH+10% Fly Ash+1% Copolymer)

It was found that low and high values of axial strains in samples 1, 2, and 3 are not precisely hyperbolic, as shown in Figures 6.183 (a, b, and c). In other words, these points can not be fitted in a straight line. However, it was possible to estimate the actual stress-strain curves by a hyperbola. Thus, it is found to have a reasonable degree of accuracy. On the other hand, the transformed hyperbolic stress-strain curve in samples 4 and 5 is hyperbolic, as shown in Figures 6.183 (d and e). In other words, these points can be best-fitted in a straight line.

The relationship between the secant modulus at 50% of maximum stress (E_{s50}) and the initial tangent modulus (E_i) of the designated mixture of high plasticity clay samples (1% copolymer and 10% fly ash-added CH) is shown in Figure 6.184.

According to the data, it can be inferred that these soil moduli refer to the hardening of 1% copolymer and 10% fly ash-added high plasticity clay samples. Thus, the initial tangent modulus increases with the increasing secant modulus at 50% of maximum stress. Furthermore, it was best suited for estimating these soil moduli by a power model.

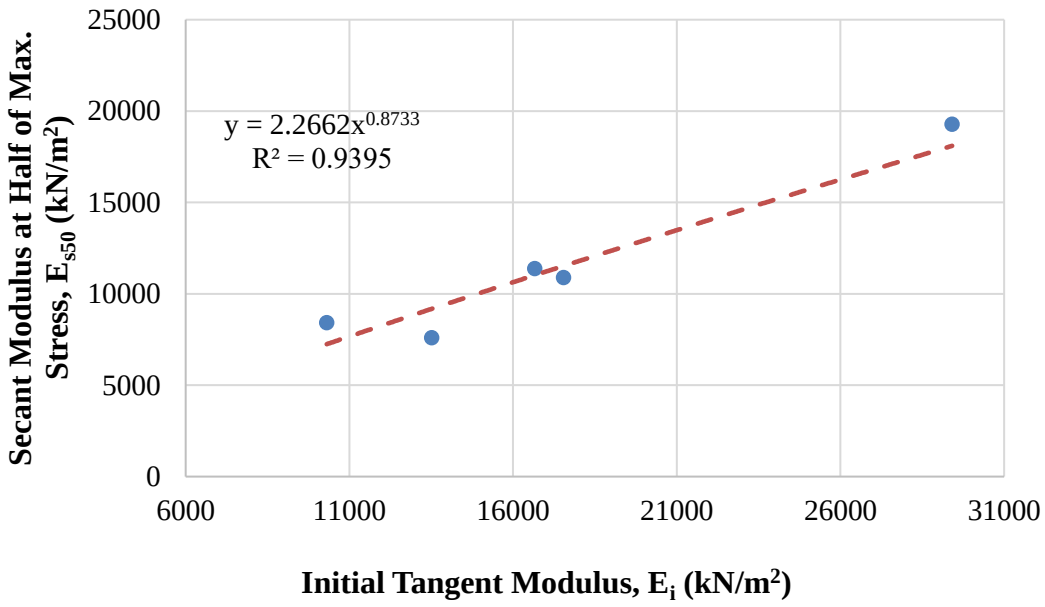

Figure 6.184 Relationship between secant modulus at 50% of maximum stress and initial tangent modulus (CH+10% Fly Ash+1% Copolymer)

The relationship between the secant modulus at failure (E_{sf}) and the tangent modulus at 50% of maximum stress (E_{t50}) of the designated mixture of high plasticity clay samples (1% copolymer and 10% fly ash-added CH) is shown in Figure 6.185.

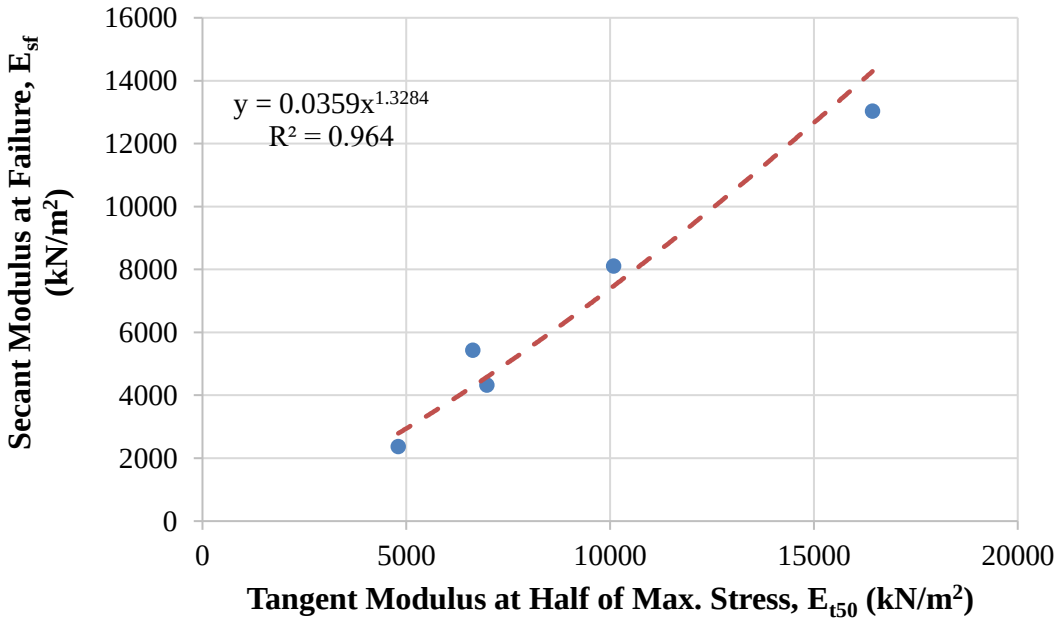

Figure 6.185 Relationship between secant modulus at failure point and tangent modulus at 50% of maximum stress (CH+10% Fly Ash +1% Copolymer)

The tangent modulus at 50% of maximum stress increases with the increasing secant modulus at failure. Thus, it was best suited for estimating these soil moduli by a power model.

Furthermore, the relationship between the initial tangent modulus (E_i) and unconfined compression strength of the designated mixture of high plasticity clay samples (1% copolymer and 10% fly ash-added CH) is shown in Figure 6.186.

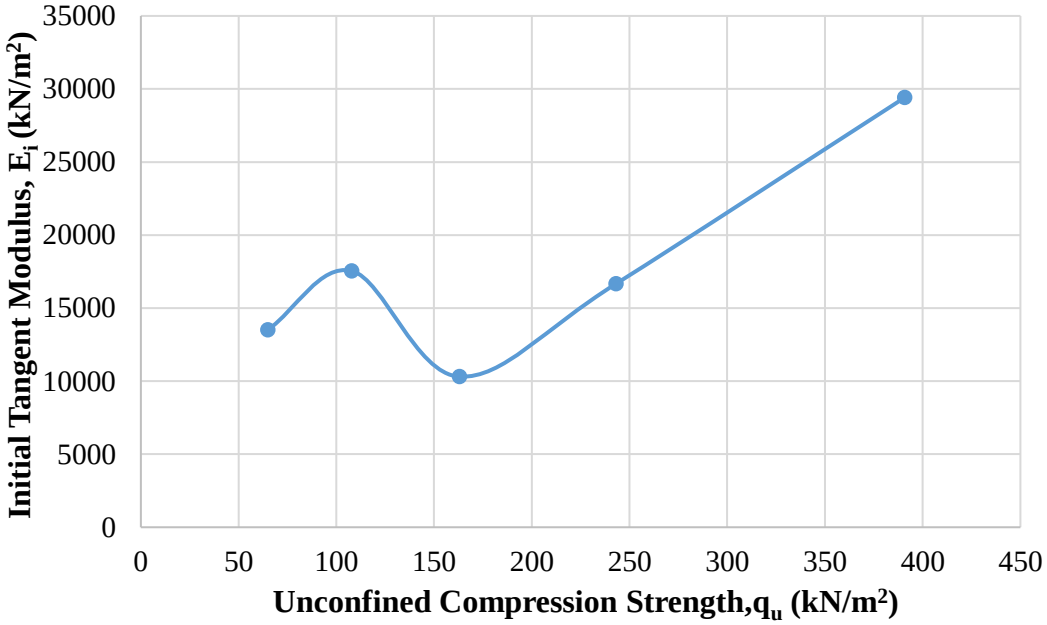

Figure 6.186 Relationship between initial tangent modulus and unconfined compression strength (CH+10% Fly Ash +1% Copolymer)

According to data, the maximum initial tangent modulus is obtained in sample 1 as 29411.8 kN/m^2 for 1% copolymer and 10% fly ash-added high plasticity clay. It should be noted that the water content is 21%, the dry unit weight is 14.71 kN/m^3, and the unconfined compression strength is 390.8 kN/m^2 when the initial tangent modulus is the maximum value for 1% copolymer and 10% fly ash-added high plasticity clay.

The relationship between secant modulus at 50% of maximum stress (E_{s50}) and unconfined compression strength of the designated mixture of high plasticity clay samples (1% copolymer and 10% fly ash-added CH) is shown in Figure 6.187.

The maximum secant modulus at 50% of maximum stress is obtained in sample 1 as 19273.8 kN/m^2 for 1% copolymer and 10% fly ash-added high plasticity clay. It should be noted that the water content is 21%, the dry unit weight is 14.71 kN/m^3, and

the unconfined compression strength is 390.8 kN/m^2 when the secant modulus at 50% of maximum stress has the maximum value of 1% copolymer and 10% fly ash-added high plasticity clay.

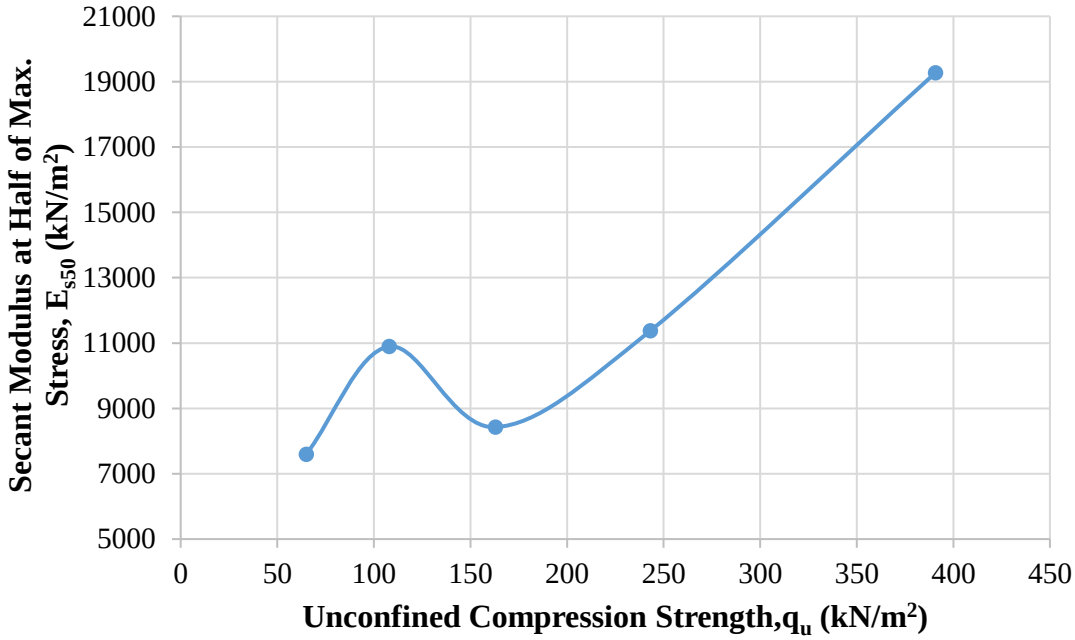

Figure 6.187 Relationship between secant modulus at 50% of maximum stress and unconfined compression strength (CH+10% Fly Ash +1% Copolymer)

On the other hand, the relationship between tangent modulus at 50% of maximum stress (E_{t50}) and unconfined compression strength of the designated mixture of high plasticity clay samples (1% copolymer and 10% fly ash-added CH) is shown in Figure 6.188.

The maximum tangent modulus at 50% of maximum stress is obtained in sample 1 as 16435.9 kN/m^2 for 1% copolymer and 10% fly ash-added high plasticity clay. It should be noted that the water content is 21%, the dry unit weight is 14.71 kN/m^3, and the unconfined compression strength is 390.8 kN/m^2 when the tangent modulus at 50% of maximum stress is the maximum value for the 1% copolymer and 10% fly ash-added high plasticity clay.

In addition, the relationship between secant modulus at failure point (E_{sf}) and unconfined compression strength of the designated mixture of high plasticity clay samples (1% copolymer and 10% fly ash-added CH) is shown in Figure 6.189.

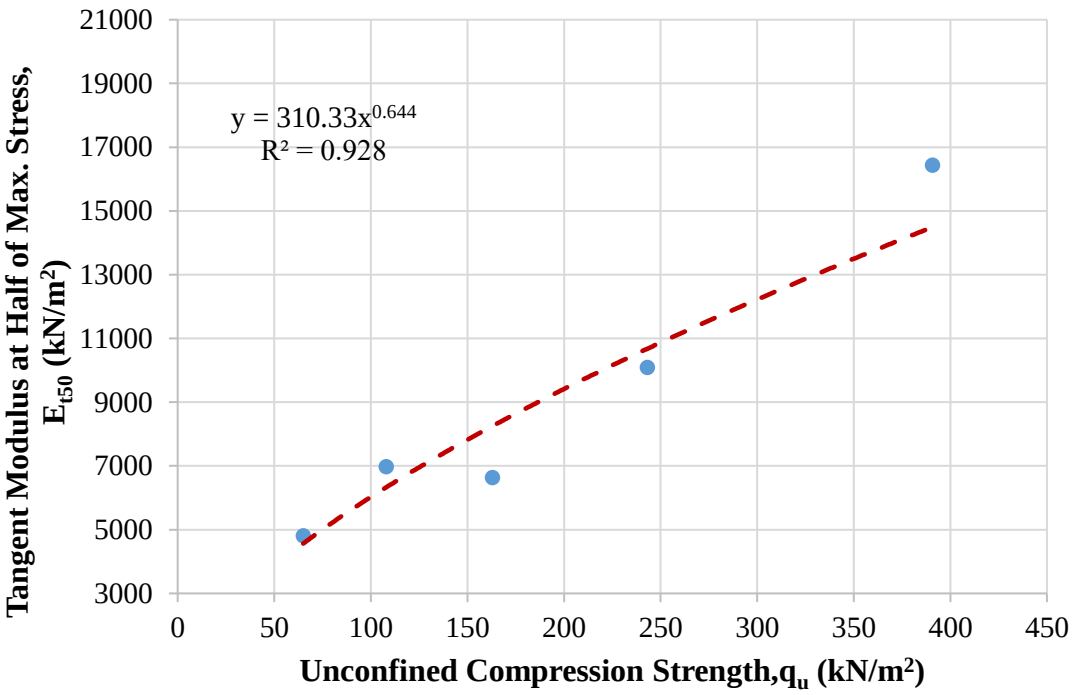

Figure 6.188 Relationship between tangent modulus at 50% of maximum stress and unconfined compression strength (CH+10% Fly Ash +1% Copolymer)

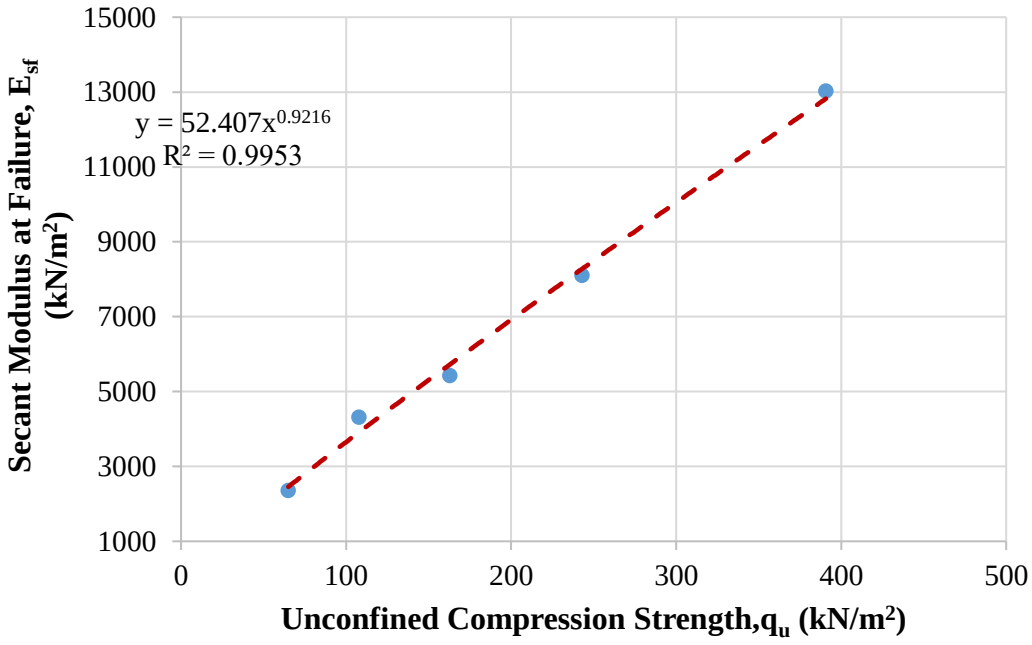

Figure 6.189 Relationship between secant modulus at failure point and unconfined compression strength (CH+10% Fly Ash +1% Copolymer)

It is obvious that the maximum secant modulus at failure point is obtained in sample 1 as 13026.7 kN/m^2 for 1% copolymer and 10% fly ash-added high plasticity clay. It should be noted that the water content is 21%, the dry unit weight is 14.71 kN/m^3, and the unconfined compression strength is 390.8 kN/m^2 when the secant modulus at failure point is the maximum value for 1% copolymer and 10% fly ash-added high plasticity clay.

With respect to the results of the all calculated moduli, it seems that the maximum values of these moduli are obtained at maximum unconfined compression strength (sample 1 for 1% copolymer and 10% fly ash-added high plasticity clay). On the other hand, when these moduli have the maximum value for 1% copolymer and 10% fly ash-added high plasticity clay, the water content is less than the optimum water content (w_{opt}=24.3%), and the dry unit weight is less than the maximum dry unit weight (γ_{dmax}=14.83 kN/m^3). Also, high plasticity clayey soil's strength and load-deformation properties are improved by reinforcing with copolymer fiber and stabilized with fly ash.

6.6.3 High Plasticity Clay Soil Mixture with 10% of Fly Ash and 1.25% of Copolymer

During the experimental program of this study, the amount of 1.25% copolymer and 10% fly ash mixed with high plasticity clay soil was used. The compaction and the unconfined compression tests were performed on the 1.25% copolymer and 10% fly ash mixed with high plasticity clay, and the outcomes of these experiments are illustrated in Table 6.56. With respect to data obtained from mentioned tests, it can be seen that the value of ω_{opt} and γ_{dmax} obtained at 23.70% and 14.77 kN/m^3, respectively.

Table 6.56 Results of experiments executed with CH+10% fly ash+1.25% copolymer

Sample No.	ω (%)	γ_d (kN/m^3)	q_u (kN/m^2)
1	16	13.57	164.4
2	21	14.77	369.3
3	25	14.77	263.1
4	28	14.26	161.5
5	31	13.77	91.8

The axial stress-axial strain curves of five different 1.25% copolymer and 10% fly ash-added high plasticity clay samples are shown in Figure 6.190. Besides, Figure 6.191 exhibits the tested 1.25% copolymer and 10% fly ash-added high plasticity clay sample, which has the highest value of the maximum unconfined compression strength. Therefore, according to data obtained from the unconfined compression test of the 1.25% copolymer and 10% fly ash-added high plasticity clay sample, it can be inferred that the maximum unconfined compression strength was obtained in the second sample, and it was obtained as 369.3 kN/m^2.

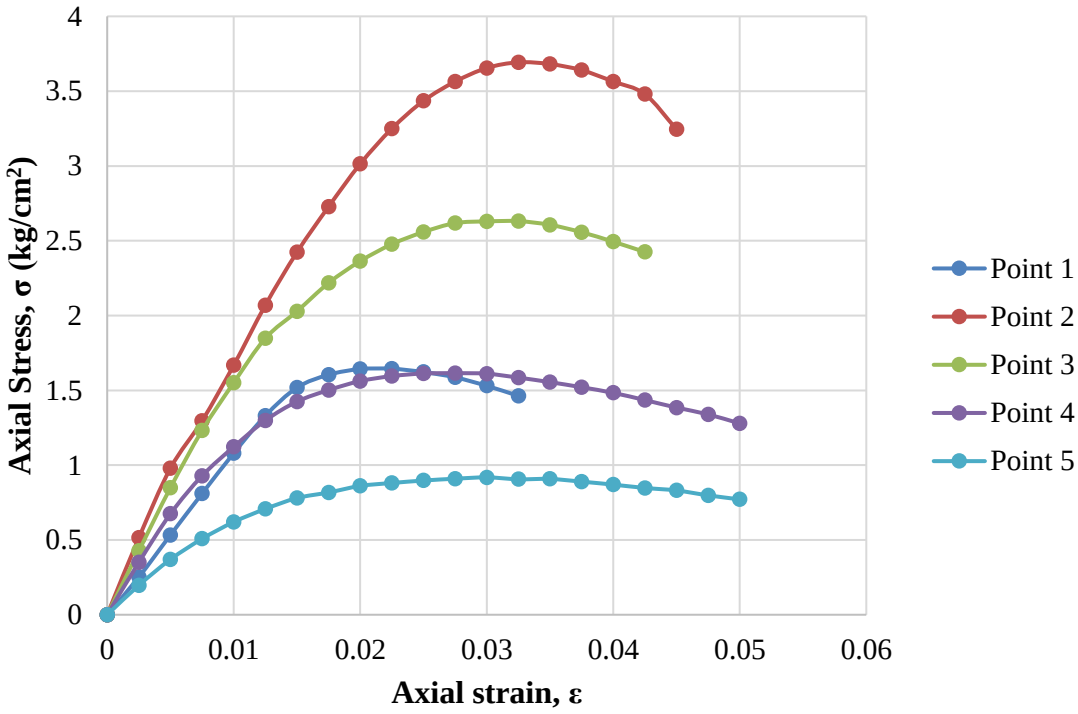

Figure 6.190 Results of unconfined compression tests of CH+10% fly ash+1.25% copolymer

Some of the required parameters were calculated to apply the modified and mentioned numerical model. Calculated engineering parameters to obtain soil moduli are given in Table 6.57.

It should be noted that the strain level of 1.25% copolymer and 10% fly ash-added high plasticity clay is classified as small strain (SS) because the maximum axial strain was determined in samples 4 and 5. The maximum axial strain was obtained as 0.05%. Thus, it can be concluded that nonlinear behaviour was observed for the tested 1.25% copolymer and 10% fly ash-added high plasticity clay samples.

Table 6.57 Calculated engineering parameters of CH+10% fly ash+1.25% copolymer

Sample No.	a (cm^2/kg)	b (cm^2/kg)	$(\sigma_1)_{ult}$ (kg/cm^2)	$(\sigma_1)_f$ (kg/cm^2)	R_f -	ε_f -	ε_{50} -
1	0.0062	0.2946	3.394	1.644	0.48	0.0225	0.0076
2	0.0046	0.1163	8.598	3.693	0.43	0.0325	0.0111
3	0.0045	0.2195	4.556	2.631	0.58	0.0325	0.0082
4	0.0052	0.3989	2.507	1.615	0.64	0.0275	0.0063
5	0.0093	0.7382	1.355	0.918	0.68	0.0300	0.0066

Initial tangent modulus (E_i), tangent modulus at 50% of maximum stress (E_{t50}), secant modulus at failure (E_{sf}), secant modulus at 50% of maximum stress (E_{s50}), and unconfined compression strength (q_u) of five different 1.25% copolymer and 10% fly ash -added high plasticity clay soil samples are given in Table 6.58.

Table 6.58 Soil moduli and unconfined compression strength of CH+10% fly ash+1.25% copolymer

Sample No.	E_i (kN/m^2)	E_{t50} (kN/m^2)	E_{sf} (kN/m^2)	E_{s50} (kN/m^2)	q_u (kN/m^2)
1	16129.0	9263.2	7306.7	10800.0	164.4
2	21739.1	13404.8	11363.1	16615.9	369.3
3	22222.2	11241.6	8095.4	16121.0	263.1
4	19230.8	8837.2	5872.7	12809.1	161.5
5	10752.7	4700.4	3060.0	6941.6	91.8

According to the data obtained, it can be concluded that the maximum modulus values are observed in the initial tangent modulus compared with other soil moduli in all five 1.25% copolymer and 10% fly ash-added high plasticity clay samples due to the initial slope of the stress-strain curve. In other words, the axial stress increases up to a certain point very sharply. Then, this sharp increasing trend suddenly starts to slow down, and during this slowing trend, the axial strain increases rapidly.

Figure 6.191 Peak point of CH+10% fly ash+1.25% copolymer

In addition, transformed hyperbolic stress-strain curves for five different 1.25% copolymer and 10% fly ash-added high plasticity clay samples are illustrated in Figure 6.192.

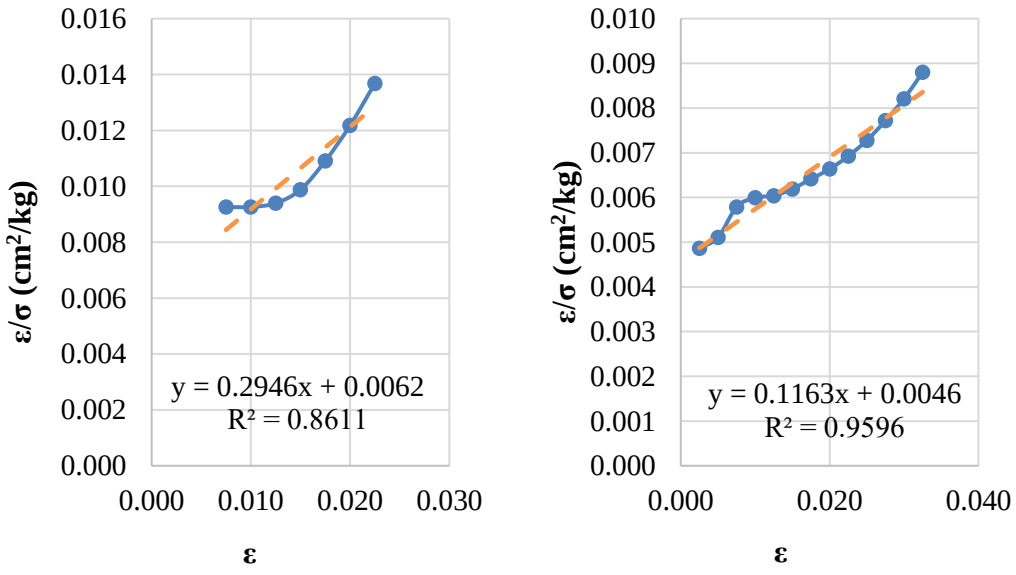

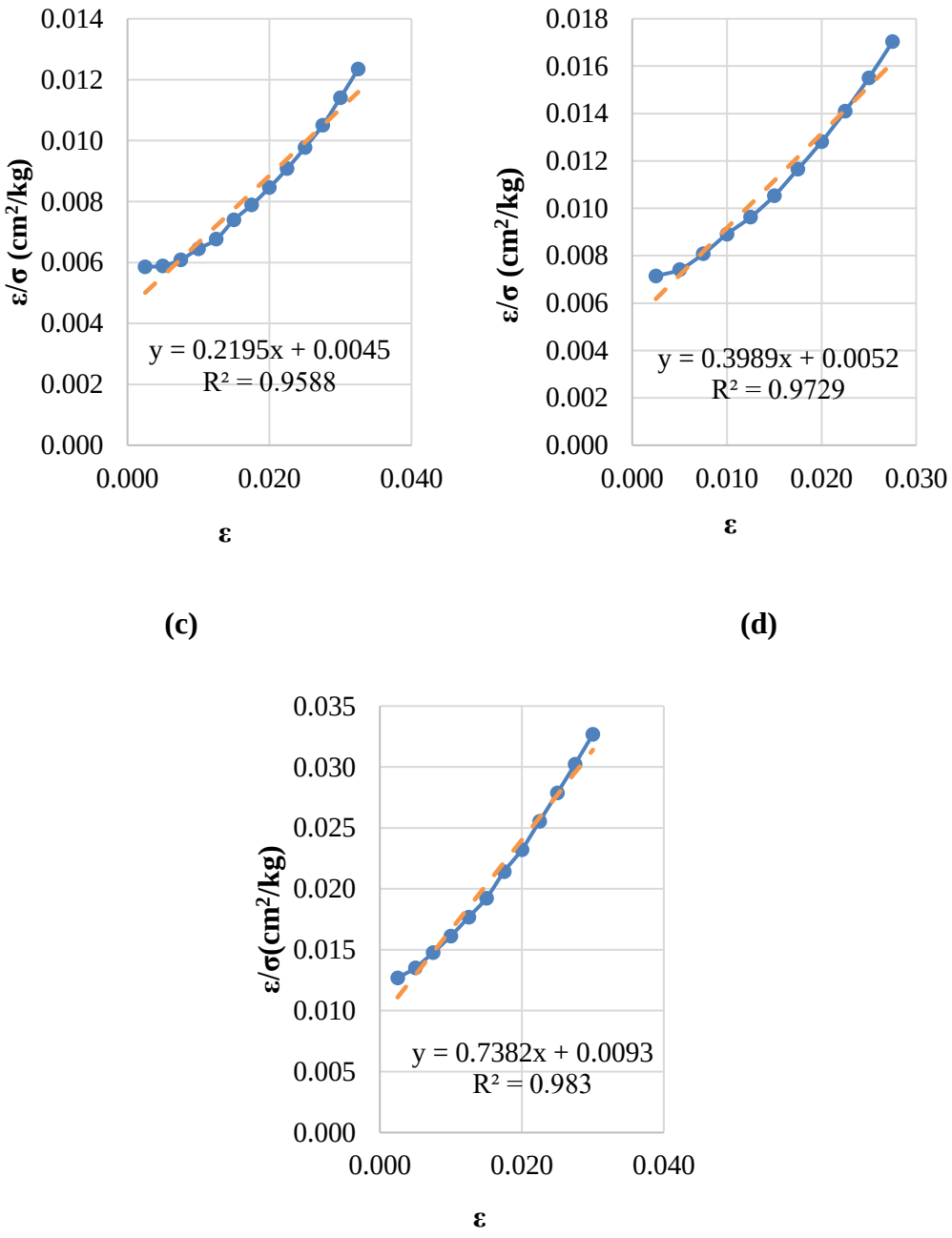

Figure 6.192 Transformed hyperbolic stress-strain curves for (a) sample 1, (b) sample 2, (c) sample 3, (d) sample 4, and (e) sample 5 (CH+10% Fly Ash+1.25% Copolymer)

It was found that low and high values of axial strains in samples 1, 2, and 3 are not precisely hyperbolic, as shown in Figures 6.192 (a, b, and c). In other words, these points can not be fitted in a straight line. However, it was possible to estimate the actual

stress-strain curves by a hyperbola. Thus, it is found to have a reasonable degree of accuracy. On the other hand, the transformed hyperbolic stress-strain curve in samples 4 and 5 is hyperbolic, as shown in Figures 6.192 (d and e). In other words, these points can be best-fitted in a straight line.

The relationship between the secant modulus at 50% of maximum stress (E_{s50}) and the initial tangent modulus (E_i) of the designated mixture of high plasticity clay samples (1.25% copolymer and 10% fly ash-added CH) is shown in Figure 6.193.

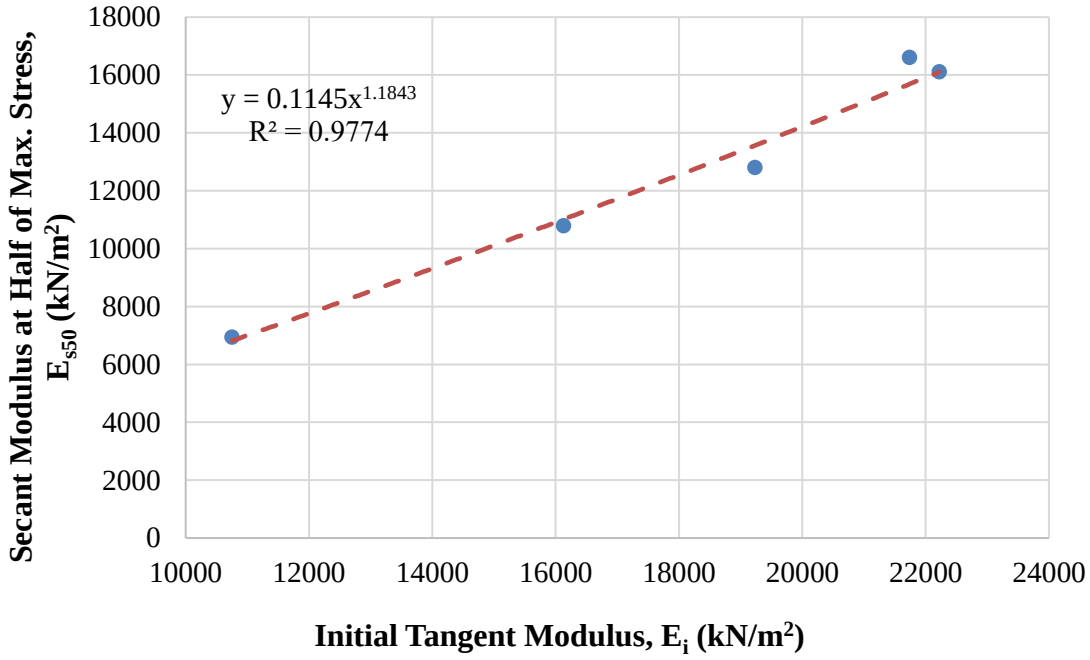

Figure 6.193 Relationship between secant modulus at 50% of maximum stress and initial tangent modulus (CH+10% Fly Ash+1.25% Copolymer)

According to the data, it can be inferred that these soil moduli refer to the hardening of 1.25% copolymer and 10% fly ash-added high plasticity clay samples. Thus, the initial tangent modulus increases with the increasing secant modulus at 50% of maximum stress. Furthermore, it was best suited for estimating these soil moduli by a power model.

The relationship between the secant modulus at failure (E_{sf}) and the tangent modulus at 50% of maximum stress (E_{t50}) of the designated mixture of high plasticity clay samples (1.25% copolymer and 10% fly ash-added CH) is shown in Figure 6.194.

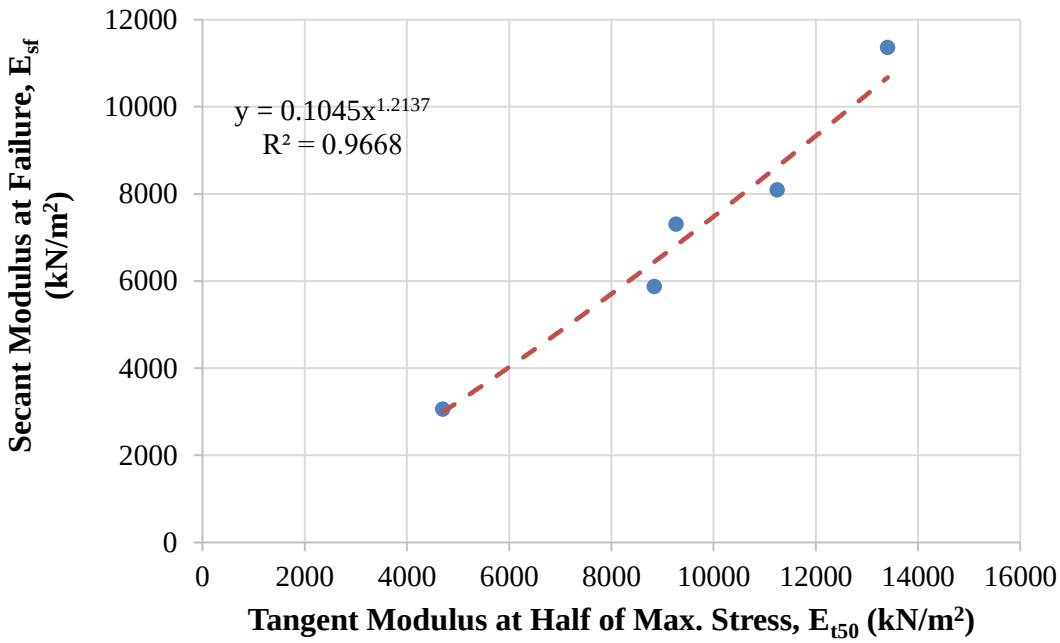

Figure 6.194 Relationship between secant modulus at failure point and tangent modulus at 50% of maximum stress (CH+10% Fly Ash +1.25% Copolymer)

The tangent modulus at 50% of maximum stress increases with the increasing secant modulus at failure. Thus, it was best suited for estimating these soil moduli by a power model.

Furthermore, the relationship between the initial tangent modulus (E_i) and unconfined compression strength of the designated mixture of high plasticity clay samples (1.25% copolymer and 10% fly ash-added CH) is shown in Figure 6.195.

According to data, the maximum initial tangent modulus is obtained in sample 3 as 22222.2 kN/m^2 for 1.25% copolymer and 10% fly ash-added high plasticity clay. It should be noted that the water content is 25%, the dry unit weight is 14.77 kN/m^3, and the unconfined compression strength is 263.1 kN/m^2 when the initial tangent modulus is the maximum value for 1.25% copolymer and 10% fly ash-added high plasticity clay.

With respect to the results, it seems that the maximum values of the initial tangent modulus are not obtained at maximum unconfined compression strength (sample 2 for 1.25% copolymer and 10% fly ash-added high plasticity clay) since the beginning of the stress-strain curve of sample 3 has rapidly increased in axial stress. On the other hand, when the calculated initial tangent modulus has the maximum value

for 1.25% copolymer and 10% fly ash-added high plasticity clay, the water content is not equal to the optimum water content (w_{opt}=23.7%), and the dry unit weight is equal to the maximum dry unit weight (γ_{dmax}=14.77 kN/m^3).

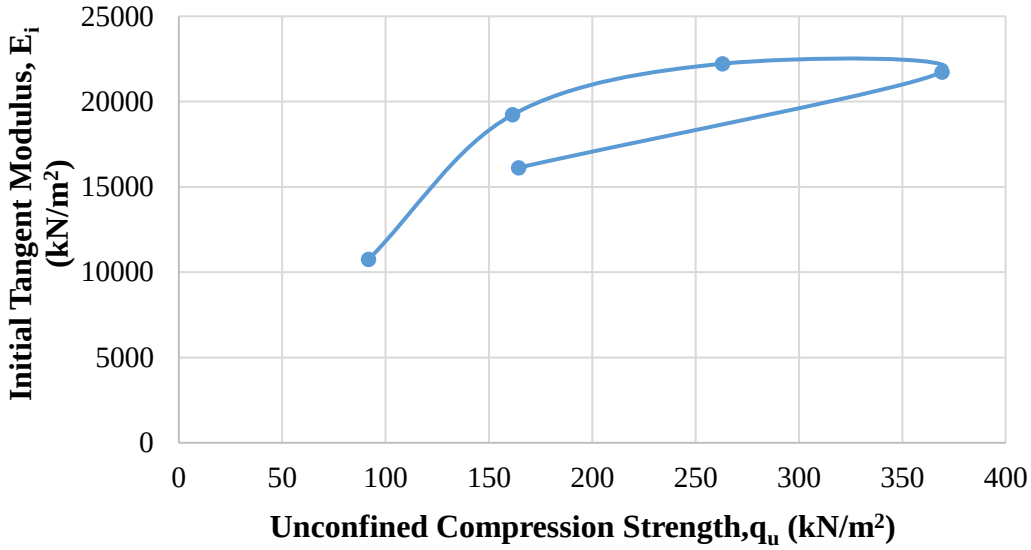

Figure 6.195 Relationship between initial tangent modulus and unconfined compression strength (CH+10% Fly Ash +1.25% Copolymer)

The relationship between secant modulus at 50% of maximum stress (E_{s50}) and unconfined compression strength of the designated mixture of high plasticity clay samples (1.25% copolymer and 10% fly ash-added CH) is shown in Figure 6.196.

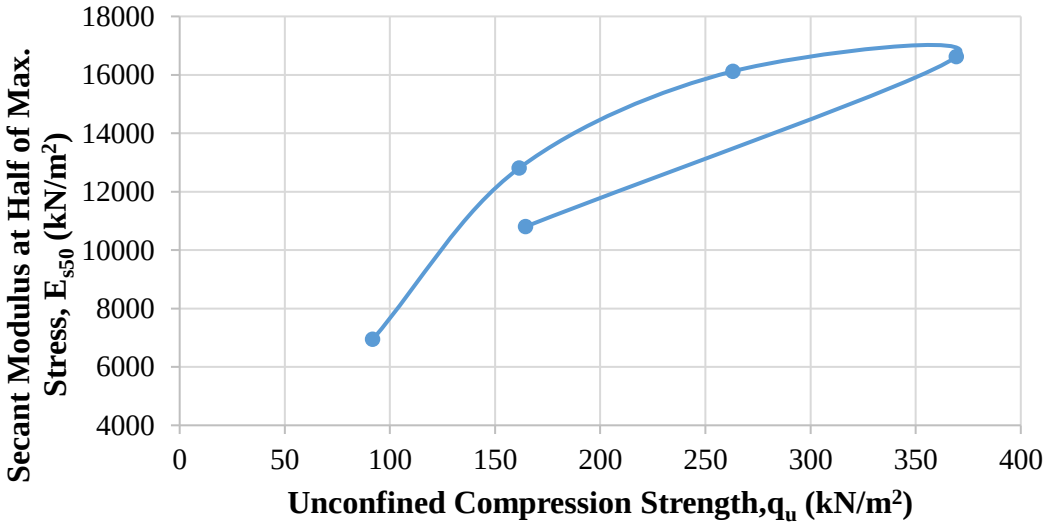

Figure 6.196 Relationship between secant modulus at 50% of maximum stress and unconfined compression strength (CH+10% Fly Ash +1.25% Copolymer)

The maximum secant modulus at 50% of maximum stress is obtained in sample 2 as 16615.9 kN/m^2 for 1.25% copolymer and 10% fly ash-added high plasticity clay. It should be noted that the water content is 21%, the dry unit weight is 14.77 kN/m^3, and the unconfined compression strength is 369.3 kN/m^2 when the secant modulus at 50% of maximum stress has the maximum value of 1.25% copolymer and 10% fly ash-added high plasticity clay.

On the other hand, the relationship between tangent modulus at 50% of maximum stress (E_{t50}) and unconfined compression strength of the designated mixture of high plasticity clay samples (1.25% copolymer and 10% fly ash-added CH) is shown in Figure 6.197.

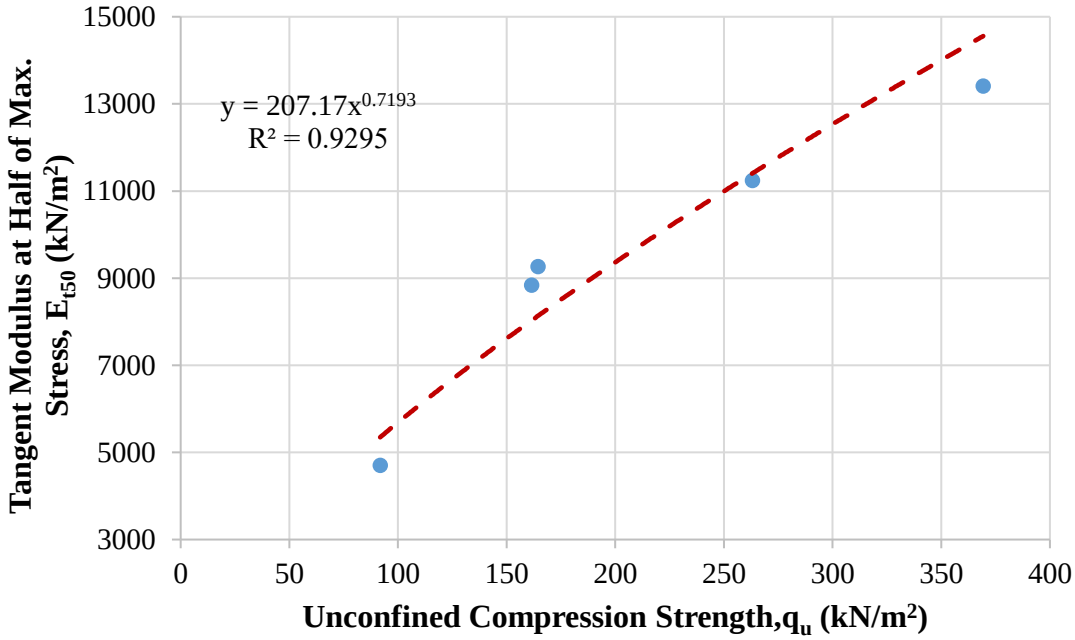

Figure 6.197 Relationship between tangent modulus at 50% of maximum stress and unconfined compression strength (CH+10% Fly Ash +1.25% Copolymer)

The maximum tangent modulus at 50% of maximum stress is obtained in sample 2 as 13404.8 kN/m^2 for 1.25% copolymer and 10% fly ash-added high plasticity clay. It should be noted that the water content is 21%, the dry unit weight is 14.77 kN/m^3, and the unconfined compression strength is 369.3 kN/m^2 when the tangent modulus at 50% of maximum stress is the maximum value for the 1.25% copolymer and 10% fly ash-added high plasticity clay.

In addition, the relationship between secant modulus at failure point (E_{sf}) and unconfined compression strength of the designated mixture of high plasticity clay samples (1.25% copolymer and 10% fly ash-added CH) is shown in Figure 6.198.

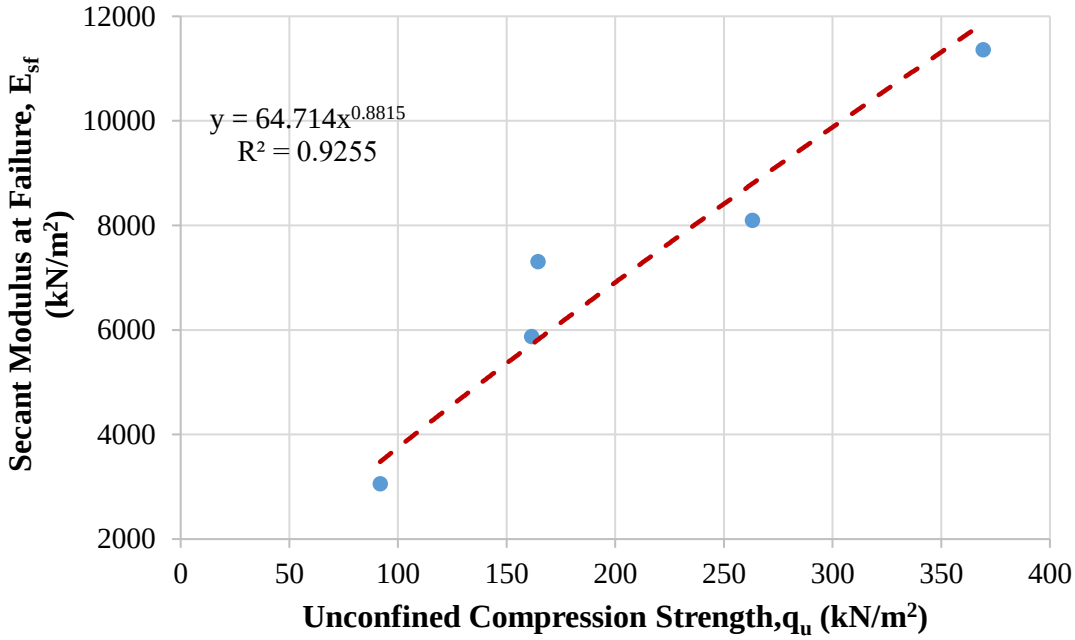

Figure 6.198 Relationship between secant modulus at failure point and unconfined compression strength (CH+10% Fly Ash +1.25% Copolymer)

It is obvious that the maximum secant modulus at failure point is obtained in sample 2 as 11363.1 kN/m^2 for 1.25% copolymer and 10% fly ash-added high plasticity clay. It should be noted that the water content is 21%, the dry unit weight is 14.77 kN/m^3, and the unconfined compression strength is 369.3 kN/m^2 when the secant modulus at failure point is the maximum value for 1.25% copolymer and 10% fly ash-added high plasticity clay.

With respect to the results of the secant modulus at 50% of maximum stress, tangent modulus at 50% of maximum stress, and secant modulus at failure point, it seems that the maximum values are obtained at maximum unconfined compression strength (sample 2 for the 1.25% copolymer and 10% fly ash-added high plasticity clay). However, the value of water content is less than the optimum water content (w_{opt}=23.7%), and the dry unit weight is equal to the maximum dry unit weight (γ_{dmax}=14.77 kN/m^3). Also, high plasticity clayey soil's strength and load-deformation

properties are improved by reinforcing with copolymer fiber and stabilized with fly ash.

6.6.4 Comparison of Three Different Fly Ash-Copolymer Mixtures with High Plasticity Clay Soil

Three different amounts of copolymer (0.75%, 1%, and 1.25%) mixed with 10% fly ash-added high plasticity clay soils were prepared to analyze deformation moduli. The soil moduli of the mentioned amounts of the copolymer and 10% fly ash-added high plasticity clay mixtures are compared with the plain high plasticity clay. Figure 6.199 exhibits the relationship between the maximum initial tangent modulus and different copolymer content of 10% fly ash-added CH mixtures.

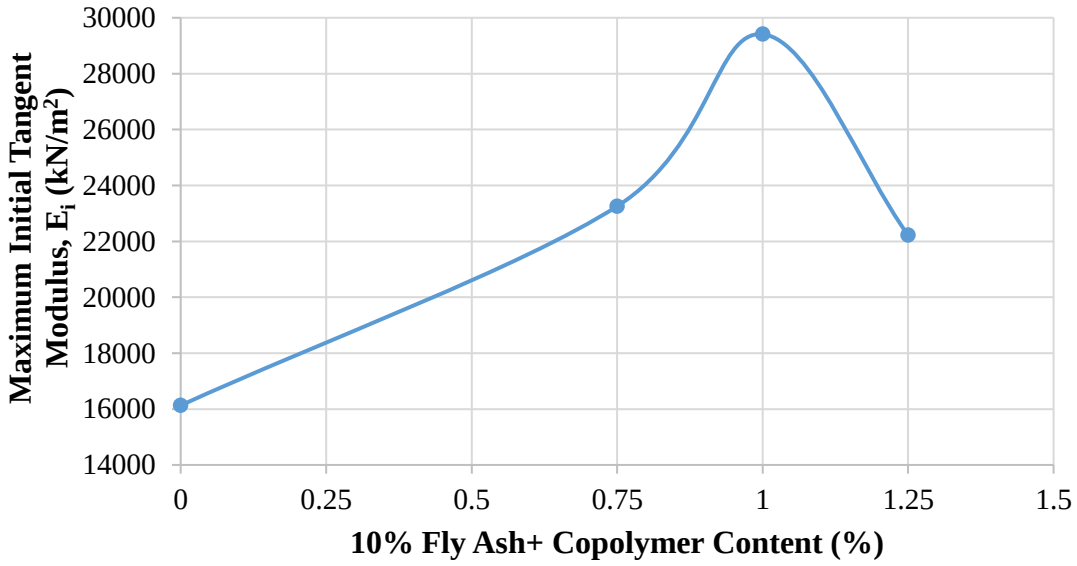

Figure 6.199 Relationship between maximum initial tangent modulus and different copolymer contents of 10% fly ash-added CH mixture

After analyzing all initial tangent modulus of amounts of the copolymer and 10% fly ash-added high plasticity clay mixtures, and comparing them in a graph, it can be seen that the maximum initial tangent modulus was obtained in the mixture with 1% of copolymer. In addition, the initial tangent modulus increases up to 82% in the mixture with 1% of copolymer. In other words, the optimum value of the initial tangent modulus was determined in the mixture with 1% copolymer and 10% fly ash-added high plasticity clay.

As the next step, all secant modulus at 50% of maximum stress of copolymer and 10% fly ash-added high plasticity clay mixtures were gathered and compared in Figure 6.200.

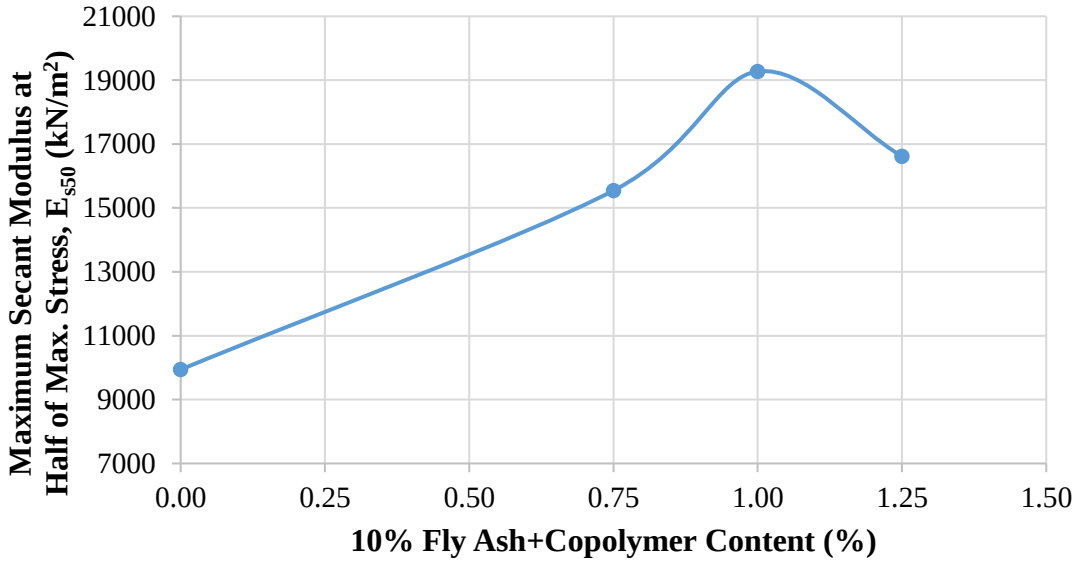

Figure 6.200 Relationship between maximum secant modulus at 50% of maximum stress and different copolymer contents of 10% fly ash-added CH mixture

It can be seen that the maximum secant modulus at 50% of maximum stress was obtained in the mixture with 1% of copolymer. In addition, the secant modulus at 50% of maximum stress increases up to 94% for the mixture with 1% of copolymer. In other words, the optimum value of the secant modulus at 50% of maximum stress was determined in the mixture with 1% copolymer and 10% fly ash-added high plasticity clay.

Furthermore, all tangent modulus at 50% of maximum stress of copolymer and 10% fly ash-added high plasticity clay mixtures were gathered and compared in Figure 6.201.

It can be seen that the maximum tangent modulus at 50% of maximum stress was obtained in the mixture with 1% copolymer. In addition, the tangent modulus at 50% of maximum stress increases up to 126% in the mixture with 1% of copolymer. In other words, the optimum value of the tangent modulus at 50% of maximum stress was determined in the mixture with 1% of copolymer and 10% fly ash-added high plasticity clay.

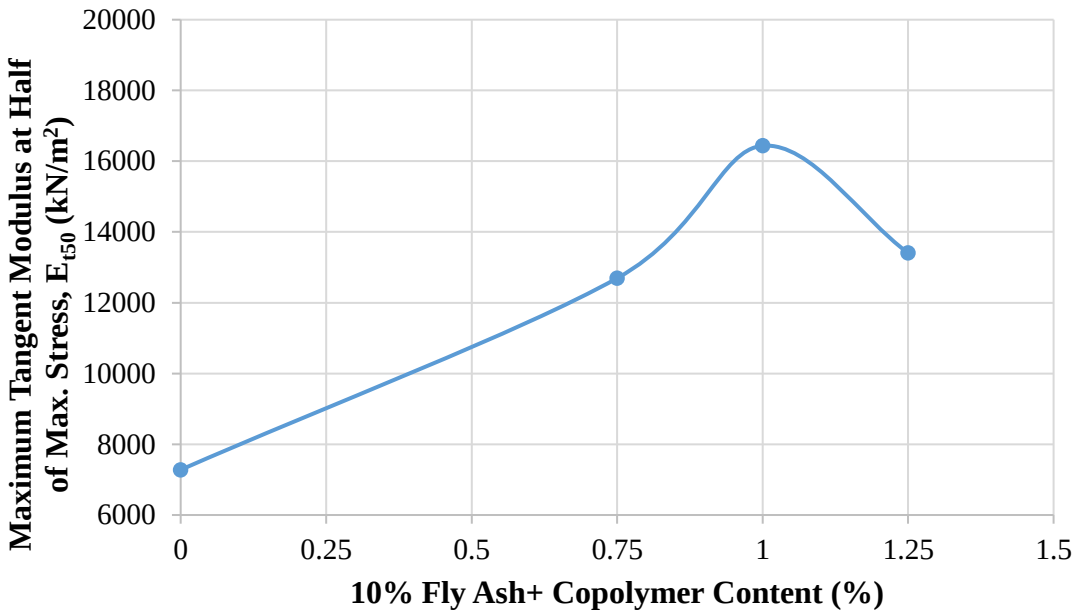

Figure 6.201 Relationship between maximum tangent modulus at 50% of maximum stress and different copolymer contents of 10% fly ash-added CH mixture

Moreover, Figure 6.202 exhibits the relationship between the maximum secant modulus at failure point and different copolymer content of 10% fly ash-added CH mixtures.

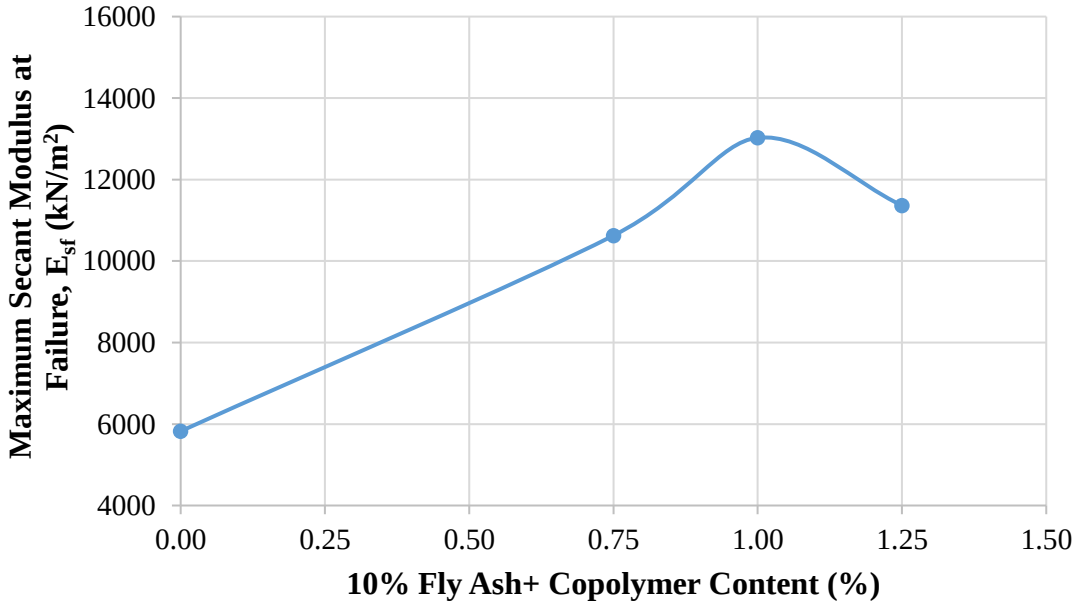

Figure 6.202 Relationship between maximum secant modulus at failure point and different copolymer contents of 10% fly ash-added CH mixture

After gathering all secant modulus at failure point of amounts of polypropylene and 10% fly ash-added high plasticity clay mixtures, and comparing them in a graph, it can be seen that the maximum secant modulus at failure point was obtained in the mixture with 1% of copolymer. In addition, the secant modulus at failure point increases up to 124% in the mixture with 1% of copolymer. In other words, the optimum value of the secant modulus at failure point was determined in the mixture with 1% copolymer and 10% fly ash-added high plasticity clay.

CHAPTER 7

7. CONCLUSIONS AND RECOMMENDATIONS

Construction of highway embankments, shallow foundations, and other earth structures requires sustainable solutions for the engineering behavior of soils. The primary problem of construction is that maintained the inadequacy of subgrade strength and cost efficiency of selected implementation. Therefore, alternative materials and applicable techniques should be investigated to develop improvement of subgrade soils. On the other hand, it is obvious that the engineering properties of clayey soils should be studied to examine how their deficiency can be limited within the scope of more complex behavior than gravels, sands, and silty soils. The clayey soils can be improved by adding soil-stabilized engineering materials to available materials. Hence, examining the deformation modulus of clayey soils allows gathering information about its deformation features, especially for cases where alternative materials are used.

The first chapter of the research has briefly described why clayey soil needs soil stabilization and which type of stabilization techniques and alternative materials can be an option for improving clayey soil. In addition, it was described how clayey soil improvement could be investigated during the experimental program from different soil moduli aspects.

During the second part of the research, the stress and strain behavior of cohesive soils, which included stress and strain states, yield surface, and effective and total stress mechanism of clayey soil, has been discussed. It should be noted that soil strength is a significant factor in the safety conditions of almost all geotechnical structures within the scope of estimating the bearing capacity of shallow foundations and piles, stress-strain characteristics of soil, stability of dams and embankments, and

lateral earth pressure on the retaining walls. Thus, the factors influencing the shear strength of cohesive soils have been described in detail. In addition, as a response to applied loading in the cohesive soils, it causes deformation in the direction of applied loading. Hence, the methods that have investigated the deformation characteristics and the strain levels of the soil through the modulus of deformation have been discussed in this chapter. Furthermore, the definition of types of soil moduli and their determination methods have also been represented, especially for application in solving specific soil mechanics problems.

In the third part of the research, several common constitutive models, which analyze the stress-strain curves using mathematical functions, fitting methods, nonlinear elasticity, and plasticity theories, have been discussed. The clayey soils exhibit the nonlinear behavior assessed with the stiffness and strength of the soil. Thus, it should be noted that setting up a numerical model of physical quantities in the clayey soil provides the estimation of deformation features, especially for cases where alternative materials are used in order to stabilize the soil. It is found that the Duncan-Chang hyperbolic model is the most common and widely used model used to determine nonlinear characteristics of clayey soils for revising under complicated stress states. Thus, the method of determination in initial tangent modulus and tangent modulus have been described in this part.

As the fourth part of the research, aims and various types of soil stabilization have been discussed. In addition, the advantages and disadvantages of globally common methods have been described. Lime and portland cement, manufactured products, are commonly used in civil engineering studies. Fly ash which is a product of the burning coal at electric power stations and recycled material used to stabilize clayey soils. Also, these alternative materials provide cementitious stabilization by adding in available soil. Other additives, such as shredded tire rubbers, natural and synthetic fibers, lead to the improvement by mixing with clayey soils.

During the fifth part of the research, performed laboratory tests and used materials, and the modeling procedure of experimental results were discussed. Laboratory tests are essential steps to determine the engineering properties and mechanical behavior of clayey soil and alternative engineering materials. Sieve and hydrometer analyses, Atterberg limits by performing liquid and plastic limit tests, and the unconfined compression tests were mentioned in this part. The unconfined compression test was used to determine the soil moduli by the proposed modified

constitutive model for investigating the amount of improvement in the stabilized clays by using alternative engineering materials, such as fly ash, polypropylene, and copolymer fibers. The chemical and physical properties of fly ash and the physical properties of polypropylene and copolymer fibers were described in detail. As a next step, the tangent modulus formulation can be obtained using derivation in the Duncan-Chang model. In other words, the modification of the Duncan-Chang model by utilizing the derivation based on the unconfined compression test conditions was achieved. The secant modulus at failure and the secant modulus at half of the maximum stress can be obtained by the expressions of the initial tangent modulus and tangent modulus at half of the maximum stress due to the unconfined compression test conditions. Hence, suggested and modified new equations of soil moduli have been mentioned in this part.

In the last part of the research, high plasticity clay soil (CH) was mixed with fly ash, polypropylene, and copolymer fibers. The soil was mixed with 5%, 10%, and 15% of class C fly ash compared to the whole mixture weight. As a second alternative additive, polypropylene fiber was used in the amount of weights 0.25%, 0.5%, 0.75%, and 1% polypropylene fiber, which stabilizes clayey soil. The copolymer with 0.5%, 0.75%, 1%, 1.25%, and 1.5% amounts added to the high plasticity clay soil. It was decided that the fly ash and each fiber were mixed to achieve better soil moduli results. The high plasticity clay was mixed with 10% of fly ash - 0.25%, 0.5%, and 0.75% of polypropylene, and with 10% of fly ash - 0.75%, 1%, and 1.25% of the copolymer. It was decided to choose a constant value of fly ash and add each fiber step by step to get better soil moduli compared with adding polypropylene and copolymer alone.

According to the results of soil moduli of plain high plasticity clay, it is concluded that the initial tangent modulus was obtained in sample 4 as 16129 kN/m^2. The maximum secant modulus at 50% of maximum stress was obtained in sample 4 as 9939.1 kN/m^2. Then, the maximum tangent modulus at 50% of maximum stress and the maximum secant modulus at failure were found in sample 3 as 7277.1 kN/m^2 and 5823.3 kN/m^2, respectively. All mentioned alternative materials as an additive mixed with plain high plasticity clay, and it was found that the best improvement result of initial tangent modulus was investigated by adding 15% of fly ash and it is equal to the 30303 kN/m^2, which showed 188% of increase compared with plain high plasticity clay. As the next analyzed soil moduli, it was found that the best improvement result of secant modulus at 50% of maximum stress was investigated by adding 10% of fly

ash, and it is equal to the 25617.8 kN/m^2, which showed 258% of increase compared with plain high plasticity clay. It should be noted that the best improvement result of tangent modulus at 50% of maximum stress was investigated by adding 10% of fly ash, and it is equal to the 21659.6 kN/m^2, which showed a 298% increase compared with plain high plasticity clay. As of the last determined soil moduli, the high plasticity clay soil mixture achieved better results of secant modulus at failure when mixed with 10% of fly ash and 0.75% of polypropylene, which reached 14706.7 kN/m^2. Also, it reached to 253% increase of secant modulus at failure compared with plain high plasticity clay.

Further studies can investigate especially large-scale tests in order to better understand the behavior of fiber-reinforced and chemically stabilized soils. In addition, further studies are essential to clarify the effect of prior treatment of fibers and the strength behavior of composite in the long term under more severe conditions. The impact of drainage on the stabilized soil's effective strength can be of particular interest, especially during large-scale laboratory test conditions. Furthermore, using the large volume of recycled waste materials and fibers can be examined to improve engineering properties by comparing plain soils. In further studies, the deformation modulus of soils can be analyzed by modifying other constitutive models. It is suggested that soil moduli can be studied step by step according to the percentages of strains in the test results.

REFERENCES

AASHTO M 295. *Standard Specification for Coal Fly Ash and Raw or Calcined Natural Pozzolan for Use in Concrete.* AASHTO.

Adam, T. H. (1988). In MSU seminar: Fly ash. *Marketing of fly ash concrete*. Michigan State University.

Ahmad, Z., Saman, H., & Tahir, P. (2010). Oil Palm Trunk Fiber as a Bio-Waste Resource for Concrete Reinforcement. *International Journal of Mechanical and Materials Engineering (IJMME)*(Vol.5), 199-207.

Anderson, D., & Stokoe, K. (1978). Shear Modulus: A Time-Dependent Soil Property. *Geology*. doi:10.1520/STP35672S

Anochie-Boateng, J. (2007). Advanced Testing and Characterization of Transportation. *Doctor o f Philosophy*. Urbana,, Illinois, USA: ProQuest LLC. UMI Number: 3301099

Araz, I., & Fitsum, T. (2011). Analysis of Deformations in Soft Clay Due to Unloading. *Master's Thesis*. Chalmers University of Technology, Sweden.

ASTM C1116-03. *Standard Specification for Fiber-Reinforced Concrete and Shotcrete.* American Society for Testing and Materials. doi:10.1520/C1116-03

ASTM C618-19. *"Standard Specification for Coal Fly Ash and Raw or Calcined Natural Pozzolan for Use in Concrete".* American Society for Testing and Materials.

ASTM D1633-00. *Standard Test Method for Compressive Strength of Molded Soil-Cement Cylinders.* USA: American Society for Testing and Materials.

ASTM D1883-21. *Standard Test Method for California Bearing Ratio (CBR) of Laboratory-Compacted Soils.* American Society for Testing and Materials.

ASTM D2166-06. *Standard Test Method For Unconfined Compressive Strength Of Cohesive Soil.* American Society for Testing and Materials.

ASTM D2850-15. *Standard Test Method For Unconsolidated-Undrained Triaxial Compression Test On Cohesive Soils.* American Society for Testing and Materials.

ASTM D4318-10. *"Standard Test Methods for Liquid Limit, Plastic Limit, and Plasticity Index of Soils".* USA: American Society for Testing and Materials.

ASTM D559-03. *Standard Test Methods for Wetting and Drying Compacted Soil-Cement Mixtures.* USA: American Society for Testing and Materials.

ASTM D560-03. *Standard Test Methods for Freezing and Thawing Compacted Soil-Cement Mixtures.* USA: American Society for Testing and Materials.

Atkinson, J. (1993). *An Introduction to the Mechanics of Soils and Foundations.* McGraw-Hill Book Company.

Atkinson, J., & Sallfors, G. (1991). Experimental determination of soil properties. *In: Proceedings of the 10th ECSMFE(vol. 3)*, 915–956. Florence.

Babu, S., & Vasudevan, K. (2008). Strength and stiffness response of coir fiber reinforced tropical soil. 571–7.

Bejarano, M. (1999). Subgrade Soil Evaluation for the Design of Airport Flexible Pavements. *Doctor of Philosophy*. Illinois: Bell & Howell Information and Learning Company. UMI Number 9952961

Bejarano, M., & Thompson, M. (1999, September). Subgrade Soil Evaluation for the Design of Airport Flexible Pavements. *DOT 95-C-001*. Federal Aviation Administration.

Bell, F. (2000). Engineering Treatment of Soils. London, UK: Taylor & Francis group.

Bishop, A., Alpan, I., Blight, G., & Donald, I. (1960). Factors controlling the strength of partially saturated cohesive soils. *In Research Conference on Shear Strength of Cohesive Soils*, 503–532. American Society of Civil Engineers.

Bosscher, P., Edil, T., & Kuraoka, S. (1997). Design of Highway Embankments Using Tire Chips. *Journal of Geotechnical and Geoenvironmental Engineering*(123), 295-304.

Briaud, J. L. (2013). *Geotechnical Engineering: Unsaturated and Saturated Soils.* New Jersey, USA: John Wiley & Sons, Inc.

Brinkgreve, R. (2005). Selection of Soil Models and Parameters for Geotechnical Engineering Application. (J. A. Yamamuro, & V. N. Kaliakin) *Soil Constitutive Models*, 69-98.

Budhu, M. (2011). *Soil Mechanics and Foundation* (3rd Edition b.). USA: John Wiley& Sons, INC.

Calvello, M. (2002, December). Inverse Analysis o f a Supported Excavation through Chicago Glacial Clays. *Doctor of Philosophy*. Illinois, Northwestern University.

Cho, W. (2007, June). Recent Stress History Effects on Compressible Chicago Glacial Clay. *Doctor of Philosophy*. Illınoıs: ProQuest LLC. UMI Number: 3298150

Clough, R., & Woodward, R. (tarih yok). Analysis of Embankment Stresses and Deformations. *Soil Mechanics & Foundation Division*(93), 529-549. doi:10.1061/JSFEAQ.0001005

Das, B. (1997). *Soil Mechanics Laboratory Manual.* UK: Oxford University Press.

Das, B. M. (2008). *Advanced Soil Mechanics, 4th Edition.* New York, USA: Taylor & Francis.

Das, B. M. (2010). *Principles of Geotechnical Engineering, 7th Edition.* Stamford, USA: Cengage Learning.

Das, B., & Ramana, G. (2011). *Principle of Soil Dynamics.* Stamford, USA: Cengage Learning.

Desai, C. S., & Christian, J. T. (1977). *Numerical Methods in Geotechnical Engineering.* USA: Mc.Graw-Hill, Inc.

Desai, C., & Christan, J. (1977). *Numerical Methods in Geotechnical Engineering.* McGraw-Hill.

Draper, N., & Smith, H. (1998). *Applied Regression Analysis* (3th Edition b.). New York: Wiley. https://doi.org/10.1002/9781118625590

Duncan, J. M., & Chang, C. Y. (1970, September). Nonlinear Analysis of Stress and Strain in Soils. *Journal of the Soil Mechanics and Foundations Division*, 1630-1653.

Duncan, J., & Dunlop, P. (1970, September). Closure to "Slopes in Stiff-Fissured Clays and Shales". *Journal of the Soil Mechanics and Foundations Division*(Vol. 96, Issue 5). doi:10.1061/JSFEAQ.0002028

Duncan, J., Monismith, C., & Wilson, E. (tarih yok). Finite Element Analyses of Pavements. *University of California*. Berkeley: Committee on Mechanics of Earth Masses and Layered Systems and presented at the 47th Annual Meeting.

Duncan, J., Wrigth, S., & Brandon, T. (2014). *Soil Strength and Slope Stability* (Second Edition b.). New Jersey: John Wiley & Sons, Inc.

Erol, B. (2008). Atık Maddelerin Yol İnşaatlarında Temel Malzemesi Olarak Kullanımı. *İstanbul Teknik Üniversitesi, Fen Bilimleri Enstitüsü, Yüksek Lisans Tezi*. İstanbul.

Etminan, E. (2012). Soft Soil Stabilization Using Fly ash, Polypropylene, Copolymer and VHP. *Istanbul Technical University, Graduate School od Science Engineering and Technology, M.Sc. Thesis*. Istanbul.

Filho, R., Joseph, K., Gravami, K., & England, G. (1999). The use of sisal fibre as reinforcement in cement based composites. *Revista Brasileira de Engenharia Agrícola e Ambiental*(3(2)), 245-256. doi:10.1590/1807-1929/agriambi.v3n2p245-256

Ghosh, A., & Dey, U. (2009). Bearing Ratio of Reinforced Fly Ash Overlying Soft Soil and Deformation Modulus of Fly Ash. *Geotextiles and Geomembranes*(27), 313-320. doi:10.1016/j.geotexmem.2008.12.002

Ghosh, A., & Subbarao, C. (2012). Deformation Modulus of Fly Ash Modified with Lime and Gypsum. *Geotech Geol Eng*(30), 299-311. doi:10.1007/s10706-011-9468-z

Gupta, R. C. (2000, February). An Approach for Estimating Deformation Moduli from Self-Boring Pressuremeter Test Data. *Soils and Foundations*(40), 23-33.

Halstead, G. (2011). Cement-Modified Soil for Long Lasting Pavements. *Annual Conference of the Transportation Association of Canada*. Edmonton, Alberta.

Hejazi, S. M., Sheikhzadeh, M., Abtahi, S. M., & Zadhoush, A. (2012). A simple review of soil reinforcement by using natural and synthetic fibers. *Construction and Building Materials*(30), 100-116.

Helmuth, R. (1987). Fly Ash in Cement and Concrete. *Portland Cement Association Publications*.

Hicher, P., & Shao, J. (2008). *Constitutive Modeling of Soils and Rock.* USA: John Wiley & Sons, Inc.

Holman, T. (2005, June). Small Strain Behavior of Compressible Chicago Glacial Clay. *Doctor of Philosophy*. Illınoıs: ProQuest LLC. doi:UMI Number: 3177732

Huang, H., Huang, M., & Ding, J. (2018, May). Calculation of Tangent Modulus of Soils under Different Stress Paths. *Mathematical Problems in Engineering*. doi:10.1155/2018/1916761

Ibanez, J. (2007). Environmental Chemistry: Fundamentals. Springer publications.

Ishihara, K. (1996/7). Soil behaviour in earthquake geotechnics. *(Vol.257)*, 338. Clarendon press.

Jamiolkowski, M., Ladd, C., Germaine, J., & Lancelotta, R. (CA(1985)). New developments in field and laboratory testing of soils. *vol. 1* (s. 57-153). San Fransisco: A.A. Balkema.

Janbu, N. (1963). The Resistance Concept Applied to Deformations of Soils. 191-196. https://www.issmge.org/publications/online-library

Janbu, N. (1963). The Resistance Concept Applied to Deformations of Soils. International Society for Soil Mechanics and Geotechnical Engineering.

Khedari, J., Watsanasathaporn, P., & Hirunlabh, J. (2005). Development of fiber-based soil–cement block with low thermal conductivity. *Cement Concrete Composision*, 111–6.

Kowaski, T., & Starry, D. (2007). Modern Soil Stabilization Techniques. *Annual Conference of the Transportation Association of Canada*.

Kumar, A., Walia, B., & Bajaj, A. (2007). Influence of Fly Ash, Lime and Polyester Fibers on Compaction and Strength Properties of Expansive Soil. *Journal of Materials in Civil Engineering*.

Labuz, J., & Zang, A. (2012, July). Mohr–Coulomb Failure Criterion. *Rock Mech Rock Eng* (45), 975–979. doi:10.1007/s00603-012-0281-7

Ladd , C., & Lambe , R. (1963). The strength of undisturbed clay determined from undrained tests. *(STP 361)*, 342–371. Ottawa: Proceedings of the ASTM-NRC Symposium on Shear Testing of Soils.

Little, D. (1995). Handbook for Stabilization of Pavement Subgrades and Base Courses with Lime. *The National Lime Association*.

Masin, D., & Josef, R. Small strain stiffness anisotropy of natural sedimentary clays: Review and a model. *Acta Geotechnica*(9(2)). doi:10.1007/s11440-013-0271-2

Mcgown, A., Andrawes, Z., & Hasani , M. (1978). Effect of inclusion properties on the behavior of sand Geotechnique.

Mesri, G. (1989). A re-evaluation of $s_{u(mob)} = 0.22\ \sigma'p$ using laboratory shear tests. *Canadian Geotechnical Journal*(26(1)), 162–164.

Moghal, A. A., Obaid, A. A., & Al-Refeai, T. O. (2014, May 5). Effect of Accelerated Loading on the Compressibility Characteristics of Lime-Treated Semiarid

Soils. *Journal of Materials in Civil Engineering*(26). doi:10.1061/(ASCE)MT.1943-5533.0000882

O'Rourke, T., & Crespo, E. (1988, October 10). Geotechnical Properties of Cemented Volcanic Soil. *Journal of Geotechnical Engineering*(114). doi:10.1061/(ASCE)0733-9410(1988)114:10(1126)

Qubain, B. (2000). Incorporating Subgrade Lime Stabilization into Pavement Design.

Rawas, A., & Goosen, M. (2006). Expansive Soils: Recent Advances in Characterization and Treatment. London, UK: Taylor & Francis group.

Robertson, P., & Campanella, R. (1983, November). Interpretation of Cone Penetration Tests. *Canadian Geotechnical Journal*(Vol. 20), No. 4.

Roscoe, K., & Burland, J. (1968). On the generalized stress-strain behaviour of 'wet' clay. *Engineering plasticity*, 535-609. Cambridge: Cambridge University Press.

Roscoe, K., Schofield , A., & Wroth , C. (1958). On the Yielding of Soils. *Géotechnique(8)*, 22-53. http://doi.org/10.1680/geot.1958.8.1.22

Savastano, H., Warden, G., & Coutts, P. (2000). Brazilian waste fibers as reinforcement for cement-based composites. Cement Concrete Compos. 379–384.

Segetin, M., Jayaraman, K., & Xu, X. (2007). Reinforcement of soil–cement building materials: manufacturability and properties. *Build Environment*, 66-79.

Skempton, A. (1957). Discussion on planning and design of the new Hong Kong airport. *Proceedings Institution of Civil Engineers*(7), 305-307.

Şenol, A., Edil, T., Acosta, H., Benson, A., & C., H. (2006). Soft Subgrades Stabilization by Using Various Fly Ashes, Resources. *Conservation and Recycling*(vol.46), 365-376.

Taiebat, H., & Carter, J. (2008). Flow rule effects in the Tresca model. *Computers and Geotechnics*, 500–503. doi:10.1016/j.compgeo.2007.06.012

Tatsuoka, F., Jardine, R., & Benedetto, H. (1997). Characterising the pre-failure deformation properties of geomaterials. 2129-2164. International Society for Soil Mechanics and Geotechnical Engineering.

TRANSPORTATION RESEARCH BOARD (TRB). (1987). State-of-the-Art Report: Lime Stabilization Research, Properties, Design, and Construction. Washington DC, USA: National Research Council.

Tutluoglu, L., Oge, İ., & Karpuz, C. (2015). Relationship Between Pre-failure and Post-failure Mechanical Properties of Rock Material of Different Origin. *Rock Mech Rock Eng*(48), 121–141. doi:10.1007/s00603-014-0549-1

CURRICULUM VITAE